DEVELOPMENT AND CHARACTERISATION OF PHOTOCATALYTIC SURFACES THAT ARE ACTIVE UNDER FLUORESCENT LIGHT

A thesis submitted in partial fulfilment of the requirements

of Manchester Metropolitan University for the degree of Doctor of Philosophy

By

SOHEYLA OSTOVARPOUR

Faculty of Science and Engineering

School of Healthcare Science

Manchester Metropolitan University

2015

Table of contents

Table of contents

List of tables

List of figures

List of figures

Abstract

Hygiene and cleaning are of paramount importance to the food and beverage industry, but they also cause considerable costs to the industry in terms of production (energy, water and chemicals) and downtime of working hours for cleaning equipment. At the same time, environmental demands urge for reduction in water consumption and the use of more environmentally friendly chemicals. Photocatalytically active metal oxides, of which TiO_2 is most often used, generate strong oxidizing conditions when illuminated with UVA light (400-315 nm). In addition, they create hydrophilic surfaces, which can be cleaned by "sheeting" water that carries the dirt away. TiO_2 coatings therefore have the potential to reduce the attachment and viability of microbial cells. TiO_2 requires UV light in order to become activated, but doping the coatings with different transition metals can improve the visible light activity. In this project the physical vapour deposition technique of magnetron sputtering was used to produce well characterised photocatalytic coatings, to see whether the addition of the transition metal dopants W (tungsten), Nb (niobium), Ta (tantalum) and Mo (molybdenum) to TiO_2 coatings enhanced photocatalytic activity and antimicrobial properties under fluorescent light. The optimum photocatalytic activity, assessed by methylene blue degradation was shown by TiO_2-Mo (7 at. %) after annealing at a temperature of 600 °C presenting a mixed phase anatase/rutile crystal structure. These materials also exhibited an antibacterial effect under fluorescent light against *Escherichia coli*. However, the TiO_2-Mo and TiO_2-W (10 at.%) coatings inactivated *E. coli* under fluorescent light over a shorter incubation time (24 hours) in comparison to TiO_2-Nb and TiO_2-W (3.80 at.%) (48 hours). The TiO_2-Nb film did not show any bactericidal effect in the dark, but the Mo and higher concentration of W doped sample inactivated the bacteria in the dark as well as in the light after 24 hours. In this study, photocatalytic and bactericidal activity of TiO_2-Mo 7 at.% , TiO_2-Nb 0.25 at.%, TiO_2-W 3.8 at.% and TiO_2-W 10 at.% are demonstrated, when irradiated with fluorescent light with some surfaces also being innately antimicrobial in the dark. The chemical and mechanical stability of TiO_2-Mo and TiO_2 surfaces were assessed for their effectiveness *in situ* in bottle filling lines in breweries prior to and after placement. The results from the brewery trials demonstrated some durability with slight loss of Mo (0.5 at.%), 50% loss of photocatalytic activity, and some loss of adhesion to the substratum. In conclusion, the bactericidal properties of TiO_2 doped coatings can be exploited in environments where surface contamination is an issue. The difference between innate (TiO_2-Mo) and photo-activated (TiO_2-Nb) antimicrobial properties can also be exploited in appropriate environments. Some additional work on batch variability and coating stability is required.

Declaration

This is to certify that the material contained in this thesis has been produced by the author and has not been accepted in substance for any other degree and is not currently submitted in candidature for any other academic award.

Soheyla Ostovarpour

Abbreviations List

Term	Description
AC	Alternating Current
CA	Contact Angle
CVD	Chemical vapour deposition
CFUBMS	Closed field unbalanced magnetron sputtering
CFU	Colony Forming Unit
DC	Direct current
eV	Electron volt
EDX	Energy Dispersive X-Ray Spectroscopy
FWHM	Full width at half maximum
MIC	Minimum Inhibitory Concentration
NBT	Nitrotetrazolium Blue Chloride
OEM	Optical emission monitor
OD	Optical Density
PA	Photocatalytic Activity
PVD	Physical Vapour Deposition
PE	Polyethylene Film
RF	Radio Frequency
SEM	Scanning Electron Microscope
TSA	Tryptone Soya Agar
UMBS	Unbalanced Magnetron Sputtering
XRD	X-Ray Diffraction

Acknowledgements

I would like to thank Professor Joanna Verran and Professor Peter Kelly for their patience and advisory and technical support and also for allowing me to develop my own ideas and opinions, while keeping me on track. I would like to give special thanks to Dr Kathryn Whitehead for her advice and support. I would also thank to Dr Leanne Fisher and Dr Paul Benson for helping me with the Microbiology experiments. In addition I would like to acknowledge my sponsors TSB for funding this project and partners, Teer coating Ltd particularly, Dr Parnia Navabpour, Crystal Global (Dr Carin Tattershal), VTT (Dr Erna Storgards) and TUT in Finland for their technical support in the project. I would like to thank Dr Ivanka Lordanova and Dr Vladimire Vishnyakove for doing XRD and Raman analysis.

I wish to thank Marina Ratova for doing photocatalytic experiments with me and being always there for me, Ziad Benyamin for helping me with changing the target and Carolin Struller for WLI, and the rest of the people in Surface Engineering group for their support and patience.

The world is meaningless without having my sister, Saeideh next to me. I would like to thank her for making this life more meaningful and enjoyable. Finally and most importantly, I would like to thank my parents and grandparents, to whom I dedicate this thesis.

Chapter 1: Background and context

1. Introduction

Cleaning of food and beverage industry process surfaces is intended to guarantee product and consumer safety and satisfaction. In addition, the goal of improving energy and water saving and reducing chemical loads in the environment gives further support to the aim of finding novel means to maintain process hygiene. A hygienic design of process equipment has a tremendous impact on diminishing the risk of contamination of foods during production, which also means the shelf life of products is improved. If the applied process equipment is of a poor hygienic design, it is difficult to clean. They may survive and multiply in the crevices and dead areas, i.e. inaccessible regions of the equipment or the process line. Poor hygienic design of process equipment and components used in the food processing industry is a risk for food contamination. The hygienic design of process equipment and components should be based on a sound combination of process and mechanical engineering as well as knowledge in microbiology.

Self-cleaning or easy-to-clean coatings on food and beverage process surfaces would also reduce costs caused by production interruptions and consumption of energy, water, chemicals and working hours. The primary aim of this research was, therefore, to develop multifunctional materials and material solutions capable of reducing/inactivating microbial attachment on surfaces in the food and beverage industry. Titanium dioxide based photocatalyst thin films are of interest as self-cleaning and antimicrobial coatings, and were the focus of this project.

The project was carried out in co-operation between VTT Technical Research Centre of Finland, Tampere University of Technology Department of Materials Science (DMS/TUT), Oy Panimolaboratorio- Bryggerilaboratorium Ab Brewing Laboratory (PBL), Millidyne Oy, Manchester Metropolitan University, School of Engineering and School of Healthcare Science (MMU), Teer Coatings Limited (TCL-Miba), and Millennium Chemicals - Cristal Global (CG). The UK partners' work was funded by the Technology Strategy Board; the Finnish partners' work was funded by Tekes.

In this component of the overall project, based at MMU, titanium dioxide coatings were deposited by reactive magnetron sputtering, then characterised and modified to improve photocatalytic activity under fluorescent light using dopants. The influence and mechanism of action of the various doping elements are discussed in this thesis. The antimicrobial activity of selected coatings was assessed. The mechanical and chemical durability of these photocatalytically active coatings were evaluated prior to installation by VTT into different brewery environments in Finland. The samples were returned to the UK by post after 3, 10, and 12 months installation. Each sample was cut into three pieces and allocated to UK partners for scratch adhesion test, contact angle measurements, assessment of photocatalytic activity and fouling. The scratch adhesion test and contact angle measurement were carried out by Teer Coatings Limited (TCL-Miba), and Millennium Chemicals - Cristal Global (CG), respectively. Microbiological testing was carried out in a separate and subsequent study by VTT.

This chapter provides an overview of the work, including information on background and motivation, a description of the main research goals to be achieved, and information about thesis layout and list of publications.

1.1 Background and motivation

The aim of self-disinfecting coatings is to reduce the number of pathogenic microorganisms on an object or in an environment. TiO_2 (titania) is a versatile photocatalyst suited to a wide variety of photocatalytic applications. One of the applications is as an antimicrobial environmental surface which could be used in the food and beverage industries. TiO_2 is an n-type wide band gap semiconductor material which can be chemically activated by the absorption of light. However, the photoefficiency of this material is ultimately limited by its large band gap. Most photocatalytic applications of TiO_2 require UV illumination because the band gaps of the anatase and rutile polymorphs are 3.2 eV (~ 385 nm) and 3.0 eV (~ 410 nm), respectively. When TiO_2 is illuminated by UV light, inter-band transition occurs [1], where an electron from a valence band (VB) is promoted to the conduction band (CB) with simultaneous generation of a photogenerated holes (h^+) in the VB and photogenerated electrons (e^-) in the CB. These holes generate hydroxyl radicals by hole trapping and the excited electrons generate superoxide anions at the surface, which degrade organic pollutants into harmless intermediate organic compounds; CO_2 and H_2O [2]. As a result of its band gap, titania can only use radiation of wavelengths less than about 390 nm, which equates to about 3-5 % of the solar spectrum which greatly limits the potential for photocatalytic applications driven by sunlight. In order to improve the photocatalytic activity by extending the utilisable wavelength range of the solar spectrum, doping with different transition metals and non-metals can be implemented [1]. When adopting this strategy, it is desirable to maintain the crystal structure (anatase) of the photocatalyst while changing its electronic structure by doping. The crystal structure of the material is directly related to the ratio of cation and anion size in the crystal lattice. It appears to be relatively easier to replace Ti^{4+} in titania with any cation than to substitute O^{2-} with any other anion due to difference in charge states and ionic

radii [3]. The incorporation of transition metals in the titania crystal lattice, through doping may result in the formation of new energy levels between the valence band and conduction band, including a shift of light absorption towards the visible light region [4].

Titania can be deposited onto substrates using physical vapour deposition (PVD). Unbalanced reactive magnetron sputtering, used in this study, is an example of a PVD technique, which will explained in detail later.

This research project is based on using the magnetron sputtering technique for the deposition of photocatalytic titanium dioxide coatings and changing their properties with the use of different transition metals as dopant, and by varying the sputtering mode.

1.2 Research aims and contributions

The overall aim of this project was to develop well characterised photocatalytic coatings that inhibit/inactivate attached microorganisms under fluorescent light, suitable for environmental use in areas such as the bottle filling lines in the brewing industry. To achieve this aim, the following objectives were carried out:

1. Develop and characterise (photochemically) a range of TiO_2 photocatalytic coatings using different transition metals (W, Mo, Ta and Nb) as dopants.
2. Assess their photocatalytic activity in terms of the degradation of an organic dye (methylene blue).
3. Evaluate the antimicrobial properties of those selected coatings using *Escherichia coli* as a model organism.
4. Assess the chemical and mechanical durability of selected coatings.
5. Identify coatings with physical properties suitable for use in the bottle filling equipment in the beverage industry.

6. Place coated active surfaces into breweries and assess their effectiveness over time in terms of photocatalytic activity, scratch adhesion testing, and water contact angle measurements.

VTT and PBL contributed in this project by installing the coated photocatalytic active surfaces into three different Finnish breweries. TCL-Miba and CG contributed by carrying out the scratch adhesion test and contact angle measurements. All other work was done by the author.

1.3 Thesis structure

The thesis is divided into eight chapters and appendix A and B. A more detailed description of the thesis structure is as follows:

Chapter 1: Defines the background of the research carried out, as well as providing an overview of research aims and contributions by the project partners.

Chapter 2: Introduces the main principle of titanium dioxide photocatalysis and its applications. The chapter also addresses the limiting factors that affect the photocatalytic activity of titanium dioxide and describes how its photoactivity might be enhanced.

Chapter 3: Presents an overview of thin films and their growth processes and introduces the techniques of thin film production. This chapter is focused on physical vapour deposition techniques and various modes of magnetron sputtering.

Chapter 4: This chapter describes the experimental set up used for coating production and the assessment of their antimicrobial activity. It also gives an overview of techniques used for analysing the thin films.

Chapter 5: Gives an overview of the transition metal doped titania coatings and discusses their structure, morphology and photocatalytic activity, and the effect of selected transition metals on the properties of the coatings.

Chapter 6: Reviews the antimicrobial activity of titanium dioxide doped with different transition metals. This chapter also discusses the effect of transition metals and their oxides on the inactivation of bacteria.

Chapter 7: Discusses the chemical and mechanical durability of selected coatings and their effectiveness by measuring their photocatalytic activity, conducting scratch adhesion testing and contact angle measurements after being installed in different brewery environments for 3, 10 and 12 months.

Chapter 8: General conclusion on photocatalytic and antimicrobial activity of doped titanium dioxide coatings which were placed *in situ* and suggests the possibilities of further research work required in this area.

Appendix A: Results relating to the accuracy of the proposed photocatalytic testing technique.

Appendix B: EDX penetration depth calculation

Appendix C: List of publications.

Chapter 2: Titanium Dioxide Photocatalysis

2.0 Introduction

2.1 Semiconductor photocatalysis

A semiconductor is a material with conducting properties between those of a good insulator and a good conductor. A photocatalyst is a semiconductor material which can be chemically activated by the absorption of light. The discovery that impacted most significantly on the field of semiconductor photocatalysis was the "Honda-Fujishima Effect" first described by Fujishima and Honda in 1972, by the splitting of water on a TiO_2 electrode under UV light [5]. Subsequent to this, work on TiO_2 has proceeded apace.

The main criterion for an efficient semiconductor photocatalyst is that the redox potential of the charge couple, *i.e.*, e^-/h^+, lies within the band gap domain of the photocatalyst (+2.53 V for titania). The photocatalytic process takes place when photons have a higher energy than the band gap value of the semiconductor photocatalyst. These photons can be absorbed and an electron is promoted to the conduction band, leaving a hole in the valence band.

The energy level at the bottom of the conduction band determines the reducing ability of photoelectrons while the energy level at the top of the valence band determines the oxidizing ability of photogenerated holes, each value reflecting the ability of the system to promote reductions and oxidations [1]. As well as having suitable band gap energy ($\leq$ 3eV), an ideal semiconductor should also be easy to produce and use, cost effective, photostable, non-hazardous for humans and the environment, and able to catalyse chemical reactions on the surface of materials effectively. Many of the reported photocatalysts have limitations, e.g., GaAs, PbS, and CdS are not sufficiently stable for catalysis as they readily undergo photocorrosion and are also toxic [6].

TiO_2 is close to being an ideal photocatalyst and is the benchmark for photocatalysis performance. Titanium dioxide, also known as titania, is a naturally occurring oxide of titanium. Wide band gap materials are defined as semiconductors with band gaps greater than 1.7 eV. Titania is an n-type wide band gap semiconductor material. It is cheap, stable, non-toxic and environmentally benign. The most common polymorphs of titania are anatase and rutile which they have different physical properties. TiO_2 has many applications, since it can be used either as nano-particles in powder form or as a thin film coating on different substrates. Its principal usage is as a white pigment in paints (in the rutile form), plastic goods, rubber, inks and paper, but it is also incorporated into a diverse range of products such as pharmaceuticals, cosmetics and food additives. TiO_2 is activated by the absorption of light, through which it has been found to decompose organic materials (in the anatase form) and inhibit bacterial growth [7].

2.2 TiO_2 photocatalysis

TiO_2 photocatalysts have received a significant amount of research interest during the last 40 years owing to the various environmentally valuable applications of such materials [5]. When a TiO_2 semiconductor is excited by photons with energy equal to or higher than its band gap energy, electrons receive energy from the photons and are thus transferred from the valance band to the conduction band. Upon light absorption, the photocatalytic TiO_2 generates pairs of electrons (e^-) and holes (h^+). The photogenerated electrons and holes can recombine within a very short time, releasing energy in the form of heat. Therefore, it is essential to avoid the recombination of electrons and holes in photocatalytic reactions. Electrons and holes that migrate to the surface of the TiO_2 semiconductor without recombination can, respectively, reduce and oxidise the reactants adsorbed by the semiconductor.

It is generally believed that the photon induced electron-hole pairs can react with O_2 dissolved in water to form $^{\bullet}OH$ radicals (equation 2.1, 2.2). These radicals can reduce or oxidize pollutants in water and air.

$$TiO_2\ (h^+_{VB}) + H_2O_{ads} \longrightarrow TiO_2 + {}^{\bullet}OH_{ads} + H^+_{aq} \qquad (2.1)$$

$$TiO_2\ (h^+_{VB}) + OH^-_{ads} \longrightarrow TiO_2 + HO^{\bullet}_{ads} \qquad (2.2)$$

Hydroxyl radicals are produced by holes (h^+) in valence bands (VB) and superoxide anions ($O_2^{\bullet -}$) are produced by excited electrons in conduction bands (CB) (equation 2.1-2.8). This reaction prevents e^-/h^+ recombination in the absence of other electron acceptors.

$$TiO_2\ (e^-_{CB}) + O_2 \longrightarrow TiO_2 + O_2^{\bullet -} \qquad (2.3)$$

Equation 2.3-2.8 shows the reaction pathways for the electrons released by irradiation of a photocatalyst with dissolved molecular oxygen.

$$TiO_2\ (e^-_{CB}) + O_2^{\bullet -} + 2H^+ \longrightarrow TiO_2 + H_2O_2 \qquad (2.4)$$

$$O_2^{\bullet -} + H^+ \longrightarrow HO^{\bullet}_2 \qquad (2.5)$$

$$O_2^{\bullet -} + 4HO^{\bullet}_2 \longrightarrow 2HO^{\bullet} + 3O_2 + H_2O_2 \qquad (2.6)$$

$$HO^{\bullet} + HO^{\bullet}_2 \longrightarrow O_2 + H_2O \qquad (2.7)$$

$$2HO^{\bullet}_2 \longrightarrow O_2 + H_2O_2 \qquad (2.8)$$

Both favourable and unfavourable effects in photocatalytic degradations can be expected from the presence of H_2O_2. Hydrogen peroxide enhances the photodegradation rate of organic adsorbed pollutants under certain conditions, probably by the formation of $HO^{\bullet}$ radicals either indirectly via superoxide ions (equation 2.9) or directly via the reduction of H_2O_2 by

conduction band electrons (equation 2.10). It is also degraded over band gap irradiated TiO_2 (equation 2.11).

$$H_2O_2 + O_2^{\bullet-} \longrightarrow O_2 + OH^- + HO^{\bullet} \quad (2.9)$$

$$TiO_2\ (e^-_{CB}) + H_2O_2 \longrightarrow TiO_2 + OH^- + HO^{\bullet} \quad (2.10)$$

$$H_2O_2 + h\nu \longrightarrow 2HO^{\bullet} \quad (2.11)$$

These reducing and oxidising agents (hydroxyl radicals and superoxide anions) can destroy organic and biological compounds (Figure 2.1). Applications of such TiO_2 photocatalytic coatings include self-cleaning coatings [8], antimicrobial coatings [9], and water purification [10].

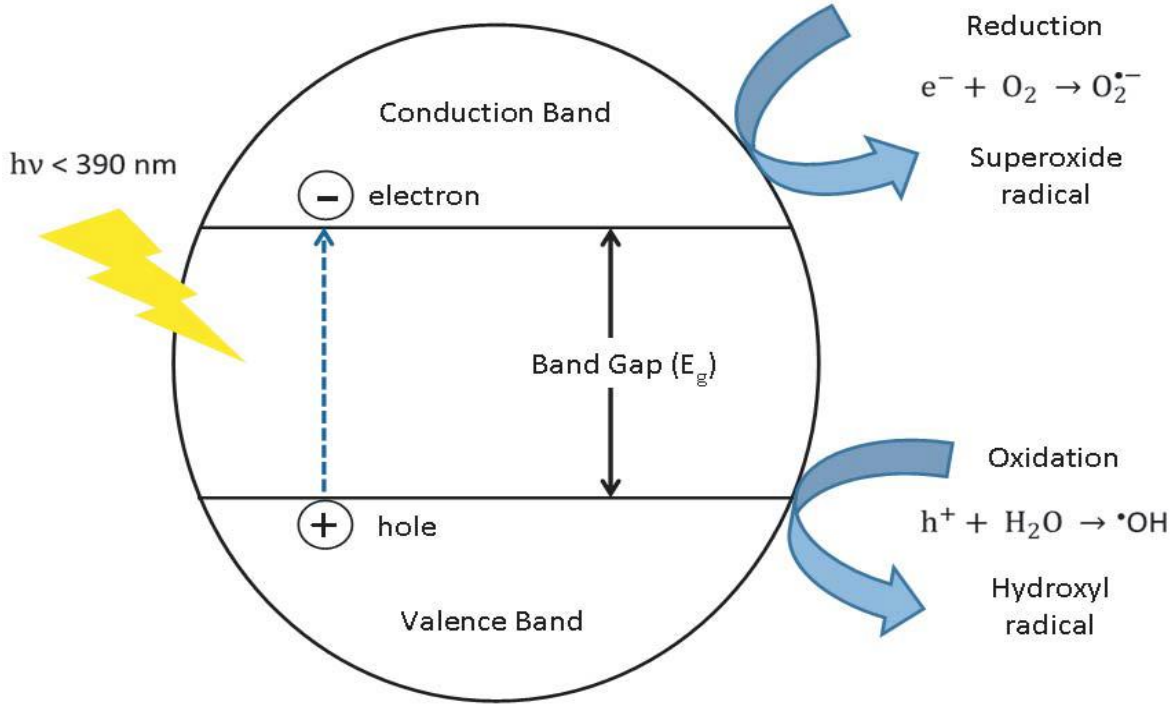

Figure 2.1: Mechanism of light absorption by TiO_2 showing how the light absorption (< 390 nm) produces electrons and holes.

2.3 Crystal structure of titanium dioxide

TiO_2 exists in three forms with different crystal lattice structures, with each having different physical properties. These are rutile, anatase and brookite. Anatase and rutile crystallize in a tetragonal system. Although anatase and rutile are chemically identical, there are differences in the arrangement of the titanium and oxygen atoms within the crystal that result in different crystal lattices. Rutile is thermodynamically the most stable form. It has a tetragonal structure and contains six atoms per unit cell. The TiO_6 octahedron is slightly distorted (Figure 2.2) [11]. Anatase also has a tetragonal structure but the distortion of the TiO_6 octahedron is slightly greater for the anatase phase than the rutile phase [12]. These differences in lattice structures cause different mass densities, electronic band structures, specific gravity, hardness, refractive index and weathering performance [13, 14]. Brookite belongs to the orthorhombic crystal system. Its unit cell is composed of eight units of TiO_2 and is formed by edge-sharing the TiO_6 octahedron. It is more complicated, has a larger cell volume and is also the least dense of the three forms (Figure 2.3) [15]. The photocatalytic activity of the rutile phase is poor. In some recent work brookite was shown to have higher photocatalytic activity compared to anatase and rutile; but it is difficult to manufacture [16]. The anatase structure is preferred over other polymorphs for photocatalytic applications due to its higher Fermi level, lower capacity to absorb oxygen and higher degree of hydroxylation [17]. The Fermi level of anatase is higher than that of rutile by 0.1 eV. This results in a higher level of hydroxyl groups on the surface and thus greater photocatalytic activity.

Although the band gap energy value of rutile is lower than that of anatase, the latter shows higher photocatalytic activity (anatase 3.23 eV > rutile 3.06 eV) [14]. The band gap is called direct if the momentum of electrons and holes is the same in both the conduction band and the valence band; an electron can directly emit a photon. In an indirect gap, a photon cannot

be emitted because the electron must pass through an intermediate state and transfer momentum to the crystal lattice. Anatase has an indirect band gap however, rutile has a direct band gap, and as a result the anatase conduction band is located away from the maximum in the valance band. This results in the ability of electrons to stabilize at the lower level of the conduction band itself, consequently giving a longer life-time and greater mobility. In a direct band gap material, the minimum in the conduction band overlaps with the maximum in the valance band, thus enabling an early return of an electron to the valance band.

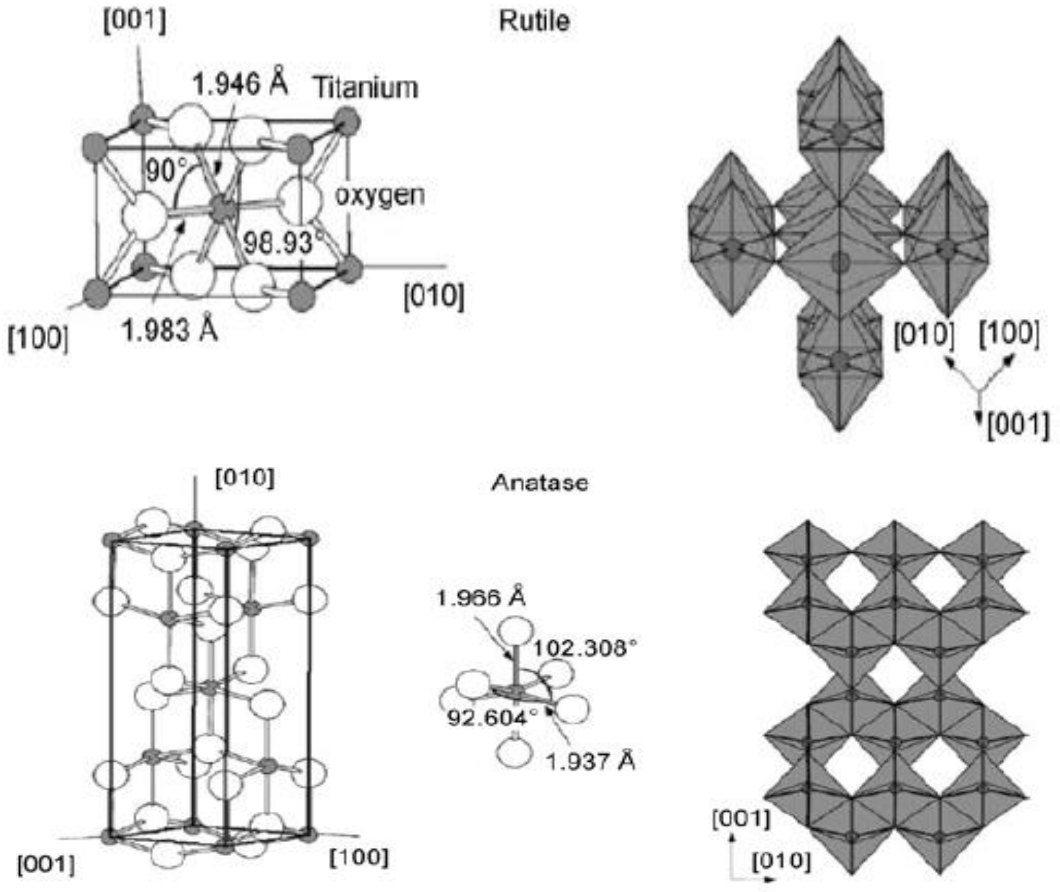

Figure 2.2: Crystal structure of the rutile and anatase phase demonstrating how titanium and oxygen atoms are arranged in the lattice [11].

Anatase has a wider optical absorption gap. Hence, it is proposed that the excitation electron mass of the outer shell electrons in anatase may be lower than in the case of rutile [18]. This may explain the higher mobility of electrons in the anatase. The wider band gap energy of anatase would also generate more hydroxyl radicals. This allows a more extensive chemisorption (reaction) of oxygen, although the difference may not be sufficient to explain the large difference in reactivity between the two crystalline forms. It was found that a anatase/rutile mixed phase was more active than a single phase [19, 20]. Mixed-phase titania catalysts showed greater photo-effectiveness due to three factors: 1) the smaller band gap of rutile extends the useful range of photoactivity into the visible region; 2) the stabilization of charge separation by electron transfer from rutile to anatase slows recombination; 3) the small size of the rutile crystallites facilitates this transfer, making catalytic hot spots at the rutile/anatase interface. [20, 21].

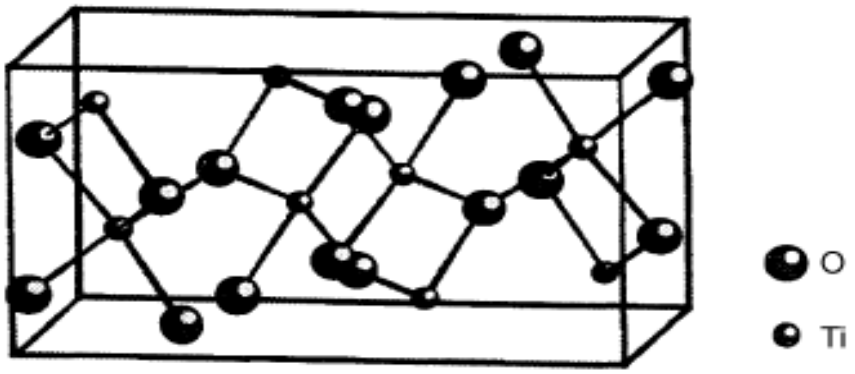

Figure 2.3: Lattice structure of brookite TiO_2 showing how titanium and oxygen atoms are arranged in the lattice [22].

2.4 Applications of photocatalytic TiO_2 coatings

2.4.1 Antimicrobial properties

Disinfection is one of the most common and important methods of controlling numbers of pathogens for the sterilization of critical instruments, water treatment, food production, and in hospitals or health care facilities. TiO_2 based photocatalysts have been used to inactivate pathogenic microbes, including bacteria, fungi and viruses [23], thus providing new approaches to disinfection. One advantage of photocatalytically sterilizing surfaces is that they operate in a passive fashion and hence function without the need for electrical power or chemical reagents only light, oxygen and water are required. Unlike chemical antibacterial agents, TiO_2 surfaces are non-toxic and will not cause environmental pollution.

There are many reports on antimicrobial activity of reactive oxygen species photogenerated upon UV and visible light irradiation at TiO_2 surfaces and TiO_2 suspended nanoparticles [24-28]. These demonstrate significant interest in this technology across a wide range of applications.

There are a variety of targets in/on the microbial cell, for the reactive oxygen species generated by TiO_2 photocatalytic reactions. In the initial studies by Jacoby *et al*. [29], a decrease in intracellular coenzyme A (CoA) in the TiO_2 treated cell was detected for various microorganisms. Cell death was caused by the direct oxidation of CoA thus inhibiting cell respiration. This mode required a direct contact between TiO_2 and the target cell to ensure the direct oxidation of cell components [30, 31]. However, the majority of studies showed that the lethal action is due to membrane and cell wall damage. These studies include microscopic and spectroscopic studies [32-36].

Kiwi *et al.* [32] investigated the peroxidation process of *Escherichia coli* using a TiO_2 photocatalyst. One of the toxic effects of reactive oxygen species is the damage to the cellular

system which is initiated by a process known as peroxidation. The destruction of *E. coli* cells on a TiO_2 porous film was followed by analysis using ATR-FTIR techniques. The decay of the polysaccharide bands, acyl bonds, $>CH_2$, $-CH_3$ bands, and amide bands by TiO_2 films was reported. The oligosaccharide bands of *E. coli* and LPS and the isolated CdC-H bands disappeared during short irradiation times. The formation of peroxidation products such as aldehydes, ketones, and carboxylic acids was detected in parallel with the disappearance of the constituents of the cell wall membranes. The FTIR spectra found that the peroxidation products of *E. coli*, LPS (lipo-polysaccharide), PE (phosphatidyl-ethanolcholine), and PGN (peptidoglycan) revealed numerous features related to the appearance of oxidation products due to the TiO_2 photocatalysis on sugar rings, lipid chains, and polypeptide molecules. The ATR-FTIR data about LPS on TiO_2 surfaces suggest the introduction of disorder in the LPS lipid layer during photocatalysis. The peroxidation of LPS on TiO_2 was faster than that of *E. coli* on TiO_2, suggesting that the order of the LPS bilayer structure determines the rate of the photocatalytic peroxidation process. The comparison of the peroxidation of three main components of the wall LPS, PE, and PGN show that PGN is the most resistant toward peroxidation. They noted that photocatalytic peroxidation induced changes of the ATR-FTIR spectra of the *E. coli* occur due to two reasons: first, the decrease of the initial bio-molecule concentration and concomitant formation of peroxidation products and second the photocatalytic induced structure modification of the wall membrane giving rise to the shift of $>CH_2$ vibration peak assigned to the fatty tails of lipid molecules. The latter peak shift is proof that structural transformation occurred in the lipid layer. This shift seems to be the precursor of the structural changes in the cell wall membranes during lipid peroxidation leading to bacterial lysis in the later stages of the photocatalysis. By laser photolysis, it was shown that the reaction of *E. coli*, LPS, or PE with the hole (h^+) competes with the

recombination reaction of the h^+ with e^-. This reaction is considered as the initial step in the chain-radical peroxidation process.

In another paper Nadtochenko *et al.* [34] found that during the initial stage of treatment with TiO_2, photokilling could be attributed to the increase in the lipid-layer fluidity of the *E. coli* cell walls. This structure and fluidity of the LPS monolayer has been reported to be very sensitive to peroxidation in the case of polar-saccharide moieties [37]. Shifting of the –CH symmetric stretching (ν_s (CH_2)) band during TiO_2 photocatalysis was found to be a valuable tool for monitoring of the progressive disorder LPS in Gram-negative *E. coli* bacteria (Figure 2.4,b) as the precursor event of the bacterial lysis.

Scanning electron microscopy (SEM), transmission electron microscopy (TEM) and atomic force microscopy (AFM) were used in order to study the effect of TiO_2 on microorganisms. Kangwansupamonkon *et al.* [35] reported the morphological disruption of bacterial cell walls by SEM on an apatite coated TiO_2 suspension after UVA irradiation for *E. coli*, MRSA, *S. aureus* and *M. luteus*. Chung *et al.* [36] studied the antibacterial effect of anatase TiO_2 by TEM and found that *S. aureus* was killed by the detachment of the cell wall from the cell membrane, while *E. coli* suffers from changes in the nucleoid pattern from relaxed to condensed state (in addition to cell wall damage).

Gram positive bacteria were found to be more resistant to photocatalytic disinfection than Gram negative bacteria [38, 39]. The difference is attributed to the difference in cell wall structure (Figure 2.4,a), since the Gram positive bacteria have a thicker peptidoglycan layer and no outer membrane whereas Gram negative bacteria have a triple layer cell wall with an inner membrane, a thin peptidoglycan layer and an outer membrane. Fungi and algae have also been shown to be susceptible to photocatalytic disinfection. However, they were found to be more resistant to photo-killing than bacteria due to differences in size and structure [40, 41].

a)

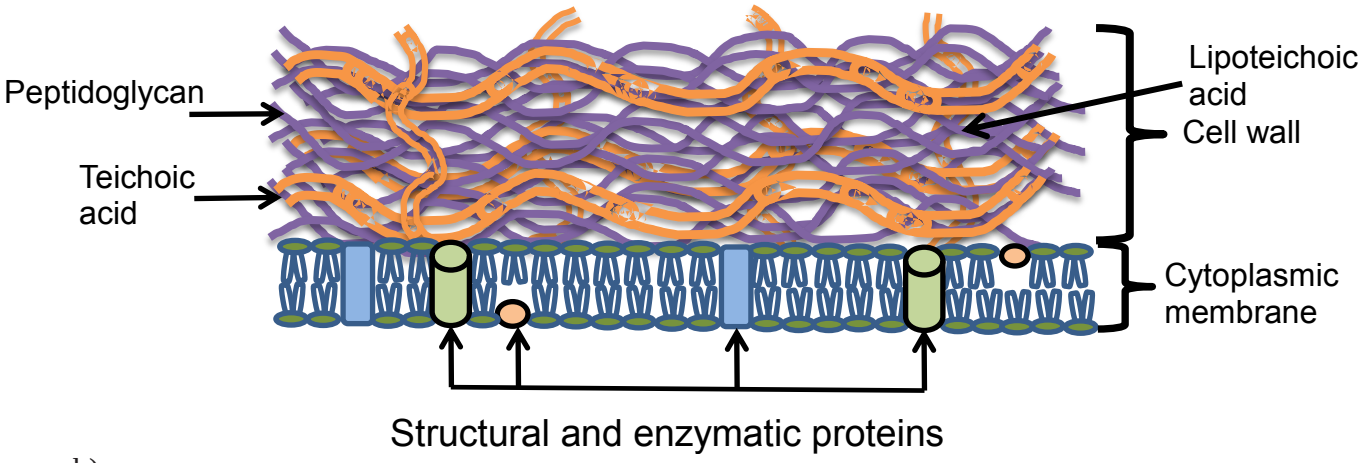

b)

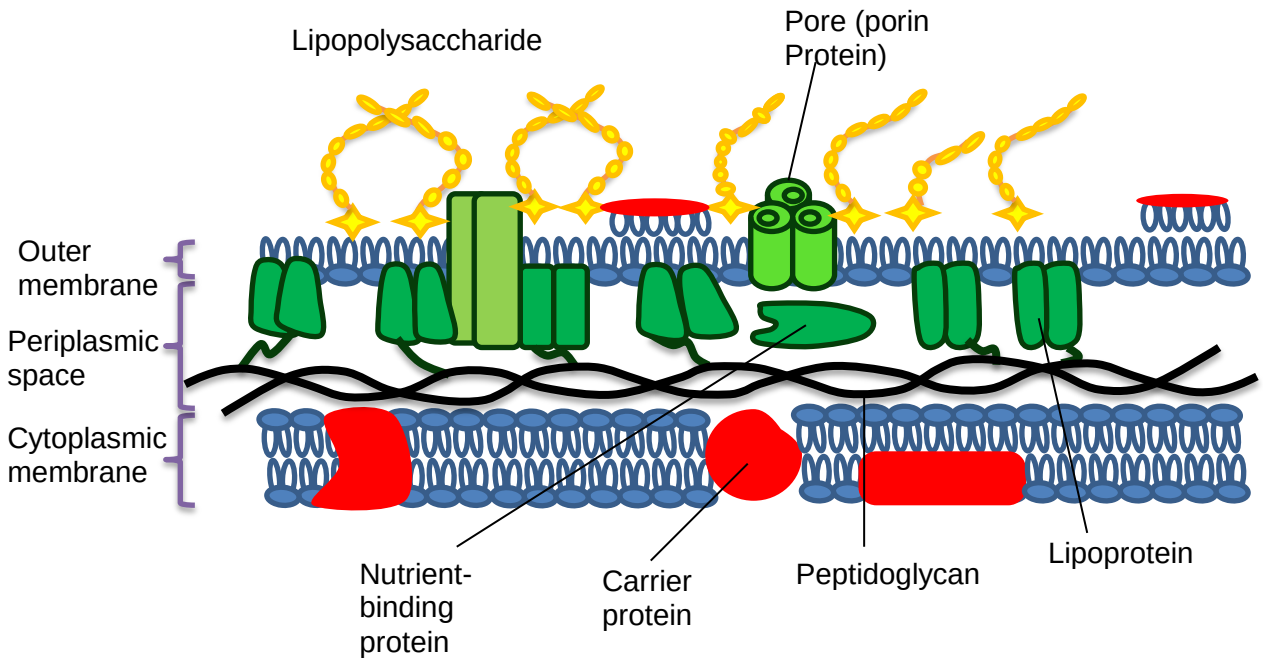

Figure 2.4: Cross section through cell walls of a) Gram positive and b) Gram negative bacteria [42].

2.4.2 Self-cleaning coatings

The technology of self-cleaning coatings and surfaces has grown quickly in recent years. This is due to a widespread variety of applications from window glass, mirrors, lenses and cements to textiles [43]. The field of self-cleaning coatings is divided into two categories: hydrophobic and hydrophilic [44]. These two types of coatings clean themselves through the action of water, the former by enhancing droplet formation and the latter by spreading water, thus removing dirt.

Toma *et al.* [45] reported the degradation of gaseous nitrogen oxide pollutants such as NO and NO_x by spray applied TiO_2 coatings. Zhang *et al.* [46] reported on anti-reflective TiO_2 - SiO_2 self-cleaning coatings that may find applications for the surfaces of solar cells. It has been reported that ceramic tile coatings incorporating TiO_2 were very effective in terms of breaking down organic and inorganic materials, as well as inactivating bacteria and it was suggested that these ceramic tiles can be used in hospitals to reduce the spread of infections particularly around patients whose immune systems have been weakened [45]. Yaghoubi *et al.* [47] produced a self-cleaning TiO_2 coating on a polycarbonate substrate by employing a chemical surface treatment method to create hydrophilic groups on the polycarbonate substrate. Beobide *et al.* [48] employed a dip coating technique to produce multi-functional coatings consisting of a mesoporous SiO_2 layer and a dense/mesoporous TiO_2 layer. This coating exhibited both anti-reflective and self-cleaning properties.

Wetting is the term used to describe how liquid behaves on a solid surface. The contact angle (θ) of water or another liquid makes with a substrate is an important parameter to define the wetting of a liquid on a solid surface. When the water contact angle θ is less than 65° the surface is hydrophilic. On a superhydrophilic surface the contact angle for water with the surface is less than 5° (Figure 2.5). The main advantage of TiO_2 - based hydrophilic surfaces

is the combined hydrophilicity- photodegradation effect, that aids cleaning process significantly [49]. The super-hydrophilisation mechanism of TiO_2 upon UV irradiation also involved electrons and holes but proceed via a different route to photocatalysis. During super hydrophilisition electrons tend to reduce the Ti (IV) cations to the Ti (III) state, and the holes oxidize the O_2^- anions. In the process, oxygen atoms are ejected, creating oxygen vacancies. Water molecules can then occupy these oxygen vacancies, producing adsorbed OH groups, which tend to make the surface hydrophilic. The longer the surface is illuminated with UV light, the smaller the contact angle for water becomes [7, 50].

The photo-induced hydrophilic effect was initially thought to involve only the photocatalytic removal of hydrocarbon contamination films. Mills *et al*. [51] studied the effect of UV/O_3, heating and strong acid pre-treatment on primarily hydrophobic samples of Pilkington Activ^{TM} glass (self-cleaning glass which has manufactured by Pilkington Ltd) and plain glass. They found that the photo-induced hydrophilicity is due to UV-driven removal of hydrophobic surface organics by photocatalytic oxidation process via the photogenerated holes. Fujishima *et al.* [7] found that titania surfaces can have more photocatalytic properties and a less superhydrophilic character, and vice versa, depending on composition and processing. It could be concluded, that the existence of photocatalytic properties does not guarantee super-hydrophilicity and vice versa [52].

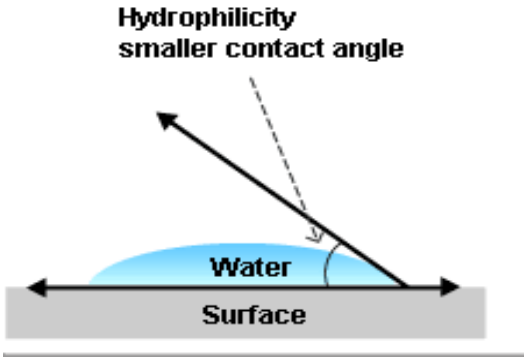

Figure 2.5: Superhydrophilic surface.

2.4.4 Other applications

Photocatalysis is an attractive approach to water treatment as this technique does not involve the consumption of chemical reagents; enables the removal of a variety of pollutants; is effective across a wide range of pollutant concentration levels, and can be achieved using solar irradiation as the sole energy input [53-55]. A suspension (TiO_2 nano powder) based system and an immobilized substrate supported system are two approaches which have been used for photocatalysis with TiO_2 nanoparticles. TiO_2 powders have higher surface areas than coatings, which results in higher photocatalytic activity [45]. However, the separation of powder from the liquid state is difficult, and also because the depth of penetration of UV light is limited due to strong absorption by both catalyst particles and dissolved organic species. To overcome these problems different substrates have been used for coatings, such as glass and stainless steel [45].

Water contaminated with metal and organic species has been treated by using TiO_2. It has been reported that Ag (I), Hg (II), Cr (VI), and Pt (II) contaminants were easily removed by photocatalytic reduction by 0.1 wt% TiO_2, whereas Cd (II), Cu (II) and Ni (II) were not removed. The ability of TiO_2 to remove metals from water was found to depend on the

standard reduction potential of the target metal [56]. Ag (I) and Hg (II) could be reduced to Ag^0 and Hg^0, respectively, and subsequently were deposited onto the catalyst surface, and can subsequently be extracted from the slurry by mechanical and/or chemical means [57].

An environmentally friendly fuel production process uses TiO_2 photocatalysts to generate hydrogen as a source of energy via splitting of water. Photocatalysis using solar energy has been widely studied as a possible system to produce hydrogen from water. The possibility of solar photoelectrolysis was demonstrated for the first time with a system in which an n-type TiO_2 semiconductor electrode was connected through an electrical load to a platinum black counter electrode. When the surface of the TiO_2 electrode was irradiated with near-UV light, photocurrent flowed from the platinum counter electrode to the TiO_2 electrode through the external circuit, showing that water can be decomposed into oxygen and hydrogen without the application of an external voltage. The direction of the current revealed that oxygen evolution occurred at the TiO_2 electrode and hydrogen evolution occurred at the Pt electrode [58].

2.5 Factors limiting the photocatalytic activity of TiO_2

Despite the positive characteristics of TiO_2, there are some disadvantages associated with its use as a photocatalyst. Firstly charge carrier recombination occurs within nanoseconds so the rate of recombination of e^-/h^+ pairs increases compared to the separation rate [59, 60]; secondly the band gap absorption threshold does not allow operation in visible light [61]. To circumvent these particular limitations, a number of strategies have been proposed to improve the light absorption features and lengthen the carrier life time characteristics of TiO_2. The photocatalytic activity of a catalyst can be influenced by its crystal structure, surface area, particle size distribution, porosity, band gap and surface hydroxyl group density [62]. Various

methods have been used to enhance the photocatalytic activity of titania including: dye sensitization, doping, coupling, and capping [63-65].

One approach to overcome these problems, is adding metal and non-metal dopants to TiO_2. Carbon, nitrogen and silicon are the most used non-metal dopants. Upon addition of N, the crystal structure and photocatalytic activity has been extended into the visible range [66]. Narrowing the band gap and improvements in the crystallinity and photocatalytic activity of TiO_2 films have been also observed at dopant concentrations of less than 10 at.% transition metals incorporation [67-70].

2.5.1 Metal – doped TiO_2 thin films

Doping of TiO_2 has been an important approach in band gap engineering to change the optical response of semiconductor photocatalysts. The main objective of doping with transition metal ions is to provide additional energy levels within the band gap of a semiconductor. Electron transfer from one of these levels to the conduction band requires lower photon energy than in the situation for an unmodified semiconductor.

Doping TiO_2 with transition metals gives rise to formation of defect sites such as Ti^{3+} in the semiconductor lattice, where the oxidation of Ti^{3+} species is kinetically fast compared with the oxidation of Ti^{4+}. The differences in photoactivity derive from the change in the diffusion length of the minority carriers (e^-/h^+) [71].

The dopant content directly influences the rate of e^-/h^+ recombination, which affects the photocatalytic activity. In a previous report, Choi *et al.* [72] found that if a dopant concentration is below the optimal value, the photoreactivity increases with an increasing dopant concentration, because there are fewer trapping sites available to suppress the recombination of electrons and holes. However, for a higher dopant concentration beyond the

optimal value, the excess trapping sites become efficient recombination centres because the average distance between the trap sites decreases with an increasing number of dopants confined within a particle. This increases the recombination rate.

Apart from the concentration of the transition metal dopants, the ionic radius of the dopant ion plays an important role in the enhancement of photocatalytic activity. Some authors [72-74] have investigated the effect of dopant ion and its ionic radius in the titanium dioxide lattice. They have shown that, if the ionic radius of dopant ions is smaller than that of titanium (0.074 nm) e.g. Mo^{6+} (0.073 nm), then the dopant ions enter the lattice of titanium dioxide in a substitutional manner, while larger doping ions enter the lattice in an interstitial manner e.g. Pd^{2+} (0.086 nm). The change of the potential level of transition metal ions in interstitial and substitutional positions is different, and they have different trapping efficiency for electrons. The effect of interstitials in distorting the potential energy is larger than that of substitutional atoms. Substitutionally incorporated dopants are less useful for disturbing the dopant energy level, which in turn affects the electron trapping efficiency. For the interstitial dopants, the potential energy can be increased negatively towards the conduction band edge because of the oxygen affinity of the dopant ions. The high oxygen affinities of interstitially located dopant ions effectively create a localized positive charge around Ti and/or form oxygen vacancies. The potential energy of dopant ions are disturbed and electrons are efficiently trapped. Therefore, the oxidation process could be improved significantly. Shah *et al.* [73] found interstitial dopants to be more photoactive. However, other research groups were found the substitutional dopants to be more photoactive [72, 74].

Shen *et al.* [75] reported that Nb doped coatings have shown an enhancement of photoactivity in the visible range. As the ionic radii of Nb^{5+} (0.074 nm) is close to that of Ti^{4+} (0.074 nm), the Nb^{5+} acts as a charge compensation mechanism in the titania lattice rather than on the induced stress, so it would reduce the amount of oxygen vacancies since it has

higher positive charge than Ti. The charge compensation of Nb^{5+} is achieved either by the creation of one vacancy per titanium site per four Nb^{5+} introduced, or by reduction of one Ti^{4+} to Ti^{3+} per Nb^{5+} introduced. Both mechanisms may be present, the latter being much more likely to occur at high temperatures. Whatever the case, the presence of a vacancy on a titanium site or the stress induced by the presence of Ti^{+3}, suggests that a higher solubility limit of niobium into TiO_2 may be found in anatase than rutile, in line with the undoped TiO_2. However, for a complete description of possible Nb-doped TiO_2 defects, the occurrence of oxygen vacancies also has to be considered [76].

Ahmad *et al.* [77] investigated the effect of niobium doping on titanium dioxide. They have found that as the concentration of Nb metal increased from 0.5 at. % to 1.5 at.%, there were fewer rutile related reflections in the XRD traces. Thus the Nb dopant stabilizes the formation of anatase in the titania lattice. As the annealing temperature increased up to 700 °C in their samples, the crystallinity became stronger and more predominant. Niobium doping caused a decrease in band gap energy and introduced an additional transition level at 2.8 eV, which corresponds well to the assumption that niobium creates shallow electron traps below the conduction band. TiO_2: Nb with Nb concentrations of up to 1 at.% showed an improvement in photocatalytic performance towards methylene blue decomposition under both types of irradiation, which was better than commercial Degussa P25 TiO_2.

Akurati *et al.* [78] reported that addition of WO_3 to TiO_2 caused an increase in the photocatalytic activity of the resultant film under UV irradiation. As the concentration of WO_3 increased in doped titania the film became less crystalline. The coordination of WO_x species changed from tetrahedral to octahedral with increasing concentration of WO_3. At a lower concentration of WO_3, highly amorphous WOx species formed on the surface of W doped TiO_2 substrate particles. This surface layer enhanced the acidity of the particles so more hydroxyl groups and more organic reactants can be adsorbed on its surface, leading to

significantly improved photocatalytic activity (as measured by the degradation of methylene blue) relative to commercial P25- TiO_2.

Molybdenum (Mo) is another transition metal dopant which has been shown to enhance photoactivity at Mo levels ≥ 1 at. % [79]. Lopez *et al.* [80] produced TiO_2/Mo powders with Mo levels of 0-5 wt. % using sol-gel methods. The samples were annealed at 500 °C. The highest photocatalytic activity was obtained at Mo levels of ca. 1 wt. %. Stengl *et al.* [81] found that incorporation of molybdenum ions into the crystal lattice of anatase TiO_2 changes the morphology of particles from spindle-like shapes to rectangular or square-like. The molybdenum addition also increases the anatase phase stability to above 900 °C by inhibiting the growth of anatase crystallite, the increase of the lattice constants of anatase; and the red shift of the optical absorption of molybdenum doped anatase. The latter effects mean that, the molybdenum addition increases the photocatalytic activity of titania in the visible region of the electromagnetic spectrum.

In summary, there is no uniform theory governing the selection of suitable doping metal to enhance the photoactivity of titania, but some examples are described in the literature [73, 74]. Thus, to decrease the band gap of titania, a transition metal is expected to be incorporated into the titania lattice, rather than form a separate phase. This suggests that the ionic radius of transition metal should be comparable to that of titanium. It is also suggested that doping of titania with transition metal cations with valences greater than 4 has a better performance on photocatalytic properties, e.g. Mo^{6+} [82].

2.5.2 Non-metal – doped TiO_2 thin film

Doping TiO_2 with different anions has been investigated by many groups in order to increase the photoactivity when irradiated with visible light [83-92]. Anions have been used as a substitute for oxygen in the TiO_2 lattice. For these anion-doped TiO_2 photocatalysts, the mixing of the 2p states of the doped anion (N, S or C) with the O 2p states shifts the valence band edge upwards, narrowing the band gap energy of TiO_2. Unlike metal cations, anions are less likely to form recombination centres and therefore, are more effective at enhancing the photocatalytic activity of TiO_2 [93].

Asahi *et al.* [83] prepared $TiO_{2-x}N_x$ films by sputtering from a TiO_2 target in an N_2 (40%)/Ar gas mixture. After being annealed at 550 °C in nitrogen for 4 hours, the films were crystalline, with features assignable to a mixed structure of the anatase and rutile crystalline phases. TiO_2 films were also prepared in a similar fashion by sputtering from a TiO_2 target in an O_2 (20%)/Ar gas mixture and subsequently annealing at 550 °C in oxygen for 4 hours. The nitrogen doped samples were more active than pure TiO_2 under visible light irradiation. They have also calculated the electronic band structure of TiO_2 containing various substitutional dopants including C, N, F, P and S. Substitutional doping with N narrowed the band gap most significantly because its p state mixed with the O 2p states[83]. Since Asahi's work nitrogen doping has been considered to be the most effective approach to improving photocatalytic activity under visible light illumination.

Di Valentin *et al.* [94, 95] investigated the mechanism of nitrogen doping. They performed DFT calculations considering two different doping models of substitutional and interstitial nitrogen doping. Their results showed that in substitutional doping the nitrogen atom is bound to three Ti atoms and replaces lattice oxygen in TiO_2. This nitrogen atom is in a negative

oxidation state (N^{2-}). In interstitial doping the nitrogen atom is bound to one lattice oxygen and therefore is in a positive oxidation state. The resulting NO species interacts with the lattice Ti atoms through its p-bonding states [94]. In preparing N-doped TiO_2 the experimental parameters will determine which doping type will dominate the structure. Interstitial doping will be preferred when there is an excess of nitrogen and oxygen in the process. In high-temperature, oxygen deficient, calcination processes N-doping will result in substitutional doping and oxygen vacancies. In both systems the formation of localized states in the band gap are found. Substitutional nitrogen states are situated above the valence band whereas interstitial nitrogen states are placed higher in the gap. Excitation from these localized states to the conduction band may result in a narrower band gap and in a red shift towards the visible light region [94].

In addition Di Valentin *et al.* [94] calculated a relative difference in core level shifts for N-doped TiO_2 samples and compared them with the experimental values based on X-ray photoelectron spectroscopy (XPS) measurements. The investigators reported that the calculated core level shift between substitutional and interstitial doping was 1.6 eV which correlated well with the experimental values for 397 eV (attributed for substitutional N) and >399eV (interstitial N) [94].

Another approach for enhancing photocatalytic activity of TiO_2 is addition of halogen elements into titania thin films. Halogen elements provide both cation and anion substitutes for Ti^{4+} and/ or O^{2-} in the TiO_2 matrix. The precursor of the doping ion will greatly influence the chemical state of the impurities of the doped samples. Fluorine, chlorine and bromine generally exist in the TiO_2 matrix with a chemical state of -1, indicating their substitutions of O^{2-} in TiO_2 crystals; however, iodine usually is present as a cation (+5 and +7) for occupying the Ti sites. They have shown good photocatalytic activity under visible light illumination [96, 97].

Chapter 3: Thin film deposition

3.0 Physical vapour deposition

Physical vapour deposition (PVD) is a term given to a group of thin film deposition processes involving physical mechanisms such as sputtering and evaporation. The evaporation process involves the heating of the solid source in a high vacuum to a point where it has a high vapour pressure; this usually requires the temperature to exceed the melting point of the solid. In sputtering, atoms are removed from a solid target by ion bombardment. The atoms and molecules are transported in the vapour state, either through vacuum or low pressure gas or a plasma environment and then condense on the substrate as thin films. The films produced during PVD can have different composition and structures depending on operating parameters [98]. PVD processes can be divided into three main types; vacuum evaporation, ion plating and sputtering [99]. Only sputtering will be described in detail, as this was the technique used in this project.

3.1 Glow discharge plasmas

Plasma is partially ionised gas, which includes a mixture of neutral particles, radicals, ions and electrons (Figure 3.1). Plasmas play an important role in several PVD coating techniques. A plasma is created when the energy contained within a material is increased to such extent to produce ionisation. When ionisation occurs there is also excitation of atoms and ions, which in turn leads to decay, and production of photons giving the plasma its characteristic ‘glow’. Plasmas can be formed by a number of methods, but the only one of great importance in this project is the plasma created in a vacuum by application of an electric field. The type

of plasma used in the sputtering process can be discussed by considering a DC diode discharge. This system consists of two electrodes (target and substrate holder) within a vacuum chamber and an external high voltage power supply to generate an electric field between the two electrodes. This system is evacuated to a base pressure in the region of 10^{-3} Pa (high vacuum). Argon gas is introduced into the chamber in order to initiate the discharge. The gas atoms are ionised via collisions with electrons accelerating from the cathode. The target is then bombarded with positive argon ions that lead to the ejection of target atoms. When the ions accelerate to the cathode (target), they also cause emission of secondary electrons, which are the main source of ionising electrons in the discharge [100]. The voltage required depends on the gas pressure, which determines the 'mean free path' of the ionised particles (electrons, ions, neutral atoms or molecules). The mean free path measures a typical distance a particle travels between collisions. When the mean free path is large, electrons travels to ground without colliding with an atom and the level of ionisation is very low, i.e. there is an optimum value/pressure for each system. The gas pressure that is required to ensure that species within the chamber will collide with one another to cause ionisation is in the region of 0.1 to 1 Pa for magnetron sputtering system. In this pressure range, the mean free path is in the range 60-6 mm.

The plasmas that are used during magnetron sputter deposition are considered to be low temperature plasmas. Low temperature plasma has a low degree of ionisation, typically 1 in 1000 to 1 in 10000 atoms are ionised so the majority of plasma consists of neutral gas atoms. The number of positive and negative species per volume is balanced in the plasma, so it remains electrically neutral overall in a state described as quasi-neutral. The plasma sustains its quasi-neutral state due to strong electrical fields. Despite being in a state described as quasi-neutral, plasmas are not neutral on a small spatial scale and when interacting with the vacuum chamber wall. This happens due to the mass difference between positively charged

particles (ions) and negative charge carriers (electrons). Electrons are also far more energetic than ions and neutral particles. Average electron energies are about 2 eV that corresponds to an effective temperature of approximately 23000 K, neutral particles and ions have energies of about 0.025 eV and 0.04 eV, corresponding to temperatures of 290 K and 400 K, respectively. Thus, electrons will respond much faster to applied electric fields and will initially leave plasma faster than ions. This results in the plasma acquiring a net positive potential, which then tends to reduce the flow of electrons and increase the flow of ions from the plasma, such that the flux of ions and electrons are equal.

Ion bombardments from glow discharges are used during magnetron sputter deposition to generate coating flux, to sputter clean the substrate prior to deposition, and to provide a source of energetic particles to bombard the growing film.

Figure 3.1: Glow discharge plasma from metal target.

3.2 Sputtering

Sputtering is a momentum transfer process in which an impinging ion impacts the target surface (cathode) with sufficient energy, to overcome the binding energy of atoms on the target surface, which is typically in the range of 2-10 eV [101]. If the incident particles have enough energy (2-10 eV), they will impact the surface causing a collision cascade, which will eventually lead to an atom of the target material being ejected into the surrounding plasma [101]. Therefore, ion bombardment can have a number of effects on the target surface:

1) Secondary electron emission from ionised target atoms (or energetic particles)
2) Collision cascades within the target material, which often lead to sputtering events
3) Photon or X-ray emission
4) De-sorption of surface gas atoms
5) Implantation of bombarding species in the target material
6) Reflection of impacting species as high energy neutral particles
7) Re-deposition of the sputtered species due to collisions with the gas species causing ionisation and acceleration back to the target

The sputtered material then moves through the plasma and condenses on the substrate (Figure 3.2). However, this process is very slow due to the small number of ions available for sputtering. The ionisation fraction is so low (0.1%) because the secondary electrons emitted from the target surface are only likely to undergo a few collisions en-route to the anode. Increasing the process gas pressure would increase the number of collisions but this also has the detrimental effect of increasing scattering of the sputtered species thus lowering the deposition rate and lowering the energy of the active species. Thus the problems of low deposition and ionisation were improved with the use of magnetic fields (section 3.3).

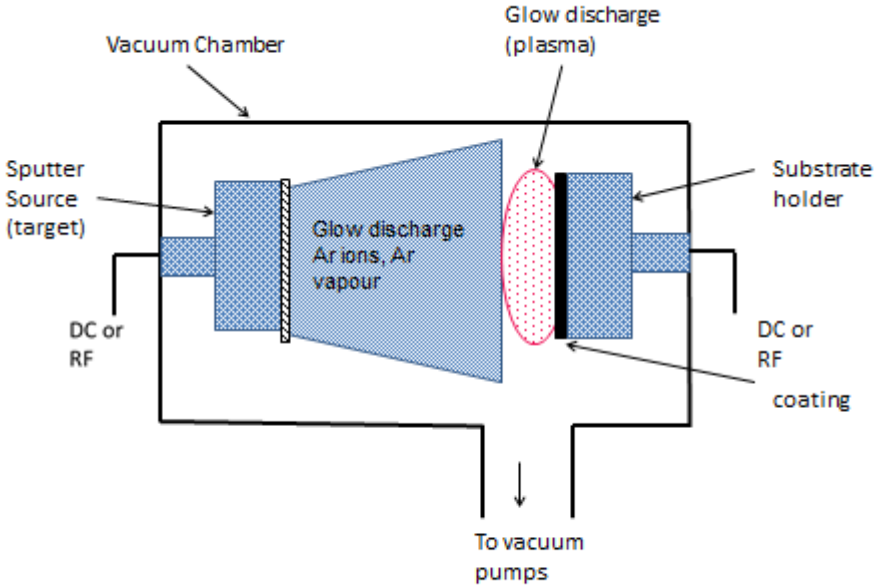

Figure 3.2: Schematic representation of basic sputtering process.

3.3 Magnetron sputtering

Magnetron sputtering was developed in the 1970s [102] by Chapin. It improves over the basic sputtering technique by introducing a magnetic field in the region of space in front of the target. Magnetic fields are used in the magnetron to control the movement of the charged particles and to produce good plasma confinement to increase the plasma density near the cathode surface and to enhance the sputtering rate (Figure 3.3). The magnetic field produces a closed system of flux, which electrons from the ionised gas travel along. The magnetic field lines travel from north to south through the target material, as the magnets are situated behind it. This entrapment of electrons creates a highly increased amount of ionisation near the target surface removing many more target atoms at a lower voltage. The dense plasma, which formed between the two poles, creates a characteristic erosion path known as the racetrack. This region is the only area of the target to be eroded significantly- typically only 30% of the

target is utilised for deposition. Magnetic fields have a considerable effect on charged particles within the plasma (the effect on electrons is 1000 × greater than ions due to their very low mass); the magnitude of this effect is dependent on the mass of the charged particle, the magnetic field strength, the velocity of the particle and its charge. In sputtering there is an electric field present, the initiator of the sputtered material (plasma), the electric field accelerates both electrons and ions on a path towards either anode or cathode. A magnetic field (B), with field lines starting and ending on the cathode surface, is used to trap electrons. The electric field (E) is always orientated normal to the surface of the cathode and perpendicular to the magnetic field. This result in an E×B drift for electrons, which gives rise to a sequence of cycloidal hopping steps parallel to the cathode face. If magnetic field lines originate and terminate on the surface, the energetic electrons travel along the field lines and get reflected at the mirror regions as they approach the cathode. As a result, the secondary electrons, which are emitted from the cathode because of ion bombardment, are confined to the near vicinity of the cathode. A higher density plasma region is produced above the target surface which causes an increase in ion bombardment of the target, giving higher sputtering rates and, thus, higher deposition rates at the substrate [103, 104].

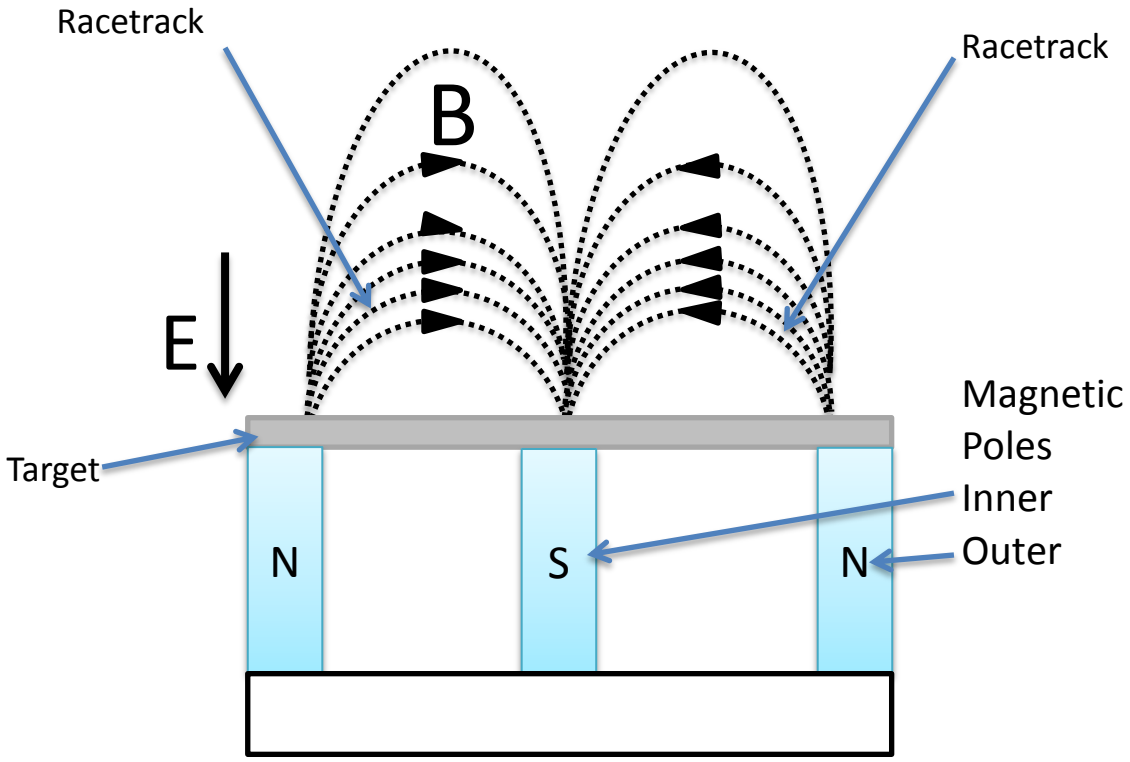

Figure 3.3: The cross section of a magnetron with the location of magnetic field lines.

3.4 Unbalanced magnetron sputtering

Magnetron sputtering is a technique where a magnetic field was introduced in the region of space in front of the target. A disadvantage of the standard magnetron is that outside a distance of approximately 60 mm from the target surface the density of the plasma drops rapidly. If the substrate is placed outside this dense plasma zone, there is little surface modification to the growing film from ion bombardment. The bombardment of the growing film by ions from the plasma is a very important process, which has been shown to influence both chemical properties such as the formation of compounds or the incorporation of gaseous atoms into the film and physical properties such as a change in grain size, density, level of residual stress, the electrical resistivity, the dielectric constant and the stability of the film

[105]. Typically the ion current density reaching the substrate in a standard magnetron is less than 1 mA/cm^2 [106]. The magnetron therefore requires a small target to substrate distance in order to have higher ion bombardment of the target, higher deposition rate at the substrate and to give improved film qualities, which is not convenient for coating 3D components or large surface areas. However, this problem was tackled by the development of the unbalanced magnetron in 1986 by Window and Savvides [107-109].

In unbalanced magnetron sputtering (UBM) the strength of outer magnet is stronger than the inner magnet (type II) which means not all the plasma is confined to the target region, but some is directed out towards the substrate. This in turn means that secondary electrons would follow the magnetic flux causing ionisation of the surrounding gas, which would then also travel towards the substrate. The dense plasma then extends out towards the substrate increasing ion bombardment (Figure 3.4). The magnitude of this increased ion bombardment will be dependent on gas pressure, target voltage, degree of unbalance and substrate bias condition, but can be in the range of 2-10 mA/cm^2. This high level of ion bombardment of the growing film results in films with good structural and physical properties [110, 111]. The UBM therefore acts as two sources at once, a magnetron with a high deposition rate and a source of a medium energy ion beam, which can be used to enhance film properties.

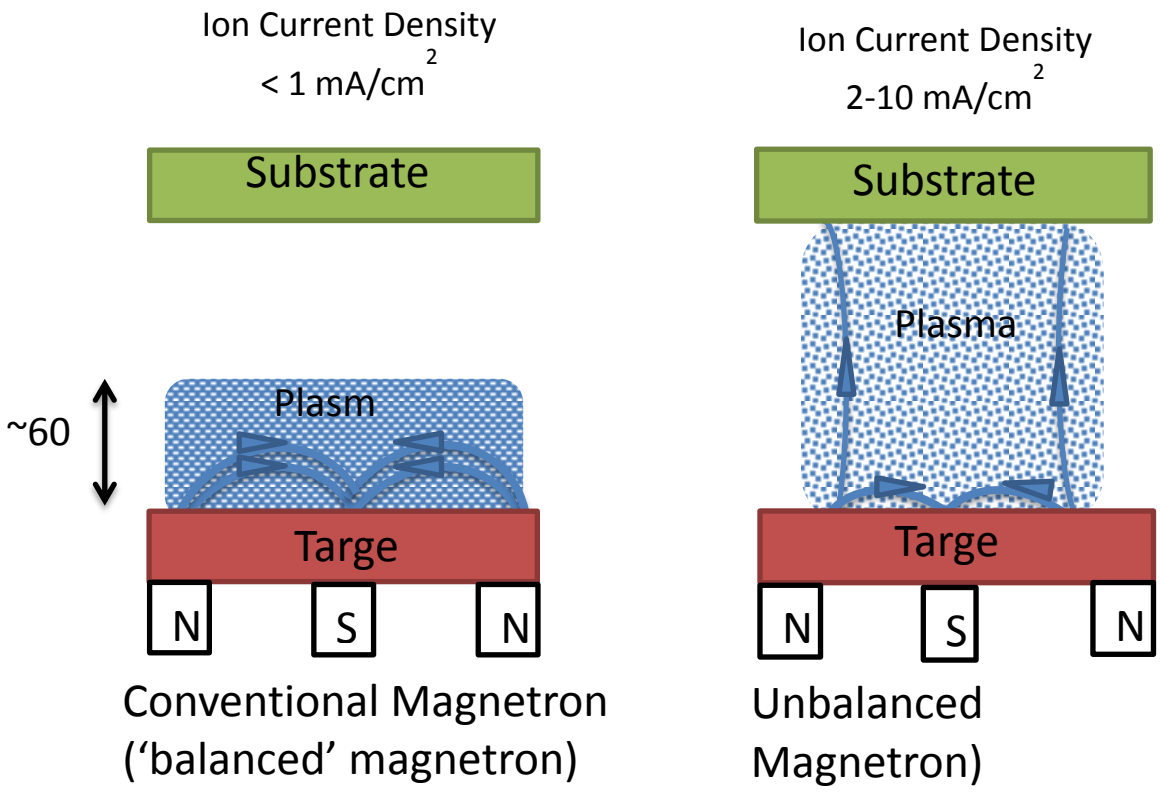

Figure 3.4: Schematic representation of the plasma confinement observed in conventional and unbalanced magnetrons.

3.5 Closed - field unbalanced magnetron sputtering

With the development of closed-field unbalanced magnetron sputtering (CFUBMS), a closed magnetic field is created by arranging adjacent magnetrons with opposite magnetic polarity, thereby resulting in much higher ion current densities (increasing ion to atom arrival ratio) and dense, well adhered coatings by enhanced chemical reaction at the substrate (Figure 3.5). Closed field systems can be configured using any even number of magnetrons. The ion to atom arrival ratio at the substrate is also dependent on the magnetic field configuration. It is possible to vary the ratio by more than a factor of ten from going from a single unbalanced

magnetron (UBM) to closed field unbalanced magnetron sputtering (CFUBMS) system and up to 60 times in changing the configuration from mirrored to closed field [112]. Increasing the ion to atom arrival ratio represents increasing ion bombardment and thus the amount of energy available to modify the growing film. Thus a high ion to atom arrival ratio is beneficial to promote adatom (deposited atoms) mobility and diffusion within the coating (section 3.10). In CFUBMS the ion to atom ratio increases with increasing target to substrate separation, this is beneficial for coating irregular large substrates with a high degree of ion bombardment. The high degree of ion bombardment promotes the formation of dense structures without the need for external heat sources or excessive substrate bias voltages [104], since the excessive substrate biasing can lead to defects in the film and increased film stress, and therefore, be detrimental to the overall film properties.

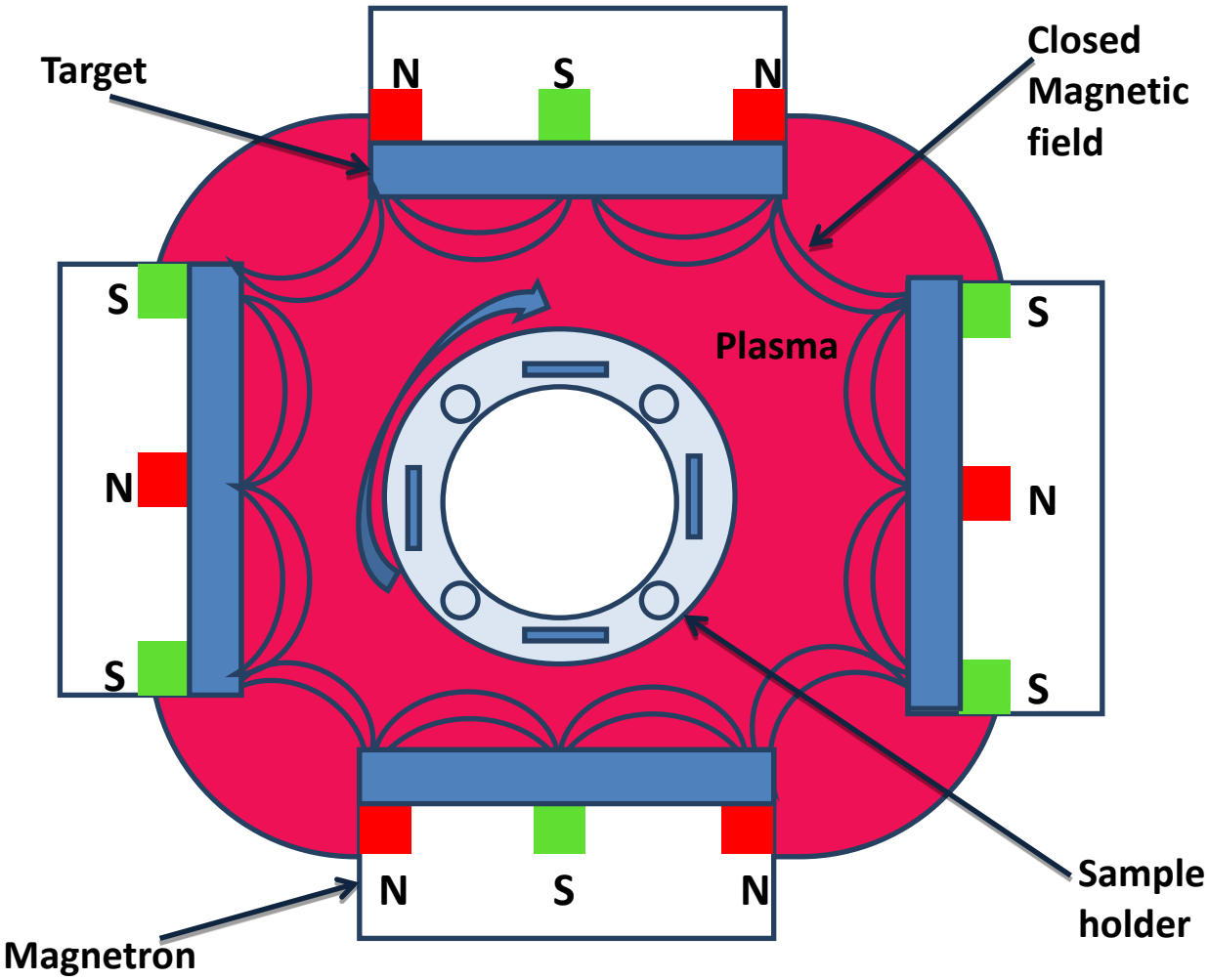

Figure 3.5: Schematic representation of closed field magnetron sputtering system.

3.6 Reactive sputtering

Reactive sputtering can be defined as ‘a method of depositing films that have a different composition to the target from which they were sputtered due to the addition of a reactive gas to the system’ [113]. In pure metal coatings only argon gas is used as the process gas, but in reactive sputtering additional reactive gases are used, such as nitrogen, butane or oxygen. Reactive sputtering can, thus, be used to deposit most nitride, carbide and oxide thin films

with desired compositions as a controlled monolithic or compositionally graded structure [104, 114].

Oxide films that are formed using the reactive sputtering process are often dielectrics (insulators). A dielectric is defined as 'a material which polarises in an electric field and remains charged when the field is terminated' [115]. The reaction between the metal target atoms and the reactive gas can take place at the target surface or at the surface of the substrate. The reacted species may also re-deposit themselves onto the target surface. In the case where the reaction takes place at the target or there is re-deposition, a build-up of possibly insulating reaction products can occur on non-eroding parts of the target surface (i.e. regions away from the racetrack). When an insulating film forms on the target surface, it can charge up electrically. If the charge reaches the breakdown voltage for the insulating film, an arc will occur.

There are two types of arcing, which can occur within a magnetron system. The first of these is a 'hard' or 'bi-polar' arc; this can occur between the cathode and a certain part of the sputtering system, typically the earth shield surrounding the cathode. Taking the supply voltage to zero normally quenches this type of arc- most DC power supplies have this facility. The second type of arc is referred to as a 'micro' or 'uni-polar' arc. These occur on the surface of the cathode and terminate on the same surface. Micro arcs are initiated by the plasma. The reason for this is that ions from the plasma bombarding the insulating (dielectric) layers, which formed on the non-eroding areas of the target surface, cause such areas to charge up. This effect is like that of a capacitor until a point which the dielectric layer breaks down, forming small self-sustaining discharge-micro arcs, which in turn can lead to the formation of a hard arc. Arcs usually result in droplets being ejected from the target surface which contaminate the growing film, and these droplets degrade the film quality.

Arcs affect the structure of the film, the process control system, deposition rate and damage the power supply. Historically, to overcome these problems, radio frequency (RF) power has been used, but RF power is more expensive to use than direct current (DC) powder. RF sputtering works due to the much higher mobility of electrons than the heavier ions. A target potential is established at V_0 with relation to the plasma, where V_0 is the mean value of the RF voltage. The mean is shifted negatively from zero to a point where the flow of electrons is equal to the flow of the slower ions. The target thus can only be positive in relation to the plasma for a small part of the RF cycle so that the flux of positive ions and negative electrons charges reaching the target surface are the same. RF power supplies cost more per watt than DC power supplies, and a matching network must be used in a RF system further adding to the overall cost. For an equivalent amount of power, the deposition rate with RF power is about half the rate for DC power [116].

3.7 DC and Pulsed DC power supply

DC power could be used for the reactive sputtering of insulating films if compound formation on the target surface could be avoided by separating the reactive gas from the target. It has been shown that if a box with a mesh opening is added around the sputtering target and the argon is introduced, while the reactive gas is introduced next to the substrate, it is possible to use DC power for reactive sputtering of insulating films [117]. The disadvantages of this technique are that it is maintenance intensive and flakes from the coated mesh may break off and lower film quality. In addition, sputtering through a mesh reduces the deposition rate. In the early to mid-1990s, pulsed DC and mid-frequency alternating current (AC) power were introduced for reactive sputtering of insulating films. Both pulsed DC (typically 2-350 kHz) and mid frequency (typically 40 kHz) AC use a voltage reversal at the cathode to offset the

charge build up on the target surface. With pulsed DC power, the polarity of the power delivered to the target is alternated between negative and positive (only for bipolar supplies) [118]. In unipolar pulsed sputtering, the target voltage is pulsed between the normal operating voltage and ground (Figure 3.6). During a negative pulse, which is the normal condition for sputtering, ions are attracted to the target to eject target atoms, while during the positive pulse electrons from the plasma are attracted to the target to discharge any charged regions. Since the magnitude and duration of the negative pulse are greater than those for the positive pulse, this type of pulsed power is known as asymmetric pulsed DC power (e.g. the positive voltage is typically10% of the negative supply voltage), and it is used most often for the reactive sputtering of insulating films (Figure 3.6).This reversal occurs at a frequency typically between 20-350 kHz with durations of 1-10 μs.

There are three key variables that can be changed in pulsed sputtering, the frequency, reverse time and reverse voltage. The frequency determines how many times per second the supply pulses on and off to neutralise charge build up on the dielectric layer. This frequency has to be set high enough to prevent the voltage climbing up causing breakdown of the dielectric layer. The reverse time determines how much of each pulse is spent in the off phase – this parameter also determines the duty cycle i.e. how much time is spent sputtering and how long spent discharging. This parameter is critical due to the fact that the time must be set carefully to be long enough to prevent breakdown of the dielectric layer and short enough to minimise loss of sputtering time. The reverse voltage has to be set high enough to enhance preferential sputtering of the dielectric layer but not too high as back sputtering may occur from chamber walls and substrate. Several authors reported the advantage of pulsed DC sputtering compared to continuous DC sputtering, since charging and arcing does not have sufficient time to occur in the poisoned regions [119, 120].

One of the arc suppression methods is the use of smart power supplies. Arcs are detected by rising currents and/or falling voltage. At very high sputter power levels, voltage drop detection is much less ambiguous than current changes. Once detected, a smart power supply shuts down the arc by interrupting the energy supply, and in some cases the voltage is reversed. Sputter conditions are restored after the arc spot region was allowed to cool down. Developers of power supplies have succeeded in reducing the duration between arc detection and shutdown to some 10 µs. However, since arc ignition and spot development are sub-microsecond events, residual damage may still occur, leading to the ejection of some macro particles [121].

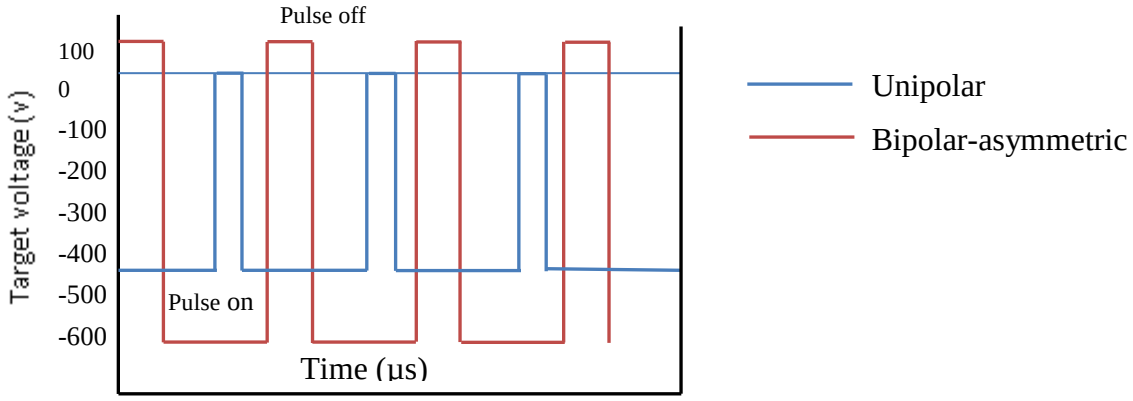

Figure 3.6: Schematic waveforms of unipolar and bipolar pulsed sputtering.

3.8 Film formation

There are three main stages in all PVD processes:

1) Formation of vapour phase species (the appropriate atomic, molecular, or ionic species) within the chamber from a solid source. The vapour phase of the material can be formed by the sputtering of the solid source in an inert gas atmosphere or heating a solid above its meting point to a temperature at which it has a significant vapour pressure. Different types of

reactive gas such as nitrogen and oxygen can be employed in order to react with the vapour species and form oxide or nitride coatings [122].

2) Transport of these species to a substrate through a reduced pressure gas medium. Gas pressure has a great influence on the energy of the atoms arriving at the substrate which in turn influences the film structure. Sputtering takes place at a higher gas pressure (0.1 to 1 Pa) compared to evaporation processes (10^{-2} Pa). What this means in terms of collisions is that, in evaporation processes there are few or no collisions between the evaporated atoms and the residual gas molecules in the chamber, in passing from source to substrate; i.e. the mean free path of the particles is large (>1m) in relation to the size of the chamber. Sputtering takes place at a higher gas pressure, which means that the mean free path of the particles is reduced (6-60 mm) from source to substrate separation, and thus more collisions take place between residual gas particles and sputtered particles. A reduction in energy of the sputtered atoms and the scattering of these atoms are caused by these gas-phase collisions.

3) Condensation of atoms on a substrate. This process takes place either directly or via a chemical and/or electrochemical reaction, to form a solid deposit. The temperature of the substrate and the energies of the impinging ions/atoms on the substrate are two important factors which affect film growth on the substrate. The adhesion, composition, stress and structure of thin films can be altered by bombardment of the substrate by energetic atoms/ions. Formation of a thin film takes place via nucleation and growth processes. Island growth, layer growth and Stranski-Krastanov growth are the three main forms of growth [106]. The predominant growth mechanism depends on the relative strength of attraction of the sputtered atoms/ions to themselves and to the substrate material.

In island growth, the mean free path of diffusing adatoms is equal to the mean island separation and adatoms will attach themselves with much higher probability to existing islands creating larger ones. Approaching coverage of about half a monolayer, islands

eventually coalesce which decreases their density. In layer growth, atoms are more strongly bound to the substrate than to each other. Faster diffusion takes place and the growth is two-dimensional and monolayers form on top of each other. In Stranski-Krastanov growth, first layer by layer growth takes place followed by growth through nucleation and coalescence of adsorbate islands. An important factor that determines the mobility of the adatoms is their energy; a high energy adatom is more likely to diffuse across the substrate material and then become trapped at low energy sites, possibly undergoing diffusion processes rather than rebounding from the substrate.

3.9 Film structure

In PVD processes, the structure of the growing film depends on various factors; such as chamber gas pressure, temperature achieved at the substrate and energy of incident particles. The first studies of film growth were carried out by Movchan and Demchishin [123]. Their initial studies explored the effect of the substrate deposition temperature, T and the melting temperature T_m of the deposited film. Their work was carried out using electron beam evaporation. They showed that the deposited film structure can be divided into three zones (Figure 3.7).

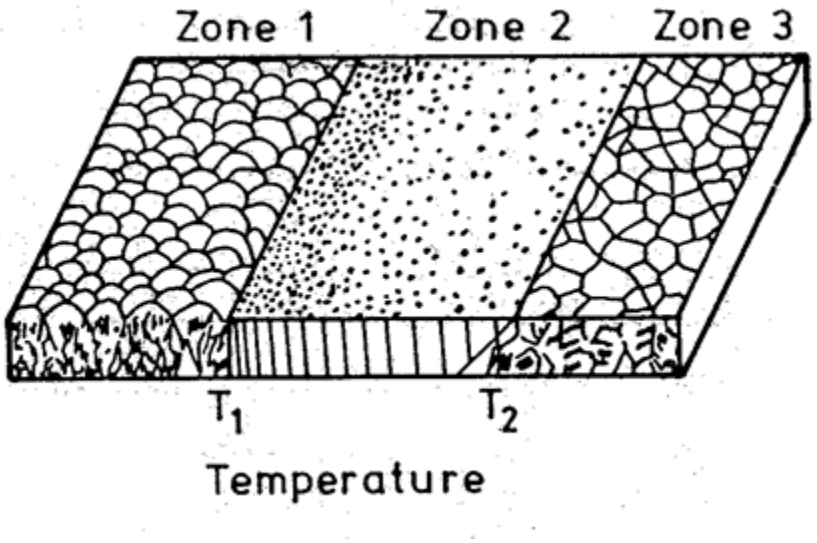

Figure 3.7: Movchan and Demchishin structure zone model [123].

Zone 1 represents structures that form at lower substrate temperatures where the deposited films have a porous columnar structure. This is due to the fact that adatoms (deposited atoms) do not have enough energy to diffuse across the surface and therefore grow in a predominantly island type growth. As the islands grow into columns, this results in shadowing effects causing the formation of voids in the growing lattice. The crystals are segregated by voids and have rounded tops on the upper surface. This structure is mechanically weak and has few applications.

In the 2nd zone, the structure becomes denser with fewer voids separating the crystalline columns, and grain size has also increased. The energy of the depositing film approaches the energy needed for surface diffusion and thus adatoms have enough energy to migrate across the surface to provide a denser structure than the 1st zone. Metallic deposits are an approximation of cast metals. This is a very common structure for sputtered coatings and has better properties that makes it much more suited to engineering applications than the zone 1 structure.

As the temperature increases in the 3rd zone, equiaxed grains and a shiny surface forms. The energy is now approaching that needed for bulk diffusion and adatoms have enough energy to diffuse within the growing film and bulk processes, such as recrystallisation and grain growth occur. The properties of metals deposited in this range represent those of a fully annealed metal. This structure is relatively rare due to the elevated temperature required for formation.

Thornton [124] further investigated structure formation during the sputtering process by incorporating process gas pressure effects (Figure 3.8). The model is similar to the previous model, however an additional zone was introduced - Zone T – which is a transitional zone between the 1st zone and the 2nd zone structures. According to Thornton's description, there are two zones of growth morphology depending on gas pressure at lower substrate temperature, which are the transition zone (zone T) and zone 1. At lower gas pressures (zone T structure); the film consists of a more dense structure with a mirror-like surface topography. At high pressure (zone 1 structure), columnar micro crystals with voids are formed. Zone 2 and 3 are the most useful structures in typical thin film coating applications.

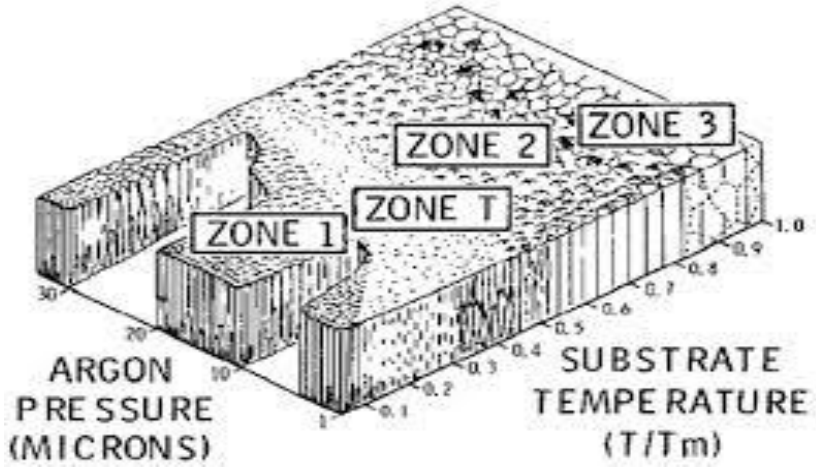

Figure 3.8: Thornton structure zone model for sputtered coatings [124].

As the magnetron sputtering technique has been developed over the years, further expansion of the Thornton zone model was needed. In the 1990s Kelly *et al.* [104] introduced a structure zone model that represents the structure of thin film deposited by the closed field unbalanced

magnetron sputtering (CFUBMS) technique. In this model parameters such as homologous temperature T/T_m (where T is the substrate temperature and T_m is the melting point of coating material) bias voltage at the substrate (ion energy) and ion to atom ratio at the substrate J_i/J_n (ion flux) were considered (Figure 3.9). This structure zone model points out that film deposited by closed field unbalanced magnetron sputtering (CFUBMS) represent fully dense columnar structures at relatively low homologous temperatures, compared to other PVD processes (zone 3 at T/T_m of 0.43, zone 2 at 0.13). Zone 1 structures are not formed. This is one of the reasons CFUBMS has become an important coating technique for many applications and was the system of choice in this study.

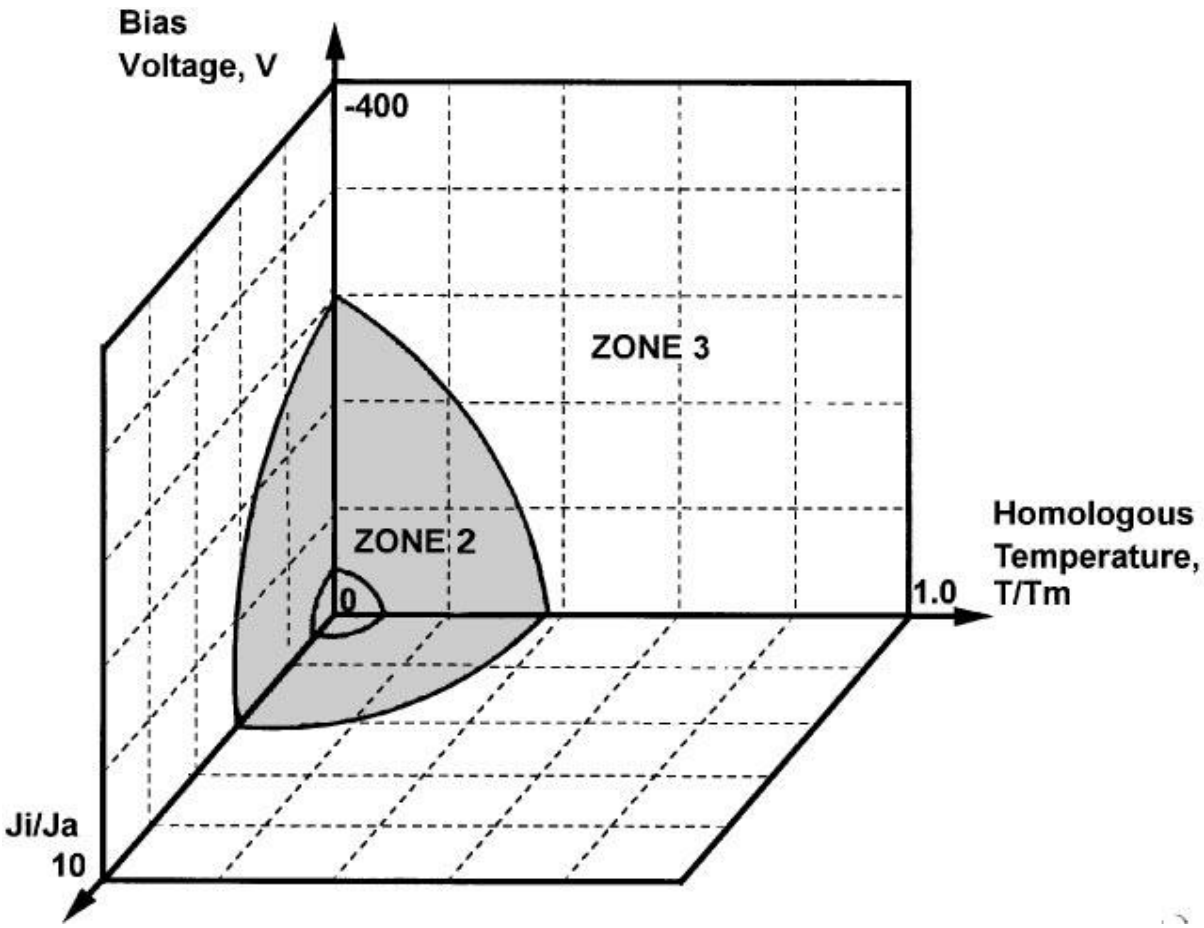

Figure 3.9: Schematic representation of structure zone model relating to closed field unbalanced magnetron sputter deposited film by Kelly *et al.*[104] .

3.10 Adhesion

The adhesion of the deposited film onto the desired substrate is one of the key properties of a thin film. The adhesion depends on the chemical nature, cleanliness, and microscopic topography of the substrate surface. In practical situations adhesion can be measured using a range of techniques such as the scratch test [125].

In order to determine the adhesion between a substrate and a film, it is important to know the type of interfacial layer formed. There are five types of interfacial layer:

1) Diffusion interfacial layer: gradual change in composition from substrate to film

transition zone. This can only occur when there is partial solubility between the two materials and when there is enough supplied energy.

2) Pseudodiffusion interfacial layer: caused by particle bombardment at high energies of materials that would not normally undergo diffusion type processes. This involves the backward scattering of gas phase substrate atoms, which mix with the vapour phase atoms/ions of the coating material, which then in turn condense and re-condense on the substrate. Ion bombardment before and during coating has the effect of roughening the surface, which in turn increases the amount of diffusion between the two layers, and thus the amount of anchoring between the two materials is also increased.
3) Chemical bonding interfacial layer: when a chemical reaction occurs between the film and substrate atoms.
4) Monolayer on monolayer: occurs as an abrupt transition from substrate to film material, when there is almost no mixing of the two materials. This mainly occurs on very smooth, dense, non-reactive substrate materials.
5) Mechanical interfacial layer: when the substrate is rough and porous, the coating fills the holes within the substrate surface and a mechanical anchoring is formed.

All of these forms of interfacial layers can happen at any one time. Pseudodiffusion is the most common form that occurs in the PVD process [125].

Chapter 4: Experimental and analytical techniques

4.0 Introduction

This chapter describes the methods used for preparing, coating and characterising the coated stainless steel. Techniques for assessment of the antibacterial activity of the coatings are also described. The background information and key principles behind each of analytical techniques is provided.

4.1 Film formation and analysis

4.1.1 Magnetron sputtering rig

The coatings were produced by unbalanced reactive magnetron sputtering in a Teer Coatings Ltd. UDP450/4 sputtering system [126]. The rig achieves high vacuum using a BOC Edwards 40 rotary pump and Edwards Diffstack 250/2000 oil diffusion pump. The pressure is monitored via a Penning gauge, two Pirani gauges and a Baratron^{TM} gauge. Three 300 mm × 100 mm vertically opposed unbalanced planar magnetrons and one blanking plate at 90° intervals around the chamber; two magnetrons were fitted with titanium targets and one with the dopant metal target (molybdenum (Mo), tantalum (Ta), niobium (Nb), or tungsten (W). All the targets were of 99.5% purity. The base pressure of the sputtering chamber was 1×10^{-3} Pa. During sputtering the flow rate of argon was controlled using a mass flow controller. The flow rate of oxygen was controlled by a Megatech Reactaflo^{TM} optical emission monitoring system (OEM) which controls the flow of oxygen into the chamber via a piezo electric valve. Operating set points were selected that were previously found to produce stoichiometric TiO_2 coatings [126] (15% of full metal signal). The OEM was used to monitor an emission line in the Ti spectrum (504 nm) and allowed O_2 into the chamber until the Ti signal fell to 15% of

the full metal signal and was held at 15% by a feedback circuit. The reactive sputtering process was carried out in an argon: oxygen atmosphere at 0.3 Pa. The commercially available AISI 304 2B finish stainless steel substrates (2 × 1 cm) were ultrasonically cleaned with isopropanol then mounted on a substrate holder after cleaning, which was rotated at 4 rpm during deposition. The target to substrate separation was 8 cm. The magnetrons with the titanium targets were in the closed field configuration and driven in pulsed DC sputtering mode using a dual channel Advanced Energy Pinnacle Plus supply at a frequency of 100 kHz and a duty cycle of 50% (in synchronous mode). The third magnetron, with the dopant metal target, was driven in either continuous DC mode (Advanced Energy MDX power supply) or pulsed DC mode. The Ti targets were operated at a constant time-averaged power of 1 kW each for all runs and the dopant target was operated at powers in the range of 60–240 W to vary the dopant content. Pulsed DC mode with the frequency ranging from (100 - 350 kHz) was also used for dopant metal target in order to change the dopant content.

An additional set of W, WO_3, Mo, MoO_3, Nb and Nb_2O_5 coatings were produced for antimicrobial assays. For transition metals and their oxides (W, WO_3, Mo, MoO_3, Nb and Nb_2O_5) coatings were deposited from one target operated in pulsed DC, at a power of 1 kW, 100 kHz and a duty cycle of 50%.

The titanium and dopant targets were cleaned before each coating run by pre-sputtering in a pure argon atmosphere for about 10 minutes. Deposition time was varied to obtain a film thickness of 800 nm - 1.2 µm. The sputtered films were annealed post deposition at two different temperatures (400 °C and 600 °C) for 30 minutes in air.

Three samples from each batch were kept in the dark (sealed in an aluminium foil) (in case there was a need for future monitoring) to monitor variation and reproducibility of the photocatalytic activity of the coatings (Appendix A).

4.2 Analytical techniques

4.2.1 Raman spectroscopy

Raman spectroscopy is a structural characterization technique. It is used in condensed matter physics and chemistry to study vibrational, rotational and related low frequency modes of a system [127]. It relies on inelastic scattering, or Raman scattering, of monochromatic light. Lasers of visible, near infrared or near ultraviolet range frequencies are typically used as a light source for the Raman spectroscopy. Photons of laser light are absorbed by the sample and re-emitted. The shift in energy provides information about rotational, vibrational and related low frequency modes of the system that provides information regarding the crystal structure of the coatings.

In a Raman spectroscopy process, a specimen is illuminated with the laser; the re-emitted light is collected via lens and directed through a monochromator. The wavelengths closely corresponding to those of the laser are filtered out to eliminate elastic Rayleigh scattering components. The remainder of the light goes to a detector in order to observe the Raman effect (Figure 4.1).

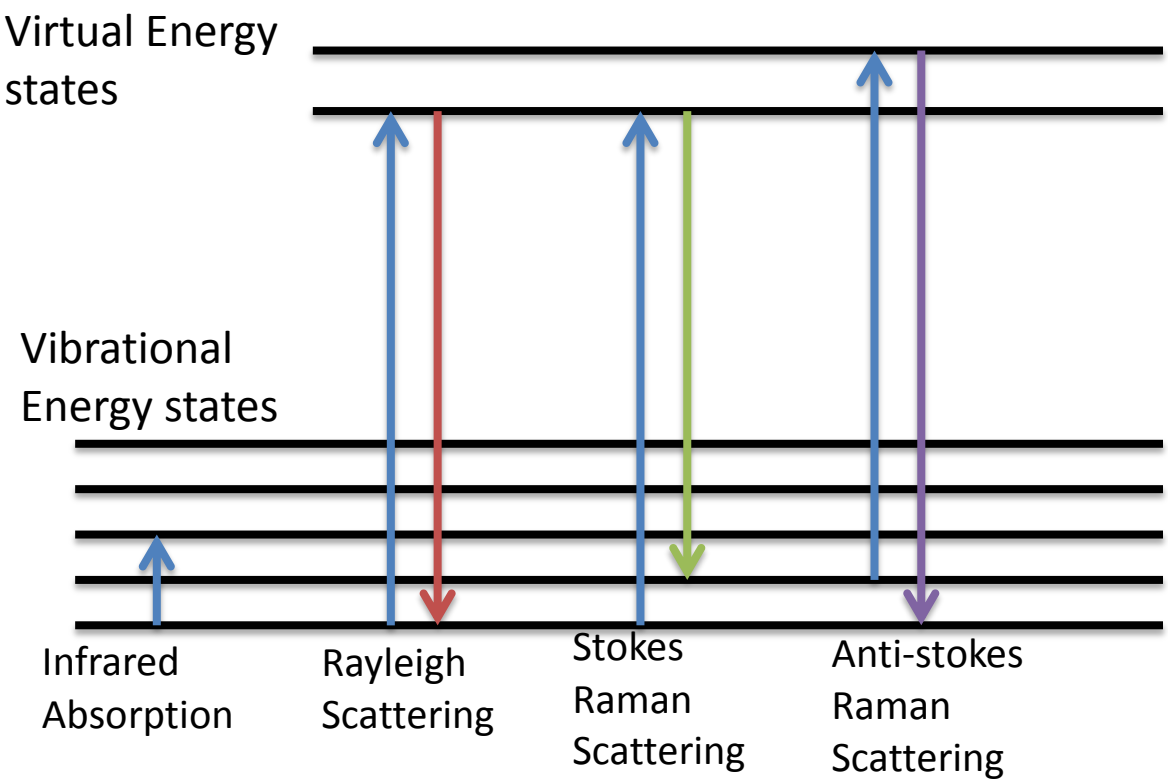

Figure 4.1: An energy diagram showing the transitions involved in Rayleigh and Raman scattering [127].

When the energy of the scattered radiation is less than the incident radiation, Stokes scattering occurs and when the energy of the scattered radiation is more than the incident radiation, Anti-Stokes scattering occurs. Anti-Stokes lines correspond to rotational relaxation whereas Stokes-lines correspond to rotational excitation (Figure 4.1) [127].

The energy increase or decrease from the excitation is related to the vibrational energy spacing in the ground electronic state of the molecule. Consequently, it directly measures the wavenumbers of the Stokes and Anti-Stokes lines and gives the vibrational state of the molecule at a specific radiation. It is the change in wavelength of the scattered photon which provides the chemical and structural information of material. Raman shifts are typically measured in wavenumbers and typically expressed in cm^{-1} (Figure 4.2).

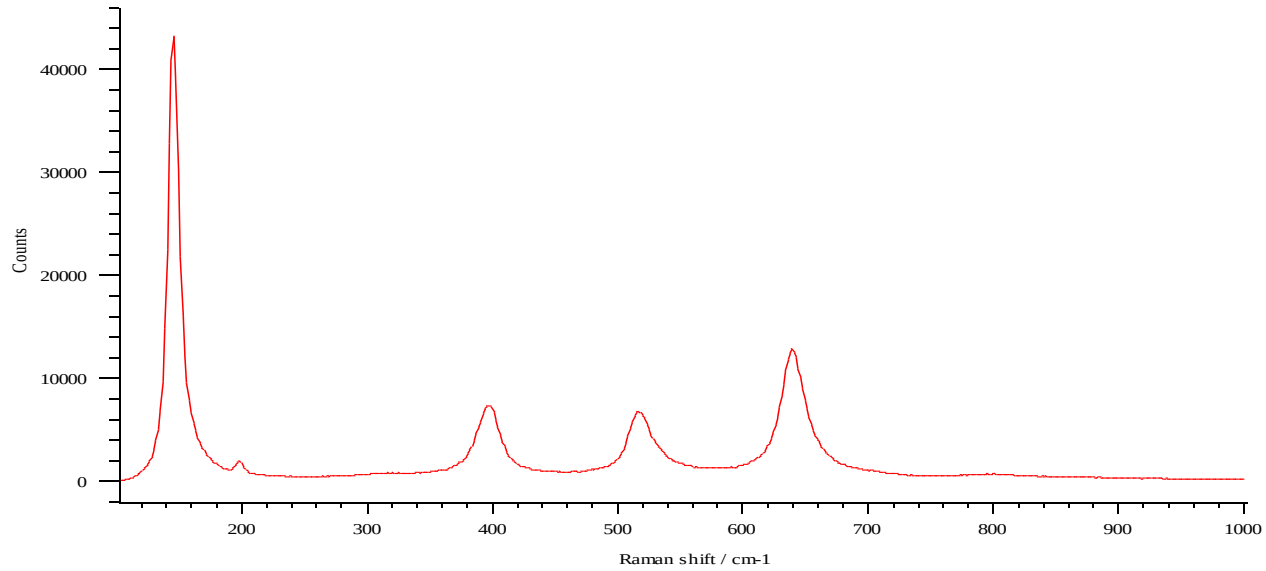

Figure 4.2: An example of the Raman spectra of the anatase phase from nanocrystalline powder.

Raman spectroscopy offers several advantages for microscopic analysis. Since it is a scattering technique, specimens do not need to be fixed or sectioned. Raman spectra can be collected from a very small volume; these spectra allow the identification of species present in that volume. In general, glass, metal or water does not interfere with Raman spectra analysis. Raman spectroscopy can be used to identify the crystal structure of a coating. As the vibrational characterisation of specific chemical bonds are known, Raman spectroscopy can be used to identify the crystal structure of a coating. The Raman system used for crystal structure determination was a Renishaw Invia system using a 514 nm laser.

4.2.2 X-ray diffraction (XRD)

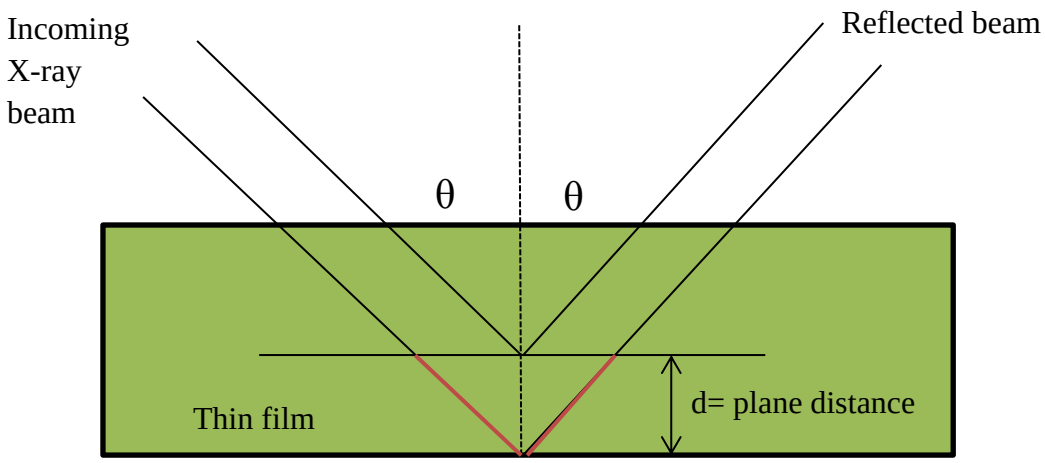

Figure 4.3: Schematic illustration of Braggs reflection.

X-ray diffraction techniques can be used to analyse the thin films crystal structure because crystalline materials diffract X-rays in a material specific manner according to the Bragg condition, equation (4.1):

$$n\lambda = 2\, d \sin\theta \qquad (4.1)$$

Where;

n is an integer

λ is the wavelength of the incident X-rays

d is the spacing between the planes in the atomic lattice, and

θ is the angle between the incident ray and the scattering planes (Figure 4.3).

Constructive interface between incident and diffracted X-rays only occurs when the multiples waves and the latter are in phase. Therefore, peaks in diffracted X-ray intensity are recorded only at diffraction angles which meet the Bragg condition, i.e. when the path difference between X-rays reflecting off adjacent crystal planes is equal to integer multiples of the X-ray wavelength. Different crystalline materials, even if they share the same unit cell type, will have different lattice spacing, determined by atomic distances and so have distinct diffraction peaks. Unknown materials may therefore be indexed either by comparison against reference patterns of known compounds, or by calculating lattice parameters and unit cell sizes from the diffraction data [128]. Phase identification is one of the most important uses of XRD techniques in thin films analysis. Figure 4.4 shows the fundamental characteristic of an XRD system, where the diffraction angle 2θ, is the angle between the incidents and diffracted X-rays. In a classic experiment the θ - 2θ mode, the diffracted intensity is measured as a function of 2θ and the orientation of the sample, which yields the diffraction pattern. X-ray diffractometry traces were obtained using a URD6 Seiferd & Co diffractrometer in the θ - 2θ mode.

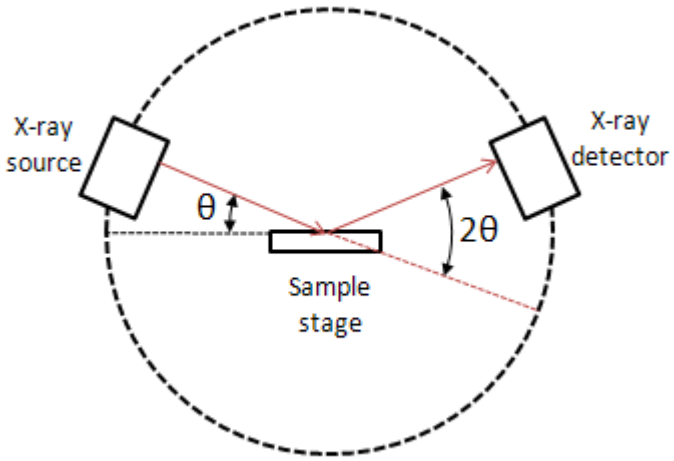

Figure 4.4: Schematic diagram of θ - 2θ XRD system.

4.2.3 UV-VIS spectrophotometer

UV-VIS spectrophotometer is used to obtain absorbance spectra of a compound in a solution or as a solid. A UV-VIS spectrometer consists of a light source, sample holder, diode array detector and a data acquisition computer. The space between the light source and detector is known as the sample compartment. The amount of ultraviolet and visible light transmitted through a sample is measured in the spectrometer. The wavelengths at which chemicals absorb light is a function of their electronic structure, therefore a UV/Vis spectrum can be used to identify some chemical species. The amount of chemical located between the detector and light source is associated with the amount of light absorbed for a particular sample/chemical. Once chemical species have been quantified after calibration, the UV-VIS spectrophotometer can be used to record the spectrum for the sample. An ultraviolet spectrum ranges from 200-400 nm while the visible spectrum is from 400 - 750 nm. A Perkin-Elmer Lambda 40 UV-Vis spectrophotometer was used for measuring the degradation of an organic dye (methylene blue), which was used as an indicator of the photocatalytic activity of the coatings produced in this project.

In spectroscopic practice, quantitative analysis is based on the Lambert Beer Law, given by the equation (4.2):

$$A = \log_{10}\left[\frac{I_0}{I}\right] = \varepsilon c l \qquad (4.2)$$

Where;

A is absorbance,

I_0 is the intensity of the incident radiation,

I is the intensity of the radiation transmitted through the sample,

ε is the molar absorptivity or molar extinction coefficient in $dm^{-3}.mol.cm^{-1}$

c is the concentration of the solution and

⌊ is the path length (cuvette).

4.2.4 Scanning electron microscope (SEM)

The SEM is one of the most flexible instruments available for the examination and analysis of the microstructural characteristics of solids. A scanning electron microscope (SEM) scans a focused electron beam over a surface to create an image. The electrons in the beam interact with the sample producing various signals that can be used to obtain information related to the surface topography and composition. The types of signals produced by a SEM include secondary electron (SE), backscattered electron (BSE), characteristic X-rays, specimen current and transmitted electrons. Secondary electrons are electrons generated as ionization products. BSEs are beam electrons that are reflected from the sample by elastic scattering. Secondary electrons and backscattered electrons are commonly used for imaging samples: secondary electrons are most valuable for showing the morphology and topography of samples and backscattered electrons are most valuable for illustrating contrasts in composition in multiphase samples.

One of the reasons for its usefulness is the high resolution image with large depth of focus that can be obtained. The latter used to the three-dimensional appearance of the specimen image. The “shadow-relief” effect of the secondary (SE) and backscattered electron (BSE) contrast also adds to the three dimensional appearance [129].

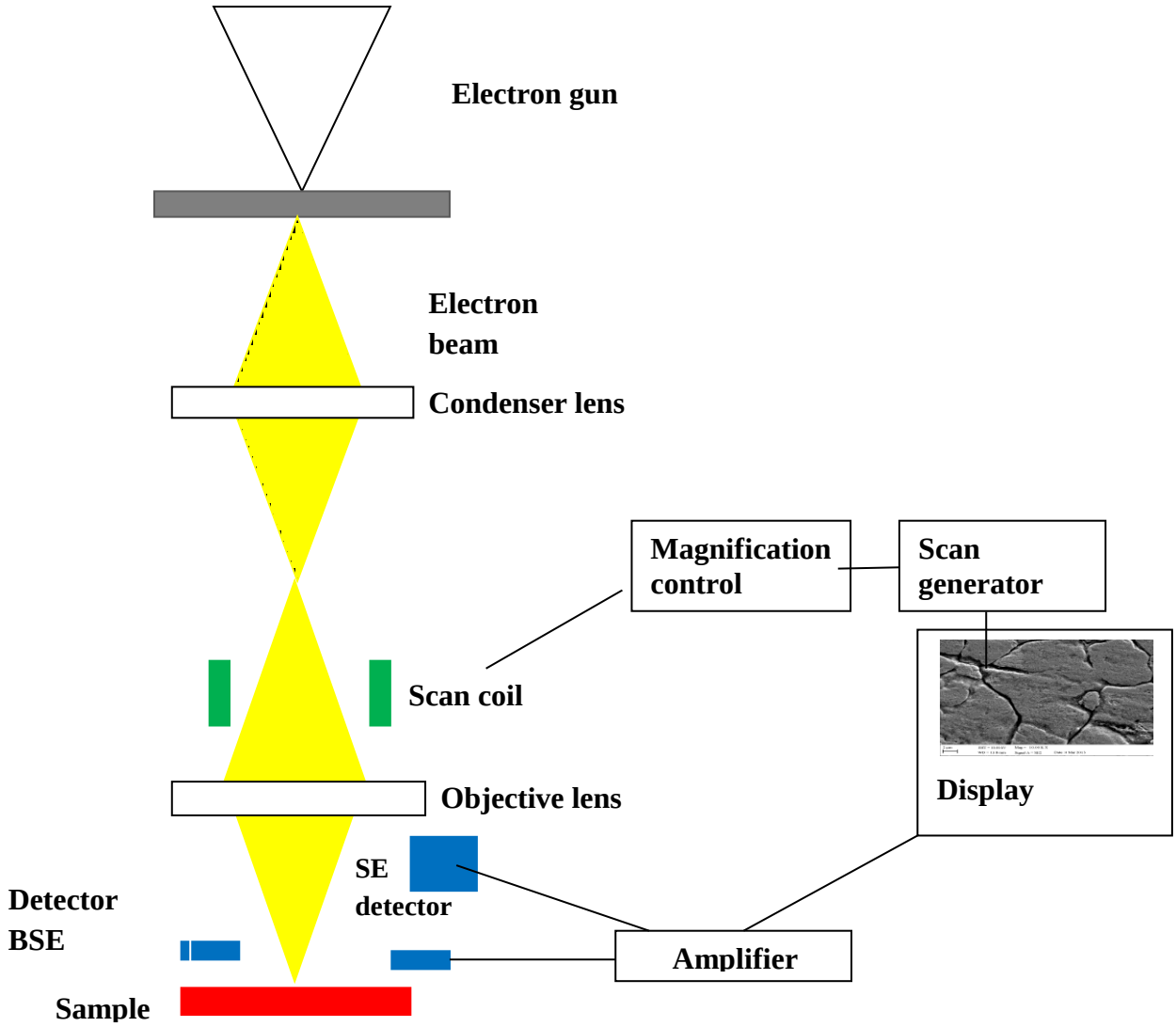

Figure 4.5: Schematic diagram of the SEM.

Another advantage of SEM is the wide variety of electron – specimen interactions that can be used to form an image and to provide qualitative and quantitative information such as surface roughness. The large depth of focus, the excellent contrast and the straightforward

preparation of solid specimens are the reasons for the considerable success and widespread use of scanning electron microscopy in the imaging of surfaces over the past decades.

Three SEMs were used in this study, one at MMU (Zeiss Supra 40 VP-FEG-SEM) and the other at TCL (Cambridge Stereoscan 200 and JEOL 7000 Field Emission SEM (FESEM)) for examination of the scratch track generated during scratch adhesion testing of the coating (see Section 4.2.11). Scanning electron microscopy (SEM) was used to investigate the morphology of the coatings (carried out by TCL). An acceleration voltage of 15 kV was utilised. The composition and elemental distributions of the coatings were investigated using a SAMX energy dispersive X-ray analyser (EDX) system, attached to the SEM. The composition was measured on a minimum of five locations and the mean ±2σ (standard deviation) values were reported. High resolution SEM images were obtained using a JEOL 7000 Field Emission SEM (FE-SEM) at an acceleration voltage of 10 kV. SEM specimens were prepared by mounting coated stainless steel substrates onto pin stubs using double-sided conductive compound adhesive tape.

4.2.5 Energy dispersive X-Ray spectroscopy (EDX)

Energy dispersive X-ray spectroscopy (EDX) is a technique used for the elemental analysis or chemical characterization of a sample. The EDX analysis system works as an integrated feature of a scanning electron microscope (SEM), and cannot operate on its own without the latter. At rest, an atom within the sample contains ground state electrons in discrete energy levels or electron shells bound to the nucleus. During EDX analysis, the specimen is bombarded with an electron beam inside the SEM. The incident beam may excite an electron in an inner shell ejecting it from the shell while creating an electron hole where the electron was. A position vacated by an ejected inner shell electron is eventually occupied by a higher

energy electron from an outer shell, and the difference in energy between the higher energy shell and the lower energy shell may be released in the form of an X-ray. The amount of energy released by the transferring electron depends on which shell it is transferring from, as well as which shell it is transferring to. Furthermore, the atom of every element releases X-rays with unique amounts of energy during the transferring process. Thus, by measuring the amounts of energy present in the X-rays being released by a specimen during electron beam bombardment, the identity of the atom from which the X-ray was emitted can be identified [130].

The output of an EDX analysis is an EDX spectrum. The EDX spectrum is a plot of how frequently an X-ray is received for each energy level. An EDX spectrum normally displays peaks corresponding to the energy levels for which the most X-rays had been received. Each of these peaks is unique to an atom, and therefore corresponds to a single element. The higher a peak in a spectrum, the more concentrated the element is in the specimen; however there is a possibility of peak overlap which would affect the result. This also depends on the mass of the atom, since the light elements $Z < 10$ cannot be detected by EDX. In order to determine the concentration of each element in a specimen line intensities of each element are measured and compared with calibration sample containing the same elements in known compositions. The EDX technique is capable of identifying the elements in concentration in order of 0.1%. Experimental analysis is often conducted with an accelerating voltage in the 15 - 20 kV range since a broad array of elements will be detected. An additional spectrum collected at 5 – 10 kV could help to avoid missing low atomic number elements at low concentrations. The accelerating voltage can subsequently be tailored to the element and shell level of the specimen. Therefore, accelerating voltage and atomic number are two factors that determine spatial resolution of and depth of signal from the specimen. The Accelerating voltage in the range of 5 - 15 kV was used which would give an estimate penetration depth of 83 nm – 1.72

μm which was depending on accelerating voltage and composition of material. Kanaya-Okayama formula [131] was used to calculate the penetration depth. Results are presented in Appendix B.

The accuracy of EDX results are around 5% of the recorded value. Composition was investigated by EDX—Edax Trident, installed on a Zeiss Supra 40 VP-FEG-SEM.

4.2.6 White light interferometry (WLI)

White light interferometry is a non-contact optical method for imaging and measuring the surface topography of a material. It provides both 2D and 3D images of specimen surface, as well as surface roughness measurements. WLI use a white light source through a filtering optical component towards a sample surface. It is possible to separate the light with a dispersive lens into its component wavelengths, each of which corresponds to a different z-coordinate in the optical axis. Therefore the visible light spectrum is now encoded with a z-coordinate as a function of varying focal distance from the end of the lens.

WLI was employed to measure the coating thickness and roughness R_a (2D average surface roughness) and S_a (3D average roughness) values after the chemical durability tests (Figure 4.6). Kapton ^{TM} tape was used during the deposition process to create a step in the coating, in order to divide the coated surface into coated and uncoated parts for thickness measurement. Analysis of the surface roughness and thickness were taken using a MicroXAM (phase shift) surface mapping microscope with an ADE phase shift XYZ 4400 ml system and an AD phase shift controller (Omniscan, Wrexham, UK). The image analysis system used was Mapview AE 2.17 (Omniscan, Wrexham, UK). Three samples of every surface were examined and five separate areas on each sample scanned to gain average values.

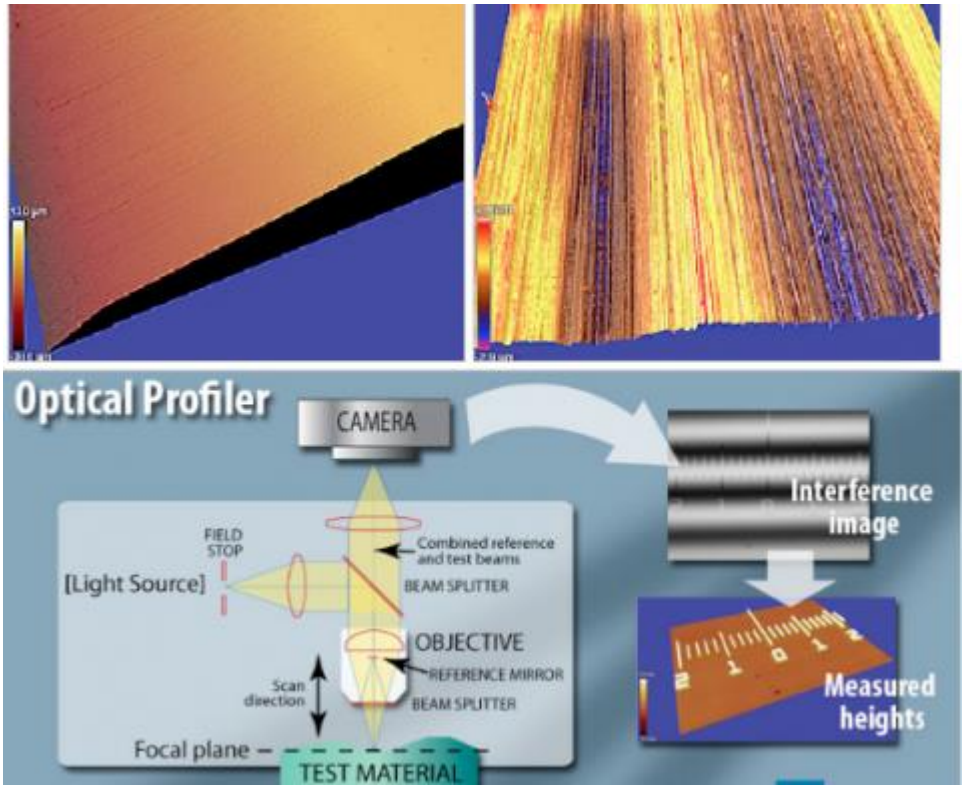

Figure 4.6: Schematic representation of white light interferometry microscope for measuring roughness and film thickness [132].

4.2.7 ICP-AES: Inductively coupled plasma atomic emission spectroscopy

ICP-AES is an analytical technique that uses emission spectrophotometry in order to detect traces of metals in liquid [133]. It is a type of emission spectroscopy that uses the inductively coupled plasma to produce excited atoms and ions that emit electromagnetic radiation at wavelengths characteristic of a particular element. The intensity of this emission is indicative of the concentration of the element within the sample.

This technique was used to quantify the amount of metal ions released in water from the surfaces used in this project because of concern about nanoparticle toxicity. A Varian Vista

AX CCD inductively coupled plasma atomic emission spectrometer (ICP-AES) (Varian Inc) was used to assess any Mo ion release from the deposited thin film coatings (since it was the only coating which had been placed *in situ*). Surfaces were individually placed into a petri dish to which 20 mL of HPLC grade water (Fisher Scientific, UK) was added and incubated under fluorescent lighting in a 20 °C incubator. At 2, 4, 8, 24, 48, 72, 96 and 168 hours surfaces were transferred to fresh HPLC grade water whilst the previous sample was kept for analysis by ICP-AES. All samples were frozen at -85 °C prior to analysis. Molybdenum ion release was calculated from calibration curves (0.1 to 5 ppm) and all tests were carried out in triplicate (samples). The accuracy of ICP-AES results are around 3% of the recorded value.

4.2.8 Contact angle measurement

The contact angle (θ) is an important term to define the wetting of a liquid on a solid surface. In an ideal situation, meaning the solid surface is smooth, rigid, chemically homogeneous, insoluble and non-reactive, the contact angle (the angle between γ_{SL} (solid/liquid) and γ_{LV} (liquid/vapour) is defined from Young's equation as following:

$$\cos\theta_Y = \frac{\gamma_{SV} - \gamma_{SL}}{\gamma_{LV}} \qquad (4.3)$$

Where θ_Y is called the Young's contact angle, γ is the surface tension that is the force per unit length of the interface. S, L and V represent solid, liquid, and vapour, respectively. Therefore, γ_{sv} is the surface tension between the solid phase and the vapour phase, γsl between the solid phase and the liquid phase, and γ_{lv} between the liquid phase and the vapour phase. γ is also often referred to as surface energy in literature (Figure 4.6). Surface energy is measured in

units of Joules per unit area J/m^2, which is dimensionally equivalent to surface tension measured in Newton per metre N/m. In dealing with liquids, it is more usual to use the term of surface tension than surface energy which is a more general term for solids. Surface tension is also often used as surface free energy [134].

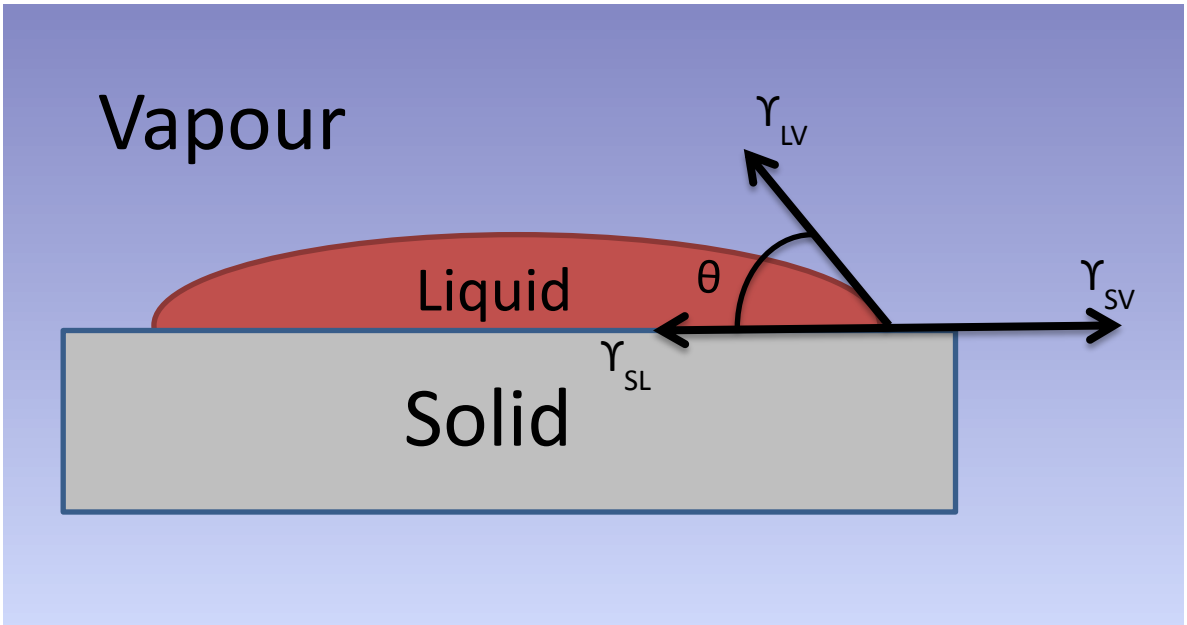

Figure 4.7: Liquid droplet on a flat surface showing the quantities in Young's equation.

When θ is 0°, the water droplet spreads completely on the solid surface, and it is called complete wetting of the surface. When θ is 180°, the water droplet stands as a sphere on the surface, and it is called non-wetting on the surface. In between 0° and 65°, it is called a hydrophilic surface and in between 90° to 180°, it is called a hydrophobic surface.

The contact angle measurements were performed on a Digidrop Contact angle measurement system from GBX Scientific Instruments by Cristal Global Ltd (Grimsby, UK). Five microlitre drops of demineralised water were placed onto the horizontal test surface. The instrument was equipped with a camera, where the images of water droplet were taken in order to measure the contact angle. The contact angle was determined using WinDrop++ software, d254 version 1.0 (GBX, Romans sur Isr, France). The contact angle was measured

conventionally (as shown in Figure 4.7), where a liquid/vapour interfaces meets a solid surface. Contact angle measurements were conducted on surfaces as received (after deposition and heat treatment), after the brewery trial (TiO_2 and TiO_2-Mo), and after wiping with 2- propanol and rinsing with water (one coupon per treatment). Measurements were conducted after exposure to light for 18 hours, either in a SUNTEST CPS+ (filtered xenon arc, 1500 W) or UVA light (Philips black light, 10-12 W/m^2), and after storage in the dark for at least 6 days. Measurements were carried out on 2 drops, and the results averaged.

4.2.9 Assessing photocatalytic activity

The photocatalytic activity of the coatings was determined via the degradation of an organic dye, methylene blue (MB) (Alfa Aesar, UK). MB is a heterocyclic aromatic dye with a molecular formula of $C_{16}H_{18}ClN_3S$, and is often used as a model organic compound to measure photoreactivity [135, 136]. ISO standard 10678 confirms the use of MB as a model organic dye for the determination of photocatalytic activity of thin films in an aqueous medium. The decomposition of MB was assessed using an initial concentration of 1.5 µMol L^{-1}. The coated samples were immersed horizontally into 20 ml of conditioning solution of MB for 30 minutes in dark conditions until adsorption/desorption equilibrium was reached.

The coated substrate was then placed into 10 mL of MB solution (glass beaker, Fisher, UK) which was irradiated with 2×15 W UV lamps (black Ray Cambridge UK, 4 mW/cm^2 at 10 cm distance) with an emission peak at 352 nm wavelength for 5 hours. The coated samples were also tested under fluorescent light via a similar set up experiments with 2×15 W Ushio fluorescent lamp (6.4 mW/cm^2 at 10 cm distance).

The beaker was covered with cling film (PVC) to avoid evaporation of the solution which can affect the concentration and peak absorbance of the MB solution. The light absorbed by cling film was measured using an Ocean Optics USB 2000+ spectrophotometer. The cling film absorbed irradiation below 200 nm, which was outside the range of interest [137]. Optical absorbance measurements of the MB solutions were taken every hour by UV-VIS spectrophotometer. The degradation of MB without contact with a photocatalyst surface in the absence and presence of UV and fluorescent light sources was measured in order to calculate the photocatalytic activity (Figure 4.8). The photocatalytic activity was measured in arbitrary units.

The overall photo-decomposition reaction of MB can be summarized as follows:

$$C_{16}H_{18}ClN_3S + 25.5\,O_2 \xrightarrow{TiO_2 + h\nu \geq 3.2\ eV} 16\,CO_2 + 3HNO_3 + H_2SO_4 + HCl + 6H_2O \quad (4.4)$$

However, it should also be recognized that when using a dye test system for assessing semiconductor photocatalysis (SPC) activity, that photo-bleaching of the dye can also occur via a dye photosensitised process in which the electronically excited state of the dye, D^*, injects an electron into the conduction band of the semiconductor (SC) to produce an oxidised dye radical ion, D^{*+} (equation 4.5), that is unstable and able to decompose to form bleached products [138, 139].

$$D^* + SC \longrightarrow D^{*+} + SC\,(e^-) \quad (4.5)$$

The injected electron can also promote this process via its subsequent reaction with O_2 to produce a number of different oxidising species, such as hydrogen peroxide. It is usually possible to discriminate between dye bleaching caused by photocatalysis or photosensitisation of the dye via the careful selection of the excitation wavelength [139]. Preferably, the wavelength of excitation should be chosen such that the semiconductor alone is able to absorb the light. MB has a minimum in its UV absorption spectrum around the

wavelength of UV light usually used (365 nm). Even though, this choice of light source minimises the risk that the observed photobleaching is due to photocatalytic reaction, it does not eliminate it and the component of the photobleaching rate will increase with decreasing the pH of MB solution. Thus, it is important to control the pH of the MB solution. In order to confirm that MB discoloration is caused by photocatalytic degradation of MB, rather than colourless leuco-methylene blue (LMB) formation (equation 4.6).

$$2e^- + H^+ + MB^+ \longrightarrow LMB \qquad (4.6)$$

LMB ($C_{16}H_{19}N_3S$) is a colourless and formed by reduction of MB^+. LMB is known to be oxidised very rapidly at pH < 4 [140]. The pH measurements of MB solution in contact with TiO_2 - Mo 7 at.%, were carried out using a calibrated pH meter in the dark, and under UV, and fluorescent light for 5 hours. The results obtained from pH measurement showed that the pH did not change (pH ~ 6), and therefore formation of LMB due to acidity of the solution was unlikely (Figure 4.9).

Aqueous MB absorbs light most strongly at about 660 nm with a molar absorptivity of 10^5 dm^3 mol^{-1} cm^{-1}. The absorbance at 660 nm versus UV or fluorescent irradiation time generated in a study of the photocatalytic decomposition of MB can be translated into a graph of peak height absorbance against irradiation time, which has an exponential form [141]. MB concentrations were calculated using the measured absorbance peak at 665 nm (equation 4.8).

A graph of absorbance at 665 nm against irradiation time was generated (Figure 4.8). An index of photocatalytic activity (P_a) was defined by comparing the degradation rate of the MB solution in contact with the coated surfaces to the rate for an irradiated MB solution with no coating present. The equation below was used to calculate the photocatalytic activity (P_a) of each of the films.

$$P_a = 1 - (C_0e^{-mx} / C_0e^{-cx}) \quad (4.7)$$

Where:

C_0 = peak height at time = 0 (ie. Initial concentration)

C_0e^{-mx} = decay rate of methylene blue with no sample present

C_0e^{-cx} = decay rate of methylene blue in contact with a photocatalytic coating

Two parameters were defined: P_{aUV} for UV radiation and P_{aFL} for fluorescent light radiation.

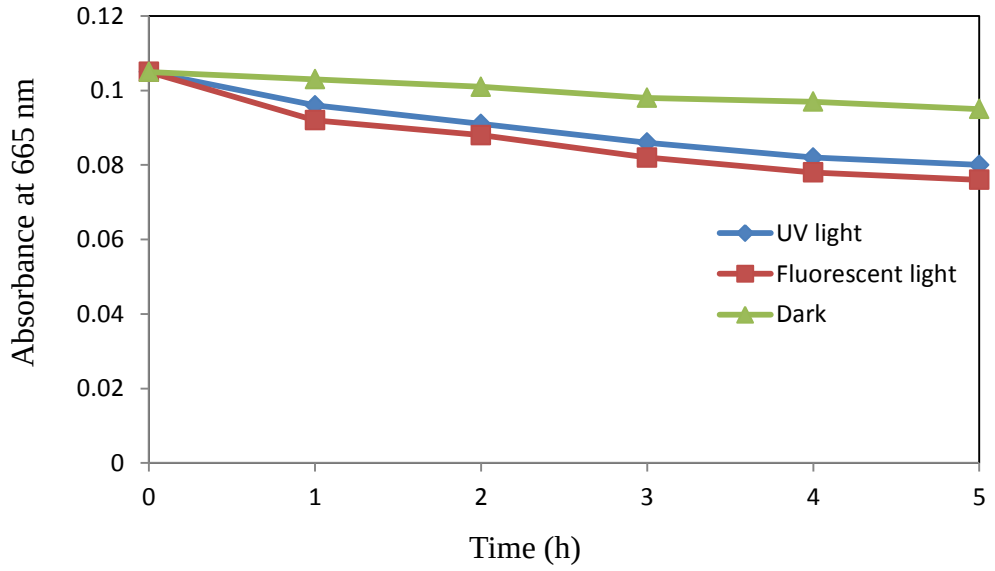

Figure 4.8: Absorbance at 665 nm versus irradiation time showing MB degradation in absence of photocatalytic surface.

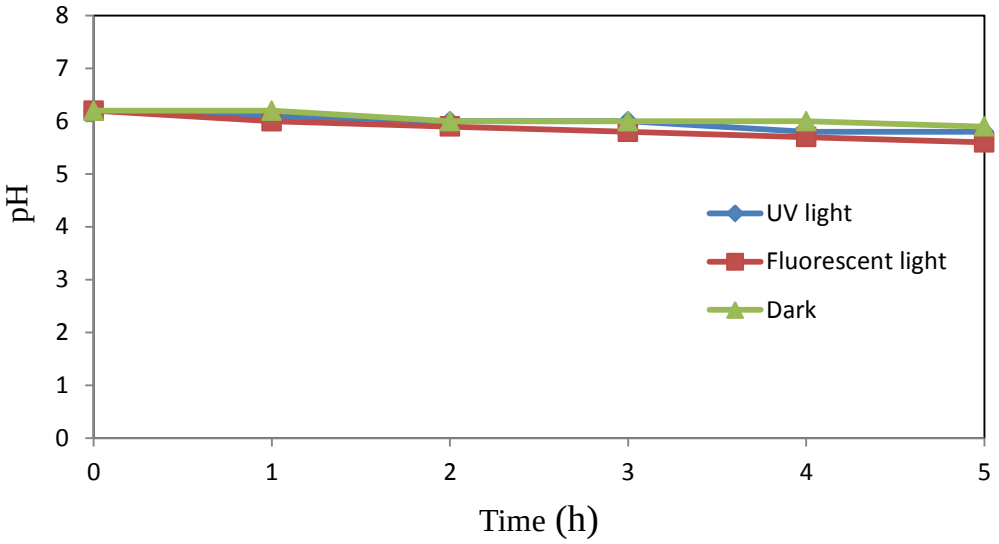

Figure 4.9: pH measurement of MB solution in dark, UV and, fluorescent light irradiation in contact with TiO_2-Mo 7 at.% after 5 hours.

The reproducibility of photocatalytic activity between batches was determined by statistical analysis (standard deviation, standard errors) which is presented in Appendix A.

4.2.10 Spectral analysis of light source (UV/Vis)

Two black light blue lamps (black Ray Cambridge, UK) with a peak emission at 352 nm and a power output of 15 W were used as a light source for UVA photocatalysis experiments (4 mW/cm^2 at 10 cm distance) and two fluorescent tubes with power output of 6.4 mW/cm^2 were used as a fluorescent light source (10 cm distance) (Figure 4.10). The UV component of the fluorescent light was measured as 0.5 mW/cm^{-2}. The Ocean Optic USB 2000+ spectrophotometer was used to measure the light intensity.

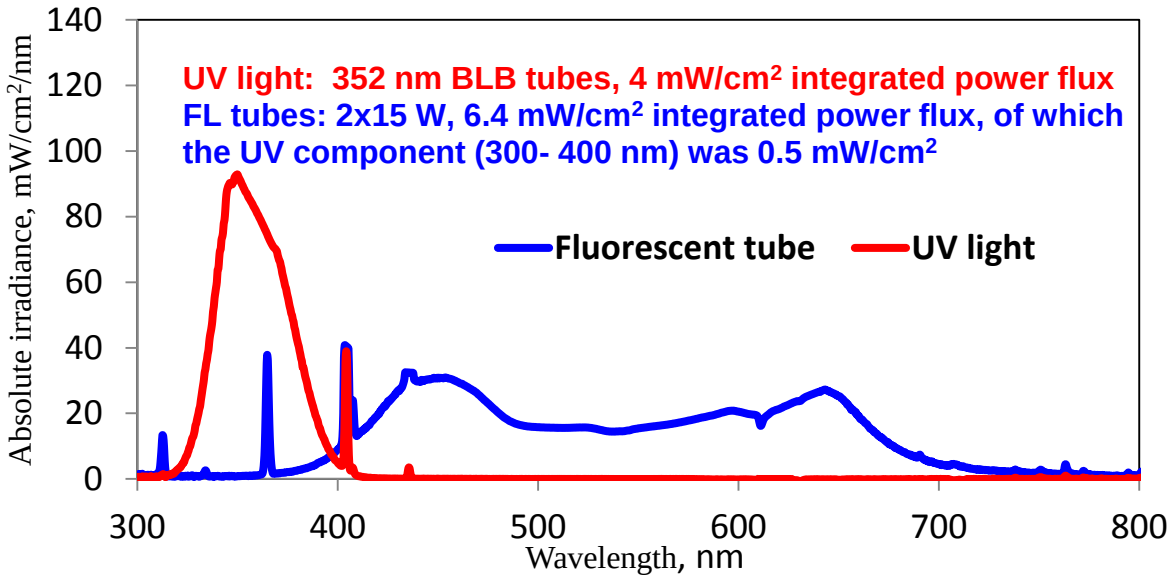

Figure 4.10: Power output spectra of fluorescent and UV light sources used during the photocatalytic testing which were obtained from an Ocean Optic USB 2000+ spectrophotometer, demonstrating part of the fluorescent tubes spectrum is in UV range.

4.2.11 Mechanical properties

Laboratory mechanical tests were done by scratching the coating surfaces using a finger nail, pencils with hardness of 2B and HB, a steel scalpel and a diamond tip. Pencil tests were carried out according to ASTM standard ASTM D3363 (Standard test method for film hardness by pencil test) [142]. Tape test were based on standard ASTM D3359 (Standard test methods for measuring adhesion by tape test) [143]. Scotch 3M invisible tape was used to carry out the test. Tests were carried out by Teer Coatings Ltd (Droitwitch,UK).

The scratch test is one of most widely used, fast, and effective methods to obtain the critical loads that are related to the adhesion properties of the coating to the substrate. The scratch adhesion test is performed by applying either a progressive (linearly increasing) or constant

load to the coated sample through an indenter [144, 145]. Scratch adhesion tests were carried out by Teer Coatings Ltd (Droitwitch,UK), with a Rockwell C- diamond tip (200 µm diameter) indenter with a load linearly increasing from 10 N to 40 N over 10 mm distance at a load rate of 10 N min^{-1} and speed of 1 mm min^{-1} [146]. Two samples of each coating were tested. The indenter is moved over a specimen surface, with a linearly increasing load, until failure. Cracking and delamination of coatings occurs at critical loads (Lc) defined by the mode of failure (Figure 4.11). The normal force (Fz) and the tangential force (Fx) are recorded. The failure events are examined by an optical microscope. Acoustic emission (AE) monitoring is also used during the test to detect cracking. Critical load is a function of the coating-substrate adhesion, stylus-tip radius, loading rate, mechanical properties of the substrate and coating, coating thickness, internal stress in the coating, flaw size distribution at substrate-coating interface, and friction between stylus-tip and the coating [147]. The data recorded from the load cells can then be used to plot a graph and thus determine the coefficient of friction of the coating and the point at which the coating fails.

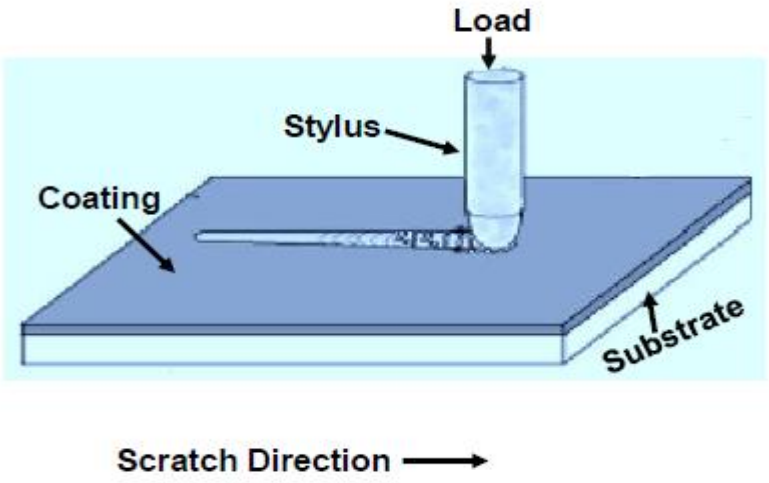

Figure 4.11: Schematic diagram of the progressive load scratch test.

Progressive load tests are suitable for rapid assessment and quality assurance of coatings, hence are more popular than constant load tests for research and development work on

coating processes. At sufficient stress levels, cracks initiate preferentially at defect sites in the coating and /or coating-substrate interface. Propagation of such cracks leads to coating failure. Adhesive failure happens due to compressive stress; the coating separates from the substrate either by cracking and lifting (buckling) or by full separation (spallation; chipping). The practical scratch adhesion value of a coating is defined as the lowest critical point at which the coating fails. It is an important parameter related to coating-substrate cohesion that can be used for comparative evaluation of coatings.

In a typical scratch test, eight failure types can be observed [147] and these are illustrated and explained in Figure 4.12.

a) Brittle tensile cracking: nested micro cracks; open to the direction of scratch; straight and semi-circular; formed behind a stylus (cohesive failure).

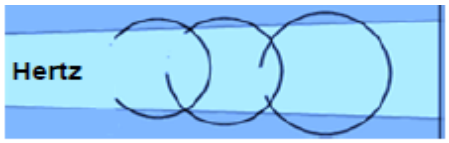

b) Hertz cracking : series of nested micro cracks within the scrach groove (cohesive failure).

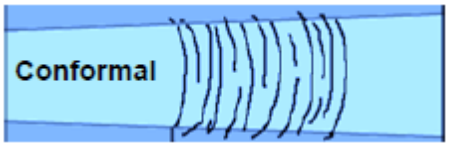

c) Conformal cracking: micro-cracks form while coating tries to conform to the groove ; open away from a direction of scratch (cohesive failure).

d) Chipping: round regions of coating removal extending laterally from the edges of the scratch groove (cohesive failure).

e) Buckling: coatings buckle ahead of the stylus tip; irregularly wide arc-shaped patches missing; opening away from scratch direction (adhesive failure).

f) Wedging: caused by delaminated region wedging ahead to separate a coating; regularly spaced annular-circular that extends beyond the edge of the groove (adhesive failure).

g) Recovery: regions of detached coating along one or both sides of the groove; produced by elastic recovery behind a stylus and plastic deformation in the substrate (adhesive failure).

h) Gross spallation: large detached regions; common in coating with low adhesion strength (adhesive failure).

Figure 4.12: Coating failure modes observed during progressive load scratch testing.

4.2.12 Chemical durability

These coatings will be cleaned using a range of chemical solutions after placement at the test locations in the brewery. Assessment of their chemical durability in basic, acidic and alcohol solutions is important, as most cleaning solutions will contain at least one of these

components [148]. Thus 0.02 M NaOH, 0.02 M HCl, 70% ethanol and distilled water were used to carry out the test [148]. Coated samples were placed into solution for two hours at room temperature, and removed and rinsed with sterilised distilled water and air dried under a hood. The surface roughness and coating thickness were measured before and after exposure to chemicals by WLI (white light interferometry) (see section 4.2.6). The photocatalytic activity was measured by methylene blue degradation (see section 4.2.9) after exposure to 0.02 M NaOH, 0.02 M HCl, 70% ethanol and distilled water.

4.2.13 *In situ* study

The samples (TiO_2 and TiO_2 -Mo4 7 at.%, two replicates from each coating) were installed in bottle filling and canning machine lines in three different Finnish breweries; A, B, and C. for the breweries B and C the product was beer and Brewery A was soft drinks and water. Filler surfaces were cleaned with saBesto spray (25-50% petroleum, 20-30% isopropanol, Würth, Riihimäki, Finland) and the samples were fixed with HV350 glue (Valco, Cincinnati, OH) (Figure 7.1). There was no special provision of lighting for the photocatalytic coatings; the process test took place under the usual brewery conditions of lighting, with coupons receiving varying amounts of light depending on their position in each machine. Two replicates of each sample were removed from the process after 3, 10 and 12 months and were sent for material characterisation by post to different partners for scratch adhesion test, photocatalytic activity measurements and contact angle measurements. Some of the samples were damaged during removal and packaging, which is likely to affect the mechanical durability and photocatalytic activity results.

The mechanical durability, chemical durability and photocatalytic activity were evaluated before and after being exposed to process conditions for 3, 10 and 12 months. The contact angle measurement was performed after three months.

4.3 Antimicrobial testing procedures

4.3.1 Culture maintenance and preparation

Escherichia coli ATCC 8739 was obtained from the American Type Culture Collection (Manasas, VA, USA). To check purity (from frozen stock), a loop of culture was streaked onto Tryptone soya agar (TSA) plate and incubated at 37 °C for 24 h. Stock plate cultures were stored at 4 °C for up to one month.

4.3.2 Bacterial inactivation using fluorescent irradiation

Measurements of the antimicrobial activity of the photocatalytic surfaces were performed using ISO 27447 as guidance (with minor modifications, such as using neutralizing solution and centrifuging cell suspensions) [149]. ISO 27447 confirmed the use of *E. coli* ATCC 8739 as a model microorganism. A loop of *E. coli* colonies from a plate was used to inoculate 10 mL of nutrient broth (NB) which was incubated aerobically for 18 h at 160 rpm in a shaker at 37 °C. Resultant suspensions were centrifuged at 3000 rpm for 10 minutes and cells were washed in Ringers solution (Oxoid, UK) prior to re-centrifugation. The density of the bacteria cells in liquid cultures was monitored by taking optical density (OD) readings at 540 nm (Jenway 6305 spectrometer, Essex, UK). An OD was selected in the range of 0.08 which corresponded to an initial concentration of bacteria of $1.0 \pm 0.2 \times 10^7$ cfu mL^{-1}.

Fifty microlitre aliquots of standardised cell suspension were inoculated onto the surface of the test substrate in a Petri dish (90 mm diameter × 12 mm height). In order to spread out the

liquid evenly without spilling over, polyethylene film (10 mm × 20 mm) (Scientific Laboratory Supplies, Nottingham, UK) was gently pressed onto the drop by sterilized tweezers. PE film was sterilized by 70% ethanol. The lid was placed on the petri dish. Four round Petri dishes plus contents were placed in one large square Petri dish (24.5 cm × 24.5 cm × 2.5 cm) which contained sterilized moistened tissues, to provide a humid environment that will prevent cultures drying out during light exposure. Aluminium foil was used to cover the dish for dark controls. The light absorbed by the Petri dish lids was measured by Lambda 40 spectrophotometer (Perkin/Elmer, USA). The Petri dish lid absorbed irradiation below 300 nm, which was outside the range of interest. The Polyethylene film (PE) absorbed light below 200 nm. Thus neither lid nor film would interfere with the photocatalytic effect under investigation.

The efficacy of photocatalytic inactivation (pure titania and doped titania coatings) was examined at four irradiation times (0, 12, 24, and 48 h). At each time (0, 12, 24, and 48 h) surfaces were removed and vortexed for 1 minute in 10 mL of neutralizing solution (20 g L^{-1} Soya Lethicin (Holland and Barrett, UK) and 30 g L^{-1} Tween 80 (Sigma Aldrich, UK) to remove attached bacteria. This neutralizing medium is considered suitable for protecting cells and maintains viability during the recovery of the cells from a coated surface [150]. This 10 ml of neutralisation solution was then diluted 1:10 in 0.9% NaCl (Fisher Scientific, UK). The viable population associated with these samples was calculated by plating serial dilutions in triplicate (to 10^{-7}) onto nutrient tryptone soya agar (TSA) (100 µL), and incubating at 37 °C for 24 h. At the end of the incubation period colonies on the agar plates were counted and the number of colony forming units (cfu) per mL was calculated. Counts were used from one dilution where agar plates showed 15 – 300 colonies [151].

In order to assess the effect of dopant metal/metal oxide on bacteria inactivation, coatings of W, WO_3, Mo, MoO_3, Nb and Nb_2O_5 were also produced. The antimicrobial activity of

transition metals and their oxides were tested using the above method but at six irradiation times (0, 6, 8, 12, 24 and 48 h). Two controls were included in each experiment; a dark control (Petri dishes covered in aluminium foil) and a light control. Three replicates were used for each treatment. Each experiment was repeated three times.

4.3.3 Light source

For the antimicrobial assays, an illuminated cooled incubator (Gallenkamp, Loughborough, UK) with six fluorescent lamps 6×8 W (Sylvania, Ontario, Canada) was used. The temperature was set at 20 °C; the lamps were used as a light source for fluorescent light irradiation of the samples (wavelength range of 300 - 700 nm). The fluorescent lamps were positioned at a distance of 15 cm from the coated surfaces inoculated with the bacteria. Lamps placed on both sides of the cabinet ensured a uniform light energy. A USB4000 Miniature Fiber Optic Spectrometer (Dunedin, USA) was used to determine the UV/Vis power at the sample distance. Samples were exposed to a portion of UV (290–400 nm) at 0.12 mW/cm^2 intensity, and visible light source (400 –7 00 nm), with intensity of 4 mW/cm^2. The light source was selected according to ISO 27447.

4.3.4 Innate antimicrobial properties of dopants

In order to assess an innate antimicrobial activity of dopants several tests were performed, metabolic activity, minimum inhibitory concentration and zone of inhibition.

4.3.4.1 Metabolic activity

The metabolic activity assay using Nitrotetrazolium Blue Chloride (NBT) (Fluka, Sigma-Aldrich, Poland, 1.0 gl^{-1}) is an alternative method for the detection of residual viable cells on the surface, and as an indication of viability [152]. *E. coli* were inoculated in 10 mL of nutrient broth (Oxoid, UK) and incubated for 16-18 hours at 37 °C with shaking at 160 rpm. The cells were centrifuged at 3000 rev min^{-1} (vortex Sigma 204, Sigma Laborcentrifugen, Germany) for 10 minutes and re-suspended in 100 mL sterilized quarter strength ringer solution, to minimise carryover of nutrient.

Ten microlitre drops of this suspension were inoculated onto 1x2 cm coated coupons (TiO_2-Mo (7 at.%), TiO_2-W (3.8 at.% and 10 at.%) and TiO_2-Nb (0.25 at.%) in a Petri dish. After 2 hours, when the inoculum had dried, molten TSA (at 45 °C) was poured over the inoculated surfaces to a depth of approximately 3 mm. The plates were incubated over night at 37 °C. Then approximately 2 mL of the respiratory NBT dye (Fluka, Sigma-Aldrich, Poland, and 1.0 gl^{-1}) was pipetted onto the agar plates, which was incubated for a minimum of 6 hours at room temperature to allow improved visibility of colonies beneath the agar. If bacteria are viable on the surface they will have grown to produce colonies. NBT stains the colonies blue and makes them easier to see.

4.3.4.2 Minimum inhibitory concentration (MIC)

The antimicrobial effectiveness of an agent is often described in terms of its MIC, the lowest concentration capable of inhibiting the growth of challenging organism.

Minimum inhibitory concentrations (MICs) of Mo, Nb and W ions (dissolved) were determined by an agar incorporation method. Stock solutions (1000 mg/L in 10% hydrochloric acid) of Mo, Nb and W standard solutions for AAS (Fluka Analytical, Sigma-

Aldrich) were serially diluted in sterilized distilled water to cover concentrations ranging from 0.5 - 5 mg/L for Mo, 5 - 25 mg/L for Nb and 0.5 - 7 mg/L for W. Since stock solutions of Mo, Nb and W also contained 10% hydrochloric acid, 2% nitric acid and 5% nitric acid respectively, serial dilutions were also performed as above using the acids alone to ensure that inhibition was due to the metal and not the acid. The same single concentration for both acids, HCl and HNO_3 was used. 2 mL of each concentration were added to 18 mL of molten isosensitest agar (ISA - Oxoid) to give a further 1:10 dilution. Agar was poured into petri dishes and left to dry before a volume 0.5 McFarland standard suspension of *E. coli* was spread onto the surface. Plates were incubated for 18 - 24 hours at 37 °C. The test was performed three times and for each experiment three replicates were used. Results agreeing on two or more occasions were adopted as the MIC of *E. coli*. The MIC was determined to be the highest concentration at which no growth was evident.

4.3.4.3 Zone of inhibition

Zone of inhibition measurements were used to determine if any antimicrobial ions leached from the coatings. 20 mL of TSA was poured in Petri dishes and 100µL of cell suspension was evenly spread over the surface with a glass spreader and left to dry for 5 minutes. The substrata (stainless steel and coatings: TiO_2-Mo 7 at.%, TiO_2-Nb 0.25 at.%, TiO_2-W 3.8 at.% TiO_2-W 10 at.%, Mo, MoO_3, W, WO_3, Nb, and Nb_2O_5) were placed with the coated side facing down in direct contact with the cells on the agar plates. Two duplicates were made and plates were incubated overnight at 37 °C. The experiment was repeated once. Only the zone of inhibition around the coupons was recorded not the absence or presence of growth beneath the coupon.

4.3.5 Investigation of pre-soiled surfaces

4.3.5.1 Re-using the surface

It is vital to know whether the photocatalytic surfaces can be reused or not, as the coating is used *in situ* over a period of time in which repeated soiling and cleaning will occur. In order to assess the effect of re-using the surface on photocatalytic function, newly prepared TiO_2 - Mo 7 at.% surfaces, and old surfaces which were used and stored in a beaker in the dark for one year, were cleaned by sonication for 2 minutes with either acetone/methanol/ethanol (AME) or 4 v/v% oxofoam (Johnson Diversey Oxofoam, Northampton, UK). Oxofoam solution contains a balanced blend of caustic alkali, surface active agents, sequestrant and hydrochlorite. Surfaces were sonicated for a further 2 minutes in distilled water to remove any residue chemicals and left to dry in a sterile class 2 cabinet. Bacteria were applied following cleaning, were irradiated and enumerated as above (section 4.3.2). Tests were performed using *E. coli.*

4.3.5.2 Effect of beer soil on antimicrobial activity of TiO_2 - Mo 7 at.%

Since the 'old' coupons described in section 4.3.5.1 above were heavily soiled in a manner unlikely to be encountered *in situ,* antimicrobial tests were performed on TiO_2 - Mo 7 at.% coatings immediately after annealing (but at room temperature) and on coatings which had been soiled with either undiluted beer or diluted beer (10% vol). Beer used to simulate soiling was a pasteurised, commercial product (Carlsberg, water, alcohol, protein, carbohydrates, vitamins and minerals). 20 µl of undiluted or diluted beer was dried onto the surfaces prior to the application of the bacterial suspension and the effect of soiling on microbial numbers was examined over an irradiation period of up to 48 hours.

4.3.5.3 Detection of residual material (bacteria and soil)

A stock solution of 3 % acridine orange (St Louis, Sigma, USA) was made up in 2 % vol glacial acetic acid (BDH, Poole, England) and stored at 4 °C, wrapped in foil until use. For staining purposes, the stock solution was diluted to 3% in 2% glacial acetic acid. The acridine orange staining was carried out after cleaning the surface with the three different cleaning solutions (Section 4.3.7), to assess whether any material was retained on the surface. Three surfaces from each cleaning solution were stained. Substrata were stained for 2 min with 3% acridine orange and rinsed. Substrata with retained cells and residual material were air dried in a laminar flow hood, in darkness to avoid leaching of the acridine orange.

Epifluorescence microscopy was used to determine the retention of bacteria and soil on the surface after cleaning using a Nikon Eclipse E600 (Nikon, Kingston Upon Thames, Surrey, UK). The microscope was mounted with a Hitachi HV-D37P colour camera (Nikon, Kingston Upon Thames, Surrey, UK) and a Lucia Image analysis package was used (Nikon,Kingston Upon Thames, Surrey, UK) to view any retained microorganisms and soil, to give a qualitative indication of cleaning.

4.3.6 Statistics

A two-tailed homoscedastic Student t-test was performed using Microsoft Excel 2010 to compare data sets. If the p value was <0.05, then results were statistically significant.

Chapter 5: Enhancing Photocatalytic Activity of TiO_2 coatings via Doping with Different Transition Metal

5.1 Introduction

As discussed earlier (chapter 2), the problems associated with the use of TiO_2 as a photocatalyst could be addressed by incorporation of transition metal and non-metal dopant elements into the titania lattice. Different methods and techniques have been used to deposit doped TiO_2 thin films, so there are various investigation in the literature focused on the determination of optimum dopant concentrations and the choice of dopant [153]. It is believed that doping TiO_2 with transition metal ions with valences higher than +4 leads to an upward shift of the Fermi level which reduces the possibility of electron-hole recombination, resulting in more efficient separation and stronger photocatalytic reaction. In addition use of doping ions with an ionic radius close to that of titanium was suggested, as ions with larger ionic radii will not incorporate into the titania lattice and would form a separate phase [74, 154, 155]. Therefore, molybdenum (Mo), niobium (Nb), tantalum (Ta) and tungsten (W) were chosen as doping ions because of their higher valence and similar ionic radius to titanium.

This chapter describes the results obtained from doping TiO_2 with various transition metals deposited onto the stainless steel substrates by closed field unbalanced magnetron sputtering.

5.2 Results

The coatings were produced by unbalanced reactive magnetron sputtering (Section 4.1) in two modes; direct current (DC) and pulsed DC modes using Advanced Energy MDX^{TM} and dual channel Advanced Energy Pinnacle^{TM} Plus power supplies. In order to develop the crystal structure samples of each coating were annealed in air for 30 minutes at two different temperatures: 400 °C and 600 °C. In order to assess the thin film crystal structure, X-ray diffraction (XRD), Raman spectroscopy, and energy dispersive X-ray (EDX) spectroscopy were employed (Chapter 4). Raman spectroscopy has a penetration depth of a few hundred nanometres, while XRD has a penetration depth of several microns. In this study, coating thicknesses were in the range 800 nm to 1.2 μm; therefore they had enough thickness to be studied by both Raman spectroscopy and XRD.

UV/Vis spectrophotometer was used to measure photocatalytic activity by methylene blue degradation. TiO_2 was doped with four different transition metals Mo, Nb, Ta and W. Tables 5.1-5.4 provide a summary of compositional properties, roughness of titania and doped titania coatings and parameters used for deposition. The same ranges of powers were applied to the four dopant targets (100 W – 240 W), but due to different sputtering rate of the materials, this resulted in very different dopant contents. Only selected results are presented here, based on coatings which showed some level of photocatalytic activity. Coatings with no activity have not been included. These tables will be referenced again later in this Results section.

Table 5.1: TiO_2-Mo films deposited on stainless steel 304-2B, with different operating parameters (power and annealing temperature) demonstrating Mo content and roughness (R_a) of coatings.

Sample type	DC Power to Mo target (W)	At.% Mo	Annealing temperature (°C)	Roughness (R_a, nm)
Stainless steel 304 2B				280
TiO_2	-	-	As deposited	290
TiO_2	-	-	400	300
TiO_2	-	-	600	305
TiO_2-Mo1(50% duty cycle)	100	1.5	400	310
TiO_2-Mo1(50% duty cycle)	100	1.5	600	315
TiO_2-Mo2	100	2.7	400	311
TiO_2-Mo2	100	2.7	600	318
TiO_2-Mo3	150	5.5	400	315
TiO_2-Mo3	150	5.5	600	327
TiO_2-Mo4	180	7	400	325
TiO_2-Mo4	180	7	600	332
TiO_2-Mo5	240	11.8	400	325
TiO_2-Mo5	240	11.8	600	335

Table 5.1 shows the parameters used for Mo-doped titania and pure titania coating. The majority of coatings were deposited in DC mode, however 50% duty cycle and 100 kHz on Mo target was used for sample TiO_2-Mo1, in order to obtain the lower amount of Mo in the coating. As-deposited coatings had lower roughness value in comparison to annealed samples. Doping of titania with molybdenum generally resulted in a slight increase in surface roughness in comparison to undoped titania coating. No remarkable changes in surface roughness value of the coatings can be seen with varying annealing temperature.

Table 5.2: TiO_2-Nb films deposited on stainless steel 304-2B, with different operating parameters (power and annealing temperature) demonstrating Nb content and roughness (R_a) of coatings.

Sample type	Power to Nb target (W)	At.% Nb	Annealing temperature (°C)	Roughness (R_a, nm)
Stainless steel 304 2B				280
TiO_2-Nb1	100	0.25	400	303
TiO_2-Nb1	100	0.25	600	310
TiO_2-Nb2	150	0.5	400	308
TiO_2-Nb2	150	0.5	600	315
TiO_2-Nb3	200	1.4	400	310
TiO_2-Nb3	200	1.4	600	318
TiO_2-Nb4	100	0.75	400	305
TiO_2-Nb4	100	0.75	600	311
TiO_2-Nb5	150	2.1	400	309
TiO_2-Nb5	150	2.1	600	315
TiO_2-Nb6	200	2.85	400	312
TiO_2-Nb6	200	2.85	600	318

The initial experimental conditions where the dopant target was deposited in DC mode (100-200 W) had produced relatively low photocatalytic activity (TiO_2-Nb4 - TiO_2-Nb6) which will be discussed in more details later on. Thus, a series of Nb doped titania coatings were deposited (TiO_2-Nb1 - TiO_2-Nb3) in pulsed DC mode at 100 kHz and 84% duty cycle in order to obtain lower Nb content in coatings (84% duty cycle was applied on Nb target) (Table 5.2). Pulsed DC mode would decrease the deposition rate, in comparison to DC mode. This can be explained in terms of the driving voltage waveform at the target (Chapter 3). Lower Nb dopant levels was chosen, as the optimum content of Nb in the coating is reported in the range of 0.1 at.% to 1 at.% [155]. However, these numbers are only estimated as

guidline, as the optimum level of dopant in the coatings depends on many factors, specifically on the deposition technique used. Doping with niobium did not significantly affect the value of surface roughness. Dopant content would be expected to be proportional to dopant target power. However, as can be observed from the table, the relationship between the target power and dopant content is not linear. Since the deposition rate for Nb is relatively low (based on composition data), this might be due to sputtered titanium cross contaminating the Nb target at lower power, so there would be less Nb in the coating.

Table 5.3: TiO_2-Ta films deposited on stainless steel 304-2B, with different operating parameters (power and annealing temperature) demonstrating Ta content and roughness (R_a) of coatings.

Sample type	Power to Ta target (W)	At.% Ta	Annealing temperature (°C)	Roughness (R_a ,nm)
Stainless steel 304 2B				280
TiO_2-Ta1 (50% duty cycle, 350 kHz)	100	0.76	400	324
TiO_2-Ta1 (50% duty cycle, 350 kHz)	100	0.76	600	330
TiO_2-Ta2 (50% duty cycle, 225 kHz)	100	1.1	400	328
TiO_2-Ta2 (50% duty cycle, 225 kHz)	100	1.1	600	337
TiO_2-Ta3	100	3.4	400	340
TiO_2-Ta3	100	3.4	600	350
TiO_2-Ta4	150	9.2	400	341
TiO_2-Ta4	150	9.2	600	348
TiO_2-Ta5	200	13.8	400	342
TiO_2-Ta5	200	13.8	600	355

For samples TiO_2-Ta1 and TiO_2-Ta2, pulsed DC mode at 350 kHz and 225 kHz and 50% duty cycle was also used to obtain lower content of Ta in the coatings (50% duty cycle was applied on Ta target) (Table 5.3). For Ta doped coatings suggested optimum dopant level is in the range of between 0.6 at.% to 1.6 at.% [156]. Higher surface roughness was achieved by increasing the Ta content in the coatings.

Table 5.4: TiO_2-W films deposited on stainless steel 304-2B, with different operating parameters (power and annealing temperature) demonstrating W content and roughness of coatings.

Sample type	DC Power to W target (W)	At.% W	Annealing temperature (°C)	Roughness (R_a ,nm)
Stainless steel 304 2B				280
TiO_2-W1	60	3.8	400	333
TiO_2-W1	60	3.8	600	340
TiO_2-W2	70	4.6	400	338
TiO_2-W2	70	4.6	600	345
TiO_2-W3	80	5.8	400	339
TiO_2-W3	80	5.8	600	347
TiO_2-W4	90	7	400	341
TiO_2-W4	90	7	600	350
TiO_2-W5	100	10	400	342
TiO_2-W5	100	10	600	351
TiO_2-W6	150	13.4	400	348
TiO_2-W6	150	13.4	600	357
TiO_2-W7	200	15.2	400	355
TiO_2-W7	200	15.2	600	360

The results from first set of coatings (100-200 W) had produced relatively high level of tungsten in the coatings (10-15.2 at.%) and low photocatalytic activity. Therefore, a second series of W-doped coatings were produced where the power to dopant target was varied over

a lower range values (60-90 W), in order to obtain a lower W concentration in the coatings, with a view to optimising the photocatalytic activity level. Doping of titania with W resulted in an increase in surface roughness, however no substantial change was observed by increasing the annealing temperature.

5.3 Raman spectroscopy results

Anatase TiO_2 has five Raman active fundamentals in the vibrational spectrum at 144, 197, 639, 399 and 519 cm^{-1}.The rutile structure has three Raman shifts at 273, 447 and 612 cm^{-1} [157, 158]. Typically, as the crystal size of TiO_2 nano-materials decreases, the characteristic Raman scattering peaks become broader. The crystal size effect on the Raman scattering in nano-crystalline TiO_2 is interpreted as originating from phonon confinement, non-stoichiometry, internal stress or surface effects [115].

By increasing the annealing temperature, the crystallinity of TiO_2 changed from an amorphous to crystalline anatase form as shown in the Raman spectra (Figure 5.1). The broader features assumed to be from amorphous regions have disappeared.

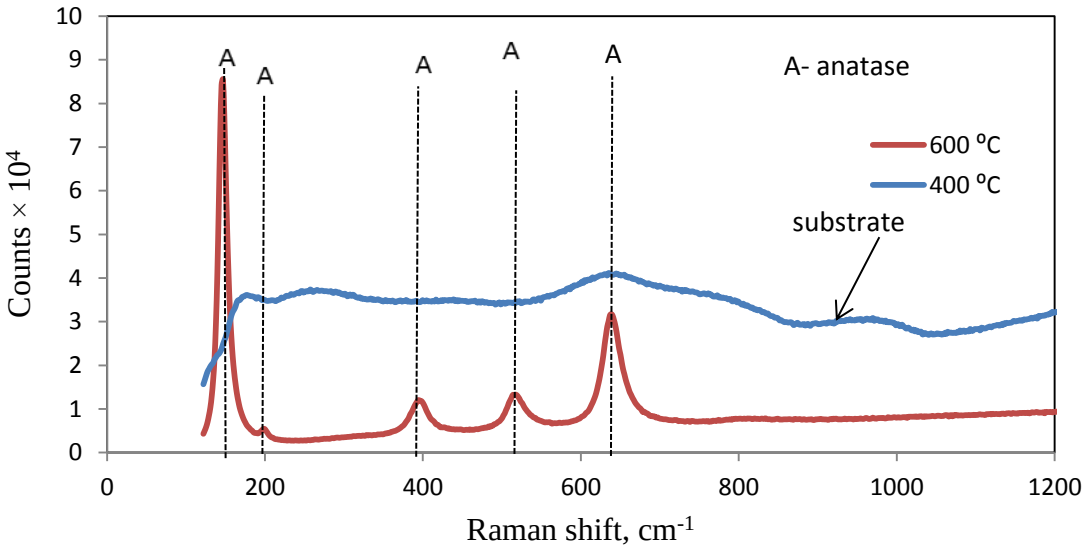

Figure 5.1: Raman spectra of TiO_2 coatings with different annealing temperatures of 400 °C, and 600 °C showing the crystal structure of the coatings (anatase and amorphous).

The Raman spectra for Mo-doped samples are presented in Figures 5.2 and 5.3; they showed anatase, mixed phase anatase/rutile and amorphous structures. After annealing at 400 °C TiO_2 - Mo1, Mo2 and Mo3 had anatase crystal structure (Figure 5.2). Further increase in Mo content resulted in the disappearance of the anatase peaks and the structure changed into amorphous for the TiO_2-Mo4 and TiO_2-Mo5 samples.

As can be seen in Figure 5.3, the coatings annealed at 600 °C demonstrated anatase and mixed anatase/rutile phase. As the annealing temperature increased from 400 °C to 600 °C for the TiO_2 -Mo4 sample, the crystal structure changed from amorphous to mixed phase anatase/rutile. As, at higher annealing temperatures, anatase crystal structure formation and improvement of crystal growth rate occurs. An increase in Mo content also resulted in anatase phase suppression. The Raman spectra of TiO_2-Mo coatings contains a peak at 972

cm^{-1} which is the marker band for Mo=O bond stretching in coatings [115], which can be attributed to some molybdenum oxide in the structure of the coating.

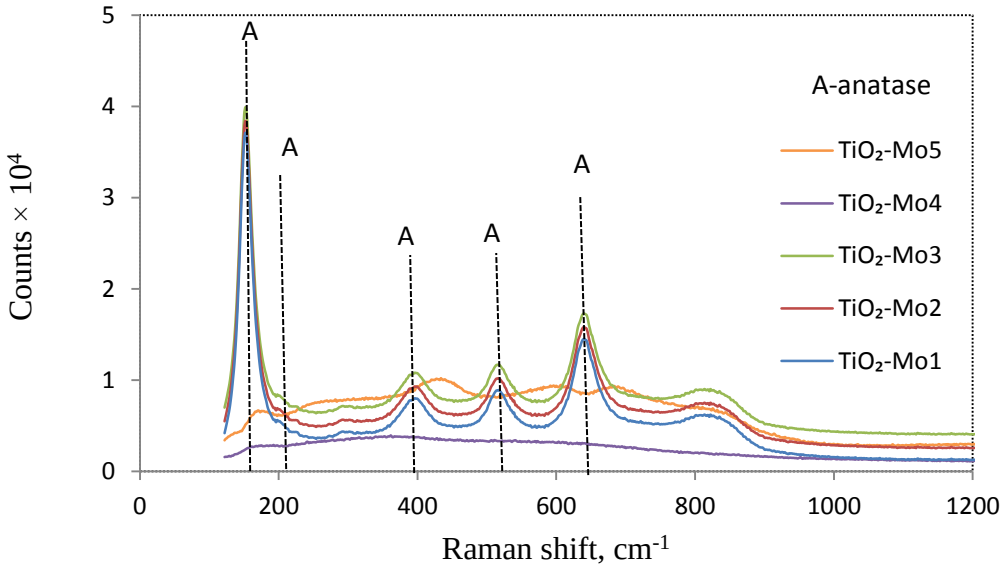

Figure 5.2: Raman spectra of TiO_2-Mo coatings post-deposition annealed at 400 °C showing the crystal structure of coatings (anatase and amorphous).

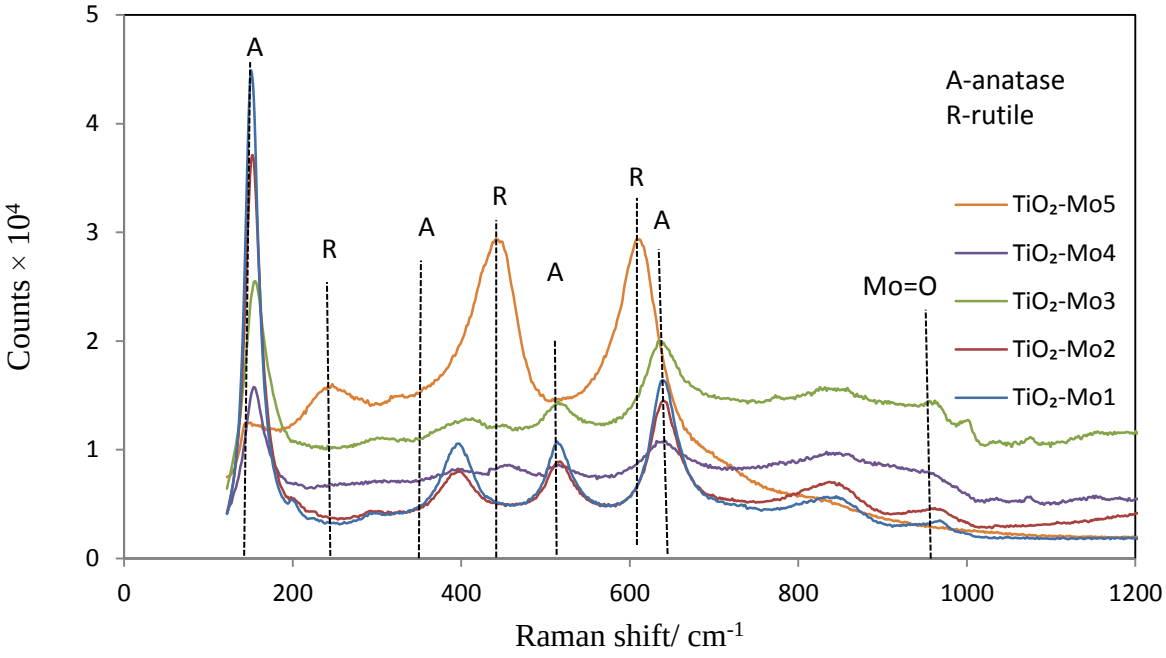

Figure 5.3: Raman spectra of TiO_2-Mo post-deposition annealed at 600 °C showing the crystal structure of coatings (anatase and rutile).

Doping of TiO_2 with Nb and post-deposition annealing at 400 °C and 600 °C (Figures 5.4, 5.5) was investigated. All of the samples showed anatase structure. Increasing annealing temperature and Nb content did not cause any significant difference in the crystal structure of TiO_2-Nb coatings, which imply the substitutional incorporation of Nb into TiO_2 lattice during deposition. However, differences in the relative intensity of the main peaks can be observed in the crystal structure as the dopant levels increased, which indicates the mixture of polycrystalline structures and small grain size.

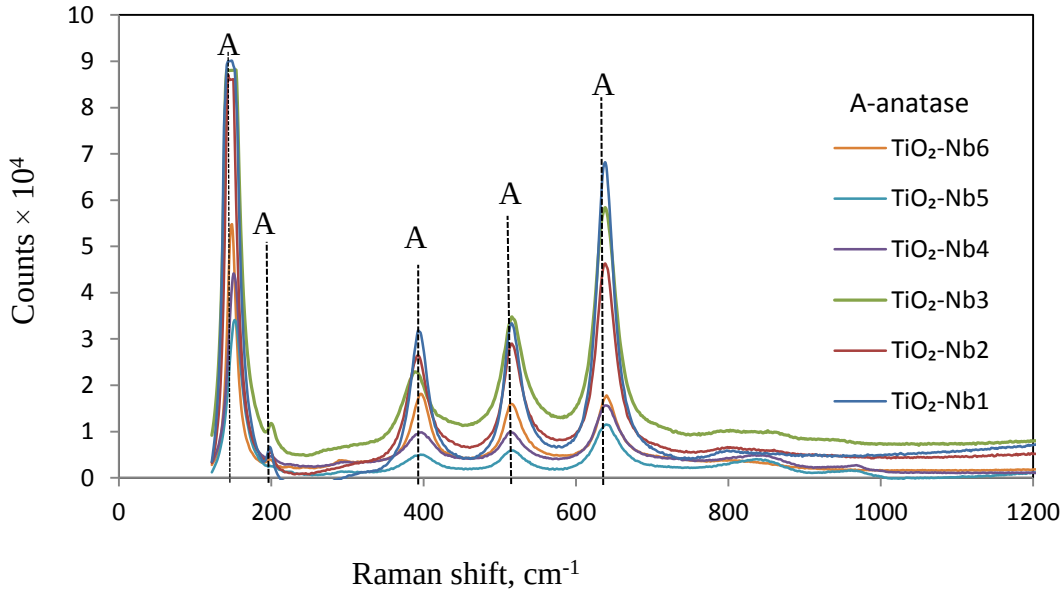

Figure 5.4: Raman spectra of TiO_2-Nb coatings post-deposition annealed at 400 °C showing the crystal structure of coatings (anatase).

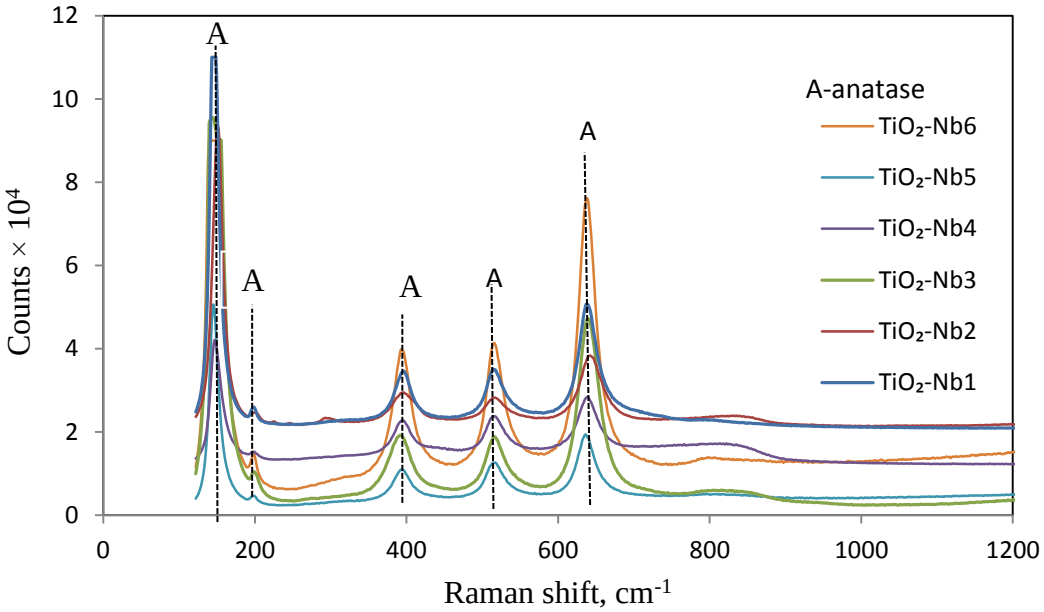

Figure 5.5: Raman spectra of TiO_2-Nb coatings post-deposition annealed at 600 °C showing the crystal structure of coatings (anatase).

The TiO_2-Ta1 and Ta2 samples which were doped with lower content of Ta showed anatase structure after annealing at 400 °C (Figure 5.6). By increasing the Ta content in the coating the structure changed from anatase to amorphous for TiO_2-Ta3, Ta4 and Ta5 samples after annealing at 400 °C. Once the samples were annealed at higher tempereture the structure changed from amorphous to anatase (Figure 5.7).

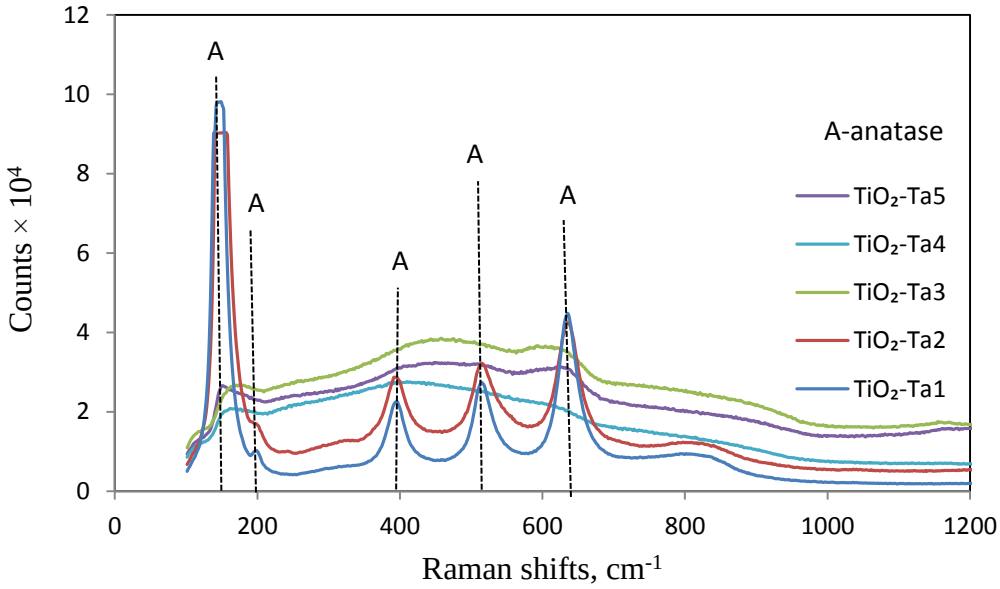

Figure 5.6: Raman spectra of TiO_2-Ta coatings post-deposition annealed at 400 °C showing the crystal structure of coatings (anatase and amorphous).

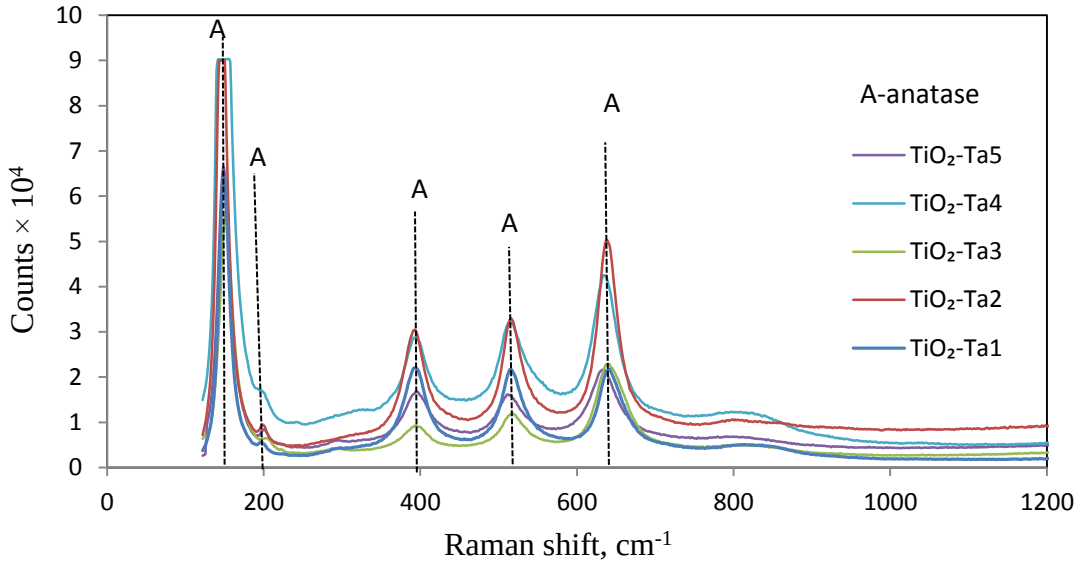

Figure 5.7: Raman spectra of TiO_2-Ta coatings post-deposition annealed at 600 °C showing the crystal structure of coatings (anatase).

The results of Raman spectroscopy for W-doped samples are presented in Figures 5.8 and 5.9. The only W-doped sample that showed an anatase structure after annealing at 400 °C was TiO_2-W1. The rest of the samples did not form any crystal structure (Figure 5.8). The samples with the lower content of W were anatase after annealing at 600 °C. As the amount of W increased from 10-15.2 at.%, the crystal structure changed from anatase to rutile (Figure 5.9). Therefore, W levels below 10 at.% promoted anatase formation and W level above 10 at.% supresses crystallinity. At higher concentrations of W, the peaks for WO_3 were observed at 968 cm^{-1} and 273 cm^{-1} that are assigned to tugsten oxide species on the surface of the coatings [115].

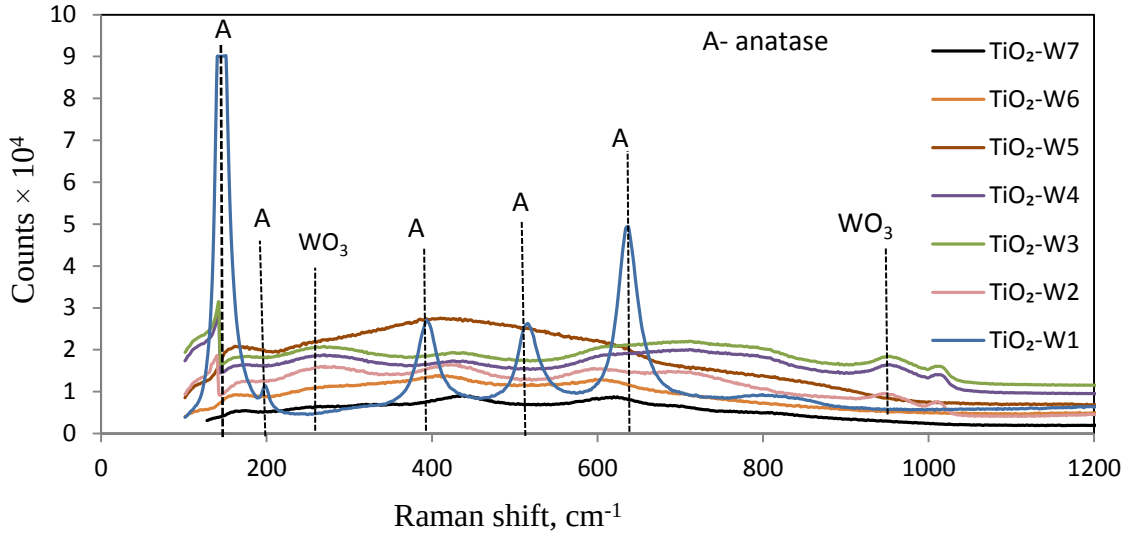

Figure 5.8: Raman spectra of TiO_2-W coatings post-deposition annealed at 400 °C showing the crystal structure of coatings (anatase, amorphous).

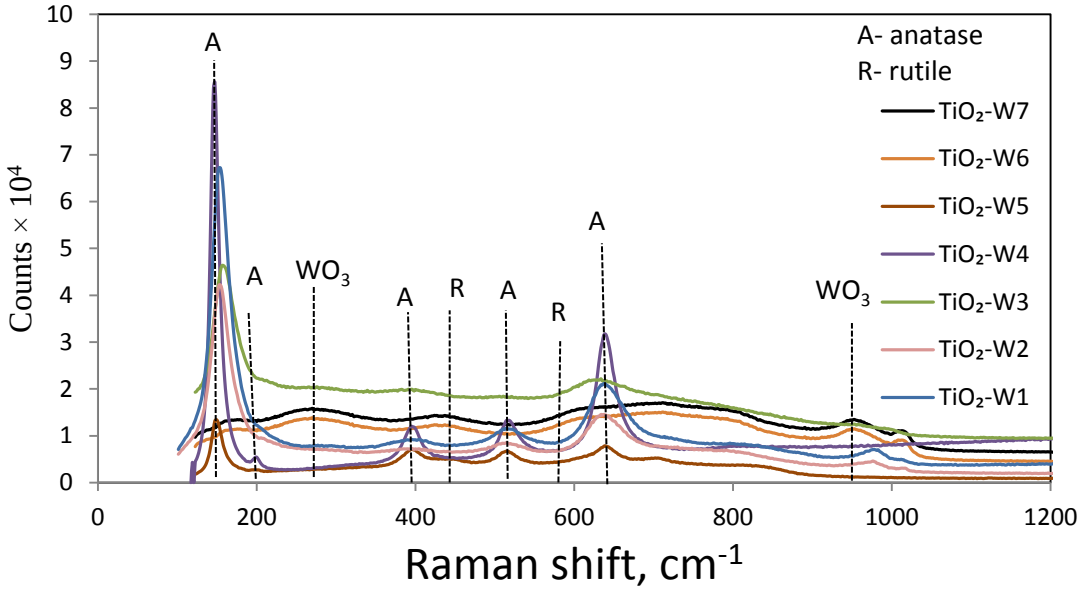

Figure 5.9: Raman spectra of TiO_2-W coatings post-deposition annealed at 600 °C showing the crystal structure of coatings (anatase, rutile).

In summary, for Mo-, Nb-, W- and Ta-doped titania coatings, with a dopant level of below 4 at.%, a strong anatase structure has clearly evolved at 400 °C which indicates that the lower dopant level promotes anatase phase growth. As the dopant content increased above 4 at.% for Ta- and W-doped coatings, the crystal structure changed from anatase to amorphous at 400 °C, it may be inferred that the higher dopant levels were suppressing crystallisation. Annealing at 600 °C results in the formation of an anatase structure for the majority of the dopants investigated, but in the case of tungsten, broad rutile peaks were also detected. Therefore, annealing at higher temperature did not promote anatase phase growth with higher dopant levels (above 10 at.%).

5.3 XRD results

X-ray diffraction patterns were collected for a number of samples. Representative XRD patterns (Figures 5.10-5.16) for pure titania and Mo-, Ta- and Nb-doped titania samples have three sharp peaks at 43.7°, 50.6°, and 75.3° degrees 2θ which are from the substrate, which in this case is stainless steel. As mentioned earlier, XRD has higher penetration depths in comparison to Raman spectroscopy; therefore substrate peaks are more evident in the XRD pattern than Raman spectra. The XRD data generally echoed the Raman data in that the majority of samples have a mixture of polycrystalline structures. Anatase (tetragonal) (JCPDS: 21-1272), rutile (tetragonal with different arrangement) (JCPDS 21-1276) and β TiO_2 are three crystalline phases that could be found in the XRD spectra. All samples, after annealing at 400 °C, and 600 °C showed a strong anatase peak at 2θ = 25.4° (101), except TiO_2-Mo4 (7 at. %). All the analysed samples also showed the presence of some monoclinic β-titania. In the XRD patterns for the TiO_2-Mo4 (7 at. %) sample annealed at 400 °C, some rutile peaks were found (Figure 5.11). In Figure 5.12, as the annealing temperature increases

to 600 °C, the TiO_2-Mo4 (7 at. %) becomes more crystalline, indicated by the sharper, more intense peaks in the trace. The anatase phase with characteristic peaks at 25.4°, 48° and rutile peaks at 27.4°, 36° and 55° were present. No additional peaks were found that could be attributed to molybdenum oxides or molybdenum clusters.

More crystalline peaks could be observed for TiO_2-Nb1 (0.25 at. %) coating in comparison to TiO_2-Nb2 (0.52 at.%) (Figures 5.13 and 5.14). Fewer anatase peaks were found, as the concentration of Nb in the coating increased for samples post annealed at 400 °C (Figure 5.13). The intensity of the 25.4° (101) peak was higher for TiO_2-Nb1 (0.25 at. %) than TiO_2-Nb2 (0.52 at. %) (Figure 5.14), which indicates a higher ratio of anatase structure in the coating. No peaks of other phases such as Nb-Ti, niobium oxides and Nb clusters were found.

The TiO_2-Ta2 sample, which was selected as a typical example of the Ta-doped coatings, showed an anatase structure once annealed at 400 °C (Figure 5.15). The Ta-doped titania coatings after annealing at 600 °C showed an anatase/rutile mixed phase structure (Figure 5.16). The XRD pattern did not exhibit any peaks that could be attributed to Ta oxide.

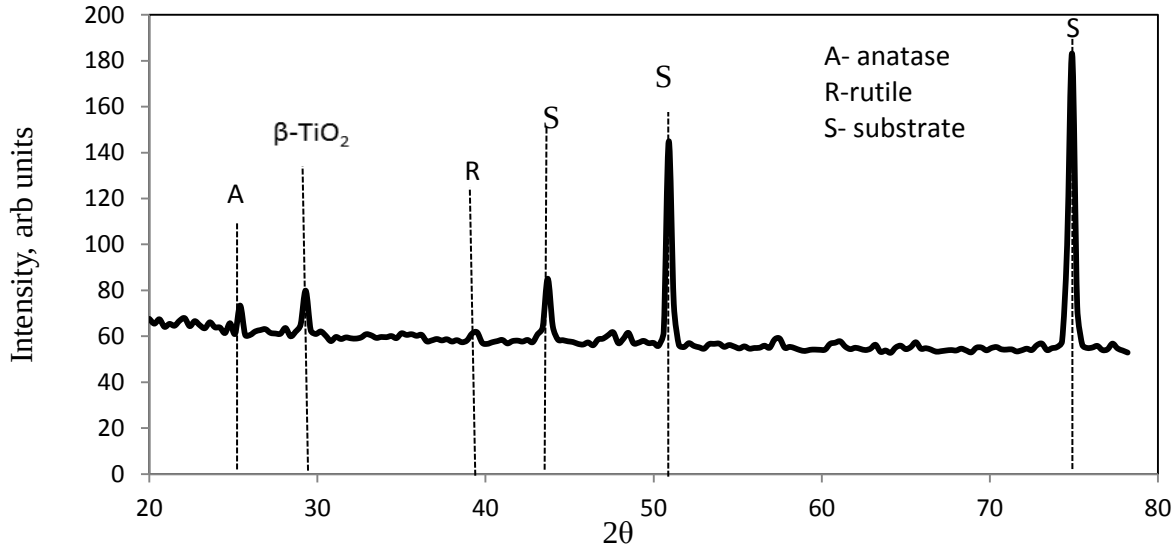

Figure 5.10: XRD pattern of TiO_2 coating post-deposition annealed at 600 °C, showing the crystal structure of coating.

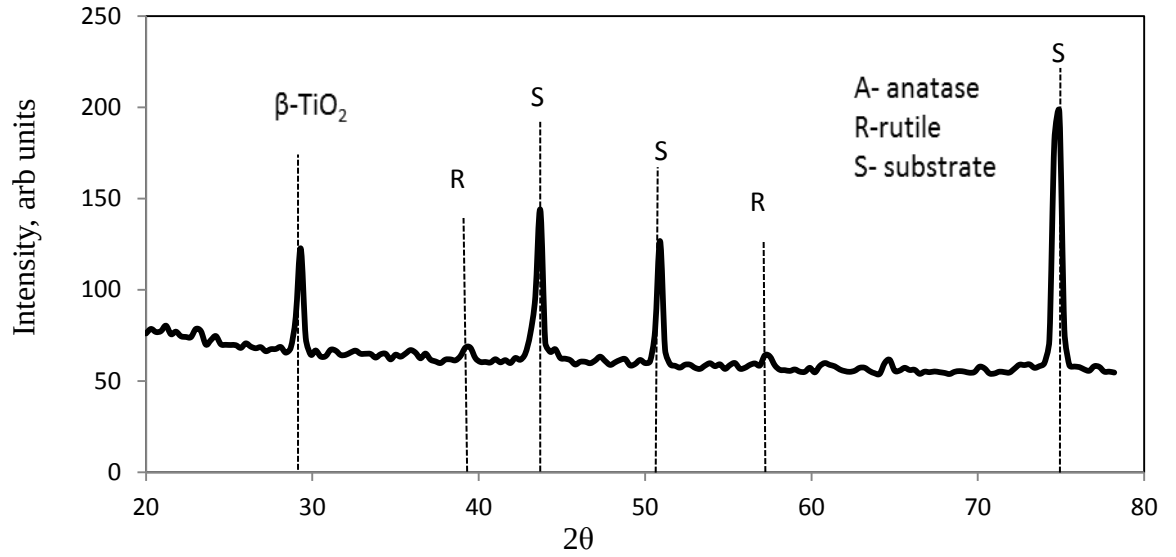

Figure 5.11: XRD pattern of TiO_2-Mo4 coating post-deposition annealed at 400 °C showing the crystal structure of coating.

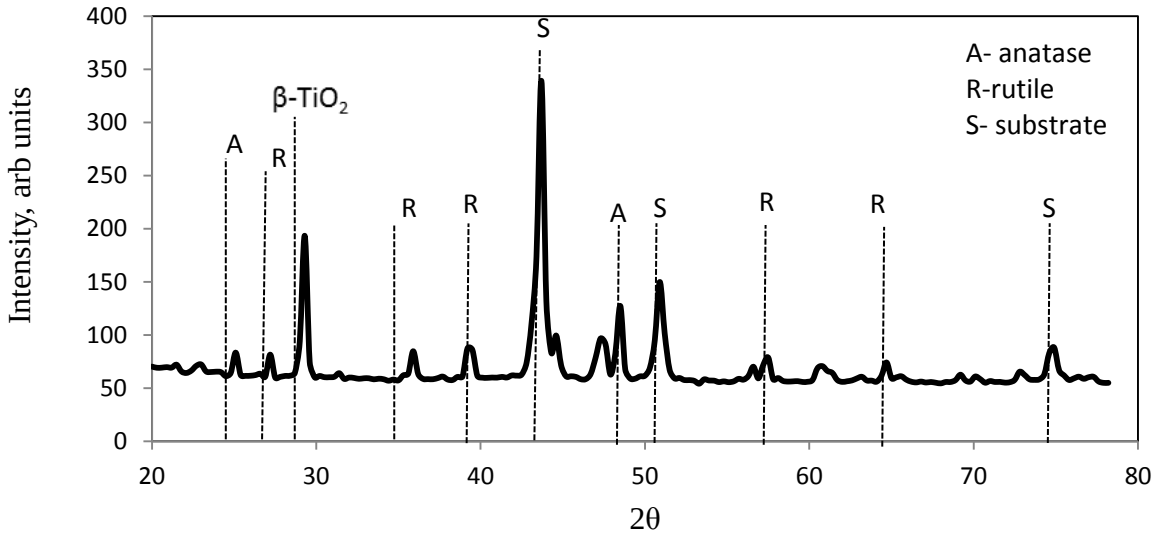

Figure 5.12: XRD pattern of TiO_2-Mo4 coating post-deposition annealed at 600 °C showing the crystal structure of coating.

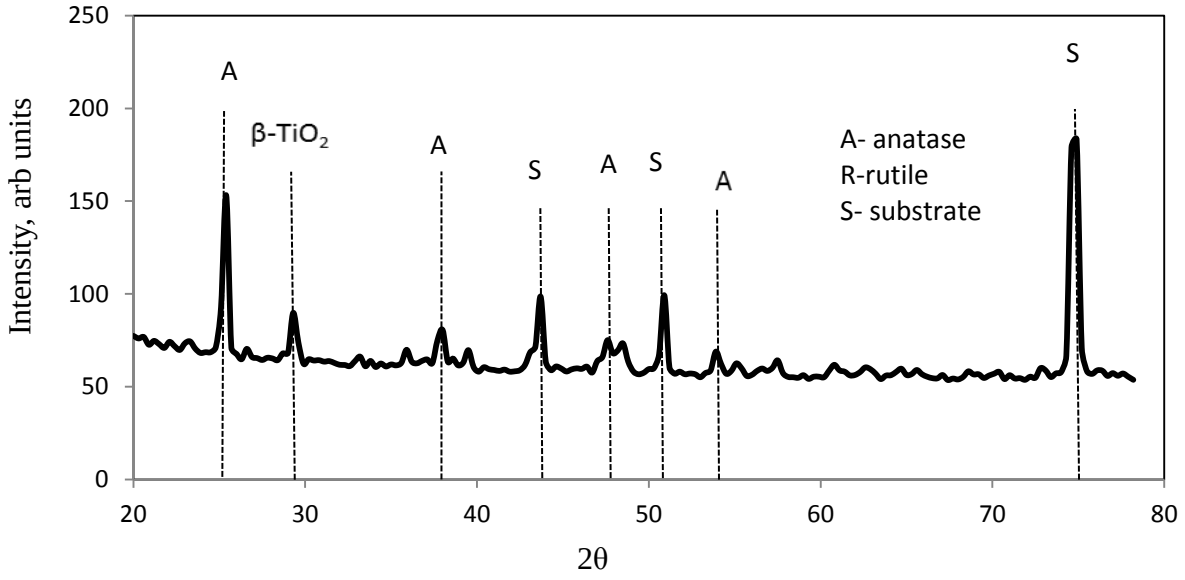

Figure 5.13: XRD pattern of TiO_2-Nb1 coating post-deposition annealed at 400 °C showing the crystal structure of coating.

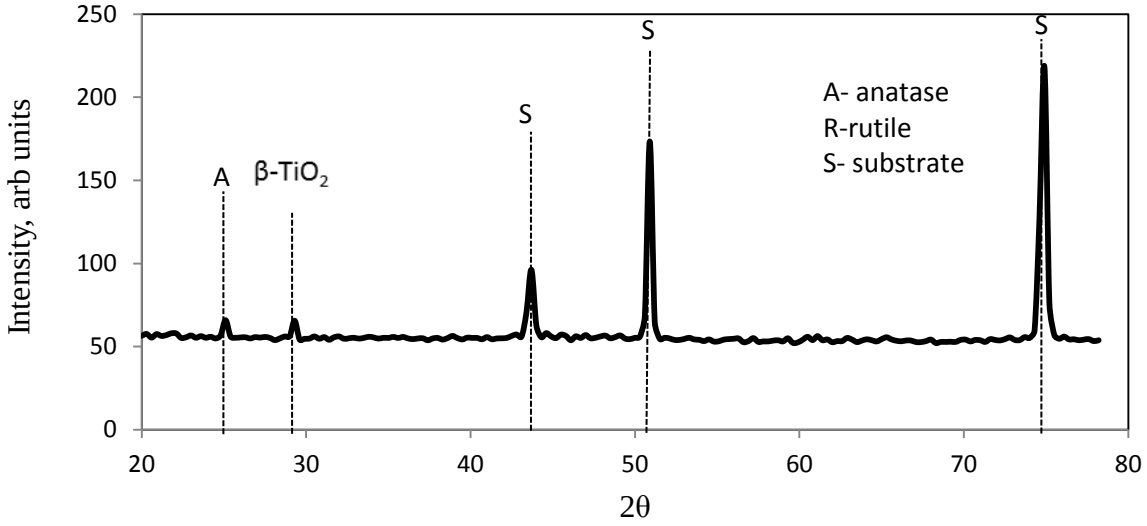

Figure 5.14: XRD pattern of TiO_2-Nb2 coating post-deposition annealed at 400 °C showing the crystal structure of coating.

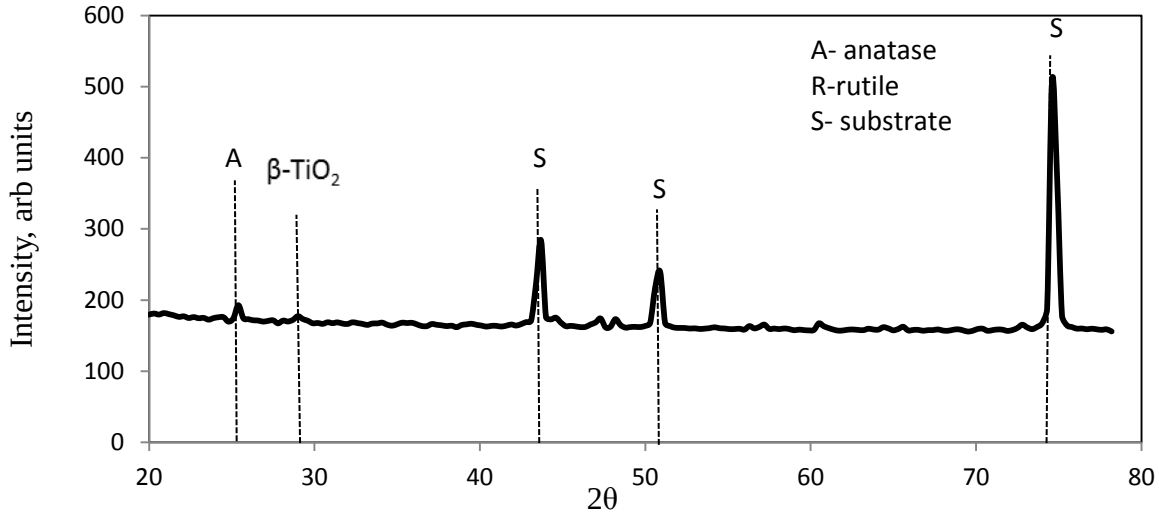

Figure 5.15: XRD pattern of TiO_2-Ta2 coating post-deposition annealed at 400 °C showing the crystal structure of coating.

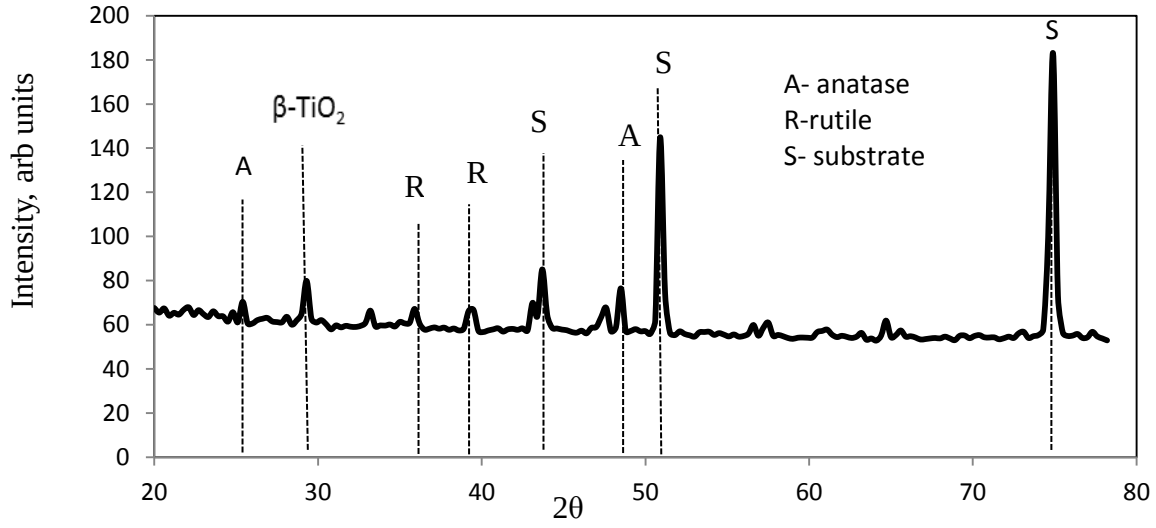

Figure 5.16: XRD pattern of TiO_2-Ta3 coating post-deposition annealed at 600 °C showing the crystal structure of coating.

5.5 Photocatalytic activity

5.5.1 TiO_2-Mo coatings

Figures 5.17 - 5.20 show methylene blue (MB) degradation versus time plots for TiO_2-Mo coatings, post annealed at 400 °C and 600 °C, under both UV and fluorescent light irradiation. It can be observed that coatings annealed at 400 °C had low photocatalytic activity, none of the Mo-doped coatings were better than TiO_2 (Figures 5.17 and 5.19). TiO_2-Mo2 coating showed the highest photocatalytic activity under UV light irradiation after annealing at 400 °C in comparison to other Mo-doped coatings. The photocatalytic activity was raised by increasing the annealing temperature to 600 °C for TiO_2-Mo2 and TiO_2-Mo3 samples with crystal structure of anatase and mixed phase anatase/rutile (Table 5.5).

As Mo content increased up to 7 at.%, photocatalytic activity increased under both UV and fluorescent light in comparison to the undoped TiO_2. The best photoactivity under both light sources was achieved with the Mo content of 7 at. %, and annealing temperature of 600 °C (Table 5.5). TiO_2-Mo4 7 at.% had a mixed phase crystal structure of anatase/rutile that may explain the strong photoactivity results, as it is reported that the mixed phase crystal structure reduces the rate of photoexcited e^-/h^+ recombination [21]. The crystal structure changed from mixed phase anatase/ rutile to rutile as the Mo content exceeded 7 at.% (Figure 5.21), therefore the photocatalytic activity was reduced. Changes in crystal structure clearly influence the photoactivity of the thin film coatings. It was found that the undoped amorphous titania coating was inactive during photocatalytic testing [1]. As expected, the amorphous Mo-doped titania coating prepared in this project also showed a low activity level for photo-decomposing MB in aqueous solution (Figure 5.17).

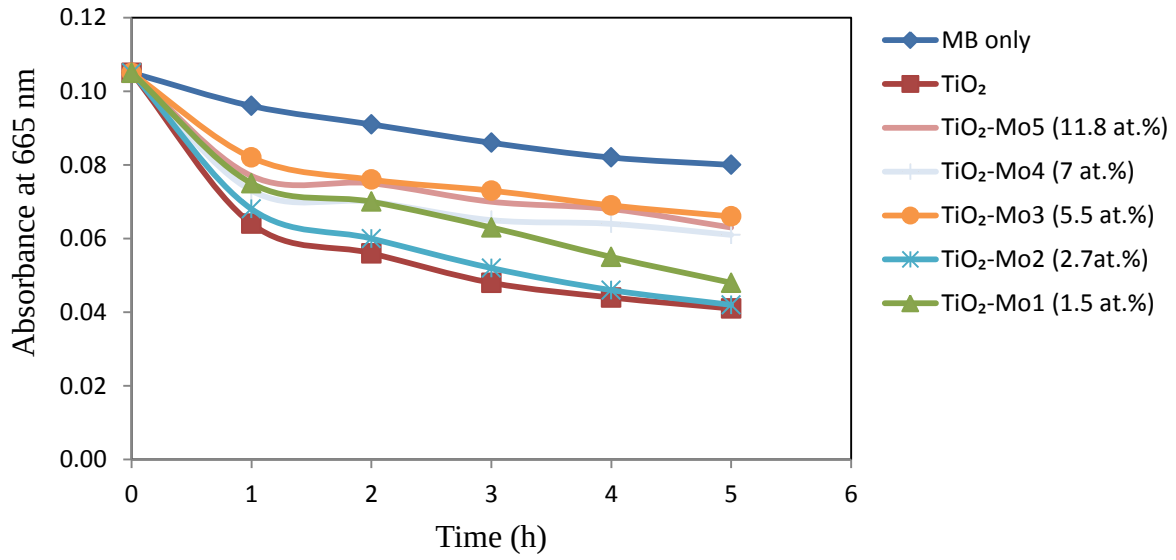

Figure 5.17: Peak methylene blue absorbance (665 nm) as a function of UV light exposure time for TiO_2-Mo coatings with different Mo level, annealed at 400 °C.

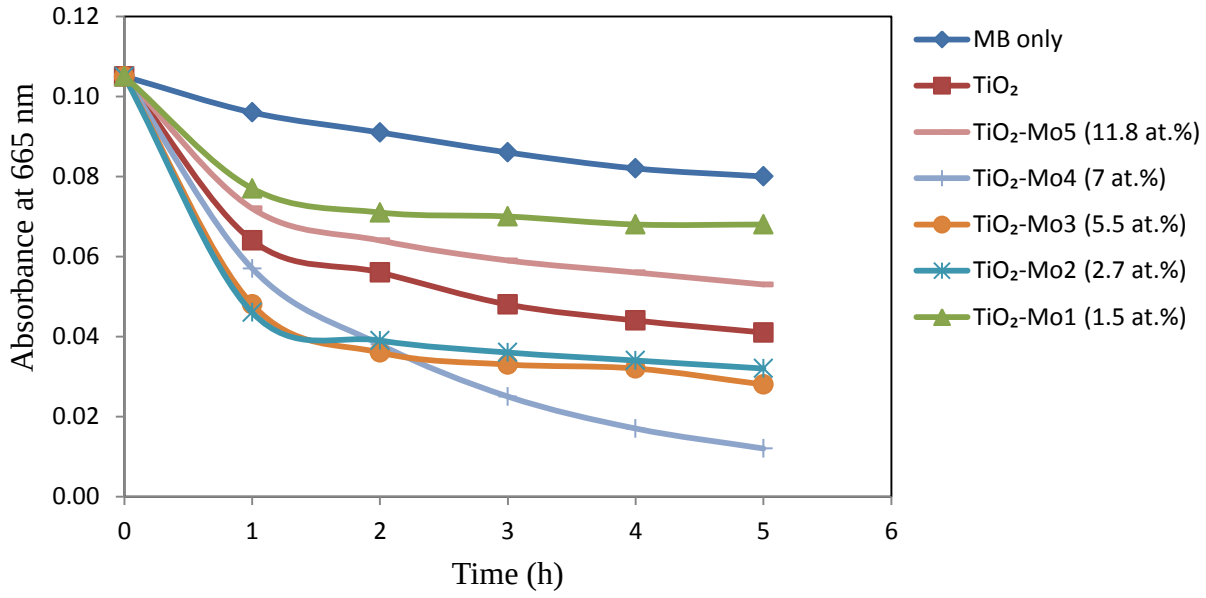

Figure 5.18: Peak methylene blue absorbance (665 nm) as a function of UV light exposure time for TiO_2-Mo coatings with different Mo level, annealed at 600 °C.

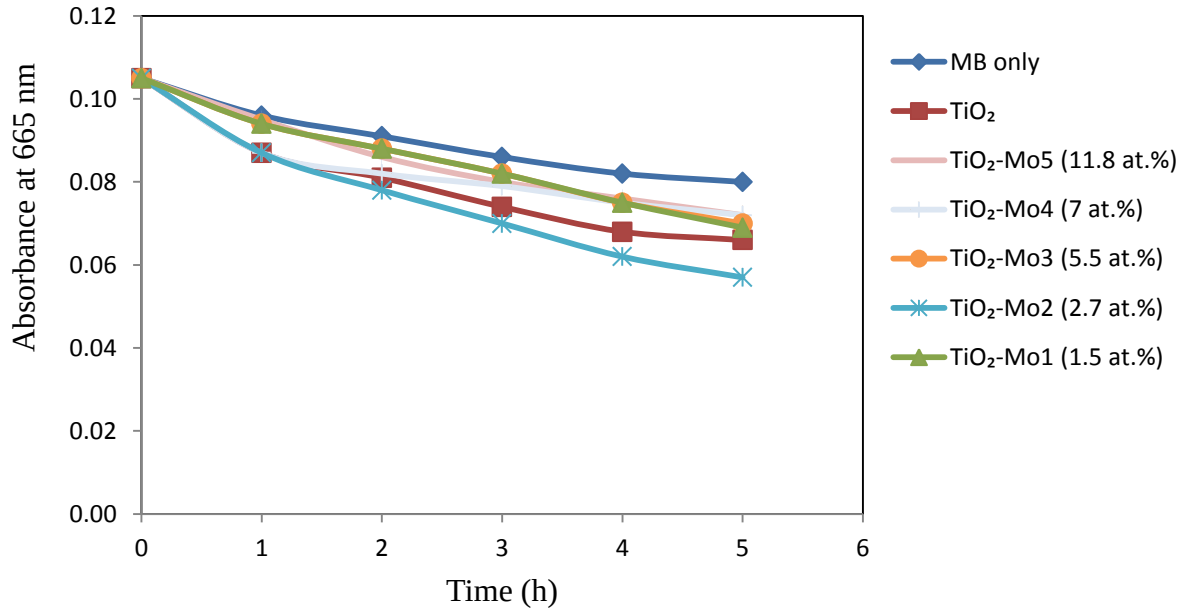

Figure 5.19: Peak methylene blue absorbance (665 nm) as a function of fluorescent light exposure time for TiO_2-Mo coatings with different Mo level, annealed at 400 °C.

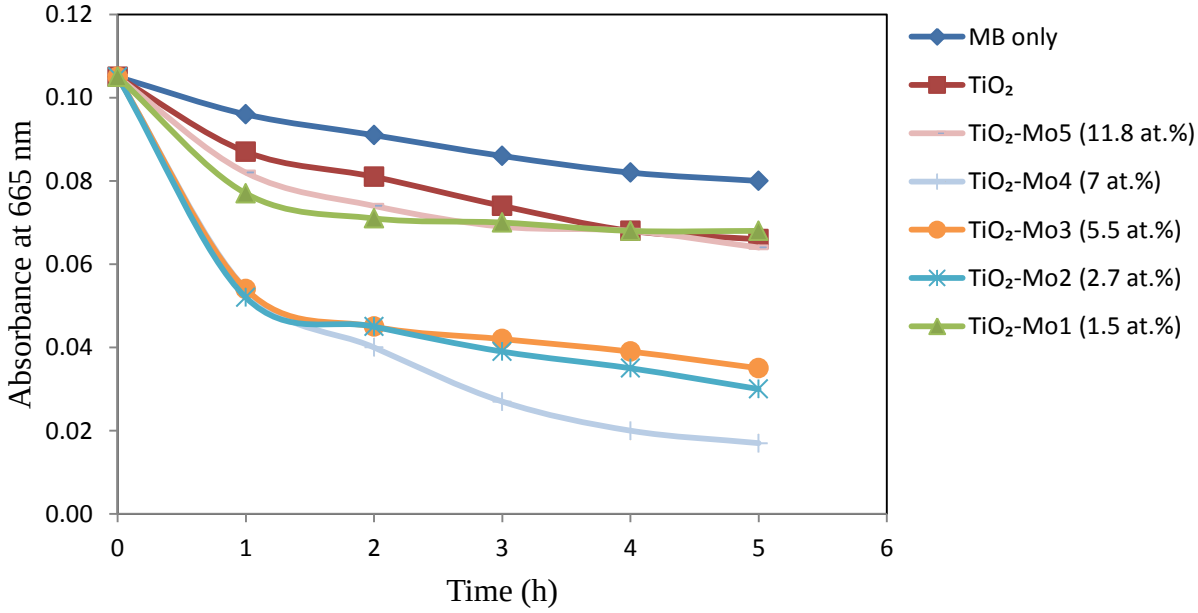

Figure 5.20: Peak methylene blue absorbance (665 nm) as a function of fluorescent light exposure time for TiO_2-Mo coatings with different Mo level, annealed at 600 °C

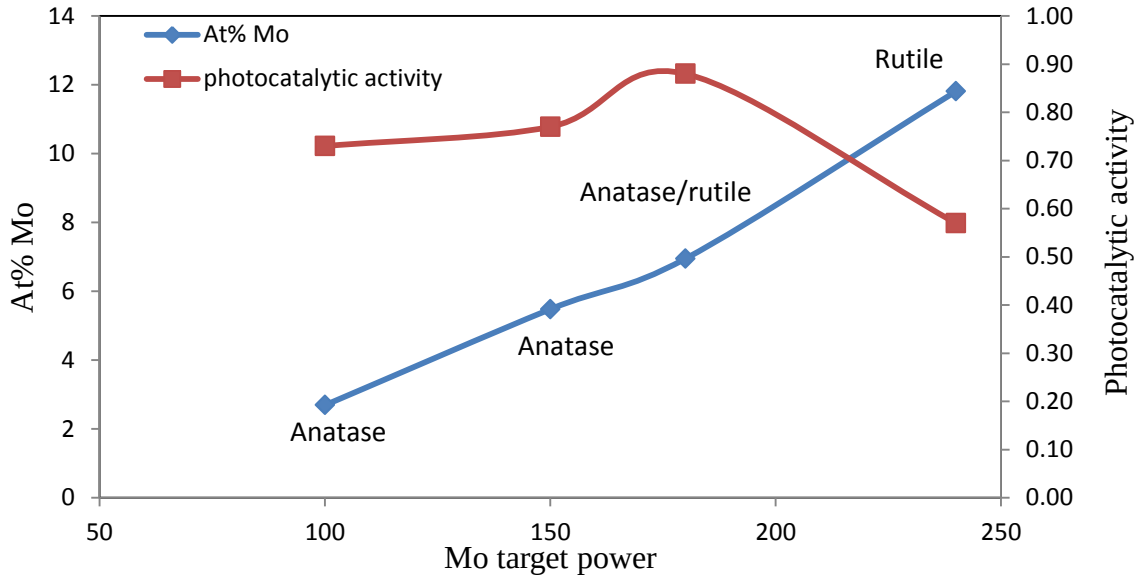

Figure 5.21: At.% and photocatalytic activity of Mo annealed at 600 °C. This figure provides a comparison of composition, structure and activity and clearly reveals that the maximum activity coincides with a dopant content of 7 at.% and a mixed phase structure.

Table 5.5: Crystal structure properties and photocatalytic activity under fluorescent and UV light irradiation for Mo-doped TiO_2 coatings.

Sample type	Mo (at.%)	Annealing temperature (°C)	Crystal structure (Raman spectroscopy)	P_{aUV}	P_{aFL}
TiO_2		As deposited	Amorphous	0.1	0
TiO_2		400	Amorphous	0.35	0.1
TiO_2		600	Anatase	0.69	0.41
TiO_2-Mo1(50% duty cycle)	1.5	400	Anatase/ rutile	0.65	0.25
TiO_2-Mo1(50% duty cycle)	1.5	600	Anatase	0.27	0
TiO_2-Mo2	2.7	400	Anatase /rutile	0.68	0.48
TiO_2-Mo2	2.7	600	Anatase	0.73	0.54
TiO_2-Mo3	5.5	400	Anatase	0.5	0.14
TiO_2-Mo3	5.5	600	Anatase/rutile	0.77	0.47
TiO_2-Mo4	7	400	Amorphous	0.52	0.17
TiO_2-Mo4	7	600	Anatase/ rutile	0.88	0.72
TiO_2-Mo5	11.8	400	Amorphous	0.47	0.14
TiO_2-Mo5	11.8	600	Rutile	0.57	0

5.5.2 TiO_2-Nb coatings

Methylene blue degradation (MB) behaviour in presence of TiO_2-Nb coatings, post annealed at 600 ℃ and 400 ℃, under UV and fluorescent light were investigated (Figures 5.22- 5.25). The TiO_2-Nb1 (0.25 at. %) coating gave the highest photocatalytic degradation of MB under UV and fluorescent light after annealing at 400 ℃ compared to other samples annealed at the same temperature. As explained earlier, the intensity of Raman spectra and XRD reflecting peaks was higher for TiO_2-Nb1 sample, which could explain the better crystallinity (more crystalline material), although all of the Nb-doped titania samples were anatase (Figure 5.26). TiO_2-Nb3 and Nb4 showed the higher photocatalytic activity in comparison to other samples annealed at 600 ℃. However, the photoactivity was not improved after annealing at 600 ℃ (Figures 5.23, 5.25). Initially, this was considered unexpected as annealing at higher temperature is frequently carried out to improve the photocatalytic activity of coatings. This could be explained by the possibility of separation of Nb from TiO_2 matrix, which resulted in reduced photoactivity of coatings. However, further investigation by XPS, EDX mapping or SIMS is needed in order to establish the distribution of Nb in coatings after annealing at different temperatures. The results of Nb doped coatings are summarised in Table 5.6.

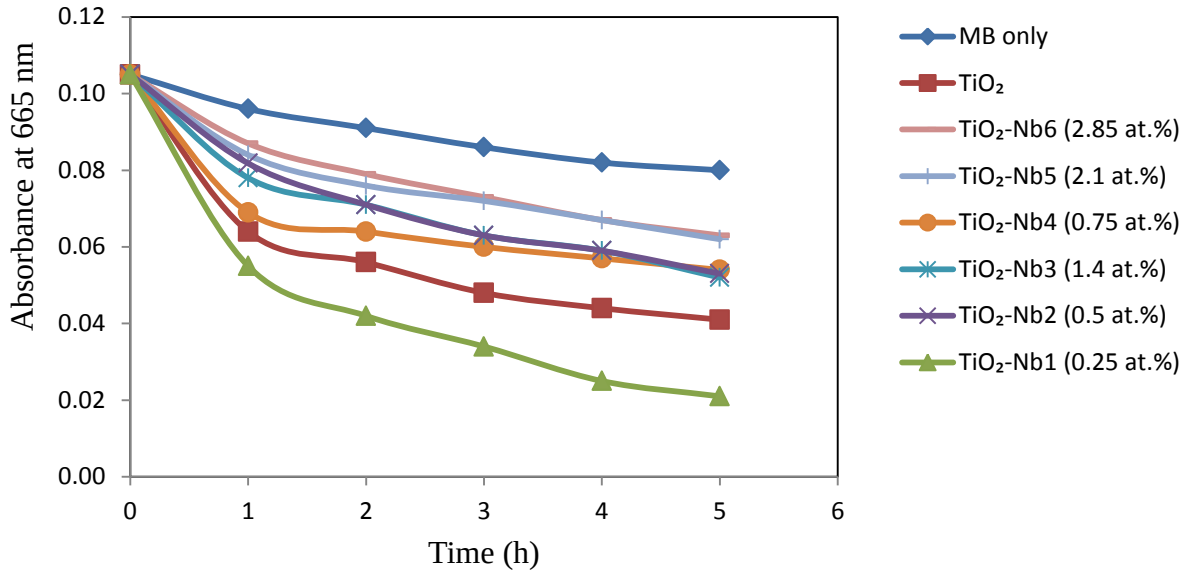

Figure 5.22: Peak methylene blue absorbance (665 nm) as a function of UV light exposure time for TiO_2-Nb coatings with different Nb level, annealed at 400 °C.

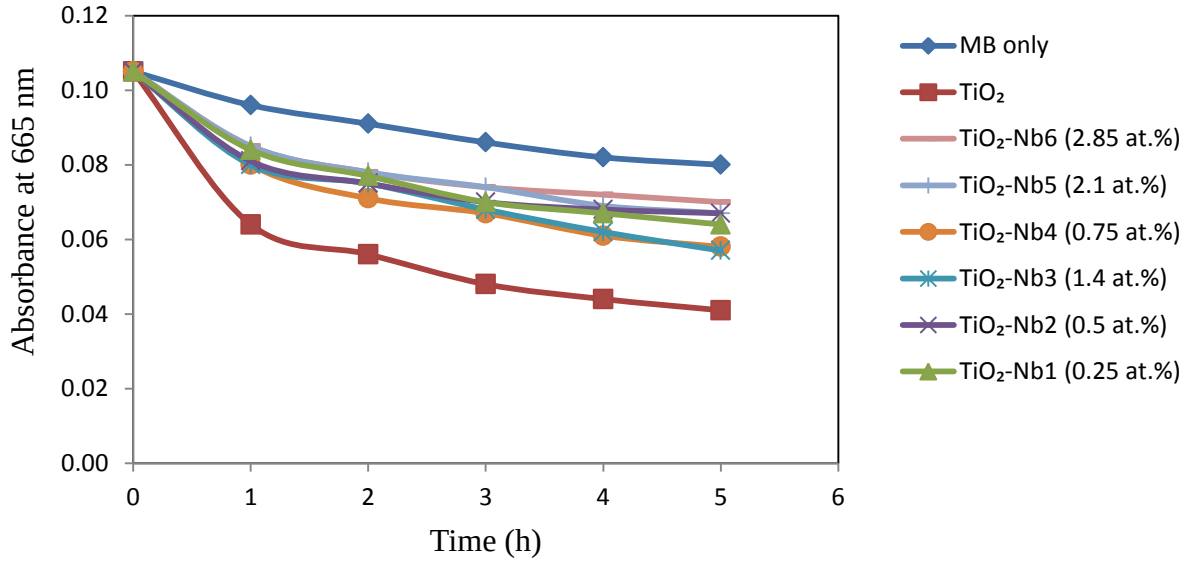

Figure 5.23: Peak methylene blue absorbance (665 nm) as a function of UV light exposure time for TiO_2-Nb coatings with different Nb level, annealed at 600 °C.

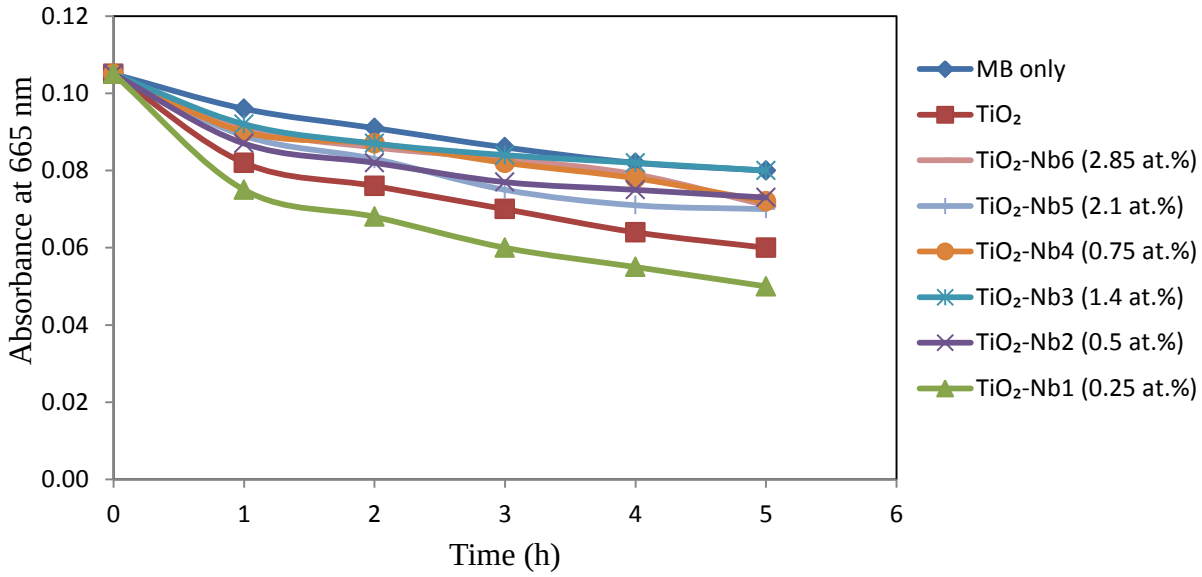

Figure 5.24: Peak methylene blue absorbance (665 nm) as a function of fluorescent light exposure time for TiO_2-Nb coatings with different Nb level, annealed at 400 °C.

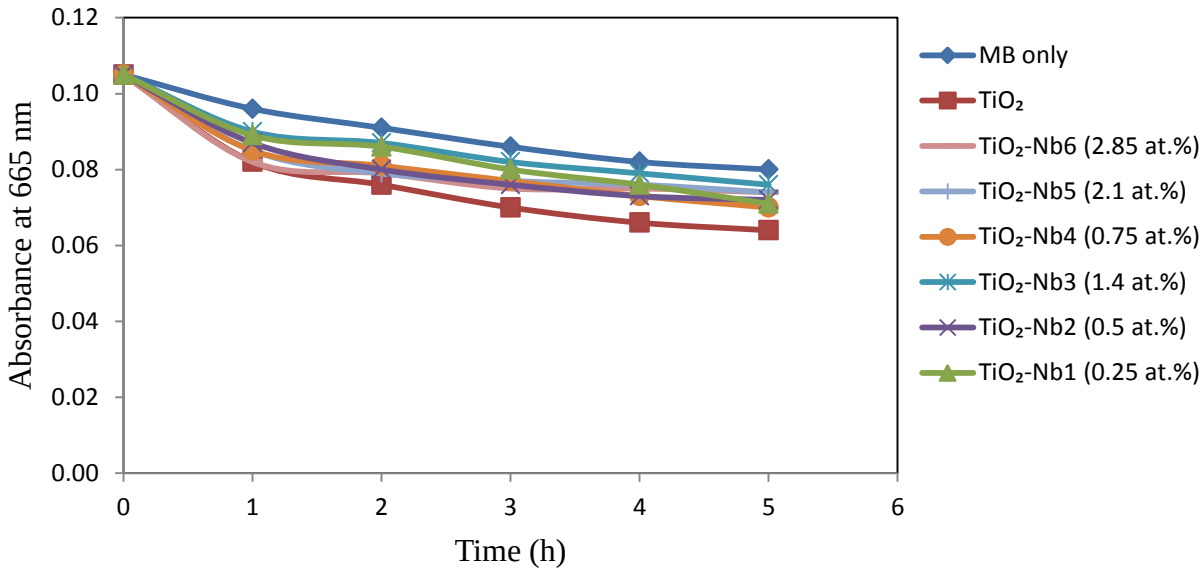

Figure 5.25: Peak methylene blue absorbance (665 nm) as a function of fluorescent light exposure time for TiO_2-Nb coatings with different Nb level, annealed at 600 °C.

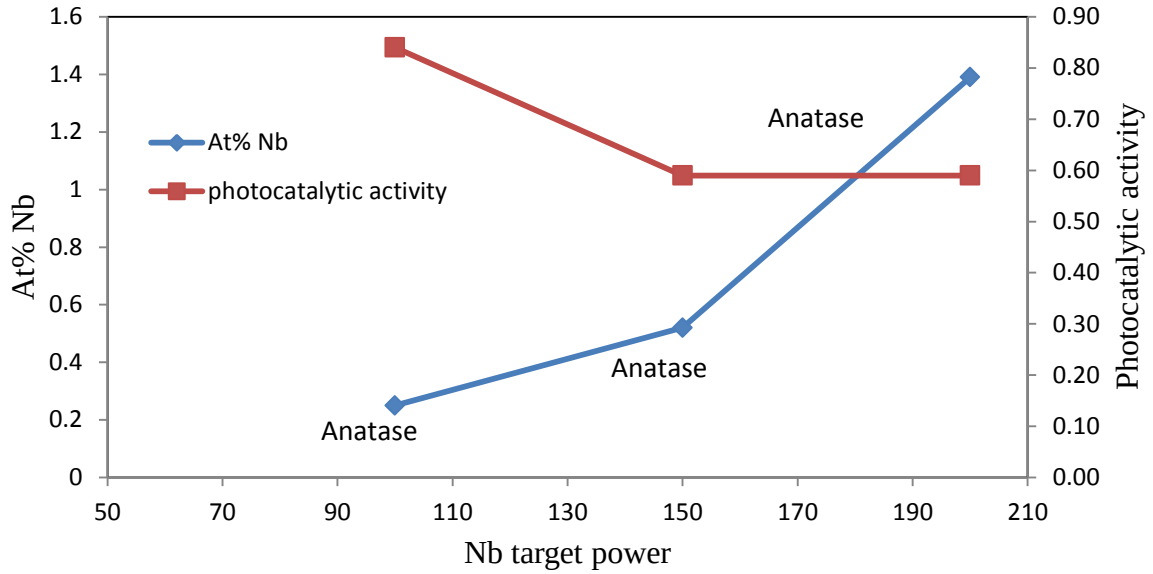

Figure 5.26: At.% and photocatalytic activity of Nb annealed at 400 °C. This figure provides a comparison of composition, structure and activity and clearly reveals that the maximum activity coincides with a dopant content of 0.25 at.% and an anatase structure.

Table 5.6: Crystal structure properties and photocatalytic activity under fluorescent and UV light irradiation for Nb-doped TiO_2 coatings.

Sample type	Nb (at.%)	Annealing temperature (°C)	Crystal structure (Raman spectroscopy)	P_{aUV}	P_{aFL}
TiO_2-Nb1	0.25	400	Anatase	0.84	0.53
TiO_2-Nb1	0.25	600	Anatase	0.45	0.27
TiO_2-Nb2	0.5	400	Anatase	0.59	0.1
TiO_2-Nb2	0.5	600	Anatase	0.35	0.22
TiO_2-Nb3	1.4	400	Anatase	0.59	0
TiO_2-Nb3	1.4	600	Anatase	0.5	0.1
TiO_2-Nb4	0.75	400	Anatase	0.57	0.1
TiO_2-Nb4	0.75	600	Anatase	0.51	0.15
TiO_2-Nb5	2.1	400	Anatase	0.44	0
TiO_2-Nb5	2.1	600	Anatase	0.36	0
TiO_2-Nb6	2.85	400	Anatase	0.42	0
TiO_2-Nb6	2.85	600	Anatase	0.3	0

5.5.3 TiO_2-Ta coatings

As can be seen from the results of photocatalytic measurements, doping with tantalum (Ta) did not enhance the photocatalytic activity under fluorescent light irradiation, compared to undoped TiO_2 (Figures 5.27- 5.30). The coatings with a Ta dopant level of 0.76 at.% and 1.1 at.% and annealing temperature of 400 °C gave the highest activity in comparison to other dopant levels (Table 5.7) under UV light irradiation. As the annealing temperature increased from 400 °C to 600 °C, an improvement in photoactivity was observed for TiO_2-Ta3, TiO_2-Ta4 and TiO_2-Ta5 samples. An enhancement in photocatalytic activity could be explained by the formation of anatase phase after annealing at 600 °C. As explained earlier, at higher annealing temperature for lower dopant levels, there is a possibility of separation of dopant metals from titania matrix, i.e. leading to the formation of tantalum oxide. However, if this happened the quantities were too low to detect, but could nevertheless affect the photocatalytic activity of coatings. Figure 5.31 represents the trend of dopant level, crystal structure and their photocatalytic activity after annealing at 400 °C, indicating that increasing the dopant levels supress both crystallinity and photocatalytic activity.

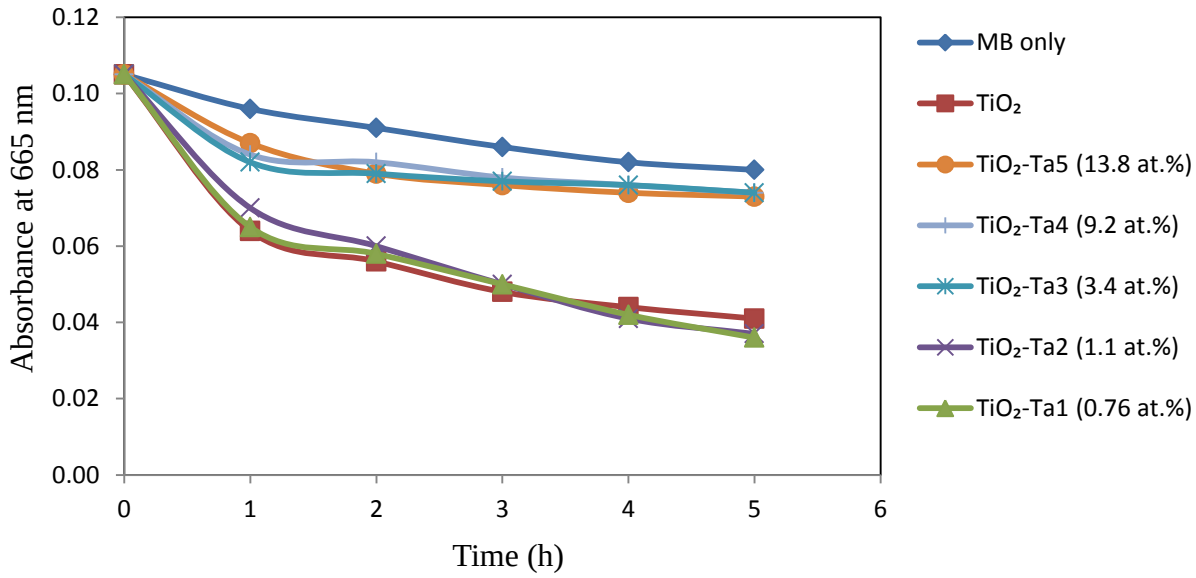

Figure 5.27: Peak methylene blue absorbance (665 nm) as a function of UV light exposure time for TiO_2-Ta coatings with different Ta level, annealed at 400 °C.

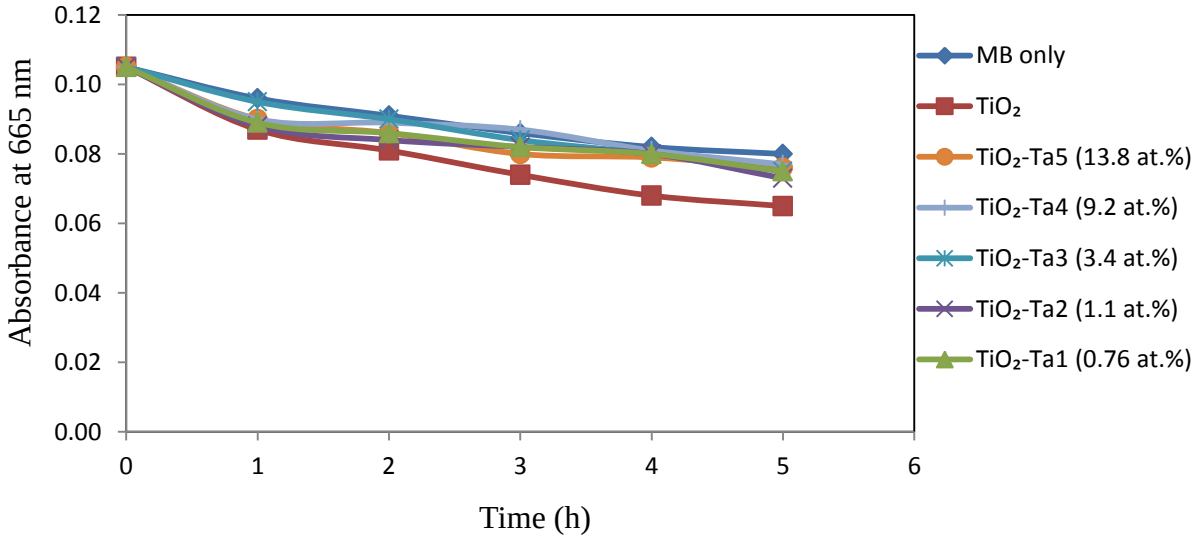

Figure 5.28: Peak methylene blue absorbance (665 nm) as a function of fluorescent light exposure time for TiO_2-Ta coatings with different Ta level, annealed at 400 °C.

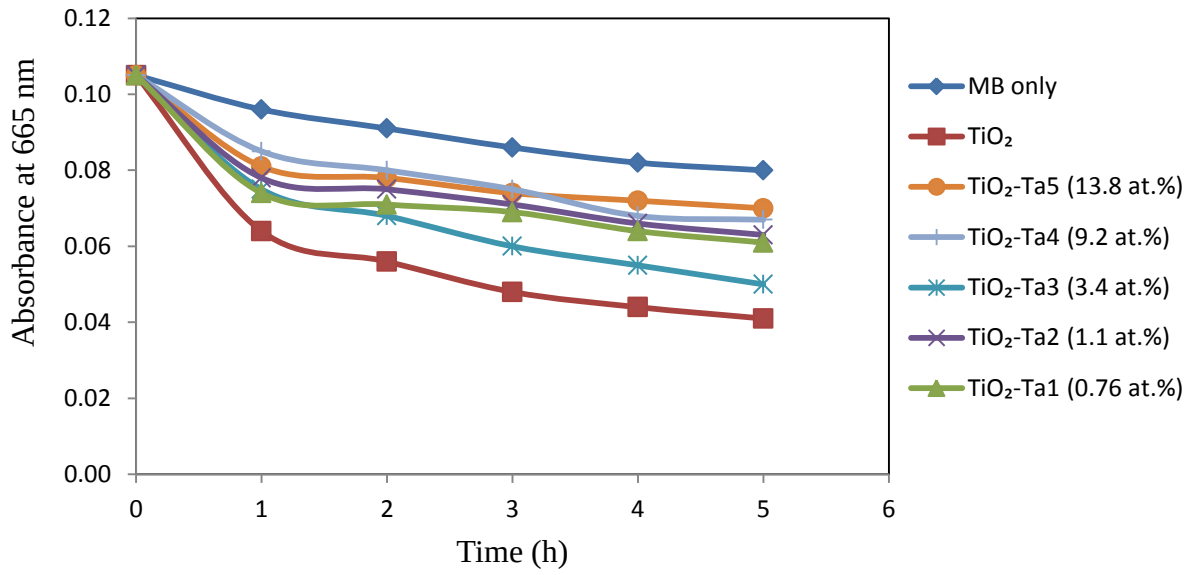

Figure 5.29: Peak methylene blue absorbance (665 nm) as a function of UV light exposure time for TiO_2-Ta coatings with different Ta level, annealed at 600 °C.

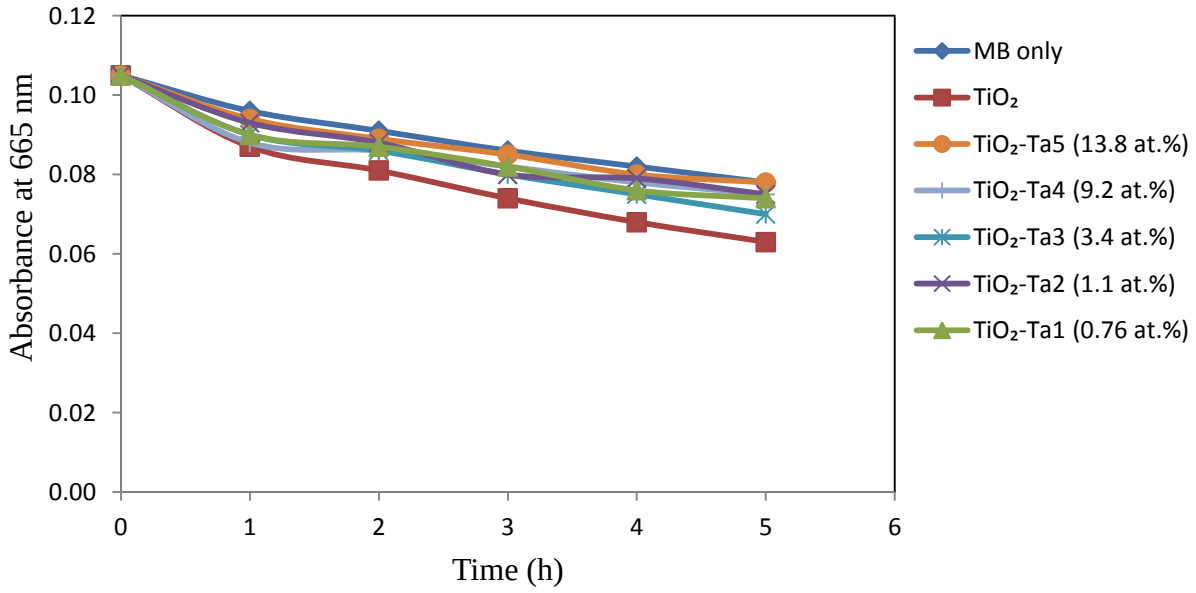

Figure 5.30: Peak methylene blue absorbance (665 nm) as a function of fluorescent light exposure time for TiO_2-Ta coatings with different Ta level, annealed at 600 °C.

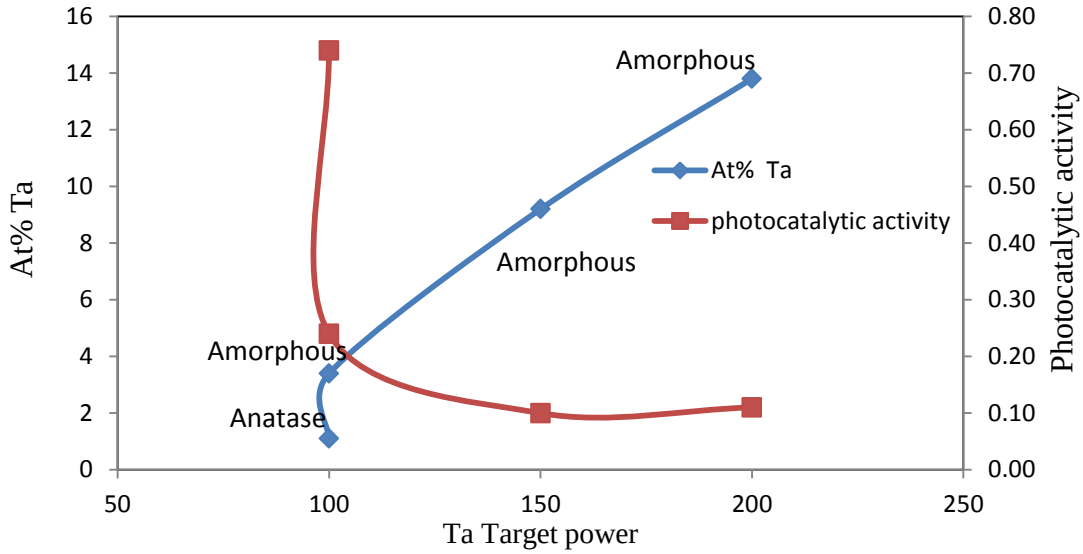

Figure 5.31: At.% and photocatalytic activity of Ta- doped coatings annealed at 400 °C. This figure provides a comparison of composition, structure and activity and clearly reveals that the maximum activity coincides with a dopant content of 1.1 at.% and an anatase structure.

Table 5.7: Crystal structure properties and photocatalytic activity under fluorescent and UV light irradiation for Ta-doped TiO_2 coatings.

Sample type	Ta (at.%)	Annealing temperature (°C)	Crystal structure (Raman spectroscopy)	P_{aUV}	P_{aFL}
TiO_2-Ta1	0.76	400	Anatase	0.73	0.03
TiO_2-Ta1	0.76	600	Anatase	0.42	0.04
TiO_2-Ta2	1.1	400	Anatase	0.74	0.13
TiO_2-Ta2	1.1	600	Anatase	0.4	0.07
TiO_2-Ta3	3.4	400	Amorphous	0.24	0
TiO_2-Ta3	3.4	600	Anatase	0.61	0.17
TiO_2-Ta4	9.2	400	Amorphous	0.11	0
TiO_2-Ta4	9.2	600	Anatase	0.37	0
TiO_2-Ta5	13.8	400	Amorphous	0.11	0
TiO_2-Ta5	13.8	600	Anatase	0.2	0

5.5.4 TiO_2-W coatings

Photocatalytic activity was not improved significantly by the addition of W into TiO_2, although it was enhanced slightly by increasing the annealing temperature from 400 ºC to 600 ºC (Figures 5.32-5.35). As the amount of W dopant increases, there is a reduction in photocatalytic activity under UV light irradiation in comparison to lower dopant levels (Figure 5.34). There is a change in crystal structure of the thin film from anatase to rutile as the content of W increased in the coating, which results in reduction of photocatalytic activity (Figure 5.36) (Table 5.8). The presence of WO_3 peaks at and 968 cm^{-1} and 273 cm^{-1} on the Raman spectra of the W-doped coatings may be taken as evidence that some quantity of tungsten exists as a separate phase of tungsten oxide. Thus, the reduction in photocatalytic activity could be due to presence of tungsten oxide species covering the surface of photocatalyst. At higher concentration, W ions can behave as recombination centres, as it can not actively trap and transfer both photogenerated electrons and holes to the surface of titania [159]. There is a slight increase in photoactivity under fluorescent light in contrast to pure titania for the TiO_2-W1 (3.8 at.%) sample (Figure 5.32).

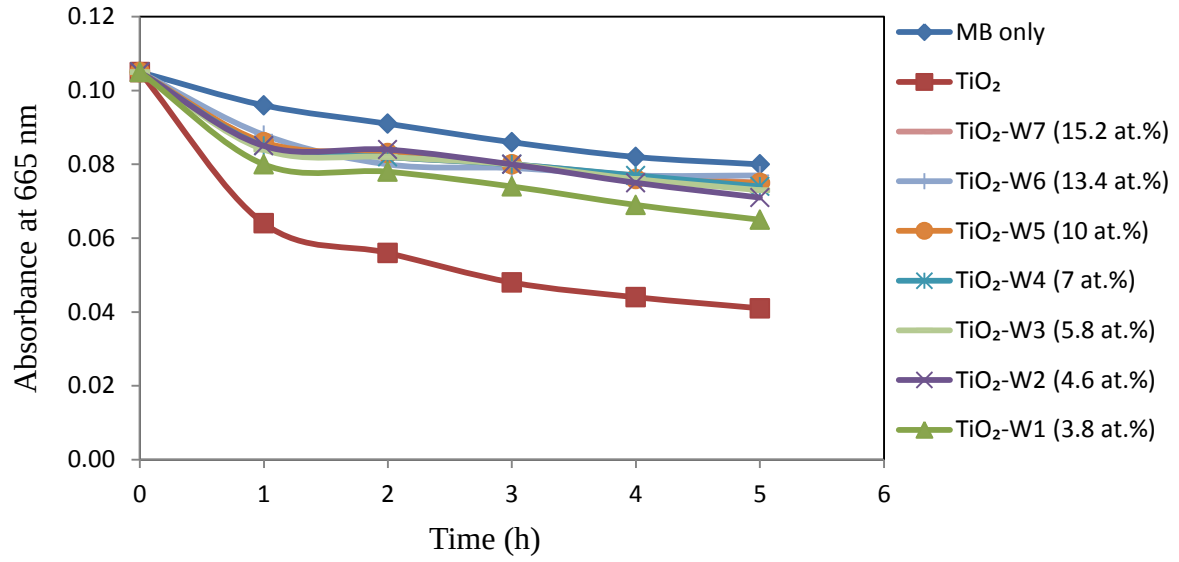

Figure 5.32: Peak methylene blue absorbance (665 nm) as a function of UV light exposure time for TiO_2-W coatings with different W level, annealed at 400 °C.

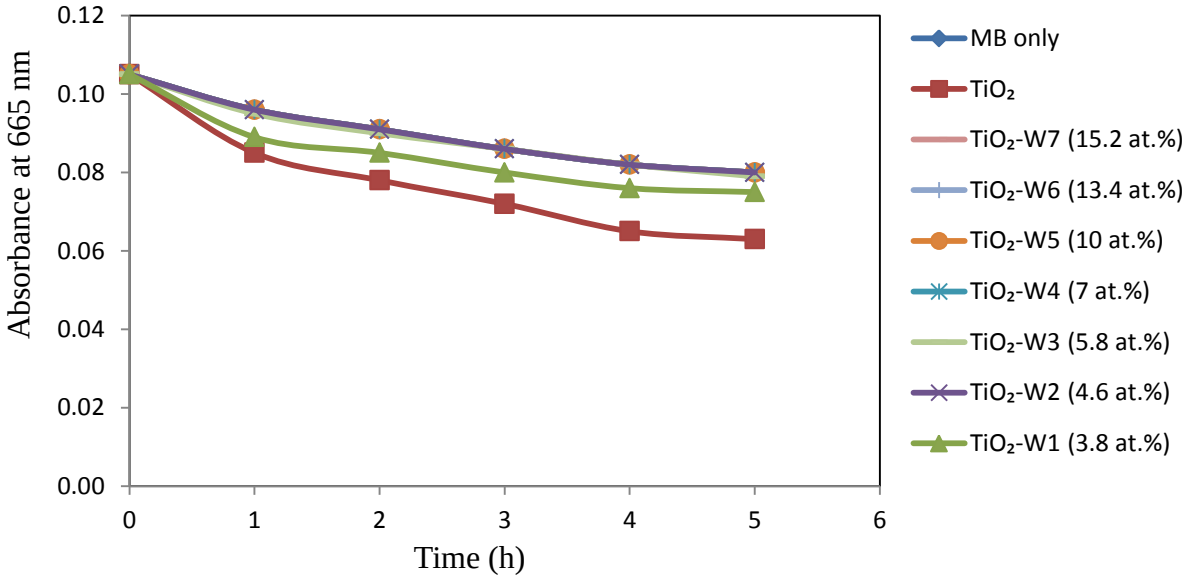

Figure 5.33: Peak methylene blue absorbance (665 nm) as a function of fluorescent light exposure time for TiO_2-W coatings with different W level, annealed at 400 °C.

.

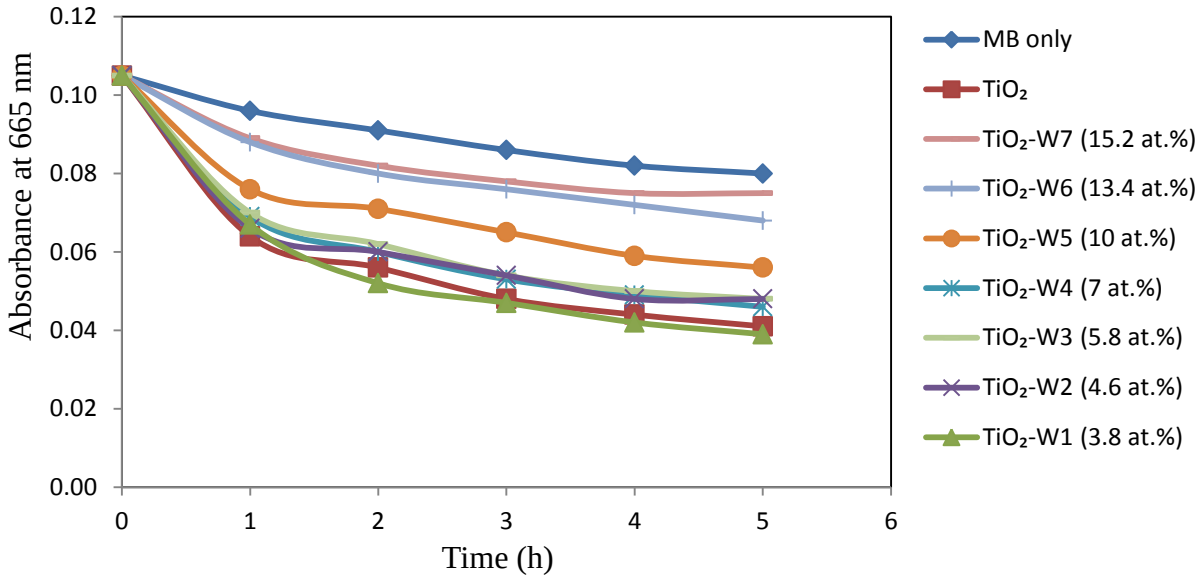

Figure 5.34: Peak methylene blue absorbance (665 nm) as a function of UV light exposure time for TiO_2-W coatings with different W level, annealed at 600 °C.

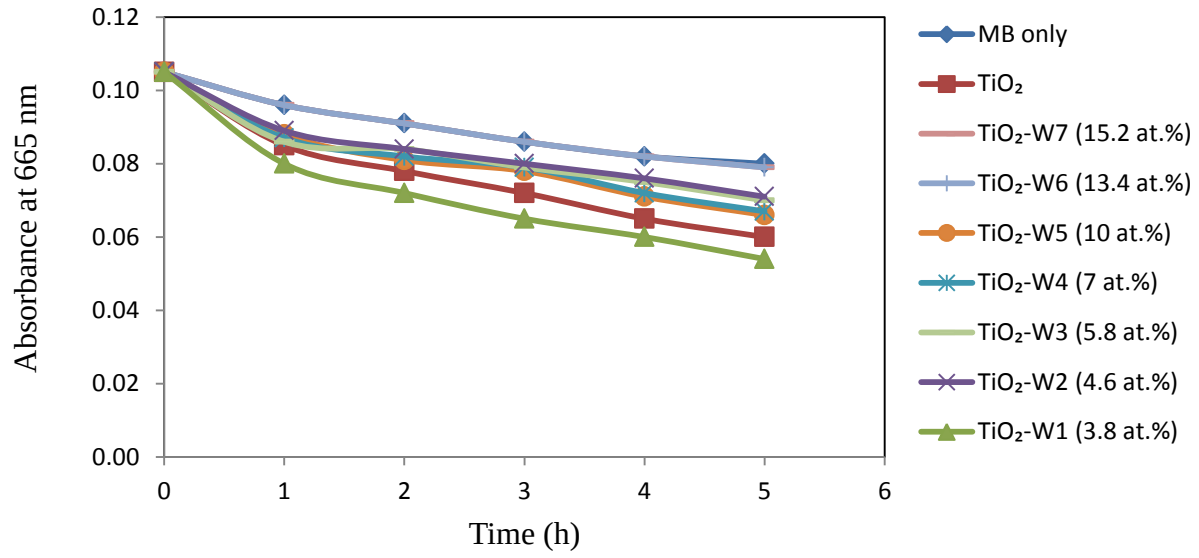

Figure 5.35: Peak methylene blue absorbance (665 nm) as a function of fluorescent light exposure time for TiO_2-W coatings with different W level, annealed at 600 °C

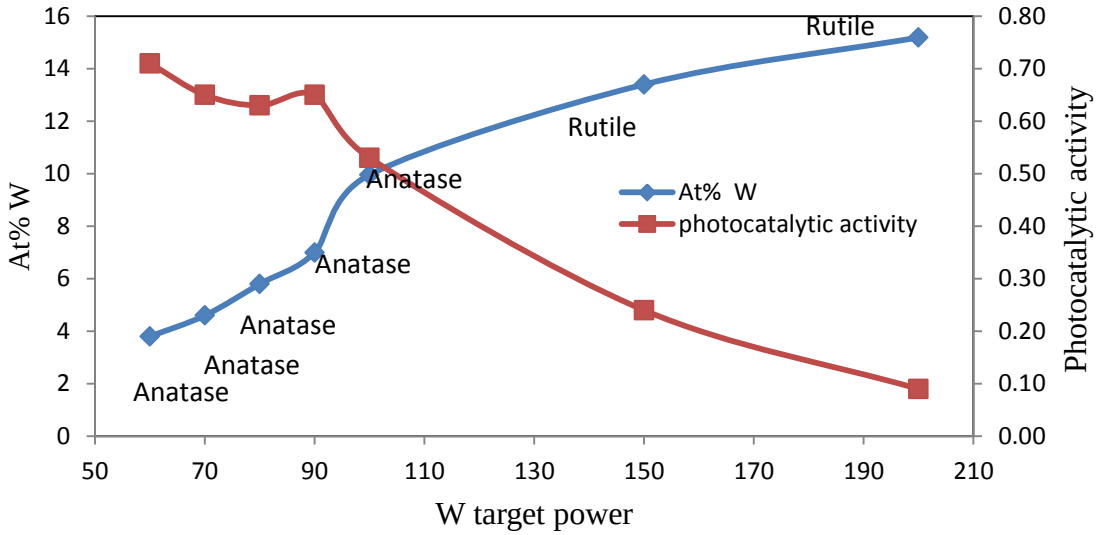

Figure 5.36: At.% and photocatalytic activity of W-doped coatings annealed at 600 °C. This figure provides a comparison of composition, structure and activity and clearly reveals that the maximum activity coincides with a dopant content of 3.8 at.% and an anatase structure.

Table 5.8: Crystal structure properties and photocatalytic activity under fluorescent and UV light irradiation for W-doped TiO_2 coatings.

Sample type	W (at.%)	Annealing temperature (°C)	Crystal structure (Raman spectroscopy)	P_{aUV}	P_{aFL}
TiO_2-W1	3.8	400	Anatase	0.36	0.1
TiO_2-W1	3.8	600	Anatase	0.71	0.45
TiO_2-W2	4.6	400	Amorphous	0.22	0
TiO_2-W2	4.6	600	Anatase	0.65	0.19
TiO_2-W3	5.8	400	Amorphous	0.14	0
TiO_2-W3	5.8	600	Anatase	0.63	0.14
TiO_2-W4	7	400	Amorphous	0.08	0
TiO_2-W4	7	600	Anatase	0.66	0.28
TiO_2-W5	10	400	Amorphous	0.11	0
TiO_2-W5	10	600	Anatase	0.53	0.24
TiO_2-W6	13.4	400	Amorphous	0.05	0
TiO_2-W6	13.4	600	Rutile	0.24	0
TiO_2-W7	15.2	400	Amorphous	0.08	0
TiO_2-W7	15.2	600	Rutile	0.09	0

5.5.6 Summary statement

In this study the dopant levels varied widely between different transition metals, since the deposition rate of different transition metals varied from target to target. However, for some of the transition metals investigated similar dopant levels were achieved. Figures 5.37 and 5.38 were plotted for various samples with similar dopant levels.

Thus, by comparing the doping level of the TiO_2-Mo4 (7 at.%) and TiO_2-W4 (7 at.%) coatings after annealing at 600 °C, it can be observed that Mo4 showed higher photocatalytic activity under both light conditions (Figure 5.37). This could be explained by the crystal structures of coatings, as TiO_2-Mo4 had a mixed phase anatase/rutile crystal structure, which was found to be more photoactive, but the structure of TiO_2-W3 was anatase. Photocatalytic activity was also higher for the TiO_2-Mo3 (5.5 at.%) coating than TiO_2-W3 (5.8 at.%) under both UV and fluorescent light. The TiO_2-Mo3 (5.5 at.%) coating also had a mixed phase anatase/rutile crystal structure but TiO_2-W3 (5.8 at.%) was anatase. This result infers that Mo had greater effect on capturing photo-generated electrons and holes than W.

For the 2.7 at.% Mo-doped coating, the photocatalytic activity was improved significantly in comparison to 2.85 at.% Nb-doped sample under both light conditions. Again, it appears that Mo had greater effect on effective charge carrier separation. Comparing the 3.8 at.% W-doped sample with 3.4 at.% Ta-doped sample, a conclusion can be drawn that tungsten was more effective at slowing the recombination rate and thus increasing the photocatalytic activity.

Figure 5.38 shows the relative photocatalytic activity of Mo-, Ta- and Nb-doped samples with similar dopant levels after annealing at 400 °C. In this case, Ta-doped samples showed higher photocatalytic activity under UV light in comparison to Nb- and Mo-doped samples. However, the photocatalytic activity of Mo-doped sample under fluorescent light irradiation

was higher than other doped samples with similar dopant level. All of the samples under investigation had anatase crystal structure, so the difference in photocatalytic activity could be due to the position of dopant within the crystal lattice of titania.

The best results obtained for each dopant can be seen in figure 5.39, in comparison to undoped titania and Pilkington Activ^{TM} glass (a commercial product) (measured by the same process). However, direct comparison with this latter standard sample should be avoided, because it is produced via a chemical vapour deposition pyrolysis route. It is also prepared on glass substrate, as it has been reported by several authors that the choice of substrates can affect photocatalytic activity [160, 161]. However, as there is no standard thin film coating on stainless steel substrate; it still serves a useful bench mark for assessment of relative activity levels. It is evident from Figure 5.40, the colour of stainless steel changed after coating.

Doping with 7 at.% molybdenum improved the photocatalytic activity under both UV (19% higher than pure TiO_2) and fluorescent light (31% higher than pure TiO_2) irradiation in comparison to undoped TiO_2 and other transition metal dopants, after annealing at 600 °C. This effect is probably due to more efficient electron-hole separation, and band gap reduction. The niobium (Nb) doped titania coating (0.25 at.%) also showed high photocatalytic activity under UV light (12% higher than pure TiO_2), however, the activity under fluorescent light was lower than the Mo doped samples. Tungsten (3.8 at.%) and tantalum (1.1 at.%) doped samples demonstrated slight enhancement in photocatalytic activity under UV light. However, the W-doped coatings showed higher photocatalytic activity than Ta-doped coating under fluorescent light. Therefore, Mo-, Nb- and W-doped tiania coatings were selected for antimicrobial assay, as they showed higher photocatalytic activity under fluorescent light in comparison to pure titania. The results will be discussed in Chapter 6.

The best performing sample (TiO_2-Mo4) was taken for placement in brewery trials. TiO_2-Mo4 also showed an antimicrobial activity, which will be discussed in the next chapter. Due to a limit on number of samples that can be installed in the brewery environment, only TiOMo 4 and pure TiO_2 were placed. This will be described in details in Chapter 7.

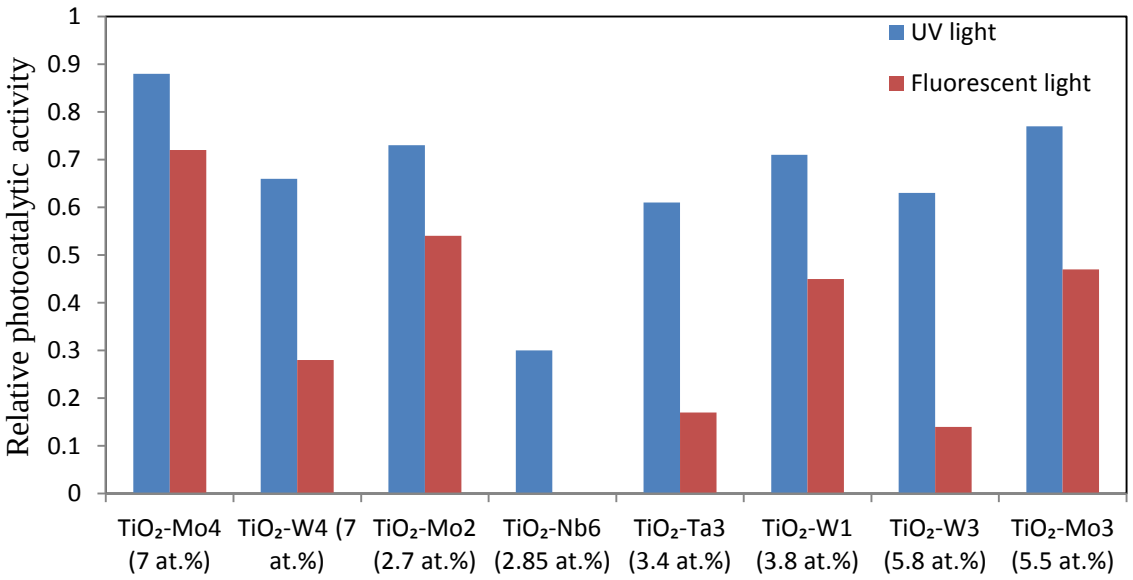

Figure 5.37: Relative photocatalytic activity for TiO_2 doped with similar dopant levels (Mo, W, Nb and Ta) after annealing at 600 °C.

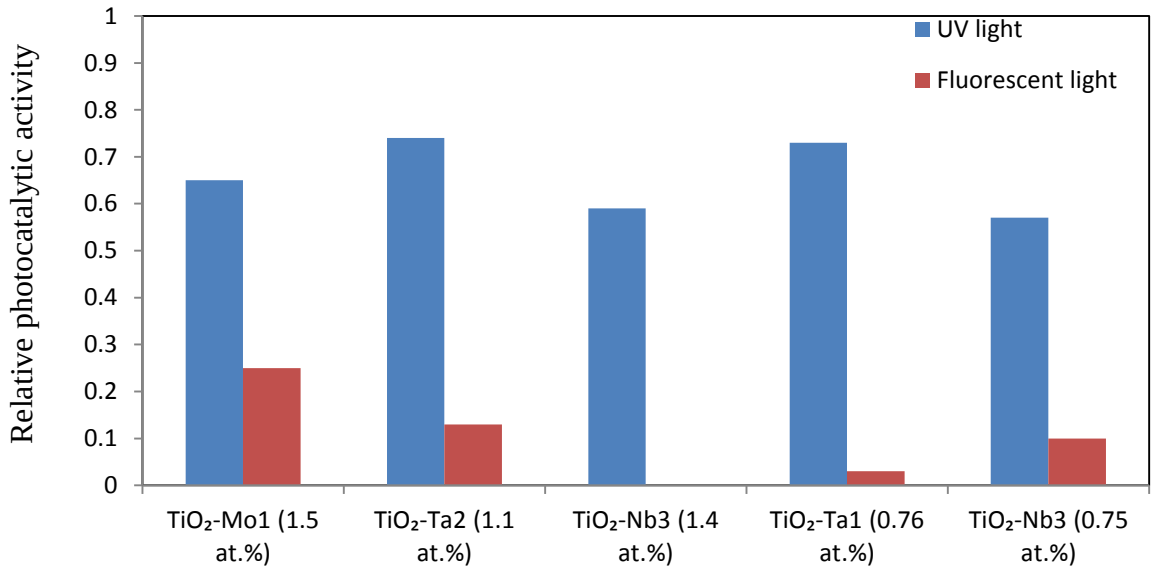

Figure 5.38: Relative photocatalytic activity for TiO_2 doped with similar dopant levels (Mo, Nb and Ta) after annealing at 400 °C.

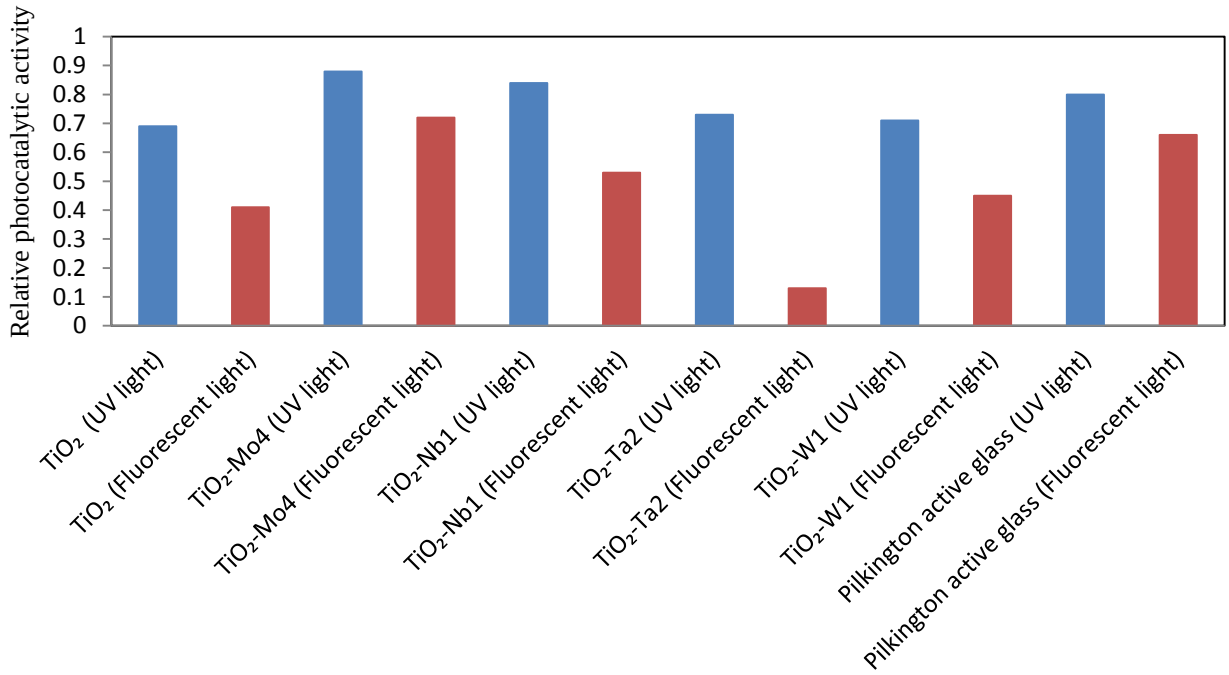

Figure 5.39: Relative photocatalytic activity for TiO_2 doped with different transition metals (Mo, Nb, W and Ta) and comparison with commercially available photocatalytic surface (Pilkington Activ^{TM}).

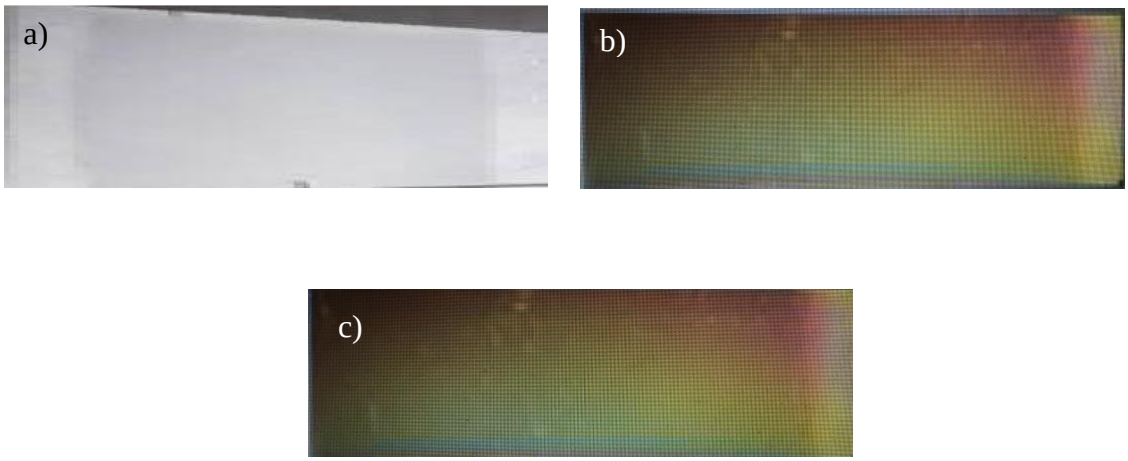

Figure 5.40: Example of coated stainless steel surface produed in this project a) uncoated stainless steel b) pure TiO_2 b) Mo-doped TiO_2.

5.7 Discussion

Different dopants (Mo, Nb, Ta, and W) at various levels in TiO_2 coatings were selected in order to investigate their effect on coating crystal structure and corresponding photocatalytic activity. This allowed for the optimisation of the coating properties. Two different annealing temperatures were selected in order to improve the crystal structure and the photocatalytic activity of doped and undoped TiO_2 thin film coatings.

The first major point to note from the results obtained is that all as-deposited coatings were amorphous, but developed a crystalline structure after annealing. The dopant content influenced the crystallisation of the coatings with some dopants tending to suppress crystallisation and others suppressing or promoting an anatase to rutile transition. Apart from crystal structure and annealing temperature, other parameters such as the electronic structure of metal ion and interaction of the latter with substrates can also influence the ion doping behaviour, which might in turn affect the optimum dopant concentration.

Although the majority of doped titania samples showed photoactivity under UV light, a large difference is observed between the different dopants, which depends on the dopant level which varied widely. The amount of dopant in the titania lattice influences the process of charge carrier trapping, separation and recombination, so when the concentration of dopant is high the electron-hole recombination process occur easily, due to short distance between charge carrier traps [161].

For the Mo-doped samples, the best photocatalytic activity was obtained with TiO_2-Mo 4 (7 at.%), with 600 °C annealing. The XRD diffraction peaks and Raman spectra indicate mixed anatase/rutile phases. It has been found in the literature that a mixed phase anatase/rutile structures are more active than pure anatase [19, 21]. No additional peaks were found that could be attributed to molybdenum oxides or molybdenum clusters, so most of the Mo dopant is substitutionally incorporated into the TiO_2 lattice. As the Mo content increased, there was an increase in photoactivity under both UV and fluorescent light irradiation. However, as the dopant concentration was increased to 11.8 at. %, a reduction in photocatalytic activity was observed. As the redox potential of Mo^{6+}/Mo^{5+} is higher than Ti^{4+}/ Ti^{3+}, Mo^{6+} is more likely to capture electrons compared to Ti^{4+}. For this reason an appropriate concentration of Mo could increase the number of photo-generated holes on the surface and consequently promote the formation of hydroxyl radicals which are highly reactive and can increase the photocatalytic activity. However, further increased levels of Mo may bring an opposite effect, due to reduction in the distance between the trap sites, the rate of recombination increases and photocatalytic activity decreases [79].

When the dopants levels are too high, Mo^{6+} cannot enter the TiO_2 lattice and it can cover the surface of titania, which leads to a decrease in photocatalytic activity. The valence bands and conduction bands of two crystals (TiO_2 and MoO_3) may be linked and charge capture centres maybe become recombination centres, so photocatalytic activity reduces [79]. At higher

annealing temperatures, the crystallinity becomes stronger and more predominant. There was no remarkable change in surface roughness as the annealing temperature increased.

As the concentration of niobium increased in the coatings their photocatalytic activity decreased. An anatase crystal structure existed for all of the samples under investigation. However, differences in the relative intensity of the main peaks were observed. The intensity of some of the samples was higher than others which indicated higher crystalline content. According to previously published works, Nb doped samples with up to 1 at.% of Nb showed the maximum photocatalytic activity [77, 155] and stabilized the formation of anatase in the titania lattice. In most of the published studies describing the photocatalytic properties of Nb, high temperatures (above 600 °C) were used to anneal the coating [77, 162]. However, in our studies, it has been shown that the good photocatalytic activity can be obtained at a lower annealing temperature (400 °C). Further investigation is required to explore the distribution of Nb in the coating after annealing at higher temperature.

Tantalum is another transition metal that was used to dope the titanium dioxide for enhancing the photoactivity of TiO_2 films. The best photocatalytic activity under UV light irradiation was achieved with TiO_2-Ta 1 (0.76 at.%) and TiO_2-Ta 2 (1.1 at.%) with a calcination temperature of 400 °C. However, no improvement in photocatalytic activity was achieved under fluorescent light irradiation. The change in calcination temperature from 400 °C to 600 °C for the TiO_2-Ta 3 and TiO_2-Ta 4 coatings caused a change in crystal structure from amorphous to anatase which resulted in an increase in photoactivity under UV light compared to the 400 °C annealing temperature. Our results are in agreement with those of Stengl *et al.* [163] who showed that tantalum doping did not improve the photocatalytic activity of TiO_2.

The W-doped titania samples were also investigated. Doping with W slightly improved the photocatalytic activity under fluorescent light illumination. The best performance was achieved with 3.8 at. % W annealed at 600 °C. There was a change in crystal structure from anatase to rutile at higher dopant concentration. It is known that the addition of W into the titania lattice also causes the formation of WO_3 which acts as a separation centre for electrons and holes due to its conduction and valence bands being lower than those of TiO_2, which leads to the photogenerated electrons being transferred to the lower-lying WO_3 conduction band, while holes accumulate in the TiO_2 valence band [164]. The presence of the Raman bands at 968 cm^{-1} and 273 cm^{-1} on the Raman spectra of W-doped samples may be taken as evidence that some quantity of tungsten exists as a separate phase of WO_3. Therefore, it would be reasonable to assume that some fraction of the doping tungsten is not incorporated into the lattice of titania as the content of dopant increased, it is considered that the tungsten oxide species would cover the surface of photocatalyst, and hence reduce the available surface area of TiO_2 would be reduced, thereby resulting in the observed reduction of photocatalytic activity.

The majority of published work reported that W-doped titania significantly improved the photocatalytic activity of titania thin film [78, 165, 166]. In the present study this has not been the case and a small enhancement in photocatalytic activity was observed. This different behaviour may be related to the choice of substrate, as ceramic and glass substrates are reported to show higher photocatalytic activity in comparison to stainless steel substrates [161]. At high annealing temperature, Fe and Cr ions from stainless steel substrate could penetrate into the film, which can have a detrimental effect on photocatalytic activity [167]. Another possible reason that was suggested in literature is that, an electrical double layer is formed when TiO_2 thin films and the substrates are in contact with each other, thus the

electrons would transfer from high Fermi level to low Fermi level. There are two typical electron double layer structures: one is the composite semiconductor structure between two semiconductors, such as a ceramic substrate, the other is the Schottky barrier structure between the metal and the semiconductor, such as titanium sheet. Since non-metal substrates have a larger band gap and lower Fermi level than the TiO_2 semiconductor, the electrons will transfer from TiO_2 semiconductor to non-metal substrates. The electron depletion layer thus will be formed in the TiO_2 film. The depletion layer of TiO_2 thin film can further serve as the trap centre of photo-excited electrons. The work function value of stainless steel is 4.51 eV, which is below the values of TiO_2 semiconductor work function (5.58 eV), so the electrons will transfer from metal to semiconductor. The accumulation layer of electrons will be formed in TiO_2 film, which would act as the trap centre of photo-excited holes [161]. Identical coatings prepared on glass substrate demonstrated higher photocatalytic activity (the results of the parallel project) [168].

The value of surface roughness did not change significantly by doping with different transition metals. Higher surface roughness could have a positive impact on photocatalytic activity [82], since an increase in surface roughness implies an increase in surface area of the coating in contact with methylene blue solution. However, this does not apply to coatings studied here, as they all were of similar surface roughness.

Chapter 6: Antibacterial Activity of TiO_2 Doped with Different Transition Metals (Mo, W and Nb)

6.1 Introduction

In food processing systems, as in nature, microorganisms become attached to solid surfaces conditioned with nutrients that may allow for their survival and growth. The development of biofilms can occur once viable microorganisms have attached to a surface; this can occur on most surfaces in any environment, given appropriate conditions for growth. Where surface fouling occurs, without biofilm growth, the term microbial fouling or biofouling is generally used. Biofouling refers to the undesirable formation of a layer of living microorganisms and/or their decomposition products as deposits on the surfaces. In the food and beverage industry, biofouling (and biofilms) cause serious problems such as impeding heat transfer, increasing the frictional resistance of a fluid over the surface and increasing the corrosion rate at the surface. These effects lead to an increase of energy use and spoilage of product [169]. In order to overcome these problems, an optimum cleaning protocol should be employed to reduce the number of attached bacteria and prevent biofouling and biofilm formation. Cleaning approaches can be classified in to two types [170]:

1) Engineering approaches: reducing energy, cost, and time in established cleaning operations.
2) Scientific approaches: achieving cleanliness or a cleaning time as a function of influencing factors; for examples, shear stress, temperature, surface type, finish, food type, and mode of action of cleaner.

Process hygiene plays a major role in ensuring the quality of products. One approach to improve cleaning is to change the surface chemistry by coating the surface. Titanium dioxide powder and thin film coatings used as photocatalytic surfaces provide complementary

technology to current drinking water treatment processes [53]. TiO_2 photocatalysts have potential for use in the food industry since they reduce requirements for consumable cleaning chemicals.

The aim of the work described in this chapter was to evaluate the antimicrobial properties of selected TiO_2 coatings doped with transition metals as well as the metals themselves and their thin film oxide coatings using *Escherichia coli* as a model organism under fluorescent light.

6.2 Antimicrobial assay results

In any study on the effect of a surface on microbial viability, it is important that the growth phase of the microorganisms is well defined. Bacteria in the exponential phase are more susceptible to injury than during the stationary phase [171, 172], but cells in any relatively hostile environment are likely to be in the stationary phase, where growth is halted. Thus, the initial bacterial inoculum used for all the experiments was of stationary phase cells. For all experiments the initial bacterial suspension was standardised to an $OD_{540\ nm}$ of 0.08. This absorbance corresponds to a cell concentration of 1.0 (± 0.2) × 10^7 cfu mL^{-1} (Section 4.3.2). The limit of detection for the bacterial viability test was 10 cells per cfu μL^{-1}.

The effect of different initial *E. coli* concentrations on susceptibility to photocatalytic treatment has been reported [27, 173]. Results indicated that a longer time is required for bacterial inactivation when the initial concentration of bacteria is higher. It can be assumed that in this work, where a high initial concentration (10^7 cfu mL^{-1}) was used, that bacteria would have been inactivated more slowly than with a lower cell concentration. However, high concentrations tend to be used in standardised assays to enable the effects of variables to be measured.

E. coli was used to assess the antimicrobial activities of TiO_2 samples doped with Mo, Nb and W samples under fluorescent light irradiation. TiO_2-Mo (7 at.%), TiO_2-Nb (0.25 at.%) and TiO_2-W (3.8 at.%) showed high photocatalytic activity under fluorescent light, however the Ta-doped titania coating did not show improved photocatalytic activity under fluorescent light. Therefore, these coatings were selected on basis of their performance which was described in Chapter 5. Higher concentration of W in the coating (10 at.%) was also selected, as the results from W and WO_3 coatings confirmed an antimicrobial activity of W in the dark.

Furthermore, transition metals and their oxides were tested by methylene blue degradation under UV and fluorescent light to investigate their photocatalytic activity. However, no trace of photoactivity was detected (results not presented). Experiments to determine the antimicrobial properties of transition metal coatings and coatings of their oxides were also carried out at different exposure times under fluorescent light irradiation. The photocatalytic inactivation of the bacteria cells was assessed by removing samples at 0, 6, 8, 12, 24 and 48 hours.

The TiO_2 coated surface was proved to be less effective against *E. coli* than doped TiO_2 coatings, reducing the number of colony forming units by 2 logs after 24 hours irradiation under fluorescent light, with no reduction of counts in the dark condition. However, the TiO_2-Mo (7 at.%) surface was proved to be more effective against *E. coli*, with counts reducing to below the limit of detection (<10 cfu cm^{-2}) within 24 hours ($p<0.05$) (Figure 6.1).

The extent of bacterial inactivation tended to increase with increased exposure time to fluorescent light (Figure 6.1). Control experiments showed no significant ($p > 0.05$) bacterial inactivation in the presence or absence of the light on stainless steel surfaces. Metal ion dopants work as charge carrier traps, effectively enhancing the separation of photoexcited electron/hole pairs and result in an increase in the surface photoreaction, which in turn results in formation of more reactive oxygen species (ROS) on the photocatalyst surface. It may be

speculated that the production of more ROS resulted in an increase of bacterial inactivation [79, 174]. Indeed, as noted in chapter 5, Mo-doped titania coating showed high photocatalytic activity.

On Mo metal and MoO_3 coatings in the absence of TiO_2, *E. coli* was inactivated within eight hours both in the dark and under fluorescent light irradiation, so the inactivation was much more rapid than for TiO_2-Mo (7 at.%) (Figure 6.2 and 6.3). Light was unnecessary for this inactivation, further suggesting that the Mo metal and MoO_3 coatings were also innately antimicrobial.

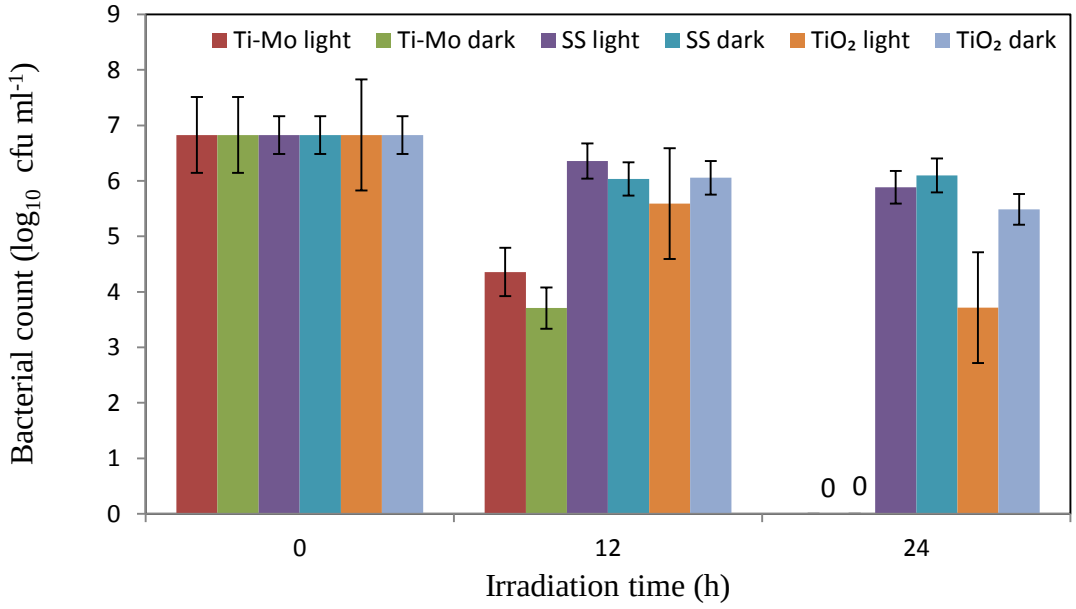

Figure 6.1: Antimicrobial effect of TiO_2 -Mo (7 at.%) photocatalyst against *E. coli* compared to stainless steel (SS) and TiO_2 over 24 hours of incubation demonstrating that TiO_2-Mo (7 at.%) was more antimicrobial than TiO_2 (<10 cfu cm^{-2} over 24 h) in both light and dark conditions, suggesting an innate antimicrobial effect other than photocatalysis.

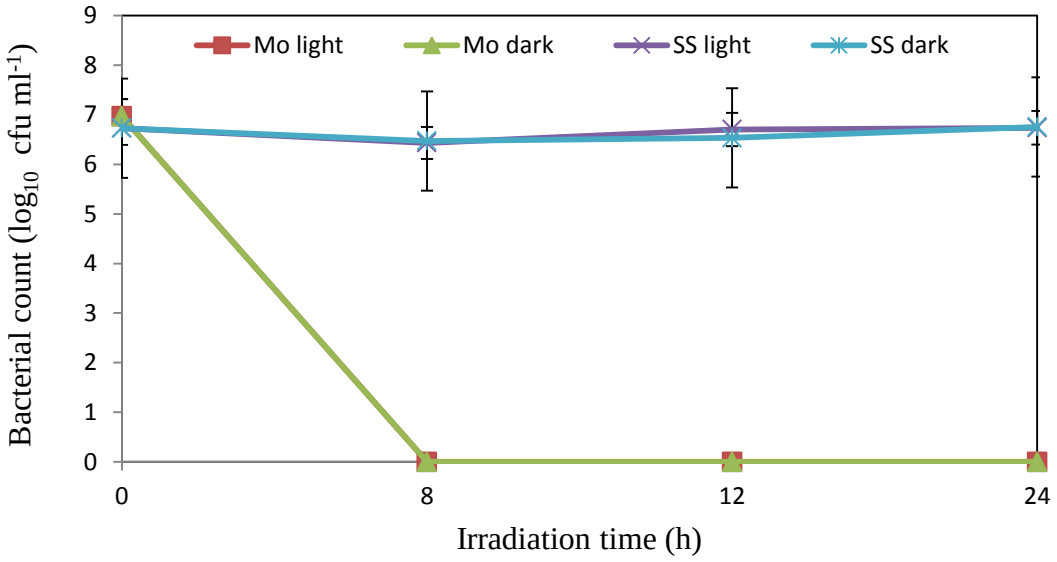

Figure 6.2: Antimicrobial effect of Mo metal coating against *E. coli* compared to stainless steel (SS) over 24 hours of incubation demonstrating that the Mo has an antimicrobial effect, and that light was not needed to activate this surface.

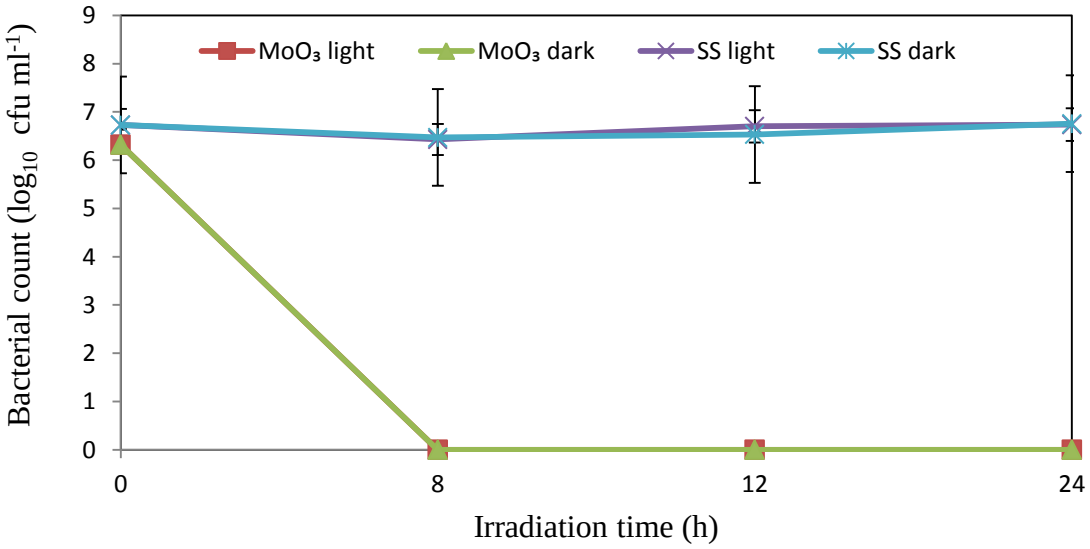

Figure 6.3: Antimicrobial effect of MoO_3 coating against *E. coli* compared to stainless steel (SS) over 24 hours of incubation demonstrating that MoO_3 had an antimicrobial effect that did not require light activation.

The fluorescent light inactivation rate for the TiO_2-Nb (0.25 at.%) coating was much lower than for the TiO_2-Mo (7 at.%) photocatalyst, taking 48 hours compared to 24 hours to reduce the bacterial count to <10 cfu cm^{-2} (Figure 6.4). This was expected because the photocatalytic activity of TiO_2-Mo (7 at.%) assessed by methylene blue was higher (Chapter 5). Nb metal and Nb_2O_5 coatings did not show any antimicrobial activity either in dark or light (Figure 6.5 and 6.6), thus Nb only acted as a photocatalytic enhancer rather than being innately antimicrobial. However, there was a small reduction in counts in the dark after 24 hours with Nb-doped TiO_2 coating. It would be intersting to investigate this further with different Nb dopant concentration.

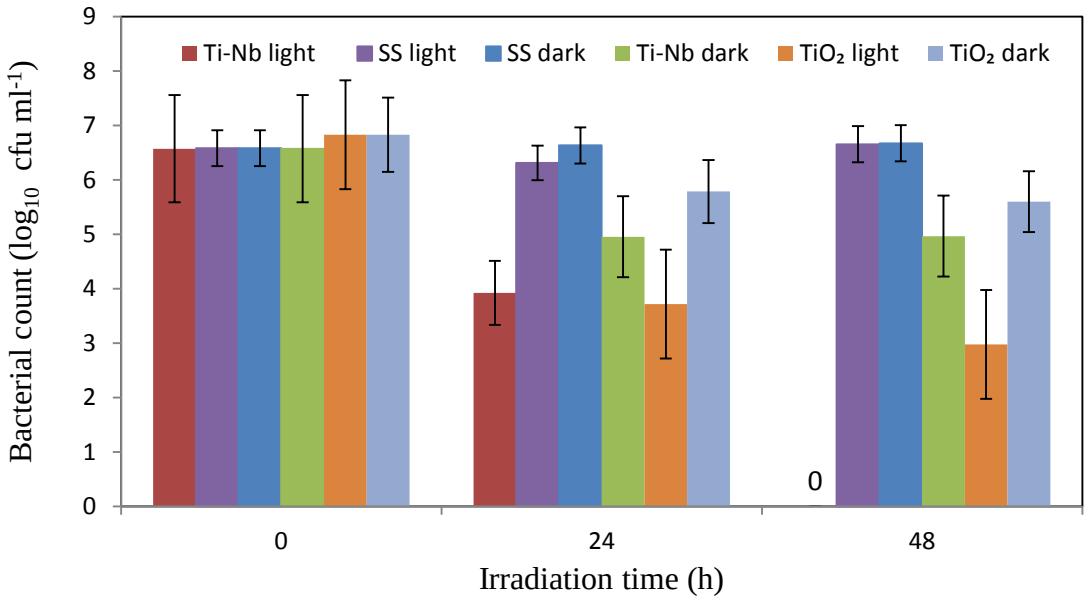

Figure 6.4: Antimicrobial effect of TiO_2-Nb (0.25 at.%) photocatalyst against *E. coli* compared to stainless steel (SS) over 48 hours of incubation demonstrating that TiO_2-Nb (0.25 at.%) was the most antimicrobial (<10 cfu cm^{-2} over 48 h) in the light.

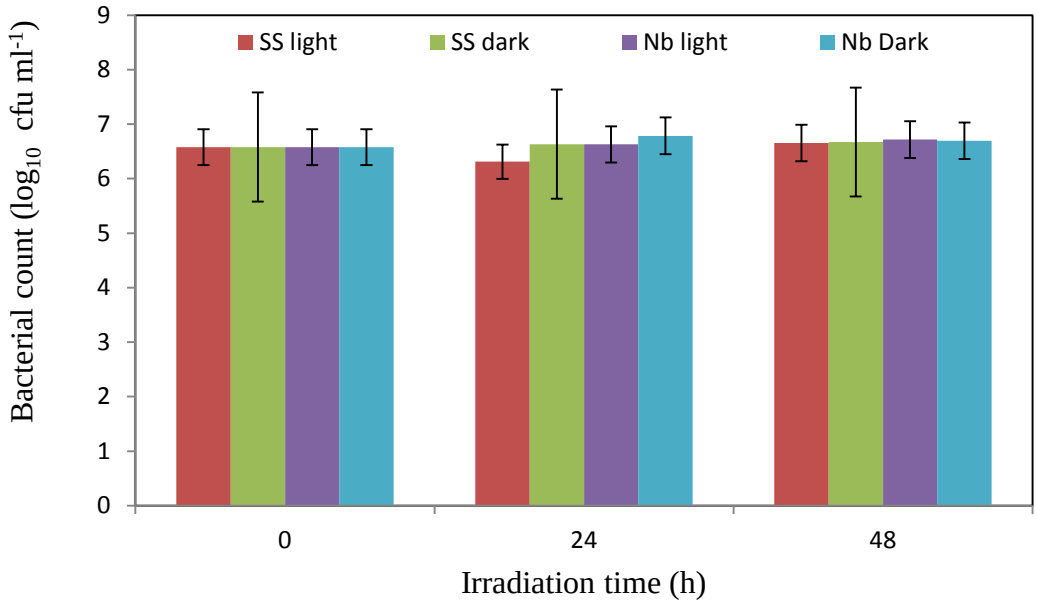

Figure 6.5: Antimicrobial effect of Nb metal coating against *E. coli* compared to stainless steel (SS) over 48 hours of incubation demonstrating no antimicrobial activity.

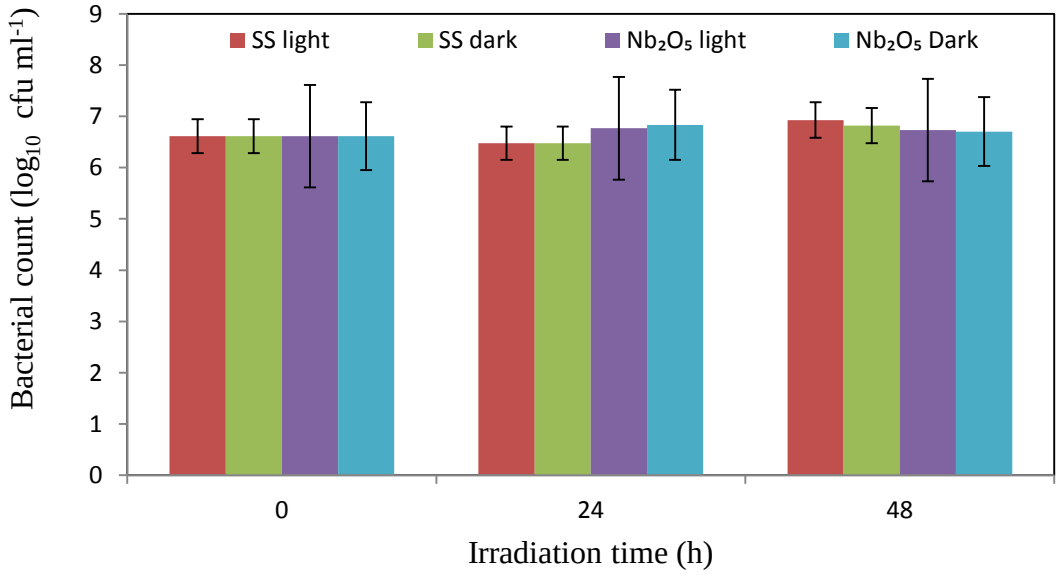

Figure 6.6: Antimicrobial effect of Nb_2O_5 coating against *E. coli* compared to stainless steel (SS) over 48 hours of incubation demonstrating no antimicrobial activity.

For the TiO_2-W (3.8 at.%) sample, there was inactivation of *E. coli* after 48 hours of incubation (Figure 6.7) but no effect in the dark. In this instance, some reduction in cell numbers on stainless steel controls was observed over time. This might be due to a not unexpected natural loss of viability, but could also be related to some batch variation in the stainless steels used which was noted but not investigated further. However, only the TiO_2-W (3.8 at.%) with different light treatment had an effect with *E. coli* over and above those of all other treatments.

W metal and WO_3 coatings were also tested for antibacterial activity (Figure 6.8 and 6.9). No *E. coli* cells survived after an incubation time of six hours in either light or dark for the WO_3 coating. The WO_3 coating was more active than the W metal coating, reducing detectable counts to zero in 6 hours instead of 12 hours. This result confirmed the antimicrobial properties of W and WO_3. Higher concentration of W in the coating (10 at.%) was also selected, as the results from W and WO_3 coatings confirmed an antimicrobial activity in the dark. With a higher concentration W in the coating (10 at.%), antibacterial activity was achieved over a shorter period of time in both the light and dark (Figure 6.10). This indicated that W possesses innate antimicrobial activity.

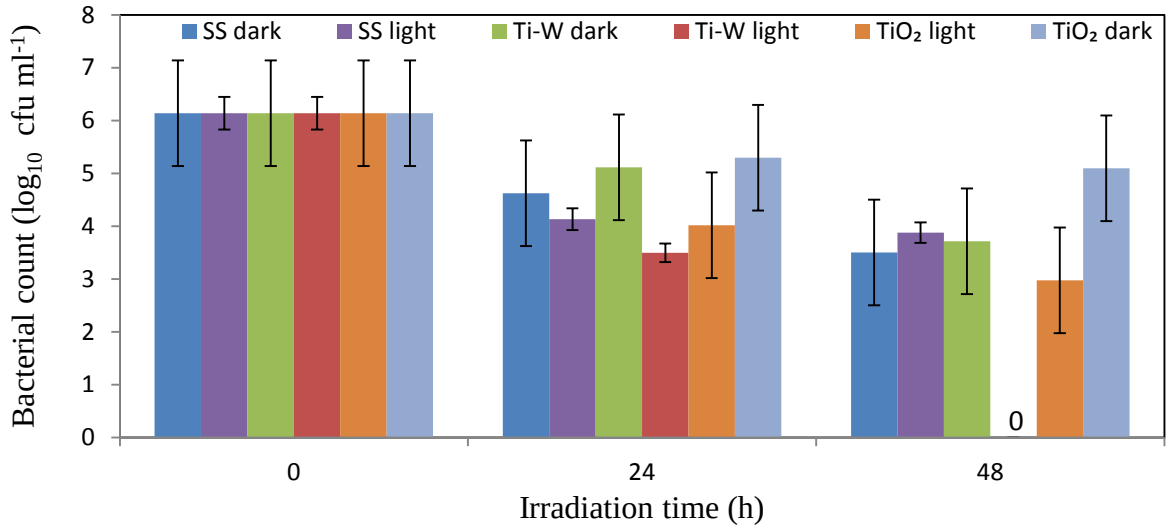

Figure 6.7: Antimicrobial effect of TiO_2-W (3.8 at.%) photocatalyst against *E. coli* compared to stainless steel (SS) over 48 hours of incubation demonstrating that TiO_2-W (3.8 at.%) under light condition showed an antimicrobial effect.

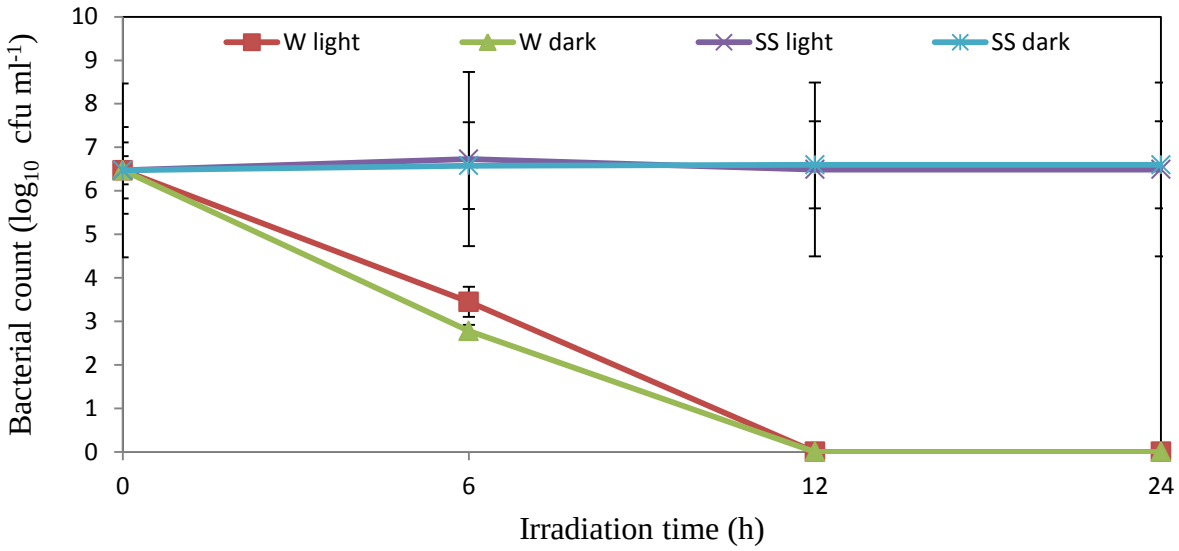

Figure 6.8: Antimicrobial effect of W metal coating against *E. coli* compared to stainless steel (SS) over 24 hours of incubation demonstrating that on a coating of W, an antimicrobial effect was observed.

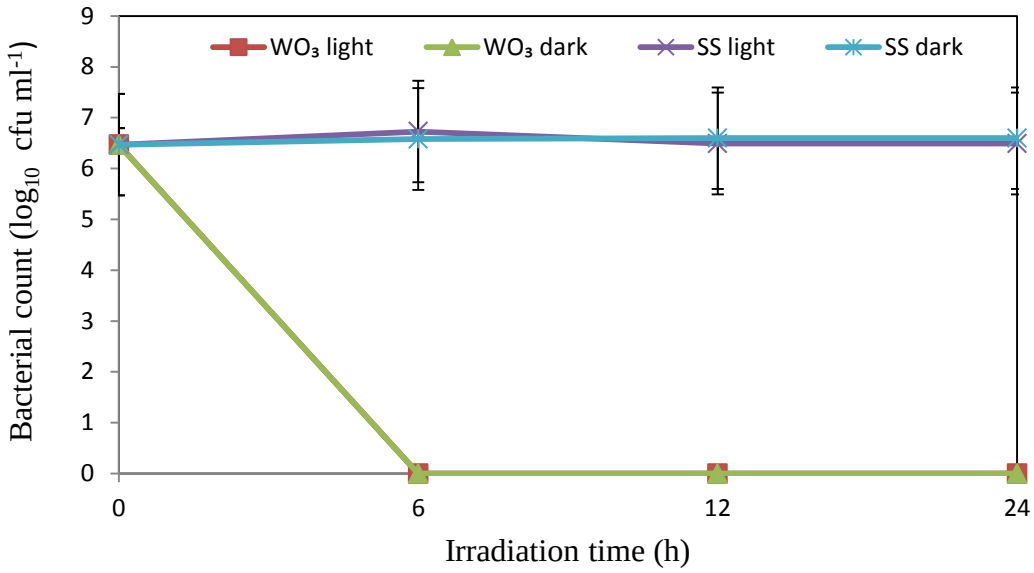

Figure 6.9: Antimicrobial effect of WO_3 coating against *E. coli* compared to stainless steel (SS) over 24 hours of incubation demonstrating that WO_3 coating had an antimicrobial activity under dark as well as light conditions.

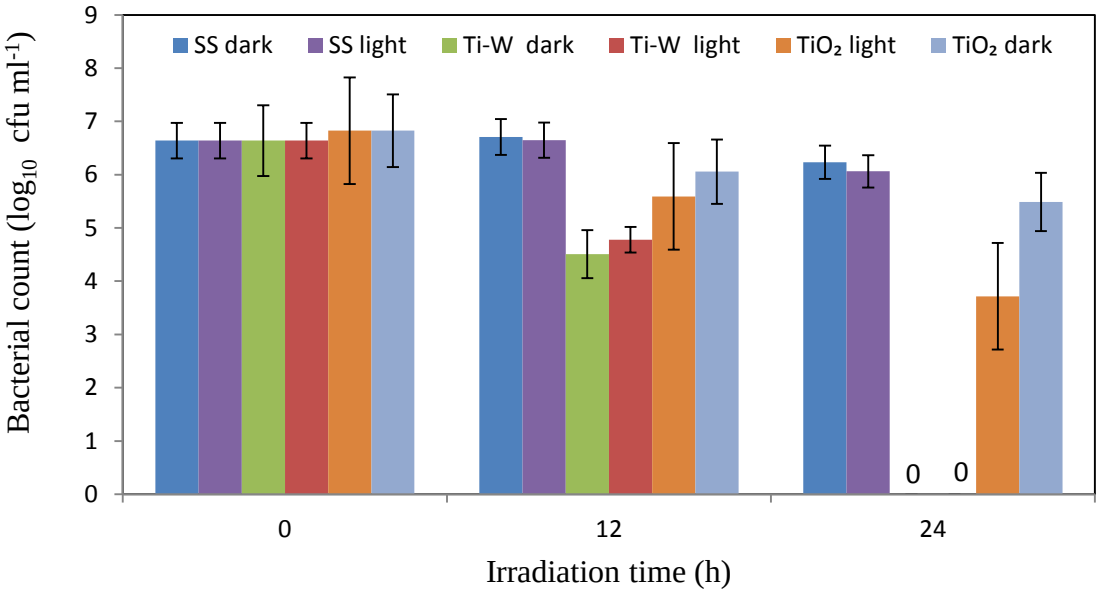

Figure 6.10: Antimicrobial effect of TiO_2-W (10 at.%) photocatalyst against *E. coli* compared to stainless steel (SS) over 24 hours of incubation demonstrating that when using a higher concentration of W, antimicrobial effect was also seen under dark condition.

6.3 Re-use of TiO_2-Mo (7 at.%) surface and cleaning assays

It is important to know whether the photocatalyst surfaces can be reused or not, since the substratum is used *in-situ* over a period of time in which repeated soiling and cleaning will occur. Because TiO_2-Mo (7 at.%) was the test surface selected for use in the brewery trials, only this surface was used for the cleaning assays. As will be noted in Chapter 7, the samples placed in three different brewery environments retained some of their photocatalytic activity, thus it was hoped that they would also retain their antimicrobial activity. A laboratory simulation of activity after one test cleaning assay was carried out as a preliminary comparison.

After cleaning the TiO_2-Mo (7 at.%) surfaces with either AME or 4 v/v % oxofoam and re-challenging with *E. coli*, counts were again reduced to below the limit of detection (<10 cfu cm^{-2}) within 24 hours (Figure 6.11 and 6.12). It would therefore appear that re-use of the surface following one cleaning cycle with oxofoam (a standard industrial cleaner) and AME (a standard laboratory cleaner) did not impact negatively on the antimicrobial ability of the coating as counts of *E. coli* were reduced. However, this process will be repeated regularly *in-situ*, and more cleaning cycles sould be investigated *in vitro* for comparison. Testing for photocatalytic activity alone after re-use would also provide a more rapid screening process.

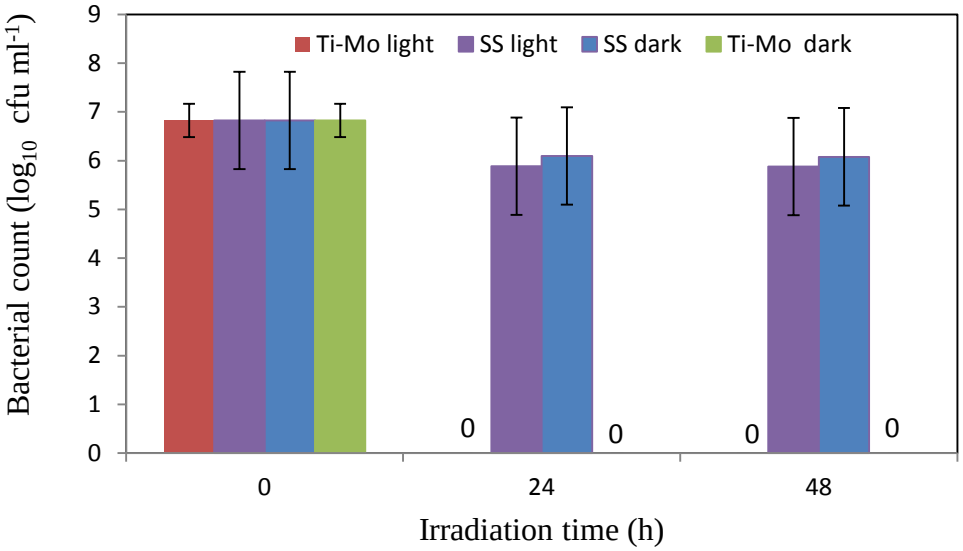

Figure 6.11: Antimicrobial effect of re-used TiO_2-Mo (7 at.%) photocatalyst against *E. coli* compared to stainless steel (SS) over 48 hours of incubation demonstrating an antimicrobial activity of TiO_2-Mo (7 at.%) under light or dark conditions after cleaning with AME solution.

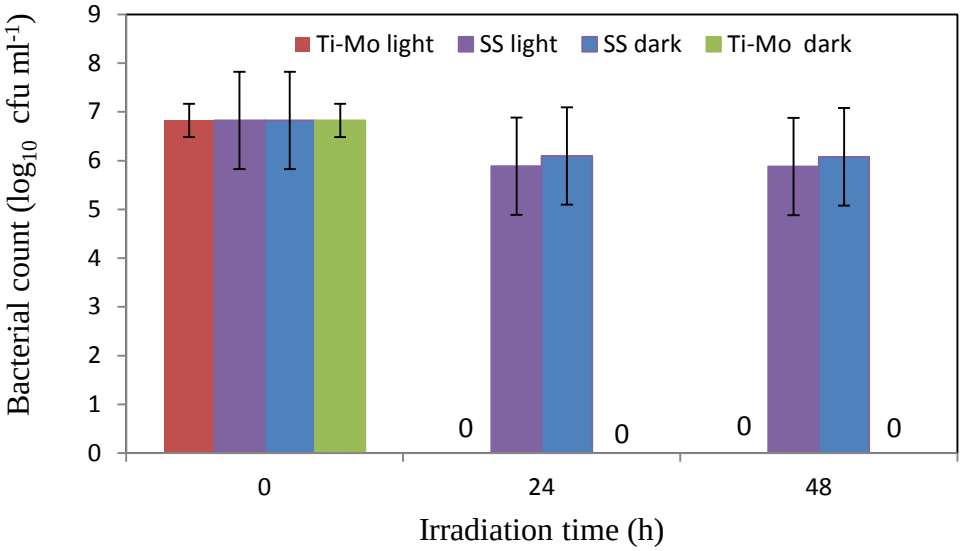

Figure 6.12: Antimicrobial effect of re-used TiO_2 -Mo (7 at.%) photocatalyst against *E. coli* compared to stainless steel (SS) over 48 hours of incubation. The surface was cleaned with 4 v/v % oxofoam solution, demonstrating that TiO_2-Mo (7 at.%) retained its antimicrobial activity after cleaning.

The new TiO_2-Mo (7 at.%) surfaces that had been tested for antimicrobial activity and were then treated with selected cleaners (4 v/v% oxofoam and AME) were stained using acridine orange to determine if any residue had been left on the surfaces. Neither residual soil nor bacteria were apparent on the surfaces (Figure 6.13 b,c), indicating that for new surfaces, one cleaning cycles is effective.

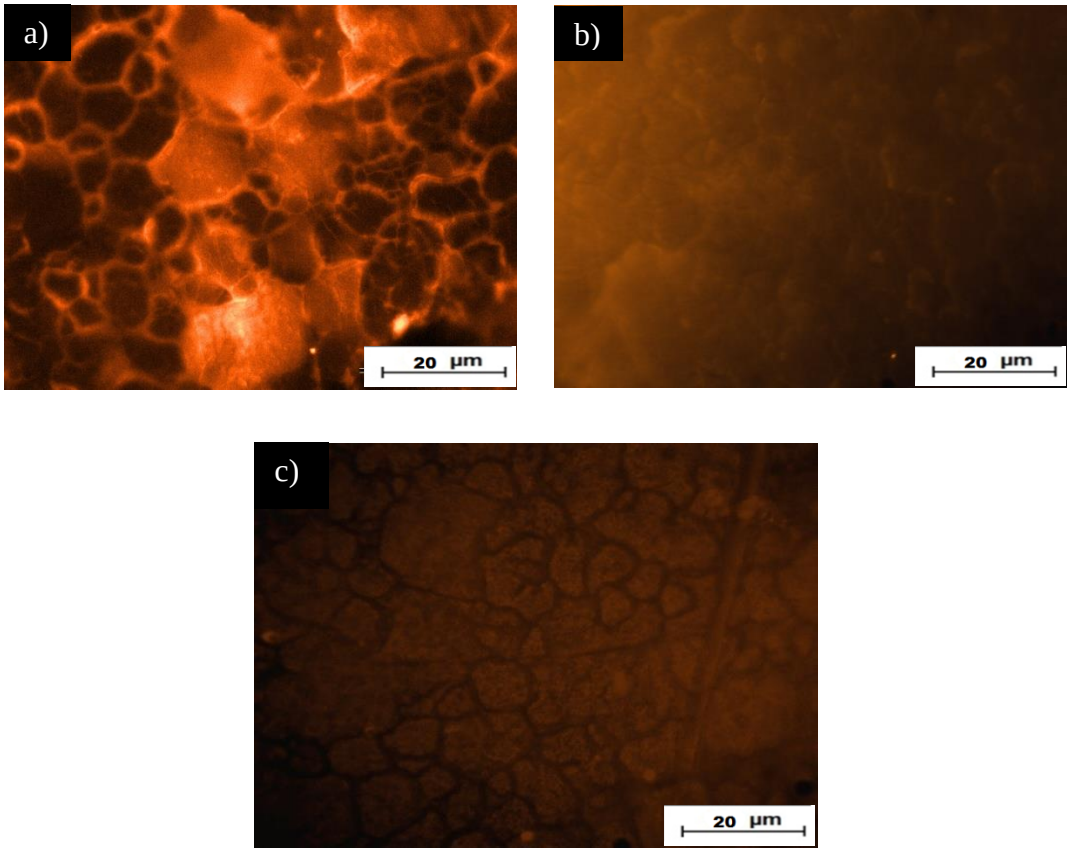

Figure 6.13: Epifluorescent microscopy image of TiO_2-Mo (7 at.%) photocatalyst stained with acridine orange a) after an assay and before cleaning and b) after cleaning with 4 v/v % oxofoam solution c) after cleaning with AME solution. Before cleaning, stained material is apparent particularly at grain boundaries. This material is essentially absent after cleaning.

An additional series of surfaces was also tested. Used surfaces from earlier assays had been discarded after immersion in neutraliser and kept in a dry beaker in the dark for up to 12 months. These were cleaned (using oxofoam 4% v/v) and tested to check whether they had retained their antimicrobial activity, under fluorescent light irradiation. There were no changes in cell counts after 48 hours, thus activity had been lost (Figure 6.14). After the assay, Mo-doped titania sample was also tested by methylene blue degradation. There was a reduction in photocatalytic activity by 30%, indicating that residual soil was masking the photocatalytic activity (result not presented). Acridine orange staining of the surface (post cleaning) demonstrated significant fouling, presumably dried out neutralising solution and

residual microbial debris (Figure 6.15). Other factors which could affect the activity of the surface over time, such as diffusion of active components from coating, or degradation of the coating over time, or through damage caused by the recalcitrant soil. It would have been useful to have removed this residue and then retested for photocatalytic and antimicrobial properties. Other cleaning regimes such as abrasion, and the use of different chemicals cleaners and sanitiser could be employed to further investigate the robustness of the coating. This finding reinforces the importance of regular cleaning regimes to ensure that photoactivity is retained.

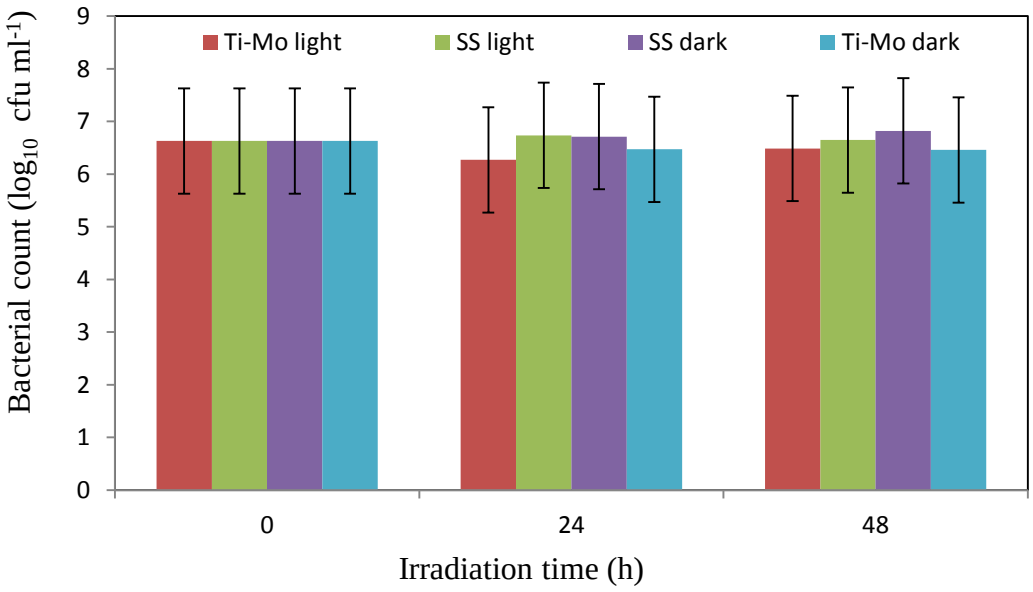

Figure 6.14: Antimicrobial effect of TiO_2-Mo (7 at.%) on *E. coli* compared to stainless steel (SS) over 48 hours of incubation. The used surface had been stored uncleaned and dry for 12 months, and was then cleaned with 4 v/v% oxofoam solution, demonstrating no antimicrobial activity.

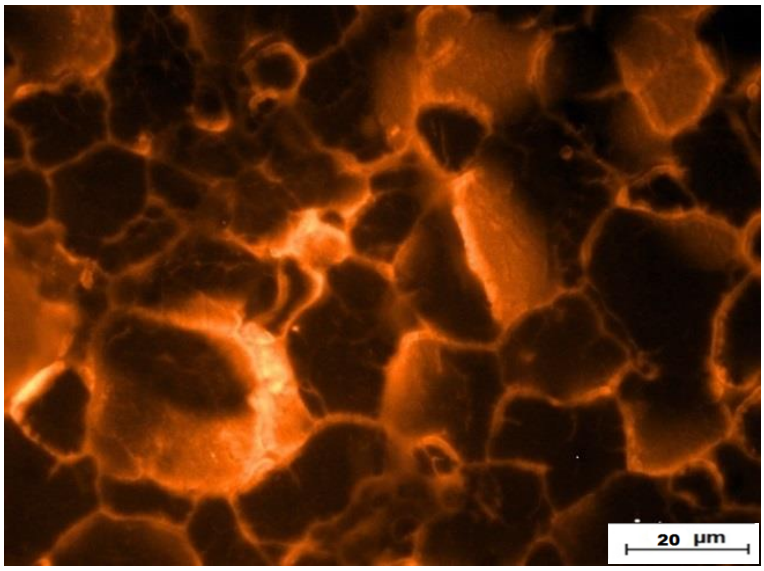

Figure 6.15: Epifluorescent microscopy image of acridine orange staining of old TiO_2 -Mo (7 at.%) photocatalyst (had been stored uncleaned and dry for 12 months) after cleaning with 4 v/v % oxofoam solution (before antimicrobial assay). Cleaning was ineffective at removing old, dried soil.

6.4 Effect of beer soil on antimicrobial activity of TiO_2-Mo 7 at.%

The effect of beer soil on antimicrobial activity demonstrated by the TiO_2-Mo (7 at.%) surfaces was investigated against *E. coli*. The presence of dilute beer (10%) on the surfaces did not reduce the antimicrobial activity of coatings (Figure 6.16). However, undiluted beer on the TiO_2-Mo (7 at.%) surfaces reduced the antimicrobial effectiveness, and no inhibition was seen (Figure 6.17). These results again show the importance of cleaning - dilute beer soil did not interfere with activity [175].

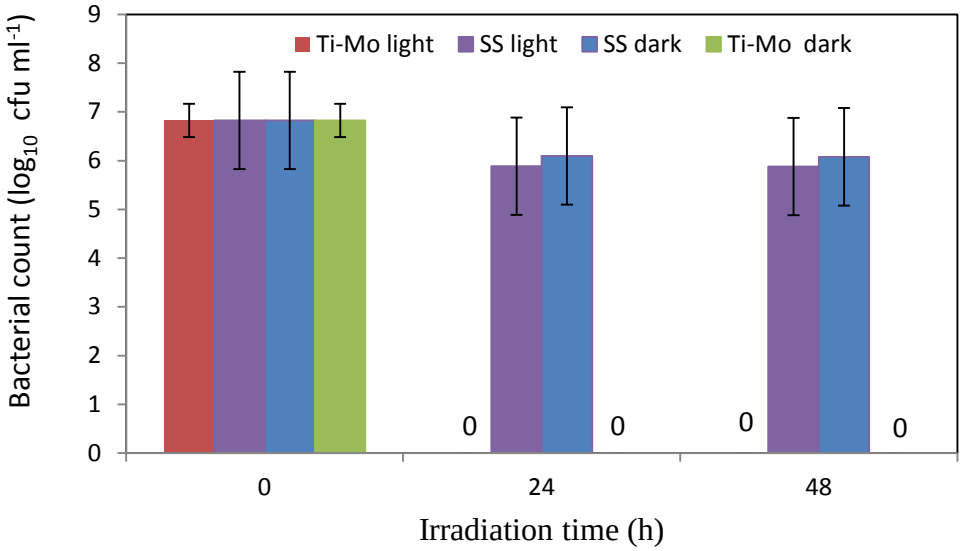

Figure 6.16: Antimicrobial effect of TiO_2-Mo (7 at.%) with dilute soil (10% beer) on *E. coli* compared to stainless steel (SS) over 48 hours of incubation demonstrating an antimicrobial activity of TiO_2-Mo (7 at.%) with diluted soil.

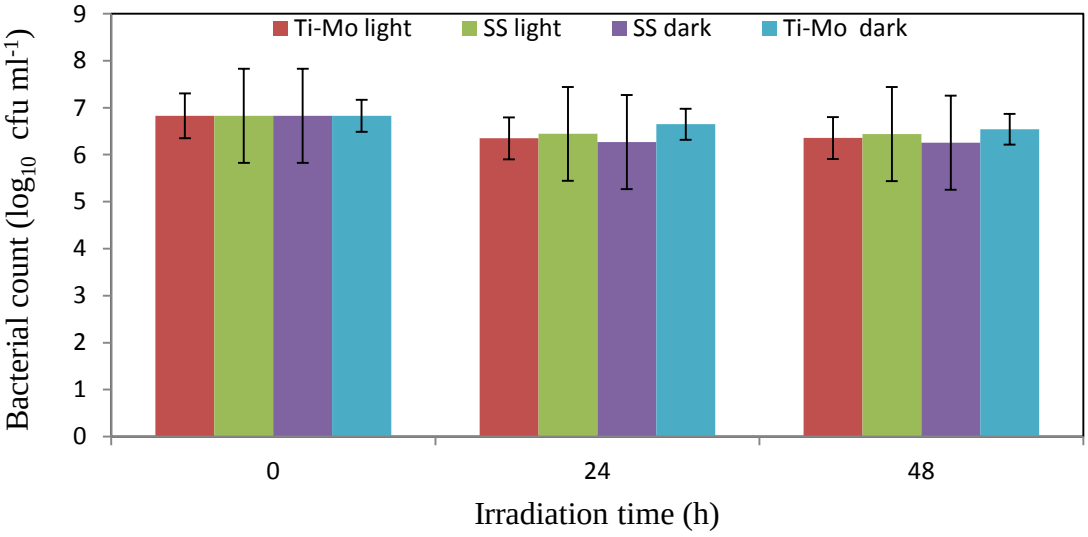

Figure 6.17: Antimicrobial effect of TiO_2-Mo (7 at.%) undiluted soil (beer) on *E. coli* compared to stainless steel (SS) over 48 hours of incubation demonstrating no antimicrobial activity.

6.5 Zone of inhibition

The zone of inhibition (ZOI) test was carried out to evaluate whether Mo, W and Nb could diffuse from the coated surfaces, and inactivate bacteria (Section 4.3.4.3). The test was performed on titania doped W and Mo samples, Nb metal was used as a control since it did not show any antibacterial activity in the dark. No zones of inhibition were observed (images not presented). These results suggest that, Mo and W ions were not leaching out from surface, or that the concentrations leaching out were too low to inhibit bacterial growth. Mo, MoO_3, W, WO_3, Nb and Nb_2O_5 coatings were also tested and no zones of inhibition were detected, although no growth beneath the surfaces were observed for Mo, MoO_3, W and WO_3 coatings.

6.6 Inhibition of metabolic activity

The nitrotetrazolium blue chloride (NBT) assay was used to evaluate whether the dopant metals (Mo, W and Nb) were sufficiently active in the TiO_2 coating to inactivate bacteria on the surface of coating. Tetrazolium redox dye scavenges electrons from microbial oxidation/reduction reactions and is intracellulary reduced to brightly chromogenic or fluorescent formazan precipitates by the electron transport system components or dehydrogenases in metabolically active cells [176].

The viability of bacteria, applied as a suspension and dried on a surface, may be determined directly by colony counts after overlaying the surface with TSA agar and allowing an appropriate incubation period in the dark. If the cells are killed by contact with Mo, W or Nb (dark), then they would not grow when subsequently exposed to TSA agar. Colonies were only apparent on TiO_2-Nb 0.25 at.% and TiO_2-W 3.8 at % thin film coatings. No colonies were observed on TiO_2-Mo 7 at. % and TiO_2-W 10 at % coatings. These results are in

agreement with findings from the antibacterial photocatalytic assays that showed the Mo and the higher concentration of W metal have innate antibacterial properties, whilst the Nb does not (Figure 6.18).

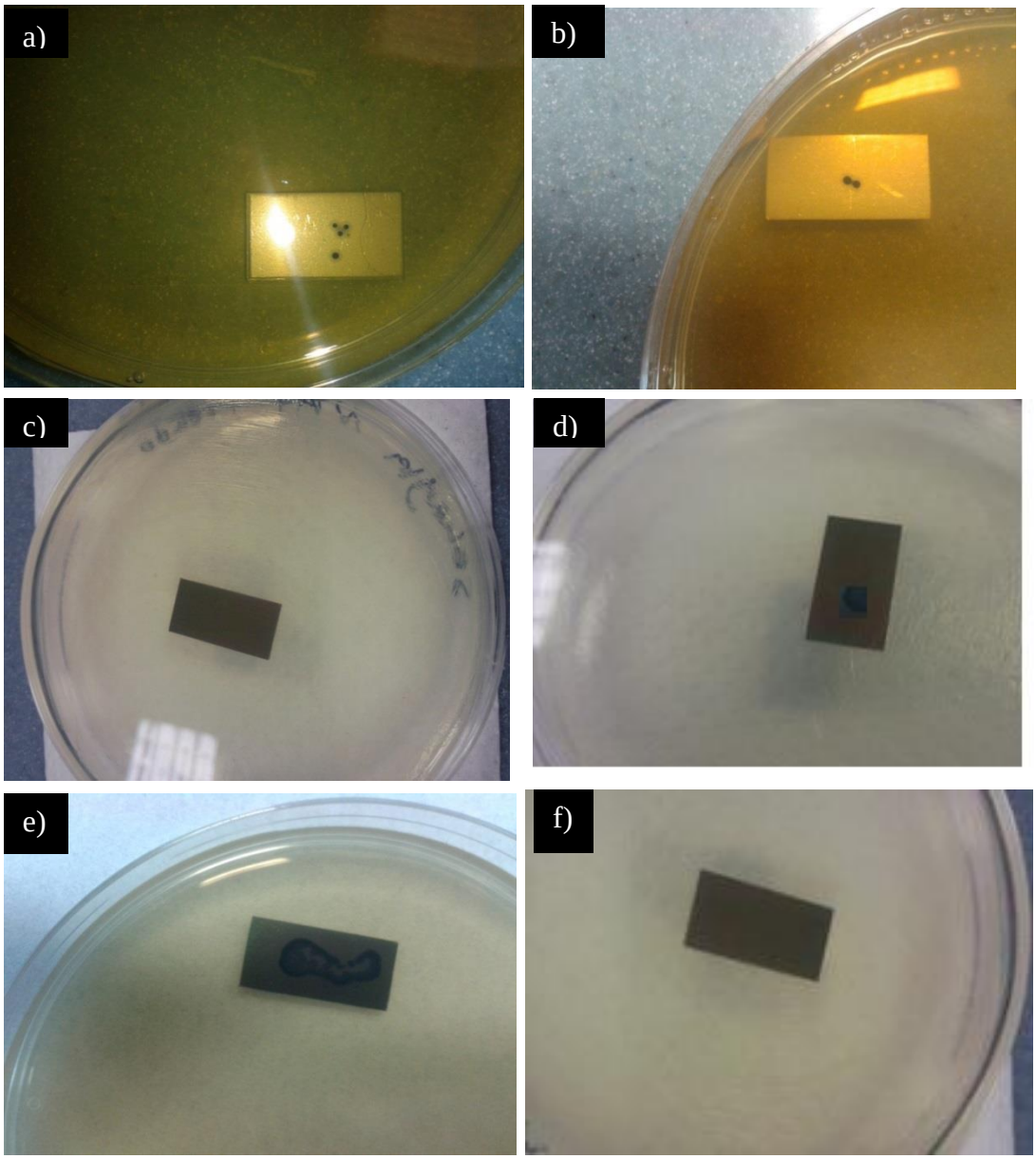

Figure 6.18: Colonies stained with NBT on stainless steel coatings to test antibacterial effect of dopant metals a and b) stainless steel (control) c) TiO_2-Mo 7 at.% d) TiO_2-W 3.8 at.% and e) TiO_2-Nb 0.25 at.% f) TiO_2-W 10 at.% .

6.7 Minimum inhibitory concentration (MIC)

Minimum inhibitory concentrations (MICs) of Mo, Nb and W ions (dissolved) were determined by an agar incorporation method to find the lowest concentration that would give no growth of bacteria (Table 6.1). Molybdenum ions inactivated *E. coli* at a lower concentration than tungsten ions and niobium ions. Bacterial growth was seen on all of the dilutions of the acid that had been used on diluent, indicating that the low percentage of acid present in the salt suspensions did not interfere with growth of *E. coli*. Metal ions are thought to exert their antimicrobial effects through a variety of mechanisms. They either accumulate on cell membranes, the permeability of which may become compromised rendering the cell unable to regulate transport through it, hence the leaking of intracellular components, and eventually causing cell death, or may penetrate membranes and accumulate intracellularly, where they may exert an effect on nucleic acid [177].

The concentration of Mo ions which was released from coatings during ICP-AES was 0.73 ppm (0.73 mg/L) during the first 48 hours which decreased to 0.04 ppm after 7 days (Chapter 7). The ion concentration released was too low to cause inhibition, which explains the results from the zone of inhibition test.

Table 6.1: MIC results for selected transition metal ions (dissolved) demonstrating the minimum concentration of ions required to inactivate the bacteria.

Strain	Tungsten (W)	Molybdenum (Mo)	Niobium (Nb)
E. coli	3-4 mg/L	2-3 mg/L	12-14 mg/L

6.8 Discussion

The antimicrobial properties of titanium dioxide (TiO_2) doped with different transition metals (Mo, Nb and W) and untreated stainless steel AISI 304 2B were measured against *E. coli* for various contact times in the absence and presence of fluorescent light. On stainless steel (SS) under either light or absence of light, there was a slight decrease in the number of viable cells ($p > 0.05$) on the surface after 6, 8, 12, 24 and 48 hours. This reduced survival is not unexpected under such conditions. The antimicrobial activity demonstrated by the TiO_2-Mo (7 at.%) surfaces was also investigated against microorganisms isolated from brewery surfaces that included *Pseudomonas rhodesiae , Serratia marcescens,* and *Wickerhamomyces anomalus.* The results are presented in Appendix C [175].

6.8.1 TiO_2-Mo 7 at. %

TiO_2-Mo 7 at. % inactivated the bacteria after 24 hours of incubation in both light and dark, which indicated a dual functionality of molybdenum doped sample, being photocatalytically active in the light and antimicrobial in the dark. Mo had a direct role in promoting increased bacterial kill under fluorescent light irradiation. There was a 7 log reduction over 24 hours in comparison to undoped titania coatings (3 logs over 24 hours). The results from methylene blue degradation assay also showed a high photocatalytic activity of Mo-doped TiO_2 coating. Thus, the presence of Mo enhances the photo-killing effect, and also makes the surface innately antimicrobial [178].

6.8.2 TiO_2-Nb 0.25 at. %

The 0.25 at.% niobium doped sample inactivated the bacteria (7 log reduction) after only 48 hours of illumination which demonstrates its photo-killing activity under fluorescent light, this activity was much higher than TiO_2 alone (4 log reduction over 48 h). However, no antimicrobial activity was observed when the TiO_2-Nb 0.25 at% coated substrate was incubated with inoculum in the dark for 48 hours, which indicates that TiO_2-Nb 0.25 at% has no innate toxic effect on bacterial cells [179].

6.8.3 TiO_2-W 3.8 at. % and 10 at.%

Two different tungsten concentrations were used to dope the TiO_2, as highest level of W and WO_3 showed antimicrobial activity in the dark pointing to W and WO_3 possessing inherent antimicrobial activity. The W-doped TiO_2 (3.8 at.%) coating showed no antimicrobial effect in the dark, but an innate antimicrobial effect was observed with TiO_2-W (10 at.%) coating in the dark. Both concentrations enhanced photo-killing in contrast to undoped TiO_2 and uncoated stainless steel. There was also an enhancement in photo-killing as the concentration of W increased. At higher concentrations of W, the Raman peaks for WO_3 were observed at 968 cm^{-1} and 273 cm^{-1} which is assigned to tungsten oxide species on the surface of the coatings (Chapter 5). The enhancement in antimicrobial activity for TiO_2-W (10 at.%) coating could be due to more WO_3 being available on the surface [180].

The photo-killing activity can be explained by the formation of hydroxyl radical and reactive oxygen species (ROS) at the surface. The passage of hydroxyl radicals towards the cytoplasmic membrane of *E. coli* is significantly hindered by the morphology of the cell envelope which differs between Gram positive and negative bacteria [35, 39]. In Gram negative bacteria, such as *E. coli*, the cytoplasmic membrane is protected by a thin layer of

peptidoglycan, followed by an outer membrane. The outer membrane presents a significant barrier to hydroxyl radical passage since it comprises a complex layer of lipids, lipopolysaccharides and proteins [35]. The outer membrane layer presents an attractive target for approaching hydroxyl radicals because of this composition. Although the outer membrane is semi-permeable, many of the hydroxyl radicals will react with the lipid constituents of the membrane rather than pass through it [32]. Once the membrane is breached, there are no further significant obstacles blocking the approach of radicals to disrupt the cytoplasmic membrane and cell death can be observed [31]. This interpretation is supported by study of the photo-killing of *E. coli* by TiO_2 thin films, where the bactericidal action was found to be a two-step process in which the outer membrane is compromised first, followed by cytoplasmic membrane [30]. However, the recent study by Kubacka *et al*. [181] showed that antimicrobial mechanisms of TiO_2 photocatalysis exhibit; i) rapid cell inactivation at the regulatory and signalling levels, ii) a strong decrease of the coenzyme-independent respiratory chains, iii) a lower ability to integrate and transport iron and phosphorous and iv) a lower capacity for the biosynthesis and degradation of heme (Fe-S cluster) groups. These activities, together with the extensive cell wall modifications, are the main factors that explain the high biocidal performance of TiO_2-based nanomaterials.

6.8.4 Antimicrobial activity of transition metals and their oxides

The antimicrobial principle of transition metals and their oxides (Mo, MoO_3, W and, WO_3) can be related to acidic surface reaction as release of hydroxynium ions [178].

$$MoO_3 + H_2O \rightleftharpoons H_2MoO_4 \qquad (6.2)$$

$$H_2MoO_4 + 2H_2O \rightleftharpoons 2H_3O^+ + MoO^{2-}{}_4 \quad (6.3)$$

$$WO_3 + H_2O \rightleftharpoons H_2WO_4 \quad (6.4)$$

$$H_2WO_4 + 2H_2O \rightleftharpoons 2H_3O^+ + WO_4{}^{2-} \quad (6.5)$$

According to the above Reactions (6.2), (6.3), (6.4) and (6.5):

First molybdic acid is formed when the surface is in contact with water. Hydroxynium ions (H_3O^+) will be released from molybdic acid and also molybdate ions ($MoO^{2-}{}_4$) will be formed once the molybdic acid mixes with water (Reactions 6.2 and 6.3). Tungstic acid will be formed in the presence of water. Further reaction with water would lead to the formation of H_3O^+ and tungstate ions ($WO_4{}^{2-}$) (Reactions 6.4, 6.5). In the equilibrium state, the molybdates and tungstates will be transformed into molybdic acid and tungstic acid [178, 182]. Acids generally inhibit molecular reactions essential to the microorganisms by increasing the hydrogen ion concentration, which results in a decrease in internal pH. This fall in internal pH is a major cause of growth inhibition by weak acids [183].

The formation of acid on the coated surface would inhibit bacterial growth [182, 184] at a pH values 3.5 - 4. Many Gram negative bacteria such as *E. coli* are killed at pH values of 5.5 and below [185]. The acid activity refers to the diffusion of H_3O^+ ions through the cell membranes [184, 186]. This results in distortion of the enzyme and transport systems of the bacteria [187]. There is also a disruption of the DNA helix [188]. It has been reported that MoO_3 interacted with *E. coli* which resulted in cell wall damage/disruption further leading to release of β-D-galactosidase and thus mediated cell death [186]. The W metal and WO_3 coatings also showed a bactericidal effect [189]. The Nb metal and Nb_2O_5 did not show any antimicrobial effect. No reduction in number of bacteria was observed after 48 hours of

incubation under light and dark conditions. These observations are in agreement with Gao *et al*.[190]. However, further work is required to explore the relationship between coatings and pH of the surrounding environment.

6.8.5 Re-use of TiO_2-Mo (7 at.%) surface and cleaning assays

The TiO_2 - Mo 7 at.% coated surface retained activity after one use *in vitro*. Two cleaning solutions were used to clean the surfaces immediately after an antimicrobial assay; Oxofoam solution, and laboratory cleaning regime acetone, methanol, ethanol (AME). Both oxofoam and AME treatments effectively cleaned these lightly soiled surfaces, and these cleaned surfaces were able to inactivate bacteria after 24 hours. *In vivo*, repeated cleaning of lightly soiled surfaces carried out. It would be interesting to carry out repeated soil and cleaning cycle on these surfaces.

Surfaces, which had been used and not cleaned and left dry in the dark for one year before cleaning did not show any antimicrobial activity. The cleaning protocol used was not effective in this unlikely scenario. Clearly, appropriate regular cleaning regime needs to be in place in order to retain photocatalytic surface.

6.8.6 Effect of beer soil on antimicrobial activity of TiO_2-Mo 7 at.%

In the dispensing and bottling section of a brewery, it is common for process surfaces to become covered by a conditioning film formed via the adsorption of various organic materials from the spilt beer [191]. The antimicrobial efficacy of the TiO_2-Mo 7 at.% surface was also examined following the deposition of soil in the form of undiluted beer on the surface. There was no decrease in cell numbers following exposure to fluorescent light for 48 hours. It would therefore appear that the presence of soil had a significant impact on the antimicrobial effectiveness of the photocatalytic surface compared to without soil. With the

contaminating population remaining viable, it is likely that the soil was acting as a nutrient source and masking the photocatalytic effects of TiO_2-Mo 7 at.%.

The contamination of surfaces with heavy soil does, however, present an unlikely exposure scenario.The application of dilute beer to the surface more closely mimics real brewery dispensing and bottling processes since automated rinsing with jets of water would dilute any spillage of product. Dilute beer applied to the TiO_2 - Mo 7 at.% surface did not reduce the antimicrobial effect and a 6-log reduction of *E. coli* was observed.

Ahmed *et al*. [192], examined the photocatalytic degradation of human serum albumin (HSA) on TiO_2 and TiO_2 - Ag films by immersing the surfaces in 0.5% w/v HSA in distilled water for 30 minutes. Raman spectroscopy indicated changes in protein conformation, consistent with denaturation and enhanced binding and oxidation, these were thought to be induced via a photocatalytic mechanism. A comparable phenomenon might be occurring with the dilute beer in contact with TiO_2-Mo 7 at.% surface, as opposed to the heavier soils.

6.8.7 Zone of inhibition, metabolic activity and MIC assays

No zones of inhibition were detected from TiO_2-Mo 7 at.% and TiO_2 - W 10 at.% coatings, presumably because the concentration of these ions released from the coating was too low to inhibit bacterial growth. Mo, MoO_3, W, WO_3, Nb and Nb_2O_5 coatings were also tested and no zones of inhibition were detected. The NBT assays also confirmed the innate antibacterial activity of TiO_2-Mo 7 at.% and TiO_2-W 10 at.% coatings. However, viable cells remained on the TiO_2-Nb 0.25 at.% and TiO_2-

W 3.8 at.% coatings and stainless steel, confirming their lack of antimicrobial properties. The MIC results also showed that Mo and W metal ions inactivated *E. coli* at lower concentration in comparison to Nb metal ion. Yasuyuki *et al.* [193] investigated the antimicrobial effect of nine pure metals on *E. coli* and *S. aureus*. The results confirmed the antibacterial properties

of molybdenum. Several authors also confirmed the antimicrobial activity of W and Nb ions [189, 194].

6.9 Conclusion

This chapter describes investigations into the antimicrobial effect of a) doped TiO_2 coatings combined with different transition metals, b) coatings of transition metals and their oxides. TiO_2-Mo 7 at.% and TiO_2-W 10 at.% coatings had an antimicrobial activity after 24 h light irradiation and incubation in the dark. TiO_2-W 3.8 at.% and TiO_2-Nb 0.25 at.% , showed no antibacterial activity in the dark, and bacteria were only killed on the surfaces in presence of fluorescent light, showing a photo-killing activity. The higher inactivation rate of Mo-doped TiO_2 coating was expected as they had shown higher photocatalytic activity than Nb- and W-doped TiO_2 coatings. Transition metals and their oxides coatings were also used in order to assess the effect of dopant metal/metal oxide on bacteria inactivation. The WO_3 coating had greater antibacterial activity in comparison to W metal coating. Both Mo and MoO_3 coatings inactivated *E. coli* after 12 hours incubation. The Nb and Nb_2O_5 coatings did not show any antimicrobial effect in the presence and absence of light. The results were confirmed by MIC assays of their ions, with the W and Mo ions having higher antibacterial activity than Nb ion. No zones of inhibition were detected for Mo- and W-doped titania coatings, indicating no/low release of ions from the surface. However, the NBT results confirmed the innate antibacterial activity of Mo and W demonstrated by contact between cell and surface. The photocatalytic and antimicrobial nature of the TiO_2-Mo 7 at.% surface significantly reduced microbial numbers even with the application of a dilute brewery soil (beer). This work has provided useful information regarding the potential of TiO_2 doped materials for food or beverage processing applications. There are some limitations for the use of these coatings,

since appropriate light sources should be available in industry to maximise the activity of these surfaces. Also more work needs to be done to identify robust cleaning and disinfection regimes. It has been confirmed that all the doped photocatalytic surfaces possess antimicrobial activity when irradiated with fluorescent light. Surfaces which additionally possessed innate antimicrobial activity might be better suited to enviromental applications to avoid contamination of food. These applications might include hard to reach industrial areas where contact with the food and beverage product is unlikely.

Chapter 7: Chemical and Mechanical Durability of TiO_2 and Molybdenum Doped TiO_2 coatings

7.1 Introduction

As discussed in earlier chapters, one way to reduce cleaning costs and to improve process hygiene could be to use self-cleaning and antimicrobial coatings, that can prevent the attachment of microorganisms and soil, or facilitate their efficient removal during the cleaning process.

As the surfaces used in the food and beverage industries are exposed to adverse environments (contact with water and beverages, cleaning solutions, abrasive wear during cleaning), scratch and corrosion resistance play important roles in their mechanical durability and chemical stability. Hence, an effective coating must satisfy several requirements, including good adhesion to the substrate, the retention of high activity and resistance to chemicals.

The adhesion of any film to its substrate is one of the most important properties of a thin film. The level of adhesion depends on the force required to separate atoms or molecules at the interface between film and the substrate. The adhesion of a film to the substrate is strongly dependent on the chemical nature, cleanliness, and microscopic topography of the substrate surface [122].

The presence of contaminants on the substrate surface may increase or decrease the adhesion depending on whether the adsorption energy is increased or decreased, respectively. Also the adhesion of a film can be improved by providing more nucleation sites on the substrate, for instance, by using a fine-grained substrate or a substrate pre-coated with suitable materials. Of the deposition processes available, magnetron sputtering has been shown to produce well-adhered and uniform coatings over wide areas [195]. In this process, the adhesion of the film to the substrate can be improved by ion-cleaning of the substrate prior to the coating

deposition as well as additional ion bombardment during coating deposition which improves adhesion by providing intermixing on an atomic scale [196]. Use of an interlayer of titanium metal would also improve the adhesion between the film and substrate.

In this work, the most effective coating was found to be (TiO_2-Mo 7 at. %), as it had the highest photocatalytic activity in comparison to the other dopants investigated. This and a pure TiO_2 coating (control) were placed in three different Finnish breweries: A, B, and C (Figure 7.1) at sites in the production process that are important in terms of maintaining good environmental hygiene, that is bottle filling and canning lines. The product line in brewery A was soft drinks and water and in brewery B and C was beer (Figure 7.1). These challenging environments will test key properties of the coatings: the retention of photocatalytic activity over time and use, good adhesion to the substrate, and resistance to chemical cleaning treatments.

This chapter describes investigation of the chemical and mechanical durability of the selected coatings, the retention of photocatalytic activity and contact angle measurement of the initial coatings (TiO_2, and TiO_2-Mo 7 at.%,) the data obtained should serve as an indicator of photocatalytic activity after they had been placed in different brewery process environments (bottle filling lines in three Finnish breweries) over a 12 month period.

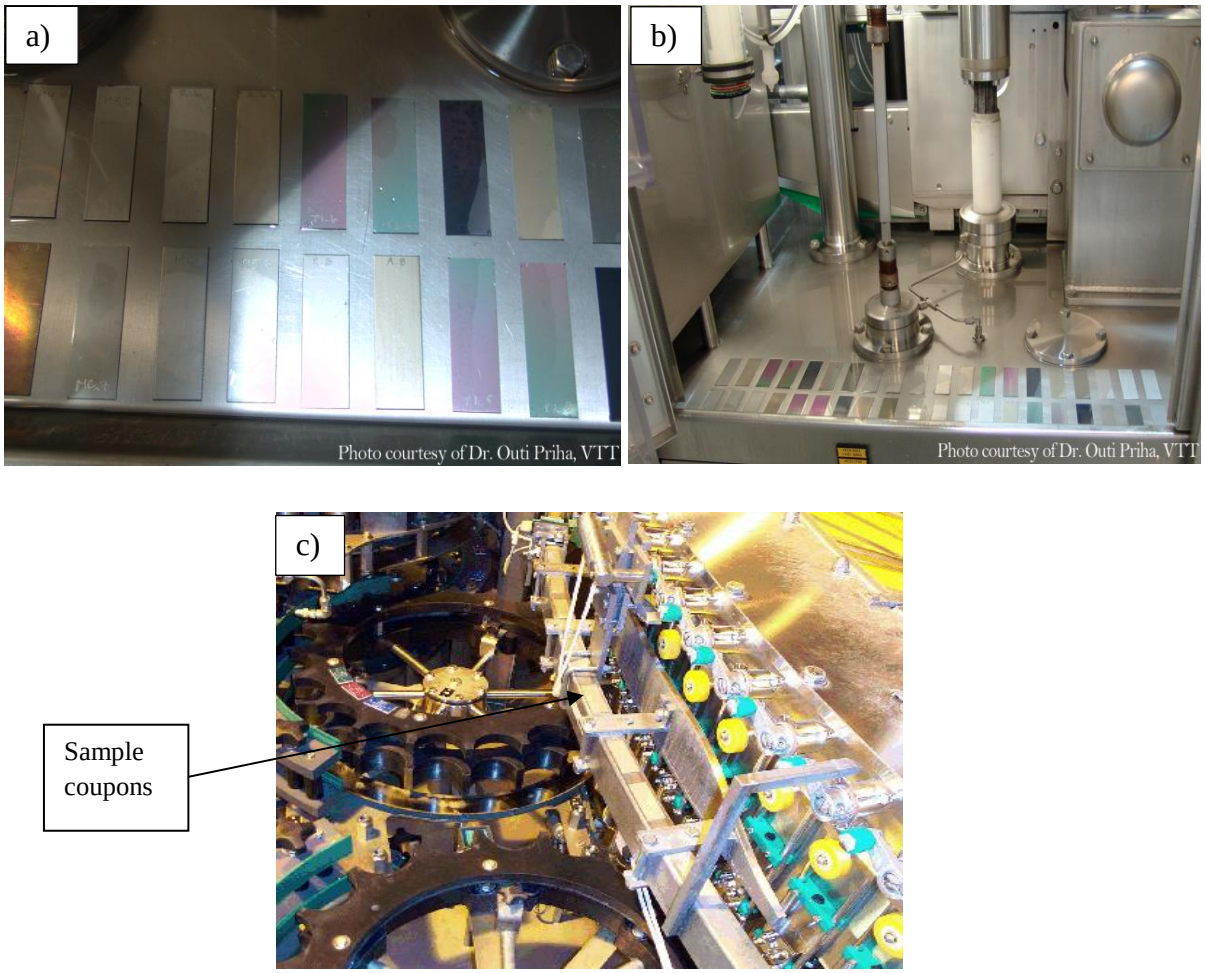

Figure 7.1: Process studies of photocatalytic coatings. Photocatalytic sample coupons were placed a) on the filler table, b) bottle line filler wheel support, and c) in the canning line at different Finnish breweries.

7.2 Chemical durability of TiO_2 and TiO_2–Mo (7 at.%) coatings

As a preliminary study, different chemical solutions (0.02 M HCl, 0.02 M NaOH, ethanol and water) were used to assess the chemical durability of annealed TiO_2 and TiO_2-Mo (7 at.%) coatings. These agents were selected on the basis of presenting neutral, alkali, acid and alcohol to the surfaces, thus representing the different types of cleaning and disinfection agents that might be encountered *in-situ.* The preliminary experiments with 2 M NaOH and 2 M HCl suggested that the stainless steel itself was attacked by the acid. Therefore, 0.02 M HCl (pH 1.7) and NaOH (pH 12.3) aqueous solutions were chosen on the basis of stainless steel corrosion resistance. The pH values of the 0.02 M reagents are more representative of the conditions which may be encountered during the brewery trial [148, 197] (Section 4.2.12). The samples were placed in these solutions for two hours at room temperature.

A representative image of a TiO_2-Mo (7 at.%) surface is shown in Figure 7.2. The image shows the two sections of the substrate, coated and uncoated part. The uncoated part was covered with Kapton tape during coating, and the tape was removed for immersion studies. The coating thickness was calculated from the step height of the cross section between these two areas. The surface roughness (R_a (2D average roughness), and S_a (3D average roughness) were also measured using WLl. As has already been noted, the R_a is a 2-dimensional measurement of the average departure of the surface profile from a mean centre line and is used as a descriptor of surface roughness. The S_a value, which is taken across an area of the surface along several lines to enable an indication of roughness over a specified area, rather than a line profile.

No significant changes were observed in surface thickness (800 nm - 1.10 µm) of the coated part after exposure to different chemicals for doped and undoped titania samples (P > 0.05) (Figures 7.3 and 7.6).

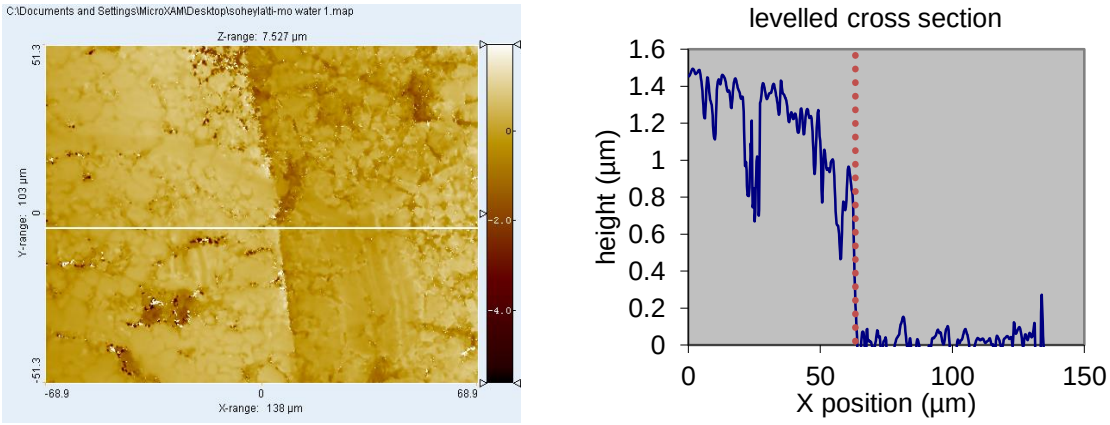

Figure 7.2: White light interferometry image of TiO_2–Mo (7 at.%), example of thickness calculation by levelled cross section. The left hand side is the coated part and right hand side is the uncoated part.

7.2.1 Chemical durability of TiO_2

No significant changes were observed in surface thickness and roughness R_a or S_a values before and after exposure to the selected chemicals (P > 0.05) (Figures 7.3 and 7.4). There is no significant difference in S_a (3D average roughness) value (p > 0.05) for pure titania coatings (Figure 7.5). These results demonstrated that surface roughness did not change after immersion in the chemical solutions. The R_a value of less than 0.8 µm is generally accepted as indicative of a hygienic surface. All surfaces had R_a values well below this level.

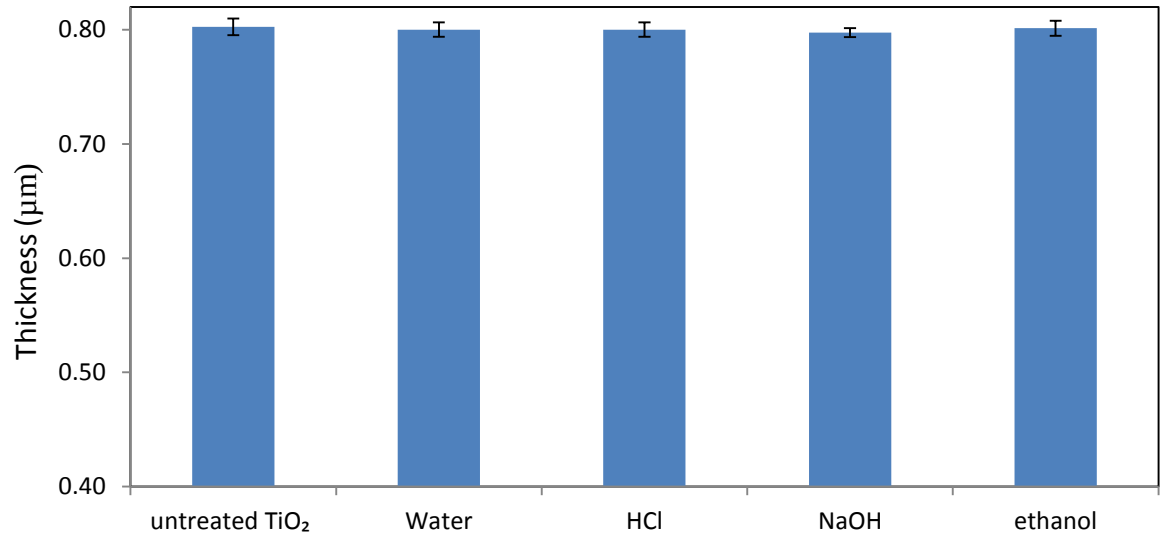

Figure 7.3: Thickness measurement of TiO_2 before and after chemical durability test.

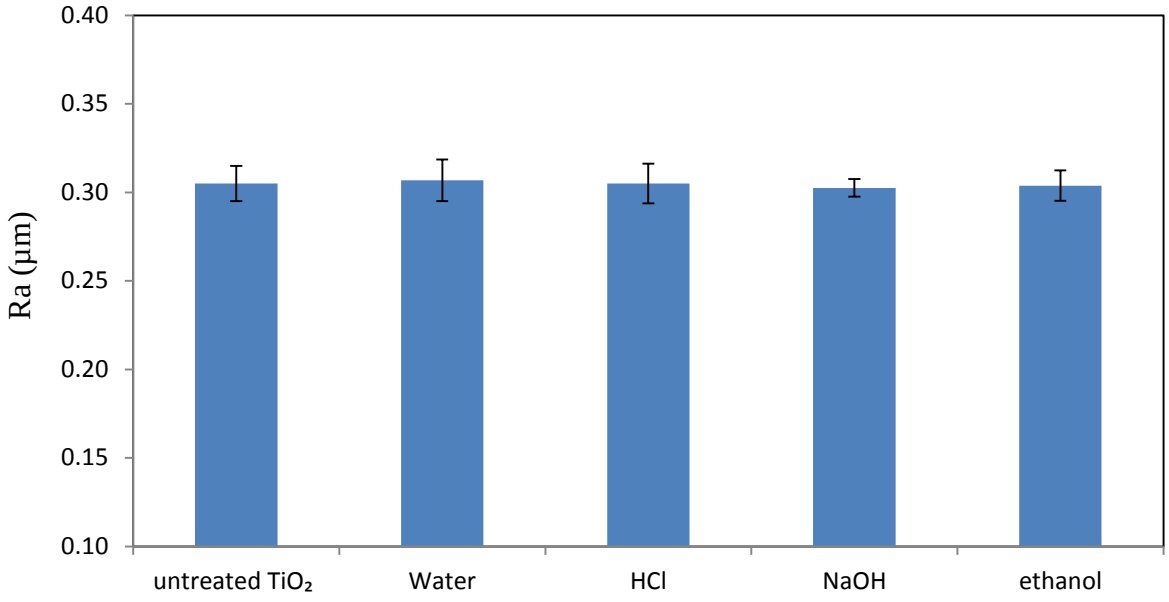

Figure 7.4: R_a values of TiO_2 before and after chemical durability test demonstrating surface roughness.

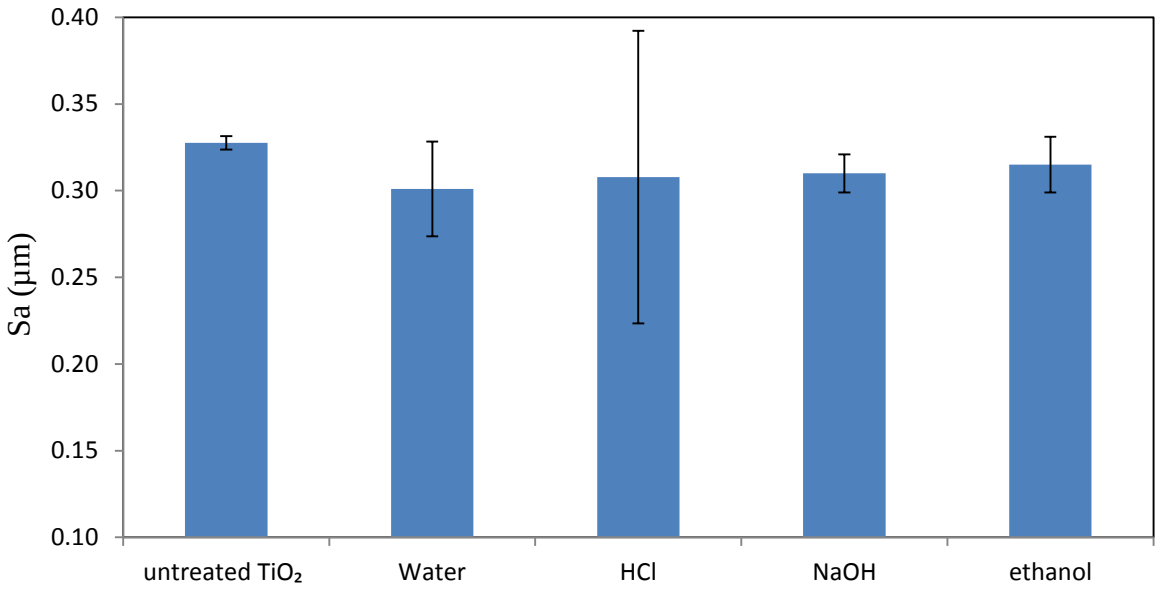

Figure 7.5: S_a values of TiO_2 before and after chemical durability test demonstrating surface roughness.

7.2.2 Chemical durability of TiO_2 -Mo 7 at.%

No significant changes were observed in surface thickness and roughness (R_a) for TiO_2-Mo 7 at.% ($p > 0.05$) after exposure to acidic, basic, neutral and alcohol environments (Figures 7.6, and 7.7). There was a slight reduction in S_a for 0.02 M NaOH ($p > 0.05$) (Figure 7.8), indicating that 0.02 M NaOH solution etched the coating more than other solutions. EDX analysis confirmed that the composition of the coatings did not change significantly after immersion in water, ethanol, acidic and basic solutions (Table 7.1).

Table 7.1: EDX results after immersion of TiO_2-Mo 7 at.% in different chemical solutions.

Chemical treatments	Dopant content, at.%
Water	7 ± 0.05
0.02 HCL	6.85 ± 0.05
0.02 M NaOH	6.8 ± 0.05
Ethanol	6.95 ± 0.05

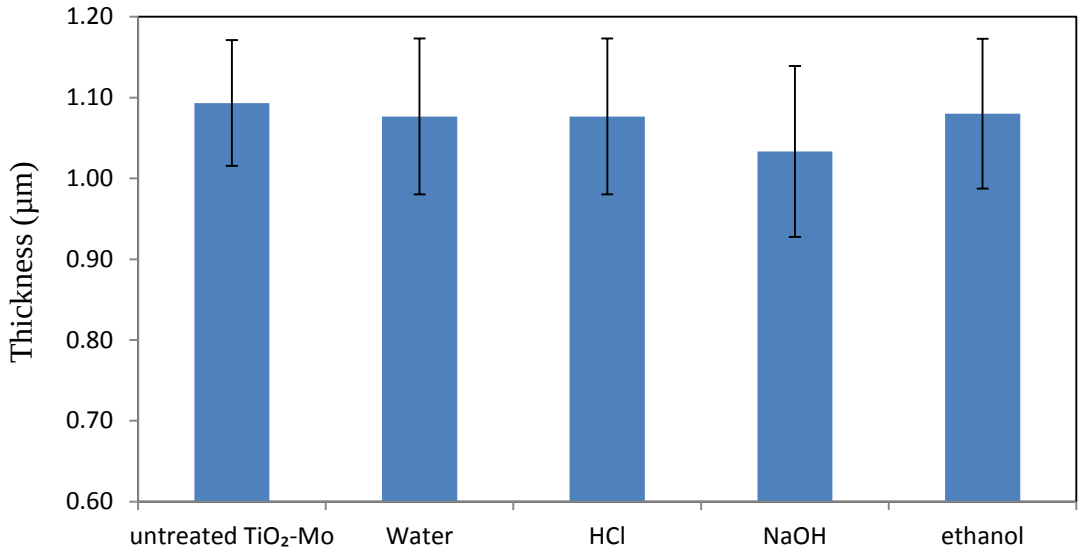

Figure 7.6: Thickness measurement of TiO_2-Mo (7 at.%) before and after chemical durability test.

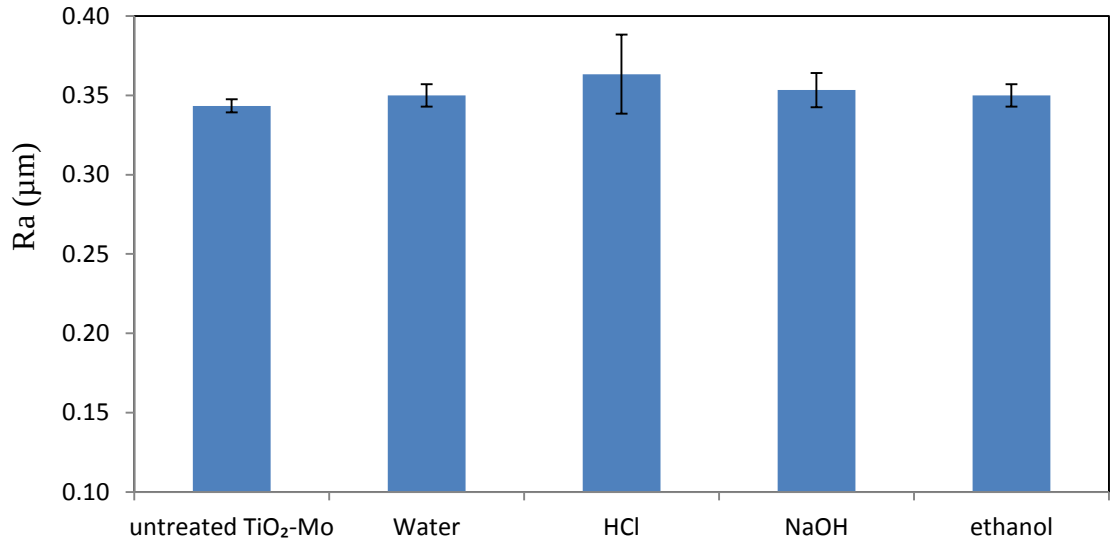

Figure 7.7: R_a values of TiO_2-Mo (7 at.%) before and after chemical durability test demonstrating surface roughness.

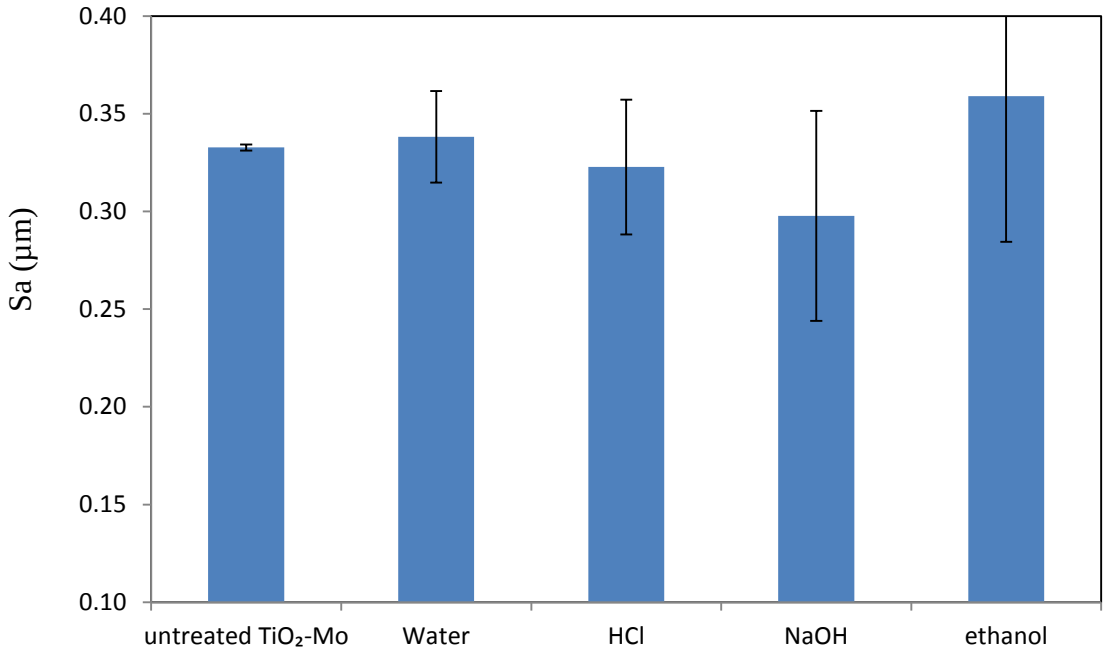

Figure 7.8: S_a values of TiO_2-Mo (7 at.%) before and after chemical durability test demonstrating surface roughness.

7.2.3 Photocatalytic activity after Chemical durability testing of TiO_2 and TiO_2-Mo (7 at.%)

The photocatalytic activity of the coatings selected for the chemical durability tests was measured by the methylene blue degradation test (Section 4.2.9) after the samples had been placed in 0.02 M HCl, 0.02 M NaOH, water and ethanol for two hours and rinsed with distilled water (Figures 7.9-7.10) and results were compared to those from reference samples. There was no significant change in photocatalytic activity of pure titania after immersion in ethanol, neutral and acidic solutions ($p > 0.05$) under UV and fluorescent light irradiation, but there was a slight reduction in photocatalytic activity for surfaces immersed in 0.02 M NaOH solutions under both irradiation conditions ($p < 0.05$) (Figure 7.9). The reduction in photocatalytic activity of pure titania coatings can be explained by adsorption of sodium onto

the coatings. It is well known that sodium has detrimental effect on photocatalytic activity [198].

For TiO_2-Mo 7 at. %, there was a significant reduction in photoactivity for both acidic and basic solutions under UV and fluorescent light illumination ($p < 0.05$) (Figure 7.10).

A reduction in surface roughness was observed after treatment with NaOH (base) for this coating, which suggests that the coating was etched. This might be expected, as a decrease in roughness value implies a decrease in surface area of the coating in contact with methylene blue solution which results in reduction in photocatalytic activity. However, there was no reduction in surface roughness for samples immersed in HCl solution which indicating that surfaces roughness cannot alone account for this 20% reduction in photocatalytic activity. There was no a significant reduction in Mo content after immersion in HCl and NaOH solutions (results recorded were 0.1 at.% and 0.15 at.%, respectively). One of the other reasons that may explain the reduction in photocatalytic activity is that after immersion of this coating in acidic (HCl) solution, there is a possibility of diffusion of chloride ion into the coatings which resulted in decreasing the photocatalytic activity. However, more chemical analysis of the surface is required to be absolutely sure of the equalities of this effect.

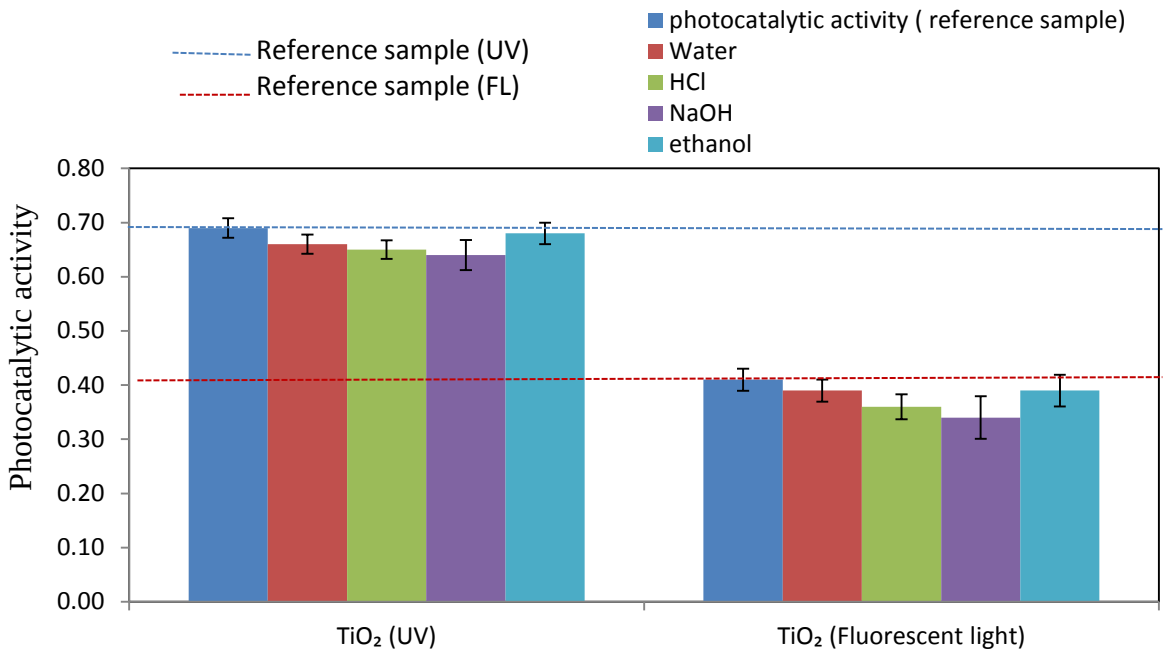

Figure 7.9: Photocatalytic activity of TiO_2 coating after being immersed in 0.02 M HCl, 0.02 M NaOH, water and ethanol.

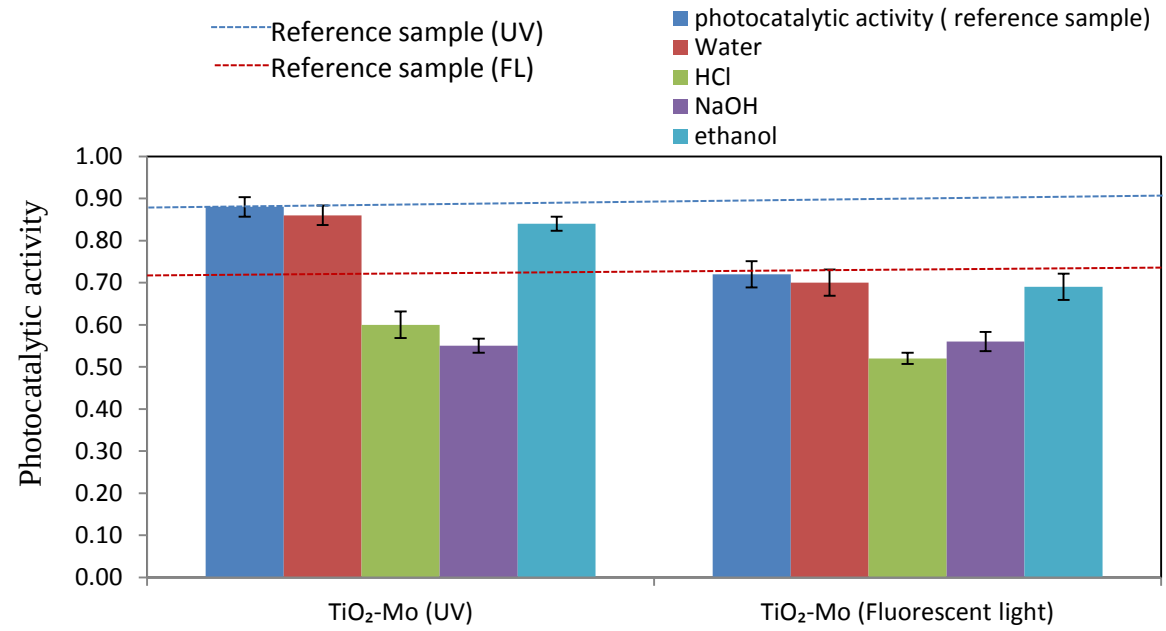

Figure 7.10: Photocatalytic activity of TiO_2-Mo (7 at.%) coating after being immersed in 0.02 M HCl, 0.02 M NaOH, water and ethanol.

7.3 Mechanical durability of TiO_2-Mo (7 at.%) and TiO_2 surfaces before the brewery trials

The TiO_2-Mo 7 at.% coating had been selected on the basis of photocatalytic and antimicrobial performance (Chapters 5 and 6). These surfaces along with TiO_2 control surfaces were placed in different brewery environments over a 12 month period. After 3, 10, and 12 months two coupons were removed for measurement of photocatalytic activity by methylene blue degradation, contact angle measurement and scratch adhesion test to assess how robust the coatings are.

Laboratory mechanical tests were done by scratching the coating surfaces using a finger nail, pencils with hardness of 2B and HB, a steel scalpel and a diamond tip. The pencil test was carried out according to ASTM D3363 (Standard test method for film hardness by pencil test). The tape test was based on standard ASTM D3359 (Standard test methods for measuring adhesion by tape test), using Scotch 3M invisible tape. The finger nail, pencil and tape tests did not cause any visible changes to the surface coatings. The scalpel test was performed by cutting the coating surface with a steel scalpel. The scalpel cut into both surfaces, as did the diamond tip.

The scratch adhesion tests were conducted using a Teer ST3001 scratch & wear tester. The coated surfaces were evaluated using a Rockwell diamond tip (radius 200 µm). In the scratch test a diamond stylus is drawn across the coated surface under an increasing load until some failure occurs due to detachment of the coating (Section 4.2.10).

The results of scratch adhesion tests performed on TiO_2, and TiO_2-Mo (7 at. %) coatings before the process trial showed no cracking or flaking around the scratch tracks (Figure 7.11). The images show the end of the scratch tracks, which is the high load end- i.e. these coatings show the scratch track at a maximum load of 40 N. Damage is inevitable but the disturbed coating shows good cohesion to the substrate.

Given the destructive nature of the scratch test and the high load levels used in this test, all coatings were deemed to show sufficient mechanical resistance for use on food and drinks processing surfaces in this trial. Further development and research would be necessary for further improvement in the quality of the coating.

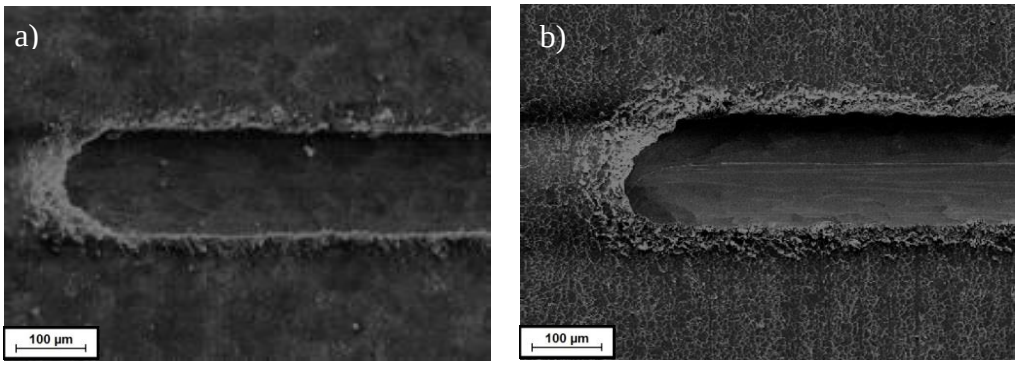

Figure 7.11: SEM image of the scratch test tracks for a) TiO_2, b) TiO_2-Mo (7 at.%) after scratch testing showing no flaking next to the scratch track.

7.4 Mechanical durability of brewery exposed surfaces

Visual inspection of the coatings before and after the three month process trial showed that all the coatings were physically present, though in some cases colour changes were apparent (Figure 7.12), indicating some of the surfaces were soiled or worn. The scratch test results from reference samples (TiO_2-Mo (7 at. %) and TiO_2) which were placed in the dark (wrapped in aluminium foil and kept at room temperature) for three months showed some flaking around the edge of the scratch tracks in comparison to pre-brewery samples. Initially, this was unexpected, as they should show the same mechanical properties as pre-brewery samples. There is a possibility of decomposition of coating in the dark over time. Further investigation of this aspect is required to reveal the underlying problems. The flaking was

less for the TiO_2-Mo (7 at.%) coating which indicates better adhesion of the coating to the substrate in contrast to pure TiO_2 (Figures 7.13, and 7.14).

The scratch test results for the samples which had been placed in three different brewery environments for three months are shown in Figures 7.15-7.23. Some of the coatings show flaking, which in most cases was confined to the area immediately next to the scratch track. Thus the exposure conditions in the breweries seemed to have affected the coatings. However, only one or two replicates were available at any time and batch variability and brewery treatments are likely to affect results, so few conclusions can be drawn. Surfaces from brewery B and C were more disrupted than those from brewery A. Some surfaces show flaking near to the scratch tracks, but for other surfaces flaking is more widespread. This could be due to heat treatment and the different unspecified methods used for cleaning the surfaces at the different breweries.

TiO_2-Mo (7 at.%) was appeared to be better adhered to the substrate than pure TiO_2 (Figure 7.15-7.23) after 3, 10 and 12 months, since more flaking was observed in the TiO_2 samples.

Figure 7.12: Images of coupons after the 3 month brewery trial. U1 = TiO_2, U2 = TiO_2-Mo (7 at.%). Control coupons (13 &14), Brewery A (1 & 2), Brewery B (5 & 6) and Brewery C (9 & 10).

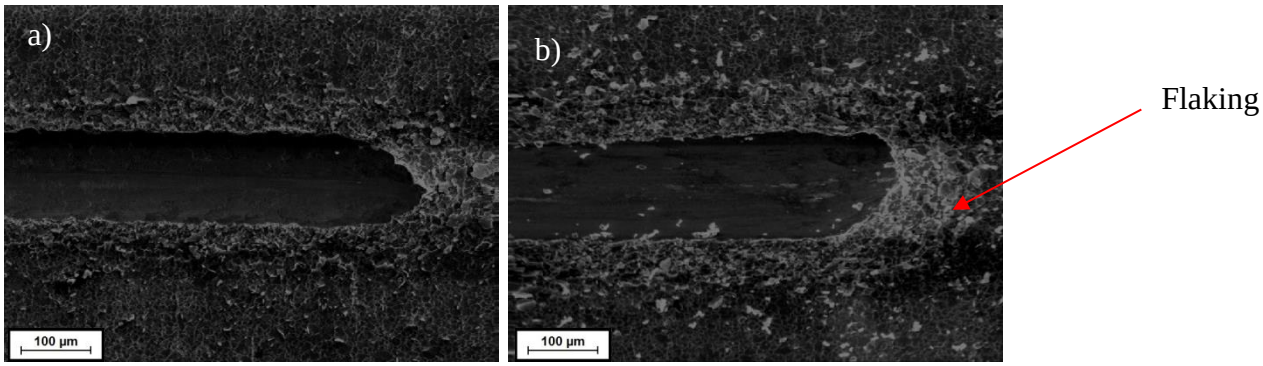

Figure 7.13: SEM image of scratch test tracks a) TiO_2 following annealing at 600 °C prior to brewery trial b) TiO_2 following annealing at 600 °C samples after storage in the dark for 3 months (reference samples) demonstrating a more widespread flaking.

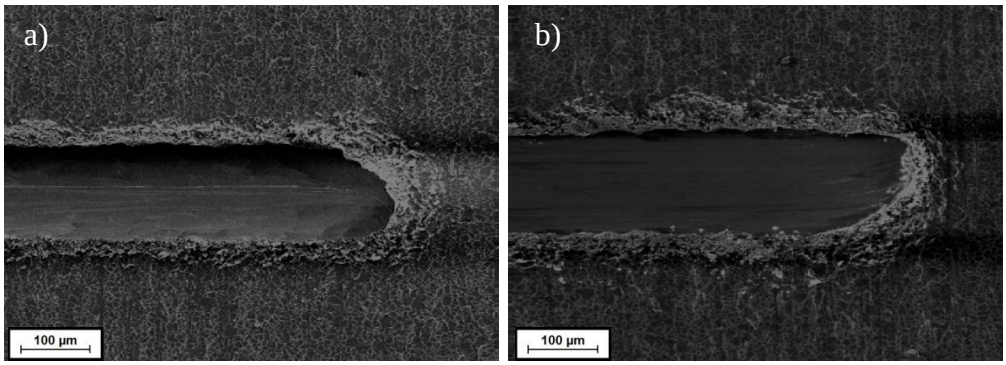

Figure 7.14: SEM image of scratch test tracks a) TiO_2 - Mo (7 at.%) following annealing at 600 °C prior to brewery trial, b) TiO_2-Mo (7 at.%) sample following annealing at 600 °C after storage in the dark for 3 months (reference samples) demonstrating slight flaking next to the scratch track.

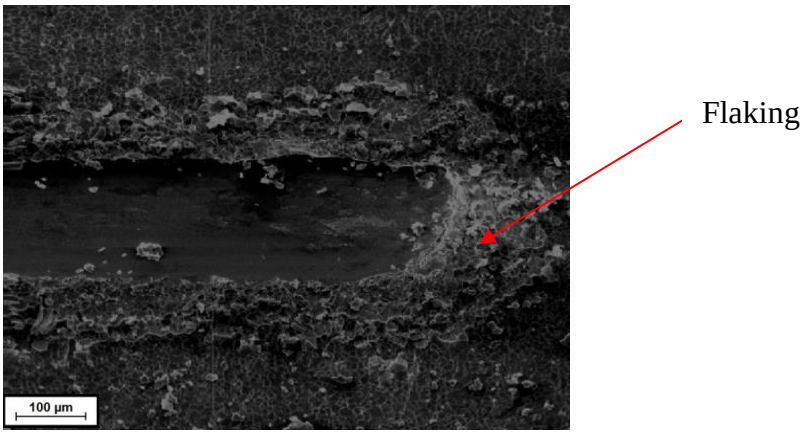

Figure 7.15: Scratch test of TiO_2 coating after use in brewery A for three months, demonstrating a more widespread flaking.

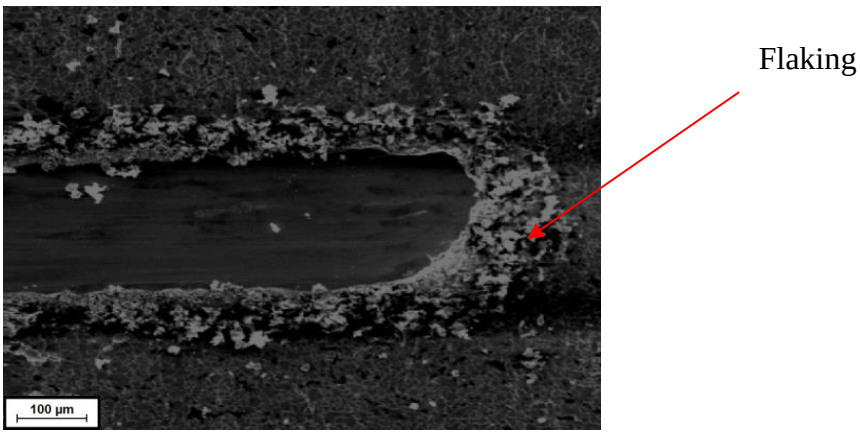

Figure 7.16: Scratch test of TiO_2-Mo (7 at.%) coating after use in brewery A for three, months demonstrating a more widespread flaking.

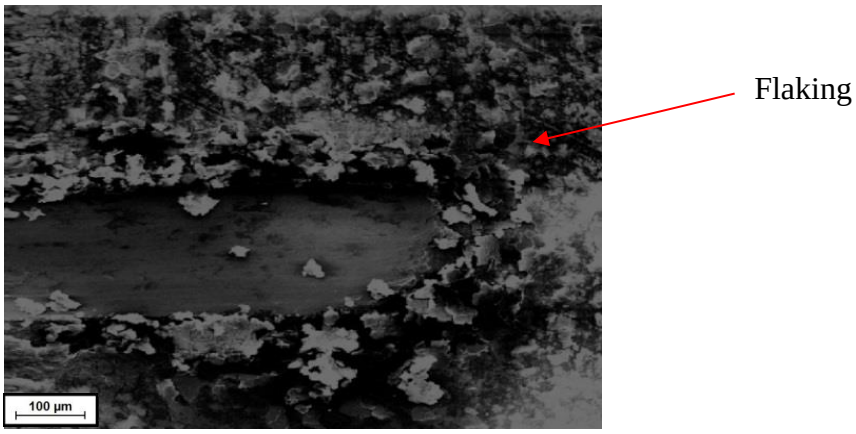

Figure 7.17: Scratch test of TiO_2 coating after use in brewery B for three months, demonstrating a more widespread flaking.

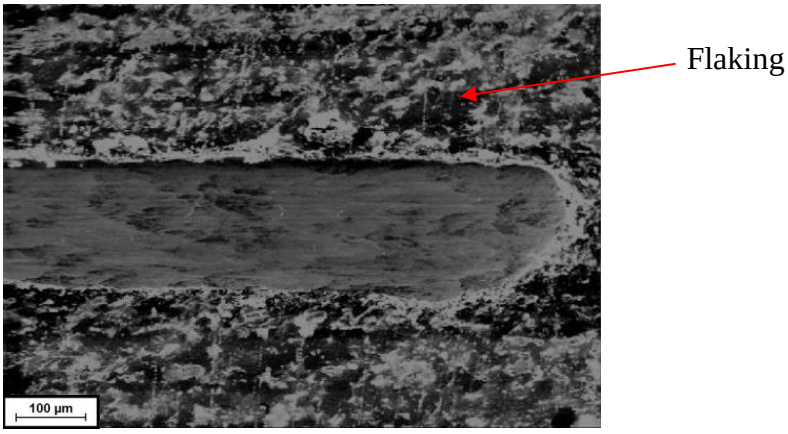

Figure 7.18: Scratch test of TiO_2-Mo (7 at.%) coating after use in brewery B for three months, demonstrating a more widespread flaking.

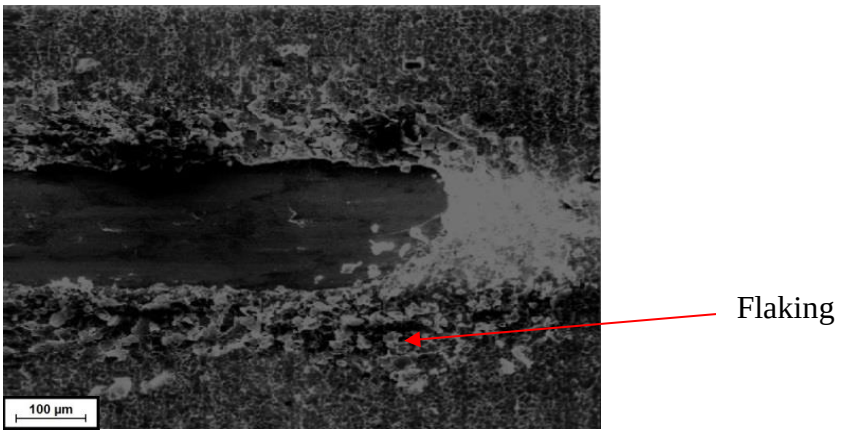

Figure 7.19: Scratch test of TiO_2 coating after use in brewery C for three months, demonstrating a more widespread flaking.

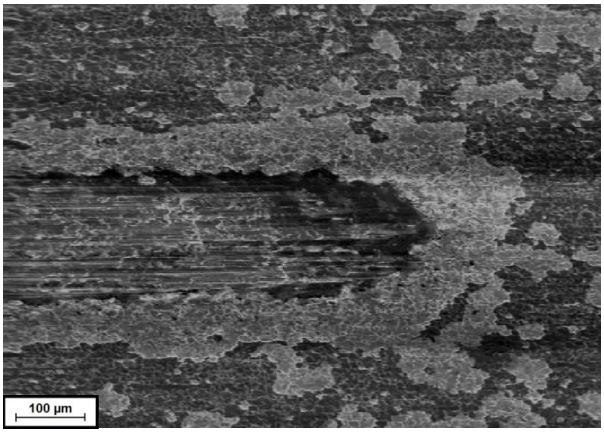

Figure 7.20: Scratch test of TiO_2 coating after use in brewery C for ten months, demonstrating a more widespread flaking.

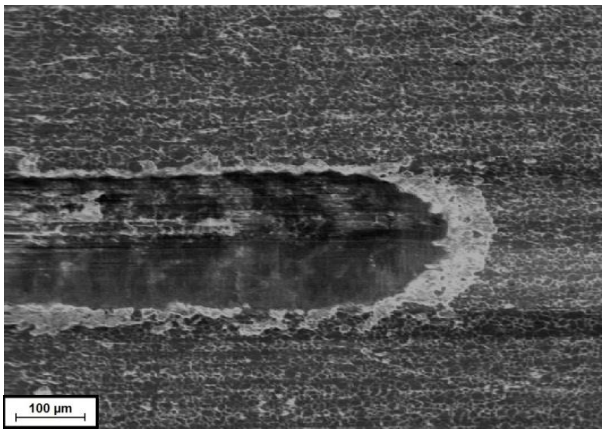

Figure 7.21: Scratch test of TiO_2-Mo (7 at.%) coating after use in brewery C for ten months, demonstrating some flaking.

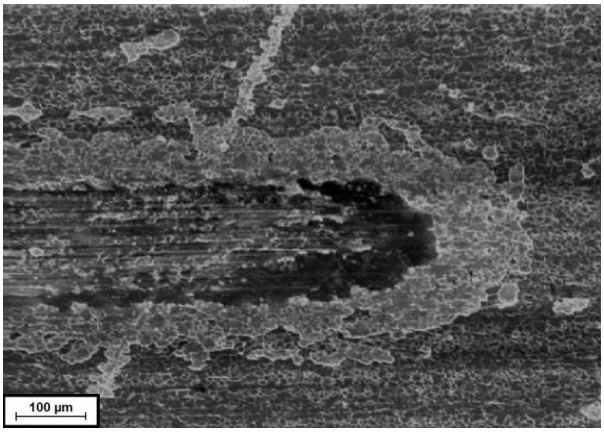

Figure 7.22: Scratch test of TiO_2 coating after use in brewery A for one year, demonstrating a widespread flaking.

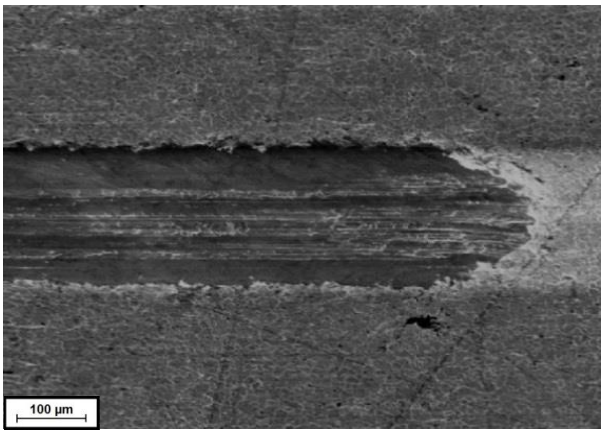

Figure 7.23: Scratch test of TiO_2-Mo (7 at.%) coating after use in brewery A for one year, demonstrating some flaking.

7.5 Photocatalytic activity of TiO_2-Mo (7 at.%) and TiO_2 after 3, 10 and 12 months installation in different breweries

The photocatalytic activities of brewery exposed coatings were monitored by their ability to degrade methylene blue (MB) dye under UV and fluorescent light irradiation (Section 4.2.9). The samples were cleaned with isopropanol (wiping) then with water prior to the MB degradation test.

Comparison of the photocatalytic properties of TiO_2 and TiO_2-Mo (7 at.%) showed that the addition of Mo to the heat-treated TiO_2 surface increased its photocatalytic activity under UV and fluorescent light and this remained the case following the process studies (Chapter 5).

A loss of activity for TiO_2 and TiO_2-Mo (7 at.%) coatings under UV and fluorescent light over time during the brewery trial was seen to varying degrees (Figures 7.24-7.26). However, some of the samples in brewery C had lost most of their activity; this might be due to damage to the coatings as observed via scratch testing, and the effect of cleaning solution, e.g. chemicals and scrubbing methods used in the different breweries, with some conditions (e.g. location, exposure, time since rinse and chemical regime) overcoming the chemical and

mechanical resistance of the coating. There was limited light available for some of the samples, which could also affect the photoactivity of the coatings. Separate light sources were not installed alongside the surfaces, so any activity *in-situ* would rely on irradiation by natural light. In this study the light intensity in the process condition was low, around 0.5 μW cm^{-2} for UV light and 34 μW cm^{-2} for visible light. The controls also lost activity following three months storage in the dark compared to the as deposited samples (UV light) (Figures 7.24-7.26).

Overall, more samples with better monitoring of process conditions should assist in interpretation of the in-use potential of these surfaces. Variability in results between breweries was as follows: In breweries A and B, the TiO_2-Mo (7 at.%) coating was more active than pure TiO_2 under UV and fluorescent light. Overall, the TiO_2 and TiO_2-Mo (7 at.%) coatings lost some of their photoactivity (40-50%) after being placed in the breweries for 10 to 12 months (Figures 7.24, and 7.26). The TiO_2 coatings were more photoactive than TiO_2-Mo (7 at.%) coating after ten months in use in the brewery C. The TiO_2 - Mo (7 at.%) coating showed higher photoactivity under UV light irradiation than TiO_2 coatings after being used for one year in brewery A.

Reduction in photoactivity may also be explained by the presence of soiling on the surface (Figure 7.27) (Section 4.3.5.3). The organic or inorganic materials present on the surface may interfere with photocatalytic activity. It has been reported, that photocatalysts are not especially useful at breaking down heavy contamination, but they are capable of destroying it as it accumulates [7], so, the existence of contaminating material on some part of the coatings coupled with the general environmental stresses will reduce photocatalytic activity.

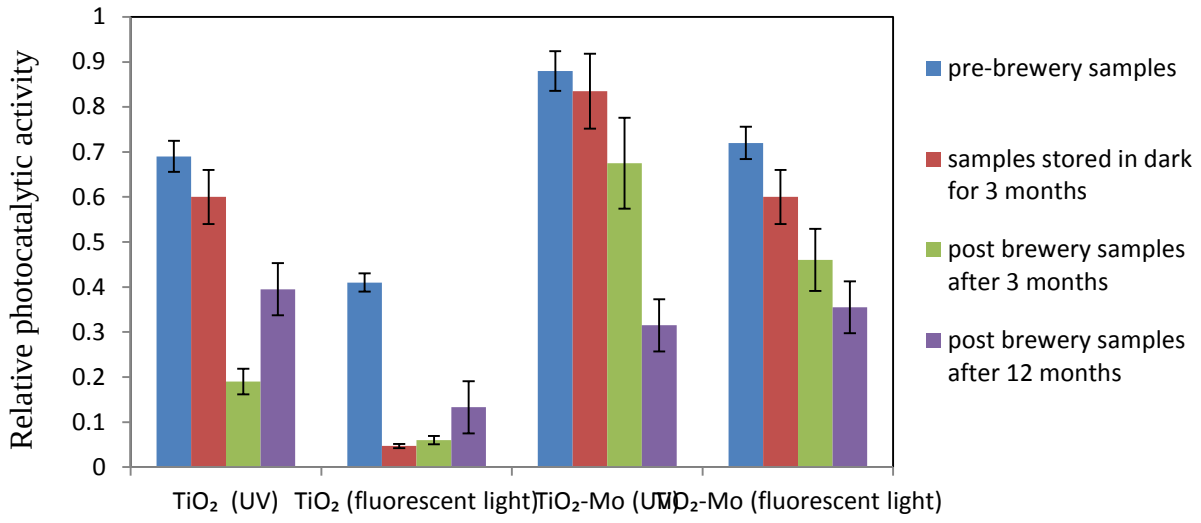

Figure 7.24: Photoactivity of TiO_2 and TiO_2-Mo (7 at.%) coatings after being placed at the brewery A for 3 and 12 months (filler table) demonstrating TiO_2-Mo (7 at.%) coatings were more photoactive than pure TiO_2.

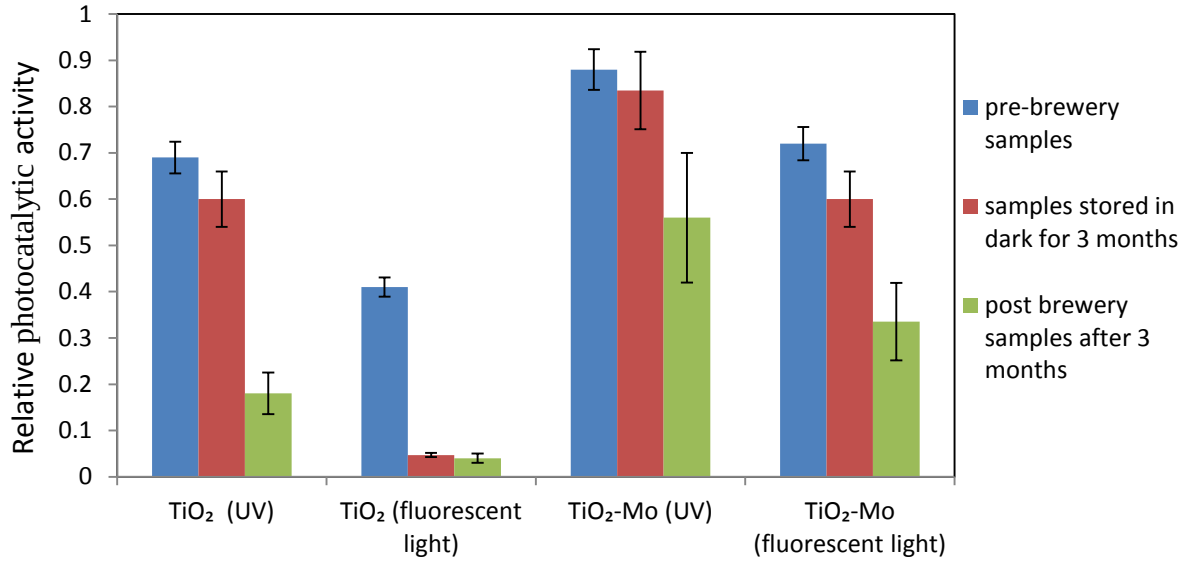

Figure 7.25: Photoactivity of TiO_2 and TiO_2-Mo (7 at.%) coatings after being placed at the brewery B for three months (filler table of the canning machine) demonstrating TiO_2-Mo (7 at.%) coatings were more photoactive than pure TiO_2.

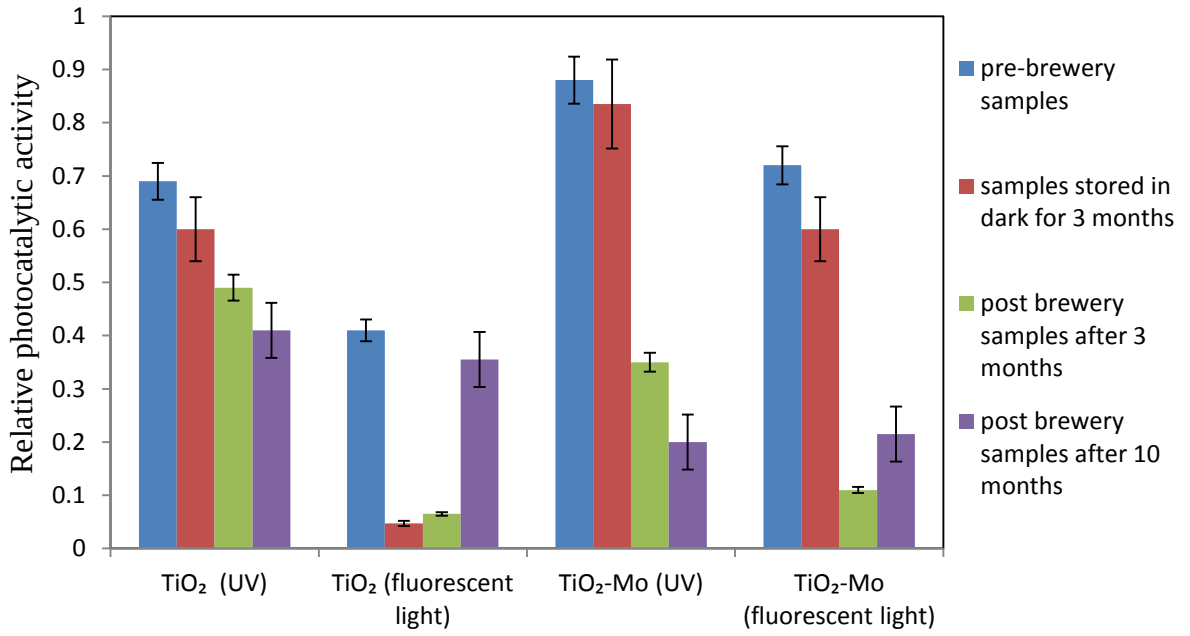

Figure 7.26: Photoactivity of TiO_2 and TiO_2-Mo (7 at.%) coatings after being placed at the brewery C for 3 and 10 months (canning machine) demonstrating pure TiO_2 coatings were more photoactive than TiO_2-Mo (7 at.%) after 10 months installation.

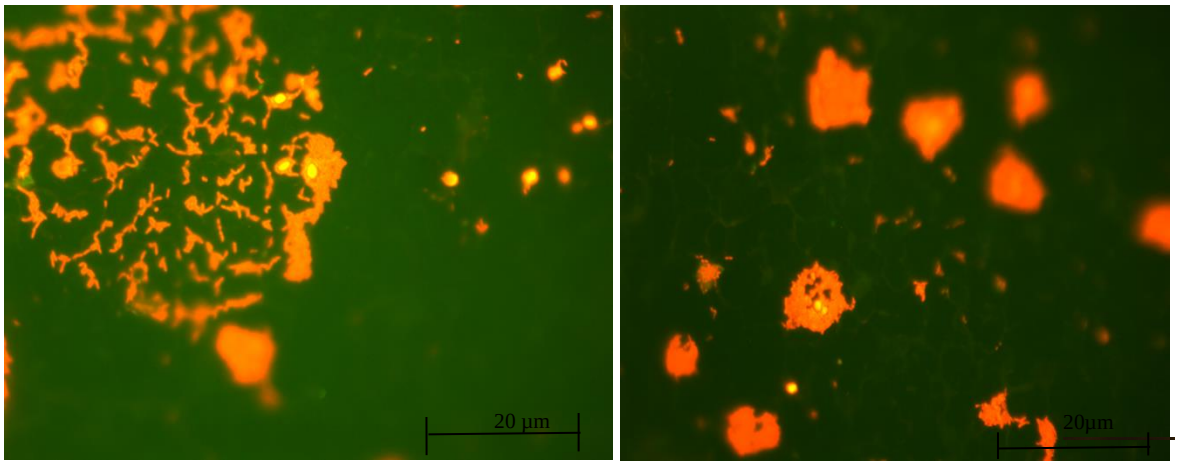

Figure 7.27: Epifluorescent microscopy image of acridine orange staining of TiO_2-Mo (7 at.%) b) TiO_2 coating after being removed from brewery C after 10 months demonstrating the likely present of bacteria and yeast on the surface.

7.6 Retention of Mo in coating after 3, 10 and 12 months detected via by energy dispersive X-ray (EDX) and ICP-AES analysis of the samples

The EDX results showed that the amount of Mo ions lost from the surface was less than 0.5 at. % after 3, 10, and 12 months, indicating a stable structure (Table 7.2). The Inductively Coupled Plasma Atomic Emission Spectroscopy (ICP-AES) analysis of Mo ion release from new coatings further confirmed the EDX results, in that Mo was generally well retained (Figure 7.28). Results show an initial burst of Mo ions release (0.73 ppm) over the first 2 hours followed by steady low level release. The low concentration of Mo ions (<0.04 ppm) being released following the initial 48 hours, suggests that the bulk of Mo is retained in the film and is not readily leachable. This is important in terms of retaining activity but minimising contamination of any product or environments with Mo. ICEP-AES is a more challenging test for assessing leaching than would be encountered *in-situ*, due to constant immersion in liquid.

Table 7.2: Energy dispersive X-ray (EDX) results after brewery trial, showing the Mo content (at. %).

Sample	Mo at.%	Mo at.%
TiO_2-Mo (after three months in dark)	6.9	6.85
TiO_2-Mo (after three months)	6.95	6.85
TiO_2-Mo (after ten months in brewery C)	6.5	6.8
TiO_2-Mo (after one year in brewery A)	6.5	6.83

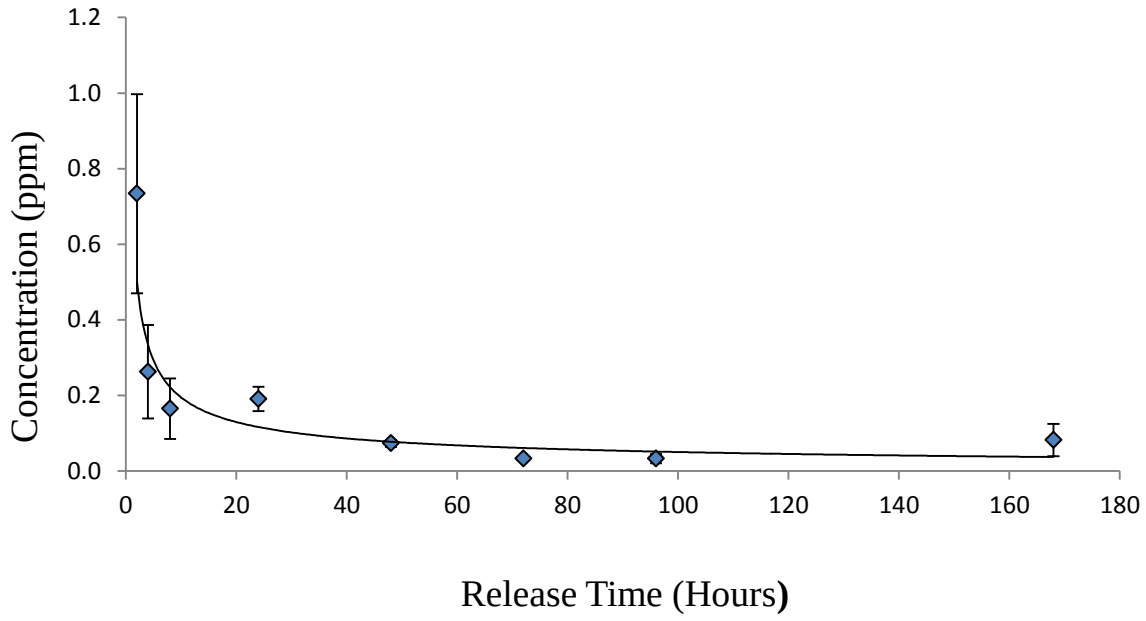

Figure 7.28: Molybdenum ion release determined by Inductively Coupled Plasma Atomic Emission Spectroscopy (ICP-AES) over 168 hour.

7.7 Water contact angle measurements of TiO_2-Mo and TiO_2 coatings after brewery trials

Water contact angles were firstly measured for the coupons immediately on unpacking (dark), and then after 20 hours irradiation. It was noticeable that many of the coupons were heavily soiled so a portion of each sample was cleaned by wiping with 2-propanol dispensed onto a soft cloth, and then with water. Contact angles were re-measured after 20 hours under UVA light, and again after 6 - 7 days in the dark. TiO_2-Mo (7 at.%) surfaces had lower water contact angle values in comparison to pure TiO_2 and hence were more hydrophilic (Figure7.29). For the control samples which were stored in the dark, after light illumination the water contact angle was reduced (i.e. surfaces became more hydrophilic). Low contact angles usually associated with photo-induced hydrophilicity were not observed, even in the cases of control samples. Little difference was noticed between light and dark contact angles. Once the samples were cleaned with isopropanol, the value of the water contact angle increased. It is difficult to interpret the water contact angle measurements due to the low number of replicates and high number of variables (including cleaning methods) because residues from the brewery trial may affect water contact angle. The samples with less soil on them had lower water contact angle values (brewery A).

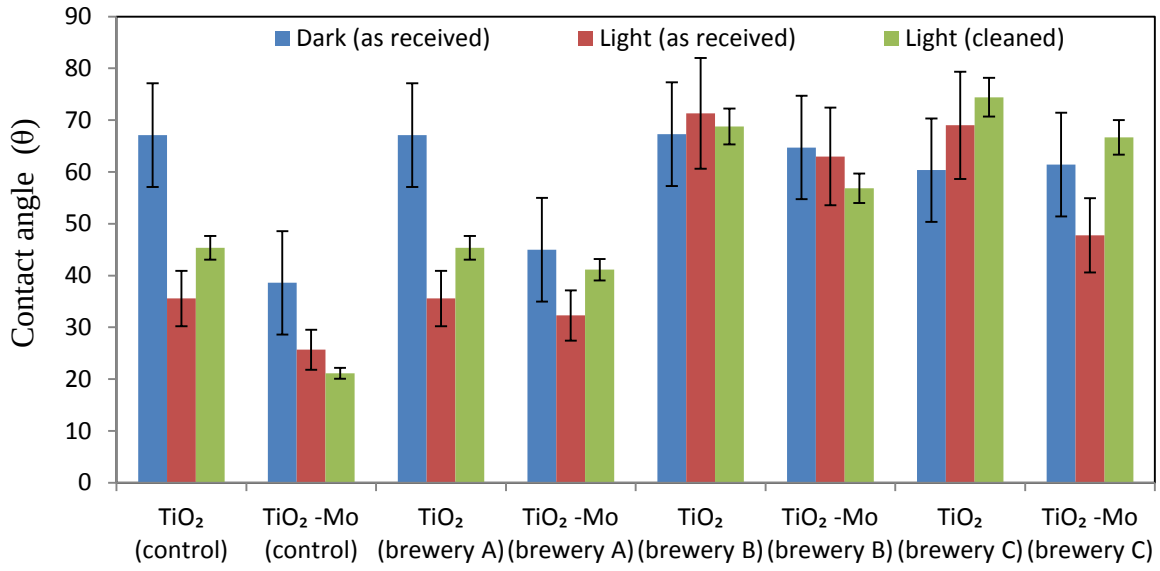

Figure 7.29: Water contact angle data for samples exposed for 3 months within Breweries A, B, C and TiO_2 and of TiO_2-Mo controls (kept in the dark for 3 months). Data for as received surfaces, light exposed surfaces and cleaned light exposed surfaces are included for each surface. It is evident that the samples from Brewery A responded more to light exposure than those for breweries B and C.

7.8 Discussion

The chemical stability of thin film coatings that might be used in the food and beverage industry is an essential parameter. These thin films typically would be exposed to a variety of cleaning agents and protocols. Such chemical solutions can accelerate the deterioration of the films, change the film physical/chemical properties and thus affect photocatalytic performance. In this study, films were treated with 0.02 M HCl, 0.02 M NaOH, ethanol and water, and changes in surface roughness and thickness were assessed. There was no change in thickness of TiO_2, and TiO_2-Mo samples and no chemical damage was observed. There was

no significant reduction in R_a (roughness) value for most of the coatings immersed in natural, basic, acidic and alcoholic solution. However, the S_a values of TiO_2-Mo coatings were slightly reduced in basic solution. These findings alone could not explain the decrease in photocatalytic activity under UV and fluorescent light illumination. One of the reasons which might explain the reduction of photocatalytic activity after surfaces being treated with HCl and NaOH could be the diffusion of chloride and sodium ions into the coatings. It has been reported by several authors that both sodium and chloride ions have detrimental effect on photocatalytic activity [198, 199]. Thus, cleaners containing this type of reagents should be avoided for these coatings and new cleaners need to be developed and recommended. However, more chemical analysis of the surfaces is required.

EDX data indicated no loss of Mo from coatings after immersion in water and alcohol, HCL and NaOH. Navabpour *et al.* [200] investigated the chemical resistance of Ag doped titania coatings by immersing the coatings in HCl and NaOH solutions. In contrast to our work, they found the migration of Ag particles to the surface after immersion in HCl which caused a reduction in the silver content of the coatings.

TiO_2, and TiO_2-Mo coatings showed good adhesion to substrate prior to brewery trials. TiO_2 and TiO_2-Mo were placed into three different Finnish breweries. After brewery use, some of the TiO_2 and TiO_2-Mo (7 at.%) coatings failed on adhesion testing, with flaking evident at the edge of scratches. The mechanical durability test performed on samples after the process trial, confirmed the visual assessment of coating appearance, as many of the surfaces were heavily soiled and worn, especially those exposed at breweries B and C. TiO_2 and TiO_2-Mo 7 at.% coatings showed some flaking, which in most cases was confined to the area immediately next to the scratch track. Some of the samples, however, showed a more widespread flaking particularly those exposed in brewery C. This may be related to significant stress experienced by coatings during the heat treatment (annealing) due to mismatch in thermal expansion

coefficients between the coating and the substrate. It has been noted that, not all of the annealed coatings were affected. This was considered to be due to variations in the environmental conditions (cleaning regime, surface contamination, location, etc.) within the breweries.

The TiO_2 and TiO_2-Mo (7 at.%) coatings were placed in canning machines at breweries B and C and on a filler table handling water and soft drinks in brewery A. The TiO_2 and TiO_2-Mo (7 at.%) lost some of their photocatalytic activity after being placed in breweries for up to 12 months. Any loss of photoactivity may be explained by the damaging effect of different cleaning protocols e.g. cleaning and disinfection chemicals and physical cleaning methods used in the different breweries and the presence of biofouling material on the coated surfaces. There was also limited light irradiation available for some of the samples; surfaces were only exposed to fluorescent light (only in day time). Fouling could mask surface active sites and cause an increase in opacity and light scattering of TiO_2 and TiO_2-Mo (7 at. %) films, which leads to a decrease in light transmission onto the photocatalyst. Epling *et al.* [201], stated that some organic or inorganic chemicals can deactivate or deteriorate the photocatalytic effect of TiO_2. In addition, even low intensity UV light exposure can make a surface more hydrophilic, which may encourage adsorption of organic materials from liquid, thus disturbing the photocatalytic activity of the coatings [201]. Thus, the photocatalytic functionality of TiO_2 may have been insufficient due to the nature of the coatings themselves, their location and treatment.

Work by others has shown that canning machines were markedly less prone to accumulation of microorganisms than bottling machines [202]. Further, horizontal surfaces are more prone to microbial accumulation and should be avoided in constructions as much as possible. Furthermore, biofilm formation occurred on certain surfaces despite daily cleaning and disinfection [202]. Thus, in these situations deposits formed by reaction processes or

microbes usually cannot be wholly removed from stainless steel with water [203]. Cleaning agents give varying degree of improvement on the latter. Treatment of clean test surfaces with a hypochlorite-based disinfectant was shown to be effective after an exposure of 10 min against all the microbes tested whereas an isopropanol-based cleaning agent was effective against all the vegetative cells tested [204]. In the presence of soil, hypochlorite was effective against *Listeria monocytogenes* and *Pseudomonas aeruginosa* [204]. If surfaces were soiled with chemical residue and not cleaned sufficiently, it is possible that this may have an effect on photocatalytic activity. Conversely over aggressive cleaners might damage the surface, as noted previously (acid and base sensitivity).

Priha *et al.* [205] investigated the effect of TiO_2 and Ag doped TiO_2 on process hygiene in the beverage industry over a 15 month period. They prepared coatings using the atomic layer deposition (ALD) method. They found that most of the Ag dissolved, and some of TiO_2 coatings were partly damaged. In our work, EDX results indicate that there was little loss of Mo ions from the coatings, after 12 month exposure within breweries. The results were confirmed by ICP-AES analysis monitoring of Mo ion release into solution after 180 hours. The majority of the Mo is retained on the surface and the metal is not readily leachable. This indicates a stable surface, with any activity of the Mo retained in the film so, this performance is better than that of Ag.

Hydrophilicity can occur when irradiated TiO_2 generates electrons and holes. The electrons tend to reduce the Ti (IV) cations to the Ti (III) state, and the holes oxidize the O_2^- anions. In the process, oxygen atoms are ejected, creating oxygen vacancies. Water molecules can then occupy these oxygen vacancies, producing adsorbed OH groups, which tend to make the surface hydrophilic [7, 206]. However, depending upon composition and processing, the surface can have more photocatalytic character and less superhydrophilic characteristics, or vice versa [207]. The synergistic effect of photocatalysis and hydrophilicity can be explained

as follows. Because more OH group can be adsorbed on the surface due to hydrophilicity, the photocatalytic activity is enhanced [208]. So, hydrophilicity can improve photocatalysis. On the other hand, the film surface can absorb contaminated compounds, which tend to turn the hydrophilic surface into a hydrophobic surface. Photocatalysis can decompose the organic compounds on the surface resulting in the restoration of hydrophilicity. Thus, photocatalysis can improve hydrophilicity and maintain this characteristic for a long time [209].

In this experiment, doping of TiO_2 with Mo had an effect on hydrophilicity. The water contact angle on TiO_2-Mo (7 at.%) was lower than pure TiO_2. The water contact angle of TiO_2-Mo (7 at.%) coating was reduced after light irradiation for all three breweries. However, the water contact angle for TiO_2 was not reduced for samples placed in brewery B and C after light irradiation. This was expected since TiO_2-Mo (7 at.%) had a higher photocatalytic activity than TiO_2 . The effect of light on wettability was more pronounced in the case of the reference surfaces than those having undergone brewery exposure conditions. The higher water contact angle in the brewery trials in comparison to the control samples might be explained by the accumulation of fouling material on the surface and the effect of cleaning agents.

7.9 Conclusion

The mechanical and chemical durability of pure TiO_2 and Mo-doped TiO_2 coatings were evaluated prior to process studies. They showed acceptable mechanical durability for *in situ* trials. All of the deposited TiO_2 - Mo (7 at.%), and TiO_2 thin films showed sufficient chemical resistance in neutral, alcohol, acidic and basic solution. No significant change in thickness was observed, which was expected. However, a reduction in roughness (S_a) value was observed. There was a small reduction in the Mo content after samples were treated with

acid and base. There was also a reduction in photocatalytic activity under UV light irradiation after the immersion of samples in acidic and basic solutions. So, when surfaces are used *in situ*, cleaning and disinfection products need to be carefully considered so as not to interfere with intended stability and photoactivity of the surface. The undoped TiO_2 and TiO_2 - Mo (7 at.%) samples were placed in the brewery environments for 12 months because they were previously shown to be the most effective under fluorescent and UV light. Both of the surfaces developed for this study undoped TiO_2 and TiO_2 - Mo (7 at.%) coatings showed adequate adhesion properties after 3, 10, and 12 months. Large area of detachment of coatings from substrate was not observed, although some of the coatings showed failure on occasion. Both coatings lost some of their photocatalytic activity after one year in brewery A. Mo was well retained in the coating.

In conclusion, the coatings have potential as robust photocatalytic materials to help reduce contaminant load over and above cleaning and disinfection procedures in the food processing environment. The final process study publication regarding microbiology assessment of these coating will be presented in appendix C of this thesis.

Chapter 8: Concluding remarks

8.1 Thesis summary

The aim of this project was to develop photocatalytic coatings that inhibit/inactivate attachment of microorganisms under fluorescent light, particularly those of interest to the brewery industry. In order to achieve this aim several tasks were carried out. The initial objective was to optimise the photocatalytic activity of the titania coatings via transition metal doping. This was to be achieved through the use of pulsed reactive unbalanced magnetron sputtering with the incorporation of various transition dopant metals and the use of pulse power supply.

All as-deposited coatings were amorphous, but developed crystalline structures after annealing. The inclusion of the dopant influenced the crystallisation of the coatings with some dopants tending to supress crystallisation and others suppressing or promoting an anatase to rutile transition.

The photocatalytic activities of Mo-doped TiO_2 coatings under fluorescent light were improved significantly (31 %) over that of pure TiO_2 annealed at the same temperature. Different transition metals with different dopant contents were separately screened for optimum photocatalytic activity. Of the transition metal dopants studied, molybdenum and niobium were found to be the most successful in enhancing the photocatalytic properties of titania under both UV and fluorescent lighting conditions. The best results for Mo and Nb doped titania were obtained with 7 at. % molybdenum and 0.25 at.% niobium, 12% improvements in photoactivity relative to pure titania under were achieved fluorescent light (annealing temperature were 600 °C and 400 °C, respectively). The UV light photoactivity of

W (3.8 at.%) and Ta (1.1 at.%) doped coatings also showed a slight improvement over pure titania coatings. However, the activity under fluorescent light was not improved. It was assumed that the optimum amounts of these transition metal dopants enhanced photoactivity by slowing the recombination rate of the photogenerated charge carriers.

The second objective was to evaluate the antimicrobial properties of selected TiO_2 coatings doped with different transition metals, as well as the metals themselves, and their thin film oxide coatings. This was investigated using *E. coli* as a model organism under fluorescent light. The antimicrobial assay for photocatalytic coatings is technically complex, primarily due to many variables neccessary different experimental conditions (UV/Vis irradiation), length of exposure, different TiO_2 photocatalysts, number of replicates and microorganisms employed). In this study the ISO:27447:2009 standard was used as a guide to develop and perfom the antimicrobial assay.

TiO_2-Mo 7 at. % and TiO_2 -W 10 at. %, inactivated *E. coli* after 24 hours in the presence and absence of light, which confirmed dual functionality of the coatings. TiO_2 -Nb 0.25 at. %, and TiO_2 -W 3.8 at. % coatings were only antimicrobial during fluorescent light illumination. Zones of inhibition was observed for any surfaces when placed on a culture of *E. coli*, indicating no diffusion of ions from surface, or concentrations were below an inhibitory level. Any innate antimicrobial effects are likely to be due to close contact between cell and coating.

Some of the transition metals and their oxide coatings also showed antimicrobial activity. W, WO_3, Mo and MoO_3 coatings inactivate *E. coli* after 6, 8, and 12 hours in the absence of TiO_2. Nb and Nb_2O_5 coatings did not show any antibacterial activity compared to other transition metals and their oxides, although an MIC of 12-14 mg/L was demonstrated. A dilute beer soil on the surface did not affect photocatalytic activity, although more heavily soiled samples lost activity. These results emphasise the importance of regular cleaning and

disinfection *in-situ* to minimise accumulation of soil. This study shows that illumination by fluorescent light is capable of activating a novel antimicrobial photocatalytic surfaces. These coatings provide a promising direction for future applications in the food and beverage industries, and in medical and other hygienic environments.

The final objective was to assess the chemical and mechanical durability of selected coatings and place them into breweries in order to assess their effectiveness over time in terms of photocatalytic activity, mechanical durability and water contact angle measurements. Pre-brewery trials confirmed that $TiO_{2,}$ and TiO_2 -Mo 7 at. % showed sufficient mechanical and chemical durability. However, there was a variation in photocatalytic activity after the chemical durability test particularly after exposure to acid and alkali, although there was no significant change in Mo content, as measured by EDX. Therefore, further work is needed to improve the chemical durability of these coatings to ensure stability in service and to cleaning procedures. Characterisation on the effect of acids and bases on the structure of the coatings maybe required in order to recommend appropriate cleaning protocols *in-situ*.

Photocatalytic activity, mechanical durability and contact angle measurement were assessed after 3, 10 and 12 months placement in three Finnish breweries. TiO_2 and TiO_2-Mo 7 at. % coatings retained approximately 50% of their photocatalytic activity after twelve months placement in the brewery. However, the results varied significantly between breweries. This was likely to be due to a number of factors including position of the samples and the cleaning regime used. The number of replicates was also too low. If surfaces were soiled with any residue and not cleaned sufficiently, this may have an effect on photocatalytic activity. The results of scratch adhesion tests performed on samples (post brewery exposure) showed some flaking, which in most cases was confined to the area immediately next to the scratch track. This may indicate that over-aggressive cleaning agents may damage the surfaces during

normal scene. Therefore, the mechanical durability of the coatings should be further improved to withstand severe conditions including cleaning with a range of known cleaning agents.

The activity of the TiO_2 -Mo 7 at. % and TiO_2 coatings in terms of inhibiting microbial colonisation on equipment surfaces at two brewery filling lines were also studied. This study was performed in order to narrow the gap between bench-scale experimental work under ideal conditions and functionality in real industrial environments. This was a final part of the project of which this work was part. The major findings from this study was that the run time after washes and location on filling lines had a significant influence on the number and type of adhering microbes on surfaces, whereas the total exposure time or coating type did not. The study also showed that the two filling lines had characteristic bacterial communities, the major species belonging to *Acinetobacter* sp., lactic acid bacteria and enterobacteria. Thus, in spite of promising *in vitro* data showing antimicrobial properties of doped photocatalytic coatings represented in this thesis (Chapter 6), no effect on microbial numbers on the surfaces was discerned *in-situ*. Most of the studies with photocatalytic coatings so far have been based on laboratory experiments. As a result, coatings with good mechanical and chemical durability and thus suitable for industrial surfaces have been developed, but the efficiency of these coatings in reducing the number of microorganisms on the surfaces in the challenging beverage process conditions demands further investigation. The results of microbiological assessment will be presented in an Appendix C of this thesis [210].

The TiO_2-Mo 7 at.% coated surfaces proved to be usable in a challenging brewery environment. In the manufacture of the surfaces, deposition parameters and surface characteristics must be controlled in order to maintain optimum photocatalytic activity. Although the Mo-doped surface is also active in the dark, there should be sufficient light in

the environment for photocatalytic activity. The lack of Mo ion leaching is of benefit and makes the coating potentially applicable for use as a hygienic surface, although perhaps not for food contact. The size of the surface that can be coated would need to be up-scaled to an industrial level and the length of time examined to establish if and how long before re-coating of the surface is required.

8.2 Conclusions

- Of the surfaces produced, the best results in terms of photoactivity under fluorescent and UV light irradiation were achieved with TiO_2 doped with 7 at.% Mo and an annealing temperature of 600 °C giving a mixed phase anatase/rutile structure.
- TiO_2-Mo 7 at.% and TiO_2 -W 10 at. %, coating showed antimicrobial activity after 24 h light irradiation and 24 h incubation in the dark. TiO_2-W 3.8 at.% and TiO_2-Nb 0.25 at.%, showed no antibacterial activity in the dark, and bacteria were only killed on the surfaces in the presence of fluorescent light, showing a photo-killing activity. TiO_2-Mo 7 at.% and TiO_2-W 10 at.% coatings present a dual function.
- TiO_2-Mo 7 at.% coating significantly reduced microbial numbers even in the presence of a typical brewery soil. Thus, the surface may act as a secondary level defence against microbial populations and proliferation between disinfection/cleaning cycles.
- W, WO_3, Mo and MoO_3 coatings inactivate *E. coli* over shorter periods of time in comparison to titania and doped titania coatings. The Nb and Nb_2O_5 coatings did not show any antimicrobial activity.
- TiO_2 and TiO_2-Mo 7 at.% coatings showed some mechanical and chemical durability for *in situ* trials, which could be improved.
- TiO_2 and TiO_2-Mo 7 at.% coatings were placed in brewery environments for 12

months. They showed overall adequate adhesion properties, although some of the coatings showed failure on occasion.

- Both coatings lost some (50%) photocatalytic activity over a 12 months period.
- Although these surfaces showed good mechanical, chemical durability and antimicrobial activity, no clear effect on microbial numbers on the surfaces showed in process study. Therefore, the effectiveness of these coatings in decreasing the number of microorganisms on the surfaces in the challenging beverage process conditions demands further investigation.

8.3 Future work

Based on the main findings of the work and the questions arising from the research carried out, in order to develop the surfaces so that they can be recommended to use *in-situ* the following work is suggested:

- Characterise the surfaces to identify the chemical and structural relationships between TiO_2 and dopants e.g. XPS and TEM. The position of the doping element in the titania crystal lattice is a factor of high importance for the modification of titania photocatalytic properties through the use of dopants. Despite widely-known suggestions [72-74] that the ionic radii of the dopants govern their position in the titania lattice, detailed structural characterisation/analysis a valuable contribution to the understanding of the structure property relationships of doped photocatalysts surfaces.
- The production method should be managed in a way that provides effective process control and reproducible results, regardless of scale up.

- No clear effect of coatings on microbial numbers in the brewery environment could be shown, there were only five replicates and a high number of variables (location, exposure, time since rinse, batch variability). Therefore for future studies, more replicates and fewer variables should be employed in order to fully understand the effect of coatings on microbial population in more challenging brewery environments and to provide statistically significant data.
- The surfaces should be optimized in terms of adhesion and durability for best use in the industrial environment, by using different substrates or surface treatments before start of deposition (such as ion assisted treatments). As it has been reported previously the choice of substrate and surface treatment can have an effect on photocatalytic and physical properties of coatings.
- The potential use of transition metal oxide coatings as antibacterial surfaces could be investigated. The transition metals and their oxide coatings (Mo, MoO_3, W and WO_3) eradicate the bacteria in dark and hence are innately antimicrobial. Further research is required to look at chemical and mechanical durability of these coatings and their potential use in different environments that require high levels of hygiene.
- Little information could be found concerning the mode of action of Mo and W as antibacterial metals. More work should be done to understand their mode of action such as using FT-IR, Raman spectroscopy, and TEM to look at the effect of Mo and W on the structure of microorganisms. FT-IR and Raman spectroscopy provides spectra of all the components in the cells, including proteins, peptides, lipids and polysaccharides.
- The activity of surfaces against different microorganisms (bacteria, viruses, fungi) should be tested in order to investigate potential application in different environments.

- More extensive surface characterisation should be performed after *in-situ* trials. Different surface characterisation techniques such as Time of Flight Secondary Ion Mass Spectroscopy or FT-IR could be employed in order to investigate the effect of cleaning, soiling and etc. on coated surfaces. Time of Flight Secondary Ion Mass Spectroscopy could provide information regarding to presence of any cleaning solutions or soil on the surface.
- In real situations surfaces are in contact with different soil and food residues. The effect of different soil on antibacterial activity of these coatings could be investigated further. Although, the photocatalytic surfaces produced in this project were used in the brewery industry, other industries might also be a potential market.
- Each industrial environment will have its own cleaning regime. Most of the cleaning solutions used in food or beverage industries have been designed for stainless steel not for photocatalytic coated stainless steel. Therefore, the most appropriate regime should be identified for these photocatalytic surfaces.

References

1. O. Carp; C. L. Huisman and A. Reller, Photoinduced reactivity of titanium dioxide. *Progress in Solid State Chemistry* **2004,** 32, 33-117.
2. Z.Y. Chen; Y. Hu; T.C. Liu; C.L. Huang and T.S. Jeng, Mesoporous TiO_2 thin films embedded with Au nanoparticles for the enhancement of the photocatalytic properties. *Thin Solid Films* **2009,** 517, 4998-5000.
3. K. Shankar; J.I. Basham; N.K. Allam; O.K. Varghese; G.K. Mor; X. Feng; M. Paulose; J.A. Seabold; K.S. Choi and C.A. Grimes, Recent advances in the use of TiO_2 nanotube and nanowire arrays for oxidative photoelectrochemistry. *The Journal of Physical Chemistry C* **2009,** 113, (16), 6327-6359.
4. K. Demeestre; J. Dewulf; T. Ohno; P.H. Salgado and H.V. Langenhove, Titanium dioxide mediated heterogeneous photocatalytic degradation of gaseous dimethyl sulfide: parameter study and reaction pathways. *Applied Catalysis B: Environmental* **2005,** 61, 140-149.
5. A. Fujishima and k. Honda, Electrochemical photolysis of water at a semiconductor electrode. *Nature* **1972,** 238, 37-38.
6. A. Mills and S.L. Hunte, An overview of semiconductor photocatalysis. *Journal Photochemistry and Photobiology A: Chemistry* **1997,** 108, 1- 35.
7. A. Fujishima; T.N. Rao and D.A.Tryk, Titanium dioxide photocatalysis. *Journal of Photochemistry and Photobiology A: Chemistry* **2000,** 1, 1-21.
8. I.P. Parkin and R.G. Palgrave, Self-cleaning coatings. *Journal of Materials Chemistry* **2005,** 15, 1689–1695.
9. L. Miao; S.Tanemura; Y. Kondo; M. Iwata; S. Toh and K. Kaneko, Microstructure and bactericidal ability of photocatalytic TiO_2 thin films prepared by rf helicon magnetron sputtering. *Applied Surface Science* **2004,** 238, 125–131.
10. D. M. Alrousan; P. S. Dunlop; T. A. McMurray and J. A. Byrne, Photocatalytic inactivation of *E. coli* in surface water using immobilised nanoparticle TiO_2 films. *Water Research* **2009,** 43, 47- 54.
11. U. Diebold, The surface science of titanium dioxide *Surface Science Reports* **2003,** 48, 53-229.

12. A.L. Linsenbigler; G. Lu and J.T. Yates, Photocatalysis on TiO_2 surfaces: principles, mechanisms, and selected results. *Chemical Reviews* **1995,** 95, 735-758.
13. D.H. Solomon and D.G. Hawthorne, Chemistry of pigments and fillers. **1983**, 51 - 80.
14. D. Chatterjee and S. Dasgupta, Visible light induced photocatalytic degradation of organic pollutants. *Journal of Photochemistry and Photobiology C: Photochemistry Reviews* **2005,** 6, 186-205.
15. T.L. Thampson and J.T. Yates, Surface science studies of the photoactivation of TiO_2 - new photochemical processes. *Chemical Reviews* **2006,** 106, 4428-4453.
16. N. Murakami; T. Kamai; T. Tsubota and T. Ohno, Novel hydrothermal preparation of pure brookite-type titanium (IV) oxide nanocrystal under strong acidic conditions. *Catalysis Communications* **2009,** 10, 963-966.
17. K. Tanaka; M.F. Capule and T. Hisanaga, Effect of crystallinity of titanium dioxide on its photocatalytic action *Chemical Physics Letters* **1991** 187, 73-76.
18. S. Banerjee; J. Gopal; P. Muraleedharan; A.K. Tyagi and B. Raj, Physics and chemistry of photocatalytic titanium dioxide: visualization of bactericidal activity using atomic force microscopy. *Current Science* **2006,** 90, (10), 1378-1383.
19. M. Boehme and W. Ensinger, Mixed phase anatase/rutile titanium dioxide nanotubes for enhanced photocatalytic degradation of methylene-blue. *Nano-Micro Letters,* **2011,** 3, 236-241.
20. D.C. Hurum; A.G. Agrios and K.A. Gray, Explaining the enhanced photocatalytic activity of Degussa P25 mixed-phase TiO_2 using EPR. *Journal of Physical Chemistry B* **2003,** 107, 4545-4549.
21. D. Jiang; S. Zhang and H. Zhao, Photocatalytic degradation characteristics of different organic compounds at TiO_2 nanoporous film electrodes with mixed anatase/rutile phases. *Environmental Science and Technology* **2007,** 41, 303-308.
22. S. Mo and W. Ching, Electronic and optical properties of three phases of titanium dioxide : Rutile, anatase and brookite. *Physical Review B* **1995,** 51, 13023-13032.

23. F. Chen; X. Yang and Q. Wu, Photocatalytic oxidation of *Escherischia coli,* Aspergillus niger, and formaldehyde under different ultraviolet irradiation conditions. *Environmental Science and Technology* **2009,** 43, 4606-4611.
24. J. Rawat; S. Rana; M. M. Sorensson and R. D. Misra, Anti-microbial activity of doped anatase titania coated nickel ferrite composite nanoparticles. *Materials Science and Technology* **2007,** 23, 97- 102.
25. K. Sunada; T. Watanabe and K. Hashimoto, Bactericidal activity of copper-deposited TiO_2 thin film under weak UV light illumination. *Environmental science & technology* **2003,** 37, 4785-4789.
26. K. Page; M. Wilson and I. P. Parkin, Antimicrobial surfaces and their potential in reducing the role of the inanimate environment in the incidence of hospital-acquired infections. *Journal of Materials Chemistry* **2009,** 19, 3819–3831.
27. L. Caballero; K.A.Whitehead; N.S Allen and J . Verran, Inactivation of *Escherichia coli* on immobilized TiO_2 using fluorescent light. *Journal of Photochemistry and Photobiology A: Chemistry* **2009,** 202, (2-3), 92-98.
28. L. Caballero; K.A. Whitehead; N.S.Allen and J. Verran, Photocatalytic inactivation of *Escherichia coli* using doped titanium dioxide under fluorescent irradiation. *Journal of Photochemistry and Photobiology A: Chemistry* **2014,** 276, 50-57.
29. A. Di Paola; G. Marcı`; L. Palmisano; M. Schiavello; K. Uosaki; S. Ikeda and B. Ohtani, Preparation of polycrystalline TiO_2 photocatalysts impregnated with various transition metal ions: characterization and photocatalytic activity for the degradation of 4-Nitrophenol. *Journal of Physical Chemistry B* **2002,** 106, 637-645.
30. K. Sunada; T. Watanabe and K. Hashimoto, Studies on photokilling of bacteria on TiO_2 thin film. *Journal of Photochemistry and Photobiology A: Chemistry* **2003,** 156, 227-233.
31. Z. Huang; P.C. Maness; D.M. Blake; E.J. Wolfrum; S.L. Smolinski and W.A. Jacoby, Bactericidal mode of titanium dioxide photocatalysis. *Journal of Photochemistry: Photobiology A: Chemistry* **2000,** 130, 163-170.
32. J. Kiwi and V. Nadtochenko, Evidence for the mechanism of photocatalytic degradation of the bacterial wall membrane at the TiO_2 interface by ATR-FTIR and laser kinetic spectroscopy. *Langmuir* **2005,** 21, 4614-4631.

33. H.A. Foster; I.B. Ditta; S. Varghese; A. Steele, Photocatalytic disinfection using titanium dioxide: spectrum and mechanism of antimicrobial activity. *Applied Microbiology and Biotechnology* **2011,** 90, 1847-1868.
34. V. Nadtochenko; A. Rincon; S. Stanka and J. Kiwi, Dynamics of *E. coli* membrane cell peroxidation during TiO_2 photocatalysis studied by ATR-FTIR spectroscopy and AFM microscopy. *Jounal of Photochemistry and Photobiology A: Chemistry* **2005,** 169, 131-137.
35. W. Kangwansupamonkon; V. Lauruengtana; S. Surassmo and U. Ruktanonchai, Antibacterial effect of apatite-coated titanium dioxide for textiles applications. *Nanomedicine: Nanotechnology, Biology, and Medicine* **2009,** 5, 240-249.
36. C. Chung; H. Lin ; C. Chou ; P. Hsieh ; C. Hsiao; Z. Shi and J. He, Inactivation of *Staphylococcus aureus* and *Escherichia coli* under various light sources on photocatalytic titanium dioxide thin film. *Surface and Coatings Technology* **2009,** 203, 1081-1085.
37. D. Naumann; C. Shultz; A. Sabisch; M. Kastowsky and H. Labischinsi, New insights into the phase behaviour of a complex anionic amphiphile: architecture and dynamics of bacterial deep rough lipopolysaccharide membranes as seen by FTIR, X-ray, and molecular modelling techniques *Journal of Molecular Structure* **1989,** 214, 213-246.
38. D.W. Sheel; L.A. Brook; I.B. Ditta; P. Evans; H.A. Foster; A. Steele and H.M. Yates, Biocidal silver and silver/titania composite films grown by chemical vapour deposition. *International Journal of Photoenergy* **2008,** 2008, 11.
39. E.V. Skorb; L.I. Antonouskaya; N.A. Belyasova; D.G. Shchukin; H. Möhwald and D.V. Sviridov, Antibacterial activity of thin-film photocatalysts based on metal-modified TiO_2 and TiO_2: In_2O_3 nanocomposite. *Applied Catalysis B: Environmental* **2008,** 84, (1), 94-99.
40. D.J. Giannantonio; J.C. Kurth; K.E. Kurtis and P.A. Sobecky, Effects of concrete properties and nutrients on fungal colonization and fouling. *International Biodeterioration & Biodegradation* **2009,** 63, (3), 252-259.
41. M. Sökmen; S. Değerli and A. Aslan, Photocatalytic disinfection of *Giardia intestinalis* and *Acanthamoeba castellani cysts* in water. *Experimental Parasitology* **2008,** 119, (1), 44-48.

42. P.R. Murray; K.S. Rosenthal; G.S. Kobayashi; M.A. Pfaller, *Medical microbiology*. Mosby: St. Louis, 2002.
43. Z. Zhao; H. Tan; H. Zhao; D. Li; M. Zheng; P. Du; G. Zhang; D. Qu; Z. Sun and H. Fan, Orientated anatase TiO_2 nanocrystal array thin films for self-cleaning coating. *Chemical Communications* **2013,** 49, 8958-890.
44. S. Nishimoto and B. Bhushan, Bioinspired self-cleaning surfaces with superhydrophobicity, superoleophobicity, and superhydrophilicity. *RSC Advances* **2013,** 3, 671-690.
45. F.L. Toma; G. Bertrand; D. Klein; C. Meunier and S. Begin, Development of photocatalytic active TiO_2 surfaces by thermal spraying of nanopowders. *Journal of Nanomaterials* **2008,** 58, 1-8.
46. X.T. Zhang; O. Sato; M. Taguchi; Y. Einaga; T. Murakami and A. Fujishima, Self-cleaning particle coating with antireflection properties. *Chemistry of Materials* **2005,** 17, 696-700.
47. H. Yaghoubi; N. Taghavinia and E. K. Alamdari, Self cleaning TiO_2 coating on polycarbonate: Surface treatment, photocatalytic and nanomechanical properties. *Surface Coating and Technology* **2010,** 204, 1562-1568.
48. R. Prado; G. Beobide; A. Marcaide; J. Goikoetxea and A. Aranzabe, Development of multifunctional sol–gel coatings: Anti-reflection coatings with enhanced self-cleaning capacity. *Solar Energy Materials and Solar Cells* **2010,** 94, 1081-1088.
49. K. Hashimoto; M. Miyauchi; M. Shimohigoshi and T. Watabe Self-cleaning member having photocatalytic hydrophilic surface Hydrophilic member and method for manufacture thereof. 2001.
50. V.A. Ganesh; A.S. Nair; H.K. Raut; T.M. Walsh and S. Ramakrishna, Photocatalytic superhydrophilic TiO_2 coating on glass by electrospinning. *RSC Advances* **2012,** 2, (5), 2067-2072.
51. A. Mills and M. Crow, A study of factors that change the wettability of titania films. *International Journal of Photoenergy* **2008,** 2008, 1-6.
52. V. Zorba; X. Chen and S.S. Mao, Superhydrophilic TiO_2 surface without photocatalytic activation. *Applied Physics Letters* **2010,** 96, (9), 3702-3703.

53. N.M. Mahmoodi and M. Arami, Degradation and toxicity reduction of textile wastewater using immobilized titania nanophotocatalysis. *Journal of Photochemistry and Photobiology B: Biology* **2009,** 94, 20-24.
54. J.C. Colmenares; P. Lisowskia and D. Łomota, A novel biomass-based support (Starbon) for TiO_2 hybrid photocatalysts: a versatile green tool for water purification. *RSC Advances* **2013,** 3, 20186-20192.
55. L. Zhu; Y.F. Xiao and X. Wang, The photocatalytic oxidation properties of La^{3+} doped and Ce^{4+}-doped ZnO-TiO_2 in treating pharmaceutical wastewater. *Advanced Materials Research* **2013,** 726-731, 2988-2992.
56. M.R. Prairie; L.R. Evans and S.L. Martinez, Destruction of organics and removal of heavy metals in water via TiO_2, photocatalysis in chemical oxidation: Technology for the nineties. *In Second International Symposium. Lancaster: Technomic Publishing Company* **1994**, 428-441.
57. J.M. Herrmann; Pichat, J. D. a. P., Photocatalytic deposition of silver on powder titania: Consequences for the recovery of silver. *Catalysis* **1988,** 113, 72-81.
58. A. Fujishima; K. Kohayakawa and K. Honda, Hydrogen production under sunlight with an electrochemical photocell. *Journal of the Electrochemical Society* **1975,** 122, 1487-1489.
59. G. Rothenberger; J. Moser; M. Grätzel; N . Serpone and D.K. Sharma, Charge carried trapping and recombination dynamics in small semiconductor particles. *Journal of the American Chemical Society* **1985,** 107, 8054-8059.
60. H. Tributsch; N. Serpone and E. Pelizzetti, *Photocatalysis: fundamentals and applications*. New York: Wiley: 1989; p 339-384.
61. N. Serpone; D. Lawless; J. Disdier and J.M. Herrmann, Spectroscopic, photoconductivity, and photocatalytic studies of TiO_2 colloids. *Langmuir* **1994,** 10, 643-652.
62. D.W. Bahnemann; E. Pelizzetti and M. Schiavello, *Photochemical conversion and storage of solar energy: Mechanisms of organic transformations on semiconductor particles*. Kluwer Academic Publishers, Netherlands 1991.
63. M. Pastore; A. Selloni; S. Fantacci and F. De Angelis, Electronic and optical properties of dye-sensitized TiO_2 interfaces. *Topics in Current Chemistry* **2014,** 347, 1-46.

64. S.S. Arbuj; U.P. Mulik and D.P. Amalnerkar, Synthesis of Ta_2O_5/TiO_2 coupled semiconductor oxide nanocomposites with high photocatalytic activity. *Nanoscience and Nanotechnology Letters* **2013,** 5, (9), 968-973.

65. H. Song; K. Jo; B.Y. Jung and G.Y. Jung, Fabrication of periodically aligned vertical single-crystalline anatase TiO_2 nanotubes with perfect hexagonal open-ends using chemical capping materials. *Nano Research* **2013,** 7, (1), 104-109.

66. J.M. Mwabora; T. Lindgren; E. Avendano; T.F. Jaramillo; J. Lu; S.E. Lindquist and C.G. Granqvist, Structure, composition, and morphology of photoelectrochemically active TiO_2-xNx thin films deposited by reactive DC magnetron sputtering. *The Journal of Physical Chemistry B* **2004,** 108, 20193-20198.

67. H. Yamashita; Y. Ichihashi; M. Takeuchi; S. Kishiguchi and M. Anpo, Characterization of metal ion-implanted titanium oxide photocatalysts operating under visible light irradiation. *Journal of Synchrotron Radiation* **1999,** 6, 451-452.

68. J.O. Carneiro; V. Teixeira; A. Portinha; L. Dupa´k; A. Magalha˜ es and P. Coutinho, Study of the deposition parameters and Fe-dopant effect in the photocatalytic activity of TiO_2 films prepared by dc reactive magnetron sputtering. *Vacuum* **2005,** 78, 37–46.

69. T.T. Cushnie; P. K. Robertson; S. Officer; P.M. Pollard; R. k. Prabhu; C. McCullagh and J.M. Robertson, Photobactericidal effects of TiO_2 thin films at low temperatures-A preliminary study *Jounal of Photochemistry and Photobiology A: Chemistry* **2010**, 1- 5.

70. W. Zhang; S. Zhu; Y. Li and F. Wang, Photocatalytic Zn-doped TiO_2 films prepared by DC reactive magnetron sputtering. *Vacuum* **2007,** 82, 328-335.

71. H.P. Maryska and A.K. Ghosh, Transition metal dopants for extending the response of titanate photoelectrolysis anodes. *Solar Energy Materials* **1979,** 1, 237-247.

72. W. Choi; A. Termin and M. R. Hoffmann, The role of metal ion dopants in quantum-sized TiO_2: correlation between photoreactivity and charge carrier recombination dynamics. *Journal of Physical Chemistry* **1994,** 51, 13669-13679.

73. S.I. Shah; W. Li; C.P. Huang; O. Jung and C. Ni, Study of Nd^{3+}, Pd^{2+}, Pt^{4+}, and Fe^{3+} dopant effect on photoreactivity of TiO_2 nanoparticles. *Proceedings of the National Academy of Sciences of the United States of America* **2002,** 99, 6482-6486.
74. J. Choi; H. Park and M.R. Hoffmann, Effects of single metal-ion doping on the visible-light photoreactivity of TiO_2. *The Journal of Physical Chemistry C* **2010,** 114, (2), 783-792.
75. Y. Shen; T. Xiong; J. Shang and K. Yang, Preparation of Nb_2O_5 and N co-doped TiO_2 photocatalysts and their enhanced photocatalytic activities under visible light. *Research on Chemical Intermediates* **2008,** 34(4), 353-363.
76. J. Arbiol; J. Cerda; G. Dezanneau; A..Cirera; F. Peiro; A. Cornet and J.R. Mornate, Effects of Nb doping on the TiO_2 anatase-to-rutile phase transition *Journal of Applied Physics* **2002,** 92, 853-861.
77. A. Ahmad; J. Thiel and S.I. Shah, Structural effects of niobium and silver doping on titanium dioxide nanoparticles. *Journal of Physics: Conference Series* **2007,** 61, 11-15.
78. K. K. Akurati; A. Vital; J.P. Dellemann; K. Michalow; T. Graule; D. Ferri and A. Baiker, Flame-made WO_3/TiO_2 nanoparticles: Relation between surface acidity, structure and photocatalytic activity. *Applied Catalysis B: Environmental* **2008,** 79, 53-62.
79. Y. Yang; X.J. Li; J.T. Chen and L.Y. Wang, Effect of doping mode on the photocatalytic activities of Mo/TiO_2. *Journal of Photochemistry and Photobiology A: Chemistry* **2004,** 163(3), 517-522.
80. R. Lo´pez and R. Go´mez, Photocatalytic degradation of 4-Nitrophenol on well characterized sol–gel molybdenum doped titania semiconductors. *Topics in Catalysis* **2011,** 54, 504-511.
81. V. Štengl and S. Bakardjieva, Molybdenum-doped anatase and its extraordinary photocatalytic activity in the degradation of orange II in the UV and vis regions. *The Journal of Physical Chemistry C* **2010,** 114(45), 19308-19317.
82. F. Kiriakidou; DI. Kondarides; XE. Verykios, The effect of operational parameters and TiO_2-doping on the photocatalytic degradation of azo-dyes. *Catalysis Today* **1999,** 54, (1), 119-130.

83. R. Asahi; T. Morikawa; T. Ohwaki; K. Aoki and Y. Taga, Visible-light photocatalysis in nitrogen-doped titanium oxides. *Science* **2001,** 293, 269-271.
84. O. Diwald; T.L. Thompson and E.G. Goralski, The effect of nitrogen ion implantation on the photoactivity of TiO_2 rutile single crystals. *Journal of Physical Chemistry B* **2004,** 108, 52-57.
85. Y. Ao; J. Xu and S. Zhang, A one-pot method to prepare N-doped titania hollow spheres with high photocatalytic activity under visible light. *Applied Surface Science* **2010,** 256, 2754-2758.
86. L. Dong; G.X. Cao and Y. Ma, Enhanced photocatalytic degradation properties of nitrogen-doped titania nanotube arrays. *Transactions of Nonferrous Metals Society of China* **2009,** 19, 1583-1587.
87. J.C. Yu; J.G. Yu and W.K. Ho, Effect of F- doping on photocatalytic activity and microstructures of nanocrystalline TiO_2 powder. *Chemistry of Materials* **2002,** 14, 3808-3816.
88. S. Sakthivel and H. Kisch, Daylight photocatalysis by carbon modified titanium dioxide. *Angewandte Chemie International Edition* **2003,** 42, 4908-4911.
89. H.U. Lee; S.C. Lee; S. Choi; B. Son; S.M. Lee; H.J. Kim and J. Lee, Efficient visible-light induced photocatalysis on nanoporous nitrogen-doped titanium dioxide catalysts. *Journal of Chemical Engineering* **2013,** 228, 756-764.
90. M. Chisaka; A. Ishihara; K. Suito; K. Ota and H. Muramoto, Oxygen reduction reaction activity of nitrogen-doped titanium oxide in acid media. *Electrochimica Acta* **2013,** 88, 697-707.
91. I. Ruzmanova; M. Ustundas; M. Stoller and A. Chianese, Photocatalytic treatment of olive mill waste water by N-doped titanium dioxide nanoparticles under visible light. *Journal of Chemical Engineering* **2013,** 32, 2233-2238.
92. M. Iwase; K. Yamada; T. Kurisaki; O. Prieto-Mahaney; B. Ohtani and H. Wakita, Visible-light photocatalysis with phosphorus-doped titanium (IV) oxide particles prepared using a phosphide compound. *Applied Catalysis B: Environmental* **2013,** 132, 39-44.
93. M. Ni; M. KH. Leung; D. YC. Leung and K. Sumathy, A review and recent developments in photocatalytic water-splitting using TiO_2 for hydrogen production. *Renewable and Sustainable Energy Reviews* **2007,** 11, 401-425.

94. C. Di Valentin; E. Finazzi; G. Pacchioni; A. Selloni; S. Livraghi; M.C. Paganini and E. Giamello, N-doped TiO_2: Theory and experiment. *Chemical Physics* **2007,** 339, (1), 44-56.
95. C. Di Valentin; G. Pacchioni; A. Selloni; S. Livraghi and E. Giamello, Characterization of paramagnetic species in N-doped TiO_2 powders by EPR spectroscopy and DFT calculations. *The Journal of Physical Chemistry B* **2005,** 109, (23), 11414-11419.
96. S. Song; J. Tu; L. Xu; X. Xu; Z. He; J. Qiu; J. Ni and J. Chen, Preparation of a titanium dioxidephotocatalyst codoped with cerium and iodine and its performance in the degradation of oxalic acid. *Chemosphere* **2008,** 73, 1401-1406.
97. D. Li; H. Haneda; S. Hishita; N. Ohashi and N.K. Labhsetwar, Fluorine-doped TiO_2 powders prepared by spray pyrolysis and their improved photocatalytic activity for decomposition of gas-phase acetaldehyde. *Journal of Fluorine Chemistry* **2005,** 126, 69-77.
98. J.M. Wu; H.C. Shih and W.T. Wu, Electron field emission from single crystalline TiO_2 nanowires prepared by thermal evaporation. *Chemical Physics Letters* **2005,** 413, 490-494.
99. J.M. Wu; H.C. Shih; W.T. Wu; Y.K. Tseng and I.C. Chen, Thermal evaporation growth and the luminescence property of TiO_2 nanowires. *Journal of Crystal Growth* **2005,** 281, 384-390.
100. F.F. Chen, *Introduction to plasma physics and controlled fusion*. Plenum Press, 1984: New York, 1984; Vol. 1.
101. N.A.G. Ahmed, *Ion plating technology: developments and applications*. John Wiley & Sons: USA, 1987.
102. J.S. Chapin, Planar magnetron. *Research-Development* **1974,** 25, 37.
103. W.D. Westwood, Sputter Deposition. *American Vacuum Society, New York* **2003**, 203-204.
104. P.J. Kelly and R.D. Arnell, Magnetron sputtering: a review of recent developments and applications. *Vacuum* **2000,** 56, 159- 162.
105. S.M. Rossnagel and J.J. Cuomo, Ion beam bombardment effects during films deposition. *Vacuum* **1988,** 38, (2), 73-81.
106. M. Ohring, *The material science of thin films* Academic press: London, 1991.

107. B. Window and N. Savvides, Unbalanced DC magnetrons as sources of high ion fluxes. *Journal of Vacuum Science and Technology A* **1986,** 4, (3), 453-456.
108. N. Savvides and B. Window, Unbalanced magnetron ion-assisted deposition and property modification of thin films. *Journal of Vacuum Science & Technology A* **1986,** 4, (3), 504-508.
109. B. Window and N. Savvides, Charged particle fluxes from planar magnetron sputtering sources. *Journal of Vacuum Science and Technology A* **1986,** 4, (2), 196-202.
110. R.P. Howson; H.A. Ja'fer and A.G. Spencer, Substrate effects from an unbalanced magnetron. *Thin Solid Films* **1990,** 193, 127-137.
111. W.D. Sproul, High-rate reactive DC magnetron sputtering of oxide and nitride superlattice coatings. *Vacuum* **1998,** 51 (4), 641-646.
112. I. Petrov; F. Adibi; J.E. Greene; W.D. Sproul and W.D. Munz, Use of an externally applied axial magnetic field to control ion/neutral flux ratios incident at the substrate during magnetron sputter deposition. *Journal of Vacuum Science and Technology A* **1992,** 10 (5), 3283-3287.
113. R.W. Berry Method of making a capacitor employing, U.S. Patent No. 2,993,266. 1961.
114. J. Musil; P. Baroch; J. Vlček; KH. Nam and JG. Han, Reactive magnetron sputtering of thin films: present status and trends. *Thin Solid Films* **2005,** 475, (1), 208-218.
115. A. Fuerte; M.D. Hernandez-Alonso; A.J. Maira; A. Martinez-Arias; M. Fernandez-Garcia; J.C. Conesa and J. Soria, Visible light-activated nanosized doped-TiO_2 photocatalysts. *Journal of Chemical Communications* **2001**, (24), 2718-2719.
116. G. Este and W.D. Westwood, A quasi-direct-current sputtering technique for the deposition of dielectrics at enhanced rates. *Journal of Vacuum Science & Technology A* **1988,** 6, 1845-1848.
117. S. Maniv; C. Miner and W.D. Westwood, High rate deposition of transparent conducting films by modified reactive planar magnetron sputtering of Cd_2 Sn alloy. *Journal of Vacuum Science and Technology* **1981,** 18, 195-198.

118. J. Szczyrbowski; G. Bräuer; G. Teschner and A. Zmelty, Antireflective coatings on large scale substrates produced by reactive twin-magnetron sputtering. *Journal of Non-Crystalline Solids* **1997,** 218, 25-29.
119. P. J. Kelly; C. F. Beevers; P. S. Henderson; R. D. Arnell; J. W. Bradley and H. Ba¨cker, A comparison of the properties of titanium-based films produced by pulsed and continuous DC magnetron sputtering. *Surface and Coatings Technology* **2003,** 174-175, 795-800.
120. P.J. Kelly ; A.A. Onifade; Y. Zhou; GC. Clarke; Bradley, M. A. a. J. W., The influence of pulse frequency and duty on the deposition rate in pulsed magnetron sputtering. *Plasma Processes and Polymers* **2007,** 4, (3), 246-252.
121. A. Anders, Physics of arcing, and implications to sputter deposition. *Thin Solid Films* **2006,** 502, (1), 22-28.
122. K. Wasa; M. Kitabatake and H. Adachi, *Thin Film Materials Technology: sputtering of control compound materials*. William Andrew Inc: Norwich, USA, 2004.
123. A. Movchan and A.V. Demchishin, Investigation of the structure and properties of thick vacuum-deposited films of nickel, titanium, tungsten, alumina and zirconium dioxide. *Physics of Metals and Metallography* **1969,** 28, 83-90.
124. J. A. Thornton, High rate thick film growth. *Annual Review of Materials Science* **1977,** 7, 239-260.
125. H.K. Pulker, *Wear and corrosion resistance coatings by CVD and PVD*. Chichester, 1989.
126. A.A. Onifade and P.J. Kelly, The influence of deposition parameters on the structure and properties of magnetron-sputtered titania coatings. *Thin Solid Films* **2006,** 494(1), 8-12.
127. E. Smith and G .Dent, *Modern Raman spectroscopy : A practical approach*. Wiley: 2005.
128. H.S. Peiser; H.P. Klug and A.J. Wilson, *X-Ray diffractions by pollycrystalline materials*. Chapman and Hall Ltd: London, New York.
129. J. Goldstein; D. Newbury; D. Joy; C. Lyman; P. Echlin; E. Lifshin; L. Sawyer and J. Micheal, *Scanning electron microscopy and X-Ray microanalysis*. new york and London, 1992.

130. P.M. Martin, *Hand book of deposition technologies for films and coatings science, applications and technology*. third edition ed.; Mass: Williams Andrew/Elsevier: Oxford, UK; Burlington, 2010.
131. K. Kanaya; S. Okayama, Penetration and energy-loss theory of electrons in solid targets. *Journal of Physics D: Applied Physics* **1972,** 5, (1), 43.
132. http://www.omniscan.co.uk/portfolio-view/white-light-interferometry/.
133. K. Asami and K. Hashimoto, Importance of initial surface film in the degradation of stainless steels by atmospheric exposure. *Corrosion Science* **2003,** 45, 2263-2283.
134. J. Genzer and K. Efimenko, Recent developments in superhydrophobic surfaces and their relevance to marine fouling: a review. *Biofouling* **2006,** 22, 339-360.
135. C.J. Tavares; S.M. Marques; T. Viseu; V. Teixeira; J.O. Carneiro; E. Alves; N.P.Barradas; F. Munnik; T. Girardeau and J.P. Riviere, Enhancement in the photocatalytic nature of nitrogen-doped PVD-grown titanium dioxide thin films. *Journal of Applied Physics* **2009,** 106, 1135.
136. S.A. Tomás; A. Luna-Resendis and L.C. Cortés-Cuautli, Optical and morphological characterization of photocatalytic TiO_2 thin films doped with silver. *Thin Solid Films* **2009,** 518, 1337-1340.
137. R. Gamble; Patch for Reducing Exposure of Skin to Ultraviolet Radiation, WO2005027859A2. 2004.
138. A. Mills and C. O'Rourke, Adsorption and destruction of methylene blue by semiconductor photocatalysis. *Green* **2011,** 1, 105-113.
139. X. Yan; T. Ohno; K. Nishijima; R. Abe and B. Ohtani, Is methylene blue an appropriate substrate for a photocatalytic activity test? A study with visible-light responsive titania. *Chemical Physics Letters* **2006,** 429, 606-610.
140. O. Impert; A. Katafias; P. Kita; A. Mills; A. Pietkiewicz-Graczyk and G .Wrzeszcz, Kinetics and mechanism of a fast leuco-Methylene Blue oxidation by copper (II)–halide species in acidic aqueous media. *Dalton Transactions* **2003**, (3), 348-353.
141. A. Houas; H. Lachheb; M. Ksibi; E. Elaloui; C. Guillard and J.M. Herrmann, Photocatalytic degradation path-way of methylene blue in water. *Applied Catalysis B: Environmental* **2001,** 31, 145-157.

142. ASTM, D3363-00, Standard test method for film hardness by pencil test. **2009**.
143. ASTM, D3359-97, Standard test methods for measuring adhesionby tape test. In 2009.
144. S.J. Bull, Failure modes in scratch adhesion testing. *Surface and Coatings Technology* **1991,** 50(1), 25-32.
145. S.J. Bull, Failure mode maps in the thin film scratch adhesion test. . *Tribology International* **1997,** 30(7), 491-498.
146. J. Stallard; S. Poulat and D.G. Teer, The study of the adhesion of a TiN coating on steel and titanium alloy substrates using a multi-mode scratch tester. *Tribology International* **2006,** 39, (2), 159-166.
147. S.J. Bull, Spallation failure maps from scratch testing. *Materials at High Temperatures* **1995,** 13, 169-174.
148. T. Goldhammer, The brewer's handbook: the complete guide to brewing beer. In KVP Publishers, Clifton: 2008.
149. International organization for standardization (ISO) 27447, *Fine ceramics (advanced ceramics, advanced technical ceramics). Test method for antibacterial activity of semiconducting photocatalytic materials, British Standard Institution, London* **2009**.
150. Y. Choi; A. Termin and M.R. Hoffmann, The role of metal ion dopants in quantum-sized TiO_2 : Correlation between photoreactivity and charge carrier recombination dynamics. *Journal of Physical Chemistry* **1994,** 98, 13669-13679.
151. H. Mehrgana; F. Elmib; M.R. Fazelib; A.R. Shahverdic and N. Samadiba, Evaluation of neutralizing efficacy and possible microbial cell toxicity of a universal neutralizer proposed by the CTPA. *Iranian Journal of Pharmaceutical Research* **2006,** 3, 173-178.
152. J. Verran; P. Airey; A. Packer and K. A. Whitehead, Microbial retention on open food contact surfaces and implications for food contamination. *Advances in Applied Microbiology* **2008,** 64, 223-246.
153. N. Gupta and B. Pal, Photocatalytic activity of transition metal and metal ions impregnated TiO_2 nanostructures for iodide oxidation to iodine formation. *Journal of Molecular Catalysis A: Chemical* **2013,** 371, 48-55.

154. J. Chen; M. Yao and X. Wang, Investigation of transition metal ion doping behaviors on TiO_2 nanoparticles. *Journal of Nanoparticle Research* **2008,** 10, 163-171.

155. K. A. Michalow; D. Flak; A. Heel; M. P. Wojtan; M. Rekas and T. Graule, Effect of Nb doping on structural, optical and photocatalytic properties of flame-made TiO_2 nanopowder. *Environmental Science and Pollution Research* **2012,** 19, 3696-3708.

156. C.M. Visinescu; R. Sanjines; F. Levy; V. Marcu and V.I. Parvulescu, Tantalum doped titania photocatalysts: Preparation by DC reactive sputtering and catalytic behavior. *Journal of Photochemistry and Photobiology A: Chemistry* **2005,** 174, (2), 106-112.

157. E. Barborini; I.N. Kholmanov; P. Piseri; C. Ducati; C.E. Bottani and P. Milani, Engineering the nanocrystalline structure of TiO_2 films by aerodynamically filtered cluster deposition. *Applied Physics Letters* **2002,** 81, (16), 3052-3054.

158. W.F. Zhang; Y.L. He; M.S. Zhang; Z. Yin and Q. Chen, Raman scattering study on anatase TiO_2 nanocrystals. . *Journal of Physics : Applied Physics D* **2000,** 33, 912-916.

159. M.A. Abdullah and F.K. Chong, Preparation and characterization of tungsten-loaded titanium dioxide photocatalyst for enhanced dye degradation. *Journal of Hazardous Materials* **2010,** 176, (1), 451-458.

160. S. Daviðsdóttir; S. Canulescu; K. Dirscherl; J. Schou and R. Ambat, Investigation of photocatalytic activity of titanium dioxide deposited on metallic substrates by DC magnetron sputtering. *Surface and Coatings Technology* **2013,** 216, 35-45.

161. M. Yao; J. Chen; C. Zhao and Y. Chen, Photocatalytic activities of Ion doped TiO_2 thin films when prepared on different substrates. *Thin Solid Films* **2009,** 517(21), 5994-5999.

162. A. Ruiz; G. Dezanneau; J. Arbiol; A. Cornet and JR. Morante, Study of the influence of Nb content and sintering temperature on TiO_2 sensing films. *Thin Solid Films* **2003,** 436, 90-94.

163. V. Štengl; V. Houšková; S. Bakardjieva; N. Murafa and P. Bezdička, Niobium and tantalum doped titania particles. *Journal of Materials Research* **2010,** 25, (10), 2015-2024.

164. M.R. Bayati; F. Golestani-Fard and A.Z. Moshfegh, Visible photodecomposition of methylene blue over micro arc oxidized WO_3–loaded TiO_2 nano-porous layers. *Applied Catalysis A: General* **2010,** 382, 322-331.

165. A. Rampaul; I.P. Parkin; S.A. O'Neill ; J. DeSouza; A. Mills and N. Elliott, Titania and tungsten doped titania thin films on glass; active photocatalysts. *Polyhedron* **2003,** 22, 35 - 44.

166. N. Farahani; PJ. Kelly; G. West; M. Ratova; C. Hill and V. Vishnyakov, An Investigation into W or Nb or $ZnFe_2O_4$ Doped Titania Nanocomposites Deposited from Blended Powder Targets for UV/Visible Photocatalysis. *Coatings* **2013,** 3, (3), 153-165.

167. I. Stambolova; V. Blaskov; S. Vassilev; M. Shipochka and A. Loukanov, Effect of substrate type, dopant and thermal treatment on physicochemical properties of TiO_2–SnO_2 sol–gel films. *Bulletin of Materials Science* **2012,** 35, (4), 645-649.

168. P.J. Kelly; G.T. West; M. Ratova; L. Fisher; S. Ostovarpour and J. Verran, Structural Formation and Photocatalytic Activity of Magnetron Sputtered Titania and Doped-Titania Coatings. *Molecules* **2014,** 19, (10), 16327-16348.

169. M.T. Criado; B. Suarez and C.M. Ferreiros, The importance of bacterial adhesion in the dairy industry. *Food Technology* **1994,** 48, 123-126.

170. A. Yang; E.B. Martin; G.A. Montague and P.J .Fryer, Towards improved cleaning of FMCG plants: a model-based approach. *Journal of Computer Aided Chemical Engineering* **2008,** 25, 1161-1166.

171. D.R. Kadavy; J J. Shaffer; SE. Lott; T.A. Wolf; C.E. Bolton; W.H. Gallimore; E.L. Martin; K.W. Nickerson and T A. Kokjohn, Influence of infected cell growth state on bacteriophage reactivation levels. *Applied and Enviromental Microbiology* **2000,** 66(12), 5206-5212.

172. L. C. Keller and R. B. Maxcy, Effect of physiological age on radiation resistance of some bacteria that are highly radiation resistant. *Applied and Enviromental Microbiology* **1984,** 47(5), 915-918.

173. A.G. Rincón and C. Pulgarin, Bactericidal action of illuminated TiO_2 on pure *Escherichia coli* and natural bacterial consortia: post-irradiation events in the dark and assessment of the effective disinfection time. *Applied Catalysis B: Environmental* **2004,** 49, 99-112.

174. M. Cho; H. Chung; W. Choi and J. Yoon, Different inactivation behaviors of MS-2 phage and *Escherichia coli* in TiO_2 photocatalytic disinfection. *Applied and Enviromental Microbiology* **2005,** 71, (1), 270-275.

175. L. Fisher; S. Ostovarpour; P. Kelly; KA. Whitehead; K. Cooke; E. Storgårds and J. Verran, Molybdenum doped titanium dioxide photocatalytic coatings for use as hygienic surfaces: the effect of soiling on antimicrobial activity. *Biofouling* **2014,** 30, (8), 911-919.

176. V.K. Bhupathiraju; M. Hernandez; Alvarez-Cohen, D. L. a. L., Application of a tetrazolium dye as an indicator of viability in anaerobic bacteria. *Journal of Microbiological Methods* **1999,** 37, 231-243.

177. M. A. Vargas-Reus; K. Memarzadeh; J. Huang; G.G. Ren and R.P. Allaker, Antimicrobial activity of nanoparticulate metal oxides against peri-implantitis pathogens. *International Journal of Antimicrobial Agents* **2012,** 40, (2), 135-139.

178. J. P. Guggenbichler; N. Eberhardt; H. Martinz and H. Wildner, Substance with an antimicrobial effect. **2010,** US 2010/0057199 A1, (12/514,404).

179. H. Gan; G. Zhang and H. Huang, Enhanced visible-light-driven photocatalytic inactivation of *Escherichia coli* by $Bi_2O_2CO_3/Bi_3NbO_7$ composites. *Journal of Hazardous Materials* **2013,** 250, 131-137.

180. T. Tatsuma; S. Takeda; S. Saitoh; Y. Ohko and A. Fujishima, Bactericidal effect of an energy storage TiO_2 WO_3 photocatalyst in dark. *Electrochemistry Communications* **2003,** 5, (9), 793-796.

181. A. Kubacka; M.S. Diez; D. Rojo; R. Bargiela; S. Ciordia; I. Zapico; J.P. Albar; C. Barbas; V. A.P. Martins dos Santos and M. Fernández-García, Understanding the antimicrobial mechanism of TiO_2-based nanocomposite films in a pathogenic bacterium. *Scientific Reports* **2014,** 4, 1-9.

182. M. Lackner and J.P.Guggenbichler, Composite material with a supporting material and an antimicrobial agent. In US Patent 20,150,104,488: 2015.

183. N. Beales, Adaptation of microorganisms to cold temperatures, weak acid preservatives, low pH, and osmotic stress: a review. *Comprehensive Reviews in Food Science and Food Safety* **2004,** 3, (1), 1-20.

184. G. Bergsson; J. Arnfinnsson; O. Steingri´msson and H. Thormar, In vitro killing of *Candida albicans* by fatty acids and monoglycerides. *Antimicrobial Agents and Chemotherapy* **2001,** 45, 3209-3212.

185. J.M. Goepfert and R. Hicks, Effect of volatile fatty acids on Salmonella typhimurium. *Journal of Bacteriology* **1969,** 97, 956-958.

186. K. Krishnamoorthy; M. Veerapandian; K. Yun and S.J. Kim, New function of molybdenum trioxide nanoplates: toxicity towards pathogenic bacteria through membrane stress. *Colloids and Surfaces B: Biointerfaces* **2013,** 112, 521-524.

187. A. Plumridge; S.J.A. Hesse; A.J. Watson; K.C. Lowe; M. Stratford and D.B. Archer, The weak acid preservative sorbic acid inhibits conidial germination and mycelial growth of *Aspergillus niger* through intracellular acidification. *Applied and Environmental Microbiology* **2004,** 70, 3506-3511.

188. C. Schüller; Y.M. Mamnun; M. Mollapour; G. Krapf; M. Schuster; B.E. Bauer; P.W.Piper and K. Kuchler, Global phenotypic analysis and transcriptional profiling defines the weak acid stress response regulon in Saccharomyces cerevisiae. *Molecular Biology of the Cell* **2004,** 15, 706-720.

189. M.A. Syed; U. Manzoor; I. Shah and S.A. Bukhari, Antibacterial effects of Tungsten nanoparticles on the *Escherichia coli* strains isolated from catheterized urinary tract infection (UTI) cases and *Staphylococcus aureus*. *The New Microbiologica* **2010,** 33, (4), 329-335.

190. B. Gao; J. Fu; K. Huo; W. Zhang; Y. Xie and P.K. Chu, Quasi aligned Ag–Nb_2O_5 nanobelt arrays with enhanced photocatalytic and antibacterial ctivities. *Journal of the American Ceramic Society* **2011,** 94, (8), 2330-2338.

191. C. Jullien; T. Benezech; C. Le Gentil; L. Boulange-Petermann; PE. Dubois; Tissier., J.; M. Traisnel and C. Faille, Physico-chemical and hygienic property modifications of stainless steel surfaces induced by conditioning with food and detergent. *Biofouling* **2008,** 24, 163-172.

192. M.H. Ahmed; T.E. Keyes; J.A. Byrne; C.W. Blackledge and J.W. Hamilton, Adsorption and photocatalytic degradation of human serum albumin on TiO_2 and Ag–TiO_2 films. *Journal of Photochemistry Photobiology A: Chemistry* **2011,** 222, 123-131.

193. M. Yasuyuki; K. Kunihiro; S. Kurissery; N. Kanavillil; Y. Sato and Y. Kikuchi, Antibacterial properties of nine pure metals: a laboratory study using *Staphylococcus aureus* and *Escherichia coli*. *Biofouling* **2010,** 26, 851-858.

194. Z. Wang; Y.H. Lee; B. Wu; A. Horst; Y. Kang; Y.J. Tang and D.R. Chen, Antimicrobial activities of aerosolized transition metal oxide nanoparticles. *Chemosphere* **2010,** 80, (5), 525-529.

195. Y.M. Sung and H.J. Kim, Sputter deposition and surface treatment of TiO_2 films for dye-sensitized solar cells using reactive RF plasma. *Thin Solid Films* **2007,** 515, 4996-4999.

196. T. Ohtani; Y. Ogawa and S. Nishimoto, Photocatalytic activity of amorphous-anatase mixture of titanium(IV) oxide particles suspended in aqueous solutions. *Journal of Physical Chemistry B* **1997,** 101, 3746-3752.

197. K.R. Goode; K. Asteriadou; P.T. Robbins and P.J. Fryer, Fouling and cleaning studies in the food and beverage industry classified by cleaning type. *Comprehensive Reviews in Food Science and Food Safety* **2013,** 12, (2), 121-143.

198. C.K. Lee; C.C. Wang; M.D. Lyu; L.C. Juang; S.S. Liu and S.H. Hung, Effects of sodium content and calcination temperature on the morphology, structure and photocatalytic activity of nanotubular titanates. *Journal of Colloid and Interface Science* **2007,** 316, (2), 562-569.

199. M. Krivec; R. Dillert; DW. Bahnemann; A. Mehle; J. Štrancar and G. Dražić, The nature of chlorine-inhibition of photocatalytic degradation of dichloroacetic acid in a TiO_2-based microreactor. *Physical Chemistry Chemical Physics* **2014,** 16, (28), 14867-14873.

200. P. Navabpour; S. Ostovarpour; J. Hampshire; P. Kelly; J. Verran and K. Cooke, The effect of process parameters on the structure, photocatalytic and self-cleaning properties of TiO_2 and Ag-TiO_2 coatings deposited using reactive magnetron sputtering. *Thin Solid Films* **2014,** 571, 75-83.

201. G. A .Epling and C. Lin, Investigation of retardation effects on the titanium dioxide photodegradation system. *Chemosphere* **2002,** 46, (6), 937-944.

202. E. Storgards; K. Tapani; P. Hartwall; R. Saleva and M. Suihko, Microbial attachment and biofilm formation in brewery bottling plants. *Journal of the American Society of Brewing Chemists* **2006,** 64, (1), 8-15.

203. G.K. Christian; P.J. Fryer and W. Liu, How hygiene happens: physics and chemistry of cleaning. *International Journal of Dairy Technology* **2006,** 59, 76-84.
204. L. Grönholm; G. Wirtanen; K. Ahlgren; K. Nordström and A.M. Sjöberg, Screening of antimicrobial activities of disinfectants and cleaning agents against foodborne spoilage microbes. *Zeitschrift für Lebensmitteluntersuchung und –Forshung A* **1999,** 208, 289-298.
205. O. Priha; J. Laakso; K. Tapani; E. Levänen; M. Kolari; T. Mäntylä and E. Storgårds, Effect of photocatalytic and hydrophobic coatings on brewery surface microorganisms. *Journal of Food Protection*® **2011,** 74, (11), 1891-1901.
206. M. Nakamura; K. Makino; L. Sirghi; T. Aoki and Y. Hatanaka, Hydrophilic properties of hydro-oxygenated TiO_2 films prepared by plasma enhanced chemical vapor deposition. *Surface and Coatings Technology* **2003,** 169, 699-702.
207. Y.C. Lee; Y.P. Hong; H.Y. Lee; H. Kim; Y.J. Jung; K.H. Ko; H.S. Jung and K.S. Hong, Photocatalysis and hydrophilicity of doped TiO_2 thin films. *Journal of Colloid and Interface Science* **2003,** 267, 127-131.
208. V. Shpovalov; E.V. Stefanovich and T.N. Truog, Nature of the excited states of the rutile TiO_2 (110) surface with adsorbed water. *Surface Science* **2002,** 498, 103-108.
209. T. Watanabe, Super hydrophilic photocatalyst and its application. *Journal of the Ceramic Society of Japan* **1996,** 31(10), 837-840.
210. O. Priha; M. Raulio; K. Cooke; L. Fisher; C. Hill; S. Hylkinen; P. Kelly; P. Navabpour; S. Ostovarpour and K. Tapani, Microbial populations on brewery filling hall surfaces–Progress towards functional coatings. *Food Control* **2015,** 55, 1-11.

Appendix A

Two experiments were carried out in order to see the reproducibility of the coatings. Since the assessment of photocatalytic activity is a time consuming process (each measurement takes 5 hours plus samples pre-treatment time), it was not possible to evaluate statistically all the photocatalytic tests carried out. Therefore, the testing precision assessment was carried out on four types of coatings, which was going to place in brewery environments; TiO_2, TiO_2-Mo 7 at.%, TiO_2-Nb 0.25 at.%, and TiO_2-W 3.8 at.% which were annealed at 600 °C and 400 °C.

Experiment 1: consequent measurements of photocatalytic activity carried out on the same piece of each coating under UV light irradiation (5 measurements) (Figure A1).

Table A.1: Statistical results of photocatalytic testing for four samples (experiment 1).

Sample	Mean	Standard deviation	Standard error
TiO_2	0.6875	0.015969	0.007984
TiO_2-Mo 7 at.%	0.875	0.023238	0.011619
TiO_2-Nb 0.25 at.%	0.8325	0.011619	0.005809
TiO_2-W 3.8 at.%	0.71	0.068702	0.034351

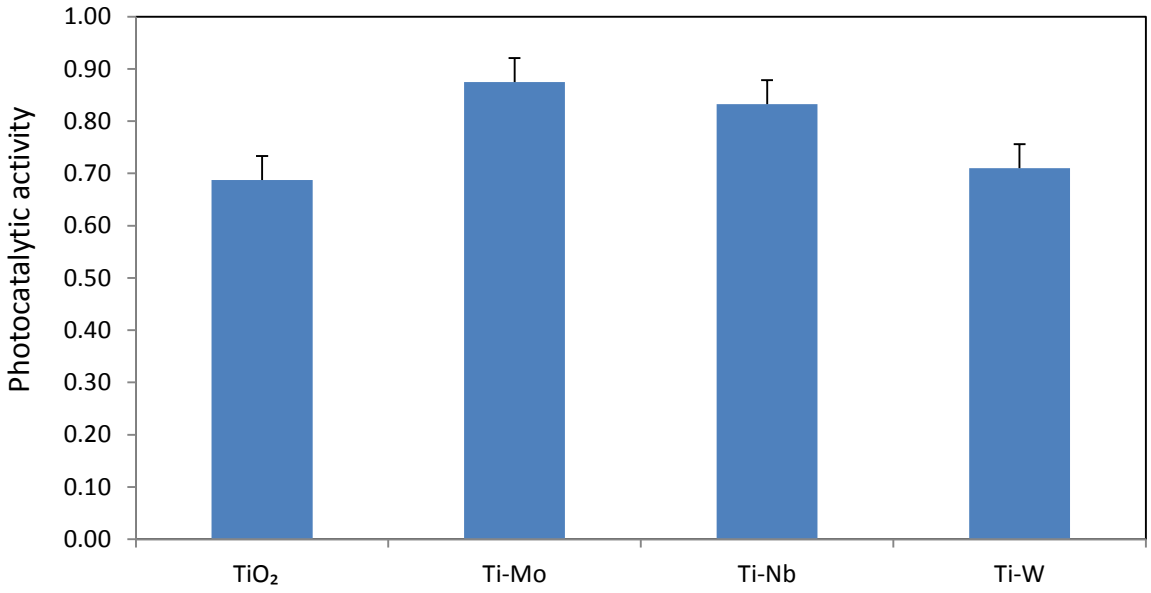

Figure A.1: Relative photocatalytic activity for experiment 1.

Experiment 2: Consequent measurements of photocatalytic activity carried out on the samples from each batch under UV light irradiation (one measurement from each batch).

Table A.2: Statistical results of photocatalytic testing for five samples (experiment 2).

Sample	Mean	Standard deviation	Standard error
TiO_2	0.6925	0.061441	0.030721
TiO_2-Mo 7 at.%	0.8775	0.034278	0.017139
TiO_2-Nb 0.25 at.%	0.835	0.057096	0.028548
TiO_2-W 3.8 at.%	0.7125	0.030578	0.015289

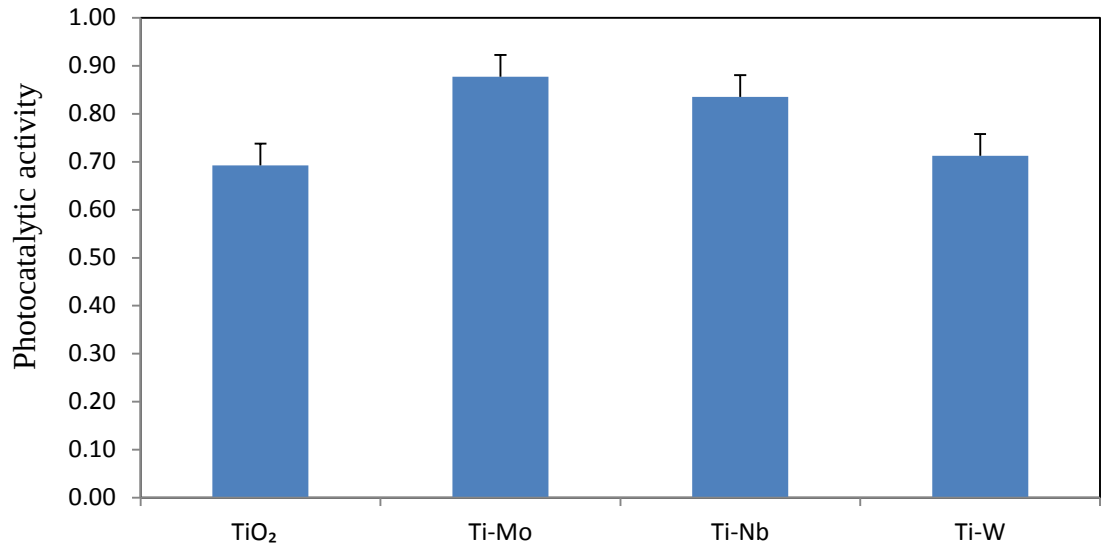

Figure A.2: Relative photocatalytic activity for experiment 2.

Based on results from statistical analysis, it can be concluded that methylene blue degradation provides precise and repeatable values for photocatalytic assessment. However, in experiment 2 where samples from each batch were tested, the standard error for all of the samples was higher than the experiment 1, which we can conclude that there is a batch variation in coatings.

Appendix B

Penetration depths of EDX were calculated according to Kanaya-Okayama formula:

$$R = \frac{0.0276\ A\ E_0^{n}}{(Z^{0.89}\ \rho)} \quad \mu m$$

R= Depth penetration

A= Atomic weight (g/mol)

n= Constant which is 1.67

E_0 = Beam energy (kV)

Z= Atomic number

ρ = Density $(g/cm)^2$

Table B.1 gives some examples of penetration depths at some energy levels of incident beams in transition metals.

Table B.1: Penetration depths at some energy levels of incident beams in Ti, Mo, Nb, Ta and W.

Beam energy kV	5	10	15
Titanium (Ti)	0.27 µm	0.87 µm	1.72 µm
Molybdenum (Mo)	0.13 µm	0.43 µm	1.02 µm
Niobium (Nb)	0.23 µm	0.74 µm	1.46 µm
Tantalum (Ta)	0.2 µm	0.64 µm	1.27 µm
Tungsten (W)	0.083 µm	0.27 µm	0.52 µm

Appendix C

List of publications

- P. Outi, M. Raulio, K. Cooke, L. Fisher, C. Hill, S. Hylkinen, P. Kelly, P. Navabpour, **S. Ostovarpour**, K. Tapani, C. Tattershall ,A. Vehvil€ainen, J. Verran , E. Storgårds. *Food Control* 55 (2015): 1-11, Microbial populations on brewery filling hall surfaces–Progress towards functional coatings.
- L. Fisher, **S. Ostovapour**, P. Kelly, K. Cooke, E. Storgårds,J. Verran Biofouling. (2014),30, 911-919 Molybdenum doped titanium dioxide photocatalytic coatings for use as hygienic surfaces - the effect of soiling on antimicrobial activity.
- P. Navabpour, **S. Ostovarpour**, K. Cooke, J. Hampshire, P. Kelly and J. Verran Thin Solid Films (2014),571,75-83 The effect of process parameters on the structure, photocatalytic and self-cleaning properties of TiO_2 and Ag-TiO_2 coatings deposited using reactive magnetron sputtering.
- P. Navabpour, **S. Ostovarpour**, C.Tattershall, K. Cooke, J. Hampshire, K. Whitehead, P. Kelly and J. Verran, Coatings (2014),4,433-449, Photocatalytic TiO_2 and doped TiO_2 coatings to improve the hygiene of surfaces used in food and beverage processing – A study of the physical and chemical resistance of the coatings.
- P.J. Kelly, G.T. West, M. Ratova, L. Fisher, **S. Ostovarpour**, and J. Verran, Molecules (2014),19, 16327-16348, Structural formation and photocatalytic activity of magnetron sputtered titania and doped-titania coatings.
- J. Verran, **S. Ostovarpour**, L. Fisher, K. Whitehead, P. Kelly, E. Storgards (2014), Investigating the potential for the use of photocatalytic surfaces in process hygiene in the brewing industry,Fouling and Cleaning in Food Processing Conference Proceedings, Cambridge.
- P.J. Kelly, P.M. Barker, **S. Ostovarpour**, M. Ratova, G.T. West, I. Iordanova, J.W. Bradley, Vacuum, (2012),86,1880-1882, Deposition of photocatalytic titania coatings on polymeric substrates by HiPIMS.

Food Control 55 (2015) 1–11

Contents lists available at ScienceDirect

Food Control

journal homepage: www.elsevier.com/locate/foodcont

Microbial populations on brewery filling hall surfaces – Progress towards functional coatings

Outi Priha [a, *], Mari Raulio [a], Kevin Cooke [b], Leanne Fisher [c], Claire Hill [d], Silja Hylkinen [e], Peter Kelly [c], Parnia Navabpour [b], Soheyla Ostovarpour [c], Kaisa Tapani [f], Carin Tattershall [d], Anna-Kaisa Vehviläinen [g], Joanna Verran [c], Erna Storgårds [a]

[a] VTT Technical Research Centre of Finland, P.O. Box 1000, FI-02044, VTT Espoo, Finland
[b] Teer Coatings Ltd., Miba Coating Group, West Stone House, Berry Hill Industrial Estate, Droitwich, WR9 9AS, UK
[c] Faculty of Science and Engineering, Manchester Metropolitan University, Chester Street, Manchester, M1 5GD, UK
[d] Cristal Pigment UK Ltd, P.O. Box 26, Grimsby, North East Lincolnshire, DN41 8DP, UK
[e] Olvi Oyj, Olvitie I-IV, 74100, Iisalmi, Finland
[f] Sinebrychoff, Sinebrychoffinaukio 1, FI-04250, Kerava, Finland
[g] Hartwall, Kasaajankatu 13, FI-15101, Lahti, Finland

ARTICLE INFO

Article history:
Received 24 October 2014
Received in revised form
12 February 2015
Accepted 16 February 2015
Available online 24 February 2015

Keywords:
Photocatalytic coatings
TiO_2
Microbial attachment
Microbial communities
DGGE
Beverage industry
Process surfaces

ABSTRACT

Microbial populations on equipment surfaces of beverage filling lines were investigated as a function of surface coating type, location and time. Photocatalytic metal-ion doped (Ag or Mo) and non-doped TiO_2 coatings deposited using reactive magnetron sputtering and spray coating methods were studied as means to reduce microbial numbers accumulating on the surfaces. The coatings were applied to stainless steel coupons, which were mounted to one canning and one glass bottle filling line for 3–5 months. After exposure microbial numbers on the coupons were evaluated by culturing, and bacterial community profiles were characterised with PCR-DGGE (denaturing gradient gel electrophoresis). The results showed that the longer the run time after washes the higher microbial numbers were detected, and that the two filling lines each had their characteristic bacterial community. The major species identified were members of *Acinetobacter* sp., lactic acid bacteria and enterobacteria. No clear effect of the different coating materials on the microbial numbers or bacterial community composition on the surfaces was shown. In conclusion, functional coatings with sufficient mechanical and chemical durability for industrial surfaces have been developed. Although these coatings have been previously reported to reduce the number of microorganisms on the surfaces *in vitro*, their efficacy in the challenging beverage process conditions was not proven.

1. Introduction

Brewery packaging equipment surfaces are constantly exposed to moisture and nutrients during production, thus being susceptible to microbial attachment and growth on surfaces. Surface-attached bacteria are problematic to process industry: they cause contaminations, degrade and/or corrode materials and affect process efficiency (e.g., filtration units or heat exchangers). Equipment surfaces are cleaned on a regular basis to reduce the microbial load to a safe level. Washing procedures cost in terms of production interruptions and consumption of energy, water, chemicals and working hours. The process industry would thus benefit from novel means for managing microbes on process surfaces. Development of functional coatings, *i.e.* coatings reducing the number of adhering microbes on surfaces, has been a growing trend in recent years especially in clinical environments (Page, Wilson, & Parkin, 2009). Such coatings could have a valuable role in improving hygiene in industrial processes, including the beverage industry.

Coatings with photocatalytically active semiconductors, especially TiO_2, have attracted attention as a method for keeping surfaces free of dirt and microbes. TiO_2 photocatalysts have been shown to kill bacteria upon illumination by UVA light (315–400 nm) (Fujishima, Zhang, & Tryk, 2008). The presently accepted view on the mode of action is that $OH^{\bullet}$ produced by TiO_2 is

* Corresponding author.
E-mail address: outi.priha@vtt.fi (O. Priha).

http://dx.doi.org/10.1016/j.foodcont.2015.02.022
0956-7135/

the primary killing agent, but that other reactive oxygen species generated in the process, such as O_2^- and H_2O_2, may be partly responsible for inactivation of bacteria (Cho, Chung, Choi, & Yoon, 2005). Because of the short half-life of $OH^•$ and its low diffusion potential, bacterial cells to be oxidized must be close to the generation site. To obtain bactericidal activity under weak UV intensity, TiO_2 films doped with antibacterial metals such as copper (Cu), silver (Ag), and other elements have been developed for combined activity (Naik & Kowshik, 2014; Ratova, Kelly, West, & Iordanova, 2013; Sunada, Watanabe, & Hashimoto, 2003).

Photooxidation of bacteria has mostly been studied using single bacterial species, like *Escherichia coli, Staphylococcus aureus, Enterobacter cloacae, Bacillus subtilis, Pseudomonas aeruginosa, P. fluorescens, Deinococcus geothermalis* or *Burkholderia cepacia* (Allion et al., 2007; Ibáñez, Litter, & Pizarro, 2003; Keskinen et al., 2006; Kühn et al., 2003; Li & Logan, 2005; Pal, Pehkonen, Yu, & Ray, 2007; Raulio et al., 2006). The photocatalytic activity has varied from 10 to 99.9999 % reduction in the number of viable bacteria depending on the light intensity, wavelength and exposure time, as well as bacterial species and whether adhered or non-adhered bacteria have been studied. Yeasts appear to be considerably more resistant than bacteria against photooxidation (Kühn et al., 2003). A few studies using mixtures of microbial species have also been reported: Rajagopal, Maruthamuthu, Mohanan, and Palaniswamy (2006) oxidised biofilms formed by natural microbiota of pond water by photocatalysis, but failed to kill all microbes. Priha et al. (2011) used a mixed culture of bacterial and yeast strains to evaluate the efficacy of atomic layer deposited (ALD) TiO_2 and $TiO_2 + Ag$ coatings in reducing the number of adhering microbes on steel, and obtained a reduction in microbial numbers adhering onto $TiO + Ag$ coatings. Due to the inadequate mechanical durability of the coatings, however, their functionality in beverage process conditions could not be evaluated.

In this study the performance of doped (Ag or Mo) and non-doped TiO_2 coatings deposited using reactive magnetron sputtering and spray coating methods was investigated in process conditions at a brewery. In preceding studies executed in laboratory, similar coatings reduced the number of bacteria compared to the non-coated stainless steel (Fisher et al., 2014; Navabpour, Ostovarpour, & Hampshire, et al., 2014). Also, the mechanical durability and retention of photocatalytic properties of these coatings has been evaluated in brewery process conditions (Navabpour, Ostovarpour, & Tattershall, et al., 2014). The aim of this study was to verify the antimicrobial activity of the coatings in real process conditions. Our hypothesis was that Ag or Mo doping would enhance the photoactivity of TiO_2, enabling the reduction in the number of adhered microbes despite the low light intensity in process conditions.

2. Materials and methods

2.1. Installation of coupons to brewery filling machines

All coatings were applied to stainless steel with bright cold rolled finish (AISI 304 2B) coupons of 18.75 cm^2 (25 × 75 × 1 mm). The properties of coatings used in this study are presented in Table 1. Details of coating preparation are given in Navabpour, Ostovarpour, and Tattershall, et al. (2014). The coated and non-coated stainless steel coupons were disinfected prior to process studies by immersion to 70% ethanol for 2 h, and air-dried. The coupons were installed onto one canning line and one glass bottle line in a randomised block design, having three blocks with five replicates of each coupon type at both filling lines, totalling 15 replicates of each coating in each filling line. Filler surfaces were cleaned with saBesto spray (25–50% petroleum, 20–30% isopropanol, Würth, Riihimäki, Finland) and the coupons were fixed with HV350 glue (Valco, Cincinnati, OH). There was no special provision of UV lighting for the photocatalytic coatings; the process test took place under the usual brewery conditions, with coupons receiving varying amounts of light depending on their location in each machine. When installing the coupons, the light intensities of UVA (LP 471 UVA probe, spectral range 315–400 nm) and VIS (LP 471 RAD Probe, spectral range 400–1050 nm) were measured with a fluorometer (HD 2102.2, DeltaOhm, Padova, Italy), and were, on average, 0.5 (±1.0) μW cm^{-2} and 34 (±38) μW cm^{-2}, respectively. All coupons underwent the normal process conditions and cleaning regimes used while being in the process. Between production batches the washing programmes of the filling lines consisted of prerinsing with cold water, soaking with alkaline foam cleaner for 10 min with concurrent manual brushing where necessary, disinfection with chlorine based cleaner for 10 min, and final rinsing with cold water. For each microbiological sampling the time from the last washing cycle was documented. In addition, less-extensive washes without brushing were done during production at 4–24 h intervals.

Table 1
The studied materials. All coatings were deposited onto stainless steel with bright cold rolled finish (AISI 304 2B).

Coupon code	Material/coating	Concentration of dopant (%)	Deposition method
R	AISI 304 2B		Control, not coated
U1	TiO_2		Reactive magnetron sputtering + heat treatment
U2	TiO_2–Mo	7.0	Reactive magnetron sputtering + heat treatment
T2	TiO_2–Ag	0.5	Reactive magnetron sputtering
MC	TiO_2		Spray-coated with TiO_2 sol

2.2. Assessing microbial attachment and retention rates

Three samplings for the assessment of the number of microbes on the coupons between two weeks and five months from the installation of the coupons were performed (Table 2). The sampling times varied between the canning and glass bottle line due to production timetables. The coupons were swabbed with sterile 5 × 10 cm nonwoven gauzes (Mesoft, Mölnlycke Health Care, Gothenburg, Sweden) placed into 10 ml of Ringer's solution (Merck, Darmstadt, Germany) immediately after swabbing. Bacteria were detached from the gauze by homogenisation for 1 min (Stomacher), and the numbers of microbes were enumerated by plate counts. For enumeration of aerobic heterotrophic bacteria, samples were cultivated on Tryptic Soy Agar (BD, Becton, Dickinson and Company, New Jersey, USA) containing 10 mg l^{-1} cycloheximide (Sigma; Sigma-Aldrich, St. Louis, MO, USA) to prevent the growth of fungi, and incubated for 3 d at 30 °C. Moulds and yeasts were detected using Potato Dextrose Agar (BD, New Jersey, USA) containing 100 mg l^{-1} chloramphenicol (Sigma; Sigma–Aldrich, St. Louis, MO, USA) and 100 mg l^{-1} chlortetracycline (Sigma; Sigma–Aldrich, St. Louis, MO, USA) to prevent to growth of bacteria, and 20 mg l^{-1}

Table 2
The sampling times of the process study.

	Days from installation of coupons (days from last washing cycle)			
	First sampling	Second sampling	Third sampling	Coupon removal
Canning line	13 (1.5)	43 (1)	84 (3)	97 (1.5)
Glass bottle line	24 (2)	43 (1.5)	149 (1)	163 (1.5)

Triton (Fluka; Sigma–Aldrich, St. Louis, MO USA) to prevent the spreading of colonies, and incubated for 7 d at 25 °C. Lactic acid bacteria were enumerated using de Man Rogosa Sharpe agar (MRS, Oxoid, Basingstoke, UK), and incubated anaerobically for 5–7 d at 30 °C.

2.3. DNA extraction and PCR-DGGE

The homogenised swab sample suspensions remaining after cultivation were filtered to Sterivex-GP 0.22 μm-pore-size filter units (Millipore, Billerica, MA, USA) and stored frozen (−20 °C) until DNA was extracted. Subsequently filters were aseptically cut into smaller pieces and transferred into DNA extraction tubes. DNA was extracted using Fast DNA Spin Kit for Soil (MP Biomedicals, USA) according to manufacturer's instructions, with the modification that the cells were homogenized in a FastPrep-24 instrument (MP Biomedicals, USA) at 6 m s^{-1} for 3 min.

For assessing bacterial community structure in the samples, a variable region of the 16S rRNA gene was amplified. In preliminary studies two primers pairs were compared: for V3 region 358F (5′-CCTACGGGAGGCAGCAG-3′) and 534R (5′-ATTACCGCGGCTGCTGG-3′) (Muyzer, De Waal, & Uitterlinden, 1993) and for V6–V8 region F-968 (5′-AACGCGAAGAACCTTAC) and R-1401 (5′-CGGTGTGTACAAGACCC-3′) (Nübel et al., 1996; Zoetendal, Akkermans, & De Vos, 1998) with a 40-bp GC clamp (5′-CGCCCGCCGCGCGCGGCGGGCGGGGCGGGGGGCACGGGGGG-3) attached to the forward primers. The primer pair 358F + 534R was shown to be more sensitive (results not shown). Due to the low DNA concentrations in the samples, the sensitivity of the assay was further improved with a two-round PCR assay, first round with primers 358F and 534R and a second round with the same primers, but a 40-bp GC clamp attached to the forward primer. The first PCR amplification was performed in 50 μl reaction volume with 1 × DynaZyme II buffer (10 mM Tris–HCl, pH 8.8, 1.5 mM $MgCl_2$, 50 mM KCl, and 1% Triton X-200; Thermo Scientific), 0.2 mM of each deoxynucleoside triphosphate, 0.4 μM of each primer, 1% formamide, 1 U of Dynazyme II polymerase (Thermo Scientific), and 5 μl of template DNA. The PCR was performed in a MasterCycler thermal cycler (Eppendorf, Germany). The PCR program consisted of a 5-min initial denaturation at 94 °C, followed by 30 cycles of 30 s at 94 °C, 30 s at 55 °C, and 45 s at 72 °C, with a final elongation step at 72 °C for 7 min. The second PCR was performed in a 50 μl reaction volume with 1 × Phusion GC-buffer (Thermo Scientific), 0.2 mM of each deoxynucleoside triphosphate, 0.4 μM of each primer, 1% formamide, 5 U Phusion Hot Start II DNA Polymerase (Thermo Scientific) and 5 μl of the PCR product from the first PCR. The PCR program consisted of 30 s initial denaturation at 98 °C, followed by 30 cycles of 10 s at 98 °C, 30 s at 65 °C, and 30 s at 72 °C, with a final elongation step at 72 °C for 7 min.

Denaturing Gradient Gel Electrophoresis (DGGE) analysis was performed with D-Code Universal Mutation detection System (Bio-Rad, California, USA). Briefly, 8% (w/v) polyacrylamide gels (16 × 16 × 1 mm) with a gradient from 30 to 70 % was run in 0.5 × TAE buffer (20 mM Tris, 10 mM acetate, 0.5 mM EDTA, pH 0.8) at 60 °C, 85 V for 16 h. The amount of PCR products (3–10 μl) loaded on the gel was adjusted according to the intensity of the bands in the agarose gel. Following electrophoresis, the gels were stained in SYBR Green I solution (Sigma; Sigma–Aldrich, St. Louis, MO, USA) for 20 min, rinsed with ultra-pure water, and documented using the Gel Doc 2000 system (Bio-Rad, California, USA). A sequence ladder consisting of PCR products of selected reference strains from VTT Culture Collection (http://culturecollection.vtt.fi/; *Leuconostoc citreum* VTT E–93497, *Acinetobacter baumannii* VTT E–022166, *Pediococcus claussenii* VTT E–022179, *Lactobacillus lindneri* VTT E–91460, *Mycobacterium hodleri* VTT E–022096 and *Kocuria kristinae* VTT E–82147) was run in parallel with the samples. Selected representative DNA bands (altogether 92) were excised from the DGGE gel using a Pasteur pipette and kept in 20 μl of PCR grade water overnight at 4 °C. The obtained gene fragments were then reamplified until a single band was obtained in DGGE. For sequencing the samples were sent to Macrogen Europe (Amsterdam, The Netherlands), for custom DNA sequencing using the EZ-

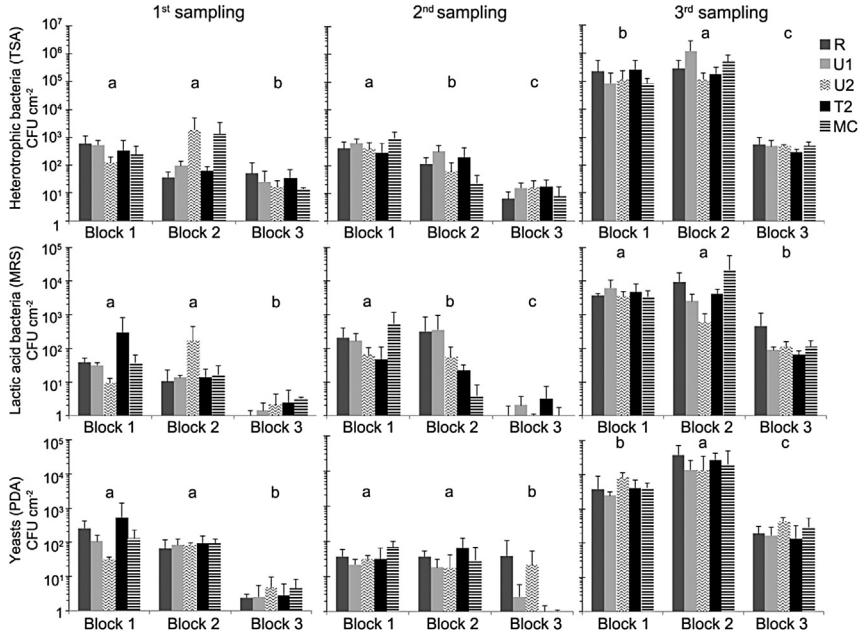

Fig. 1. The number of microbes on coated (Table 1) and non-coated AISI 304 2B stainless steel coupons after 13, 43 and 84 d exposure in a canning line seamer in a brewery. Fifteen replicates of each coating were divided into three blocks in a randomised block design and installed in the seamer of a canning machine. The number of adhered microbes was determined by swabbing and culturing on three different agar plates to detect heterotrophic and lactic acid bacteria, and yeasts. The results are shown as average CFU cm^{-2} of five replicates on each block. Bars show standard deviations, and letters show significant ($P \leq 0.05$) differences between blocks.

purification service. The obtained sequences were trimmed in Geneious software R6 (Biomatters, Auckland, New Zealand) and compared against GenBank sequences with a Megablast search (McGinnis & Madden, 2004).

For comparing community profiles of different samples the gel data were transferred into BioNumerics ver 5.10 software (Applied Maths, Sint-Martens-Latem, Belgium). Pearson's curve-based correlations were calculated, and clustering was done with the unweighted pair group with arithmetic mean (UPGMA). The band classes were searched with the band matching algorithm of the BioNumerics software.

2.4. Microscopy

At the end of the process study the coupons were removed for microscopy. They were rinsed gently twice with sterile MilliQ water and stained with acridine orange (BD 212536, 0.1 g l^{-1} in 0.5 M acetate buffer; New Jersey, USA) for 10 min in the dark for epifluorescence microscopy. Acridine orange is a nucleic acid selective fluorescent cationic dye. The coupons were examined with Axio Imager.M2 epifluorescence microscope and using a 63 × /1.4 or 100 × /1.40 Oil Plan-Apochromat objective lens (Zeiss, Oberkochen, Germany, λex = 470 ± 40, λem = 525 ± 50). Images were captured using AxioCam MRm camera and AxioVision 4.8.2 software (Zeiss, Oberkochen, Germany). One parallel coupon of each coating type at bottle filling line was immediately after removal fixed in phosphate (0.1 M, pH 7.2) buffered 2.5% glutaraldehyde for 3 h, and rinsed with phosphate buffer three times. Subsequently dehydration was carried out with an ethanol series from 30%, 50%, 70%, 85%–96% and absolute, followed by hexamethyldisilazane (Fluka, Buchs, Switzerland). Coupons were coated with Au/Pd (10 nm, 208 HR High Resolution Sputter Coater, Cressington Scientific Instruments Inc, Cranberry, PA, USA) and examined with FESEM (Hitachi S-4800, Tokyo, Japan) operated at 1 kV.

2.5. Statistical analyses

Significant ($P \leq 0.05$) differences of the means within each sampling were tested with two-way analysis of variance with block and coating as fixed factors, and subsequent Tukey's post hoc test using IBM SPSS Statistics version 21 software. The cfu counts were log transformed to fulfil the assumptions of variance analysis.

3. Results

The numbers of heterotrophic bacteria, lactic acid bacteria, and yeasts on each block of the canning line at three different time points are shown in Fig. 1. The results from the glass bottle line are shown in Fig. 2. From the glass bottle line most of the coupons from block 1 became detached in the middle of the study, and these

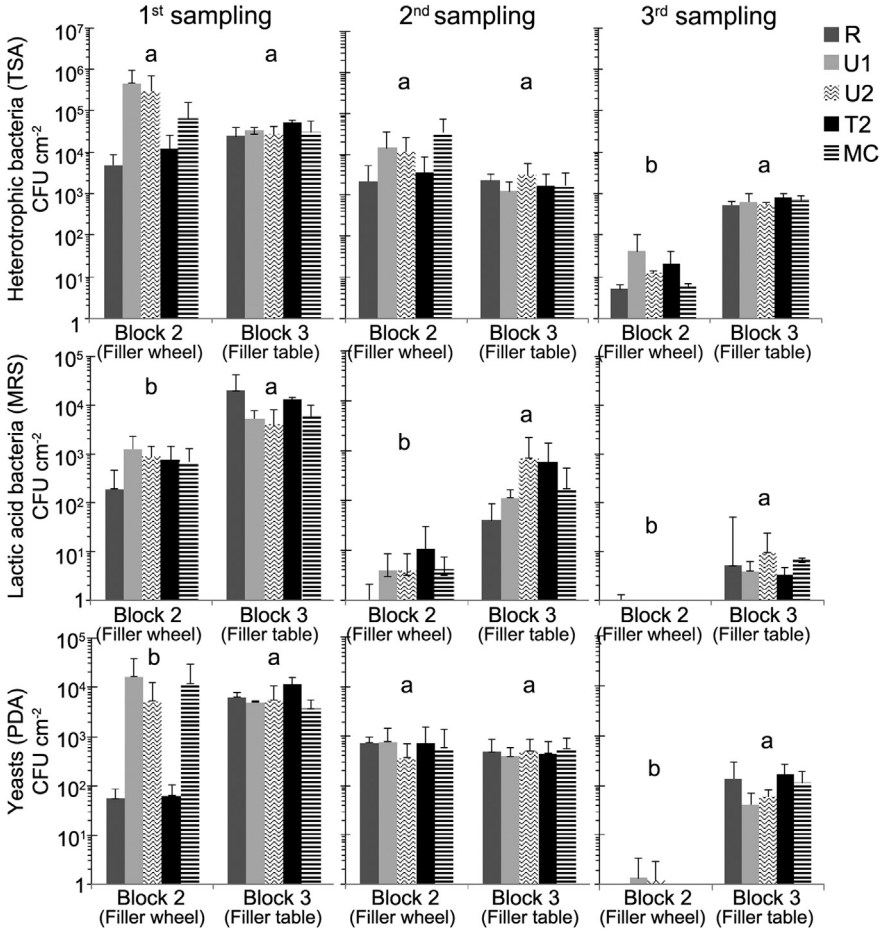

Fig. 2. The number of microbes on coated (Table 1) and non-coated AISI304 2B stainless steel coupons after 24, 43 and 149 d exposure in a glass bottling line in a brewery. Ten replicates of each coating were divided into two blocks and installed on the filler wheel and on the filling table of a glass bottling machine. The number of adhered microbes was determined by swabbing and culturing on three different agar plates to detect heterotrophic and lactic acid bacteria and yeasts. The results are shown as average CFU cm^{-2} of five replicates on each block. Bars show standard deviations, and letters show significant ($P \leq 0.05$) differences between blocks.

results are not included. Both lines were filling beer prior to each sampling time, but the filling time after the previous washing cycle varied from 1 to 3 d (Table 2).

The results show that the run time after washing had a clear effect on the number of microbes on the coupons. At the canning machine the numbers of adhering heterotrophic bacteria, lactic acid bacteria and yeast were up to 3 logs higher on the last sampling with a 3-day run, as compared to the 1st and 2nd second sampling with 1–1.5 d runs after washing cycles (Fig. 1). At the glass bottle line the numbers of attached microbes also followed the run time after the last washing cycle, with highest numbers after the 1st sampling with a 2-day run and lowest after the 3rd sampling with a 1-d run after the last washing cycle (Fig. 2). On the filler wheel the numbers of heterotrophic bacteria, lactic acid bacteria and yeasts were up to 4 logs higher after 2 d production compared to the 1 d production time.

Location on the filling line (block) also had a statistically significant effect on microbial numbers. At the canning line numbers of heterotrophic bacteria, lactic acid bacteria and yeasts were statistically significantly lower in block 3 at each sampling as compared to block 1 and 2. At the glass bottle line numbers of all microbial groups were statistically significantly higher at the filler table as compared to filler wheel at each sampling, except for heterotrophic bacteria in the 1st and 2nd sampling and yeasts in the 2nd sampling.

Despite these differences in bacterial numbers on the coupons, no clear effect of the coating type on the numbers of microbes on the surfaces could be shown.

Several microbial cells resembling bacteria, filamentous fungi and yeasts adhering to the steel surface were observed on surfaces after 96 days, using epifluorescence microscopy (Fig. 3). In SEM rod shaped bacteria tightly attached to steel surface embedded in debris and slime were seen (Fig. 4).

The bacterial community profiles generated by PCR-DGGE were clearly clustered according to the filling line; the canning and glass bottle lines separated from each other (Fig. 5). Also the location on the filling line (block) showed some clustering, as well as the sampling time. No clustering was observed due to the coating type, thus the different coatings did not have an effect on the bacterial communities attaching to surfaces. A few representative bands from each band group were sequenced for identification of bacteria (Fig. 6). The relatively short sequence amplified permitted identification to the genus level. Especially *Acinetobacter* sp. and lactic acid bacteria (*Lactobacillus* sp., *Lactococcus* sp., *Weissella* sp., and *Leuconostoc* sp.) were frequently detected (Table 3). Members of enterobacteriaceaea (e.g. *Enterobacter* sp., *Serratia* sp., *Citrobacter* sp.) were also common.

4. Discussion

In this study the microbial populations on equipment surfaces at two brewery filling lines were investigated as a function of coating, location and exposure time. The results showed clearly that the run time after washes and location on the filling line had a significant influence on the number and type of adhering microbes on surfaces, whereas the total exposure time or coating type did not.

The coupons at block 3 in the canning machine had lowest numbers of microbes at each sampling time compared to the other two blocks. Blocks 1 and 2 were placed next to each other, at a location in which open cans arrive at the seamer, allowing spills of

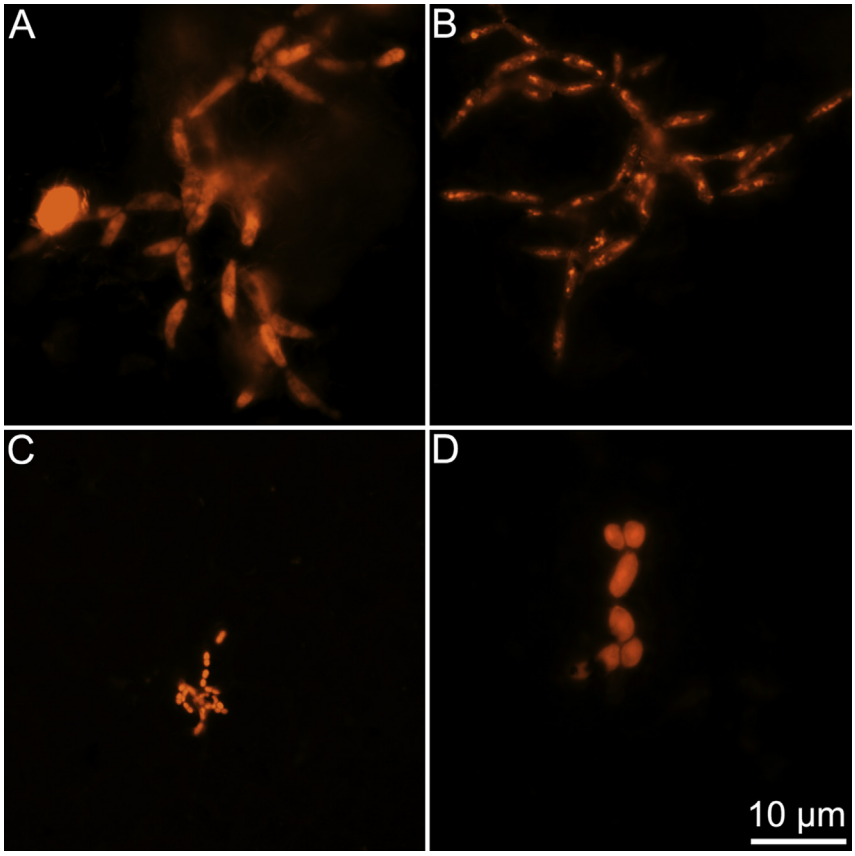

Fig. 3. Epifluorescence micrographs of AISI 304 stainless steel coupon from block one of the canning line, exposed to brewery process conditions for 97 d. The coupon was stained with acridine orange. The images show yeast (Panels A, B and D) and bacterial cells (Panel C) adhered on the surface of the steel coupon.

product onto the coupons. Block 3 was situated on the other side of the seamer, where the cans are sealed and less beer was dispensed in the water covering the coupons. At the glass bottle line, microbial numbers were higher on the filler table as compared to the filler wheel. The coupons on the filler table were continuously submerged in dilute beer, whereas the coupons on the filler wheel only had occasional sprays of product on them. The nutrients coming from spills of product thus have expectedly a clear increasing effect on microbial numbers.

Run time after the last washing cycle had a clear effect on microbial numbers on the surfaces; at both lines the numbers of adhering microbes were up to 4 logs higher after 2-3-d runs than after a 1-d run. Microbes thus proliferate and/or accumulate on surfaces between washing cycles, suggesting that relatively short production time and frequent cleaning are necessary for appropriate process hygiene. It has been shown previously that the first bacteria appear on the surfaces within hours after restarting the production (Storgårds, Tapani, Hartwall, Saleva, & Suihko, 2006). SEM examination of the coupons revealed that the bacteria adhering on filling machine surfaces are embedded in a matrix of extracellular polymeric substances. This might be the reason for colonisation after cleaning, since extracellular polymeric substances may anchor the bacterial cells on the surfaces, and protect them from external physical (shear forces) and chemical (cleaning and disinfection chemicals) stress factors (Flemming, 2011).

Photocatalytic TiO_2 and TiO_2 doped with Ag or Mo coatings deposited on steel using reactive magnetron sputtering and spray coating methods were investigated as antimicrobial surfaces for beverage filling process. In preceding studies executed in laboratory $TiO_2 + Mo$ coatings similar to those used in this study caused a 5-log reduction in bacterial (*E. coli*, *Serratia marcescens*, and *Pseudomonas rhodesiae*) counts and a 1-log reduction in yeast *Wickerhamomyces anomalus* count (Fisher et al., 2014), and the $TiO_2 + Ag$ coatings caused a 4-log reduction in *E. coli* counts (Navabpour, Ostovarpour, & Hampshire, et al., 2014). No clear effect of coatings, however, on microbial numbers could be shown in these process studies. There are several factors which may influence the functioning of photocatalytic coatings in this context: 1) the functioning parameters and durability of the coating, 2) the characteristics of microbial species adhering, 3) the wavelength and intensity of light, and 4) the presence of organic and inorganic substances on the surface. In addition, there were only five replicates and a high number of variables (location, exposure, time since rinse). Overall, it seems that the challenging factory environment has masked the effect previously demonstrated in the laboratory.

When antimicrobial coatings are applied on surfaces in industrial environment, essential characteristics in addition to their function is their durability in process conditions. In previously reported brewery process study $TiO_2 + Ag$ coatings, prepared using atomic layer deposition (ALD) technique, were damaged, and the Ag was dissolved from the surface, and the activity of the coating could not be evaluated (Priha et al., 2011). Prior to the present brewery study, the chemical and mechanical durability of the coatings were evaluated in a separate process study. These coatings deposited using reactive magnetron sputtering showed better mechanical durability and retention of active surface components

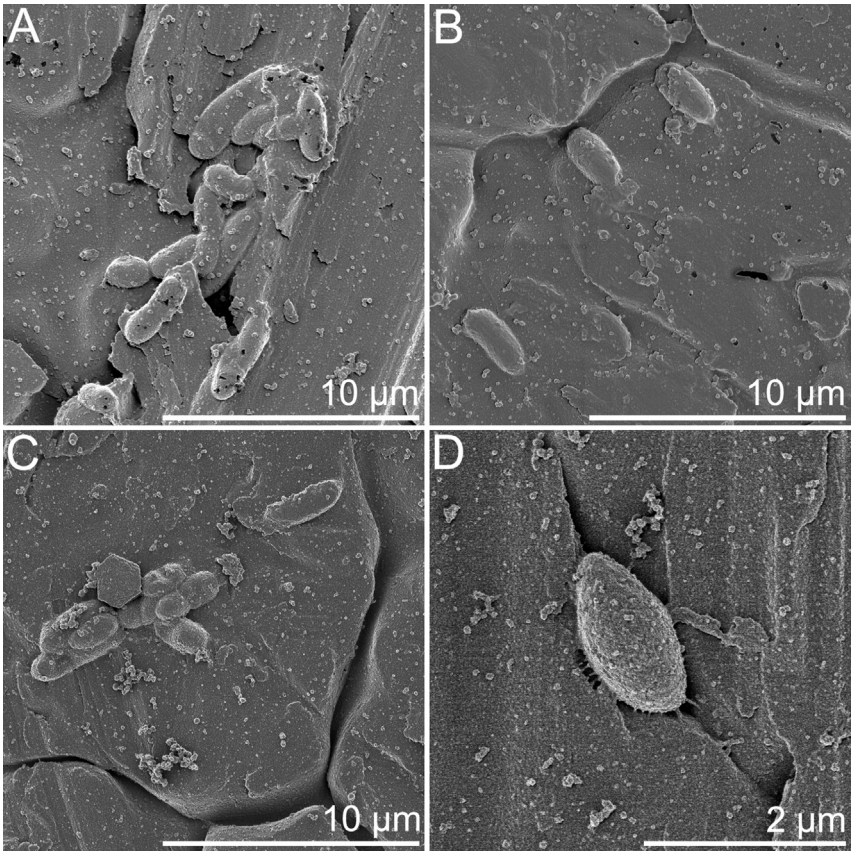

Fig. 4. FESEM micrographs of AISI 304 stainless steel coupon, exposed to brewery process conditions for 163 d on the filler table of a glass bottle line (block 3). Images show microbial cells adhered on the surface of the coupons as microcolonies. In panel A, a microcolony consisting of rod shaped bacteria (1 μm × 2–4 μm) adhered on crevice of stainless steel is shown. Three rod shaped bacteria (1 μm × 2 μm) adhered on the steel surface close to a grain boundary with organelles resembling stalk are shown in Panel B. Panel C shows a group of rod shaped bacteria (1 μm × 2–3 μm) tightly adhering on the coupon surface. Panel D shows high magnification micrograph of single bacterium adhered on the edges of a crevice with multiple pilus type organelles.

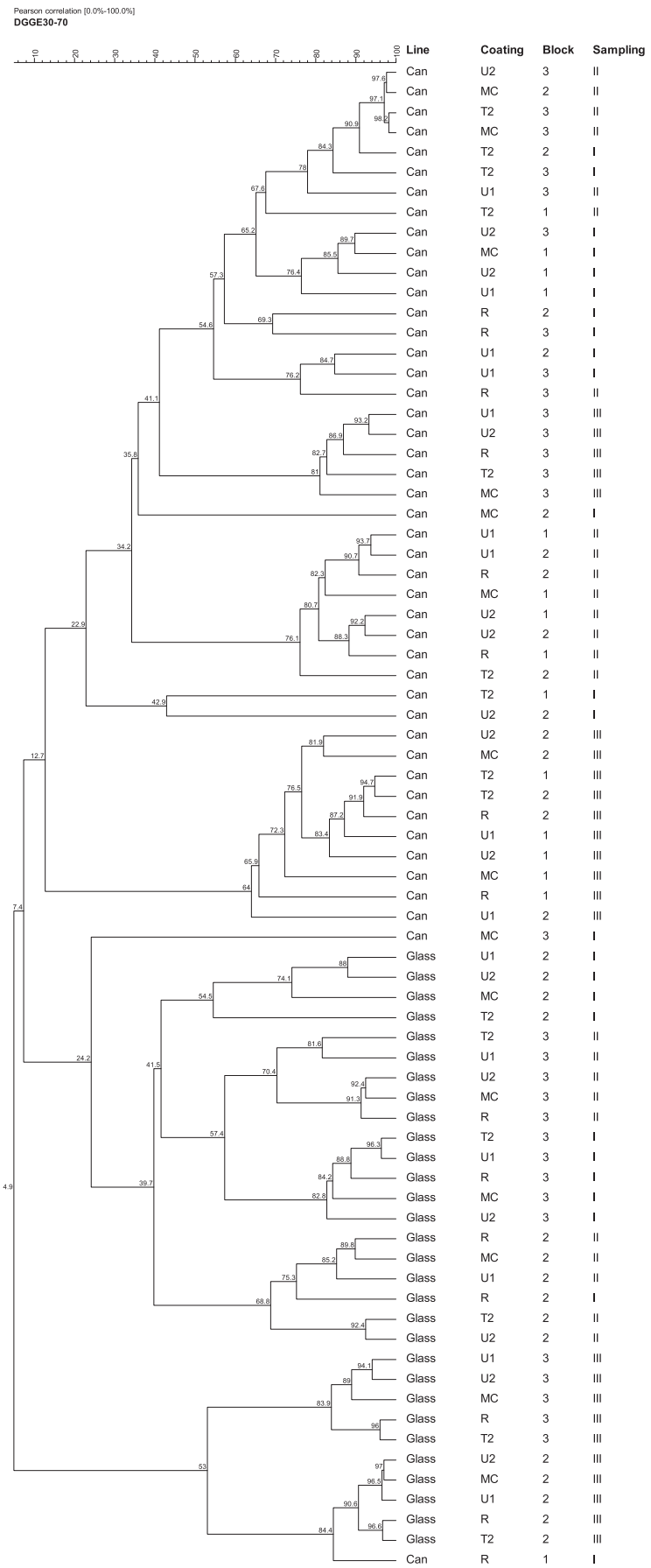

Fig. 5. Cluster analysis of DGGE profiles of the samples (Table 1 and 2). Pearson's correlation and UPGMA were used to construct the dendrogram. Numbers in branch nodes show similarity values.

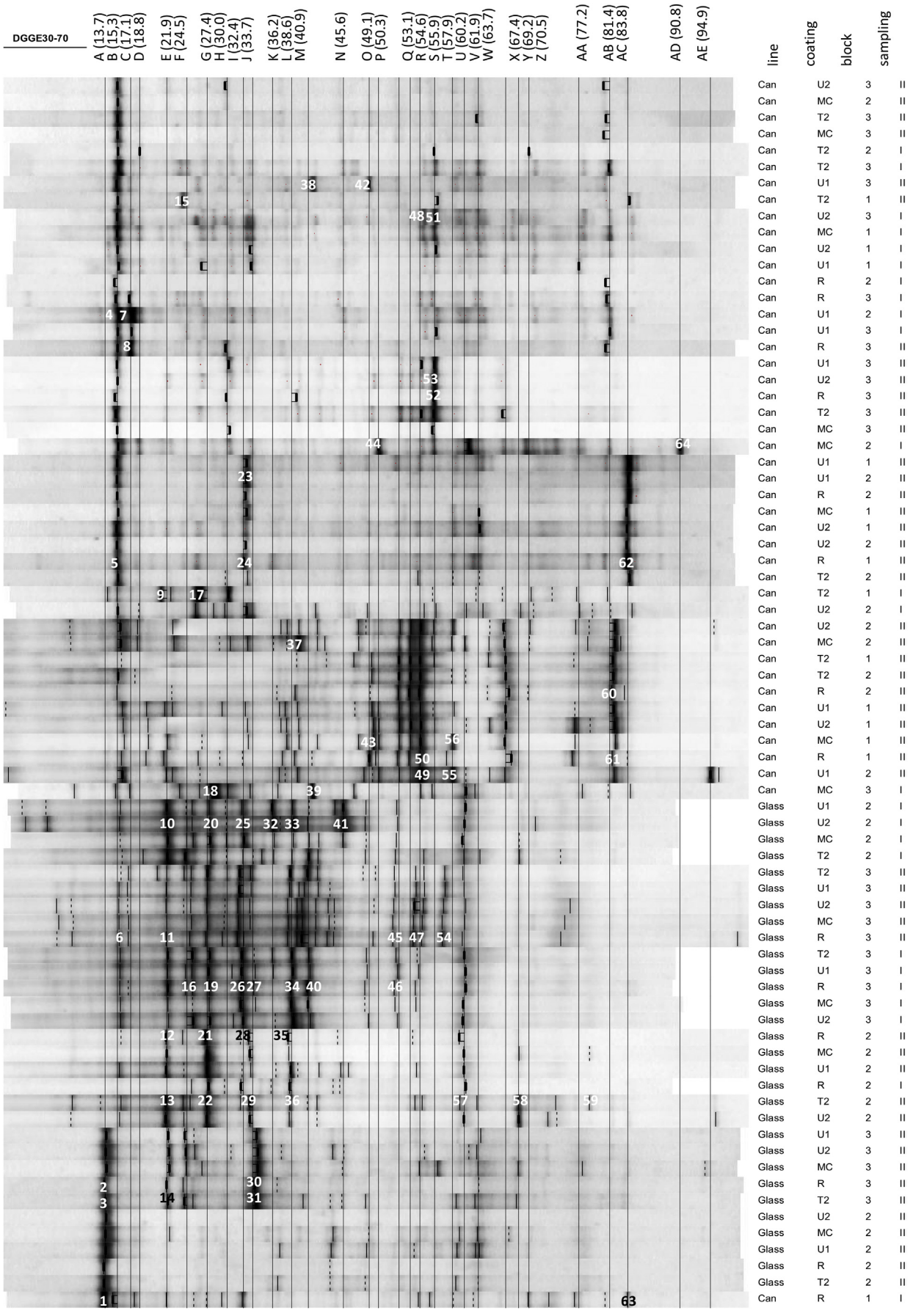

Fig. 6. DGGE gels of the samples (Tables 1 and 2). The letters on top show band classes, and the numbers in brackets after the letters show the percentage distance of the band class (The whole gel length is 100%). Numbers in the gel identify the sequenced bands shown in Table 3.

Table 3
Sequenced fragments from DGGE gels.

Band group	Band group, %	Band no	bp	Closest megablast hits	% Similarity
A	13.7	1	171	Eukaryotes	
		2	166	Eukaryotes	
		3	170	Eukaryotes	
B	15.3	4	169	Eukaryotes	
		5	168	Eukaryotes	
		6	186	*Pedobacter* sp.	99
C	17.1	7	194	*Weissella* sp.	100
		8	152	*Weissella* sp.	99
D	18.8		[a]		
E	21.9	9	192	*Leuconostoc* sp.	99
		10	168	Eukaryotes	
		11	170	Eukaryotes	
		12	168	Eukaryotes	
		13	168	Eukaryotes	
		14	109	Eukaryotes	
F	24.5	15	164	Eucaryotes	
		16	131	*Chryseobacterium* sp.	100
G	27.4	17	167	Eukaryotes	
		18	142	*Lactobacillus* sp.	100
		19	103	*Acinetobacter* sp.	100
		20	192	*Acinetobacter* sp.	100
		21	192	*Acinetobacter* sp.	99
		22	108	*Acinetobacter* sp.	100
H	30.0		[a]		
I	32.4	23	144	*Lactobacillus* sp.	100
		24	115	*Lactobacillus* sp.	100
		25	164	*Pseudomonas* sp.	100
		26	194	*Pseudomonas* sp.	100
J	33.7	27	169	*Brevundimonas* sp.	100
		28	192	uncultured	99
		29	128	*Acinetobacter* sp.	100
		30	100	uncultured	97
		31	186	uncultured	100
K	36.2	32	195	*Acinetobacter* sp.	100
L	38.6	33	195	*Acinetobacter* sp.	100
		34	192	*Acinetobacter* sp.	100
		35	110	*Acinetobacter* sp.	98
		36	108	*Acinetobacter* sp.	100
M	40.9	37	115	*Lactococcus* sp.	100
		38	192	*Lactococcus* sp.	100
		39	194	*Lactococcus* sp./*Lactobacillus* sp.	100
		40	105	*Lactococcus* sp.	100
N	45.6	41	194	*Exigiobacterium* sp.	100
O	49.1	42	191	*Escherichia* sp./*Shigella* sp.	100
		43	145	*Serratia* sp./*Yersinia* sp./*Rahnella* sp.	99
P	50.3	44	111	*Sphingomonas* sp.	99
Q	53.1	45	80	*Sphingomonas* sp./*Azospirillum* sp.	100
		46	118	*Comamonas* sp.	100
R	54.6	47	169	*Brevundimonas* sp.	100
S	55.9	48	130	*Mesorhizobium* sp.	100
		49	190	*Enterobacter* sp.	100
		50	124	*Citrobacter* sp.	98
T	57.9	51	139	uncultured	100
		52	177	uncultured	99
		53	191	uncultured	99
U	60.2	54	82	*Sphingomonas* sp.	100
		55	184	*Enterobacter* sp./*Salmonella* sp.	99
		56	93	*Pantoea* sp./*Enterobacter* sp./*Shigella* sp.	100
V	61.9	57	169	uncultured a-proteobacterium	99
W	63.7		[a]		
X	67.4		[a]		
Y	69.2	58	59	*Microbacterium* sp.	100
Z	70.5		[a]		
AA	77.2	59	86	*Streptomyces* sp.	100
	81.4	60	115	*Enterobacter* sp.	97
		61	85	*Enterobacter* sp.	97
AB	83.8	62	74	*Propionibacterium* sp.	100
		63	177	*Propionibacterium* sp.	99
AC	90.8	64	169	uncultured	100
AD	94.9		[a]		

[a] No successful sequences obtained.

than the spray coated sol–gel surfaces, whilst the spray-deposited coatings showed enhanced retention of photocatalytic properties Navabpour, Ostovarpour, & Hampshire, et al., 2014). In addition to the manufacturing method, coating thickness and barrier layers also have a role in determining the functioning of the coating. With ALD prepared TiO_2 coatings it has been shown that 500 nm thick coating reduced bacterial adhesion more efficiently than 250 nm thick (Allion et al., 2007). SiO_2 barrier layers between stainless steel and TiO_2 films have also been shown to increase photocatalytic activity Evans, English, Hammond, Pemble, & Sheel, 2007).

Most studies showing the microbial killing effect of photocatalytic and/or antimicrobial coatings have been done in laboratory with single microbial species, and the reductions vary from rather insignificant (10%) to even 6 logs (Allion et al., 2007; Kühn et al., 2003; Li & Logan, 2005; Raulio et al., 2006). The susceptibility of different microbial species to photocatalysis or silver nanoparticles varies: *Pseudomonas* sp. have repeatedly been shown to be more resistant to both than *E. coli*; Gram positive bacteria are more resistant than Gram negative bacteria; and yeasts are more resistant that bacteria (Kühn et al., 2003; Naik & Kowshik, 2014; Pal et al., 2007). Despite the innate antimicrobial properties of molybdenum and silver and the photocatalytic properties of the TiO_2, it is apparent that the genuine process conditions with multispecies bacterial communities and high numbers of yeasts are considerably more challenging to the coatings than the laboratory studies.

Comparison of UVA activation intensities required for TiO_2 coatings to kill microorganisms are complicated by variable light intensities and spectral ranges applied, and sometimes even failure to report them. In some studies showing the microbial killing effect of TiO_2 coatings the reported UVA intensities vary from 100 $\mu W\ cm^{-2}$ (Raulio et al., 2006) to 4600 $\mu W\ cm^{-2}$ (Li & Logan, 2005). In the ISO standard for studying the antibacterial activity of photocatalytic materials a maximum UV intensity of 250 $\mu W\ cm^{-2}$ is recommended to avoid damage of microbes by UV irradiation only (ISO 27447:2009). In this study, the light intensity in the process conditions was low, around 0.5 $\mu W\ cm^{-2}$ for UVA and 34 $\mu W\ cm^{-2}$ for VIS. Our hypothesis was thus that the activity of the coatings in the process conditions relies mostly on antibacterial components instead of photoactivity. It was, however, expected that the combination of antibacterial metals and TiO_2 could also have caused some photocatalysis in weak UV intensity, as shown by Sunada et al. (2003) for Cu/TiO_2 coatings at UV intensity of 1 $\mu W\ cm^{-2}$.

It has been previously reported that organic or inorganic chemicals may retard the photocatalytic effect of TiO_2 (Epling & Lin, 2002). In this study the coatings received spills of product on the filler machines, which could also decrease the activity of the coatings. Our observation that the most important factor affecting microbial numbers was run time after washes – a few days – rather than the total duration of exposure – some months – indicates the effectiveness of cleaning procedures, and suggests that experiments monitoring the effect of novel surfaces and treatments might need only to be carried out over shorter times, using run time after washes as the key parameter.

The bacterial communities remained characteristic to each filling line and location on the filling line throughout the study. The relatively short amplicon, ~200 bp, created with the Muyzer primers (Muyzer et al., 1993) did not allow identification to species level, and also permitted the amplification of eukaryotic DNA. The advantage of these primers is their high sensitivity with low DNA concentrations. The previous studies reporting microbial communities on beverage process surfaces are few. Timke,Wang-Lieu, Altendorf, and Lipski (2005), Timke, Wolking, Wang-Lieu, Altendorf, and Lipski (2005) showed that biofilms on two conveyor belts included the genera *Acidovorax*, *Achromobacter*, *Acinetobacter*,

Bacillus, *Brevundimonas*, *Citrobacter*, *Chryseobacterium*, *Enterobacter*, *Erwinia*, *Klebsiella*, *Microbacterium*, *Pseudomonas, Rhizobium* and *Stenotrophomonas*. Storgårds et al. (2006) studied filling machines of three breweries, and isolated and identified members of the genera *Acetobacter*, *Achromobacter*, *Bacillus*, *Enterococcus*, *Klebsiella*, *Lactobacillus*, *Lactococcus*, *Mycobacterium*, *Pantoea*, *Pediococcus*, *Pseudomonas* and *Serratia*. The present study is in accordance with the data reported previously; especially *Acinetobacter* sp., lactic acid bacteria (*Lactobacillus* sp., *Lactococcus* sp., *Weissella* sp., *Leuconostoc* sp.) and enterobacteria were shown to be common on the surfaces (Table 3). The frequent encounter of *Acinetobacter* spp. is interesting, since in a study analysing the organisms first appearing on cleaned brewery surfaces, *Acinetobacter* spp. accounted for up to 71% of all detected microbes, and was shown to adhere more readily and firmly to stainless steel than most other microorganisms (Lipski, 2005) . Thus this bacterium is probably providing a foundation on which other microorganisms can settle and proliferate. *Chryseobacterium* spp. was detected in our study, and it has also been thought to be involved in the rapid recolonisation of cleaned surfaces and biofilm formation in beer bottling plants (Herzog, Winkler, Wolking, Kämpfer, & Lipski, 2008). Since beer is a hostile environment for most microorganisms, only a few species are known to cause spoilage of beer, mainly bacteria representing the genera *Lactobacillus*, *Pediococcus*, *Pectinatus* and *Megasphaera* (Storgårds & Priha, 2009). It is assumed that beer-spoilage organisms themselves are not the primary colonisers of process surfaces, but instead they benefit from the biofilm formation initiated by other species (Back, 1994). The solution to biofilm-related problems should thus be the prevention of microbial adhesion – an aim which could be established with functional coatings.

5. Conclusion

In summary, this study showed that increasing run time after washes and nutrients provided by beer spilled on the coupons increased microbial numbers on them. The study also showed that the two filling lines had their characteristic bacterial communities, the major species belonging to *Acinetobacter* sp., lactic acid bacteria and enterobacteria. In spite of promising *in vitro* data showing antimicrobial properties of doped photocatalytic coatings in a previous study, no effect on microbial numbers on the surfaces was discerned *in situ*. Most of the studies with photocatalytic coatings so far have been based on laboratory experiments. This study was performed to narrow the gap between experimental work and functionality in real industrial environments. As a result, coatings with good mechanical and chemical durability and thus suitable for industrial surfaces have been developed, but the efficiency of these coatings in reducing the number of microorganisms on the surfaces in the challenging beverage process conditions demands further investigation.

Acknowledgements

This work was part of the MATERA + Project “Disconnecting”, ref MFM-1855. Funding from the Finnish Funding Agency for Technology and Innovation (Tekes, Funding decision 40306/10) and Technology Strategy Board, Project No. 620015 the UK's innovation agency, is gratefully acknowledged. The authors would like to thank Oy Panimolaboratorio–Bryggerilaboratorium Ab (PBL Brewing Laboratory) for their financial support and for the time and resources provided, and Tarja Nordenstedt and Merja Salmijärvi for technical assistance. Dr Riikka Juvonen is thanked for providing the DGGE sequence ladder.

References

Allion, A., Merlot, M., Boulangé-Petermann, L., Archambeau, C., Choquet, P., & Damasse, J.-M. (2007). Thin photocatalytic TiO_2 coatings: impact on bioadhesion and cell viability. *Plasma Processes and Polymers, 4*, S374–S379.

Back, W. (1994). Secondary contaminations in the filling area. *Brauwelt International, 12*, 326–333.

Cho, M., Chung, H., Choi, W., & Yoon, J. (2005). Different inactivation behaviors of MS-2 phage and *Escherichia coli* in TiO_2 photocatalytic disinfection. *Applied and Environmental Microbiology, 71*, 270–275.

Epling, G., & Lin, C. (2002). Investigation of retardation effects on the titanium dioxide photodegradation system. *Chemosphere, 46*, 937–944.

Evans, P., English, T., Hammond, D., Pemble, M. E., & Sheel, D. W. (2007). The role of SiO_2 barrier layers in determining the structure and photocatalytic activity of TiO_2 films deposited on stainless steel. *Applied Catalysis A: General, 321*, 140–146.

Fisher, L., Ostovarpour, S., Kelly, P., Whitehead, K. A., Cooke, K., Storgårds, E., et al. (2014). Molybdenum doped titanium dioxide photocatalytic coatings for use as hygienic surfaces – the effect of soiling on antimicrobial activity. *Biofouling, 30*, 911–919.

Flemming, H.-C. (2011). The perfect slime. *Colloids and Surfaces B: Biointerfaces, 86*, 251–259.

Fujishima, A., Zhang, Z., & Tryk, D. A. (2008). TiO_2 photocatalysis and related surface phenomena. *Surface Science Reports, 63*, 515–582.

Herzog, P., Winkler, I., Wolking, D., Kämpfer, P., & Lipski, A. (2008). *Chryseobacterium ureilyticum* sp. nov., *Chryseobacterium gambrini* sp. nov, *Chryseobacterium pallidum* sp. nov., *Chryseobacterium molle* sp. nov., isolated from beer-bottling plants. *International Journal of Systematic and Evolutionary Microbiology, 58*, 26–33.

Ibáñez, J. A., Litter, M. I., & Pizarro, R. A. (2003). Photocatalytic and bactericidal effect of TiO_2 on *Enterobacter cloacae* Comparative study with other Gram (-) bacteria. *Journal of Photochemistry and Photobiology A: Chemistry, 157*, 81–85.

ISO 27447:2009(E).Fine ceramics (advanced ceramics, advanced technical ceramics) – Test method for antibacterial activity of semiconducting materials. International Standard.

Keskinen, H., Mäkelä, J. M., Aromaa, M., Keskinen, J., Areva, S., Teixeira, C. V., et al. (2006). Titania and titania-silver nanoparticle deposits made by liquid flame spray and their functionality as photocatalyst for organic- and biofilm removal. *Catalysis Letters, 111*, 127–132.

Kühn, K. P., Chaberny, I. F., Massholder, K., Stickler, M., Benz, V. W., Sonntag, H.-G., et al. (2003). Disinfection of surfaces by photocatalytic oxidation with titanium dioxide and UVA light. *Chemosphere, 53*, 71–77.

Li, B., & Logan, B. E. (2005). The impact of ultraviolet light on bacterial adhesion to glass and metal oxide-coated surface. *Colloids and Surfaces B: Biointerfaces, 41*, 153–161.

Lipski, A. (2005). New focus in combating biofims: the pioneer organisms on cleaned surfaces. *Brauerei Forum, 20*, 178–179 (In German).

McGinnis, S., & Madden, T. L. (2004). BLAST: at the core of a powerful and diverse set of sequence analysis tools. *Nucleic Acids Research, 32*, W20–W25.

Muyzer, G., De Waal, E. C., & Uitterlinden, A. G. (1993). Profiling of complex microbial populations by denaturing gradient gel electrophoresis of polymerase chain reaction-amplified genes coding for 16S rRNA. *Applied and Environmental Microbiology, 59*, 695–700.

Naik, K., & Kowshik, M. (2014). Anti-biofilm efficacy of low temperature processed AgCl–TiO_2 nanocomposite coating. *Materials Science and Engineering, C 34*, 62–68.

Navabpour, P., Ostovarpour, S., Hampshire, J., Kelly, P., Verran, J., & Cooke, K. (2014). The effect of process parameters on the structure, photocatalytic and self-cleaning properties of TiO_2 and Ag-TiO_2 coatings deposited using reactive magnetron sputtering. *Thin Solid Films, 571*, 75–83.

Navabpour, P., Ostovarpour, S., Tattershall, C., Cooke, K., Kelly, P., Verran, J., et al. (2014). Photocatalytic TiO_2 and doped TiO_2 coatings to improve the hygiene of surfaces used in food and beverage processing – a study of the physical and chemical resistance of the coatings. *Coatings, 4*, 433–449.

Nübel, U., Engelen, B., Felske, A., Snaidr, J., Wieshuber, A., Amann, R. I., et al. (1996). Sequence heterogeneities of genes encoding 16S rRNAs in *Paenibacillus polymyxa* detected by temperature gradient gel electrophoresis. *Journal of Bacteriology, 178*, 5636–5643.

Page, K., Wilson, M., & Parkin, I. P. (2009). Antimicrobial surfaces and their potential in reducing the role of the inanimate environment in the incidence of hospital-acquired infections. *Journal of Materials Chemistry, 19*, 3819–3831.

Pal, A., Pehkonen, S. O., Yu, L. E., & Ray, M. B. (2007). Photocatalytic inactivation of gram-positive and gram-negative bacteria using fluorescent light. *Journal of Photochemistry and Photobiology A: Chemistry, 186*, 335–341.

Priha, O., Laakso, J., Tapani, K., Levänen, E., Kolari, M., Mäntylä, T., et al. (2011). Effect of photocatalytic and hydrophobic coatings on brewery surface microorganisms. *Journal of Food Protection, 74*, 1891–1901.

Rajagopal, G., Maruthamuthu, S., Mohanan, S., & Palaniswamy, N. (2006). Biocidal effects of photocatalytic semiconductor TiO_2. *Colloids and Surfaces B: Biointerfaces, 51*, 107–111.

Ratova, M., Kelly, P. J., West, G. T., & Iordanova, I. (2013). Enhanced properties of magnetron sputtered photocatalytic coatings via transition metal doping. *Surface & Coatings Technology, 228*, S544–S549.

Raulio, M., Pore, V., Areva, S., Ritala, M., Leskelä, M., Lindén, M., et al. (2006). Destruction of *Deinococcus geothermalis* biofilm by photocatalytic ALD and sol-gel TiO_2 surfaces. *Journal of Industrial Microbiology and Biotechnology, 33*, 261–268.

Storgårds, E., & Priha, O. (2009). Biofilms and brewing. In P. M. Fratamico, B. A. Annous, & N. W. Gunther, IV (Eds.), *Biofilms in the food and beverage industries* (pp. 432–454). Oxford: Woodhead Publishing Limited.

Storgårds, E., Tapani, K., Hartwall, P., Saleva, R., & Suihko, M.-L. (2006). Microbial attachment and biofilm formation in brewery bottling plants. *Journal of the American Society of Brewing Chemists, 64*, 8–15.

Sunada, K., Watanabe, T., & Hashimoto, K. (2003). Bactericidal activity of copper-deposited TiO_2 thin film under weak UV light illumination. *Environmental Science and Technology, 37*, 4785–4789.

Timke, M., Wang-Lieu, N. Q., Altendorf, K., & Lipski, A. (2005). Community structure and diversity of biofilms from a beer bottling plant as revealed using 16S rRNA gene clone libraries. *Applied and Environmental Microbiology, 71*, 6446–6452.

Timke, M., Wolking, D., Wang-Lieu, N. Q., Altendorf, K., & Lipski, A. (2005). Microbial composition of biofilms in a brewery investigated by fatty acid analysis, fluorescence in situ hybridisation and isolation techniques. *Applied Microbiology and Biotechnology, 66*, 100–107.

Zoetendal, E. G., Akkermans, A. D. L., & De Vos, W. (1998). Temperature gradient gel electrophoresis analysis of 16S rRNA from human fecal samples reveals stable and host-specific communities of active bacteria. *Applied and Environmental Microbiology, 64*, 3854–3859.

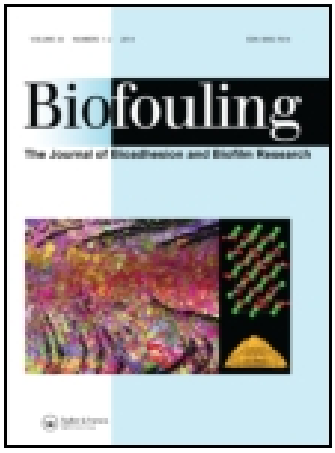

Biofouling: The Journal of Bioadhesion and Biofilm Research
Publication details, including instructions for authors and subscription information:
http://www.tandfonline.com/loi/gbif20

Molybdenum doped titanium dioxide photocatalytic coatings for use as hygienic surfaces: the effect of soiling on antimicrobial activity

L. Fisher[a], S. Ostovapour[ab], P. Kelly[b], K.A. Whitehead[a], K. Cooke[c], E. Storgårds[d] & J. Verran[a]
[a] School of Healthcare Science, Manchester Metropolitan University, Manchester, UK
[b] Surface Engineering Group, Manchester Metropolitan University, Manchester, UK
[c] Miba Coating Group, Teer Coatings Ltd, Droitwich, UK
[d] VTT Technical Research Centre of Finland, Espoo, Finland
Published online: 02 Sep 2014.

To cite this article: L. Fisher, S. Ostovapour, P. Kelly, K.A. Whitehead, K. Cooke, E. Storgårds & J. Verran (2014) Molybdenum doped titanium dioxide photocatalytic coatings for use as hygienic surfaces: the effect of soiling on antimicrobial activity, Biofouling: The Journal of Bioadhesion and Biofilm Research, 30:8, 911-919

To link to this article: http://dx.doi.org/10.1080/08927014.2014.939959

Biofouling, 2014
Vol. 30, No. 8, 911–919, http://dx.doi.org/10.1080/08927014.2014.939959

Taylor & Francis
Taylor & Francis Group

Molybdenum doped titanium dioxide photocatalytic coatings for use as hygienic surfaces: the effect of soiling on antimicrobial activity

L. Fisher[a], S. Ostovapour[a,b], P. Kelly[b], K.A. Whitehead[a], K. Cooke[c], E. Storgårds[d] and J. Verran[a]*

[a]*School of Healthcare Science, Manchester Metropolitan University, Manchester, UK;* [b]*Surface Engineering Group, Manchester Metropolitan University, Manchester, UK;* [c]*Miba Coating Group, Teer Coatings Ltd, Droitwich, UK;* [d]*VTT Technical Research Centre of Finland, Espoo, Finland*

(*Received 14 November 2013; accepted 21 June 2014*)

Titanium dioxide (TiO_2) surfaces doped with molybdenum (Mo) were investigated to determine if their photocatalytic ability could enhance process hygiene in the brewery industry. Doping TiO_2 with Mo showed a 5-log reduction in bacterial counts within 4 to 24 h and a 1-log reduction in yeast numbers within 72 h. The presence of a dilute brewery soil on the surface did not interfere with antimicrobial activity. The TiO_2–Mo surface was also active in the dark, showing a 5-log reduction in bacteria within 4 to 24 h and a 1-log reduction in yeast numbers within 72 h, suggesting it could have a novel dual function, being antimicrobial and photocatalytic. The study suggests the TiO_2–Mo coating could act as a secondary barrier in helping prevent the build-up of microbial contamination on surfaces within the brewery industry, in particular in between cleaning/disinfection regimes during long production runs.

Keywords: photocatalytic surfaces; titanium dioxide; molybdenum; antimicrobial activity; brewery microorganisms; soiling

Introduction

The photocatalytic properties of titanium dioxide (TiO_2) are well documented (Fujishima et al. 2000; Foster et al. 2011), and its use in the degradation of pollutants in water and air is well established (Fujishima & Honda 1972; Frank & Bard 1977). Titanium dioxide is a semiconductor with a wide band gap (3.2 eV), which can be excited by ultraviolet (UV) irradiation ($\lambda < 380$ nm). Photons with energy equal to or higher than their band gap can promote an electron from the valence band to the conduction band, producing electron-hole pairs. The photogenerated electrons react with molecular oxygen (O_2) to produce superoxide radical anions ($^{\bullet}O_2^-$), and the photogenerated holes react with water to produce hydroxyl ($^{\bullet}OH$) radicals (Fujishima et al. 2000; Daviðsdóttir et al. 2013). UV light and reactive radical species are able to decompose organic compounds and inactivate microorganisms. Immobilized TiO_2 particles deposited as thin films on substrata can also become superhydrophilic after UV illumination, making residual material easily displaced with water. Thus, TiO_2 surfaces can also have a self-cleaning effect (Fujishima et al. 2000) as well as being able to degrade pollutants and microorganisms through photocatalysis.

It is widely recognized that environmental surfaces can act as reservoirs for microbial fouling, and in recent years there have been many publications regarding photocatalytic disinfection with reports referring to the destruction of Gram-positive and Gram-negative bacteria as well as fungi, algae, protozoa, endospores, and viruses (Foster et al. 2011). Both the photocatalytic disinfection and the self-cleaning properties of TiO_2 surfaces make them potentially applicable to areas where microbial fouling can arise, for example, in hospital settings or in the food and beverage industry. Within a brewery environment, the hygienic status of process surfaces plays a major role in ensuring the quality of the beer. Beer production and dispensing often take place in closed systems, where in-place cleaning procedures are applied (Storgards 2000). The cleaning and disinfection regimes employed are essential for removing product deposits and microbial populations. However, long production runs between cleaning cycles are typical, making such systems more susceptible to bacterial accumulation. The accumulation of bacteria on surfaces can lead to the development of biofilms, which may consist of multiple communities of microorganisms (Costerton et al. 1995). The secretion of an extracellular matrix by these organisms helps protect them against disinfection, thus biofilms, once established, can be difficult to eradicate from surfaces (Costerton et al. 1995). Hard-to-reach areas can also be problematic. The use of photocatalytic surfaces under such circumstances could help towards inhibiting the build-up of microbial populations during long production runs and in between disinfection cycles, and provide a greener and more cost-effective disinfection

*Corresponding author. Email: J.Verran@mmu.ac.uk

strategy by reducing energy, water, and chemical consumption. However, since UV light is required to activate photocatalytic surfaces, the use of TiO_2 in indoor situations is limited.

Doping TiO_2 with transition metals causes a shift reduction in the band gap, enabling surfaces to become active under visible light (Wilke & Breuer 1999). TiO_2 doped with a transition metal can be deposited as a thin film coating onto surfaces such as stainless steel, typically used in breweries. In a study by Ratova et al. (2013), thin films of TiO_2 were doped with different amounts of the transition metals molybdenum (Mo), niobium (Nb), tungsten (W), and tantalum (Ta) onto glass substrata using reactive magnetron co-sputtering. The films were analysed in terms of their composition and structure by energy-dispersive X-ray spectroscopy (EDX) and Raman spectroscopy, and their photocatalytic activity was assessed by the degradation of the organic dye methylene blue under UV and fluorescent light sources. The study reported that, after annealing in air at 600°C, TiO_2 coatings doped with Mo exhibited the highest photocatalytic activity under both light sources. This was attributed to the presence of an anatase crystalline phase and a 'red-shift' in band-gap energy towards the visible spectrum (Ratova et al. 2013). However, the photocatalytic effect against bacteria was not examined.

The aim of the current study was to develop a novel photocatalytic surface by applying an Mo-doped TiO_2 coating to a stainless steel substratum and to determine whether process hygiene in the brewery industry could be improved. The first stage was to identify an optimal doping level to ensure photoactivity under fluorescent/visible light. Following this, the efficacy of the surface was tested against *Escherichia coli* (a model organism) and then microrganisms isolated from brewery surfaces to determine whether a brewery (beer) conditioning film reduced the activity of the TiO_2-doped surface.

Materials and methods

Production of photocatalytic thin films

Stainless steel (AISI 304-2B) was used as a substratum upon which thin films of TiO_2 doped with Mo were deposited by a closed field unbalanced magnetron sputter ion plating technique (Teer Coatings Ltd, Droitwich, UK) (Laing et al. 1999). The production of the thin films was as described by Ratova et al. (2013). In brief, three 300 mm × 100 mm vertically opposed unbalanced planar magnetrons and one blanking plate were installed in the chamber, and two magnetrons were fitted with titanium (Ti) targets and one with the Mo dopant metal target. All targets were of 99.5% purity. The magnetrons with the titanium targets were in the closed field configuration and driven in pulsed DC sputtering mode using a dual-channel Advanced Energy Pinnacle Plus supply at a frequency of 100 kHz and a duty of 50% (in synchronous mode). The Mo metal target was driven in continuous DC mode (Advanced Energy MDX). The Ti targets were operated at a constant time-averaged power of 1 kW, and the dopant target was operated at powers in the range of 0–240 W, selected to produce a range of dopant levels in the coatings. The base pressure of the sputtering chamber was 1×10^{-3} Pa. The flow rate of argon was controlled through a mass flow controller, and the flow rate of oxygen was controlled by an optical emission monitor set to 15% of the full metal (Ti) signal, which had been previously determined to produce stochiometric TiO_2 coatings (Ratova et al. 2013). Stainless steel samples (2 × 1 cm) were mounted on a substratum holder, which was rotated between the magnetrons at 4 rpm during deposition. The target to substratum separation was 8 cm. The Ti and Mo targets were cleaned by pre-sputtering in a pure argon atmosphere for 10 min. Deposition times were adapted to obtain a film thickness of 800 nm to 1 µm. The sputtered films were post-deposition annealed at 600°C for 30 min in air.

Coating characterization

Energy dispersive X-ray spectroscopy (EDX – Edax Trident, Mahwah, NJ) was employed to analyse the coating compositions and determine the dopant level. Previous experience had shown that the as-deposited coatings would be amorphous. Thus, the TiO_2 and TiO_2–Mo thin films were annealed at 600°C and then analysed by X-ray diffraction (XRD) in the θ–2θ mode (URD6 Seifert & Co. diffractometer with $CuK\alpha_1$ radiation at 0.154 nm) and by Raman spectroscopy (Renishaw Invia, 514 nm laser) to obtain information regarding their crystalline structure.

Photocatalytic activity

Photocatalytic activity levels were determined *via* the degradation of the organic dye methylene blue (MB) (Alfa Aesar, Lancaster, UK), since MB is a dye often used as a model organic compound to measure photoreactivity (Ratova et al. 2013). Aqueous MB absorbs light most strongly at about 660 nm with a given molar absorptivity of 10^5 dm^3 mol^{-1} cm^{-1}. The absorbance at 660 nm *vs* the UV or fluorescent irradiation time can be translated into a graph of peak height absorbance against irradiation time, which has an exponential form (Houas et al. 2001). MB concentrations were calculated using the measured absorbance peak around 663 nm. The formula below was used to calculate the photocatalytic activity of each of the films. Two parameters were defined: P_{aUV} for UV irradiation and P_{aFL} for fluorescent light irradiation.

$$P_a = 1 - [C_0 e^{-mx} / C_0 e^{-ex}]$$

where: C_0 is the peak height at time = 0 (ie the initial concentration), $C_0 e^{-mx}$ is the decay rate of MB with no sample present, and $C_0 e^{-cx}$ is the decay rate of MB in contact with a photocatalytic coating

The decomposition of MB was assessed using an initial concentration of 0.105 mmol l^{-1}. Annealed TiO_2 and TiO_2–Mo samples were placed in 10 ml of MB solution, which was irradiated at an integrated power flux of 4 mW cm^2 with 2 × 15 W 352 nm UV tubes (Black Ray, Cambridge, UK) or at an integrated power flux of 6.4 mW cm^2 with 2 × 15 W fluorescent tubes, of which the UV component (300–400 nm) was 0.5 mW cm^2. A 10 cm distance between the light source and MB solution was used, and a UV/Vis spectrophotometer (PerkinElmer, Seer Green, UK) was employed to measure the absorbance peak height. Measurements were taken every hour over a total of 5 h.

Using the above approach, photoactivity values were recorded for all the TiO_2 and TiO_2–Mo coatings, and from those results, the optimal dopant level was identified. Samples with that composition were then tested in the presence of soiling (20 µl dried on undiluted beer) under UV and fluorescent light.

Antimicrobial activity

Microorganisms

Escherichia coli (ATCC 8,739) was used as a model organism in the first instance. Microorganisms isolated from brewery surfaces were obtained from VTT Culture Collection and included *Pseudomonas rhodesiae* E-031,889, *Serratia marcescens* E-031,888, and *Wickerhamomyces anomalus* C-02,470. *E. coli*, *P. rhodesiae*, and *S. marcescens* were cultured on Nutrient agar (Oxoid, Basingstoke, UK) and *W. anomalus* on YM agar (Difco, Detroit, MI). Incubation was at 37°C for *E. coli*, 30°C for *P. rhodesiae* and *S. marcescens*, and 25°C for *W. anomalus* for 24–48 h.

Light source

For the antimicrobial assays, surfaces were illuminated (wavelength range of 300–700 nm) in a cooled incubator (Gallenkamp, Loughborough, UK) fitted with six fluorescent lamps (Sylvania, Ontario, Canada) with an energy output of 6.4 mW cm^2. The intensity of irradiation was previously determined at the surface of the coating. The temperature was set at 20°C.

Antimicrobial assay

Measurements of the antimicrobial activity of the TiO_2–Mo photocatalytic surfaces were performed using ISO 27447:2009 as guidance (with minor modifications). A single colony of each organism was placed in 10 ml of Nutrient broth (Oxoid) or YM broth (Difco) for *W. anomalus* and incubated for 18–24 h at the appropriate temperature in a shaker incubator set at 150 rpm. Suspensions were centrifuged at 1,560 *g* for 10 min and the cells were washed in Ringer's solution (Oxoid) prior to re-centrifugation. An OD_{540} of 0.08 (Jenway 6305 Spectrophotometer) in Ringer's solution was obtained and a 1:10 dilution performed prior to inoculating 50 µl onto the 2 × 1 cm surfaces (~10^5 cfu ml^{-1}) contained within a Petri dish. A 2 × 1 cm polyethylene film (Scientific Laboratory Supplies, Nottingham, UK) was placed over the bacterial suspension to ensure even distribution and the surfaces were placed in a tissue culture tray (Corning, Halstead, UK) with the lid on and placed under fluorescent light set up in a 20°C incubator under static conditions. The humidity was carefully maintained to avoid suspensions drying on the surface. At selected time points (0, 12, 24 and 48 h), surfaces were removed and vortexed for 1 min in a neutralizing broth (20 g l^{-1} Soya Lectin (Holland and Barrett, London) and 30 g l^{-1} Tween 80 (Sigma Aldrich, Irvine, UK) to remove attached bacteria (Caballero et al. 2010). The bacteria removed from the surface were diluted 1:10 in 0.9% sodium chloride (Fisher Scientific, Fair Lawn, NJ) as appropriate and 100 µl inoculated and spread onto the appropriate pre poured agar plate. Colony counts were performed after overnight incubation. All tests were carried out in triplicate. Stainless steel was used as a 'light control', and a set of coated surfaces was kept in dark conditions to serve as 'dark controls'.

Tests were performed on the 2 × 1 cm TiO_2–Mo coatings immediately after annealing and on coatings that had been soiled with either undiluted beer or diluted beer (10%). Beer used to simulate soiling was a pasteurized, commercial product (water, alcohol, protein, carbohydrates, vitamins, and minerals). Twenty microlitres of undiluted or beer diluted in sterile distilled water was dried onto the surfaces prior to the application of 50 µl of 10^5 cfu ml^{-1} bacterial suspension. The effect of soiling on microbial inactivation was examined over an irradiation period of up to 96 h.

Minimum inhibitory concentration determination

In order to determine the minimum inhibitory concentrations (MICs) of Mo, an agar incorporation method was used (Wiegand et al. 2008). Stock solutions (1,000 mg l^{-1}) of Mo standard for AAS (Sigma Aldrich, Dorset, UK) in liquid form were serially diluted to cover concentrations ranging from 0.25 to 5 mg l^{-1}. Since stock solutions of Mo also contained 10% hydrochloric acid, serial dilutions were also performed as above using hydrochloric acid (Fisher Scientific) alone (1.02 Mol) to ensure the MICs

Table 1. Dopant levels, predominant crystalline structure, and photocatalytic activity levels under UV and fluorescent light (FL) irradiation for Mo-doped titania coatings deposited onto stainless steel substrata.

Sample type	Power to Mo target (W)	At.% Mo	Annealing temperature (°C)	Crystal structure	P_{aUV}	P_{aFL}
TiO_2	0	0	600	Anatase	0.69	0.41
TiO_2–Mo	100	2.69	600	Anatase	0.73	0.54
TiO_2–Mo	150	5.48	600	Anatase/rutile	0.77	0.47
TiO_2–Mo	180	6.95	600	Anatase/rutile	0.88	0.72
TiO_2–Mo	240	11.81	600	Amorphous	0.57	0

P_a = photocatalytic activity values under UV light and FL light.

were due to the metal and not the acid. A 0.5 McFarland standard suspension (~1.5×10^8 cfu ml^{-1}) of each of the test cultures was made, and a swab stick was dipped into the suspension and spread onto the surface of a portion of the Mo incorporated agar. The bacterial suspension was left to dry prior to incubation at the appropriate temperature for 24 h. The test was performed three times, and results showing the concentration where no visible microbial growth was evident, which agreed on two or more occasions, were adopted as the MIC.

Measurement of molybdenum ion release by inductively coupled plasma atomic emission spectroscopy (ICP-AES)

A Varian Vista AX CCD inductively coupled plasma atomic emission spectrometer (ICP-AES) (Varian Inc., Yarnton, UK) was used to assess any Mo ion release from the deposited thin film coatings. Surfaces were individually placed into a Petri dish to which 20 ml of HPLC-grade water (Fisher Scientific) were added and incubated under fluorescent lighting in a 20°C incubator. At 2, 4, 8, 24, 48, 72, 96, and 168 h, surfaces were transferred to fresh HPLC-grade water whilst the previous sample was kept for analysis by ICP-AES. All samples were frozen at –85°C prior to analysis. Molybdenum ion release was calculated from calibration curves (0.1–5 ppm), and all tests were carried out in triplicate.

Statistics

A two-tailed homoscedastic Student *t*-test was performed using Microsoft Excel 2010 to compare datasets. If the *p* value was <0.05, then results were statistically significant.

Results

Coating characterization and photocatalytic activity

TiO_2 and TiO_2–Mo coatings were deposited as thin films onto stainless steel substrata using magnetron sputtering. The Mo dopant levels, determined by EDX analysis, increased with increasing power delivered to the Mo target and ranged from 2.69 to 11.81 at% (Table 1). Photocatalytic activity levels (P_{aUV} and P_{aFL} values) for the annealed coatings, determined from the MB tests, are also listed in Table 1. From these data, it can be seen that the highest activity under both light sources was achieved by the coatings doped at 6.95 at% of Mo.

The annealed TiO_2–6.95 at% Mo coatings were analysed by XRD (Figure 1) and Raman spectroscopy (Figure 2). The XRD pattern showed the presence of the (1 0 1) anatase peak at $2\theta = 25.4°$ and the (1 1 0) rutile

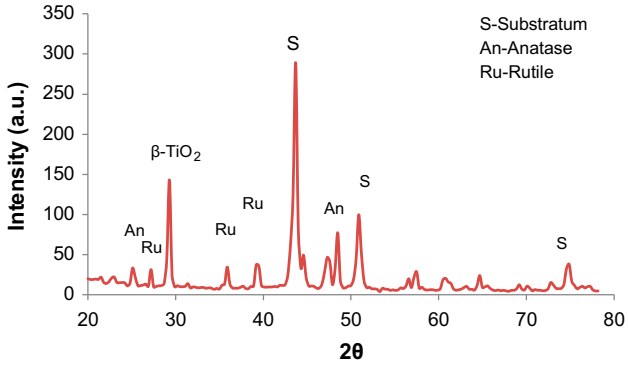

Figure 1. XRD pattern of a 6.95 at.% TiO_2–Mo surface showing the anatase/rutile mix structure.

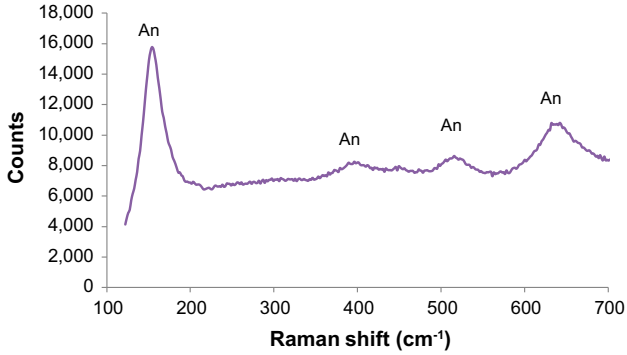

Figure 2. Raman spectra of a 6.95 at.% TiO_2–Mo surface annealed at 600°C showing the crystal (anatase) structure of the coating.

peak at $2\theta = 27.4°$ and several other minor peaks. The sample also showed the presence of some monoclinic β-titania. In contrast, the Raman spectrum showed only anatase peaks at 144, 389, 515, and 638 cm^{-1}. Based on these analyses, the assumption must be that the structure of the TiO_2–6.95 at% Mo coatings after annealing in air at 600°C was a mixed phase, anatase/rutile structure, but the relative proportions of each phase were not determined.

The photocatalytic activity of soiled surfaces

Photocatalytic activity of the TiO_2–Mo surface in the absence and presence of soiling (undiluted beer) was demonstrated *via* the degradation of MB (Table 2). Doping TiO_2 with Mo considerably improved photoactivity under fluorescent light. The apparent increase in photoactivity of soiled surfaces under fluorescent irradiation will require further investigation.

Table 2. Photocatalytic activity values of TiO_2 and TiO_2–Mo surfaces as determined by the degradation of MB, under UV and fluorescent light (FL).

Surface coating	Treatment	P_{aUV}	P_{aFL}
TiO_2	Unconditioned	0.69	0.41
TiO_2–Mo	Unconditioned	0.88	0.72
TiO_2–Mo	Conditioned	0.77	0.77

P_a = photocatalytic activity values under UV light and FL light.

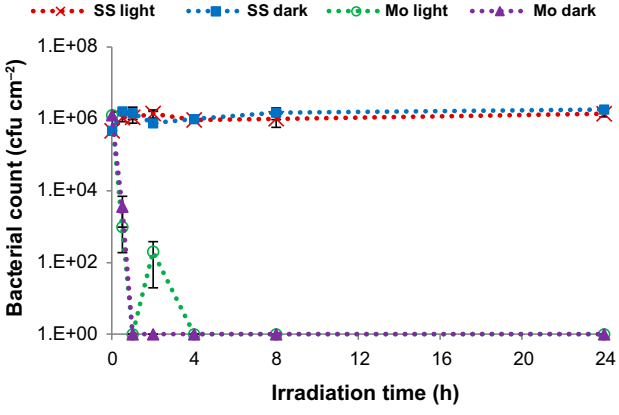

Figure 3. Antimicrobial effect of TiO_2–Mo surfaces on *E. coli* without soil. Stainless steel surfaces were used as controls, and light and dark conditions were investigated. The assay was performed in triplicate, and each point represents the mean with the SD. SDs may not be visible at every point, as they were very small, and some lines may superimpose each other.

Antimicrobial activity

The antimicrobial activity demonstrated by the TiO_2–Mo surfaces was investigated against *E. coli* and microorganisms isolated from brewery surfaces that included *P. rhodesiae*, *S. marcescens*, and *W. anomalus*. The TiO_2–Mo-coated surface proved effective against the model organism *E. coli* with counts from an unsoiled surface reducing to below the limit of detection (<10 cfu cm^{-2}) within 1–4 h (Figure 3). *P. rhodesiae* (Figure 4a) counts were also reduced to <10 cfu cm^{-2} and

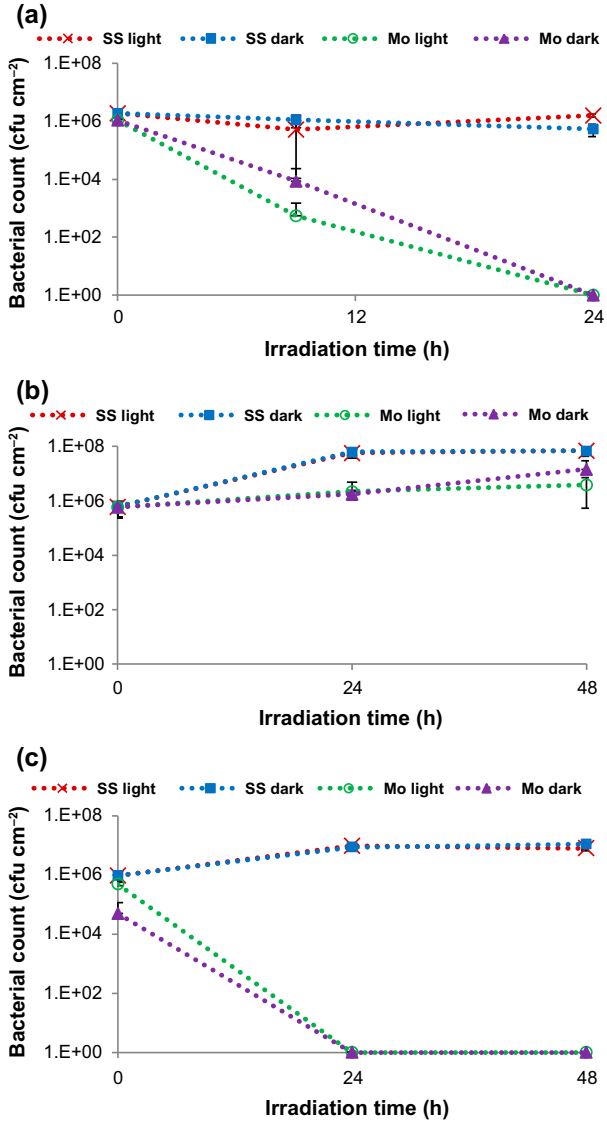

Figure 4. Antimicrobial effect of TiO_2–Mo surfaces on *P. rhodesiae* (a) without soil, (b) with undiluted soil (beer), and (c) with dilute soil (10% beer). Stainless steel surfaces were used as controls, and light and dark conditions were investigated. The assay was performed in triplicate, and each point represents the mean with the SD. SDs may not be visible at every point, as they were very small.

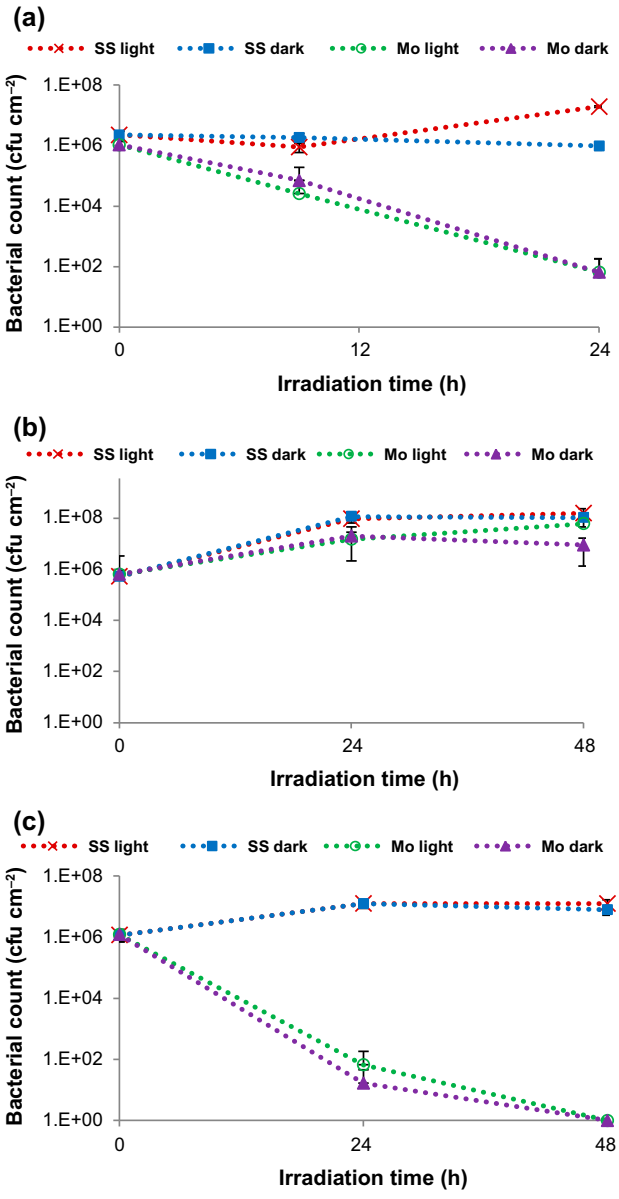

Figure 5. Antimicrobial effect of TiO_2–Mo surfaces on *S. marcescens* (a) without soil, (b) with undiluted soil (beer), and (c) with dilute soil (10% beer). Stainless steel surfaces were used as controls, and light and dark conditions were investigated. The assay was performed in triplicate, and each point represents the mean with the SD. SDs may not be visible at every point, as they were very small, and some lines may superimpose each other.

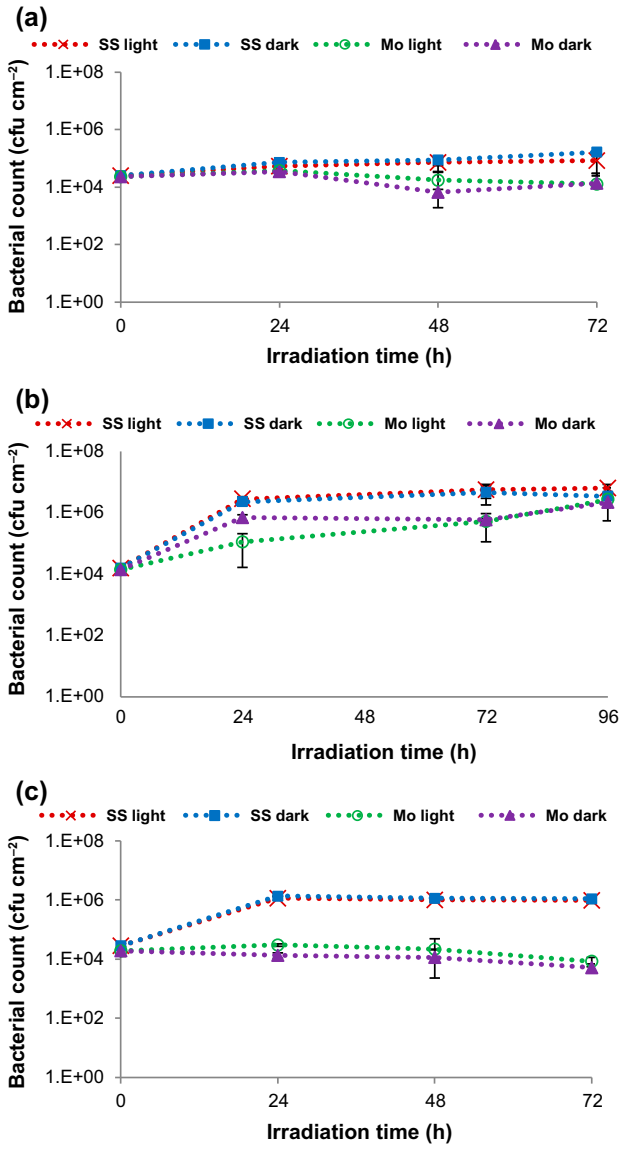

Figure 6. Antimicrobial effect of TiO_2–Mo surfaces on *W. anomalus* (a) without soil, (b) with undiluted soil (beer), and (c) with dilute soil (10% beer). Stainless steel surfaces were used as controls, and light and dark conditions were investigated. The assay was performed in triplicate, and each point represents the mean with the SD. SDs may not be visible at every point, as they were very small, and some lines may superimpose each other.

S. marcescens (Figure 5a) to 65 cfu cm^{-2} within 24 h. Further tests need to be conducted against *P. rhodesiae* and *S. marcescens* to investigate the rate of kill over shorter irradiation times. *W. anomalus* (Figure 6a) counts at 72 h were reduced by ~ 1-log to $>10^4$ cfu cm^{-2}. The presence of brewery soil in the form of undiluted beer on the TiO_2–Mo surfaces reduced the antimicrobial effectiveness, and growth of all brewery organisms rather than inhibition was seen (Figures 4b, 5b, 6b). The presence of dilute beer (10%) on the surfaces did not reduce the antimicrobial activity of the coatings. No viable *P. rhodesiae* cells (Figure 4c) were recovered from the TiO_2–Mo coatings after 24 h irradiation, and <70 cfu cm^{-2} of *S. marcescens* (Figure 5c) remained. *W. anomalus* (Figure 6c) counts after 72 h irradiation were $>10^3$ cfu cm^{-2}, although this was a significant ($p < 0.05$) decrease compared with the non-antimicrobial surface.

Table 3. Minimum inhibitory concentration (MIC) of Mo against *E. coli*, *P. rhodesiae*, *S. marcescens*, and *W. anomalus.*

	MIC (mg l^{-1})
E. coli	2–3
P. rhodesiae	2–3
S. marcescens	2–3
W. anomalus	10–15

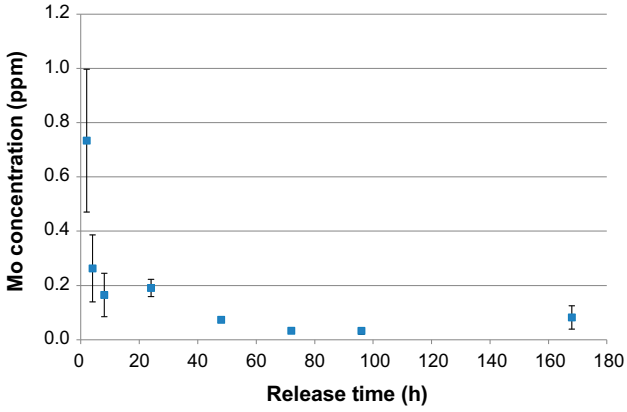

Figure 7. Molybdenum ion release determined by ICP-AES over 168 h. Tests were performed in triplicate, and each point represents the mean with the SD.

Bacteria were inactivated more readily than the yeast, and the TiO_2–Mo surfaces were also as active in dark conditions as in the light.

MIC determination and molybdenum ion release by inductively coupled plasma atomic emission spectroscopy (ICP-AES)

The MIC results showed that *E. coli*, *P. rhodesiae* and *S. marcescens* were more susceptible to Mo than *W. anomalus* (Table 3). ICP-AES was used to detect Mo ion release from the thin film coating over a duration of 7 days (Figure 7). An initial burst of Mo ions (0.73 ppm) over the first 2 h was recorded followed by a sudden decline and then a steady low concentration release. The low concentration of Mo ions (<0.04 ppm) being released after the initial 48 h suggests that Mo is retained on the surface and is not readily leachable.

Discussion

The development of novel functional photocatalytic surfaces that are activated using fluorescent light could play an important role in aiding the reduction of microbial contamination within environments such as the brewing industry. It is well known that microbial numbers decrease when in contact with a TiO_2 surface that has been illuminated with UV light. For example, Kikuchi et al. (1997), found that a suspension of *E. coli* (3×10^4 cfu ml^{-1}) deposited onto TiO_2-coated glass was eradicated within 1 h of exposure to UV light (1 mW cm^{-2}). The use of UV lighting in indoor environments can, however be hazardous; thus, in this work, by doping TiO_2 with Mo, photocatalytic activity under fluorescent lighting was enhanced, as determined by the degradation of MB (Table 2). The crystal structure of the TiO_2–Mo coating was in the mixed phase anatase/rutile form. Despite the anatase form being known as the most photoactive, in this instance it appeared that the mixed phase structure helped improve photoactivity. Other researchers have also shown that mixtures of anatase and rutile show a synergistic effect and enhanced photocatalytic activity (Boehme & Ensinger 2011). The Degussa P-25 TiO_2 powder (Evonik Degussa GmbH), a standard material used for photocatalytic reactions, has enhanced activity owing to the rutile/anatase mixed phase ratio of 1:4 (Ohno et al. 2001).

The antimicrobial effect of the TiO_2–Mo photocatalytic coatings was first tested using *E. coli* as a model organism. Since counts were reduced from $>10^5$ cfu cm^{-2} to <10 cfu cm^{-2} within 1–4 h, tests were performed to examine the photocatalytic effect on microbial brewery isolates. Within 24 h of irradiation under fluorescent light, *P. rhodesiae* and *S. marcescens* counts decreased by 5 logs. Longer irradiation times were investigated to determine whether complete microbial kill could be achieved and to reflect the time between cleaning procedures in an industrial setting following a typical long production run. *W. anomalus* counts after longer fluorescent light exposure (72 h) were still $>10^4$ cfu cm^{-2}. However, this was less than the non-antimicrobial surface. The fact that higher numbers of yeast cells remained attached to the surface could be due to differences in the cell wall structure, or the larger size and increased complexity of the eukaryotic cells, which could make them more resistant in nature to oxidative agents, compared with bacterial cells, and thus more resistant to killing. It was also noted that the Mo MIC for *W. anomalus* was >4 times higher than for the bacterial strains used. The TiO_2–Mo surfaces were also active in the dark. This suggests that the coating could have a dual function, being both photoactive under visible light as determined by the degradation of MB (Table 2) and antimicrobial.

With the ability of microorganisms to adapt to a variety of environmental situations, it is not surprising that resistance to broadly used disinfectants has been reported (McDonnell & Russell 1999). The photocatalytic mode of killing through the formation of radical species targets no particular site within a microbe and avoids the potential of resistance development (Page et al. 2009). As the Mo-doped surface also proved to be antimicrobial, resistance development, however, should not be an issue, since metal antimicrobials may target multiple sites in

the cell (Yasuyuki et al. 2010), and to the authors' knowledge, no case of microbial resistance to Mo metal has been reported. Nevertheless, the importance of monitoring for signs of the emergence of resistance to Mo over long exposure times should be highlighted and always considered when introducing new strategies for disinfection.

In the dispensing and bottling section of a brewery, it is common for process surfaces to become covered by a conditioning film formed by the absorption of various organic materials (Jullien et al. 2008) from residual beer. The application of dilute beer to the surface closely mimics an *in situ* brewery environment, where in the dispensing and bottling process cleaning procedures, including rinsing with jets of water, would cause residual beer to become diluted. Dilute beer applied to the TiO_2–Mo surface resulted in a 5-log reduction in *P. rhodesiae* and *S. marcescens* and a 2-log reduction in *W. anomalus*. Numerous articles have been published with conflicting data regarding the effects of conditioning films on bacterial attachment. Barnes et al. (1999) treated stainless steel coupons with skimmed milk and subsequently challenged them with bacteria. They found milk reduced the adhesion of bacteria compared with untreated surfaces. Conversely, Verran and Whitehead (2006), found that significantly higher numbers of cells were retained on stainless steel surfaces treated with bovine serum albumin than on those without. In a study by Ahmed et al. (2011), the photocatalytic degradation of 0.5% w/v human serum albumin (HSA) on TiO_2 and TiO_2–Ag films was examined. Changes in protein conformation consistent with denaturation and enhanced binding and oxidation, thought to be induced through a photocatalytic mechanism, were found by Raman spectroscopy. The ability of photocatalysis to break down a low concentration of HSA may indicate a similar process with the dilute beer on the TiO_2–Mo surface. This will be investigated in future work. Likewise, Fujishima et al. (2000) state that photocatalysts are not especially useful at breaking down large volumes of soilage, but they are capable of destroying it as it accumulates, and Araújo et al. (2013) report on how, in the presence of interfering substances, the antimicrobial effectiveness of quaternary ammonium compounds was reduced and depended on the type of interfering substance. To the authors' knowledge, no other reports have been published specifically relating to the effect a brewery soil on a TiO_2–Mo photocatalytic surface has on microbial numbers.

As the TiO_2–Mo surfaces were equally active in the dark as in the light, it was difficult to discern whether photocatalysis or the innate antimicrobial nature of Mo had the greater effect on reducing microbial numbers. In previous unpublished work by the authors, the addition of niobium to TiO_2 demonstrated photocatalytic activity against *E. coli* (5-log reduction) under fluorescent light but not in the dark. However, surfaces were not tested in the presence of a conditioning film. With the Mo-doped surfaces, the MB results (Table 2) clearly showed increased visible light activity, confirming photocatalytic activity. In addition, the activity demonstrated against the bacteria in the dark conferred a dual-functioning surface with an antimicrobial ability.

The photocatalyic and antimicrobial approach to reducing microbial fouling in the brewery environment could have many beneficial effects. Preventing the accumulation of microbial populations on process surfaces during long production runs would also reduce current cleaning costs owing to lower energy, water, and chemical consumption (Priha et al. 2011). Reducing production downtime as a result of potentially less frequent or shorter cleaning times, as cleaning is made easier owing to the hydrophilic nature of the surface, would enable greater product throughput. This would be beneficial economically, environmentally, and in terms of reducing human exposure to harsh chemical disinfection regimes. Additionally, the sustainable nature of the photocatalytic technology makes the use of such surfaces an environmentally friendly process. The TiO_2–Mo-coated surfaces also proved to be usable in a wet environment. However, fouling build-up over time needs to be monitored, as too much fouling makes the surface less effective. Surfaces need to be further assessed to ensure they are robust, as good environmental stability of the coating is crucial for long-term durability, and surfaces would require tests to ensure they can withstand in-place cleaning protocols. In the manufacture of the surfaces, deposition parameters and surface characteristics must be controlled in order to maintain optimum photocatalytic activity, and although the Mo-doped surface is also active in the dark, there should be sufficient light in the environment for photocatalytic activity. The size of the surface that can be coated would need to be upscaled to an industrial level and the length of time examined to establish if and how long before recoating of surface is required. Investigations to enhance the hygienic status of process surfaces in the brewing industry by application of the TiO_2–Mo coating in comparison with stainless steel are currently underway.

A similar study carried out by Priha et al. (2011) to determine whether process hygiene in the beverage industry could be improved by applying TiO_2 to stainless steel with or without added antimicrobial compounds (silver) was investigated in laboratory attachment tests and in a 15-month process study. Photocatalytic coatings containing silver reduced microbial coverage in laboratory studies and in some process samples, but some of the TiO_2 coatings were damaged, and most of the precipitated Ag had eluted. The TiO_2–Mo coatings used in this study showed an initial release of Mo ions followed by a decline to low steady-state concentrations (<0.04 ppm). The lack of Mo ions leaching from the surface would be

of benefit in process trials, and this would ensure that undesirable chemicals would not reach the end product.

In conclusion, the study describes the development of a functional surface consisting of a thin film coating of TiO_2 doped with Mo deposited by magnetron sputtering, for use in enhancing the hygienic status of surfaces in environments where microbial fouling and surface conditioning are likely. The original intention of doping with Mo was to bring photocatalytic activity into the visible spectrum. Microbiological studies additionally demonstrated an antimicrobial effect of the Mo; thus the coating presents a dual function. The coating significantly reduced microbial numbers even in the presence of a typical brewery soil. Thus, the surface may act as a secondary level defence against microbial populations and proliferation between disinfection/cleaning cycles.

Acknowledgements

Funding for this work from the Technology Strategy Board is gratefully acknowledged. The work reported in this paper formed part of the Matera+ project, 'Disconnecting microbes from food and beverage process surfaces' carried out in partnership with a complementary study in Finland, which was funded by the Finnish Funding Agency for Technology and Innovation (Tekes). Partners in the larger project were Teer Coatings Ltd, Cristal (UK), and VTT Technical Research Centre of Finland, Tampere University of Technology, Millidyne surface technology and PBL Brewing Laboratory (Finland), to whom thanks are also given.

References

Ahmed MH, Keyes TE, Byrne JA, Blackledge CW, Hamilton JW. 2011. Adsorption and photocatalytic degradation of human serum albumin on TiO_2 and Ag–TiO_2 films. J Photochem Photobiol A Chem. 222:123–131.

Araújo PA, Lemos M, Mergulhão F, Melo L, Simões M. 2013. The influence of interfering substances on the antimicrobial activity of selected quaternary ammonium compounds. Int J Food Sci. 237581:1–9.

Barnes LM, Lo MF, Adams MR, Chamberlain AHL. 1999. Effect of milk proteins on adhesion of bacteria to stainless steel surfaces. Appl Environ Microbiol. 65:4543–4548.

Boehme M, Ensinger W. 2011. Mixed phase anatase/rutile titanium dioxide nanotubes for enhanced photocatalytic degradation of methylene-blue. Nano Micro Lett. 3:236–241.

Caballero L, Whitehead KA, Allen NS, Verran J. 2010. Photoinactivation of *Escherichia coli* on acrylic paint formulations using fluorescent light. Dyes Pigm. 86:56–62.

Costerton JW, Lewandowski Z, Caldwell DE, Karber DR, Lappin Scott H. 1995. Microbial biofilms. Annu Rev Microbiol. 49:711–745.

Daviðsdóttir S, Canulescu S, Dirscherl K, Schou J, Ambat R. 2013. Investigation of photocatalytic activity of titanium dioxide deposited on metallic substrates by DC magnetron sputtering. Surf Coat Tech. 216:35–45.

Foster HA, Ditta IB, Varghese S, Steele A. 2011. Photocatalytic disinfection using titanium dioxide: spectrum and mechanism of antimicrobial activity. App Microbio Biotech. 90:1847–1868.

Frank SN, Bard AJ. 1977. Heterogeneous photocatalytic oxidation of cyanide ion in aqueous solutions at TiO_2 powder. J Am Chem Soc. 99:303–304.

Fujishima A, Honda K. 1972. Electrochemical photolysis of water at a semiconductor electrode. Nature. 238:37–38.

Fujishima A, Rao TN, Tryk DA. 2000. Titanium dioxide photocatalysis. J Photochem Photobiol C Photochem Rev. 1:1–21.

Houas A, Lachheb H, Ksibi M, Elaloui E, Guillard C, Herrmann J-M. 2001. Photocatalytic degradation pathway of methylene blue in water. Appl Catal B Env. 31:145–157.

International organization for standardization [ISO] 27447:2009. Fine ceramics (advanced ceramics, advanced technical ceramics). Test method for antibacterial activity of semiconducting photocatalytic materials.

Jullien C, Benezech T, Le Gentil C, Boulange-Petermann L, Dubois PE, Tissier JP, Traisnel M, Faille C. 2008. Physicochemical and hygienic property modifications of stainless steel surfaces induced by conditioning with food and detergent. Biofouling. 24:163–172.

Kikuchi Y, Sunada K, Lyoda T, Hashimoto K, Fujishima A. 1997. Photocatalytic bactericidal effect of TiO_2 thin films: dynamic view of the active oxygen species responsible for the effect. J Photochem Photobiol A Chem. 106:51–56.

Laing K, Hampshire J, Teer D, Chester G. 1999. The effect of ion current density on the adhesion and structure of coatings deposited by magnetron sputter ion plating. Surf Coat Techn. 112:177–180.

McDonnell G, Russell AD. 1999. Antiseptics and disinfectants: activity, action, and resistance. Clin Microbiol Rev. 12:147–179.

Ohno T, Sarukawa K, Tokieda K, Matsumura M. 2001. Morphology of a TiO_2 photocatalyst (Degussa, P-25) consisting of anatase and rutile crystalline phases. J Catal. 203:82–86.

Page K, Wilson M, Parkin IP. 2009. Antimicrobial surfaces and their potential in reducing the role of the inanimate environment in the incidence of hospital-acquired infections. J Mater Chem. 19:3819–3831.

Priha O, Laakso J, Tapani K, Levanen E, Kolari M, Mantyla T, Storgards E. 2011. Effect of photocatalytic and hydrophobic coatings on brewery surface microorganisms. J Food Prot. 74:1891–1901.

Ratova M, Kelly PJ, West GT, Iordanova I. 2013. Enhanced properties of magnetron sputtered photocatalytic coatings via transition metal doping. Surf Coat Tech. 228:S544–S549.

Storgårds E. 2000. Process hygiene control in beer production and dispensing. Espoo: VTT Technical Research Centre of Finland, University of Helsinki.

Verran J, Whitehead KA. 2006. Assessment of organic materials and microbial components on hygienic surfaces. Food Bioprod Proc. 84:260–264.

Wiegand I, Hilpert K, Hancock REW. 2008. Agar and broth dilution methods to determine the minimal inhibitory concentration (MIC) of antimicrobial substances. Nat Protoc. 3:163–175.

Wilke K, Breuer HD. 1999. The influence of transition metal doping on the physical and photocatalytic properties of titania. J Photochem Photobiol A Chem. 121:49–53.

Yasuyuki M, Kunihiro K, Kurissery S, Kanavillil N, Sato Y, Kikuchi Y. 2010. Antibacterial properties of nine pure metals: a laboratory study using *Staphylococcus aureus* and *Escherichia coli*. Biofouling. 26:851–858.

Thin Solid Films 571 (2014) 75–83

Contents lists available at ScienceDirect

Thin Solid Films

journal homepage: www.elsevier.com/locate/tsf

The effect of process parameters on the structure, photocatalytic and self-cleaning properties of TiO_2 and Ag-TiO_2 coatings deposited using reactive magnetron sputtering

P. Navabpour [a,*], S. Ostovarpour [b], J. Hampshire [a], P. Kelly [b], J. Verran [b], K. Cooke [a]

[a] Teer Coatings Ltd, Miba Coating Group, West Stone House, Berry Hill Industrial Estate, Droitwich WR9 9AS, UK
[b] Manchester Metropolitan University, Faculty of Science and Engineering, Chester Street, Manchester M1 5GD, UK

ARTICLE INFO

Article history:
Received 12 November 2013
Received in revised form 7 October 2014
Accepted 7 October 2014
Available online 16 October 2014

Keywords:
Reactive magnetron sputtering
Silver
Titanium dioxide
Photocatalysis
Antimicrobial property

ABSTRACT

This article reports on the morphology, structure, wettability, photocatalytic and mechanical properties of TiO_2 and Ag-TiO_2 thin films, with the latter also displaying antimicrobial activity. The coatings were deposited using reactive closed field unbalanced magnetron sputtering. It was possible, by varying the process parameters, to tailor the structure and composition of the coatings. TiO_2 coatings which were deposited from a single titanium target (thickness ~1 μm) were relatively dense with low crystallinity and a mixed anatase and rutile structure. The addition of silver resulted in the formation of submicron sized silver particles dispersed throughout the coating. TiO_2 coatings deposited from two titanium targets (thickness ~2 μm) had a mixed anatase and rutile structure with a less dense topography. Ag-TiO_2 coatings deposited using this process showed a uniform dispersion of silver throughout the coating. All coatings presented excellent adhesion to the substrate and high photocatalytic activity under fluorescent light. Annealing at 600 °C had a detrimental effect on the photocatalytic activity as well as the mechanical properties of the coatings. The coatings deposited from a single Ti target were evaluated for their antimicrobial potential against *E. coli*. No reduction in the number of bacteria was observed using TiO_2. Ag-TiO_2 coatings, however, showed antimicrobial properties in the dark as well as light conditions, as a result of the innate antimicrobial potential of silver.

1. Introduction

Titanium dioxide is a widely studied semiconductor. It can be found in anatase, rutile and brookite crystal structures, with a band gap ranging between 3.0 for the rutile and 3.2 for the anatase structures [1]. Two main properties result from the presence of the TiO_2 band gap: photoelectrochemical energy conversion (as a semiconductor) and photocatalytic function [2]. The photoelectrochemical properties open up applications for this semiconductor in photovoltaics. On the other hand, its photocatalytic properties mean that TiO_2 can catalyse the degradation of pollutants and microbial organisms, making it attractive where there is a demand for hygiene and cleanliness. The applications include food and beverage process surfaces as well as medical devices and surfaces [3,4].

Several studies have been carried out to investigate the effect of crystal structure of TiO_2 on its photocatalytic performance. Whilst some studies have found a higher activity in the anatase form [5,6], others have reported the mixed phase anatase/rutile to show a better photocatalytic performance [7]. Comparative studies of single phase anatase and rutile TiO_2 have concluded that the photocatalytic activity is dependent on the reaction being studied and different kinetics and intermediaries may be produced in each case [8,9].

Due to its wide band gap, TiO_2 is only active under UV irradiation. It is possible to reduce the band gap of TiO_2 using one or more dopants to shift the activity to the visible range. The use of nitrogen as a dopant has been reported to result in enhanced visible light photocatalytic activity and hydrophilicity of TiO_2 [10,11]. Iron [12] and iron oxide [13] as well as a number of other dopants such as carbon nanotubes [14] and graphene [15] have been reported to increase the photocatalytic activity of TiO_2. Silver has been used both as a dopant to shift the activity of TiO_2 to visible light and as an antimicrobial agent [16–18].

TiO_2 and doped-TiO_2 films can be produced using a number of methods including sol-gel, chemical vapour deposition (CVD) and magnetron sputtering.

Reactive magnetron sputtering has several advantages over other coating methods such as sol-gel and CVD. Firstly, it eliminates the need to use the hazardous chemicals found in some of the other processes. Also, it is a versatile process in which, by varying the deposition conditions, both highly dense and porous columnar structures can be produced depending on the requirements. Furthermore, the deposition of double layer and multilayer coatings is easily achieved by the use

* Corresponding author. Tel.: +44 1905 827550; fax: +44 1905 827551.
E-mail address: Parnia.navabpour@miba.com (P. Navabpour).

http://dx.doi.org/10.1016/j.tsf.2014.10.040
0040-6090/

of different targets and rotation speeds [19]. Reactive magnetron sputtering has been widely investigated for the deposition of photocatalytic TiO_2 coatings. Several groups have described the effect of process parameters [20], such as total and oxygen partial pressures [21,22], deposition temperature [23], annealing [24] and doping [12,16] on the structure and photocatalytic properties of magnetron sputtered TiO_2. Deposition rates of up to 15 nm min^{-1} have been reported and unbalanced magnetron sputtering has been shown to produce a higher deposition rate than the balanced mode [25].

Closed field unbalanced magnetron sputtering (CFUBMS) is capable of producing coatings with high deposition rate and is readily scalable, making it a suitable process for the deposition of photocatalytic and self-cleaning coatings for industrial applications, such as food and beverage processing and medical devices. In this paper, we report on the deposition of TiO_2 and Ag-doped TiO_2 onto stainless steel substrates using reactive CFUBMS. The effect of process parameters on the coating structure, hydrophilicity, photocatalytic and mechanical properties, as well as the antimicrobial potential of the coatings were investigated.

2. Materials and methods

2.1. Preparation of coatings

TiO_2 and Ag-TiO_2 coatings were deposited using reactive magnetron sputtering in a Teer Coatings UDP 450 coating system. One or two titanium targets (99.5% purity) were used for the deposition of TiO_2. Argon (99.998% purity) was used as the working gas and oxygen (99.5% purity) as the reactive gas. An additional silver (99.95% purity) target was used for the co-deposition of silver during the process. Advanced Energy Pinnacle Plus pulsed DC power supplies were used to power the titanium targets and to bias the substrates. An Advanced Energy DC power supply was used to power the silver target. The substrate material was 304 stainless steel with a 2B finish ($75 \times 25 \times 1.6$ mm^3). All substrates were ultrasonically cleaned in acetone and dried prior to loading into the chamber in order to remove surface contaminants. The substrates were aligned on a flat plate parallel to the surface of the metal targets at a distance of 150 mm from the target plane. A high rotational speed of 10 rpm was applied to the substrates to ensure enhanced mixing of silver and titanium within the coatings rather than the preferential formation of multilayer coatings.

The substrates were ion-cleaned for a period of 20 min prior to the coating deposition using a bias voltage of −400 V and a low current of 0.2–0.35 A on the targets. The coatings were deposited at a bias voltage of −40 V. The amount of oxygen was controlled using an optical emission monitor and, to obtain stoichiometric TiO_2, the Ti metallic emission line intensity was set to 25% of the non-reactive deposition value. The deposition time was 60 min for all coatings.

2.2. Heat treatment

When used, post deposition heat treatment of the samples was carried out at 600 °C in air using a Prometheus kiln for 30 minutes, after which they were taken out of the kiln and cooled down at room temperature.

2.3. Characterisation of the coatings

Scanning electron microscopy (SEM) (Cambridge Stereoscan 200) was used to investigate the morphology of the coatings. An acceleration voltage of 15 kV was utilised. The composition and elemental distributions of the coatings were investigated using a SAMX energy dispersive X-ray analyser (EDX) system, attached to the SEM. The composition was measured on a minimum of five locations and the mean $\pm 2\sigma$ values were reported. High resolution SEM images were obtained using a JEOL 7000 Field Emission SEM (FE-SEM) at an acceleration voltage of 10 kV.

Raman spectroscopy (Renishaw Invia, 514 nm laser) and X-ray diffraction (XRD) (Bruker D8 Advance X-ray Diffractometer) were used to evaluate the crystal structure of the coatings. XRD measurements were performed using a Cu K_α radiation ($\lambda = 0.154$ nm) in 2θ steps of 0.014°, and a low scan speed of 0.01° s^{-1}.

2.4. Mechanical properties

The scratch and wear resistance of the coatings were assessed using a Teer ST3001 scratch–wear tester [26]. The coated surfaces were evaluated using a Rockwell diamond tip (radius 200 μm). A load rate of 100 N min^{-1} and a constant sliding speed of 10.0 mm min^{-1} were used with the load increasing from 10 to 40 N. The scratch tracks were examined using SEM in order to detect any flaking.

2.5. Contact angle measurements

Advancing drop contact angle measurements with water were carried out at room temperature on the as deposited coatings using a contact angle measuring instrument developed in-house. At least 6 measurements were taken for each surface and the reported values are mean $\pm 2\sigma$.

2.6. Photocatalytic properties

The photocatalytic activity of coatings was determined via the degradation of an organic dye — methylene blue (MB) (Alfa Aesar, UK). MB is a heterocyclic aromatic dye with a molecular formula of $C_{16}H_{18}ClN_3S$, and is often used as a model organic compound to measure photoreactivity [27,28]. Aqueous MB absorbs light most strongly at about 664 nm wavelength. The absorbance at 664 nm is proportional to the concentration, C, of MB, according to the Beer-Lambert law. A graph of C/C_0 against irradiation time can, therefore, be plotted which has an exponential form [29].

The coated substrate was inserted into 10 ml of MB solution (concentration of 0.105 mMol/l) and left in the dark for 30 min to allow the equilibrium adsorption level of the dye on the surface to be reached. The surface was then irradiated with 2×15 W fluorescent tubes at an integrated power flux of 6.4 mW/cm^2 (of which the UV component (300–400 nm) was 1.3 mW/cm^2) for 5 h. The beaker was covered with cling film to avoid evaporation of the solution which could otherwise affect the concentration and peak absorbance of the MB solution. Optical absorbance measurements of the MB solutions were taken every 1 h.

2.7. Antimicrobial assays

For the antimicrobial assays, an illuminated cooled incubator (Gallenkamp, Loughborough, UK) was used. The incubator was fitted with six fluorescent lamps (Sylvania, Ontario, Canada) with a wavelength

Table 1
Parameters used for the deposition of TiO_2 and Ag-TiO_2 coatings.

Coating	Ti (A)	Ti (-V)	Ag (A)	Ag (-V)	Thickness (μm)	Deposition time (min)
Ti-I Coatings						
Ti1	1 × 6	1 × 410	0.00	0	1.0	40
Ti1-Ag1	1 × 6	1 × 390	0.25	300	1.1	40
Ti1-Ag2	1 × 6	1 × 390	0.60	330	1.9	40
Ti-II Coatings						
Ti2	2 × 6	2 × 415	0.00	0	2.0	60
Ti2-Ag1	2 × 6	2 × 415	0.50	215	2.0	60
Ti2-Ag2	2 × 6	2 × 415	0.70	230	2.1	60
Ti2-Ag3	2 × 6	2 × 430	0.90	330	3.0	60

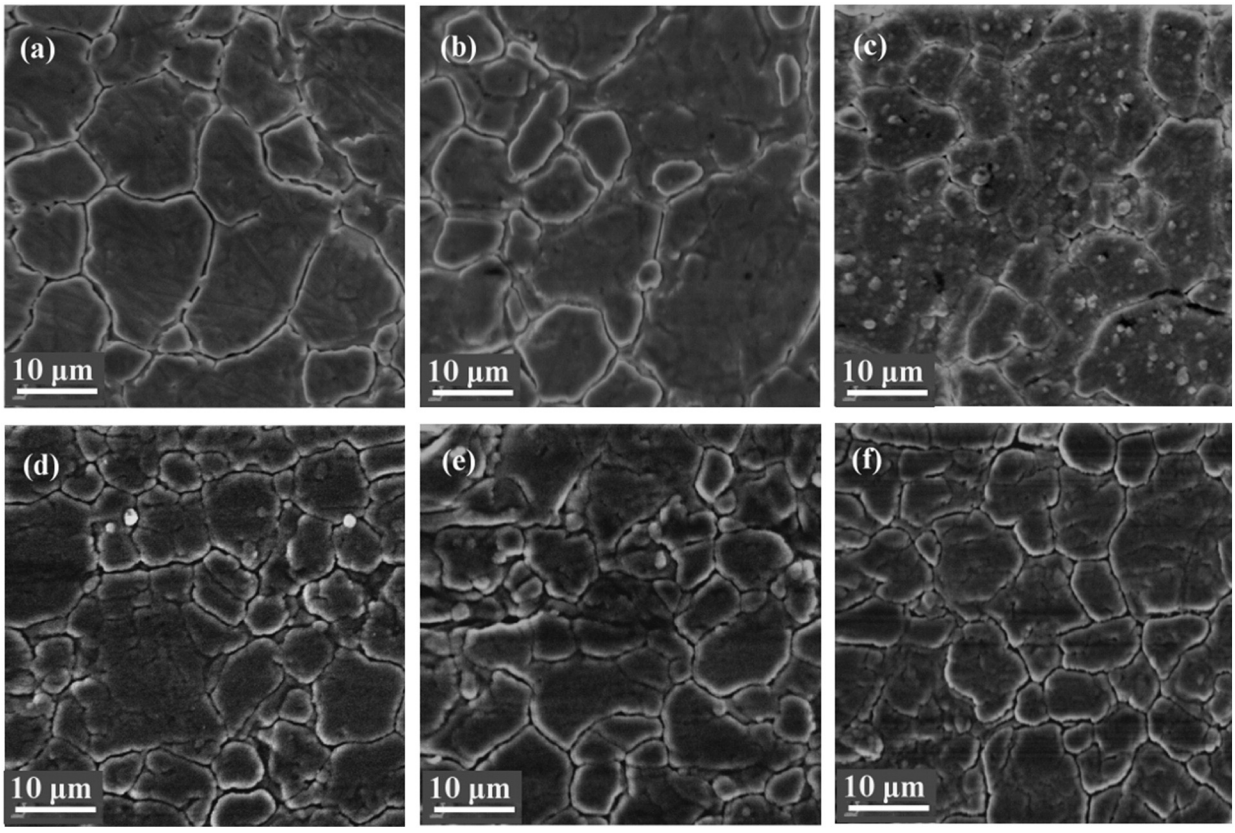

Fig. 1. SEM images of the as-deposited coatings on 304 2B stainless steel substrates: (a) Ti1, (b) Ti1-Ag1, (c) Ti1-Ag2, (d) Ti2-Ag1 (e) Ti2-Ag2 and (f) Ti2-Ag3.

range of 300-–700 nm and an energy output of 6.4 mW/cm^2. The temperature was set at 20 °C.

Escherichia coli ATCC 8739 was used throughout the study. Fifty microliter aliquots of the cell suspension were inoculated onto the surface of both the photocatalyst and 304 2B stainless steel control surfaces (1 cm x 2 cm) in a Petri dish. In order to spread out the liquid evenly, a polyethylene film was gently pressed onto the drop. The lid was then placed on the Petri dish. Four round Petri dishes plus contents were placed in one large square Petri dish which contained sterilized moistened tissues, to prevent cultures drying during light exposure. The efficiency of photocatalytic inactivation was examined at four irradiation times (0, 12, 24 and 48 h). At each time cells were collected from the sample surface and polyethylene film by dry swabbing. The swabs were transferred into 10 ml of neutralizing solution 20 g l^{-1} Soya Lethicin (Holland and Barrett, UK) and 30 g l^{-1} Tween 80 (Sigma Aldrich, UK) and vortex mixed. The viable population associated with these samples was enumerated by plating serial dilutions (to 10^{-7}) onto nutrient tryptone soya agar (TSA), and incubating at 37 °C for 24 h. At the end of the incubation period colonies on the agar plates were counted and the number of colony forming units (CFU) per mL was calculated. Counts were used from agar plates showing 15–300 colonies [30].

Table 2
Relative metallic composition of the Ag-TiO_2 coatings (i.e. ignoring oxygen content).

Coating	Ti (at%)	Ag (at%)
Ti1-Ag1	82.1 ± 1.6	17.9 ± 1.6
Ti1-Ag2	48.2 ± 12.0	51.8 ± 12.0
Ti2-Ag1	96.4 ± 1.0	3.6 ± 1.0
Ti2-Ag2	94.3 ± 1.8	5.7 ± 1.8
Ti2-Ag3	47.5 ± 1.2	52.5 ± 1.2

Two controls were included in each experiment; dark control (Petri dishes covered by aluminium foil) and a light control (uncoated stainless steel). Three replicates were used for each treatment time. Each

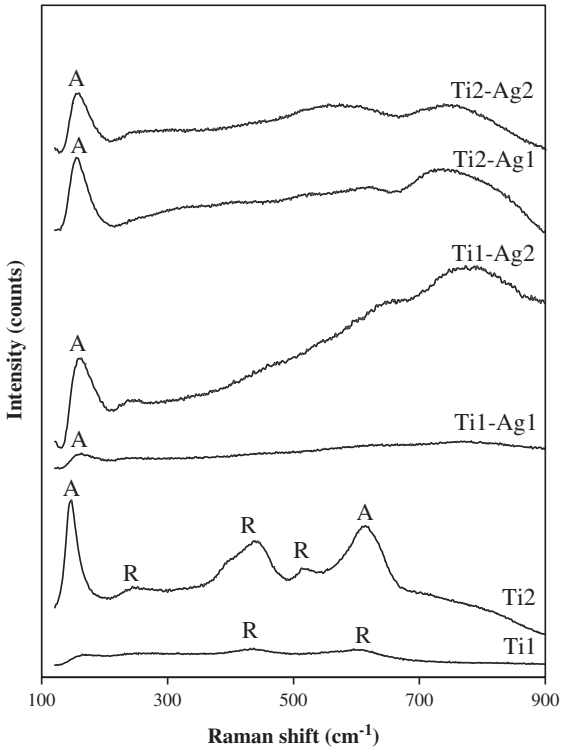

Fig. 2. Raman spectra for as-deposited coatings (a) Ti1, (b) Ti2, (c) Ti1-Ag1, (d) Ti1-Ag2, (e) Ti2-Ag1 and (f) Ti2-Ag2 indicating the position of anatase and rutile peaks.

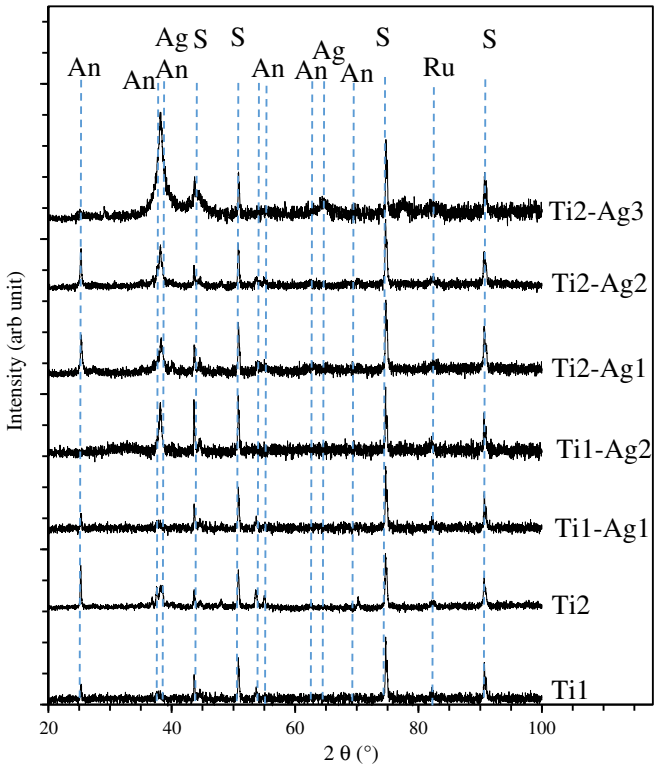

Fig. 3. XRD patterns of the as-deposited TiO_2 and Ag-TiO_2 coatings (S – substrate, An – anatase, Ru – rutile, Ag – silver).

experiment was repeated three times. Student two tail t- tests were performed to test the significance of the results. If the p value is less than 0.05, results are statistically significant.

3. Results and discussion

Table 1 shows the parameters used for the deposition of TiO_2 and Ag-TiO_2 coatings. Coatings were deposited either from one titanium target (Ti-*I* oxide coatings) or two titanium targets (Ti-*II* oxide coatings) with a (time-averaged) pulsed DC (pulse width: 500 ns, frequency: 50 kHz, giving a duty cycle of 97.5%) current of 6 A. The current applied to the silver magnetron was varied between 0.25 and 0.9 A in order to obtain a range of silver loadings. Deposition rates varied between 25 nm min^{-1} for Ti-*I* coatings and 50 nm min^{-1} for Ti2-Ag3, which were much higher than the sputtered TiO_2 coatings reported in the literature [16,25], showing the viability of this process for industrial applications. SEM micrographs of the coatings (Fig. 1) showed that, in Ti-*I* coatings, increasing the power applied to the silver target resulted in the formation of microparticles within the coating. EDX confirmed that the microparticles were formed of silver. The separation of silver could not be detected in the case of the Ti-*II* coatings and a much improved silver distribution was obtained. The relative Ti and Ag contents in the coatings are given in Table 2. The silver content in Ti1-Ag2 and Ti2-Ag3 was similar, confirming that the reason for the different morphologies observed was the variation in the coating process.

The structure of the as-deposited coatings was analysed using Raman spectroscopy (Fig. 2) and XRD (Fig. 3). The Raman spectrum for Ti1 showed low crystallinity with small peaks at 440 and 610 cm^{-1} which are characteristic of the rutile structure, whilst Ti2

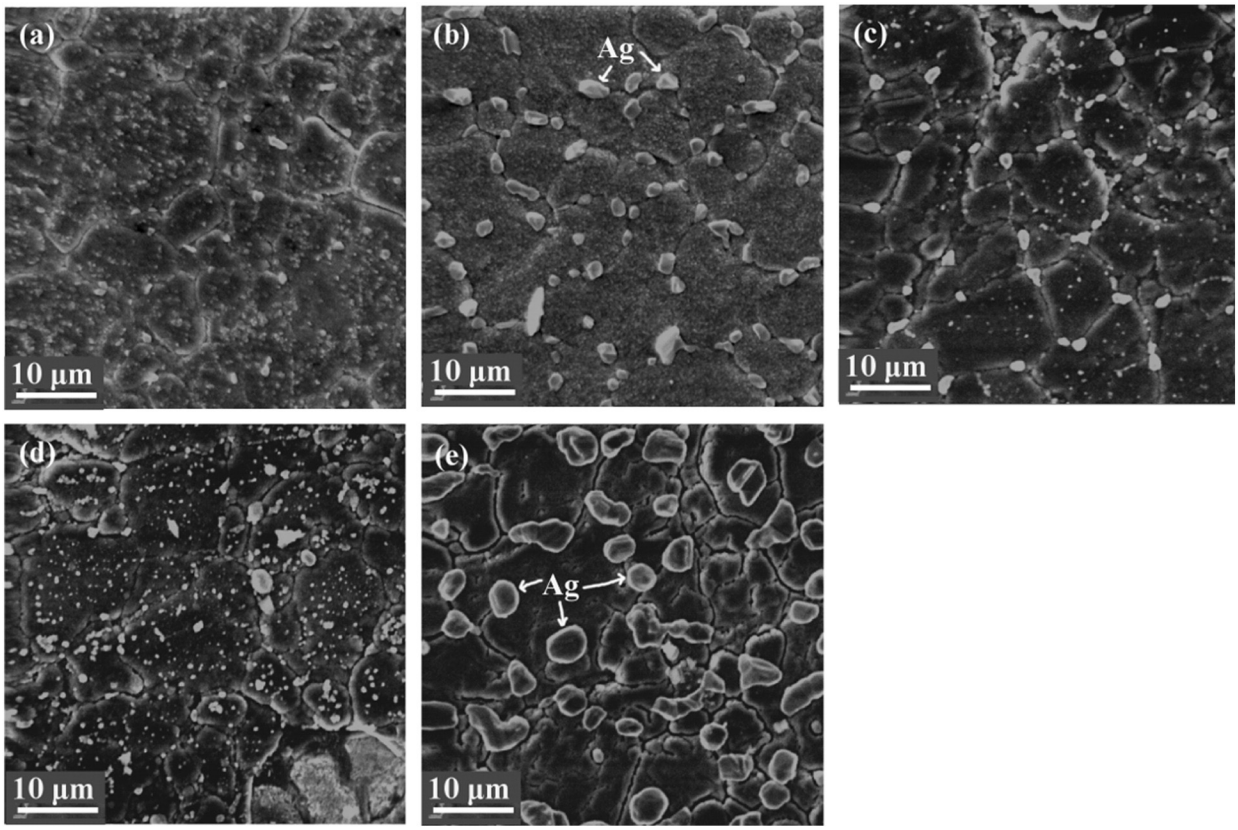

Fig. 4. Scanning electron micrographs of coatings after annealing (a) Ti1-Ag1, (b) Ti1-Ag2, (c) Ti2-Ag1, (d) Ti2-Ag2 and (e) Ti2-Ag3.

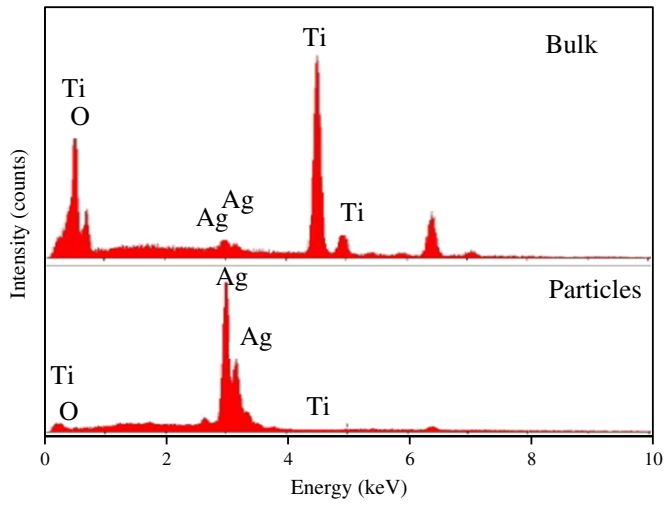

Fig. 5. EDX spectra showing the Ti, O and Ag Gaussian peaks for the bulk and islands on Ti1-Ag2 coating after annealing.

had strong peaks characteristic of a mixed rutile and anatase structure. All Ag-TiO_2 coatings showed low crystallinity of the TiO_2 phase. XRD confirmed these findings. Furthermore, the XRD patterns for Ag-TiO_2 coatings showed characteristic peaks for silver, which increased in intensity with increasing the silver content. All of the silver appeared to be in metallic form with no characteristic peaks from silver oxides. The higher crystallinity of Ti2 may be related to the higher temperature and deposition rate of this coating compared to Ti1, resulting from the use of two targets, which caused increased substrate bias current and hence power dissipation in the growing films. It has been suggested that an amorphous matrix allows silver to diffuse more easily and to form larger silver particles than a crystalline matrix [31]. The improved

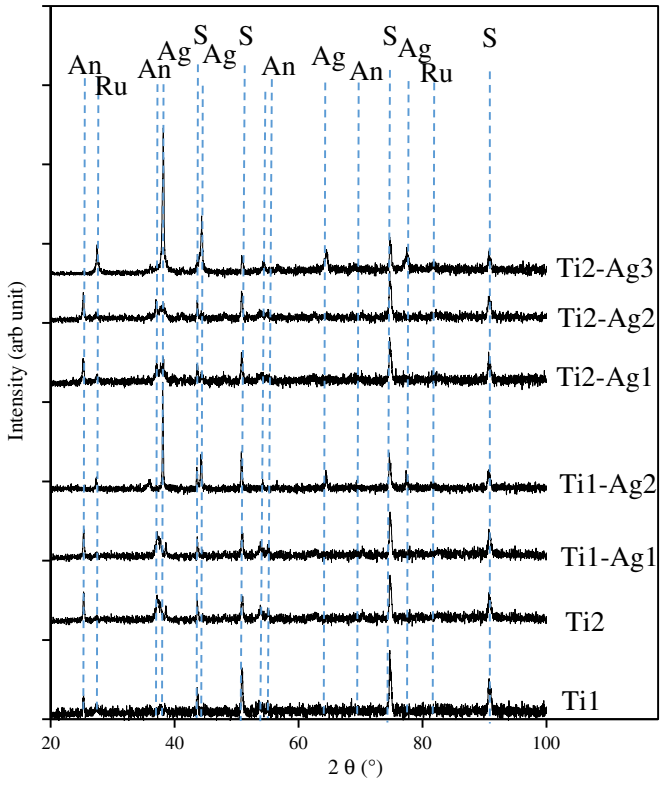

Fig. 6. XRD patterns of the coatings after annealing (S – substrate, An – anatase, Ru – rutile, Ag – silver).

Table 3
Water contact angle on coatings before and after heat treatment.

Coating	Water contact angle (°)	
	As deposited	After heat treatment
Ti1	20.0 ± 2.1	21.9 ± 1.9
Ti1-Ag1	27.0 ± 1.5	25.4 ± 1.2
Ti1-Ag2	58.1 ± 1.1	31.1 ± 1.7
Ti2	21.1 ± 1.8	20.9 ± 1.1
Ti2-Ag1	20.5 ± 0.9	23.7 ± 1.2
Ti2-Ag2	21.0 ± 2.0	24.3 ± 1.5
Ti2-Ag3	20.7 ± 1.3	35.9 ± 1.8

silver dispersion in the Ti2- coatings may be a result of the higher crystallinity of the matrix in these coatings.

Annealing has been reported to increase the crystallinity and photocatalytic properties of coatings [32,33]. Hence, the coatings were annealed in air at 600 °C and characterised using SEM, Raman and XRD. Annealing caused most of the silver to dissociate from TiO_2 and form separate islands, as seen from the SEM images (Fig. 4) and confirmed by EDX analysis (Fig. 5). This is expected due to the high diffusion rate of silver at high temperatures and its high affinity with itself, compared to the TiO_2 matrix which leads to its migration to the surface of the coatings.

Fig. 6 shows the XRD patterns of the annealed coatings. No significant change was observed in the XRD patterns of TiO_2 coatings. The crystallinity of the silver phase in the Ag-TiO_2 coatings, however, increased after annealing as observed from the increased sharpness and intensity of the silver peaks compared to those of the substrate.

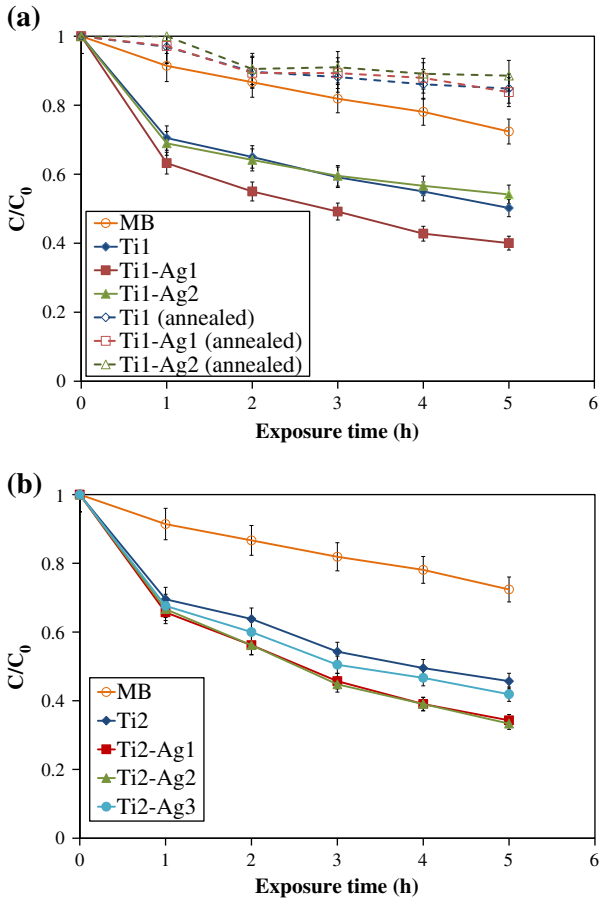

Fig. 7. Methylene blue absorption peak (664 nm) in the absence of photocatalyst and in the presence of TiO_2 and Ag-doped TiO_2 coatings under fluorescent light: (a) coatings from one Ti target, as-deposited and after annealing at 600 °C, and (b) coatings from two Ti targets (as deposited).

Additionally, Ti1-Ag1 and Ti2-Ag3 appeared to develop a rutile structure after annealing.

Water contact angle measurements were carried out as an additional method to characterise the surface of the coatings. Light-induced superhydrophilicity is widely associated with TiO_2 and it has been suggested to aid the self-cleaning properties of this material [2]. It may be expected that the TiO_2 and doped TiO_2 surfaces could be more effective in an aqueous environment (such as those in food and beverage processing), if there was a higher affinity between the surface and water, thus increasing the contact of the surface with the water-borne contaminants. Water contact angle was measured on the coatings before and after heat treatment (Table 3). For Ti-*I* coatings, increasing the silver in the coatings resulted in an increase in the water contact angle. This can be explained in terms of the effect of silver particles present on the surface of these coatings (water contact angle is ~90° on silver [34] and ~20° on TiO_2). For Ti-*II* coatings, where the dispersion of silver in the coating was uniform, the coatings behaved similarly to the bulk TiO_2 and the contact angle did not increase with increasing silver content. It may therefore be expected that the Ti2-Ag coatings would be more efficient self-cleaning surfaces than Ti1-Ag surfaces at the same silver loading, due to their higher hydrophilicity. Heat treatment led to the separation of silver from the TiO_2 matrix in both coating sets, resulting in similar surface composition, topography and hence water contact angle.

The photocatalytic properties of the coatings were evaluated through the measurement of the rate of MB degradation in the presence of coated surfaces under fluorescent light irradiation (Fig. 7). All the as-deposited coatings were active. The activity of Ti2 was higher than Ti1 (C/C_0 values were 0.45 and 0.50, respectively, after 5 h of irradiation). The addition of small amounts of silver improved the photocatalytic activity, most likely due to the reduction of the band gap by the silver dopant as reported previously in the literature [16]. Increasing the silver loading had a negative effect on the activity which may be related to the replacement of the photoactive TiO_2 with silver. Annealing had a detrimental effect on the photocatalytic activity of all surfaces. Initially, this was considered unexpected as annealing is frequently carried out to improve the crystallinity and hence the photocatalytic activity of coatings. The differences between the photocatalytic activities in Ti1 and Ti2, as well as the annealing effect on both coatings may be related to the difference in the coatings' crystallinity and surface area. Surface area is an important property of a catalyst as it affects the total catalyst available to the reacting compound [20], i.e. MB in this case. In order to investigate the surface morphology of the coatings in more detail, FE-SEM was used (Fig. 7). Comparison of Ti1 and Ti2 images (Fig. 8a and b) showed that Ti2 had a more columnar and less dense structure than Ti1. This is in agreement with the work reported in the literature which showed that thicker TiO_2 was more crystalline with higher surface roughness [16]. The higher surface area resulting from the more complex topography of Ti2 together with its higher crystallinity than Ti1 resulted in the higher activity of this coating compared to Ti1. Fig. 8 further shows that annealing produced denser coatings with reduced surface roughness (Fig. 7c and d), which combined with the separation of silver from the TiO_2 matrix, resulted in the reduced activity of the coatings.

The adhesion of the as deposited coatings to the substrate was evaluated by scratch testing. All coatings showed good adhesion (critical load >40 N) with no flaking observed under loads progressing to 40 N (Fig. 9). After annealing, all coatings showed flaking to varying extents adjacent to the scratch track (Fig. 10). In some coatings, extensive flaking was observed all over the surface. This may be related to the

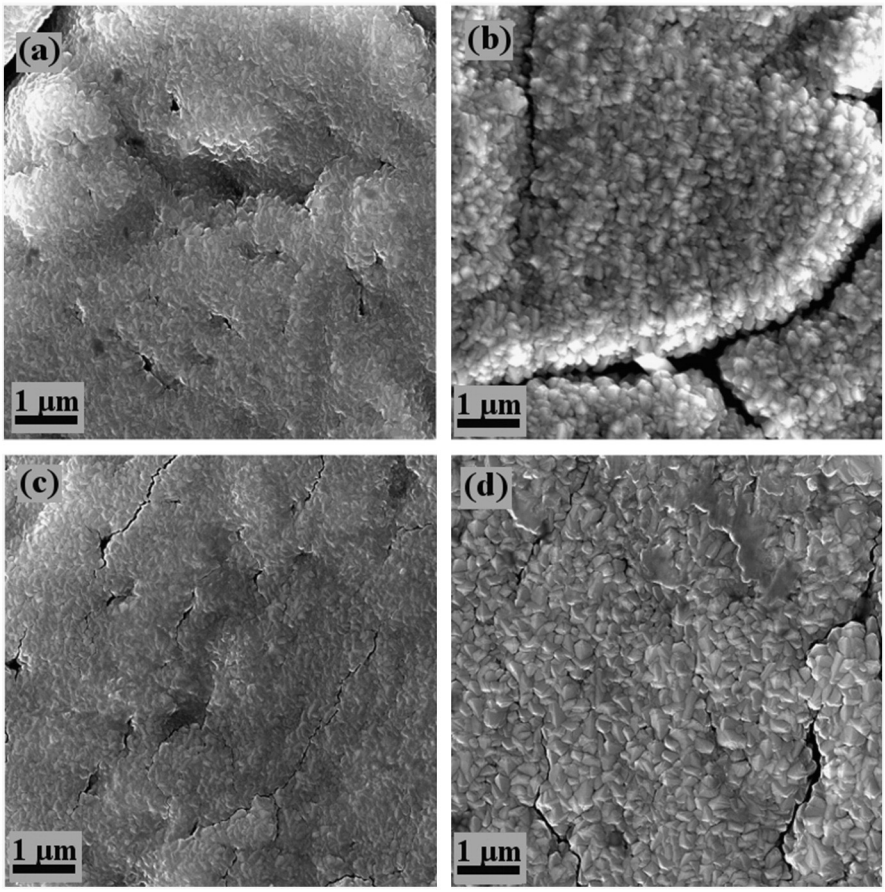

Fig. 8. FE-SEM images of (a) as-deposited Ti1, (b) as-deposited Ti2, (c) annealed Ti1 and (d) annealed Ti2.

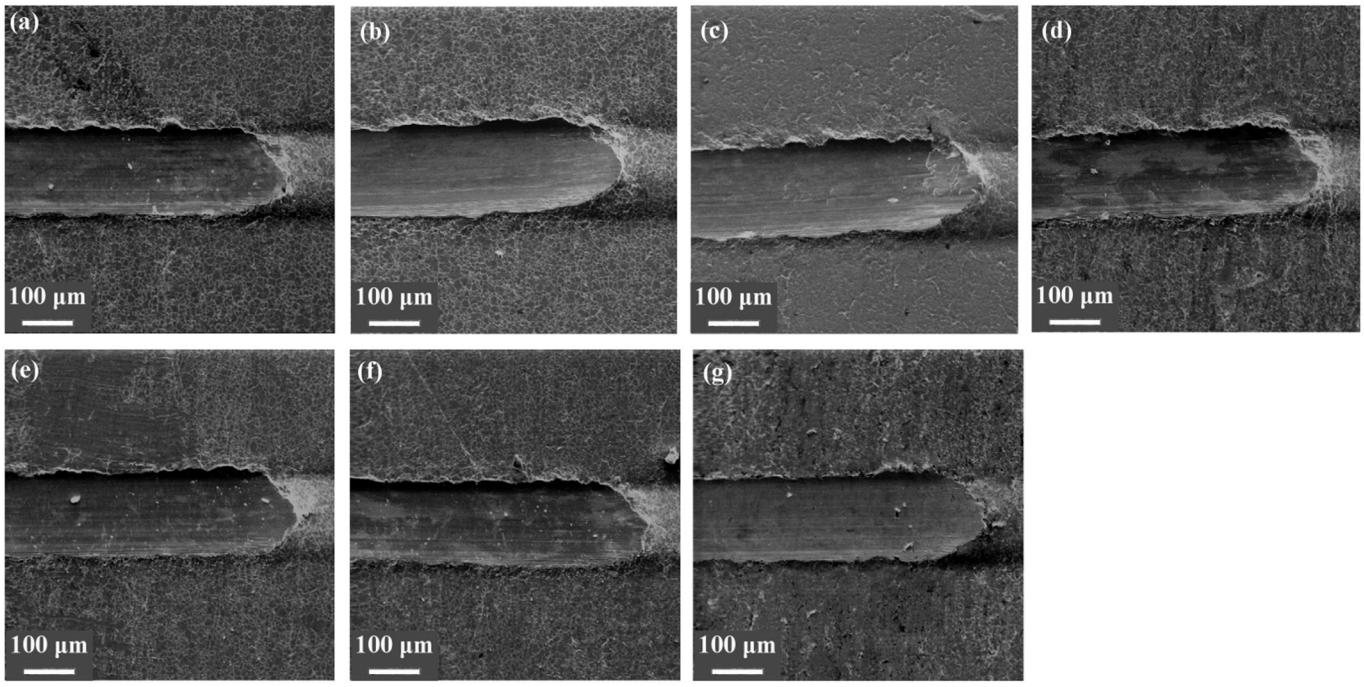

Fig. 9. scratch tracks of the as-deposited coatings, indicating no flaking at loads of up to 40 N: (a) Ti1, (b) Ti1-Ag1, (c) Ti1-Ag2, (d) Ti2, (e) Ti2-Ag1, (f) Ti2-Ag2 and (g) Ti2-Ag3.

significant stress experienced by the coating during the heat treatment due to a mismatch in thermal expansion coefficients between the coating and the substrate.

In applications which require high levels of cleanliness, such as food and medical applications, it is important that the coatings can withstand exposure to cleaning substances. In this work, the chemical resistance of Ag-TiO_2 coatings was investigated by immersing the coatings for 2 h in 0.02 M HCl and NaOH solutions. The immersion of coatings in NaOH solution did not affect their morphology or composition. Fig. 11 and Table 4 present the structure and composition of the coatings after the HCl immersion tests. HCl solution did not affect the morphology of the coatings with low silver contents. SEM and EDX analysis of the coatings with high silver loading (Ti1-Ag2 and Ti2-Ag3) displayed the migration of silver particles to the coating surface after HCl immersion tests. In terms of coating composition, HCl exposure caused a small reduction in the silver content in Ti1-Ag1 and Ti1-Ag2 coatings, although in the case of Ti1-Ag1, the change was within the measurement error. The composition of the Ti2- coatings did not change after their exposure to HCl, possibly due to the enhanced crystallinity of these coatings and better distribution of the silver, which reduced the penetration of HCl as

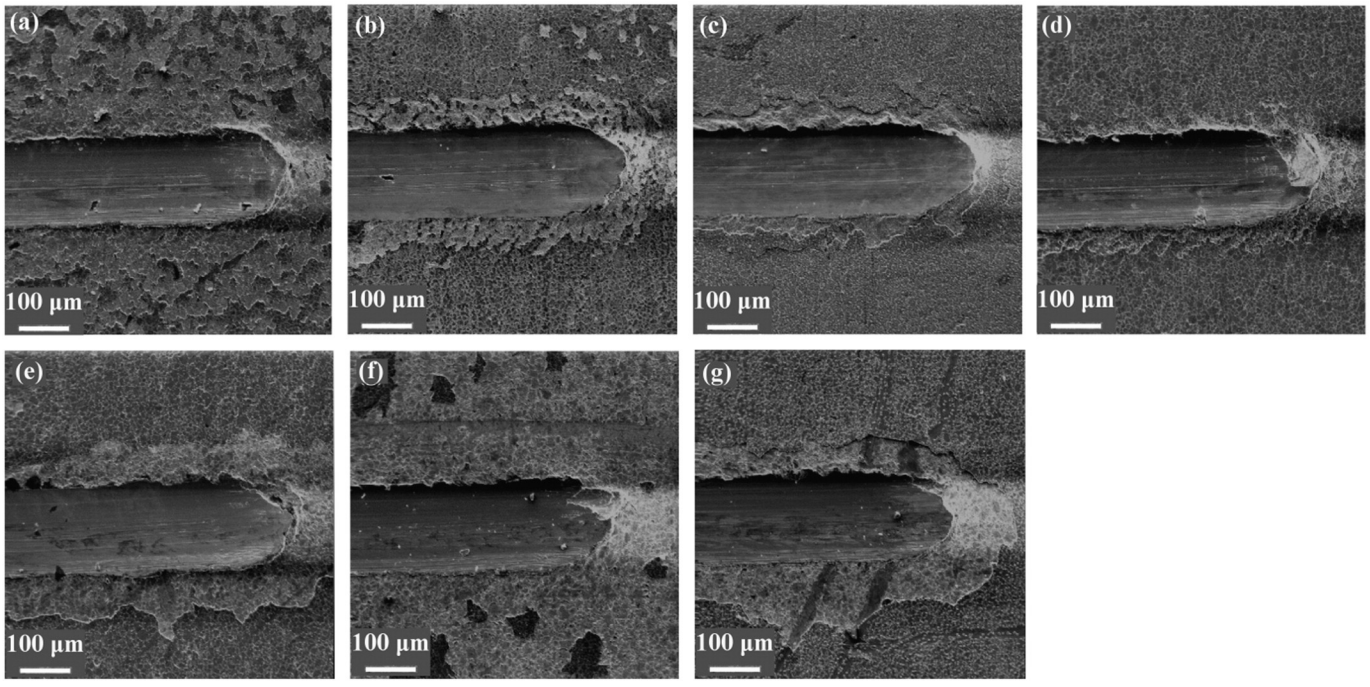

Fig. 10. Scratch tracks of coatings after annealing, showing the coating flaking and delamination around the scratch tracks: (a) Ti1, (b) Ti1-Ag1, (c) Ti1-Ag2, (d) Ti2, (e) Ti2-Ag1, (f) Ti2-Ag2 and (g) Ti2-Ag3.

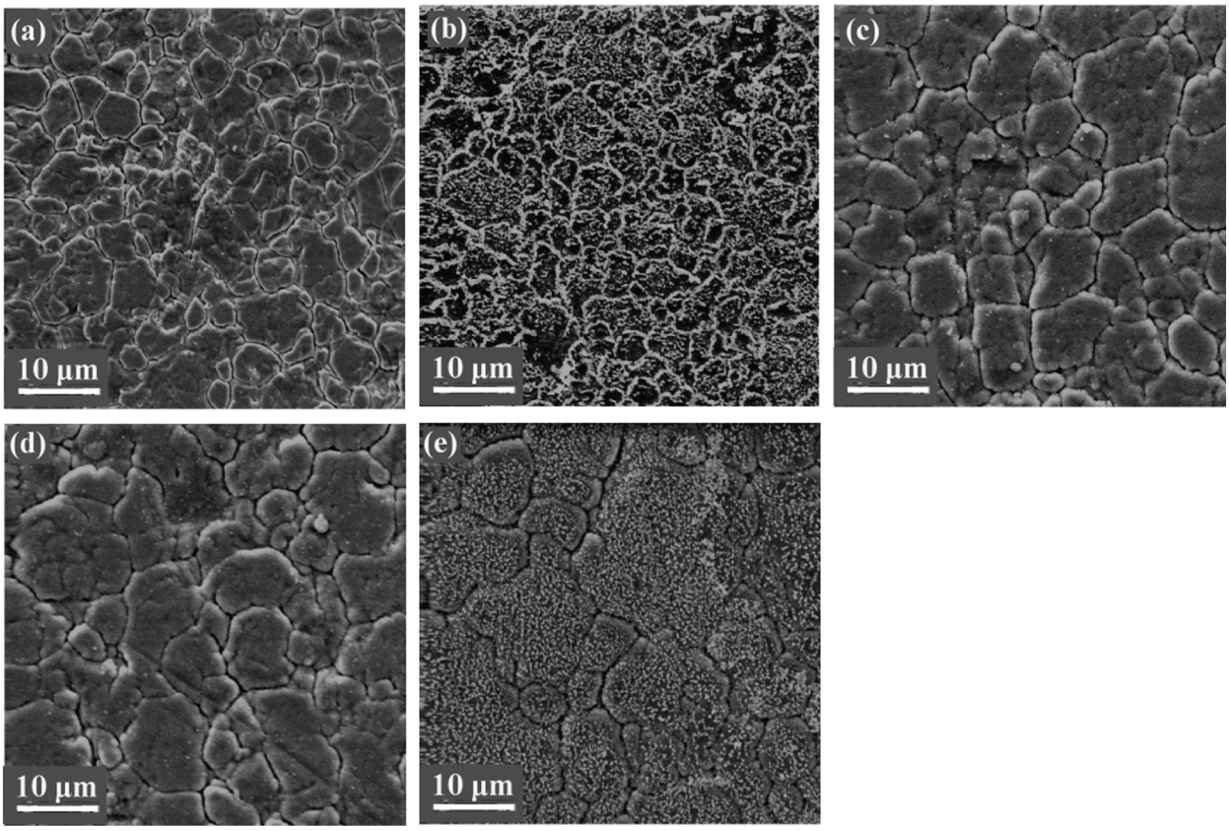

Fig. 11. SEM micrographs of the as-deposited (a) Ti-Ag1, (b) Ti1-Ag2, (c) Ti2-Ag1, (d) Ti2-Ag2 and (e) Ti2-Ag3 after exposure to HCl.

well as diffusion of silver from the bulk of coating to the surface. In Ti2-Ag3, which initially had a uniform silver distribution, silver appeared to diffuse out of the TiO_2 matrix after HCl exposure, with the apparent formation of submicron particles covering the surface (Fig. 11e). EDX analysis confirmed that these particles were formed of silver.

The antimicrobial potential of coatings are relevant to their self-cleaning properties and can affect their use in surfaces used within food and medical environments [35,36]. Initial investigations were carried out on Ti-*I* coatings against *E. coli* (Fig. 12). In the case of control stainless steel surfaces, some natural reduction in the number of bacteria was observed over time. Ti1 did not show antimicrobial properties in either dark or after irradiation with fluorescent light. Ti1-Ag1 and Ti1-Ag2 coatings had high antimicrobial properties and eradicated the bacteria within 12 hours both in the dark and light conditions. The effect can be related to the innate antimicrobial properties of silver, irrespective of irradiation [16,37], which is likely to be a result of the release of silver ions from the coatings [38,39]. Further investigation of the mechanisms involved in the antimicrobial properties of the Ag-TiO_2 coatings, silver ion release from the coatings and the effect of the process parameters on these properties are the subject of a further study.

Table 4
Ag content in the coatings before and after exposure to HCl and NaOH.

Coating	Ag (at%, i.e. referenced to the metallic content only)		
	As deposited	After HCl exposure	After NaOH exposure
Ti1-Ag1	17.9 ± 1.6	14.6 ± 0.8	16.2 ± 1.6
Ti1-Ag2*	51.8 ± 12.0	48.5 ± 5.4	52.0 ± 9.8
Ti2-Ag1	3.6 ± 1.0	3.5 ± 1.0	3.1 ± 0.6
Ti2-Ag2	5.7 ± 1.8	5.7 ± 1.8	5.8 ± 0.6
Ti2-Ag3	52.5 ± 1.2	53.7 ± 4.0	52.1 ± 1.0

* The large variation in silver content in Ti1-Ag2 is due to the phase separation of silver from the matrix TiO_2.

4. Conclusions

TiO_2 and Ag-TiO_2 coatings were deposited using reactive closed field unbalanced magnetron sputtering. The coatings were deposited from one or two titanium targets and coatings without and with varying silver loadings were produced.

The use of two targets for the deposition of TiO_2 (Ti2) resulted in a coating with higher crystallinity and surface area than the use of a single Ti target (Ti1). The addition of silver to Ti1 produced coatings with submicron-sized silver islands with increased hydrophobicity. The addition of silver to Ti2, however, led to a more uniform distribution of silver and the coatings were hydrophilic. All coatings displayed good adhesion to the substrate and high photocatalytic activity under fluorescent light.

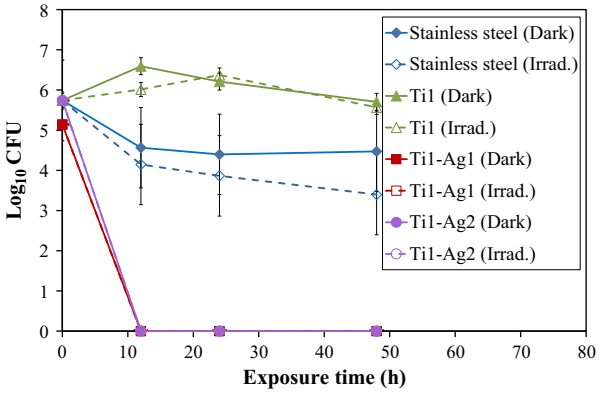

Fig. 12. The effect of exposure time on the attachment of *E. Coli* to stainless steel control and as-deposited TiO_2 and Ag-TiO_2 coatings with and without irradiation. The graphs for Ti1-Ag1 (Dark) and Ti1-Ag2 (Dark) are not visible as they overlap with Ti1-Ag1 (Irrad.) and Ti1-Ag2 (Irrad.), respectively.

Coatings with small amounts of silver gave the best photocatalytic performance. Annealing at 600 °C led to the separation of silver from the bulk TiO_2. It also had a detrimental effect on the photocatalytic activity and the mechanical properties of the coatings.

Ag-TiO_2 coatings with non-uniform silver distribution underwent silver loss after immersion in a 2 M aqueous HCl solution. Coatings which initially had a more uniform silver distribution performed better in chemical resistance tests with no loss of silver after immersion in HCl for two hours. In the coating with high silver loading (Ag: 52 at%, Ti: 48 at%), however, silver separated from the matrix and formed islands on the surface after immersion in HCl solution.

Ti1 coating did not show antimicrobial potential against *E. coli*, whilst the Ag-TiO_2 coatings eradicated the bacterium within 12 hours without the need for light.

It is therefore concluded that an oxide coating deposited from two titanium targets with a small amount of silver (Ag/Ti atomic ratio of 3/97–6/94) provides the best combination of mechanical, photocatalytic and antimicrobial properties and chemical resistance. Hence it may be suitable as a self-cleaning and innately antimicrobial surface with potential for use in food processing and medical environments.

Acknowledgements

This work was part of the MATERA+ Project “Disconnecting”, ref MFM-1855, Project No. 620015. Funding from the Technology Strategy Board, the UK's innovation agency, is gratefully acknowledged. The authors would also like to thank Dr Xiaoying Li from the University of Birmingham for her help with the XRD and FE-SEM analysis.

References

[1] C.W. Dunnil, I.P. Parkin, Nitrogen-doped TiO_2 thin films: photocatalytic applications for healthcare environments, Dalton Trans. 40 (2011) 1635.
[2] A. Fujishima, T.N. Rao, D.A. Tryk, Titanium dioxide photocatalysis, J. Photochem. Photobiol. C Photochem. Rev. 1 (2000) 1.
[3] M. Machida, K. Norimoto, T. Kimura, Antibacterial activity of photocatalytic titanium dioxide thin films with photodeposited silver on the surface of sanitary ware, J. Am. Ceram. Soc. 88 (2005) 95.
[4] C. Maneerat, Y. Hayata, Antifungal activity of TiO_2 photocatalysis against Penicillium expansum in vitro and in fruit tests, Int. J. Food Microbiol. 107 (2006) 99.
[5] L. Miao, S. Tanemura, Y. Kondo, M. Iwata, S. Toh, K. Kaneko, Microstructure and bactericidal ability of photocatalytic TiO_2 thin films prepared by rf helicon magnetron sputtering, Appl. Surf. Sci. 238 (2004) 125.
[6] S. Tanemura, L. Miao, W. Wunderlich, M. Tanemura, Y. Mori, S. Toh, K. Kaneko, Fabrication and characterization of anatase/rutile–TiO_2 thin films by magnetron sputtering: a review, Sci. Technol. Adv. Mater. 6 (2005) 11.
[7] D. Jiang, S. Zhang, H. Zhao, Photocatalytic degradation characteristics of different organic compounds at TiO_2 nanoporous film electrodes with mixed anatase/rutile phases, Environ. Sci. Technol. 41 (2007) 303.
[8] M. Andersson, L. Österlund, S. Ljungström, A. Palmqvist, Preparation of nanosize anatase and rutile TiO_2 by hydrothermal treatment of microemulsions and their activity for photocatalytic wet oxidation of phenol, J. Phys. Chem. B 106 (2002) 10674.
[9] H. Yin, Y. Wada, T. Kitamura, S. Kambe, S. Murasawa, H. Mori, T. Sakata, S. Yanagida, Hydrothermal synthesis of nanosized anatase and rutile TiO_2 using amorphous phase TiO_2, J. Mater. Chem. 11 (2001) 1694.
[10] M.-S. Wong, W.-C. Chu, D.-S. Sun, H.-S. Huang, J.-H. Chen, P.-J. Tsai, N.-T. Lin, M.-S. Yu, S.-F. Hsu, S.-L. Wang, H.-H. Chang, Visible-light-induced bactericidal activity of a nitrogen-doped titanium photocatalyst against human pathogens, Appl. Environ. Microbiol. 72 (2006) 6111.
[11] H. Irie, S. Washizuka, N. Yoshino, K. Hashimoto, Visible-light induced hydrophilicity on nitrogen-substituted titanium dioxide films, Chem. Commun. (2003) 1298.
[12] W. Zhang, Y. Li, S. Zhu, F. Wang, Fe-doped photocatalytic TiO_2 film prepared by pulsed dc reactive magnetron sputtering, J. Vac. Sci. Technol. A 21 (2003) 1877.
[13] O. Akhavan, R. Azimirad, Photocatalytic property of Fe_2O_3 nanograin chains coated by TiO_2 nanolayer in visible light irradiation, Appl. Catal. A 369 (2009) 77.
[14] O. Akhavan, M. Abdolahad, Y. Abdi, S. Mohajerzadeh, Synthesis of titania/carbon nanotube heterojunction arrays for photoinactivation of E. coli in visible light irradiation, Carbon 47 (2009) 3280.
[15] O. Akhavan, E. Ghaderi, Photocatalytic reduction of graphene oxide nanosheets on TiO_2 thin film for photoinactivation of bacteria in solar light irradiation, J. Phys. Chem. C 113 (2009) 20214.
[16] J. Musil, M. Louda, R. Cerstvy, P. Baroch, I.B. Ditta, A. Steele, H.A. Foster, Two-functional direct current sputtered silver-containing titanium dioxide thin films, Nanoscale Res. Lett. 4 (2009) 313.
[17] B.S. Necula, L.E. Fratila-Apachitei, S.A.J. Zaat, I. Apachitei, J. Duszczyk, In vitro antibacterial activity of porous TiO_2–Ag composite layers against methicillin-resistant Staphylococcus aureus, Acta Biomater. 5 (2009) 3573.
[18] S.-Q. Sun, B. Sun, W. Zhang, D. Wang, Preparation and antibacterial activity of Ag-TiO_2 composite film by liquid phase deposition (LPD) method, Bull. Mater. Sci. 31 (2008) 61.
[19] P.J. Kelly, R.D. Arnell, Magnetron sputtering: a review of recent developments and applications, Vacuum 56 (2000) 159.
[20] B.R. Weinberger, R.B. Garber, Titanium dioxide photocatalysts produced by reactive magnetron sputtering, Appl. Phys. Lett. 66 (1995) 2409.
[21] D.R. Costa, A.I. Martínez, A.A. López, C.R. Magaña, Titanium dioxide thin films: the effect of the preparation method in their photocatalytic properties, J. Mol. Catal. A 228 (2005) 183.
[22] B. Liu, X. Zhao, Q. Zhao, C. Li, X. He, The effect of O_2 partial pressure on the structure and photocatalytic property of TiO_2 films prepared by sputtering, Mater. Chem. Phys. 90 (2005) 207.
[23] Y. Zhang, X. Ma, P. Chen, D. Yang, Effect of the substrate temperature on the crystallization of TiO_2 films prepared by DC reactive magnetron sputtering, J. Cryst. Growth 300 (2007) 551.
[24] B. Karunagaran, D. Mangalaraj, K. Kim, B. Hong, Y. Roh, C.S. Park, J. Yi, Effect of calcination on the crystallinity of sputtered TiO_2 thin films as studied by Raman scattering, Cryst. Res. Technol. 40 (2005) 222.
[25] R. Hippler, S. Wrehde, V. Straňák, O. Zhigalov, H. Steffen, M. Tichy, M. Quaas, H. Wulff, Characterization of a magnetron plasma for deposition of titanium oxide and titanium nitride films, Contrib. Plasma Phys. 45 (2005) 348.
[26] J. Stallard, S. Poulat, D.G. Teer, The study of the adhesion of a TiN coating on steel and titanium alloy substrates using a multi-mode scratch tester, Tribol. Int. 39 (2006) 159.
[27] C.J. Tavares, S.M. Marques, T. Viseu, V. Teixeira, J.O. Carneiro, E. Alves, N.P. Barradas, F. Munnik, T. Girardeau, J.-P. Riviere, Enhancement in the photocatalytic nature of nitrogen-doped PVD-grown titanium dioxide thin films, J. Appl. Phys. 106 (2009) 113535.
[28] S.A. Tomás, A. Luna-Resendis, L.C. Cortés-Cuautli, D. Jacinto, Optical and morphological characterization of photocatalytic TiO_2 thin films doped with silver, Thin Solid Films 518 (2009) 1337.
[29] A. Houas, H. Lachheb, M. Ksibi, E. Elaloui, C. Guillard, J.-M. Herrmann, Photocatalytic degradation pathway of methylene blue in water, Appl. Catal. B Environ. 31 (2001) 145.
[30] H. Mehrgan, F. Elmi, M.R. Fazeli, A.R. Shahverdi, N. Samadi, Evaluation of neutralizing efficacy and possible microbial cell toxicity of a universal neutralizer proposed by the CTPA, Iran. J. Pharm. Res. 5 (2006) 173.
[31] R.C. Adochite, D. Munteanub, M. Torrell, L. Cunha, E. Alves, N.P. Barradas, A. Cavaleiro, J.P. Riviere, E. Le Bourhis, D. Eyidi, F. Vaz, The influence of annealing treatments on the properties of Ag:TiO_2 nanocomposite films prepared by magnetron sputtering, Appl. Surf. Sci. 258 (2012) 4028.
[32] K. Eufinger, D. Poelman, H. Poelman, R. De Gryse, G.B. Marin, Effect of microstructure and crystallinity on the photocatalytic activity of TiO_2 thin films deposited by dc magnetron sputtering, J. Phys. D Appl. Phys. 40 (2007) 5232.
[33] M. Ratova, P.J. Kelly, G.T. West, I. Iordanova, Enhanced properties of magnetron sputtered photocatalytic coatings via transition metal doping, Surf. Coat. Technol. 228 (2013) S544.
[34] F.W. Sears, M.W. Zemansky, University Physics, 2nd edition Addison-Wesley Pub. Co., Cambridge, Mass, 1955.
[35] P. Teixeira, D. Rodrigues, Antibiofilm Strategies in the Food Industry, in: K.P. Rumbaugh, I. Ahmed (Eds.), Antibiofim Agents, Springer Series on Biofilms, vol. 8, Springer-Verlag, Berlin Heidelberg, 2014, p. 359.
[36] P.L. Tran, A.N. Hamood, T.W. Reid, Antibiofilm Strategies on Medical Devices, in: K.P. Rumbaugh, I. Ahmed (Eds.), Antibiofim Agents, Springer Series on Biofilms, vol. 8, Springer-Verlag, Berlin Heidelberg, 2014, p. 175.
[37] K. Sornsanit, M. Horprathum, C. Chananonnawathorn, P. Eiamchai, S. Limwichean, K. Aiempanakit, Jakrapong Kaewkhao, Fabrication and characterization of antibacterial Ag-TiO_2 thin films prepared by DC magnetron co-sputtering technique, Adv. Mater. Res. 770 (2013) 221.
[38] O. Akhavan, E. Ghaderi, Self-accumulated Ag nanoparticles on mesoporous TiO_2 thin film with high bactericidal activities, Surf. Coat. Technol. 204 (2010) 3676.
[39] M.I. Majia, G. Restrepo, J.M. Marin, R. Sanjines, C. Pulgarin, E. Mielczarski, J. Mielczarski, J. Kiwi, Magnetron-sputtered Ag surfaces. New evidence for the nature of the Ag ions intervening in bacterial inactivation, Appl. Mater. Interfaces 2 (2010) 230.

Coatings **2014**, *4*, 433-449; doi:10.3390/coatings4030433

OPEN ACCESS

coatings

ISSN 2079-6412

www.mdpi.com/journal/coatings

Article

Photocatalytic TiO_2 and Doped TiO_2 Coatings to Improve the Hygiene of Surfaces Used in Food and Beverage Processing—A Study of the Physical and Chemical Resistance of the Coatings

Parnia Navabpour [1,*], Soheyla Ostovarpour [2], Carin Tattershall [3], Kevin Cooke [1], Peter Kelly [2], Joanna Verran [2], Kathryn Whitehead [2], Claire Hill [3], Mari Raulio [4] and Outi Priha [4]

1 Teer Coatings Ltd., Miba Coating Group, West Stone House, Berry Hill Industrial Estate, Droitwich WR9 9AS, UK; E-Mail: kevin.cooke@miba.com

2 Faculty of Science and Engineering, Manchester Metropolitan University, Chester Street, Manchester M1 5GD, UK; E-Mails: soheyla.ostovarpour@stu.mmu.ac.uk (S.O.); peter.kelly@mmu.ac.uk (P.K.); j.verran@mmu.ac.uk (J.V.); k.a.whitehead@mmu.ac.uk (K.W.)

3 Cristal Pigment UK Ltd., P.O. Box 26, Grimsby, North East Lincolnshire, DN41 8DP, UK; E-Mails: carin.tattershall@cristal.com (C.T.); claire.hill@cristal.com (C.H.)

4 VTT Technical Research Centre of Finland, P.O. Box 1000, FI-02044 VTT Espoo, Finland; E-Mails: mari.raulio@tikkurila.com (M.R.); outi.priha@vtt.fi (O.P.)

* Author to whom correspondence should be addressed; E-Mail: parnia.navabpour@miba.com; Tel.: +44-1905-827-550; Fax: +44-1905-827-551.

Received: 3 April 2014; in revised form: 23 June 2014 / Accepted: 1 July 2014 / Published: 15 July 2014

Abstract: TiO_2 coatings deposited using reactive magnetron sputtering and spray coating methods, as well as Ag- and Mo-doped TiO_2 coatings were investigated as self-cleaning surfaces for beverage processing. The mechanical resistance and retention of the photocatalytic properties of the coatings were investigated over a three-month period in three separate breweries. TiO_2 coatings deposited using reactive magnetron sputtering showed better mechanical durability than the spray coated surfaces, whilst the spray-deposited coating showed enhanced retention of photocatalytic properties. The presence of Ag and Mo dopants improved the photocatalytic properties of TiO_2 as well as the retention of these properties. The spray-coated TiO_2 was the only coating which showed light-induced hydrophilicity, which was retained in the coatings surviving the process conditions.

Keywords: photocatalytic; TiO_2; magnetron sputtering; spray coating; beverage processing

1. Introduction

In aquatic environments, microorganisms have a tendency to attach to surfaces along with organic and inorganic soil. For example in breweries, microorganisms have been shown to accumulate on sterile stainless steel surfaces within hours after the start of production [1].

Consumer demand is driving the development of a new group of more sensitive beverages with less alcohol, hop substances, and preservatives; however, these products are more prone to spoilage than are traditional drinks [2]. There are numerous operations involved in making beer. Each stage has a level of cleanliness that needs to be achieved and fouling is encountered at each stage [3]. Attachment of primary colonizers to stainless steel has been shown to be increased by sugars and sweeteners [1]. Thus removal of these deposits is essential since conditioning of a surface may be followed by biofilm formation. Biofilms on bottling plant surfaces are considered as serious sources for potential product spoiling microorganisms in the brewing industry [4]. Further, Fornalik [5] noted that minor fouling organisms resistant to cleaning in place (CIP) may become more resistant with time. Rheological studies indicated that increasing the temperature of the deposit generated a more elastic deposit which may decrease cleanability [3]. Thus, regular daily cleaning is needed. The following media are usually used in the cleaning process in brewing industry: water and steam, peroxide and alcohol based disinfectants, alkaline and acidic detergents and organic solvents [6,7]. There are however numerous drivers for a revision of CIP operations including the need to minimise utility usage (energy and water) and production downtime, minimisation of waste and greenhouse gas (GHG) emissions, and the need for product safety and quality [3].

One way to reduce cleaning costs and to improve process hygiene could be to use self-cleaning and antimicrobial coatings which can prevent the attachment of microorganisms and soil, or facilitate their efficient removal in the cleaning process.

TiO_2 is a widely used semiconductor. It has many different applications in optics [8], the environment [9], photovoltaics and solar cells [10,11], self-cleaning [12,13] and antimicrobial coatings [14]. In the self-cleaning and antimicrobial applications, the intended mechanism of action is often photocatalytic; in which the action of light on the TiO_2 coating generates active species that may be detrimental to microbes. For these applications, thin TiO_2 films with submicron thicknesses are usually employed. Several studies have been carried out to investigate the effect of crystal structure on the photocatalytic performance of TiO_2. Whilst some studies have found a higher activity of the anatase form [15,16], others have reported the mixed phase anatase/rutile to show a better photocatalytic performance [17]. Comparative studies of single phase anatase and rutile TiO_2 have concluded that the photocatalytic activity is dependent on the reaction being studied and different kinetics and intermediaries may be produced in each case [18,19]. As the surfaces used in the food and beverage industries are exposed to adverse environments (contact with water and beverages, cleaning solutions, abrasive wear during cleaning), scratch and corrosion resistance play important roles in their mechanical durability and

chemical stability. Hence, it is important to satisfy several requirements, including good adhesion to the substrate, the retention of high activity and resistance to chemicals.

The adhesion of any film to its substrate is one of the most important properties of a thin film. The level of adhesion depends on the force required to separate atoms or molecules at the interface between film and substrate. The adhesion of a film to the substrate is strongly dependent on the chemical nature, cleanliness, and microscopic topography of the substrate surface [20]. The presence of contaminants on the substrate surface may increase or decrease the adhesion depending on whether the adsorption energy is increased or decreased, respectively. Also the adhesion of a film can be improved by providing more nucleation sites on the substrate, for instance, by using a fine-grained substrate or a substrate pre-coated with suitable materials. Of the deposition processes available, magnetron sputtering has been shown to produce well adhered and uniform coatings over wide areas [11]. In this process, the adhesion of the film to the substrate can be improved by ion-cleaning of the substrate prior to the coating deposition as well as additional ion bombardment during coating deposition which improves adhesion by providing intermixing on an atomic scale [21].

It has been shown throughout the literature that the chemical and structural properties of the active film have a profound impact on the overall photocatalytic performance. Photocatalytic performance is influenced by film characteristics including; composition, bulk and surface structure and nanostructure, atomic to nanoscale roughness, hydroxyl concentration, and impurity concentration (e.g., Fe and Cr) [22–25].

The work described in this paper investigates the chemical and mechanical durability, wettability and the retention of photocatalytic activity of selected coatings after being placed in different brewery process environments, in this case bottle/can filling lines in three Finnish breweries.

2. Experimental Section

2.1. Preparation of Coated Surfaces

The substrate material for all coatings was stainless steel AISI 304 2B (75 × 25 × 1.6 mm^3). Coatings were produced using either closed field unbalanced magnetron sputtering (CFUBMS) [21] or by spray-coating with a TiO_2 sol. Table 1 shows the coatings produced.

Table 1. Preparation method of coated surfaces.

Code	Coating	Deposition Method
T1	TiO_2	Reactive magnetron sputtering
T2	TiO_2-Ag (low)	–
T3	TiO_2-Ag (high)	–
U1	TiO_2	Reactive magnetron sputtering + heat treatment
U2	TiO_2-Mo	–
MC	TiO_2	Spray-coated with TiO_2 sol

Coatings T1–T3 were deposited using reactive magnetron sputtering in a Teer Coatings UDP 450 coating system. One titanium target (99.5% purity) was used for the deposition of TiO_2. Argon (99.998% purity) was used as the working gas and oxygen (99.5% purity) as the reactive gas. The working pressure was 1 mbar. Ag (99.95% purity) was used as the dopant. Advanced Energy Pinnacle Plus pulsed DC

power supplies were used to power the titanium magnetrons and bias the substrates. An Advanced Energy DC power supply was used to power the silver target. 10–30 substrates were ultrasonically cleaned in acetone prior to loading into the chamber in order to remove surface contaminants. The substrates were aligned on a flat plate parallel to the surface of the metal targets at a distance of 150 mm from the target plane. A high rotational speed of 10 rpm was applied to the substrates to ensure enhanced mixing of silver and titanium within the coatings rather than the preferential formation of multilayer coatings. The substrates were ion-cleaned for a period of 20 min prior to the coating deposition using a bias voltage of −400 V and a low current of 0.2–0.35 A on the targets. The coatings were deposited at a bias voltage of −40 V. A thin layer of Ti was initially deposited as the adhesion layer prior to the introduction of oxygen to the deposition chamber. The amount of oxygen was controlled using an optical emission monitor, using conditions known to produce stoichiometric TiO_2 [26]. A pulsed-DC power of 2.5 kW was used on the Ti target at frequency 50 kHz and a duty of 97.75% (in synchronous mode). A continuous DC power of 70 W in the case of T2 and 150 W in the case of T3 was applied to the Ag target to vary the dopant content. The deposition rate was 17–22 nm/min depending on Ag content and coatings with thickness of 0.8–1 μm were produced. No additional heating was used during the coating process and the temperature did not exceed 200 °C during the process.

U1 and U2 coatings were deposited using reactive magnetron sputtering in a Teer Coatings UDP 450 coating system as described above. Two opposing magnetrons were fitted with titanium targets and one with the Mo dopant metal target (99.5% purity). The magnetrons with the titanium targets were in the closed field configuration and driven in pulsed DC sputtering mode using a dual channel Advanced Energy Pinnacle Plus supply at a frequency of 100 kHz and a duty of 50% (in synchronous mode). The Mo metal target was driven in a continuous DC mode (Advanced Energy MDX). The Ti targets were operated at a constant time-averaged power of 1 kW and the dopant target was operated at 180 W. Stainless steel samples were mounted on a substrate holder, which was rotated between the magnetrons at 4 rpm during deposition. The target to substrate separation was 8 cm. The titanium and Mo targets were cleaned by pre-sputtering in a pure argon atmosphere for 10 min. Deposition times were adapted to obtain a film thickness of 0.8–1 μm (deposition rate was 7.5 nm/min). The sputtered films were post deposition annealed at 600 °C for 30 min. in air.

Coating MC was prepared by spray-coating with a proprietary water-based TiO_2 sol using the following method. This transparent, neutral sol contained 2% TiO_2 (as anatase). Degreased stainless steel coupons were fixed to aluminium panels (approximately 150 × 100 mm^2). The panels with attached coupons were accurately weighed. The TiO_2 sol (0.2–0.3 g) was sprayed onto the aluminium panel with the attached coupons in a slow, steady motion, sweeping the panel in horizontal stripes from top to bottom, using a Badger Airbrush 200-3 model spray kit (Badger Air-Brush Co., Franklin Park, IL, USA). After air-drying for at least 15 min, the spraying procedure was repeated until 0.8–1.0 g/m^2 of TiO_2 sol was delivered to the surface. After air-drying overnight, the aluminium panel with the attached stainless steel coupons was re-weighed to give an accurate measurement of the weight per area of the coating.

2.2. Wettability

Water contact angle measurement is a practical tool to determine the wettability of a surface. Contact angle values were measured using a Digidrop instrument. At least two drops were measured for each

surface and the measurements averaged. Measurements were conducted after exposure in light, either SUNTEST CPS+ (xenon arc, filtered with special window glass, 550 W/m^2 across the irradiance range 320–800 nm) or UVA light (Philips blacklight, 10–12 W/m^2 across the irradiance range 350–400 nm), or after storage in the dark.

2.3. Adhesion of Coatings

The scratch and wear resistance of the coatings were assessed using a Teer ST3001 scratch–wear tester (Teer Coatings Ltd, Droitwich, UK) [27]. The coated surfaces were evaluated using a Rockwell diamond tip (radius 200 μm). A load rate of 100 N·min^{-1} and a constant sliding speed of 10.0 mm·min^{-1} were used with the load increasing from 10 to 40 N. The scratch tracks were examined using a Cambridge Stereoscan 200 scanning electron microscope (Cambridge Instruments, Cambridge, UK) in order to detect any flaking.

2.4. Photocatalytic Characterization of Coatings

The photocatalytic activities of the coatings were analyzed using the methylene blue (MB) degradation assay under UV and fluorescent light sources. In brief, MB solutions were made up to an initial concentration of 0.0105 mMol·L^{-1}. Photocatalytic surfaces were placed in 10 mL of the MB solution and irradiated at an integrated power flux of 40 W/m^2 with two 15 W UV lamps (365 nm wavelength). Tests were also carried out using two 15 W fluorescent tubes in place of the UV tubes to simulate typical lighting environments. The integrated power flux to the coatings with the fluorescent tubes was 64 W/m^2, of which the UV component (300–400 nm) was 13 W/m^2. A 10 cm distance between the light source and MB solution was used. Samples of the MB solution were taken before testing and at 1 hour intervals up to a total of 5–8 h. and analyzed using a UV-Vis spectrophotometer (Perkin Elmer, Waltham, MA, USA). Spectra were taken in the range of 650–668 nm and the height of the absorption peak in this region was monitored.

A graph of peak height absorbance against irradiation time, which has an exponential form was generated. An index of photocatalytic activity (*Pa*) was defined by comparing the degradation rate of the MB solution in contact with the coated surfaces to the rate for an irradiated MB solution with no coating present. The equation below was used to calculate the photocatalytic activity of each of the films. Two parameters were defined: Pa_{UV} for UV irradiation and Pa_{FL} for fluorescent light irradiation [28].

$$Pa = 1 - C_0\left[\mathrm{e}^{-mx} \Big/ \mathrm{e}^{-cx}\right] \tag{1}$$

where C_0 = peak height at time = 0; $C_0\mathrm{e}^{-mx}$ = decay rate of methylene blue; $C_0\mathrm{e}^{-cx}$ = decay rate of methylene blue in contact with photocatalytic coating.

2.5. Process Tests

Coated stainless steel pieces were placed on process surfaces within three breweries for a period of three months. Figure 1 shows an example of samples in location. Details of the location of test pieces in each brewery are given in Table 2. There was no special provision of lighting for the photocatalytic coatings; the process test took place under the usual brewery conditions of lighting, with coupons

receiving varying amounts of light depending on their position in each machine. Furthermore, all samples underwent the normal process conditions and cleaning regimes used in each brewery which included acid and alkaline cleaning chemicals such as acetic acid and sodium hydroxide, ethanol, steam and mechanical brushing. For each coating, two replicates were used in each of the breweries. Additionally, two replicates were retained as controls and were kept in the dark for the same period. After three months, each replicate was cut into six sections. The mechanical durability, photocatalytic activity and wettability were evaluated each on two of these sections.

Figure 1. Samples in location at Brewery B.

Table 2. Coatings evaluated in process tests (for a period of three months).

Coating	Control	Brewery A [1]	Brewery B [2]	Brewery C [3]
TiO_2 (T1)	T1-R1 T1-R2	T1-1 T1-2	T1-3 T1-4	T1-5 T1-6
TiO_2-Ag (low) (T2)	T2-R1 T2-R2	T2-1 T2-2	T2-3 T2-4	T2-5 T2-6
TiO_2-Ag (high) (T3)	T3-R1 T3-R2	T3-1 T3-2	T3-3 T3-4	T3-5 T3-6
TiO_2 (U1)	U1-R1 U1-R2	U1-1 U1-2	U1-3 U1-4	U1-5 U1-6
TiO_2-Mo (U2)	U2-R1 U2-R2	U2-1 U2-2	U2-3 U2-4	U2-5 U2-6
TiO_2 (MC)	MC-R1 MC-R2	MC-1 MC-2	MC-3 MC-4	MC-5 MC-6

[1] Filler table of beer canning machine; [2] Seamer of beer canning machine; [3] Filler table of a water and soft drinks PET line, inclined 10°.

3. Results and Discussion

This work compared three TiO_2 surfaces: as-deposited and heat-treated coatings deposited by reactive magnetron sputtering (T1 and U1, respectively), and a spray-coated TiO_2 (MC). Two dopants (Ag and Mo) were also investigated. Ag was used as it is a well-known antimicrobial material which could impart additional antimicrobial functionality to the coating. Mo was used as a dopant to reduce the band gap of TiO_2 in order to improve the visible light activity of TiO_2. Mo-TiO_2 has been reported to shift the band gap of TiO_2 by −0.20 eV [28]. The photoactivity and mechanical properties of the surfaces were studied for the as-prepared coatings and those having undergone process conditions. The effect of the process conditions on the properties of the coatings was investigated.

3.1. As Prepared Coatings

SEM and EDX were used to analyze the topography and dopant concentration (as atomic percent of total metals) in the as-prepared doped coatings. Ag-TiO_2 and Mo-TiO_2 surfaces showed small submicron sized particles which were characterized by EDX as silver rich phases, suggesting that the dopant separated from the matrix TiO_2. The silver content was 0.50 ± 0.05 at% in T2 and 30.0 ± 3.1 at% in T3. The Mo content in U2 was 7.0 ± 0.8 at %. The structure of coatings was analysed using XRD (Figure 2). The as-deposited TiO_2 coating (T1), showed an anatase structure. Ag-TiO_2 coatings showed strong silver peaks. The heat treated TiO_2 and Mo-TiO_2 (U1 and U2) showed anatase and rutile peaks as well as monoclinic β-TiO_2 which were very strong in the case of the doped coating.

Figure 2. Microstructure of coatings as evaluated using XRD, (**a**) as deposited TiO_2 and Ag-TiO_2 coatings (T1–T3); and (**b**) TiO_2 and Mo-TiO_2 coatings after heat treatment (U1 and U2) (S—substrate, An—anatase, Ru—rutile).

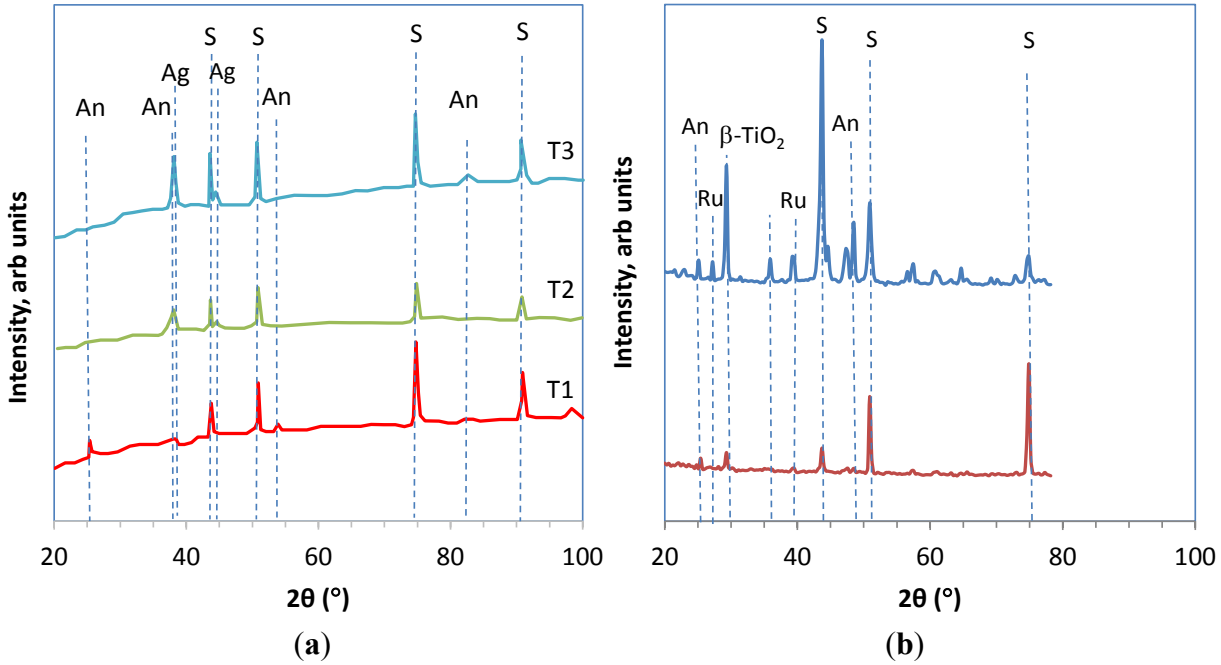

Figure 3 shows the photocatalytic activity for the as-prepared coatings and compares these values with those obtained for Pilkington Activ™ as a standard commercial product. As can be seen, all coatings showed high photocatalytic activity. In the case of T3, a change was also observed in the colour of the solution. This was thought to have been caused by leaching of silver from the surface. SEM analysis of the coating was performed before and after immersion in water for 2 h and showed the presence of microparticles on the surface which EDX confirmed to be silver (Figure 4). The silver microparticles in the as deposited coating were embedded in the matrix. Immersion in water resulted in the silver particles to protrude from the surface and EDX showed a reduction in the silver content, confirming that silver was indeed diffusing out of the coating.

Figure 3. Photocatalytic activity of the as-deposited coatings and comparison with a commercially available photocatalytic surface (Pilkington Activ™).

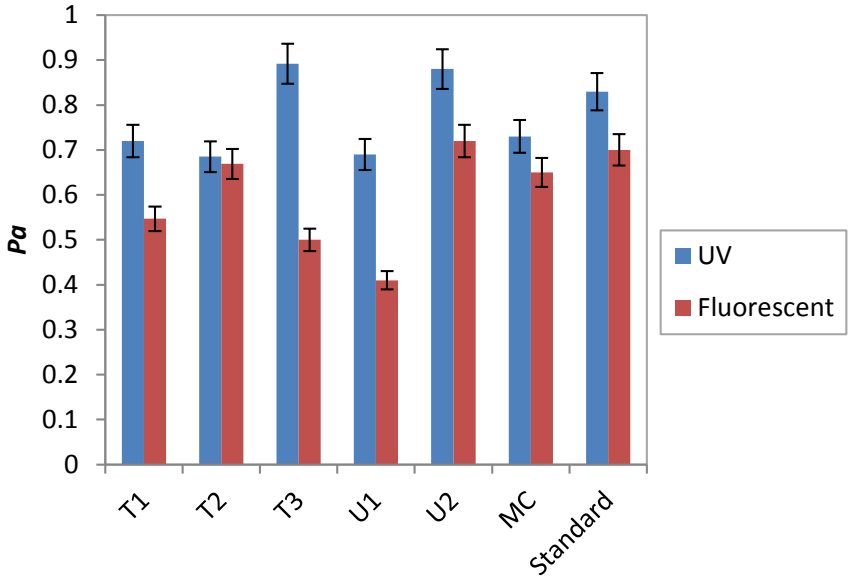

Figure 4. SEM micrographs of T3, (**a**) as deposited coating; and (**b**) after being under water for 2 h.

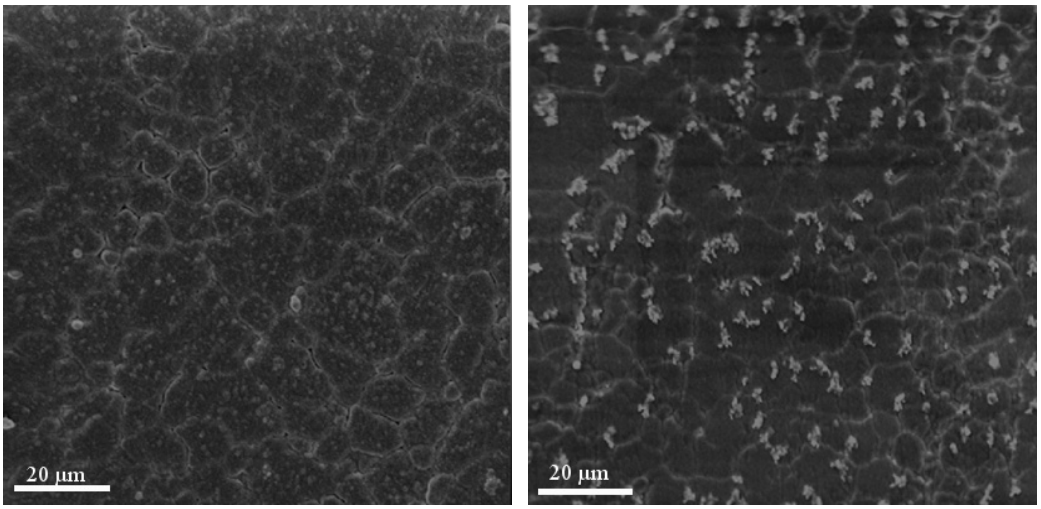

(**a**) (**b**)

Mechanical resistance of the coatings was analyzed using scratch testing. Figure 5 shows the scratch tracks of the coatings after production, as observed using the SEM. Coatings T1–T3 and MC showed excellent adhesion to the stainless steel substrate and no flaking was observed around the scratch tracks. Slight flaking was observed in U1 and U2, which was localized to the area immediately next to the scratch track. This may have been caused by the lack of a Ti adhesion layer in these coatings or due to the stresses applied to the coating during annealing. Given the destructive nature of the scratch test and the high load levels used in this test, all coatings were deemed to show sufficient mechanical resistance for use on food and drinks processing surfaces.

Figure 5. Progressive load scratch tracks of (**a**) T1; (**b**) T2; (**c**) T3; (**d**) U1; (**e**) U2 and (**f**) MC.

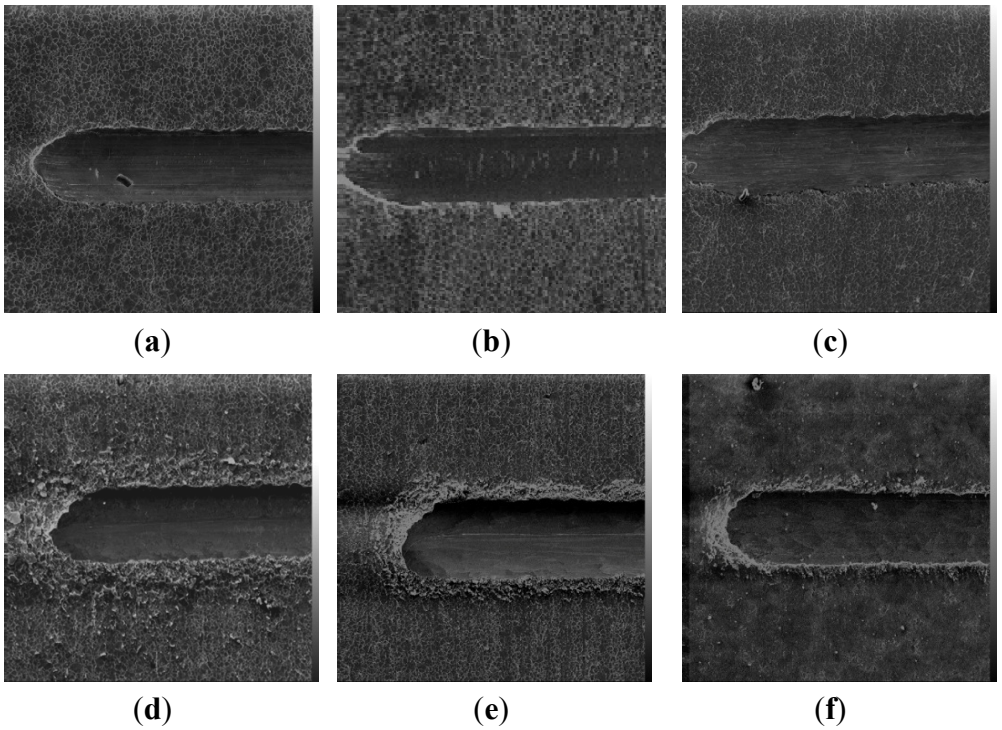

3.2. Properties of the Surfaces after Process Tests

Visual inspection of the coatings after the three months process trial and their comparison with the control surfaces showed that all coatings prepared by magnetron sputtering (T1, T2, T3, U1 and U2) were physically present, although some color changes were apparent (Figure 6). The TiO_2 sol coating (MC) appeared to be still present after the process test at Brewery C but was at least partially removed at the other two breweries. It was noticeable that many of the surfaces were heavily soiled, particularly those that had been on trial at Breweries A and B.

Figure 6. Images of coupons after the three month brewery trial. See Table 2 for sample descriptions.

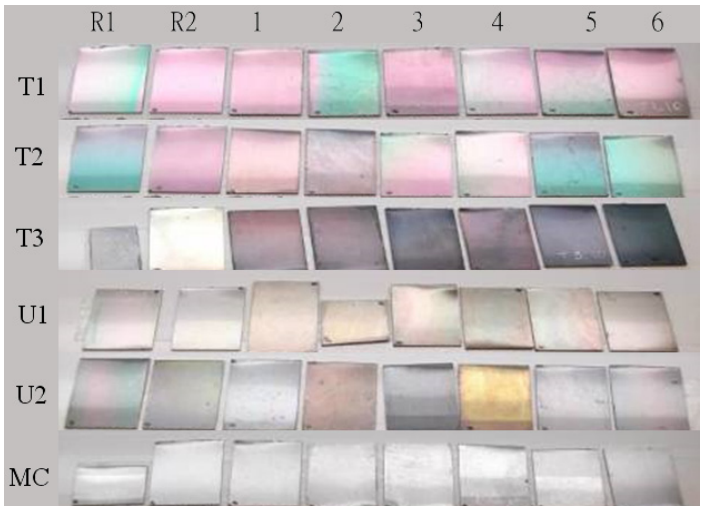

3.3. Mechanical Durability of the Coatings

The results of scratch adhesion tests performed on samples after the process trial confirmed the observations made on the appearance of coatings. Representative results are shown in Figure 7. T1–T3 coatings showed good adhesion with no flaking after the process studies. U1–U2 coatings showed some flaking, which in most cases was confined to the area immediately next to the scratch track. Some of the samples, however, showed a more widespread flaking. This was most likely caused by the lack of a Ti base layer, which can enhance the adhesion of TiO_2 to the stainless steel substrate or alternatively could be a result of the heat treatment. The MC coating from Breweries A and C showed some flaking near the scratch track. Samples removed from Brewery B showed no flaking. EDX analysis of these samples showed a Ti peak which had been greatly reduced compared to that of the control samples, suggesting that the coating had been heavily worn. This could be due to the different cleaning regimes, e.g., chemicals and scrubbing methods used in the different breweries, with some conditions exceeding the chemical and mechanical resistance of the coating.

Figure 7. SEM micrographs showing the scratch tracks of coatings before and after process tests at Brewery C.

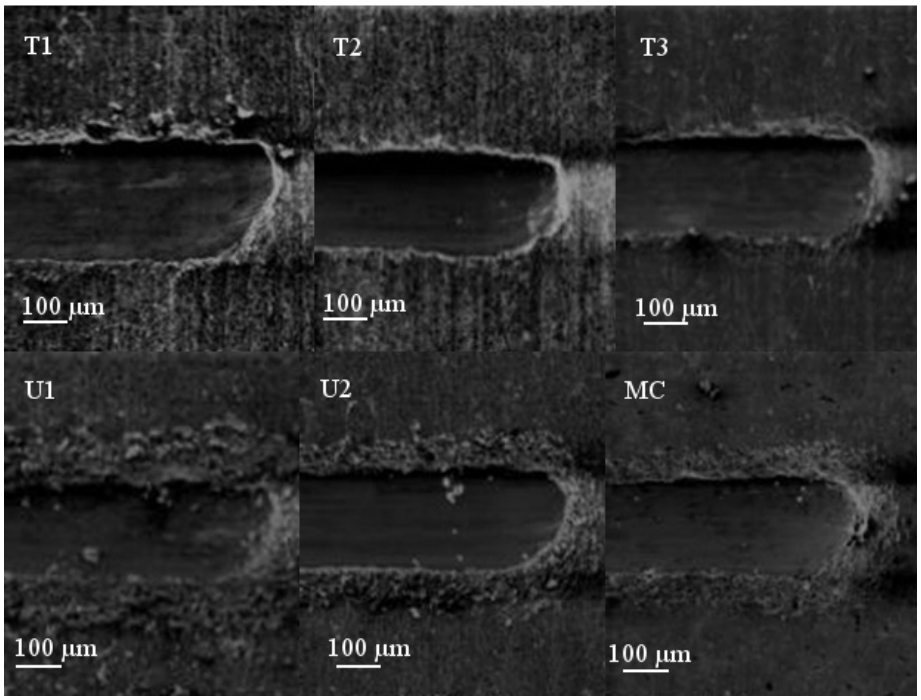

3.4. Composition of the Coatings

EDX results showed that the Ag content in T2 remained fairly constant. T3 showed a high level of Ag leaching possibly caused due to the poor dispersion and segregation of Ag within the coating as was seen from the SEM image of this coating (Figure 3). U2 showed a fairly constant concentration of Mo, except that in the areas where coating had been partially removed, it was not possible to measure the relative concentration of Mo in the coatings due to the weak signal and overlapping of the emission lines from the coating with those from the substrate (Table 3).

Table 3. Concentration of dopant as analysed using EDX (error in the measurements was ±10%).

Coating	As Deposited	Control		Brewery A		Brewery B		Brewery C	
		R1	R2	1	2	3	4	5	6
TiO_2-Ag (low Ag) (T2)	0.5	0.5		0.2	0.1	0.3	0.6	0.7	0.1
TiO_2-Ag (high Ag) (T3)	30.0	32.0	34.0	1.8	1.6	9.2	1.1	3.6	10.3
TiO_2-Mo (U2)	7.0	7.3	7.2	–	–	–	8	8.1	8.0

3.5. Photocatalytic Properties

Figure 8 shows the photocatalytic activity of the coatings under fluorescent and UV irradiation.

Figure 8. Photoactivity of TiO_2 and doped TiO_2 coatings under UV (blue bars) and fluorescent light (red bars) irradiation. (**a**) T1; (**b**) T2; (**c**) T3; (**d**) U1; (**e**) U2; (**f**) MC.

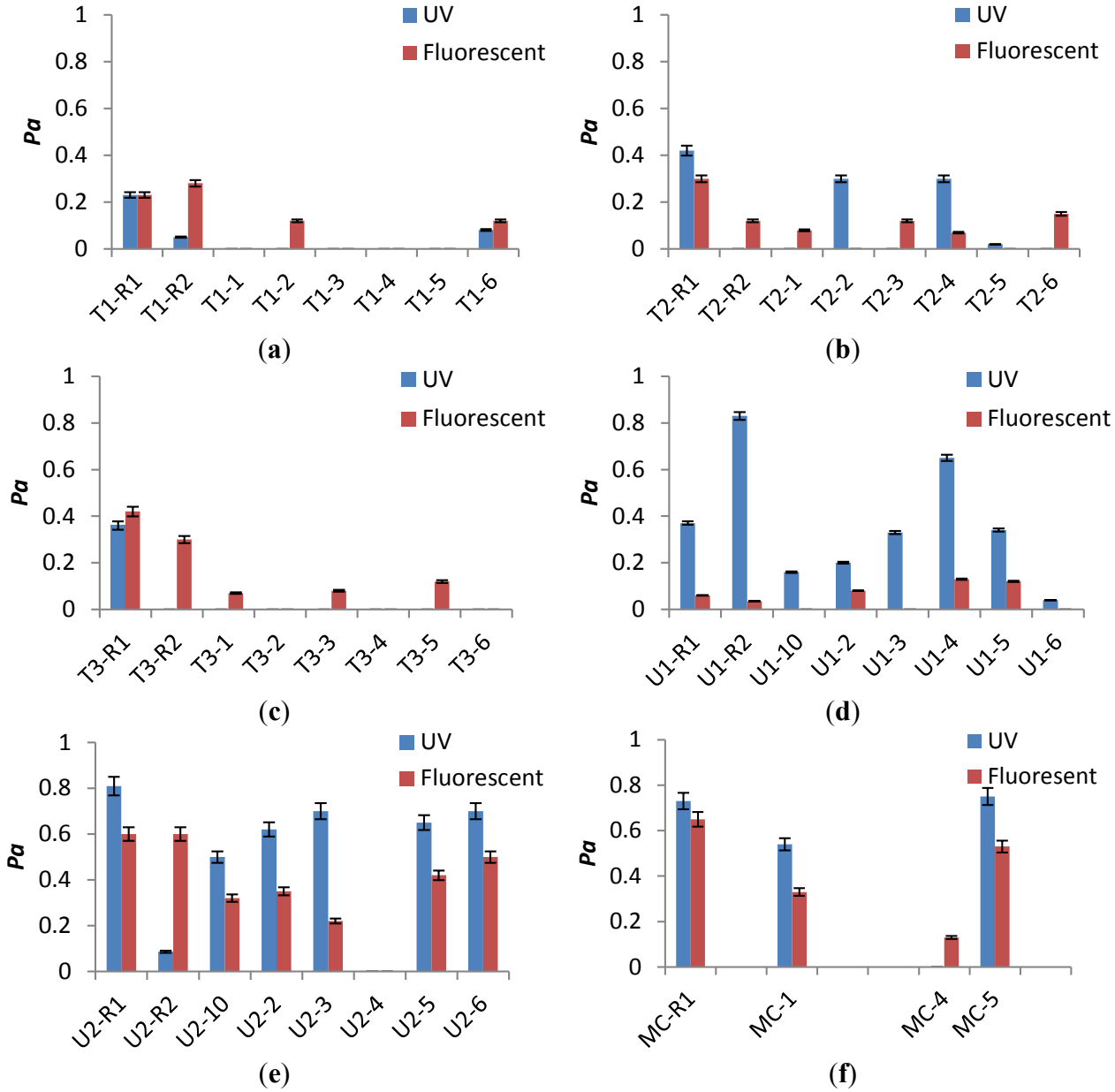

A loss of activity for T1–T3 coatings under UV light following the brewery trials was seen to varying degrees. The lower content TiO_2-Ag surface (T2) retained the most activity with the exception of samples received from Brewery C. A greater loss of photocatalytic properties of the higher doped Ag coatings was seen, possibly due to the leaching of silver during the process studies. The controls also lost activity following three months storage in the dark compared to the as-deposited samples (UV light). Similar results were seen when photocatalytic activity was assessed under fluorescent light. Comparison of the photocatalytic properties of U1 and U2, showed that the addition of Mo to the heat-treated TiO_2 surface increased its photocatalytic activity under UV and fluorescent light and this remained the case following the process studies. Photoactivity was largely retained for Mo-doped surfaces from all breweries with the exception of one of the two samples received from Brewery B. TiO_2 alone retained some of its photoactivity to varying degrees when irradiated with UV, although values between the duplicate samples differ. Less activity was shown under fluorescent light exposure, as expected and controls also showed lower photocatalytic activity compared to the as-deposited samples. Compared to the controls stored in the dark, the MC TiO_2 surfaces retained much of their photocatalytic activity, with the exception of samples received from Brewery B (under UV), where scratch test and EDX results had shown very little coating had been left on the substrate surface after the trial. As a small area of the substrate remained uncoated during the spray coating process, duplicate samples were not available in the case of MC surfaces.

The differences in photocatalytic activities of the surfaces received from the breweries could be due to the position of the samples and the cleaning regimes used. Work by others has shown that canning machines were markedly less prone to accumulation of microorganisms than bottling machines which use recycled glass bottles [1]. Further, it has been suggested that horizontal surfaces were prone to microbial accumulation and should be avoided in constructions as much as possible. Biofilm formation has also been shown to occur on certain surfaces despite daily cleaning and disinfection [1]. Thus, deposits formed by reaction processes or microbes usually cannot be wholly removed with water from stainless steel [29]. Various cleaners may have different success. In a surface test without soil a hypochlorite-based disinfectant was shown to be effective after an exposure of 10 min against all the microbes tested whereas an isopropanol-based cleaning agent was effective against all the vegetative cells tested [30]. In the presence of soil, hypochlorite was effective against *Listeria monocytogenes* and *Pseudomonas aeruginosa* [30]. The nature of clean may also affect efficacy. At 30 and 50 °C water rinsing at the flow velocities investigated could remove up to 85% of a yeast deposit. At a water rinsing temperature of 70 °C, less yeast deposit could be removed overall [3]. If surfaces were soiled with chemical residue and not cleaned sufficiently, it is possible that this may have an effect on photocatalytic activity. Conversely over aggressive cleaners might damage the surface, as noted previously.

3.6. Wettability

Photo-induced hydrophilicity is often associated with photocatalytic TiO_2 coatings [31]. Large differences in the wettability of TiO_2 coatings after irradiation by light or after storage in the dark are believed to be due to the generation of hydrophilic radicals on the TiO_2 surface by the action of light. Measurement of contact angle had been found to be an effective and easy method of detecting the presence of the TiO_2 sol coating, MC. In addition, it is expected that the contact of contaminants with the

surface is enhanced in the case of hydrophilic surfaces, resulting in an increase in the effect of the photocatalyst. Thus water contact angle measurements were made on each test coupon listed in Table 3 to help determine the presence and activity of each coating.

Contact angles were firstly measured for the coupons immediately on unpacking (dark), and then after 20 hours irradiation. It was noticeable that many of the coupons were heavily soiled so a portion of each sample was cleaned by wiping with 2-propanol on a soft cloth and then with water. Contact angles were re-measured after 20 h. under UVA light, and again after 6–7 days in the dark. The results are shown in Figures 9–11.

Figures 9–11 show that for most coatings, the effect of light on the wettability was more pronounced in the case of the reference surfaces than those having undergone the processing conditions. This may indicate changes in the coating activity resulting from the exposure to the cleaning chemicals *etc.* used during the processing.

Figure 9. Water contact angle measurements for (**a**) TiO_2 (T1); and (**b**) TiO_2-Ag (low) (T2) coupons after three-month Brewery Trial.

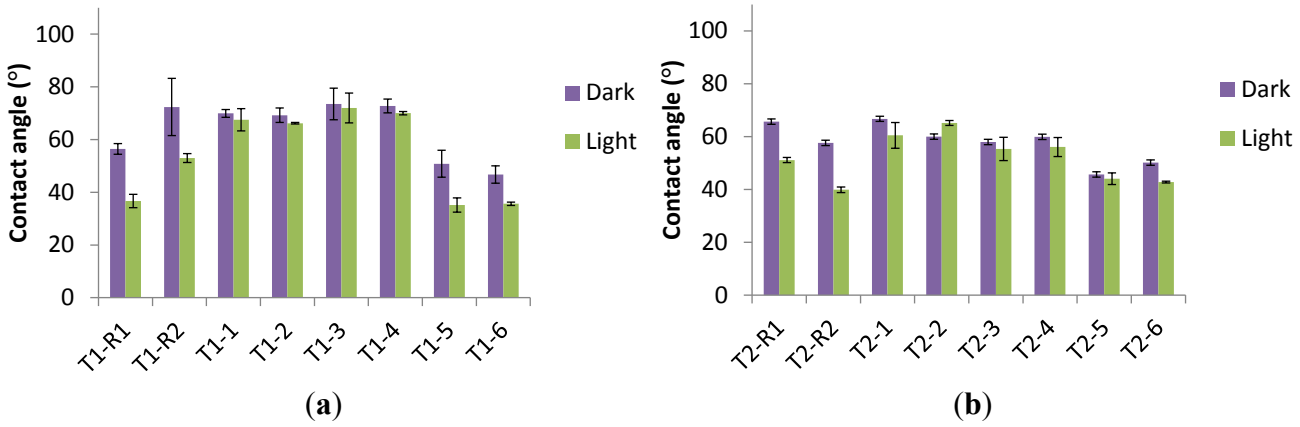

Figure 10. Water contact angle measurements for (**a**) TiO_2-Ag (high) (T3) and (**b**) TiO_2 (U1) coupons after three month Brewery Trial.

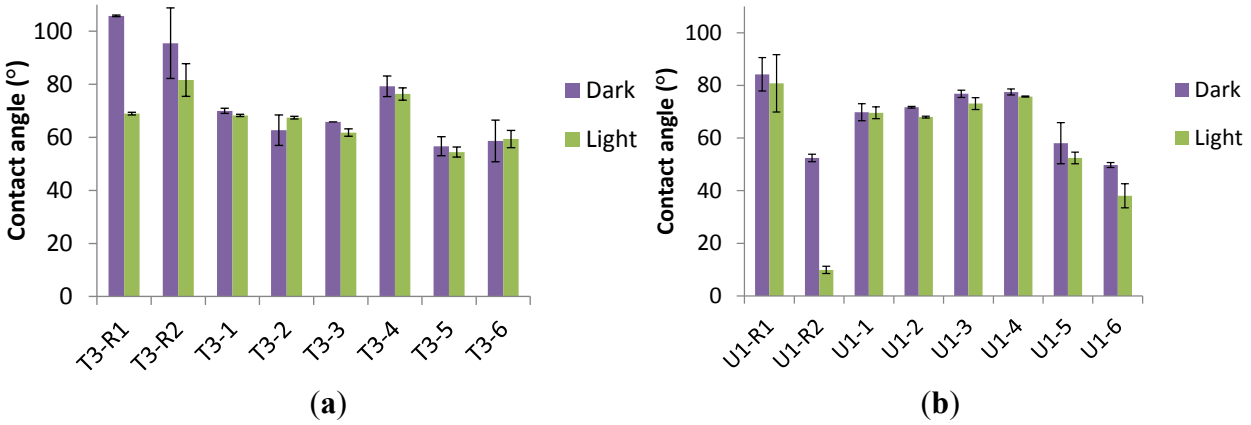

For the TiO_2 sol coating, MC, the two coupons sited at the Brewery C showed similar wettability to the control sample (MC-R2), after cleaning, both in the dark and the light. Visual inspection of the coupons sited at the other two breweries showed that the coating was wholly or partly removed from

these coupons, and the contact angle measurements reflect this loss of coating (Figure 11b). Contact angle values on blank stainless steel surfaces after cleaning were 70°–80°.

Figure 11. Water contact angle measurements for (**a**) TiO_2-Mo (U2); and (**b**) TiO_2 (MC) coupons after three month Brewery Trial (Coated area of MC-R1 was too small to test).

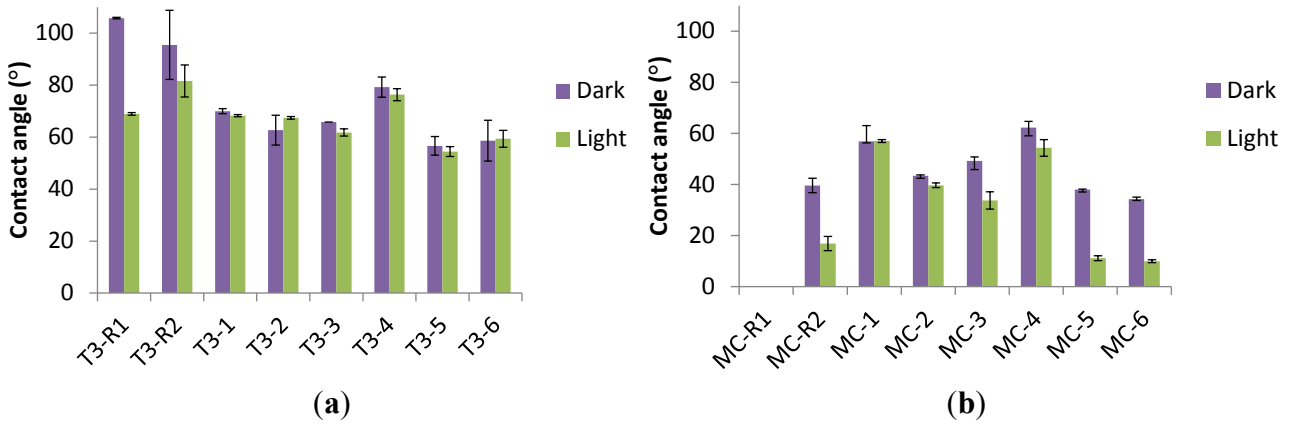

4. Conclusions

TiO_2 coatings were deposited either using reactive magnetron sputtering, both with and without subsequent heat treatment, or prepared by spray coating. Photocatalytic activity, determined by methylene blue degradation, was high under UV irradiation. The coatings were also active under fluorescent irradiation. Doping of magnetron sputtered TiO_2 with Ag- (0.5 at%) and Mo- (7 at%) increased the activity under fluorescent light. High Ag loading (~30%) had a detrimental effect on the fluorescent light induced photoactivity, possibly due to the replacement of Ti atoms in the TiO_2 matrix with Ag. The coatings were placed in three different breweries for three months. The magnetron sputtered TiO_2 surfaces which had not undergone heat treatment showed the best mechanical resistance, whilst the spray coated TiO_2 and Mo-TiO_2 showed the best retention of photoactivity. Irradiation of the coatings resulted in an increase in wettability, but the spray-coated TiO_2 was the only coating showing light-induced hydrophilicity after the process trial.

This work presented the potential of magnetron sputtered TiO_2 and doped TiO_2 coatings for surfaces used in food and beverage processing where there is a requirement for robust coatings. Selection of the optimum deposition parameters and dopants can lead to coatings which retain photoactivity and are durable in harsh processing conditions. The use of spray coatings is preferred on surfaces which do not experience severe mechanical wear and abrasion.

Acknowledgments

This work was part of the MATERA+ Project “Disconnecting”, refer MFM-1855, Project No. 620015. Funding from the Technology Strategy Board, the UK’s innovation agency and Finnish Funding Agency for Technology and Innovation (Tekes) is gratefully acknowledged. The authors would also like to thank Oy Panimolaboratorio - Bryggerilaboratorium Ab (PBL Brewing Laboratory) for their collaboration in this work.

Author Contributions

Parnia Navabpour, Kevin Cooke, Soheyla Ostovarpour, Peter Kelly, Joanna Verran and Kathryn Whitehead provided the planning and experimental work on magnetron sputtered coatings and the sections of the paper on these coatings. Teer Coatings authors also carried out the scratch tests and SEM work on all coatings and were responsible for writing the sections of the manuscript on these results. Manchester Metropolitan University authors were responsible for the photocatalytic tests, as well as the manuscript sections on these results. Carin Tattershall and Claire Hill carried out the work on MC coating and contact angle analysis and wrote the article sections on these results. Outi Priha and Mari Raulio were responsible for coordinating and performing the process tests. All authors contributed in the discussion and improvement of the paper. Parnia Navabpour coordinated the writing of the overall manuscript.

Conflicts of Interest

The authors declare no conflict of interest.

References

1. Storgårds, E.; Tapani, K.; Hartwall, P.; Saleva, R.; Suihko, M. Microbial attachment and biofilm formation in brewery bottling plants. *J. Am. Soc. Brew. Chem.* **2006**, *64*, 8–15.
2. Priha, O.; Laakso, J.; Levänen, E.; Kolari, M.; Mäntylä, T.; Storgårds, E. Effect of photocatalytic and hydrophobic coatings on brewery surface microorganisms. *J. Food Prot.* **2011**, *11*, 1788–1989.
3. Goode, K.R.; Asteriadou, K.; Fryer, P.J.; Picksley, M.; Robbins, P.T. Characterising the cleanign mechanisms of yeast and the implicaitons for Cleaning In Place (CIP). *Food Bioprod. Proc.* **2010**, *88*, 365–374.
4. Timke, M.; Wang-Lieu, N.Q.; Altendorf, K.; Lipski, A. Identity, beer spoiling and biofilm forming potential of yeasts from beer bottling plant associated biofilms. *Antonie Van Leeuwenhoek* **2008**, *93*, 151–161.
5. Fornalik, M. Biofouling and process cleaning: A practical approach to understanding what is happening on the walls of your pipes. *Master Brew. Assoc. Am. Tech. Q.* **2008**, *45*, 340–344.
6. Storgårds, E. Process Hygiene Control in Beer Production and Dispensing. Available online: http://www.vtt.fi/inf/pdf/publications/2000/P410.pdf (accessed on 8 July 2014).
7. Rezić, T.; Rezić, I.; Blaženović, I.; Šantek, B. Optimization of corrosion processes of stainless steel during cleaning in steel brewery tanks. *Mater. Corros*. **2013**, *64*, 321–327.
8. Farahani, N.; Kelly, P.J.; West, G.; Ratova, M.; Hill, C.; Vishnyakov, V. Photocatalytic activity of reactively sputtered and directly sputtered titania coatings. *Thin Solid Films* **2011**, *520*, 1464–1469.
9. Caballero, L.; Whitehead, K.A.; Allen, N.S.; Verran, J. Inactivation of E.coli on immobilized TiO_2 using fluorescent light. *J. Photochem. Photobiol. A* **2009**, *202*, 92–98.
10. Bandaranayake, K.M.P.; Indika Senevirathna, M.K.; Prasad Weligamuwa, P.M.G.M.; Tennakone, K. Dye-sensitized solar cells made from nanocrystalline TiO_2 films coated with outer layers of different oxide materials. *Coord. Chem. Rev.* **2004**, *248*, 1277–1281.

11. Sung, Y.M.; Kim, H.J. Sputter deposition and surface treatment of TiO_2 films for dye-sensitized solar cells using reactive RF plasma. *Thin Solid Films* **2007**, *515*, 4996–4999.
12. Pakdel, E.; Daoud, W.A.; Wang, X. Self-cleaning and superhydrophilic wool by TiO_2/SiO_2 nanocomposite. *Appl. Surf. Sci.* **2013**, *275*, 397–402.
13. Samal, S.S.; Jeyaraman, P.; Vishwakarma, V. Sonochemical Coating of Ag-TiO_2 Nanoparticles on Textile Fabrics for Stain Repellency and Self-Cleaning- The Indian Scenario: A Review. *J. Miner. Mater. Charact. Eng.* **2010**, *9*, 519–525.
14. Hájková, P.; Špatenka, P.; Krumeich, J.; Exnar, P.; Kolouch, A.; Matoušek J.; Koči, P. Antibacterial effect of silver modified TiO_2/PECVD films. *J. Eur. Phy. D* **2009**, *54*, 189–193.
15. Miao, L.; Tanemura, S.; Kondo, Y.; Iwata, M.; Toh, S.; Kaneko, K. Microstructure and bactericidal ability of photocatalytic TiO_2 thin films prepared by rf helicon magnetron sputtering. *Appl. Surf. Sci.* **2004**, *238*, 125–131.
16. Tanemura, S.; Miao, L.; Wunderlich, W.; Tanemura, M.; Mori, Y.; Toh, S.; Kaneko, K. Fabrication and characterization of anatase/rutile-TiO_2 thin films by magnetron sputtering: A review. *Sci. Technol. Adv. Mater.* **2005**, *6*, 11–17.
17. Jiang, D.; Zhang, S.; Zhao, H. Photocatalytic Degradation Characteristics of Different Organic Compounds at TiO_2 Nanoporous Film Electrodes with Mixed Anatase/Rutile Phases. *Environ. Sci. Technol.* **2007**, *41*, 303–308.
18. Andersson, M.; Österlund, L.; Ljungström, S.; Palmqvist, A. Preparation of nanosize anatase and rutile TiO_2 by hydrothermal treatment of microemulsions and their activity for photocatalytic wet oxidation of phenol. *J. Phy. Chem. B* **2002**, *106*, 10674–10679.
19. Yin, H.; Wada, Y.; Kitamura, T.; Kambe, S.; Murasawa, S.; Mori, H.; Sakata, T.; Yanagida, S. Hydrothermal synthesis of nanosized anatase and rutile TiO_2 using amorphous phase TiO_2. *J. Mater. Chem.* **2001**, *11*, 1694–1703.
20. Wasa, K.; Kitabatake, M.; Adachi, H. *Thin Film Materials Technology: Sputtering of Control Compound Materials*; William Andrew Inc.: Norwich, CT, USA, 2004.
21. Laing, K.; Hampshire, J.; Teer, D.G.; Chester, G. The effect of ion current density on the adhesion and structure of coatings deposited by magnetron sputter ion plating. *Surf. Coat. Technol.* **1999**, *112*, 177–180.
22. Ohtani, T.; Ogawa, Y.; Nishimoto, S. Photocatalytic Activity of Amorphous-Anatase Mixture of Titanium(IV) Oxide Particles Suspended in Aqueous Solutions. *J. Phy.Chem. B* **1997**, *101*, 3746–3752.
23. Yu, J.; Zhao, X.; Du, J.; Chen, W. Preparation, microstructure and photocatalytic activity of the porous TiO_2 anatase coating by sol-gel processing. *J. Sol Gel Sci. Technol.* **2000**, *17*, 163–171.
24. Nam, H.; Amemyima, T.; Murabayashi, M.; Itoh, K. Photocatalytic Activity of Sol-Gel TiO_2 Thin Films on Various Kinds of Glass Substrates: The Effects of Na^+ and Primary Particle Size. *J. Phy. Chem. B* **2004**, *108*, 8254–8259.
25. Kubacka, A.; Colón G.; Fernández-García, M. Cationic (V, Mo, Nb, W) doping of TiO_2–anatase: A real alternative for visible light-driven photocatalysts. *Catal. Today* **2009**, *143*, 286–292.
26. Onifade, A.A.; Kelly, P.J. The influence of deposition parameters on the structure and properties of magnetron-sputtered titania coatings. *Thin Solid Films* **2006**, *494*, 8–12.

27. Stallard, J.; Poulat, S.; Teer, D.G. The study of the adhesion of a TiN coating on steel and titanium alloy substrates using a multi-mode scratch tester. *Tribol. Int.* **2006**, *39*, 159–166.
28. Ratova, M.; Kelly, P.J.; West, J.T.; Iordanova, I. Enhanced properties of magnetron sputtered photocatalytic coatings via transition metal doping. *Surf. Coat. Technol.* **2013**, *228*, S544–S549.
29. Christian, G.K.; Fryer, P.J.; Liu, W. How hygiene happens: Physics and chemistry of cleaning. *Int. J. Dairy Technol.* **2006**, *59*, 76–84.
30. Grönholm, L.; Wirtanen, G.; Ahlgren, K.; Nordström, K.; Sjöberg, A.-M. Screening of antimicrobial activities of disinfectants and cleaning agents against foodborne spoilage microbes. *Z. Lebensm. Unters. Forshung A* **1999**, *208*, 289–298.
31. Fujishima, A.; Rao, T.N.; Tryk, D.A. Titanium dioxide photocatalysis. *J. Photochem. Photobiol. C* **2000**, *1*, 1–21.

Molecules **2014**, *19*, 16327-16348; doi:10.3390/molecules191016327

OPEN ACCESS

molecules

ISSN 1420-3049

www.mdpi.com/journal/molecules

Review

Structural Formation and Photocatalytic Activity of Magnetron Sputtered Titania and Doped-Titania Coatings

Peter J. Kelly [1,*], Glen T. West [1], Marina Ratova [2], Leanne Fisher [3], Soheyla Ostovarpour [1,3] and Joanna Verran [3]

[1] Surface Engineering Group, Dalton Research Institute, Manchester Metropolitan University, Manchester M1 5GD, UK; E-Mails: g.west@mmu.ac.uk (G.T.W.); soheyla.ostovarpour@stu.mmu.ac.uk (S.O.)

[2] School of Chemistry and Chemical Engineering, Queen's University Belfast, Belfast BT9 5AG, UK; E-Mail: marina_ratova@hotmail.com

[3] School of Healthcare Science, Manchester Metropolitan University, Manchester M1 5GD, UK; E-Mails: l.fisher@mmu.ac.uk (L.F.); j.verran@mmu.ac.uk (J.V.)

* Author to whom correspondence should be addressed; E-Mail: peter.kelly@mmu.ac.uk; Tel.: +44-161-247-4643; Fax: +44-161-247-4693.

External Editor: Pierre Pichat

Received: 27 August 2014; in revised form: 25 September 2014 / Accepted: 2 October 2014 / Published: 13 October 2014

Abstract: Titania and doped-titania coatings can be deposited by a wide range of techniques; this paper will concentrate on magnetron sputtering techniques, including "conventional" reactive co-sputtering from multiple metal targets and the recently introduced high power impulse magnetron sputtering (HiPIMS). The latter has been shown to deliver a relatively low thermal flux to the substrate, whilst still allowing the direct deposition of crystalline titania coatings and, therefore, offers the potential to deposit photocatalytically active titania coatings directly onto thermally sensitive substrates. The deposition of coatings via these techniques will be discussed, as will the characterisation of the coatings by XRD, SEM, EDX, optical spectroscopy, *etc.* The assessment of photocatalytic activity and photoactivity through the decomposition of an organic dye (methylene blue), the inactivation of *E. coli* microorganisms and the measurement of water contact angles will be described. The impact of different deposition technologies, doping and co-doping strategies on coating structure and activity will be also considered.

Keywords: titanium dioxide; photocatalytic coatings; magnetron sputtering; doping; methylene blue; HiPIMS; antimicrobial activity

1. Introduction

Photocatalytic titania-based surfaces and coatings have many potential applications, including "self-cleaning" windows, anti-fogging screens or lenses, air cleaning and water purification devices and "self-sterilizing" antibacterial tiles [1–6]. Although it is relatively straightforward to demonstrate the effectiveness of these coatings in a laboratory environment, producing highly photoactive coatings in a commercially viable process is more challenging, and this has limited the exploitation of this technology to date. Titania can be produced in nanoparticle form for incorporation into paints and other building products [7], or as slurries and suspensions for water treatment [8,9]. Whilst the latter arrangement provides high surface areas of active material, there is usually a requirement for downstream filtration of the particles, limiting its practicality. In other applications, such as windows, lenses or tiles, a titania thin film or coating is the preferred option, where the reduced surface area is compensated for by high transparency and durability.

There are a number of physical and chemical deposition techniques that can be used to produce titania and doped-titania coatings. These include pulsed laser deposition [10], magnetron sputtering [11–13], reactive evaporation [13], ion beam assisted deposition [14], chemical vapour deposition [15], sol-gel [16], dip-coating [17], hydrothermal synthesis [18] and atomic layer deposition [19,20]. The characteristics of each process have a major bearing on deposition parameters, such as substrate temperature (and thereby, choice of substrate material) and throughput and coating properties, such as adhesion, crystallinity, grain size, lattice defects, transparency and surface roughness, and in general, the performance of the coating is inextricably linked to the choice of deposition process. The production of photoactive titania coatings is further complicated by the requirement for the coating to be predominantly in the anatase crystal form (mixed phase anatase/rutile structures have also been reported as being effective [10,20]). Titania coatings deposited at ambient temperature tend to be amorphous [12], though and the formation of anatase structures usually requires elevated temperatures (~400 °C) during deposition or post-deposition annealing, which imposes additional processing costs and restricts the use of thermally sensitive substrate materials.

Of the deposition techniques available, magnetron sputtering is widely used for the production of high quality coatings for applications ranging from Low-E and solar control glazing products, tool coatings, micro- and opto-electronic components, data storage media and thin film photovoltaics. Indeed, the scalability and versatility of the magnetron sputtering process and the uniformity and repeatability of the resulting coatings has made this the process of choice for many commercial applications [21].

The magnetron sputtering process has been described in detail elsewhere [21] and the finer nuances of magnetron design and process control are beyond the scope of this paper. In simple terms, though, it is a physical vapour deposition process in which positively charged ions from a glow discharge plasma are accelerated towards a negatively biased target plate of the material to be deposited, which is mounted on the magnetron body. The incident ions remove or "sputter" atoms from the surface of the

target through a momentum exchange mechanism. The process takes place in a reduced pressure (typically 0.1 to 0.5 Pa) atmosphere, usually of argon, in which the plasma can be readily maintained. The sputtered atoms diffuse across the chamber and condense on the substrate as a thin film. Reactive gases, such as oxygen or nitrogen can be introduced with the argon in order to form compound films of oxides or nitrides. However, during the deposition of dielectric materials, such as oxides, the build-up of positive charges on the target can result in arc events, which are detrimental to the stability of the process and the quality of the coating. This problem can be negated by powering the magnetron in the mid-frequency (20–350 kHz) pulsed DC mode, where the polarity of the target alternates rapidly between positive and negative voltages. Again, this process has been described elsewhere [22].

Another variant of pulsed sputtering is the recently introduced HiPIMS (high power impulse magnetron sputtering) technique, which utilises lower pulse frequencies (50–1000 Hz), higher peak voltages (−500 to −1000 V) and very high peak currents (up to 1000 A). This results in similar time-averaged powers, but at much lower duty cycles, compared to pulsed DC magnetron sputtering, giving very high current densities at the target and leading to significant ionisation of the deposition flux. HiPIMS has been reported to enhance the film structure and make possible the deposition of crystalline thin films, including titania, without additional heat treatment [23,24]. Furthermore, the present authors have demonstrated that the thermal energy flux delivered to the substrate during HiPIMS deposition is several times lower than for DC or pulsed DC magnetron sputtering at the same time-averaged power [25]. This work was extended to demonstrate for the first time that photocatalytically active titania coatings can be deposited directly onto polymeric substrates by HiPIMS in a single stage process [26].

Sputtering systems can be configured with multiple magnetrons fitted with different target materials in order to deposit doped coatings, in which the dopant level is controlled by the relative power delivered to each magnetron. Alternatively, in a single magnetron system an alloy target can be used to produce doped coatings directly, although the dopant level in this case is fixed to that of the target material.

The ability to produce doped coatings is of great importance in this context, because the relatively high band gap of anatase (3.2 eV) means that it requires UV light (<390 nm) for activation. Photocatalytic activity can be both increased and extended into the visible range, though, by doping with different metallic elements (e.g., W, Mo, Nb, Ta) or non-metallic elements (e.g., N, C, S). Doping titanium dioxide with non-metal atoms narrows the band gap due to a mixing of the dopant p-states with the p-states of oxygen forming the valence band of titanium dioxide [27]. Of the range of possible non-metal dopants, nitrogen is one of the most described in literature for improving the photocatalytic activity of titanium dioxide [28–30] and extending its activity into the visible range. The nitrogen atom has a size comparable with the size of an oxygen atom, thus it can be easily introduced into the titania structure in either substitutional or interstitial positions [31].

Doping with transition metal ions is reported to create impurity levels near the conduction band that may perform as trapping centres, which extend the lifetime of photogenerated electrons and holes [32]. It is reported that the best results for transition metal doping can be achieved when the ionic radius of the doping metal is close to that of titanium [33] to enable incorporation into the titania lattice. Of the variety of candidate metals described in the literature, transition metals such as tungsten [34], chromium [35], vanadium [36] and molybdenum [37] are mentioned as efficient dopants for shifting the activity to the visible range.

Both of these doping strategies, and the idea of simultaneously co-doping titania with metallic and non-metallic elements, have been extensively investigated by many researches in the past few years [32,38]. Despite this, at present, there is no uniform theory explaining the optimum choice of dopant element(s) and doping level to maximise the photocatalytic properties in the visible range. This paper gives an overview of studies of doping and co-doping strategies conducted by the authors on magnetron sputtered titania coatings [25,39–43]. The influence of different elements on structural formation is considered and the production of as-deposited anatase coatings using the HiPIMS process is also described. Attempts to optimise the photoactivity of the coatings under UV, fluorescent and visible light irradiation are discussed.

2. Experimental Section

2.1. Coating Deposition Process

All the coatings described here were deposited by reactive magnetron sputtering in a Teer Coatings Ltd. (Droitwich, UK) UDP 450 system (Figure 1). Up to three 300 mm × 100 mm unbalanced planar magnetrons were installed vertically opposed through the chamber walls. Depending on the experimental array the system was configured with either two magnetrons fitted with titanium targets (99.5% purity) and one with a metallic dopant target (W, Mo, Ta or Nb—all 99.9% purity) [39–41], or for the HiPIMS array, a single magnetron was used with either a titanium target or a 5 at% W-doped Ti target installed [25,42,43].

Figure 1. Schematic representation of the Teer Coatings Ltd. UDP450 sputtering rig with three planar magnetrons installed.

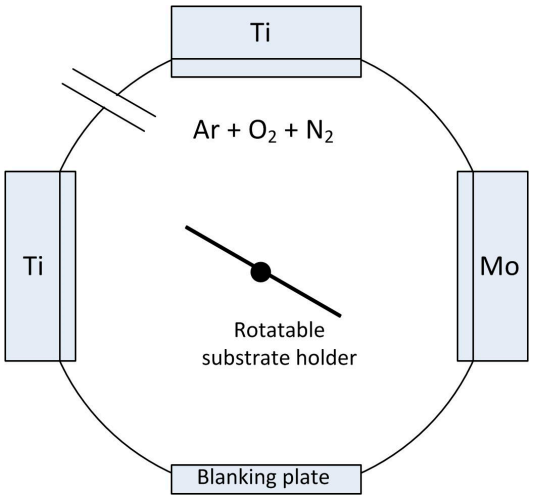

For the multiple magnetron configuration, the magnetrons with the titanium targets were driven in mid-frequency pulsed DC mode using a dual channel Advanced Energy Pinnacle Plus supply at a frequency of 100 kHz and a duty of 50% (in synchronous mode) at a constant time-averaged power of 1 kW per channel. In order to vary the doping level, the magnetron with the dopant target was driven at powers in the range 100–180 W in continuous DC mode using an Advanced Energy MDX power supply. The reactive sputtering process was carried out in an argon:oxygen atmosphere at 0.3 Pa, and was controlled by optical emissions monitoring using an operating set point (15% of the full metal

signal) previously found to produce stoichiometric TiO_2 coatings [44]. The substrates (microscope slides initially, but later 20 × 10 mm^2 304 2B stainless steel coupons were also coated for antimicrobial testing) were ultrasonically pre-cleaned in propanol and placed onto the electrically floating substrate holder, which was rotated continuously during the deposition process at 4 rpm at a distance of 100 mm from the magnetrons. During the nitrogen and co-doping experiments, the nitrogen flow was controlled using a mass flow controller in the range from 0 to 10 sccm to vary dopant levels [41]. Coating thicknesses were in the range 500 nm to 1 μm. Initial experiments showed that the as-deposited pulsed DC coatings were amorphous. Therefore, these coatings were post-deposition annealed in air at either 400 or 600 °C for 30 min and then allowed to cool in air.

For the HiPIMS experiments, the magnetron was driven at time-averaged powers of 600 W and 880 W using a Huettinger HMP1/1_P2 HiPIMS power supply. The working pressure was varied in the range of 0.13 to 0.93 Pa. Pulse frequency (100–300 Hz) and pulse width (50–200 μs) were used as two other process variables. Sputtering was carried out in an argon:oxygen atmosphere of 2:3 for all deposition runs (10 sccm of Ar and 15 sccm of O_2), which corresponded to the poisoned mode for this system. The thresholds of these variable parameters were chosen to maintain stable plasma discharge conditions and, thereby, control over the deposition process. The coatings were initially deposited onto soda-lime glass substrates. Coating thickness measurements were obtained by means of surface profilometry. All coatings deposited in this mode were of the order of 100 nm. Optimised operating conditions were then used to deposit coatings onto 100 μm PET (polyethylene terephthalate) web and PC (polycarbonate) substrates. The HiPIMS coatings were analysed in the as-deposited condition and were not annealed.

2.2. Coating Characterization

The coatings were typically analyzed by Raman spectroscopy (Renishaw Invia, 514 nm laser) and X-ray diffraction (XRD) in θ–2θ mode (Philips PW1729 diffractometer with CuKα1 radiation at 0.154 nm) to ascertain their crystalline structure. Composition was investigated by energy dispersive X-ray spectroscopy (EDX—Edax Trident, installed on a Zeiss Supra 40 VP-FEG-SEM). The surface roughness and surface areas of the coatings were determined using a MicroXAM white light surface profilometer. Finally, values of the optical band gaps of the coatings were calculated using the Tauc plot method [45], by plotting $(\alpha h\nu)^{1/2}$ *vs.* $h\nu$ and extrapolating the linear region to the abscissa (where α is absorbance coefficient, *h* is Plank's constant, *v* is the frequency of vibration).

2.3. Assessment of Photocatalytic Activity and Hydrophilicity

The determination of photocatalytic activity was carried out using the methylene blue (MB) degradation test. MB is an organic dye with molecular formula $C_{16}H_{18}ClN_3S$, and is often used as an indicating organic compound to measure the activity of photocatalysts. In fact, ISO10678 confirms the use of methylene blue as a model dye for surface photocatalytic activity determination in aqueous medium [46].

An aqueous solution of MB shows strong optical absorption at approximately 665 nm wavelength. Changes in the absorption peak height are used for monitoring the concentration of MB, and hence its degradation in contact with a photocatalytic surface.

Prior to the photocatalytic measurements, coating samples of equal size (15 × 25 mm^2) were immersed in a conditioning solution of methylene blue for pre-absorption of MB on the test surfaces to exclude the effect of absorption during the photocatalytic experiment. The photocatalytic measurements were carried out for 1 h in continuous mode. The absorption peak height of the methylene blue solution was measured with an Ocean Optics USB 2000+ spectrometer with continuous magnetic stirring.

Each coating was tested both under UV and fluorescent light sources; 2 × 15 W 352 nm Sankyo Denki BLB lamps were used as the UV light source (integrated power flux to the sample = 4 mW/cm^2) and 2 × 15 W Ushio fluorescent lamps as the fluorescent light source (integrated power flux to the sample = 6.4 mW/cm^2). Selected coatings were additionally tested under a visible light source. The visible light source was simulated by combining a fluorescent light source with a Knight Optical 395 nm long pass UV filter. The natural decay rate of methylene blue (without the photocatalyst present) under each type of light source was measured for reference purposes, as well as the degradation rate of methylene blue in contact with photocatalytic surface but without light irradiation (*i.e.*, in the dark). In both cases the decay rate of methylene blue was of zero order and, thus was neglected in the following calculations, meaning any changes in the absorption peak height could be attributed to the photocatalytic activity [37]. The experimental setup for the MB tests is shown schematically in Figure 2.

Figure 2. Schematic of methylene blue photocatalytic testing equipment.

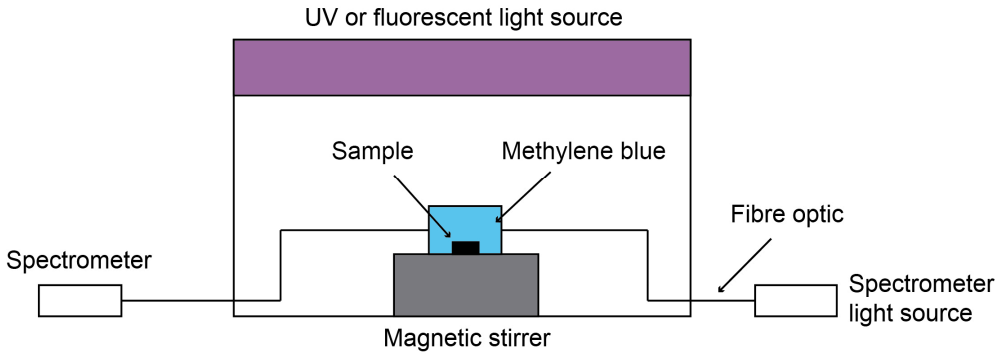

According to the Lambert-Beer law, the concentration of dye, c, is proportional to the absorbance value:

$$A = \varepsilon cl \quad (1)$$

where A is absorbance, ε is the molar absorbance coefficient; l is the optical length of the cell where the photocatalyst is immersed into MB.

The photocatalytic decomposition of MB was approximated to first order kinetics, as shown in the equation:

$$ln\left[\frac{C_0}{C}\right] = k_a t \quad (2)$$

where C_0 and C are the concentrations of MB solution at time 0 and time t of the experiment, respectively. If the ratio of absorption decay is proportional to the concentration decay, the first order reaction constant, k_a can be found from the slope of the plot $ln(A_0/A)$ against time.

The hydrophilic properties of the coatings were estimated via measurements of contact angles of deionised water droplets on the surface of the coating made with a Kruss goniometer.

2.4. Assessment of Antimicrobial Properties

Escherichia coli (ATCC 8739) was used as a model organism in these experiments. Measurements of the antimicrobial activity of selected coatings deposited onto 304 2B stainless steel substrates were performed using ISO 27447:2009 as guidance (with minor modifications) [47]. Stainless steel was selected because it is the material of choice in the food and beverage production industries and the coatings were developed for field trials in industrial facilities [48,49]. In brief, 50 µL of suspension containing approximately 10^5 colony forming units (cfu) per mL of bacterial cells were placed on the surfaces and a polyethylene film was placed over the bacterial suspension to ensure even distribution. Surfaces were illuminated (wavelength range of 300–700 nm) in a 20 °C incubator (Gallenkamp, Loughborough, UK) fitted with six fluorescent lamps (Sylvania, ON, Canada) with an energy output of 6.4 mW/cm^2. At selected time points (0, 12, 24 and 48 h), surfaces were removed and vortexed for 1 min in neutralizing broth (20 g·L^{-1} Soya Lectin (Holland and Barrett, Nuneaton, UK) and 30 g·L^{-1} Tween 80 (Sigma Aldrich, Gillingham, UK) to remove any surviving bacteria. Bacteria were enumerated by plate counts. All tests were carried out in triplicate. Stainless steel was used as a light control and a set of coated surfaces were also kept in dark conditions to serve as further controls.

3. Results

3.1. Transition Metal-Doped Pulsed DC Coatings

3.1.1. Structures and Compositions

The coatings produced by pulsed DC sputtering had dense, defect-free structures, with relatively smooth surfaces. A typical example is shown in Figure 3, which is a SEM micrograph showing the fracture section and surface topography of a Mo-doped (2.44 at%) coating after annealing at 400 °C. The sputtering rates of the dopant metals investigated increased in order Nb < Mo < Ta < W. Thus, the dopant content increased in this order when the same given power was applied to the dopant target (see Table 1), meaning some calibration of the process is required if coatings with the same dopant content are required. However, that was not the overriding concern with these experiments, which were more focused on structural formation and photocatalytic activity.

Figure 3. SEM micrograph of the fracture section of 2.44 at% Mo-doped titania coating deposited onto a glass substrate.

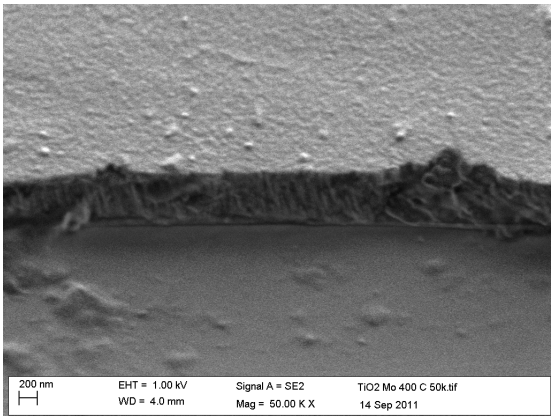

Table 1. Dopant levels and band gap values for transition metal-doped titania coatings deposited on glass substrates and annealed.

Dopant	Power on Dopant Target W	Dopant Content at%	Coating Thickness nm	Annealing Temperature °C	Band Gap eV	$k_a \times 10^{-5}$, s^{-1} UV light	$k_a \times 10^{-5}$, s^{-1} fluor. light	Crystal Structure
none (pure TiO_2)	-	-	586	400	3.12	1.0	0.5	anatase
				600	3.15	1.7	0.6	anatase
Nb	100	0.74	607	400	3.16	2.0	0.5	anatase
				600	3.16	0.6	0.3	anatase
	150	1.94	697	400	3.15	1.8	0.5	anatase
				600	3.15	0.6	0.4	anatase
	180	2.67	712	400	3.13	1.5	0.9	anatase
				600	3.13	0.4	0.0	anatase
Mo	100	2.44	685	400	3.17	4.0	1.9	anatase
				600	3.00	2.8	1.8	anatase
	150	5.37	727	400	3.11	0.6	0.3	anatase
				600 *	2.95	-	-	anatase
	180	6.96	754	400	3.09	0.5	0.2	amorphous
				600 *	2.97	-	-	anatase
W	100	10.03	814	400	3.22	0.6	0.4	amorphous
				600	3.02	2.2	1.6	anatase
	150	13.87	889	400	3.22	0.6	0.7	amorphous
				600	3.00	1.4	0.8	anatase/rutile
	180	15.84	896	400	3.22	0.4	0.3	amorphous
				600	2.98	0.9	0.6	rutile
Ta	100	3.07	594	400	3.08	0.6	0.4	anatase
				600	3.09	1.3	0.6	anatase
	150	9.10	786	400	3.20	0.7	0.0	amorphous
				600	3.16	1.0	0.0	anatase
	180	13.51	943	400	3.28	0.9	0.0	amorphous
				600	3.24	0.7	0.0	rutile

* coatings delaminated from substrate and were not tested.

As mentioned above, the as-deposited coatings were assumed to be amorphous on the basis of analysis by XRD and Raman spectroscopy. This concurs with previous work, which showed that for pure titania coatings, strongly crystalline anatase structures formed for coatings annealed at 400 °C and that this structure persisted up to 600 °C before evidence of rutile was observed [50]. For doped titania coatings, the dopant element has an important influence on structural formation during the annealing of these coatings. This is illustrated in Figures 4 and 5, which show XRD spectra of selected doped-titania coatings annealed at 400 and 600 °C, respectively. The dopant compositions are indicated in Table 1. For Mo-, Ta- and Nb- doped coatings, a strong anatase structure has clearly evolved at 400 °C, whereas, doping with W appears to suppress the formation of this structure. Annealing at 600 °C results in the formation of an anatase structure for all the dopants investigated, but in the case of tungsten, broad rutile peaks were also detected in the Raman spectra for these samples (Figure 6),

indicating a mixed-phase structure. This finding also highlights the different sensitivities of Raman spectroscopy and XRD for thin film analysis.

Figure 4. XRD analysis of selected doped-titania coatings deposited on glass substrates and annealed at 400 °C.

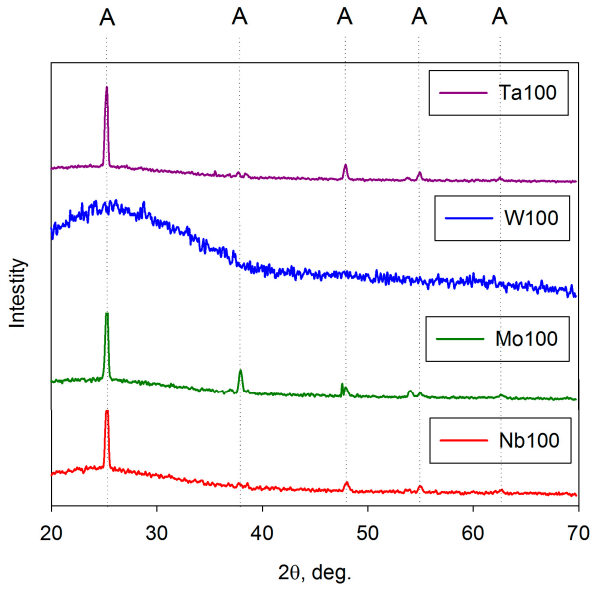

Figure 5. XRD analysis of selected doped titania coatings on glass substrates and annealed at 600 °C.

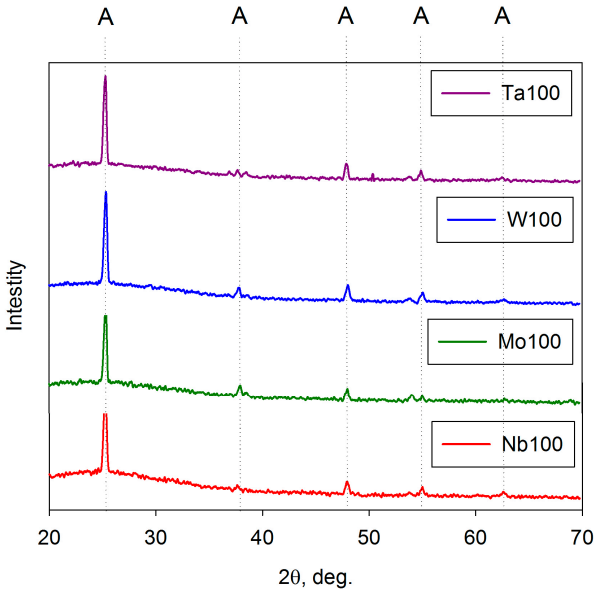

The choice of dopant material and annealing temperature also influenced the band gap of the resulting coating. Again, some typical examples are given in Table 1. Annealing at 400 °C produced very small red shifts for Mo-doped coatings, but small blue shifts for the other dopants. In contrast, annealing at 600 °C resulted in more significant red shifts for most of the combinations tested, and particularly for the Mo- and W- doped coatings (up to 0.2 eV).

Figure 6. Raman spectra showing structural variations as a function of W-content for W-doped titania coatings after annealing at 600 °C.

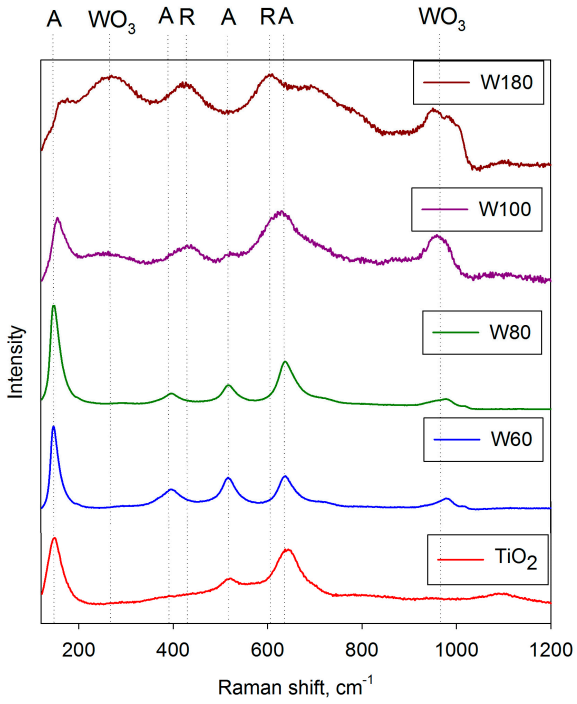

3.1.2. Photocatalytic Activity

As a benchmark for the doped titania coatings, the rate constants for the decomposition of methylene blue for pure titania coatings annealed at 400 °C and 600 °C sources were $1.0 \times 10^{-5} \cdot s^{-1}$ and $1.7 \times 10^{-5} \cdot s^{-1}$ under UV radiation and $0.5 \times 10^{-5} \cdot s^{-1}$, and $0.6 \times 10^{-5} \cdot s^{-1}$ under fluorescent light, respectively. As might be expected from the structural data shown in Figure 4, for the coatings annealed at 400 °C, Nb-doped coatings (best result: $k_a = 2.0 \times 10^{-5} \cdot s^{-1}$ with 0.7 at% Nb) and Mo-doped coatings (best result: $k_a = 4.0 \times 10^{-5} \cdot s^{-1}$ at 2.4 at% Mo) proved most effective at increasing photocatalytic activity under UV radiation. Only the 2.4 at% Mo-doped coating showed any notable improvement in fluorescent light activity ($k_a = 2.8 \times 10^{-5} \cdot s^{-1}$), which again would be expected from the observed band gap shifts. Ta- and W- doped coatings showed a reduction in activity under both light sources.

For the coatings annealed at 600 °C, now both Nb and Ta proved ineffective as dopant elements, with reduced activities compared to pure titania. In this case, Mo-doped coatings and W-doped coatings showed the greatest increases in activity. The best rate constants obtained with 2.4 at% Mo were $2.8 \times 10^{-5} \cdot s^{-1}$ and $1.8 \times 10^{-5} \cdot s^{-1}$ for UV and fluorescent light radiation, respectively. The equivalent values for coatings with 10.0 at% W were $2.2 \times 10^{-5} \cdot s^{-1}$ and $1.6 \times 10^{-5} \cdot s^{-1}$.

3.1.3. Optimisation of Tungsten Dopant Level

Although the W-doped coatings showed enhanced activity, it was recognised that the initial experimental conditions had produced relatively high levels of tungsten in the coatings (10–15 at%). Thus, a second series of W-doped coatings were produced where the power to the dopant target was varied over a lower range of values (60–90 W), to produce lower W dopant levels, with a view to optimising the activity level.

Other than the range of dopant target powers, the additional W-doped coatings were deposited under identical conditions to the initial batch of coatings, as described in Section 2.1. The coatings were then annealed at 600 °C. The dopant content and thickness of these and the previous W-doped coatings are given in Table 2. After annealing, these coatings showed a transition from anatase structures at low-W levels, through a mixed phase structure to rutile structures at higher W levels. Evidence for the formation of tungsten oxides was also identified for the higher W dopant levels. This structural transition with dopant content is illustrated in Figure 6, which shows selected Raman spectra for these coatings.

Table 2. Compositional data, band gap values and photocatalytic activity results for tungsten-doped titania coatings deposited on glass substrates and annealed at 600 °C.

Sample ID	Power on Dopant Target W	Dopant Content at%	Coating Thickness nm	Band Gap eV	$k_a \times 10^{-5}$, s^{-1} UV light	$k_a \times 10^{-5}$, s^{-1} fluor. light	Crystal Structure
TiO_2	-	-	586	3.15	1.7	0.6	anatase
W60	60	3.83	702	3.12	4.0	1.0	anatase
W70	70	4.64	746	3.09	5.6	1.2	anatase
W80	80	5.89	758	3.09	9.9	2.7	anatase
W90	90	7.09	793	3.05	6.4	2.1	anatase
W100	100	10.03	814	3.02	2.2	1.6	anatase
W150	150	13.87	889	3.00	1.4	0.8	anatase/rutile
W180	180	15.84	896	2.98	0.9	0.6	rutile

Once again, photocatalytic activity was assessed in terms of the degradation rate of methylene blue and band gap shifts were calculated from Tauc plots [40]. The results are also included in Table 2, together with surface area measurements calculated from white light profilometer scans. The rate constants obtained from the MB tests under UV and fluorescent light sources are also shown graphically as a function of W content in Figure 7, together with the surface area values for both sets of coatings. A clear, sharp peak in activity occurred at 5.9 at% W, with the k_a values showing an approximately five-fold increase compared to the values for pure titania coatings. Further increases in W content beyond 5.9 at% lead to a rapid fall off in activity levels. The peak in activity appears to almost coincide with the peak in surface area of these coatings (as determined by white light profilometry). Whilst increased surface area would be expected to contribute to an increase in activity, due to the greater area in contact with the MB, consideration of the data presented shows that the maximum to minimum variation in surface area is only around 2%, which cannot alone account for the 500% increase in activity. Furthermore, the band gap of the coatings decreased progressively with W-content, from 3.12 at 3.8 at% to 2.98 at 15.8 at%, implying that the increased activity is not linked in this instance to a reduction in band gap energy.

A mechanism has been forward by a number of authors to account for the increase in activity at specific tungsten dopant levels [51]. When the photocatalyst is irradiated, the photogenerated electrons will be transferred into the tungsten oxide conduction band, which is located lower than the corresponding band of titanium dioxide (2.5–2.8 eV). Conversely, the holes will accumulate on the valence band of titania, promoting efficient charge separation. In the case of coatings with higher W

content, excessive levels of dopant act as recombination centres for photogenerated electrons and holes. Additionally, the formation of a separate phase of tungsten oxide reduces the surface area of titanium dioxide, as proved by the surface morphology results, and thus reduces the area of contact between the pollutant and the photocatalyst. These factors result in a significant loss of photocatalytic activity for higher W-content coatings.

Figure 7. Variation in MB degradation rates for UV and fluorescent light irradiation and surface area, as functions of W content for W-doped titania coatings after annealing at 600 °C.

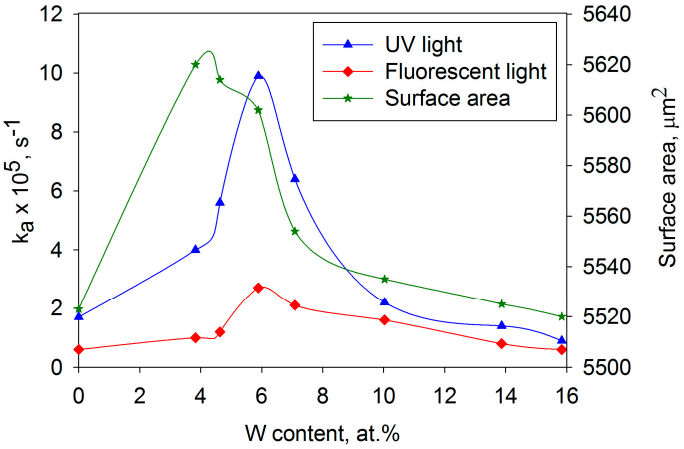

3.1.4. Synergistic Effects of Co-Doping with Molybdenum and Nitrogen

To investigate the potential of co-doping with two elements, a batch of Mo-doped coatings were produced, which also incorporated varying levels of nitrogen. Coatings with the previously determined optimum Mo dopant level of 2.4 at% were used for these experiments. Coatings doped only with nitrogen were also produced for comparison purposes. Details of the coating compositions are given in Table 3. Once again, these coatings were post-deposition annealed at 600 °C prior to testing. Despite using the same range of flow rates, it can be seen that the nitrogen content was significantly lower in the N-doped only coatings, compared to the co-doped coatings. Indeed, the nitrogen content in coatings N1–N5 was too low to be quantified with the techniques used here (XPS and EDX). Co-doping with N and Mo is known to increase the solubility limits of both N and Mo in TiO_2 [31]. This effect is described as being more pronounced in the case of nitrogen, as the solubility of N in titania is usually very low. The data presented here are in good agreement with this finding. Further detailed interpretation of the XPS analyses has been given elsewhere [41].

Raman analysis of the coatings confirmed an anatase structure for the annealed coatings, which XRD indicated had a strong (1 0 1) texture (not shown here) [41]. Band gap values and MB degradation rates are listed in Table 4. For the N-doped only coatings, samples N1 and N3 show some increase in UV activity, compared to the undoped titania coating, but apart from these two results, the effect of N-doping alone is negligible. However, the results for the co-doped coatings show a progressive increase in UV and fluorescent activity, with coating MoN7 demonstrating the highest activity under both light sources. This coating showed an increase in UV light activity of >4× and an increase in fluorescent light activity of >9× that of the pure titania coating. The equivalent values when compared to the Mo-only doped coating are both approximately a 3× increase in activity. Furthermore, visible

light testing (using the 395 nm long pass filter) demonstrated that these coatings also exhibited some activity under this light source, while for undoped/N-doped titania coatings no activity was recorded.

Table 3. Compositional properties and thickness of titania coatings doped with nitrogen ("N" series) and co-doped with molybdenum/nitrogen ("MoN" series).

Dopant	Sample ID	Flow of Nitrogen, Sccm	Content of Nitrogen, at%	Coating Thickness, nm
Mo	TiO_2 + Mo	-	-	685
N	N1	1	<1%	654
	N3	3	<1%	657
	N5	5	<1%	654
	N7	7	1.09	658
	N10	10	3.67	661
Mo + N	MoN1	1	1.22	760
	MoN3	3	3.08	764
	MoN5	5	4.95	758
	MoN7	7	7.13	761
	MoN10	10	9.12	766

Table 4. Band gap values and MB degradation rate constants for N-doped and Mo-N co-doped titania coatings.

Sample ID	Band Gap eV	Band Gap Shift (Compared to TiO_2)	$k_a \times 10^{-5}$, s^{-1} UV Light	$k_a \times 10^{-5}$, s^{-1} Fluor. Light	$k_a \times 10^{-5}$, s^{-1} Vis. Light
TiO_2	3.15	-	1.7	0.6	0
TiO_2 + Mo	3.00	−0.15	2.8	1.8	0.6
N1	3.22	+0.07	3.6	0.9	0
N3	3.22	+0.07	2.9	1.6	0
N5	3.20	+0.05	1.7	1.1	0
N7	3.14	−0.01	1.7	1.0	0
N10	3.08	−0.07	1.4	0.9	0
MoN1	3.09	−0.06	1.0	0.6	0
MoN3	3.09	−0.06	4.9	1.7	0.4
MoN5	3.05	−0.10	6.9	2.1	0.7
MoN7	3.04	−0.11	7.5	5.6	1.2
MoN10	3.07	−0.08	5.6	3.7	1.0

The results of photocatalytic tests showed that doping with nitrogen only had at best a moderately positive effect on photocatalytic activity, while co-doping with nitrogen and molybdenum resulted in significant improvements in photocatalytic activity. The efficiency of N-doped coatings under UV light, compared to that of undoped titania, was higher by a factor of 2 at most and generally lower than this. However, despite widely published information about N-doping as an efficient method of improving the photocatalytic properties under fluorescent/visible light [30,52], the N-doped titania coatings studied in this work had only a marginally higher efficiency of MB degradation under the fluorescent light source. As no noticeable band gap shift towards the visible range was observed, the increased photocatalytic activity under the fluorescent light source could only be attributed to improved electron-hole separation and the extended lifetime of charge carriers, as a result of nitrogen incorporation.

The observed increase in activity of the co-doped coatings can be assumed to be a result of more efficient electron-hole separation, compared to undoped or singly Mo- or N-doped titania coatings, due to the synergistic effect of Mo-N co-doping. A mechanism of explaining more efficient charge carrier separation was proposed by Cheng *et al.*, who observed similar results for Mo-N co-doped coatings prepared by a hydrolysis-precipitation method [38]. In the proposed mechanism nitrogen and molybdenum create local energy levels within the titania band gap, and therefore several ways of charge carrier excitation are available, and consequently more photo-induced charge carriers can be efficiently separated to participate in the photocatalytic process. Co-doped coatings with optimum content of nitrogen and molybdenum demonstrate significantly higher photocatalytic activity, due to more efficient charge carrier separation and their extended lifetimes. A shift of the band gap towards the visible range, compared to undoped titania, enables the presence of photocatalytic activity under fluorescent and visible light sources.

3.2. Characterisation of As-Deposited HiPIMS Titania Coatings

In a preliminary study using the HiPIMS process, coatings were deposited from a single titanium target and a Ti target containing 5 at% W [42]. Analysis by Raman spectroscopy of the as-deposited coatings indicated that the pure titania samples had formed a mixed anatase/rutile structure, whereas the W-doped coatings had only a weakly crystalline anatase structure. Example spectra are shown in Figure 8. These spectra imply that the presence of tungsten in the coating has suppressed the formation of a crystalline structure, as observed previously for the coatings deposited by pulsed DC sputtering. The band gap data and photocatalytic activity rate constants for these coatings are listed in Table 5. A number of interesting points emerge from these data. Firstly, the UV light rate constants (k_a values ~2.0 to 2.4 × 10^{-5}·s^{-1}) are noticeably higher than those obtained for pulsed DC titania coatings after annealing (typically k_a = 1.7 × 10^{-5}·s^{-1}). It was also observed that the presence of W reduced the band gap of these coatings quite considerably (by 0.14–0.15 eV), which in turn lead to a 2 to 4 fold improvement in the level of fluorescent light activity for the doped coatings. Finally, the W-doped HiPIMS titania coatings displayed visible light activity levels very close to the values measured under fluorescent light sources.

Figure 8. Raman spectra of as-deposited W-doped (TiO_2-W) and undoped titania (TiO_2) coatings deposited by HiPIMS on glass substrates.

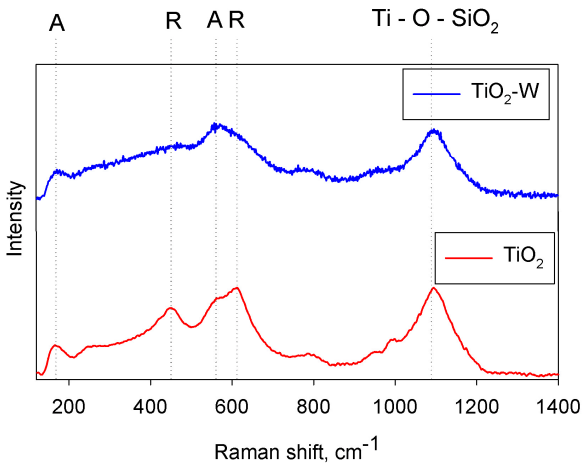

Table 5. Overview of deposition conditions and properties of titania and W-doped titania coatings deposited on glass substrates by HiPIMS.

Coating ID	Mean Sputtering Power kW	W at%	Band Gap eV	Surface Roughness µm	Surface Area µm²	$k_a \times 10^{-5}$ UV Light, s^{-1}	$k_a \times 10^{-5}$ Fluorescent Light, s^{-1}	$k_a \times 10^{-5}$ Visible Light, s^{-1}
TiO_2	44	-	3.21	0.084	5521	2.0	0.3	-
TiO_2W	44	5.67	3.04	0.092	5524	2.1	1.2	0.9

Having demonstrated the potential of the HiPIMS process, further studies were carried out to attempt to optimise the performance of the coatings produced by this technique [43]. Process variables including deposition pressure, pulse width (*i.e.*, duration of the power pulse delivered to the target) and pulse frequency were varied and their impact on photocatalytic activity and water contact angle was investigated. Of these variables, deposition pressure emerged as the most influential. This is clearly illustrated in Figure 9, which compares the variation with coating pressure of contact angle and the photocatalytic activity rate constants for MB degradation under UV light irradiation. Following these experiments, coatings were deposited directly onto PET and polycarbonate (PC) substrates under optimised conditions. Within experimental accuracy, the same values of first order rate constants were obtained for these coatings, independent of the substrate materials tested (glass, PET and PC).

Figure 9. Variation in water contact angle and UV light photocatalytic rate constant as a function of deposition pressure for titania coatings deposited on glass substrates by HiPIMS. Images of the water droplets are included for samples deposited at 0.16 and 0.93 Pa.

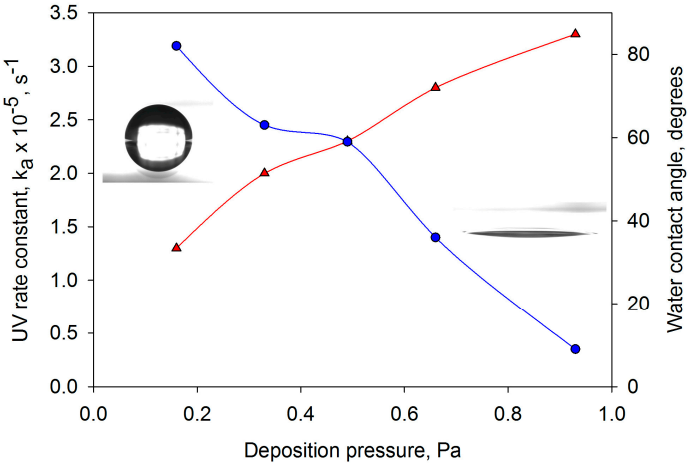

3.3. Antimicrobial Activity

The antimicrobial activity against *E. coli* of selected Mo- and W- doped titania coatings was assessed and compared to pure titania coatings and stainless steel controls. As mentioned earlier, 304 2B stainless steel was chosen for its compatibility with industrial processing. The coatings were deposited by pulsed DC magnetron sputtering, using the conditions described earlier, and then annealed at 600 °C. Interestingly, for this choice of substrate material, a higher molybdenum content (6.9 at%) was found to provide the greatest photocatalytic activity from MB tests (compared with

2.44 at% for glass), so this dopant content was used, along with coatings doped with 3.8 at% W, which were also found to be optimal in this case. This finding concurs with other studies that have shown that the choice of substrate material (particularly whether it is electrically conductive or not) influences photocatalytic activity [53].

The stainless steel controls did not reduce the number *E. coli* colony forming units in light or dark conditions in a 48 h period (Figure 10). The pure titania coatings showed only a weak photocatalytic effect in reducing the number of colony forming units by 2-logs in this time period. However, coatings doped with Mo eradicated *E. coli* within 24 h in both light and dark conditions. The activity displayed in the dark suggests that the surface is dual functioning, being both photocatalytic (as determined by the degradation of MB) and innately antimicrobial. W-doped coatings also reduced microbial counts by 5-logs within 48 h in the light but not the dark, *i.e.*, only photocatalytic behaviour was observed. All doped surfaces displayed an ability to inactivate *E. coli* when tested under visible light and, in the Mo case, when in the dark, highlighting the potential use of such surfaces for indoor applications, allowing a choice between a coating with an active antimicrobial function (Mo), or one which is inert unless irradiated (W), depending on requirements and regulations.

Figure 10. Antimicrobial effect of TiO_2, TiO_2-Mo and TiO_2-W surfaces on *Escherichia coli* Stainless steel surfaces were used as controls and light and dark conditions were investigated.

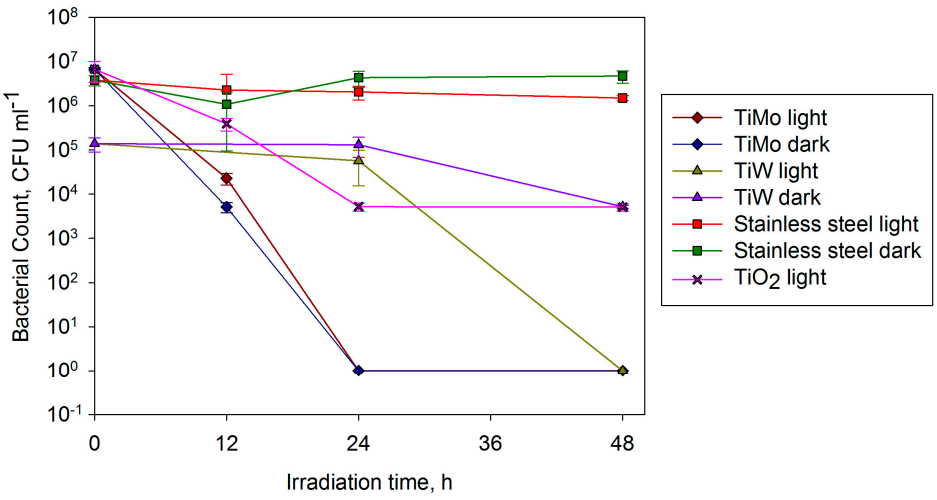

4. Discussion

This paper has considered a number of deposition and doping strategies for the production of titania-based photocatalytically active thin films. Reactive magnetron sputtering is a versatile, flexible technique for the production of high quality, fully dense coatings. When operating in pulsed DC mode, it provides a stable, arc-free process for the deposition of dielectric materials, such as titania. Furthermore, the coatings can be readily doped via transition metals, or via non-metal gaseous species, or a combination of both. In each case, control of the dopant level is straightforward. However, when operating in this mode, the as-deposited coatings were found to be amorphous and, therefore, showed no activity. Effective annealing temperatures for structural formation varied with dopant element. Mo-doped coatings annealed at 400 °C were found to demonstrate significantly higher activities than pure titania coatings annealed at the same temperature, whereas a temperature of 600 °C was required

to achieve the same result for the W-doped coatings. Figure 11 additionally shows that the synergistic effect obtained by co-doping with Mo and N also produced coatings with a UV activity, close to that of the W-doped coatings, and a noticeably higher activity in fluorescent light. The UV and fluorescent light activities of the W-doped and MoN co-doped coatings also exceed the values shown in Figure 11 obtained for a sample of Pilkington's Activ, which is a commercially available product. Direct comparisons with this sample should be avoided, because it is produced via a chemical vapour deposition pyrolysis route and is significantly thinner than the sputtered coatings. However, as there is a dearth of "standard samples" in this field, it still serves as a useful guide to relative activity levels. A mixed anatase/rutile phase was detected for the samples with the highest levels of tungsten doping in the pulsed DC study, although the best photocatalytic results were still found for anatase coatings. In contrast, for the pure titania deposited via HiPIMS, a mixed phase structure gave superior photocatalytic activity [43]. This, of course, is not a new finding and several researchers have proposed that the mixed phase structure is optimal for photocatalytic activity [10,20].

Figure 11. Bar chart of maximum rate constants obtained for the decomposition of methylene blue under UV and fluorescent light sources for pure titania coatings, transition metal doped titania coatings, Mo and N co-doped coatings deposited by pulsed DC magnetron sputtering (annealed at 600 °C) and titania and W-doped titania coatings deposited by HiPIMS (as-deposited).

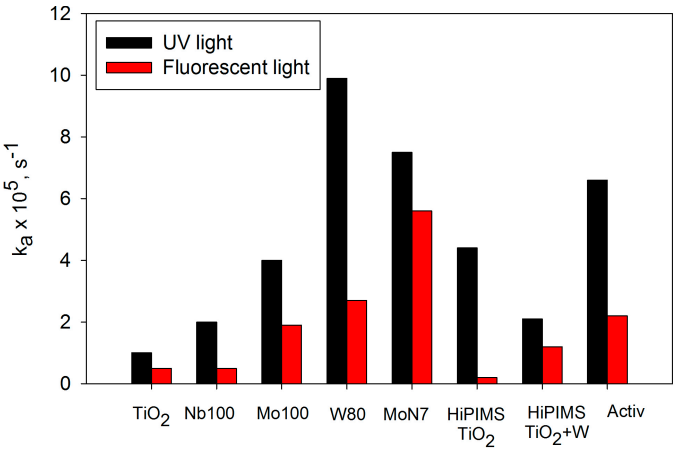

The HiPIMS process is still in the development stage and there remain issues with power supply stability and process control. Nevertheless, the potential of this process to produce, at least, semi-crystalline coatings in the as-deposited state is a clear advantage over other deposition processes. Furthermore, the low net deposition temperature makes it a suitable technique for deposition onto thermally sensitive materials, as demonstrated here with PET and PC substrates. The data presented in Figure 11 indicates that, when optimised, the HiPIMS pure titania coatings could achieve approximately twice the UV activity rate of the annealed pulsed DC coatings. The W-doped HiPIMS showed a reduction in UV activity, attributed to the weaker crystalline structure, but higher fluorescent light activity, attributed to a substantial band gap shift.

The capacity to break down organic compounds, as modelled here with methylene blue, is just one of the phenomena associated with photocatalytic coatings. The inactivation of microorganisms is another important ability. Numerous researchers have claimed antimicrobial activity for their coatings,

but care must be taken in assessing these claims. The test method for antibacterial activity of photocatalytic materials is complex, requiring specific experimental conditions to be met and multiple repeat experiments if results are to be tested for reproducibility and compared to other published data. The results presented here are a case in point. A limited number of replicates were tested and only one microorganism was used; the Gram-negative *E. coli*. Ideally, more replicates would be tested and a Gram-positive microorganism, such as *Staphylococcus aureus*, would also be investigated. Despite this, the doped titania coatings showed the ability to eradicate *E coli* within 24 to 48 h. There was also an interesting distinction between the dopant elements, with the Mo-doped coatings being effective in light and dark and the W-doped coatings only being effective in the light. These results certainly merit more detailed investigation in the future. The recent introduction of antibacterial testing under indoor lighting (ISO 17094:2014) [54] has now allowed for visible light active photocatalytic surfaces to be tested more precisely, however, a more rapid antimicrobial testing method which could be performed by non-microbiologist would still be valuable.

5. Conclusions

Reactive magnetron sputtering techniques have been used to produce a range of titania and doped titania coatings. Choice of deposition technique (pulsed DC sputtering or HiPIMS) and choice of dopant element had a significant influence on structural formation and, subsequently, photocatalytic activity for these coatings. Pulsed DC coatings were amorphous in the as-deposited state, with no measurable activity against methylene blue, whereas the HiPIMS coatings were weakly crystalline as-deposited with moderate levels of activity. The benefits of this technique were further demonstrated by depositing active coatings onto polymeric substrates in a single stage process. Of the transition metals investigated as dopant elements, molybdenum and tungsten were the most effective. The highest UV activity recorded in these experiments was achieved by coatings doped with 5.9 at% W after annealing at 600 °C. This was slightly higher than the UV activity of MoN-doped coatings after annealing, but the co-doped coatings showed a higher level of activity under fluorescent light irradiation. Although only limited tests were performed, the Mo- and W- doped coatings also demonstrated the ability to inactivate *E. coli*. In the former case, the coatings were both antimicrobial (active in the dark) and photocatalytic (active in the light), whereas the W-doped coatings only displayed photocatalytic activity.

Acknowledgments

Funding for some of the antimicrobial aspects of this work from the Technology Strategy Board (UK) is gratefully acknowledged. The authors would also like to thank Xiaohong Xia and Yun Gao from the Faculty of Materials Science and Engineering, Hubei University, China for providing XPS analysis of selected coatings.

Author Contributions

Kelly was the main author of this paper and part of the supervisory team for the experimental programmes described here. West and Verran were also part of the project supervisory teams. Ratova conducted the majority of the experimental work on the production and testing of the

photocatalytic coatings. Fisher and Ostovarpour were responsible for the production and testing of the antimicrobial coatings.

Conflicts of Interest

The authors declare no conflict of interest.

References

1. Paz, Y. Application of TiO_2 photocatalysis for air treatment: Patents' overview. *Appl. Catal. B Environ.* **2010**, *99*, 448–460.
2. Vidal, A. Developments in solar photocatalysis for water purification. *Chemosphere* **1998**, *36*, 2593–2606.
3. Fujishima, A.; Zhang, X. Titanium dioxide photocatalysis: Present situation and future approaches. *CR Chim.* **2006**, *9*, 750–760.
4. Markowska-Szczupak, A.; Ulfig, K.; Morawski, A.W. The application of titanium dioxide for deactivation of bioparticulates: An overview. *Catal. Today* **2011**, *169*, 249–257.
5. Fujishima, A.; Rao, T.N.; Tryk, D.A. Titanium dioxide photocatalysis. *J. Photochem. Photobiol. C Photochem. Rev.* **2000**, *1*, 1–21.
6. Yang, Y.; Li, X.J.; Chen, J.T.; Wang, L.Y. Effect of doping mode on the photocatalytic activities of Mo/TiO_2. *J. Photochem. Photobiol. A* **2004**, *163*, 517–522.
7. Allen, N.S.; Edge, M.; Verran, J.; Stratton, J.; Maltby, J.; Bygott, C. Photocatalytic titania based surfaces: Environmental benefits. *Polym. Degrad. Stab.* **2008**, *93*, 1632–1646.
8. Braham, R.J.; Harris, A.T. Review of major design and scale-up considerations for solar photocatalytic reactors. *Ind. Eng. Chem. Res.* **2009**, *48*, 8890–8905.
9. McCullagh, C.; Robertson, P.K.J.; Adams, M.; Pollard, P.M.; Mohammed, A. Development of a slurry continuous flow reactor for photocatalytic treatment of industrial waste water. *J. Photochem. Photobiol. A* **2010**, *211*, 42–46.
10. Zhao, L.; Han, M.; Lian, J. Photocatalytic activity of TiO_2 films with mixed anatase and rutile structures prepared by pulsed laser deposition. *Thin Solid Films* **2008**, *516*, 3394–3398.
11. Musil, J.; Herman, D.; Sicha, J. Low-temperature sputtering of crystalline TiO_2 films. *J. Vac. Sci. Technol.* **2008**, *24*, 3793–3800.
12. Šícha, J.; Musil, J.; Meissner, M.; Čerstvý, R. Nanostructure of photocatalytic TiO_2 films sputtered at temperatures below 200 °C. *Appl. Surf. Sci*. **2008**, *254*, 3793–3800.
13. Frach, P.; Glöß, D.; Metzner, C.; Modes, T.; Scheffel, B.; Zywitzki, O. Deposition of photocatalytic TiO_2 layers by pulse magnetron sputtering and by plasma-activated evaporation. *Vacuum* **2006**, *80*, 679–683.
14. Zhang, F.; Wolf, G.K.; Wang, X.; Liu, X. Surface properties of silver doped titanium oxide films. *Surf. Coat. Technol.* **2001**, *148*, 65–70.
15. Yates, H.M.; Brook, L.A.; Ditta, I.B.; Evans, P.; Foster, H.A.; Sheel, D.W.; Steele, A. Photo-induced self-cleaning and biocidal behaviour of titania and copper oxide multilayers. *J. Photochem. Photobiol. A* **2008**, *197*, 197–205.

16. Yaghoubi, H.; Taghavinia, N.; Alamdari, E.K. Self-cleaning TiO_2 coating on polycarbonate: Surface treatment, photocatalytic and nanomechanical properties. *Surf. Coat. Technol.* **2010**, *204*, 1562–1568.
17. Yang, J.H.; Han, Y.S.; Choy, J.H. TiO_2 thin-films on polymer substrates and their photocatalytic activity. *Thin Solid Films* **2006**, *495*, 266–271.
18. Wei, F.; Ni, L.; Cui, P. Preparation and characterization of N-S-codoped TiO_2 photocatalyst and its photocatalytic activity. *J. Hazard. Mater.* **2008**, *156*, 135–140.
19. Lee, C.S.; Kim, J.; Son, J.Y.; Choi, W.; Kim, H. Photocatalytic functional coatings of TiO_2 thin films on polymer substrate by plasma enhanced atomic layer deposition. *Appl. Catal. B Environ.* **2009**, *91*, 628–633.
20. Kääriäinen, M.L.; Cameron, D.C. The importance of the majority carrier polarity and p-n junction in titanium dioxide films to their photoactivity and photocatalytic properties. *Surf. Sci.* **2012**, *606*, L22–L25.
21. Kelly, P.J.; Arnell, R.D. Magnetron sputtering: A review of recent developments and applications. *Vacuum* **2000**, *56*, 159–172.
22. Kelly, P.J.; Bradley, J.W. Pulsed magnetron sputtering—Process overview and applications. *J. Optoelectron. Adv. Mater.* **2009**, *11*, 1101–1107.
23. Lundin, D.; Sarakinos, K. Smoothing of discharge inhomogeneities at high currents in gasless high power impulse magnetron sputtering. *J. Mater. Res.* **2012**, *27*, 780–792.
24. West, G.; Kelly, P.; Barker, P.; Mishra, A.; Bradley, J. Measurements of deposition rate and substrate heating in a HiPIMS discharge. *Plasma Process. Polym*. **2009**, *6*, S543–S547.
25. Sarakinos, K.; Alami, J.; Konstantinidis, S. High power pulsed magnetron sputtering: A review on scientific and engineering state of the art. *Surf. Coat. Technol.* **2010**; *204*, 1661–1684.
26. Kelly, P.J.; Barker, P.M.; Ostovarpour, S.; Ratova, M.; West, G.T.; Iordanova, I.; Bradley, J.W. Deposition of photocatalytic titania coatings on polymeric substrates by HiPIMS. *Vacuum* **2012**, *86*, 1880–1882.
27. Asahi, R.; Morikawa, T.; Ohwaki, T.; Aoki, K.; Taga, Y. Visible-light photocatalysis in nitrogen-doped titanium oxides. *Science* **2001**, *293*, 269–271.
28. Tavares, C.J.; Marques, S.M.; Viseu, T.; Teixeira, V.; Carneiro, J.O.; Alves, E.; Barradas, N.P.; Munnik, F.; Girardeau, T.; Rivière, J.P. Enhancement of the photocatalytic nature of nitrogen-doped PVD-grown titanium dioxide thin films. *J. Appl. Phys.* **2009**, *106*, 113535.
29. Chiu, S.M.; Chen, Z.S.; Yang, K.Y.; Hsu, Y.L.; Gan, D. Photocatalytic activity of doped TiO_2 coatings prepared by sputtering deposition. *J. Mater. Process. Technol.* **2007**, *192–193*, 60–67.
30. Wong, M.S.; Pang, C.H.; Yang, T.S. Reactively sputtered N-doped titanium oxide films as visible-light photocatalyst. *Thin Solid Films* **2006**, *494*, 244–249.
31. Pelaez, M.; Nolan, N.T.; Pillai, S.C.; Seery, M.K.; Falaras, P.; Kontos, A.G.; Dunlop, P.S.M.; Hamilton, J.W.J.; Byrne, J.A.; O'Shea, K.; *et al.* A review on the visible light active titanium dioxide photocatalysts for environmental applications. *Appl. Catal. B Environ.* **2012**, *125*, 331–349.
32. Liu, H.; Lu, Z.; Yue, L.; Liu, J.; Gan, Z.; Shu, C.; Zhang, T.; Shi, J.; Xiong, R. Mo-N co-doped TiO_2 for enhanced visible-light photoactivity. *Appl. Surf. Sci.* **2011**, *257*, 9355–9361.

33. Choi, W.; Termin, A.; Hoffmann, M.R. The role of metal ion dopants in quantum-sized TiO_2: Correlation between photoreactivity and charge carrier recombination dynamics. *J. Phys. Chem.* **1994**, *98*, 13669–13679.
34. Li, X.Z.; Li, F.B.; Yang, C.L.; Ge, W.K. Photocatalytic activity of WO_x-TiO_2 under visible light irradiation. *J. Photochem. Photobiol. A* **2001**, *141*, 209–217.
35. Peng, Y.H.; Huang, G.F.; Huang, W.Q. Visible-light absorption and photocatalytic activity of Cr-doped TiO_2 nanocrystal films. *Adv. Powder Technol.* **2012**, *23*, 8–12.
36. Akbarzadeh, R.; Umbarkar, S.B.; Sonawane, R.S.; Takle, S.; Dongare, M.K. Vanadia–titania thin films for photocatalytic degradation of formaldehyde in sunlight. *Appl. Catal. A Gen.* **2010**, *374*, 103–109.
37. Štengl, V.; Bakardjieva, S.; Murafa, N. Preparation and photocatalytic activity of rare earth doped TiO_2 nanoparticles. *Mater. Chem. Phys.* **2009**, *114*, 217–226.
38. Heng, X.; Yu, X.; Xing, Z. Characterization and mechanism analysis of Mo–N-co-doped TiO_2 nano-photocatalyst and its enhanced visible activity. *J. Colloid Interface Sci.* **2012**, *372*, 1–5.
39. Ratova, M.; Kelly, P.J.; West, G.T.; Iordanova, I. Enhanced properties of magnetron sputtered photocatalytic coatings via transition metal doping. *Surf. Coat. Technol.* **2013**, *228*, S544–S549.
40. Ratova, M.; West, G.T.; Kelly, P.J. Optimization study of photocatalytic tungsten-doped coatings deposited by reactive magnetron co-sputtering. *Coatings* **2013**, *3*, 194–207.
41. Ratova, M.; West, G.T.; Kelly, P.J.; Xia, X.; Gao, Y. Synergistic effect of doping with nitrogen and molybdenum on the photocatalytic properties of thin titania films. *Vacuum* **2014**, in press.
42. Ratova, M.; West, G.T.; Kelly, P.J. HiPIMS deposition of tungsten-doped titania coatings for photocatalytic applications. *Vacuum* **2014**, *102*, 48–50.
43. Ratova, M.; West, G.T.; Kelly, P.J. Optimisation of hipims photocatalytic titania coatings for low temperature deposition. *Surf. Coat. Technol.* **2014**, *250*, 7–13.
44. Onifade, A.A.; Kelly, P.J. The influence of deposition parameters on the structure and properties of magnetron-sputtered titania coatings. *Thin Solid Films* **2006**, *494*, 8–12.
45. Tauc, J.; Grigorovici, R.; Vancu, A. Optical properties and electronic structure of amorphous germanium. *Phys. Status Solidi* **1966**, *15*, 627–637.
46. *ISO10678. Fine Ceramics, Advanced Technical Ceramics—Determination of Photocatalytic Activity of Surfaces in an Aqueous Medium by Degradation of Methylene Blue*; International Organisation for Standards: Geneva, Switzerland, 2010.
47. *ISO27447. Fine Ceramics (Advanced Ceramics, Advanced Technical Ceramics). Test Methods for Antibacterial Activity of Semiconducting Photocatalytic Materials*; International Organisation for Standards, Geneva, Switzerland, 2009.
48. Fisher, L.; Ostovarpour, S.; Kelly, P.; Whitehead, K.A.; Cooke, K.; Stogråds, E.; Verran, J. Molybdenum doped titanium dioxide photocatalytic coatings for use as hygienic surfaces—The effect of soiling on antimicrobial activity. *Biofouling* **2014**, *30*, 911–919.
49. Navabpour, P.; Ostovarpour, S.; Tattershall, C.; Cooke, K.; Kelly, P.; Verran, J.; Whitehead, K.; Hill, C.; Raulio, M.; Priha, O. Photocatalytic TiO_2 and Doped TiO_2 Coatings to Improve the Hygiene of Surfaces Used in Food and Beverage Processing—A Study of the Physical and Chemical Resistance of the Coatings. *Coatings* **2014**, *4*, 433–449.

50. Kulczyk-Malecka, J.; Kelly, P.J.; West, G.; Clarke, G.C.; Ridealgh, J.A. Characterisation Studies of the Structure and Properties of As-Deposited and Annealed Pulsed Magnetron Sputtered Titania Coatings. *Coatings* **2013**, *3*, 166–176.
51. Lorret, O.; Francová, D.; Waldner, G.; Stelzer, N. W-doped titania nanoparticles for UV and visible-light photocatalytic reactions. *Appl. Catal. B Environ.* **2009**, *91*, 39–46.
52. Qin, H.L.; Gu, G.B.; Liu, S. Preparation of nitrogen-doped titania with visible-light activity and its application. *CR Chim.* **2008**, *11*, 95–100.
53. Yao, M.; Chen, J.; Zhao, C.; Chen, Y. Photocatalytic activities of ion doped TiO_2 thin films when prepared on different substrates. *Thin Solid Films* **2009**, *517*, 5994–5999.
54. *ISO17094. Fine Ceramics (Advanced Ceramics, Advanced Technical Ceramics). Test Methods for Antibacterial Activity of Semiconducting Photocatalytic Materials under Indoor Lighting Environments*; International Organisation for Standards: Geneva, Switzerland, 2014.

INVESTIGATING THE POTENTIAL FOR THE USE OF PHOTOCATALYTIC SURFACES IN PROCESS HYGIENE IN THE BREWING INDUSTRY

Joanna Verran[1], Soheyla Ostovarpour[1,2], Leanne Fisher[1*], Kathryn Whitehead[1], Peter Kelly[2], Outi Priha[3], Mari Raulio[3], Erna Storgårds[3]
[1] *School of Healthcare Science, Manchester Metropolitan University, UK*
[2] *School of Research, Enterprise and Innovation, Manchester Metropolitan University, UK*
[3] *VTT Technical Research Centre of Finland, Espoo, Finland*

ABSTRACT

Process hygiene plays a major role in ensuring beer quality. One approach to the reduction of fouling in this industry - and in any other associated with food production - is the use of photocatalytic surfaces such as those including titania (titanium dioxide), which is active under UV light. These coatings are inert when not photoactive, and their self-cleaning attributes are ecologically and toxicologically desirable. TiO_2 coatings can be doped with transition metals (in this case, molybdenum, tungsten and niobium) to extend activity under fluorescent light. The aim of this study was to produce doped coatings on stainless steel and to explore their potential for use in the brewing industry.
Coatings were produced using magnetron sputtering. Characterisation indicated the presence of photoactive phases of titania (anatase and rutile) as well as the presence of dopants. Assessment of photocatalytic activity was via degradation of methylene blue. Tests for chemical resistance to acid and alkali (components of potential cleaning products) indicated that the coatings were robust, well attached to the substratum, and that they retained their photoactivity. Photocatalytic antimicrobial activity was explored using three brewery isolates and Escherichia coli (following ISO 27447:2009).
The addition of molybdenum to the coating enhanced activity under fluorescent (visible) light in comparison to titania alone, but the surface was also antimicrobial in the dark. This innate antimicrobial activity was attributed to the presence of molybdenum. Thus these coatings presented dual function: antimicrobial and photoactive. The addition of niobium enhanced activity under fluorescent light, but no innate (dark) activity was noted. Any effect of tungsten was concentration dependent.
Titania-molybdenum surfaces were placed in the brewery environment (around filling lines) for 12 months, and were tested three times for photocatalytic activity and stability of coating. The use of small numbers of samples precluded statistical analysis of data, but there was evidence that photoactivity was retained to varying extents, and molybdenum was also largely retained on the coating. There was also some damage visible in terms of coating stability on occasion. Longer term studies investigating any antimicrobial or antifouling properties of the surface failed to demonstrate significant effects, again likely attributable to the very low numbers of replicate samples.
Overall, findings indicate potential for these doped surfaces in enhancing plant hygiene and complementing existing cleaning and disinfection protocols, whilst offering both innate (antimicrobial in the dark) and photoactive properties. Further work will explore the stability of these coatings, batch variability, and the development of additional in vitro tests prior to in situ investigations.

INTRODUCTION

It is widely recognised that environmental surfaces can act as reservoirs for microbial fouling and in recent years there have been many publications regarding photocatalytic disinfection with reports referring to the destruction of Gram positive and Gram negative bacteria as well as fungi, algae, protozoa, endospores and viruses (Foster *et al*., 2011). Titanium dioxide (TiO_2) as a photocatalyst is a semiconductor with a wide band gap (3.2 eV), which can be excited by ultraviolet (UV) irradiation (λ <380 nm). Photons with energy equal to or higher than its band gap can promote an electron from the valence band to the conduction band, producing electron-hole pairs. The photogenerated electron-hole pairs react with molecular oxygen and water to produce radical species (Fujishima *et al*., 2000; Daviðsdóttir *et al*., 2013). These reactive radical species are able to decompose organic compounds and inactivate microorganisms. Both the photocatalytic disinfection and self-cleaning properties of TiO_2 surfaces make them potentially applicable to areas where microbial fouling can arise, for example, in the food and beverage industries.

Within a brewery environment, the hygienic status of process surfaces plays a major role in ensuring the quality of beer. Beer production and dispensing often takes place in closed systems, where in-place cleaning procedures are applied (Storgårds, 2000). The cleaning and disinfection regimes employed are essential for removing product deposits and microbial populations. However, long production runs between cleaning cycles are typical, making such systems more susceptible to bacterial accumulation. The accumulation of bacteria on surfaces can lead to the development of biofilms, which once established, can be difficult to eradicate from surfaces using conventional disinfection regimes. The use of photocatalytic surfaces under such circumstances could help towards discouraging the build-up of microbial populations during long production runs and in between disinfection cycle. However, since UV light is required to activate photocatalytic surfaces, the use of TiO_2 in indoor situations is limited.

Doping TiO_2 with transition metals causes a shift reduction in the band gap, enabling surfaces to become more active under visible light (Wilke and Breuer, 1999). Titanium dioxide doped with a transition metal can be deposited as a thin film coating onto surfaces such as stainless steel, typically used in breweries. The aim of this study was to produce doped coatings on stainless steel and to characterize and explore their potential for use in the brewing industry.

EXPERIMENTAL

Production of photocatalytic thin films

Stainless steel (AISI 304-2B) was used as a substrate upon which thin films of TiO_2 doped with molybdenum (Mo), niobium (Nb) and tungsten (W) were deposited by a closed field unbalanced magnetron sputtering (Teer Coatings Ltd, Droitwich, UK) (Laing *et al*., 1999). The production of the thin films was as described by Ratova *et al*., 2013. Deposition times were adapted to obtain a film thickness of 800 nm - 1 μm and the sputtered films were post deposition annealed at either 400 °C or 600 °C for 30 minutes in air.

Coating characterization

Energy dispersive X-ray spectroscopy (EDX – Edax Trident) was employed to analyse the coating compositions and determine the dopant levels. X-ray diffraction (XRD) in the θ-2θ mode (URD6 Seiferd & Co diffractometer with $CuK\alpha_1$ radiation at 0.154 nm) and Raman

spectroscopy (Renishaw Invia, 514 nm laser) were used to obtain information regarding the coatings crystalline structure. To determine coating adhesion to substrate, scratch adhesion testing was carried out using a ST3001 scratch tester (Teer Coatings Ltd, UK). A scratch track was produced using a 200 µm diameter diamond indenter under continuous progressive loads of 10-30 N at a load rate of 10 N min^{-1} and speed of 1 mm min^{-1}. Scratch tracks were examined using SEM in order to evaluate any flaking caused by the scratch test. All procedures were performed post annealing.

Photocatalytic activity

Photocatalytic activity levels were determined via the degradation of the organic dye methylene blue (MB) (Alfa Aesar, UK) as described by Ratova *et al*., 2013, since MB is a dye often used as a model organic compound to measure photoreactivity. Photoactivity values were recorded for all the pure titania and the doped coatings and from those results, the optimal dopant level was identified.

Antimicrobial activity

Escherichia coli (ATCC 8739) was used as a model organism in the first instance. Microorganisms isolated from brewery surfaces were obtained from VTT Culture Collection and included *Pseudomonas rhodesiae* E-031889, *Serratia marcescens* E-031888, and *Wickerhamomyces anomalus* C-02470. Measurements of the antimicrobial activity of the doped annealed photocatalytic surfaces were performed using ISO 27447:2009 as guidance (with minor modifications). In brief, approx 10^5 cfu ml^{-1} of bacterial cells were placed on the surfaces and a polyethylene film was placed over the bacterial suspension to ensure even distribution. Surfaces were illuminated (wavelength range of 300-700 nm) in a 20 °C incubator (Gallenkamp, Loughborough, UK) fitted with six fluorescent lamps (Sylvania, Ontario, Canada) with an energy output of 6.4 mW cm^2. At selected time points (0, 12, 24 and 48 hours), surfaces were removed and vortexed for 1 minute in neutralizing broth (20 g l^{-1} Soya Lectin (Holland and Barrett, UK) and 30 g l^{-1} Tween 80 (Sigma Aldrich, UK)). Bacteria were enumerated by plate counts. Acridine orange staining was performed on the surfaces following vortexing and enumeration to check bacterial removal efficacy. All tests were carried out in triplicate. Stainless steel was used as a light control and a set of coated surfaces were also kept in dark conditions to serve as further controls.

Brewery trials

Doped surfaces revealing the best antimicrobial and photocatalytic ability (TiO_2-Mo) and pure titania coatings were placed in a brewery environment (around filling lines) for 12 months, and were tested three times for photocatalytic activity and stability of coating. A further series of surfaces were assessed for antifouling ability over a period of 3 months.

RESULTS AND DISCUSSION

Production of photocatalytic thin films and photocatalytic activity

Magnetron sputtering was used to deposit TiO_2 doped with varying percentages of Mo, Nb and W onto stainless steel. A range of operating parameters and annealing temperatures were investigated and the dopants with the highest photocatalytic activity under visible light, as determined by the degradation of MB, were selected for further investigation and are shown in Table 1. Visible light activity was enhanced by the addition of all transition metals, with the Mo doped coating showing the highest photocatalytic activity value.

Table 1. Dopant levels, predominant crystalline structure and photocatalytic activity levels under UV and fluorescent light irradiation for Mo-doped titania coatings deposited onto stainless steel substrates

Sample	at% dopant	Power to dopant target (W)	Annealing temperature (°C)	Crystal structure	P_{aUV}	P_{aFL}
TiO_2	0	0	600	Anatase	0.69	0.41
Ti-Mo	6.95	180	600	Anatase /rutile	0.88	0.72
Ti-Nb	0.25	100	400	Anatase	0.84	0.53
Ti-W	3.8	60	600	Anatase	0.71	0.45

Coating characterization

The annealed TiO_2 doped surfaces were analysed by XRD and Raman spectroscopy (Figure 1). For Mo, the XRD pattern showed the presence of the (1 0 1) anatase peak at $2\theta = 25.4°$ and the (1 1 0) rutile peak at $2\theta = 27.4°$ and several other minor peaks, whilst the Nb doped surface showed the presence of peaks corresponding to anatase only. In contrast, the Raman spectrum showed only anatase peaks at 144, 389, 515 and 638 cm^{-1} for all surfaces. Based on these analyses, the assumption must be that the structure of the TiO_2-Mo coatings after annealing is a mixed phase, anatase/rutile structure, whilst TiO_2-Nb and TiO_2-W are anatase.

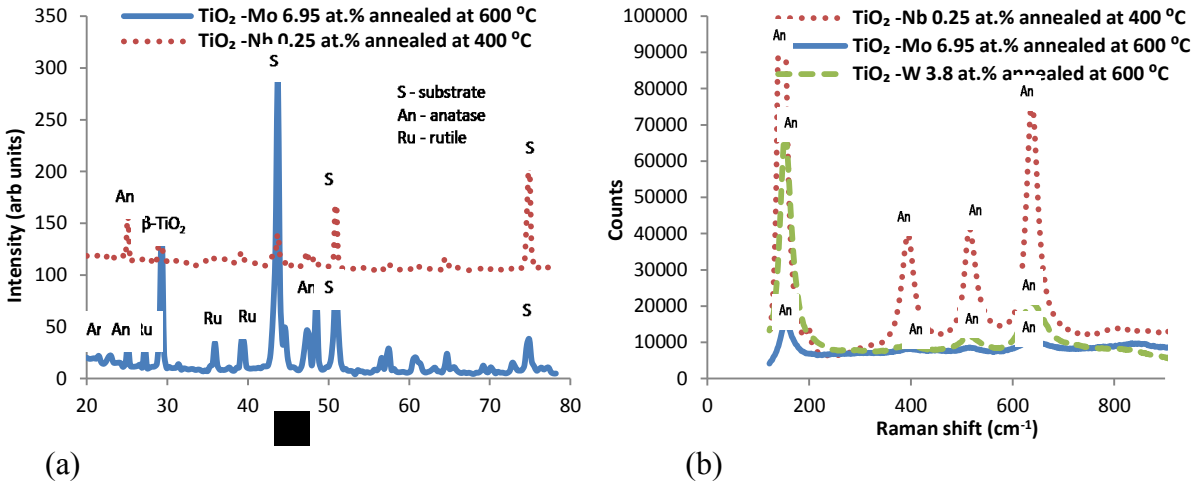

Figure 1. (a) XRD pattern of TiO_2-Mo and TiO_2-Nb surfaces showing the anatase/rutile mix and anatase alone structure respectively and (b) Raman spectra of TiO_2-Nb, TiO_2-Mo and TiO_2-W surface showing the crystal (anatase) structure of the coating.

To investigate coating adherence to substratum, scratch tests were performed on all annealed surfaces. SEM images of the scratch tracks (Figure 2) show good adhesion of the coating and little flaking, which is of fundamental importance in the final application.

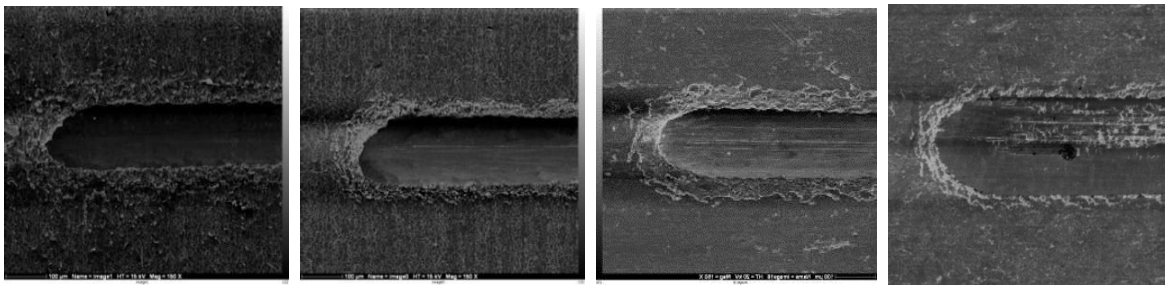

(a) (b) (c) (d)

Figure 2. SEM images of scratch test tracks performed on annealed (a) TiO_2, (b) TiO_2-Mo, (c) TiO_2-Nb and (d) TiO_2-W surfaces.

Antimicrobial activity

All 3 annealed coatings were tested for their antimicrobial activity against *E. coli*. The Mo doped surface proved the most effective and eradicated *E. coli* within 1 - 4 hours, whilst the Nb and W surfaces had a time kill of 48 hours. The Mo surface was also antimicrobial in the dark, whilst the Nb or W surfaces were not.

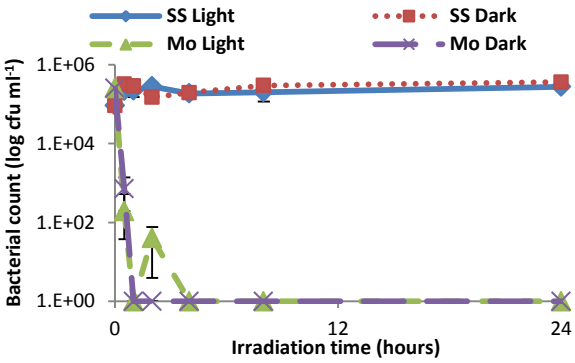

(a)

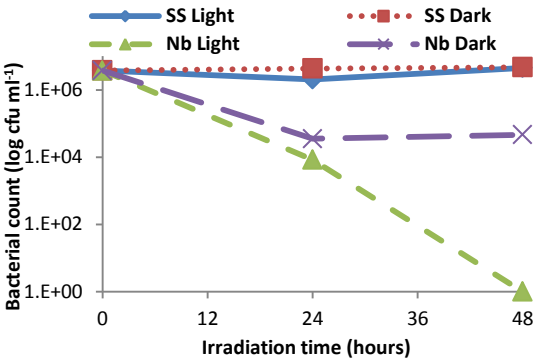

(b)

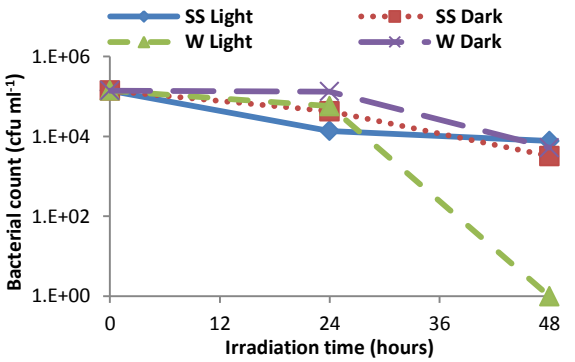

(c)

Figure 3. Antimicrobial effect of TiO_2 coated surfaces doped with (a) molybdenum (Mo), (b) niobium (Nb) and (c) tungsten (W) against *Escherichia coli*. Stainless steel surfaces were used as controls and light and dark conditions were investigated.

The most antimicrobially active coating (TiO_2-Mo) was challenged further with the brewery organisms, *P. rhodesiae*, *S. marcescens* and *W. anomalus* (Figure 4).

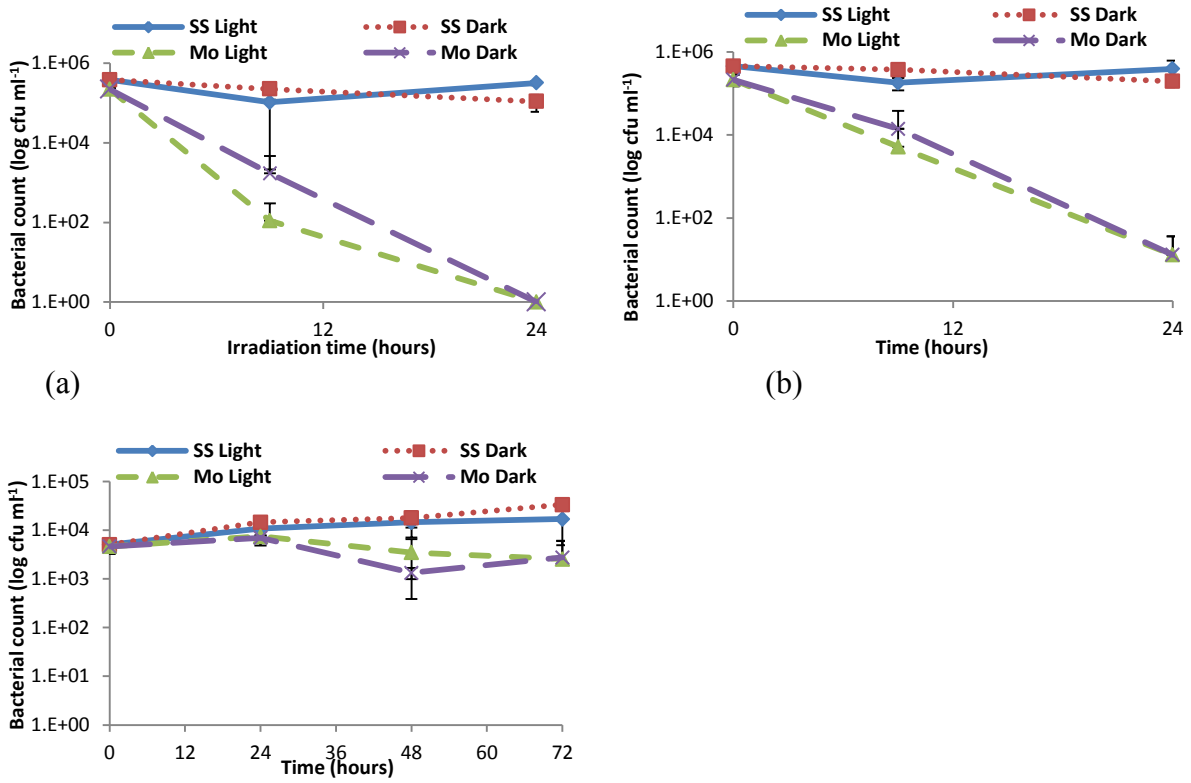

Figure 4. Antimicrobial effect of TiO_2 coated surfaces doped with molybdenum (Mo) on (a) *Pseudomonas rhodesiae* (b) *Serratia marcescens* and (c) *Wickerhamomyces anomalus*. Stainless steel surfaces were used as controls and light and dark conditions were investigated.

P. rhodesiae and *S. marcescens*, counts reduced to 0 cfu and <15 cfu ml^{-1} respectively within 24 hours in both light and dark conditions. *W. anomalus* counts reduced by 1-log compared to non-antimicrobial surfaces, but $>10^3$ cfu ml^{-1} remained following longer irradiation times. The fact that yeast were less easily inactivated could be due to differences in the cell wall structure and the larger size and increased complexity of a eukaryotic cell which could make them more resistant in nature to oxidative agents, compared to bacterial cells and more resistant to killing. In a study by Yasuyuki *et al*., 2010, metals including titanium and molybdenum were tested for their antibacterial properties. The results showed titanium did not exhibit antibacterial properties, but molybdenum did. TEM images showed that metal accumulation resulted in the disruption of the bacterial cell wall and other cellular components which, was attributed to the presence of molybdenum. Similarly Zollfrank *et al*, 2011, report on antimicrobial properties of transition metal acids molybdic acid (H2MoO4), which is based on molybdenum trioxide (MoO3) and show the antimicrobial activity is based on the formation of an acidic surface deteriorating cell growth and proliferation. Results suggest the TiO_2-Mo coating could have a dual function, being both photoactive according to MB tests and have innate antimicrobial ability.

Brewery trials

The pure TiO_2 and TiO_2-Mo surfaces were placed in the brewery environment (around filling lines) for 12 months, and were tested three times for photocatalytic activity and stability of coating. Figure 5 shows the photoactivity levels (in duplicate post brewery trial) as determined by the degradation of MB under UV and visible light, Mo remaining on the surface determined by EDX and coating adhesion following 12 months in a brewery trial

using the scratch test. There was evidence that some photoactivity was retained to varying extents and, that Mo was also largely retained on the coating. Some damage to the coating and flaking was visible on occasion but less so on the Mo doped coating compared to the TiO_2 alone.

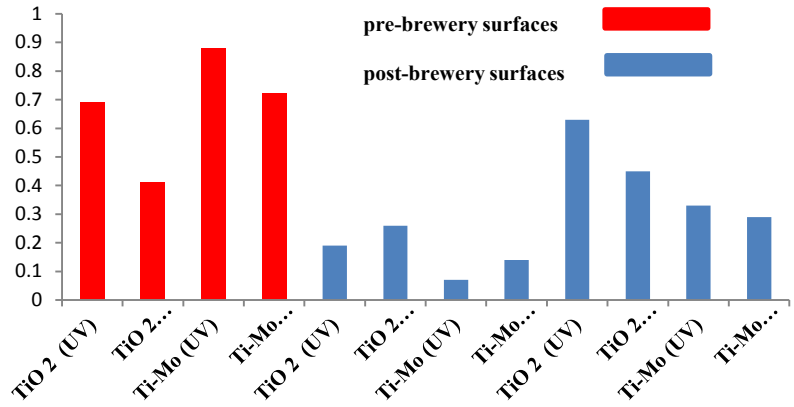

(a)

	Mo %
Pre brewery trial	6.95
Post brewery trial (Surface 1)	6.50
Post brewery trial (Surface 2)	6.83

(b)

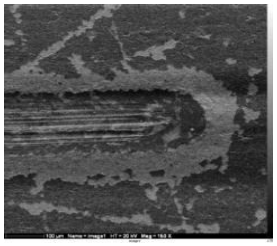

(c)

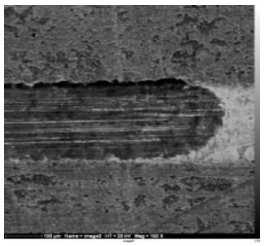

(d)

Figure 5. (a) photoactivity levels, (b) Mo percentages and coating adhesion images of (c) TiO_2 and (d) TiO_2-Mo following 12 months in a brewery trial.

In addition, 3 month fouling studies revealed low numbers of microorganisms on the surfaces, but no clear effect of the coatings on microbial numbers or bacterial community profiles could be seen in these process studies. This could be attributable to the very low numbers of replicate samples

CONCLUSIONS

Titanium dioxide coatings doped with optimized percentages of Mo (6.95 at.%), Nb (0.25 at.%) and W (3.8 at.%) were successfully produced using magnetron sputtering and showed anatase or anatase/rutile photoactive phases and improved photocatalytic activity under fluorescent lighting. Scratch test results revealed the coatings showed good adhesive properties and all surfaces showed some antimicrobial ability, with the TiO_2-Mo surface showing the best antimicrobial ability in the shortest time against *E. coli*. Tests carried out on the TiO_2-Mo surfaces with brewery organisms, found within 24 hours under light and dark conditions, *P. rhodesiae* and *S. marcescens* counts decreased by 5-logs, with *P. rhodesiae* counts reducing to below the limit of detection. *W. anomalus* counts after longer exposure (72 hours) were $>10^3$ cfu ml^{-1}. Results suggest the TiO_2-Mo coating could have a dual function, being photoactive and possessing innate antimicrobial ability.

Following brewery trails, the TiO_2-Mo surfaces retained some photocatalytic activity and scratch tests revealed some minor flaking and visible damage but less so than the TiO_2 alone. Little in terms of loss of Mo from the surface was also found. Overall findings indicate potential for TiO_2-Mo surface in enhancing plant hygiene and complementing existing cleaning and disinfection protocols, whilst offering both innate (antimicrobial in the dark) and photoactive properties. Further work will explore the stability of these coatings, batch variability, and the development of additional *in vitro* tests prior to *in situ* investigations.

ACKNOWLEDGEMENTS

Funding for this work, from the Technology Strategy Board, is gratefully acknowledged. The work reported in this paper formed part of the Matera+ project, 'Disconnecting microbes from food and beverage process surfaces' carried out in partnership with a complementary study in Finland, which was funded by the Finnish Funding Agency for Technology and Innovation (Tekes). Partners in the larger project were: Teer Coatings Ltd, Cristal (UK), and VTT Technical Research Centre of Finland, Tampere University of Technology, Millidyne surface technology and PBL Brewing Laboratory (Finland), to whom thanks are also given.

REFERENCES

Daviðsdóttir. S., Canulescu. S., Dirscherl. K., Schou. J. and Ambat. R. (2013) Investigation of photocatalytic activity of titanium dioxide deposited on metallic substrates by DC magnetron sputtering. Surf Coat Tech., **216**, 35-45.

Foster. H.A., Ditta. I.B., Varghese. S, and Steele. A. (2011) Photocatalytic disinfection using titanium dioxide: spectrum and mechanism of antimicrobial activity. App Microbio Biotech., **90**, 1847-1868.

Fujishima. A., Rao. T.N. and Tryk. D.A. (2000) Titanium dioxide photocatalysis. J Photochem Photobiol C Photochem Rev., **1**, 1-21.

International organization for standardization (ISO) 27447:2009. Fine ceramics (advanced ceramics, advanced technical ceramics). Test method for antibacterial activity of semiconducting photocatalytic materials.

Laing. K., Hampshire. J., Teer. D. and Chester. G. (1999) The effect of ion current density on the adhesion and structure of coatings deposited by magnetron sputter ion plating. Surf Coat Techn., **112**, 177-180.

Ratova. M., Kelly. P.J., West. G.T. and Iordanova. I. (2013) Enhanced properties of magnetron sputtered photocatalytic coatings via transition metal doping. Surf Coat Tech., **228**, 544-549.

Storgårds. E. (2000) Process hygiene control in beer production and dispensing. VTT Technical Research Centre of Finland: University of Helsinki

Wilke. K. and Breuer. H.D. (1999) The influence of transition metal doping on the physical and photocatalytic properties of titania. J Photochem Photobiol A Chem., **121**, 49-53.

Yasuyuki. M., Kunihiro. K., Kurissery. S., Kanavillil. N., Sato. Y. and Kikuchi. Y. (2010) Antibacterial properties of nine pure metals: a laboratory study using *Staphylococcus aureus* and *Escherichia coli*. Biofouling., **26**, 851-858.

Zollfrank. C., Gutbrod. K., Wechsler. P. and Guggenbichler. J.P. (2012) Antimicrobial activity of transition metal acid MoO3 prevents microbial growth on material surfaces. Materials Science and Engineering: C., **32**, 47-54.

Vacuum 86 (2012) 1880–1882

Contents lists available at SciVerse ScienceDirect

Vacuum

journal homepage: www.elsevier.com/locate/vacuum

Rapid communication

Deposition of photocatalytic titania coatings on polymeric substrates by HiPIMS

P.J. Kelly [a,*], P.M. Barker [a], S. Ostovarpour [a], M. Ratova [a], G.T. West [a], I. Iordanova [b], J.W. Bradley [c]

[a] Surface Engineering Group, Manchester Metropolitan University, Manchester M1 5GD, UK
[b] Department of Solid State Physics and Microelectronics, University of Sofia, Bulgaria
[c] Department of Electrical Engineering and Electronics, University of Liverpool, Brownlow Hill, Liverpool L69 3GJ, UK

ARTICLE INFO

Article history:
Received 16 April 2012
Received in revised form
2 May 2012
Accepted 3 May 2012

Keywords:
HiPIMS
Titania coatings
Photocatalytic coatings

ABSTRACT

Titania coatings have been deposited onto PET substrates by reactive magnetron sputtering in the HiPIMS (high power impulse magnetron sputtering) mode and for comparison, pulsed DC mode. In the latter case, the substrate showed evidence of melting, but the HiPIMS results were dependent on the characteristics of the power supply when operating under nominally identical conditions. A coating deposited by one of the HiPIMS supplies was found to have a mixed phase structure and to demonstrate a level of photocatalytic activity comparable to conventional coatings which had been post-deposition annealed.

1. Introduction

Upon being irradiated with UV light, titania coatings can act as photocatalysts and cause the disassociation of pollutant organic compounds and the decomposition of bacterial cells [1–4]. The superhydrophilic nature of the surfaces then enhances the removal of residual material. The photocatalytic activity is, though, limited by the crystalline structure of the films, which are very sensitive to processing conditions and it is only the anatase form (or anatase/rutile mixed phases) that shows useful levels of photocatalytic activity.

In fact, there is a large body of research describing the sensitivity of the structure and properties of titania coatings to deposition conditions (see [5] for a review). The general consensus is that substrate temperatures of the order of 250–300 °C or post-deposition annealing are required to form the anatase phase. This poses processing issues (cost, uniformity, etc.) when coating, for example, large area glazing, and is clearly a major obstacle when seeking to deposit high-performance titania films on polymeric materials.

The present authors were the first to demonstrate that HiPIMS (high power impulse magnetron sputtering) can be considered to be a low temperature deposition process, compared to conventional DC and pulsed DC magnetron sputtering. Measurements showed that for the same net deposition rate, the thermal flux at the substrate was lower in HiPIMS mode by a factor of 2 compared to DC sputtering and by a factor of 10 compared to pulsed DC sputtering, under similar operating conditions [6]. This work has now been extended to demonstrate that photocatalytically active titania coatings can be deposited directly onto polymeric substrates by HiPIMS in a single stage process.

Coatings were deposited via reactive magnetron sputtering from a single 300 mm × 100 mm 99.5% pure Ti target in an argon/oxygen atmosphere at 0.3 Pa. The oxygen flow rate was controlled by optical emission monitoring. The substrates were 75 mm × 25 mm pieces of PET (polyethylene terephthalate) sheet (100 μm thick), which were mounted on a substrate holder that was electrically floating. Three power supplies were used to drive the magnetron: an Advanced Energy Pinnacle Plus pulsed DC supply (PPlus); a Chemfilt Synex 3 HiPIMS supply (Synex); and a Huettinger HMP1/1 HiPIMS supply (Huettinger). The PPlus was operated at 100 kHz pulse frequency with a duty factor of 0.5 and both HiPIMS supplies were operated at 200 Hz pulse frequency with a 200 μs duration pulse. The same time average power of 1.5 kW was used in each case. Due to the differences in deposition rate between the pulsed DC and HiPIMS supplies, run times were adjusted to give coating thicknesses of approximately 100 nm, as measured by a Dektak profilometer from step heights on glass microscope slides coated simultaneously with the PET samples. The deposition rates estimated for each supply were 28.6, 9.1 and 22.2 nm/min for the PPlus, Synex and Huettinger, respectively.

Following deposition the PET samples were examined visually for signs of thermal damage during the coating process. It was immediately obvious that the samples coated using the PPlus and

* Corresponding author.
E-mail address: Peter.Kelly@mmu.ac.uk (P.J. Kelly).

0042-207X/$ – see front matter © 2012 Elsevier Ltd. All rights reserved.
doi:10.1016/j.vacuum.2012.05.003

the Synex supplies were thermally damaged. The substrates were distorted and aluminium foil covering the substrate holder had stuck to the melted plastic. In contrast, the sample coated using the Huettinger supply appeared to be completely undamaged by the process. These differences can be clearly seen in Fig. 1. It is interesting to note the different results obtained from the two HiPIMS supplies, despite operating them at the same pulse frequency, pulse duration and average power. Examination using a digital oscilloscope of the I-V waveforms at the target during the pulse-on phase, shown in Fig. 2, indicates that the pulse shapes of the two supplies are very different. The Synex supply delivers a shorter, more intense pulse, with much higher peak voltages and currents than the Huettinger, under the same operating parameters. Despite setting the pulse duration to 200 μs in both cases, the Synex voltage pulse has effectively decayed after 100 μs, whereas the Huettinger pulse is sustained for the full duration of the pulse. The mechanistic route through which these differences change the deposition conditions at the substrate has not yet been determined, but since the discharge characteristics are dependent on the power supply characteristics, the performances of the two HiPIMS supplies must, at this stage, be attributed to their differing I-V characteristics.

The damaged samples were not analysed further, but the undamaged sample was analysed by X-ray diffraction (XRD) in the grazing incidence asymmetric Bragg diffraction (GIABD) mode at an incident angle $\alpha = 5^\circ$ (URD6 Seiferd & Co diffractometer with CuKα_1 radiation at 0.154 nm). The results of this analysis, shown in Fig. 3, indicate that the coating had a mixed phase structure in the as-deposited condition. Rather surprisingly a peak from the brookite pattern was identified at $2\theta = 49.4^\circ$ (JCPDS file number 29-1360). This phase is not commonly reported in thin films. Of more relevance to this study is the broad peak at approximately $2\theta = 27^\circ$. This peak actually consists of two overlapping peaks, which when deconvoluted (shown inset in Fig. 3), can be identified as the {110} rutile peak (JCPDS file number 21-1276) and the {101} anatase peak (JCPDS file number 21-1272), with the former having the greater intensity.

The photocatalytic activity of this sample was assessed in terms of the degradation of an organic dye (methylene blue). Methylene blue (MB) is a heterocyclic aromatic dye with a molecular formula of $C_{16}H_{18}ClN_3S$, and is often used as a model organic compound to measure photoreactivity [7–9]. When dissolved in distilled water, the MB UV–visible spectrum shows a strong absorption peak at approximately 662 nm wavelength. Changes in this reference peak height can be used to monitor the photocatalytic degradation of MB by titania coatings. The photocatalytic activity of the HiPIMS

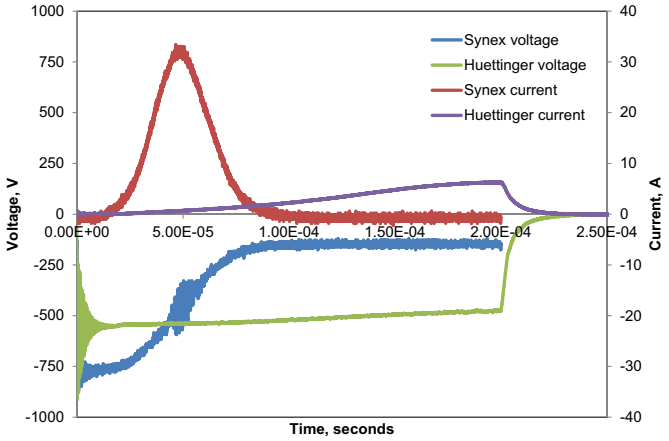

Fig. 2. I-V characteristics during the pulse on phase for the Synex and Huettinger HiPIMS supplies operating at 200 Hz pulse frequency, 200 μs pulse duration and 1.5 kW average power.

coating was studied under UV radiation at room temperature. The integrated power flux to the coating was 4 mW/cm^2 for the UV light tubes (2 × 15 W 365 nm Sankyo Denki BLB lamps). The test sample was fully immersed in 10 ml of MB solution. A Perkin–Elmer UV–Vis spectrophotometer was used for measuring the absorption peak height. Measurements were taken before irradiation and then every hour for a total time of 5 h. This technique has been used by the present authors to test other magnetron sputtered titania coatings (deposited on glass substrates), which were post-deposition annealed at 400 °C [10]. Fig. 4 presents a comparison of an as-deposited and an annealed pulsed DC titania coating (both on glass substrates) with the as-deposited HiPIMS coating (PET substrate). Also shown on the figure is the natural degradation of methylene blue when exposed to UV radiation with no photocatalytic sample present. The as-deposited pulsed DC coating shows negligible photocatalytic activity, whereas the as-deposited HiPIMS coating shows an activity which is comparable to that of the annealed pulsed DC coating. By subtracting the natural degradation of MB under UV radiation, the increased degradation rate due to the photocatalytic activity of the titania samples can be estimated. On this basis, the as-deposited HiPIMS coating has approximately 2/3rd of the activity of the pulsed DC coating annealed at 400 °C. The pulsed DC coating had a predominantly anatase structure after annealing [10], which may well account for its higher activity.

Fig. 1. PET samples coated with titania via reactive magnetron sputtering operating in A) pulsed DC mode; B) HiPIMS mode with a Synex power supply; and C) HiPIMS mode with a Huettinger power supply.

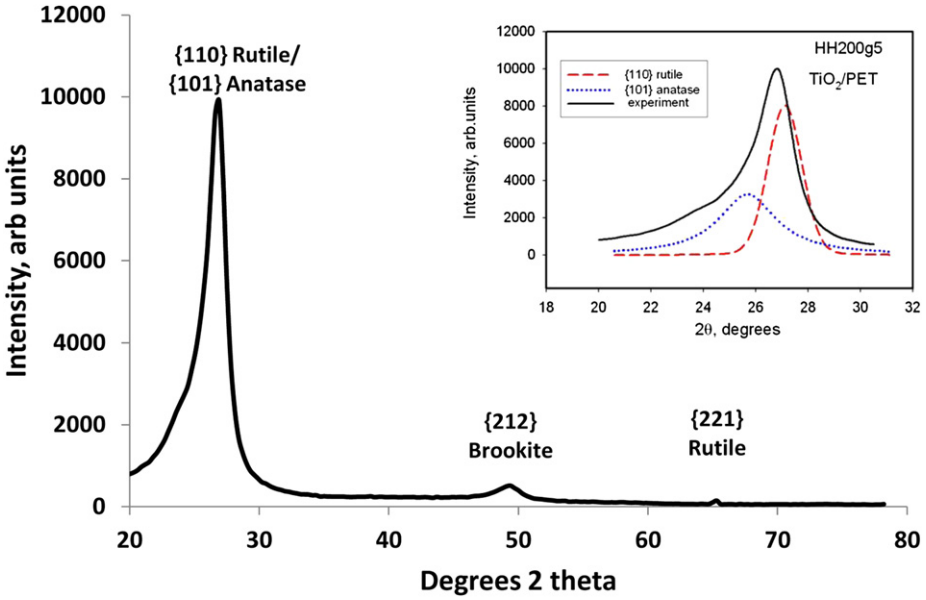

Fig. 3. GIABD mode XRD pattern for titania coating deposited onto PET substrate by HiPIMS using a Huettinger power supply. The inset figure shows the deconvolution of the {110} rutile and {101} anatase peaks.

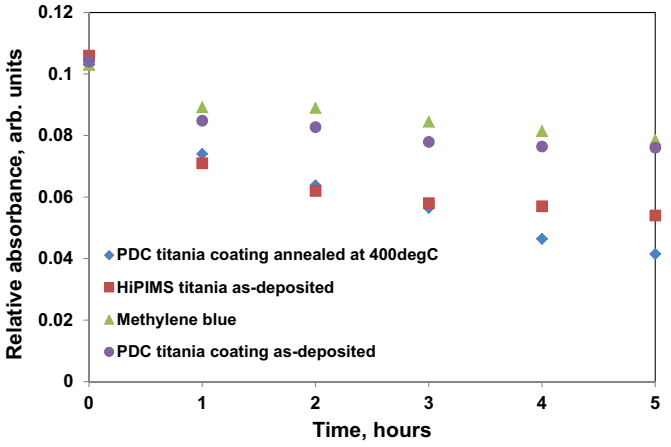

Fig. 4. Degradation of methylene blue 662 nm absorption peak as a function of exposure time to 365 nm UV radiation for pulsed DC (PDC) titania samples as-deposited and annealed at 400 °C and an as-deposited HiPIMS titania sample, compared to the natural degradation rate of methylene blue with no sample present. (For interpretation of the references to colour in this figure legend, the reader is referred to the web version of this article.)

In summary, this work demonstrates that HiPIMS can be used to deposit titania coatings onto PET substrates, but that the outcome is strongly dependent on the I-V characteristics of the power supply. Operating under identical conditions, a Synex supply with relatively high peak voltages and currents caused melting of the PET, whereas a Huettinger supply with lower, more sustained outputs left the substrate undamaged. Furthermore, in the latter case, the titania coating had a mixed phase structure and showed photocatalytic activity in the as-deposited condition which was of the order of 67% of that shown by a conventionally deposited coating that had been annealed at 400 °C. This result demonstrates the potential of the HiPIMS technique to deposit functional films directly onto thermally sensitive substrate materials and to produce active coatings in a single stage process.

References

[1] Gloss D, Frach P, Zywitzki O, Klinkenberg S, Gottfried C. Surf Coat Technol 2005;200:967.
[2] Tavares CJ, Marques S, Lanceros-Mendez S, Sencadas V, Teixeira V, Carneiro JO, et al. Thin Solid Films 2008;516:1434.
[3] Yates HM, Brook LA, Ditta IB, Evans P, Foster HA, Sheel DW, et al. J Photochem Photobiol A Chem 2008;197:197.
[4] Zhang W, Li Y, Zhu S, Wang F. J Vac Sci Technol 2003;A21(6):1877.
[5] Musil J, Herman D, Sicha J. J Vac Sci Technol 2006;A24(3):521.
[6] West GT, Kelly PJ, Barker P, Mishra A, Bradley JW. Plasma Process Polym 2009; 6:S543.
[7] Tavares CJ, Marques SM, Viseu T, Teixeira V, Carneiro JO, Alves E, et al. J Appl Phys 2009;106:113535.
[8] Tomás SA, Luna-Resendis A, Cortés-Cuautli LC, Jacinto D. Thin Solid Films 2009;518:1337.
[9] Wu M, Yang B, Lv Y, Fu Z, Xu J, Guo T, et al. Appl Surf Sci 2010;256:7125.
[10] Ratova M, Kelly PJ, West GT, Iordanova I. Surf Coat Technol; 2012. doi:10.1016/j.surfcoat.2012.04.037.